Vol. 139, July 1, 1982
Complete in one issue

ISSN 0003-2670

ANALYTICA CHIMICA ACTA

International journal devoted to all branches of analytical chemistry

ELSEVIER SCIENTIFIC PUBLISHING COMPANY

ANALYTICA CHIMICA ACTA

International journal devoted to all branches of analytical chemistry
Revue internationale consacrée à tous les domaines de la chimie analytique
Internationale Zeitschrift für alle Gebiete der analytischen Chemie

PUBLICATION SCHEDULE FOR 1982

	J	F	M	A	M	J	J	A	S	O	N	D
Analytica Chimica Acta	134	135/1	135/2	136	137	138	139	140	141	142	143	144

Scope. *Analytica Chimica Acta* publishes original papers, short communications, and reviews dealing with every aspect of modern chemical analysis, both fundamental and applied.

Submission of Papers. Manuscripts (three copies) should be submitted as designated below for rapid and efficient handling:

Papers from the Americas to: Professor Harry L. Pardue, Department of Chemistry, Purdue University, West Lafayette, IN 47907, U.S.A.

Papers from all other countries to: Dr. A. M. G. Macdonald, Department of Chemistry, The University, P.O. Box 363, Birmingham B15 2TT, England. Papers dealing particularly with computer techniques to: Professor J. T. Clerc, Universität Bern, Pharmazeutisches Institut, Sahlistrasse 10, CH-3012 Bern, Switzerland.

Submission of an article is understood to imply that the article is original and unpublished and is not being considered for publication elsewhere. Upon acceptance of an article by the journal, authors resident in the U.S.A. will be asked to transfer the copyright of the article to the publisher. This transfer will ensure the widest dissemination of information under the U.S. Copyright Law.

Information for Authors. Papers in English, French and German are published. There are no page charges. Manuscripts should conform in layout and style to the papers published in this Volume. Authors should consult Vol. 132, p. 239 for detailed information. Reprints of this information are available from the Editors or from: Elsevier Editorial Services Ltd., Mayfield House, 256 Banbury Road, Oxford OX2 7DH (Great Britain).

Reprints. Fifty reprints will be supplied free of charge. Additional reprints (minimum 100) can be ordered. An order form containing price quotations will be sent to the authors together with the proofs of their article.

Advertisements. Advertisement rates are available from the publisher.

Subscriptions. Subscriptions should be sent to: Elsevier Scientific Publishing Company, P.O. Box 211, 1000 AE Amsterdam, The Netherlands.

Publication. *Analytica Chimica Acta* appears in 11 volumes in 1982. The subscription for 1982 (Vols. 134–144) is Dfl. 1815.00 plus Dfl. 220.00 (postage) (total approx. US $814.00). Journals are sent automatically by airmail to the U.S.A. and Canada at no extra cost and to Japan, Australia and New Zealand for a small additional postal charge. All earlier volumes (Vols. 1–133) except Vols. 23 and 28 are available at Dfl. 182.00 (U.S. $72.80), plus Dfl. 14.00 (U.S. $5.60) postage and handling, per volume.

Claims for issues not received should be made within three months of publication of the issue, otherwise they cannot be honoured free of charge.

Customers in the U.S.A. and Canada who wish to obtain additional bibliographic information on this and other Elsevier journals should contact Elsevier Science Publishing Company Inc., Journal Information Center, 52 Vanderbilt Avenue, New York, NY 10017. Tel: (212) 867-9040.

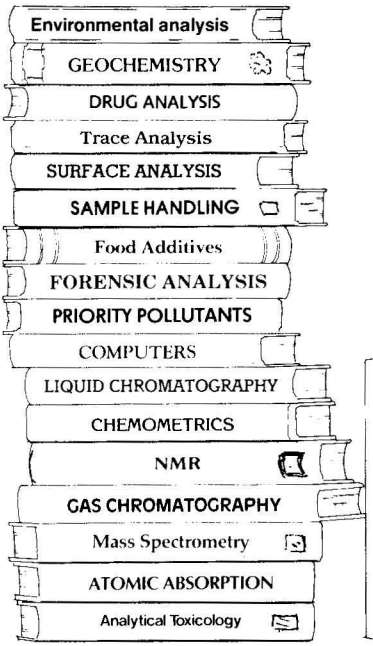

Let TrAC cover the whole of analytical chemistry for you!

A SAMPLE COPY IS NOW AVAILABLE IN YOUR LIBRARY

TrAC trends in analytical chemistry

TrAC - Trends in Analytical Chemistry is a topical monthly which provides you with an easy-to-read interdisciplinary digest of current developments and new ideas in the analytical sciences.

TrAC's authors are leading scientists, its articles practically oriented, its coverage international.

TrAC covers the broader issues which affect those who develop and use analytical methods, such as the impact of computers on the analytical laboratory and the implications of new governmental regulations.

TrAC comes from the publishers of the **Journal of Chromatography** and **Analytica Chimica Acta.**

Subscription Information
Personal edition: 12 issues -
U.K. £20.00, USA and Canada US$42.50, Europe 91.50 Dutch guilders, Rest of World 95.50 Dutch guilders.

Library edition: Vol. 1 (16 issues) -
US$ 133.25 or 260 Dutch guilders.

Prices include air delivery worldwide.

Send now for a free sample copy to

Elsevier Scientific Publishing Company

P.O. Box 330
1000 AH Amsterdam
The Netherlands

52 Vanderbilt Avenue
New York, NY 10017
U.S.A.

Elite-Inn Yushima IF
3-28-1 Yushima, Bunkyo-ku,
Tokyo 113, Japan

7242A

ANALYTICA CHIMICA ACTA
VOL. 139 (1982)

ANALYTICA CHIMICA ACTA

International journal devoted to all branches of analytical chemistry

ELSEVIER SCIENTIFIC PUBLISHING COMPANY

Analytica Chimica Acta, 139 (1982) 1—51
Elsevier Scientific Publishing Company, Amsterdam — Printed in The Netherlands

Review

THEORY AND APPLICATIONS OF ION-SELECTIVE ELECTRODES PART 4[a]

JIŘÍ KORYTA

J. Heyrovský Institute of Physical Chemistry and Electrochemistry, Czechoslovak Academy of Sciences, Opletalova 25, 110 00 Prague 1 (Czechoslovakia)

(Received 23rd November 1981)

SUMMARY

This review of ion-selective electrodes is arranged in the same way as earlier reviews in this series. The growth of the whole subject approaches a steady state. Some mechanistic studies have deepened theoretical understanding. Better insight into the mechanism of liquid-membrane systems has been gained by electrolysis at the interface of two immiscible electrolyte solutions. In this field some interesting analytical applications are noted. A steady growth is shown by publications on ion-selective field-effect transistors. Otherwise the same proportion is preserved among well-established electrode types. About 800 papers published between the end of 1978 and the beginning of 1981 are mentioned.

CONTENTS

[a]Part 3: Anal. Chim. Acta, 111 (1979) 1.

While the number of publications in ion-selective electrodes increased steadily up to 1978, the period afterwards is characterized by a constant rate of some 400 publications per year. The proportion of general papers, particularly of a review character, has increased while the ratio of the numbers of original papers on solid and liquid membranes has remained constant. Part 1 of Theory and Applications of Ion-selective Electrodes [1] covered the literature to the beginning of 1972. In addition to the general theory of membrane potentials of various types, the theory of the potential of ion-selective electrodes and a survey of applications of non-glass ion-selective electrodes, Part 1 also included the theory of the glass electrode and dealt in some detail with the general properties of ion-carriers. The subject matter of Part 2 [1], which covered about 1200 papers published before mid-1976, was restricted to non-glass membrane systems (with the exception of chalcogenide glasses). Part 3 [1] dealt with more than 800 papers published to the end of 1978. The present review again covers about two and a half years (from the end of 1978 to the beginning of 1981) and is concerned with about 800 papers from this period. The subject is treated in an order similar to that used previously. First, progress in theory is dealt with, then problems of methodology are discussed, and finally new information on the basic properties of various types of electrodes, together with their analytical application, is reviewed.

Between the end of 1978 and the beginning of 1981 several symposia took place, and several books as well as numerous reviews were published [1—140]. The 2nd Symposium on Ion-selective Electrodes took place in Warsaw in 1979 [31], the 3rd Scientific Session on Ion-selective Electrodes, in Mátrafüred in 1980 [116] and an International Symposium on Electroanalysis in Clinical, Environmental and Pharmaceutical Chemistry, in Cardiff in 1981 [56]. A symposium on ion-selective microelectrodes and their use in excitable tissues was held in Prague in 1980 [114a]. Bailey published the 2nd edition of Analysis with Ion-selective Electrodes [3]. The English version of Cammann's Working with Ion-selective Electrodes appeared in 1979 [13] and Covington edited two volumes on ion-selective electrode methodology [23, 24]. The second volume of Freiser's Ion-selective Electrodes in Analytical Chemistry [36] appeared in 1980. The classic worker on the subject, Nikolskii, together with Materova, published a Russian monograph on ion-selective electrodes [99]. A monograph devoted to ion-selective microelectrodes for intracellular use was written by Thomas [118] and a book on medical and biological applications of electrochemical devices was mainly devoted to ion-selective electrodes [74].

A new journal, Ion-selective Electrode Reviews, started publication in 1979 [59]. Several bibliographies of ion-selective electrodes were published [11, 16, 17, 18, 91], and the IUPAC Analytical Chemistry Division published a table of selectivity coefficients [62] and rules for publication of data on ion-selective electrodes [63]. A number of general, mainly analytically oriented, reviews were published [9, 14, 19, 22, 25, 27, 33, 35, 41—44, 50, 53, 54, 60, 72, 76, 85, 93, 102, 112, 120, 123, 125, 126, 128, 130, 131]. The specialized reviews are listed in Table 1.

TABLE 1

Specialized reviews on ion-selective electrodes

Subject	Reference
Microelectrodes	1, 8, 52, 96, 119, 132, 138
Industrial applications	3, 29
Medical and biological applications	4, 28, 39, 86, 87, 90, 97, 103, 104
Enzyme sensors	5, 47, 48, 70, 80, 94, 95, 106, 111, 124, 136
Gas monitors	6
Trace analysis	7, 61
Solid-state systems	10, 51, 115, 127
Instrumentation	12
Coated wire electrodes	15, 37, 129
Water analysis, including waste water	20, 32, 46, 55, 75, 77, 84, 98, 100, 107, 108, 133, 134, 139
Food analysis	21
Liquid-state systems	26, 101
Phosphate rock analysis	30
Soil and plant analysis	40, 140
Plastic film systems	45, 92
Electrode surface effects	49
Steel industry applications	78
Pharmaceutical analysis	57, 58, 137
ISFET	64, 65, 82, 83
Environmental analysis	66, 117, 122
Anion-selective electrodes	67
Fermentation process applications	68
Paper industry applications	69
Macrocyclic compound based systems	71
Electrolysis at the interface of two immiscible electrolyte solutions	73
Gran plot and known additions	79
Cholinesterase study	81
Detection limit	88, 89
Non-aqueous solvents	105
Organic analysis	109, 110, 121
Liquid chromatographic detectors	113
Plating bath analysis	114
Automatic analysis	135

THEORY OF MEMBRANE PHENOMENA AT ION-SELECTIVE ELECTRODES

Extensive advances have been made in the understanding of membrane phenomena [73, 141—177].

In continuation of their investigations referred to in Part 3, Buck and his coworkers [142, 143, 151—153, 169, 170] have studied the properties of ion-exchanger type liquid membranes. The effect of co-ion penetration into the membrane on membrane potential has been predicted [169] and the theory has been subjected, together with the method of site concentration determination, to experimental verification [143]. A model liquid membrane based on Aliquat nitrate dissolved in nitrobenzene, with cellulose triacetate, PVC—acrylonitrile, polypropylene and teflon as supports, has been investigated with respect to its electrical properties (impedance, geometrical capacitance, electrical relaxation time constants and permittivities) together with the properties of the ion-exchanger solution alone [152]. The impedance analysis of this membrane demonstrated slow kinetics of nitrate transfer across the interface between the membrane and bathing solution, the effects of the supports, and the time course of the support hydration [152]. These investigations were concluded by a discussion of the detection limit and selectivity of the electrode [153]. Non-zero current properties of the electrode for an ion-exchanger liquid membrane with interfacial permselectivity breakdown have also been predicted [170]. In a theoretical paper [168], the time constants of the response of the ion-exchanger liquid membrane have been predicted for current- and voltage-step perturbation and for a small stepwise activity change. The current-step disturbs the whole system (both interfaces and the interior of the membrane) whereas the activity step has its main impact on one side of the membrane. In connection with previous investigations (see Part 3 [1]) the surface kinetics of the rotating Ag_2S/Ag electrode have also been studied by the impedance method [158]. All this work has been summarized by Buck [142].

Van Mau and Gavach [171—173] have investigated the mechanism of the calcium ion-selective electrode without and with current flow. They also measured the degree of dissociation of the ion exchanger, calcium didecylphosphate, in the membrane.

The effect of the diffusion layer on the selectivity coefficients of solid-state ion-selective electrodes (see ref. 92 of Part 3 [1]) has been described in a new paper [147]. The influence of the speed of rotation on the potential of rotating cyanide ion-selective electrodes has been studied [141]. The impedance of fluoride ion-selective electrodes has been studied [155].

Among theoretical studies dealing with ion-selective electrodes based on neutral carriers, Iyo et al. [150] deduced the multiple chain rule for the selectivity coefficients of a series of cations when a hydrophobic anion is present in the membrane

$$k_{1,n}^{\mathrm{Pot}\prime} = K_{1,2}^{\mathrm{Pot}}\, K_{2,3}^{\mathrm{Pot}}\, K_{3,4}^{\mathrm{Pot}} \ldots K_{n-1,n}^{\mathrm{Pot}} \qquad (1)$$

This equation is valid when the same stoichiometry is preserved with all carrier-cation complexes. In the case of differing stoichiometry, the selectivity coefficient strongly depends on the carrier concentration in the membrane (see Fig. 1). In a study of the rate of partition of neutral carriers [157] between a plastic ("solvent-polymeric") membrane and the bathing solution, it has been established that the transfer of ligands with low lipophilicity is fast, and therefore controlled by diffusion in the membrane phase, whereas mixed kinetics (heterogeneous transfer reaction together with diffusion) controls the process in the case of highly lipophilic ligands.

In a series of papers [163—167, 174—177], the Leningrad group has investigated the properties of ion-selective electrodes based on neutral carriers. They have studied the distribution of ions of different charge number between a valinomycin-containing membrane and the solution [176], and the coupled transport of valinomycin, of the alkali-metal ion and, in some cases, of the lipophilic anion to the membrane/solution interface [163, 164, 167, 174, 175, 177]; the responses of such membranes to anions have been discussed [165] (cf. refs. 169 and 170 of Part 2 [1]). The mechanism of a tetranactin-based ion-selective electrode has been studied [166].

A key to understanding the processes taking place at a liquid membrane/electrolyte solution interface is the study of processes at the interface of two immiscible electrolyte solutions, ITIES (for several earlier papers dealing with the theory, see Parts 2 and 3 [1]). A new picture of the water/organic solvent interface has been proposed [144—146]. The electrical double-layer at this interface consists of two diffuse double-layers, the compact double-

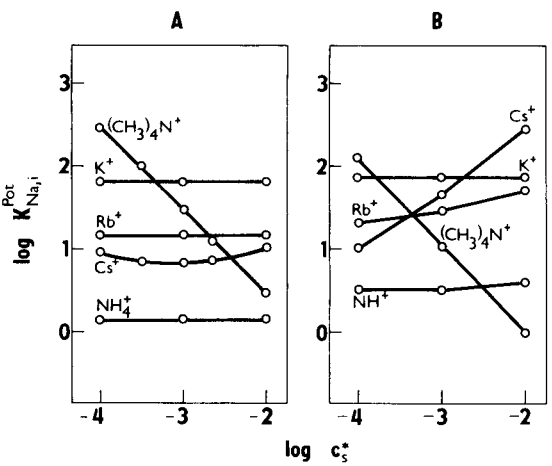

Fig. 1. Dependence of the selectivity coefficient of the ion indicated at each curve with respect to sodium ion on concentration of the neutral carrier, dibenzo-18-crown-6, in the membrane phase [150]. Membrane solvent is nitrobenzene (A) or dichloroethane (B).

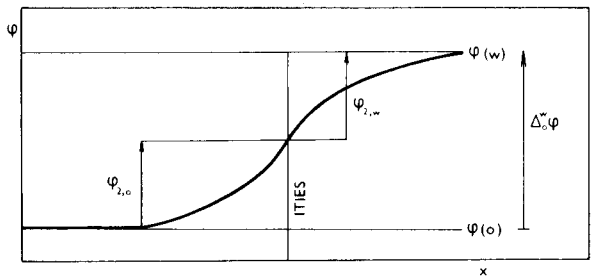

Fig. 2. The electrical double-layer structure at the interface between two immiscible electrolytes (ITIES). The total potential difference between the aqueous and the organic phase is indicated as $\Delta_o^w\varphi$ (= ΔV) = $\varphi_w - \varphi_o$. The potential quantities φ_w and φ_o are the electrical potentials in the aqueous and in the organic phase, respectively, $\varphi_{2,w}$ and $\varphi_{2,o}$ are the potential differences in the diffuse double-layers in the aqueous and in the organic phase.

layer between them being negligible (Fig. 2). This finding is of paramount importance for kinetics of ion-transfer across ITIES as will be shown in some detail.

The potential difference imposed on ITIES from an external voltage source can be defined by

$$\Delta V = \varphi_w - \varphi_o = \varphi_{2,w} + \varphi_{2,o} \quad (2)$$

where φ_w and φ_o are the electrical potentials outside the diffuse double-layers in the aqueous and in the organic phase, respectively, and $\varphi_{2,w}$ and $\varphi_{2,o}$ are the electrical potentials in the diffuse double-layer in the aqueous and in the organic phase (see Fig. 2). It should be stressed that the same potential distribution exists at ITIES when the potential difference is the Nernst potential, i.e., when it is determined by the activities of a given ion in both the phases or when the ITIES has the properties of an ideally polarized interface. Furthermore, in the case where no charge is present in the double-layer, the potential difference is equal to zero. Remarkably enough, the zero charge potential ($\Delta V = 0$) approximately coincides with the zero of the scale of standard potential differences across the water/nitrobenzene interface (see ref. 148 of Part 2 and ref. 98c of Part 3 [1]) based on the TATB assumption (see ref. 110c of Part 3 [1]).

According to the Gouy-Chapman theory of the diffuse double-layer, the charge per unit area of the double-layer is given in the case of a uni-univalent electrolyte with concentration c by the equation

$$q = -(8\epsilon RTc)^{1/2} \sinh(F\varphi_2/2RT) \quad (3)$$

where ϵ is the permittivity of the solution. As the sum of the charge in the double-layer in the aqueous phase and of the charge in the organic phase is equal to zero, $q_w = -q_o$. Combination of this equivalence with Eqn. (3) gives

$$\sinh [F \varphi_{2,w}/2RT] / \sinh [F \varphi_{2,o}/2RT] = (\epsilon_w c_w/\epsilon_o c_o)^{1/2} \quad (4)$$

where ϵ_w and ϵ_o are the permittivities of the aqueous and organic phases, respectively, and c_w and c_o are the concentrations of the uni-univalent electrolyte in each of the phases. With the help of Eqn. (2), both $\varphi_{2,w}$ and $\varphi_{2,o}$ can be calculated. For $\Delta V \gg RT/F$

$$\varphi_{2,w} = \frac{1}{2} \Delta V \pm (RT/2F) \ln (\epsilon_w c_w / \epsilon_o c_o) \quad (5)$$

where the plus sign applies to $\Delta V > 0$ and the minus sign to $\Delta V < 0$.

The simple relationship (5) completely describes the potential distribution at an ideally polarized ITIES as well as at the surface of the ion-selective electrode, of course, in the framework of the Gouy-Chapman theory. In the case of current flow, the basic step is the charge transfer across the plane dividing the aqueous and organic phases. In contrast to electro-chemical kinetics at metallic electrodes, the rate of this ion "jump" is not immediately dependent on ΔV. Only the concentrations of particles transferred at this plane between the water and organic phases depend on the corresponding electrical potential differences in the diffuse double-layers

$$c^*_{i,w} = c_{i,w} \exp (z_i F \varphi_{2,w}/RT) \quad (6)$$

$$c^*_{i,o} = c_{i,o} \exp (-z_i F \varphi_{2,o}/RT) \quad (7)$$

In view of Eqns. (2), (6) and (7), the equation given earlier in Part 3 [1] for current density at ITIES (for a univalent-ion transfer) must be modified so that it reads

$$\begin{aligned} j &= F k_i^o \{ c^*_{i,w} \exp (-\alpha F \Delta^w_o \varphi_i^o/RT) - c^*_{i,o} \exp [(1-\alpha) F \Delta^w_o \varphi_i^o/RT] \\ &= F k_i^o \{ c_{i,w} \exp (-\alpha F \Delta^w_o \varphi_i^o/RT) \exp (F \varphi_{2,w}/RT) \\ &\quad - c_{i,o} \exp [(1-\alpha) z_i F \Delta^w_o \varphi_i^o/RT] \exp (-F \varphi_{2,o}/RT)\} \end{aligned} \quad (8)$$

where k_i^o is the standard transfer rate constant for the ith ionic species, α is the charge-transfer coefficient and $\Delta^w_o \varphi_i^o$ is the standard electrical potential difference between the aqueous and organic phase for the ith ion. The formal validity of Eqn. (8) follows from the fact that for the equilibrium situation ($j = 0$) the usual form of the equation for the Nernst potential is obtained.

Now let us assume that the univalent ion that is transferred is present in concentrations $c_{i,w}$ and $c_{i,o}$ while the larger indifferent electrolyte concentrations are c_w and c_o. It is the indifferent electrolyte alone that determines the potential differences in the diffuse double-layers. When the relationships for the electrical potential differences in the diffuse double-layers are applied for $|\Delta V| \gg RT/F$ (Eqn. 5), then

$$j = Fk^{o} \left[\epsilon_{w} c_{w} / \epsilon_{o} c_{o}\right]^{\pm 1/2} \exp\left[\left(\frac{1}{2} - \alpha\right) F/(RT)\, \Delta_{o}^{w} \varphi_{i}^{o}\right]$$

$$\times \{c_{i,w} \exp\left[F/(2RT)\,(\Delta V - \Delta_{o}^{w} \varphi_{i}^{o})\right] - c_{i,o}$$

$$\times \exp\left[-F/(2RT)\,(\Delta V - \Delta_{o}^{w} \varphi_{i}^{o})\right]\} \qquad (8a)$$

where the plus sign in the exponent of the first expression in square brackets applies to $\Delta V > 0$ and the minus sign applies to $\Delta V < 0$.

In this way, an equation analogous to the basic equation of electrochemical kinetics (eqn. 4 of Part 3 [1]) is obtained where $\alpha = 1/2$. This value of the charge-transfer coefficient does not follow, of course, from the symmetry of the potential energy barrier, as is the case in electrode kinetics, but exclusively from the fact that the overall electrical potential difference between the two phases consists only of the electrical potential differences in the diffuse double-layers.

The theory as well as the experimental results of electrolysis at ITIES have been reviewed [73, 161]. The classical Nernst-Riesenfeld approach (polarization of ITIES, originally in distribution equilibrium, in the absence of an indifferent electrolyte [156]) has been generalized [154] and rectification effects have been predicted [149]. The electron transfer across ITIES has been described [159, 162] and a method for analysis of cyclic voltammetric curves elaborated [160]. The equilibrium situation in a general case of several ionic types present in the liquid/liquid system together with complexation and ion-pair formation has been analysed and the formulae for equilibrium potential differences at ITIES deduced [146a].

In a detailed study of the pCO_2 gas-sensing probe [148], Ross's theory of potentiometric gas sensing probes (see ref. 192, of Part 2 [1]) has been extended to systems with silicone-rubber membranes where diffusion across the polymer matrix characterized by the concentration-dependent diffusion coefficients must be taken into account.

TECHNOLOGY OF ION-SELECTIVE ELECTRODES

The technology of ion-selective electrodes has been studied extensively [1, 8, 12, 15, 37, 45, 52, 64, 73, 79, 82, 83, 88, 89, 92, 96, 105, 118, 119, 129, 132, 138, 161, 178–305].

Construction of ion-selective electrodes

Many papers have dealt with the construction of electrodes [15, 37, 45, 92, 129, 190, 194, 199, 201, 204, 205, 207, 215, 218, 228, 229, 233, 247, 271, 275].

The construction of heterogeneous membrane, carbon-supported and coated-wire ion-selective electrodes has been reviewed [15]. Other reviews have been devoted to plastic-film ion-selective electrodes [45, 92]. Butadiene—styrene rubber with triallylphosphate cross-linking has been used

for the calcium ion-selective electrode [194, 199]. A polymeric membrane for a zinc ion-selective electrode has been developed [201]. The preparation of neutral carrier-based plastic membranes by pressure-controlled solvent evaporation has been described [271].

Coated-wire ion-selective electrodes have been reviewed [37] and their application to the titration of pharmaceutically important substances has been described [129]. This type of ion-selective electrode has been recommended for student laboratories [247]. Miniature coated-wire ion-selective electrodes can be used for Br^-, K^+, Cl^- and SCN^- determinations [207].

Remarkable new electrode materials [233] are the synthetic zeolites, particularly Zeolite A ($NaAlLiO_4 \cdot nH_2O$) and mordenite ($CsAlLi_{6.4}O_{14.8} \cdot nH_2O$). Figure 3 shows a projection of the structure of mordenite. The mordenite membrane shows Nernstian response towards cesium in the concentration range $0.1—3 \times 10^{-5}$ M. The selectivity coefficients for sodium and potassium with respect to cesium are 0.067 and 0.47, respectively.

A magnetic-stirrer type electrode has been introduced for hot-pressed ceramic membrane studies [218]. An oxonium-selective electrode has been based on a cation exchanger membrane and used for the analysis of pickling solutions containing nitric and hydrofluoric acids [229]. Multi-enzyme electrodes have been constructed by asymmetrical coupling of enzymatic systems on collagen membranes [190].

The problem of ion-selective electrodes with internal metallic contact has been discussed in several papers [204, 205, 215, 228, 275]. For the fluoride electrode, an Ag/AgF contact has been proposed [204]. The effect of oxygen diffusion to the contact on the potential of plastic-membrane ion-selective electrodes has been discussed [215, 275]. As expected, the all-solid state electrodes with Cu/Ag/AgX contacts show behavior identical to that of the corresponding second-kind electrodes [228].

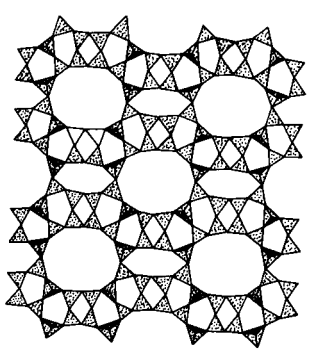

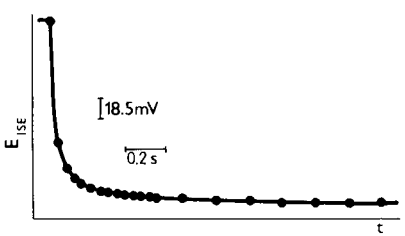

Fig. 3. Projection of the structure of mordenite [233, 402]. The structure is made up from tetrahedra of AlO_4 which are linked together by the common oxygens at the corners.

Fig. 4. Experimental time dependence of the potential of the iodide ion-selective electrode after a concentration change (full circles) [193]. The line indicates the hyperbolic course of this dependence.

Calibration and detection limit

Various aspects have been discussed [88, 89, 227, 237, 250, 251, 260, 266, 281, 286, 297].

A table of single-ion activities in aqueous solution similar to seawater has been compiled for ion-selective electrode calibration [266]. Calibration at low concentrations, calibration by means of metal buffers [286], calibration at non-Nernstian response [250] and calibration in biological fluids by means of the standard addition technique [281] have been reviewed (see also [227]). An exponential dilution flask for ion-selective electrode calibration has been designed [297]. The determination of the limit of detection in analyses with ion-selective electrodes has been discussed in several review articles [88, 89, 227, 237, 250, 251, 260, 266, 286]. Equations have been derived [88, 89] that express the limit of detection in terms of the random error of measurement and the factors that determine the deviation of the electrode response from Nernstian response (reagent blanks, solubility products and interferences).

Response time

For the response time of chloride and iodide ion-selective electrodes it is important whether the concentration is varied from higher values to lower ones or in the opposite direction. The creeping potential change is removed by suitable treatment of the electrode surface. The response time decreases with increasing temperature [192]. The response-time equations have been reviewed but none of them, with the exception of those presented earlier (see refs. 225 and 229 of Part 2 [1]), fits the experimental results obtained with an AgI—Hg_2S electrode which shows a hyperbolic course of the potential—time dependence [193] (Fig. 4). The effects of temperature and hydrodynamic flow on the valinomycin-based potassium electrode have been studied [200].

Measuring procedures

Measuring procedures have received some attention [79, 188, 189, 208—211, 222—226, 231, 234, 239, 248, 261, 263, 264, 267, 268, 277, 285, 288, 292, 295, 303, 304].

Several papers [79, 188, 189, 248, 304] have been concerned with the standard addition method. Gran plots have again been discussed [79, 189, 231]. The precision of direct potentiometry [222], of multiple standard additions [223] (see also [292]) and of potentiometric titrations [224] has been examined. Single-point potentiometric titrations with ion-selective electrodes have been studied [225].

Differential potentiometric titration with two indicator electrodes has been applied to the analysis of binary halide mixtures, to determinations of hexacyanoferrate(III) in the presence of fluoride, and of thiocyanate in the presence of fluoride [234]. Differential titration based on transient ion-selective electrode response has been proposed [295].

In two-phase titrations [181, 208—211], the aqueous phase which is analyzed is in contact with a nitrobenzene layer containing the titrant ion and functioning as an indicator ion-selective electrode. In this way, alkylsulfates, cationic dyes and tetraalkylammonium salts have been titrated with picrate [181, 208, 211], organic bases like papaverin, dimedral and others with laurylsulfate [210] and phenols with crystal violet picrate [209].

Flow injection analysis with ion-selective electrodes has been intensively studied [263, 267, 268]. The analysis of flowing systems with ion-selective electrodes has been described [264]. A flow-through electrode unit has been designed [261].

The fluoride, divalent copper and cadmium ion-selective electrodes have been used as reference electrodes [277]. Selection of suitable reference electrodes for analysis with ion-selective electrodes has been discussed [303]. The law of propagation of errors also applies in analyses with ion-selective electrodes [285]. A system of processing numerical data obtained in ion-selective electrode measurements has been described [288].

Automatic procedures

Significant work has appeared in this area [12, 179, 183, 186, 191, 198, 202, 203, 206, 214, 230, 236, 238, 240, 241, 246, 255—257, 272—274, 276, 282, 283, 296, 305].

Several reviews covering important topics of the field have been published, including general features [12], line analysis in clinical chemistry [276] and optimization of detector systems [240]. The triangle-programmed titration technique has been worked out [256, 257]. In gradient titrations, ion-selective electrodes have been used as end-point detectors [183, 198] and also in manual and computer-controlled flow-injection systems [283]. Ion-selective electrodes have been applied to continuous analysis in rapid-flow systems [179] and during surgical operations [274]. Computer automation of potentiometric analysis [236, 246, 282] as well as an automatic data acquisition system [296] have been discussed. Numerous multi-channel automatic analyzers based on ion-selective electrode potentiometry, particularly for clinical applications, have been described and evaluated [186, 191, 202, 203, 206, 214, 238, 272, 273] (for a review, see [255]). Ion-selective electrodes have been used as detectors in high-pressure liquid chromatography [230] and in gas-chromatographic determination of the Cl/Br ratio in organic compounds [241] (cf. ref. 356 of Part 3 [1]).

Ion-selective electrodes in non-aqueous media

The application of ion-selective electrodes in non-aqueous solvents has been reviewed [105]. A method for determination of methanol in binary methanol—water mixtures by ion-selective electrodes has been described [235].

Ion-selective field-effect transistors

The ISFET has shown a steady though not explosive growth of publications since the last review [64, 65, 82, 83, 178, 182, 185, 187, 212—214, 232, 244, 249, 258, 265, 280, 284, 287, 298—302a]. Besides several general papers [64, 65, 82, 83, 232, 298], attention has been paid particularly to systems sensitive to oxonium ions [178, 182, 187, 211a, 244, 258, 265, 299, 301, 302], halides [185, 213, 250, 300], potassium, sodium and calcium [211a, 214, 249, 265, 284, 287, 302a].

A simple method for silicon nitride growth has been suggested [212, 213]. An oxonium ISFET with a Ta_2O_5 gate has been described [178]. A penicillin-sensitive system is based on an oxonium ISFET [187]. A potassium ion-selective diode with a photoresistive membrane containing valinomycin has been designed [302a]. A portable system for simultaneous measurements of blood electrolytes based on ISFETs has been described [214]. Transient phenomena in ISFETs have been studied [284].

In an ion-selective microelectrode for intracellular potassium measurements (Fig. 5), an oxonium ISFET is used as a reference electrode. The ion-exchanger solution in the tip of the micropipette is in contact with a buffer solution contacting the ISFET. This arrangement shows a better performance with respect to noise than conventional potassium ion-selective microelectrode systems [211a].

Electrolysis at the interface of two immiscible electrolyte solutions (ITIES)

Besides reviews [73, 161, 243] and theoretical papers [144—146, 154, 159, 160, 162], several results of analytical relevance have been obtained [219, 220, 242, 269, 293, 294]. An improved version of the electrolyte-dropping electrode [269] has been designed (Fig. 6). The picrate [220], perchlorate, octoate and dodecylsulfate anions [293] and acetylcholine and choline cations [294] show waves with peak or limiting currents, respectively; the currents are proportional to concentration when investigated by means of cyclic voltammetry or polarography with an electrolyte dropping electrode at ITIES water/nitrobenzene. Neutral ion-carriers of the macro-

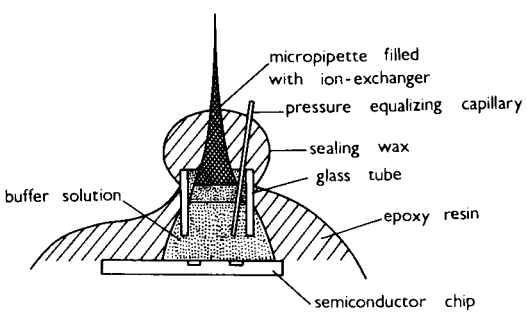

Fig. 5. A potassium ion-selective microelectrode with an oxonium ISFET as reference electrode [211a].

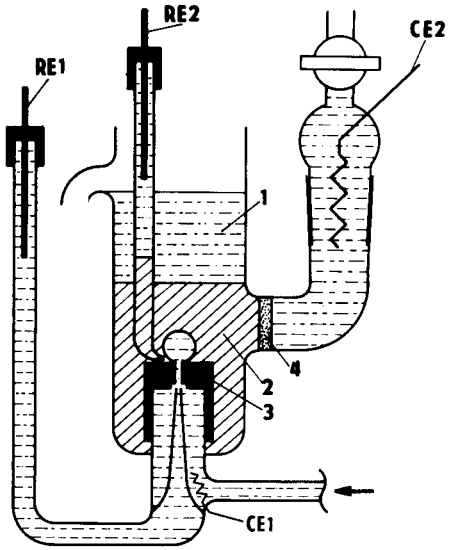

Fig. 6. A new version of the electrolyte dropping electrode [269]. The aqueous electrolyte drop is formed at the orifice of a teflon capillary (3) in a nitrobenzene solution (2). The aqueous solution after dropping off is accumulated in the layer (1). A glass frit separates the nitrobenzene solution (2) from the aqueous electrolyte of counter electrode CE2. RE1 and RE2 are the reference electrodes, both immersed in aqueous solutions.

tetrolide or cyclic polyether type dissolved in the organic phase show peaks proportional to their concentration in cyclic voltammetry [219, 242] when the aqueous solution contains alkali metal chlorides in considerably higher concentration than that of the carrier in the organic phase. The current is controlled by diffusion of the carrier to ITIES where a complex is formed.

The rate of decomposition of acetylcholine in the presence of choline esterase has been studied with this method [294].

Ion-selective microelectrodes

These devices, of great importance for electrophysiological research, have been reviewed in several books and papers [1, 8, 52, 96, 118, 119, 132, 138]. The applications will be dealt with in a later section. An ion-selective electrode with an ISFET reference electrode was described above [211a]. A coaxial low-impedance microelectrode system [289, 290] has been designed. A triple-barrelled ion-selective microelectrode for K^+ and Na^+ activity and membrane potential measurements in kidney proximal tubules has been described [221].

Miscellaneous

Comparisons of ion-selective electrode potentiometry and flame photometry for alkali-metal determinations for clinical purposes have been dealt with in several papers [86, 180—190a, 262]. The potentiometric method shows distinct advantages, as mentioned in Part 3 [1].

The surface structure changes of a copper(II) ion-selective electrode have been studied by means of Auger [252] and x-ray photoelectron [195, 196] spectroscopy. The life-time of neutral carrier-based ion-selective electrodes has been estimated [259]. Effects of light on ion-selective electrode sensitivity have been studied [291]. The problem of the asymmetry potential of ion-selective electrodes has also been investigated [270]. The response of potentiometric enzyme electrodes has been theoretically evaluated [184, 254].

A simple solid-state electrometer for pH and ion-activity determination has been designed [197]. A microprocessor-based millivoltmeter for applications of ion-selective electrodes has been evaluated [253]. A solid-state ion-selective electrode body has been described [217]. The effect of the indicating error of the potential measuring device on the reproducibility of the measurement with liquid-membrane ion-selective electrodes has been discussed [216]. Various methods for inorganic and organic microanalysis [278, 279] and analysis of pharmaceutical products [245] have been described.

FIXED-SITE ION-SELECTIVE ELECTRODES

As in Parts 2 and 3 [1], all fixed-site systems except the silicate glass electrodes are included in this section. The fixed-site ion-selective electrodes have been the subject of two reviews [10, 127], and numerous original papers have been published [141, 192, 195, 196, 204, 230, 235, 252, 277, 306—568].

Silver halide electrodes and similar systems

Several papers have dealt generally with the properties of ion-selective electrodes based on silver halides [383, 443, 445, 483, 488, 504, 506, 536]. Halide determinations with ion-selective electrodes have been reviewed [483]. Silver telluride membranes coated with silver halide can be used for halide ion-selective electrodes [443, 445]. The halide electrodes can be used for titrimetric microdetermination of quinones [383]. Determinations of halogen-substituted thiazole derivatives by means of halide ion-selective electrodes have been described [488]. Microtitration of various anions with quaternary ammonium halides and halide ion-selective electrodes has been suggested [504]. The application of halide ion-selective electrodes as gas chromatographic detectors has been described [241, 506]; cf. ref. 356 of Part 3 [1]. The halide ion-selective electrodes have been used in the analysis of microliter samples by thin-layer potentiometry [536].

Chloride-selective electrodes. Various applications of these electrodes are listed in Table 2. A general paper is available [521]. Modifications of the electrode based on incorporation of mercury(I) chloride into a Ag_2S [415] or HgS [561] membrane have been described (cf. refs. 310 and 446 of Part 3 [1]). The ionic and electronic conductivity of the $AgCl/Ag_2S$ solid electro-

TABLE 2

Applications of chloride-selective electrodes

Use	Reference	Use	Reference
Chloride determination			
in rocks	307, 529	in milk	400, 475
in pharmaceuticals	309, 543	in cheese	400
in water	416, 434	in liver	404
in seawater	310	in marine sand	407
in wastewaters	312, 401, 410, 567	in sweat	328, 450, 451
in gaseous inorganic compounds	324	in beer	478, 509
in fluids of polyamide fibre production	331	in infusion solutions	492
		in soil extracts	497, 512
in pure chemicals	356	in wort	509

lyte has been determined [547]. The response time of the electrode in a streaming solution has been studied [192] (see also above). The effects of bromide [498] and of bromide and iodide in plasma or serum [317] on the electrode have been investigated. The continuous monitoring of chlorides by means of the chloride-selective electrode has been described [370]. Thermodynamic measurements with the system sodium glass electrode/chloride selective electrode have been carried out in the range of pressures 0.1—60 MPa at temperatures of 0—25°C [422]. The behavior of the electrode in the presence of trimethylhexadecylammonium bromide and other surfactants has been investigated [532].

Bromide-selective electrodes. Determination of traces of bromide in rocks [308] and methyl bromide residues [425] by the bromide-selective electrode has been described. The electrode has been used for studying the self-oscillating bromate—propanedioic acid system [421].

The ionic and electronic conductivity of the $AgBr/Ag_2S$ solid electrolyte has been determined [547]. A disproportionation mechanism for the bromide-selective electrode based on a Hg_2Br_2/HgS mixture has been proposed [390].

Iodide-selective electrodes. Various applications of these electrodes are listed in Table 3. A general study has been published [508]. Another version of the electrode contains a Ag_2HgI_4—Ag_2S membrane [503]. The silver/silver iodide film electrode [400] has been studied using kinetic methods [481, 482]. The function of the Ag_2S/AgI electrode for mercury(II) has been evaluated [456] and the behavior at low iodide concentrations [391] and in the presence of iodine [411] has been studied. Attention has been paid to the effect of light on iodide determinations [323]. The behavior of the electrode in iodide titration of palladium(II) has been studied [372]. A student laboratory experiment with the electrode has been described [476].

Cyanide-selective electrodes. Applications of these electrodes are listed in Table 4. A general study has been reported [340]. The effect of rotation speed on the rotating cyanide electrode has been studied [141]. The effect of pH on the response of the electrode has been investigated [376] (cf. Part 1 [1]).

TABLE 3

Applications of iodide-selective electrodes

Use	Reference	Use	Reference
Iodide determination,		Mo(VI) and V(V) catalytic	
—, in organic compounds after combustion	342	determination	405, 406
—, in water	368, 464	Microsomal thyroxine	
—, in rice	368	determination	440
—, in environmental samples	368	L-Amino acids, alcohols and glucose	
—, in serum at low concentration	374	determination based on oxidase	
—, in milk	427, 556	enzyme effect	436
—, in phosphate rocks	430	Potentiometric titration of	
—, in nutritional beverage		halide mixtures	453
products	442	Potentiometric titration of	
—, in pharmaceuticals	543	L-ascorbic acid, *p*-(methylamino)-	
Residual chloride determination,[a]		phenol sulfate and hydroquinone	454
—, in waters	479	Sulfide determination in industrial	
—, automatic	491	wastewaters and sewages	469
—, in conc. H_2SO_4	329	Sulfur determination in steel	507
SO_2 determination in wastewater	359	Mercury determination in	
Nitric acid esters determination		wastewater	527
by indirect titration	403	H_2S and HS^- determination	468

[a]Cf. ref. 422 in Part 3 [1].

TABLE 4

Applications of cyanide-selective electrodes

Use	Reference
Cyanide determination, in water	489, 533
—, in wastewaters	311, 459, 563
—, in presence of mercaptans	322
—, in blood	412
—, in contaminated soil	459
Kinetic determination of formaldehyde and hexamethylene tetramine	420
Amygdalin determination in blood	465

Silver sulfide ion-selective electrodes

The applications of sulfide-selective electrodes are listed in Table 5. The electrode has been modified for flow injection analysis of sulfides and thiols [362]. An Ag_2S electrode with conductive resin support has been designed [431].

Divalent metal chalcogenide electrodes

Entirely solid-state ion-selective electrodes based on lead, silver, copper and cadmium halide and chalcogenide mixtures have been described [565].

Copper ion-selective electrodes. The applications of these electrodes are listed in Table 6. The properties of these electrodes have been reviewed [477]. The preparations of copper ion-selective electrodes based on a CuSe electroplated layer [461], on a CuTe film [444], on a Ag_2Se/Cu_2Se

TABLE 5

Applications of sulfide-selective electrodes

Use	Reference
Sulfide determination, in water	452
—, in wastewater	471, 501, 539
—, in rumen	409
—, in blood	400
Microgram quantities by titration with Pb^{2+}	366
Hg^{2+} determination (Ag_2Se electrode)	314
H_2S determination	316, 418
Various titrations	348
Ag^+ determination by titration with NH_4SCN,	373
—, in silver minerals	447
Ag molybdate and tungstate solubility determination	377
Co(II) determination by titration with ethyldithiocarbonate	419
Pyritic soil analysis by titration with Cd^{2+}	511
Pb^{2+} determination in aqueous and nonaqueous media	486

TABLE 6

Applications of copper ion-selective electrodes

Use	Reference	Use	Reference
Copper(II) determination,		Detector in high-performance liquid chromatography	230
—, in concentrated electrolytes	389	Various titrations	348, 413, 426, 531
—, in minerals	423	As a reference electrode in halide determination	277
—, in soil	423, 499	Fulvic acid ligand sites determination	371
—, in waters (as hydroxo and carbonato complexes)	516, 517	Stability constant determination of Cu-3,6-dioxaoctane-*N,N,N',N'*-tetraacetic acid binuclear complex	473
—, in electrochemical reactors	552	Fe(III), Cu(II)—EDTA complexes study	485
—, in seawater	555	Cu(II)—NTA ternary complexes stability	518
Cu molybdate and tungstate solubility determination	377	Cu(II)—thiosemicarbazide stability	524
Cu(II)—ethylenediamine complexes, study in H_2O/methanol and H_2O/acetonitrile	306	Precipitation titration of oxalate	525
Ca and Mg determination by chelatometric titration,	315	Cu(II)—polycarboxylate complexes study	559, 560
—, in magnesite	449		
Partition equilibria study	349		
Water hardness determination	347		
Amino acid titration	379		
Hydrazine microdetermination	384		
Successive Cu(II) and Zn(II) titrations	500		

mixture [320] and on a polycrystalline membrane [328] have been described. The presence of $Ag_{1.55}Cu_{0.45}S$ (a jalpaite structure) in mixed sulfide materials for copper ion-selective electrodes has been established [397] and the conductivity of this material determined [394]. The surface properties of the copper ion-selective electrode have been studied by means of Auger spectroscopy [252], e.s.c.a. [350] and x-ray photoelectron spectroscopy (x.p.s.) [195, 196, 484]. In the last-mentioned study, the formation of $CuSO_4$ caused by the effect of oxidants has been detected and regeneration by ascorbic acid solution has been suggested (see also [437]).

The behavior of the electrode in metal buffers [380, 457] where some anomalies occur [502, 537] has been described. The problems of chloride influence on the copper ion-selective electrode (cf. Part 1 [1]) have been re-examined [387, 388, 429]. The response of the electrode to solutions of different composition and of different ionic strength has been described [335]. Gran plots are useful in titrations with this electrode [519].

Iron(III) can also be determined by means of the copper selenide/telluride electrode [566]. In a study of the carbonatomonohydrogen complex of copper, the simultaneous presence of Cu(II) and Cu(I) has resulted in errors in the copper activity [551]. The electrode has been used in Cu(II), Cd(II), Co(II), Ni(II) and Zn(II) titrations [426]. It can function as a reference electrode for halide determination [277].

Lead ion-selective electrodes. Applications of lead ion-selective electrodes are listed in Table 7. The preparation of the PbS/Ag_2S electrode has been described [398] and the material characterized as a solid solution [398]. The effects of surface structure, electrode thickness, adsorption at the electrode and permittivity of the solution on the behavior of the electrode have been studied [338, 339, 343]. The influence of temperature on the potential of the electrode in water—alcohol mixtures has been investigated [496]. The microdetermination of selenium in organic compounds can be achieved by potentiometric titration of selenite using the lead ion-selective electrode

TABLE 7

Applications of lead ion-selective electrodes

Use	Reference
Lead(II) determination, in pharmaceuticals	309
—, in organic lead compounds	333
Sulfate determination,	375, 541
—, in food coal tar dyes	399
—, in differential flow systems	534
Penicillamine determination	360
Divalent sulfur determination	381
Penicillin determination	385
Vitamin B_1 determination	386

[332]. A lead-sensitive electrode based on a silver arsenic sulfide glass preparation is suitable for sulfate determination [326].

Cadmium ion-selective electrodes. The formation and properties of a mixed CdS/Ag_2S membrane (and of a mixed HgS/Ag_2S membrane) have been examined [540]. The response of the cadmium ion-selective electrode to solutions of different composition and ionic strength has been investigated [335]. The electrode has been used for potentiometric determination of sulfate in fertilizers [337], of sulfur in waters, chemicals, iron, steel and fly ash [336], of vanadyl ions by EDTA titration using the Cd—EDTA complex as indicator [460], of analytically significant reagents like 8-quinolinol and dithizone [550] and of Cu(II), Cd(II), Co(II), Ni(II) and Zn(II) [426]. The determination of chloramphenicol with this electrode has been compared with spectrophotometry and atomic absorption spectrometry [382]. The electrode has also been applied to determination of stability constants of rare earths with nitrilotriacetic acid [458].

Fluoride ion-selective electrodes

A general paper has been published [352]. Entirely solid-state fluoride electrodes have been described [204, 562]. The effect of europium [313] and calcium [546] doping of the LaF_3 single crystal on the electrode response has been studied. An improved version of the electrode has been suggested [515]. Buffers for electrode calibration at low concentration levels [538], dynamic calibration and memory effects of the fluoride electrode [538], and the effect of ionic strength on fluoride determination [325] have been described. The linear-response reagent method has been applied to fluoride determinations [435]. Analysis for fluoride by continuous flow methods has been reviewed [428]. Low-level fluoride concentrations have been determined after preconcentration on a zirconium(IV)-loaded cation-exchange resin column [417]. Methods for fluoride determination in nanogram and subnanogram quantities [358] and microliter and nanoliter volumes [346, 548, 549] have been described.

Applications of the fluoride ion-selective electrode are listed in Table 8. The determination of fluoride by the ion-selective method and by an acidimetric method have been compared [334]. A comparative study of fluoride determination in urine and blood by ion-selective electrode potentiometry and by molecular absorption spectrometry of aluminum monofluoride has been reported [345]. Potentiometric titrations of fluoride, sulfate, chromate, molybdate, tungstate, pyrophosphate, oxalate and hexacyanoferrate(II) with lead salt solutions and a fluoride indicating electrode have been described [364]. Fluoride titration with potentiometric indication can be used for the determination of aluminum, lanthanum and thorium [522].

The response of the fluoride electrode in organic solvents has been investigated [351] and applied to fluoride determinations [467]. It can also be exploited for the determination of methanol in methanol—water mixtures [235].

TABLE 8

Applications of fluoride-selective electrodes

Use	Reference	Use	Reference
Fluoride determination,			
—, in waters	318, 369, 462, 470, 553, 554, 568	—, in solids	495
—, in minerals and rocks	319, 355, 357, 408, 432, 493, 505, 523, 526	—, in teeth	513, 514
		—, in sodium monofluorophosphate solutions	520
—, in conc. sulfuric acid	330	—, in vegetation	542
—, in wastewater	344, 432, 466, 487, 494	—, in gypsum	544
		Selenium titrimetric determinations	321
—, in fertilizers	344, 432	Aluminum determination,	
—, in urine	345, 353, 396, 530	in soil	341
—, in blood and serum	345, 353, 363, 396, 510, 557	—, in paper-making industry	472
		Sodium monofluoroacetate in biological tissues	365
—, in food	354		
—, in bones	355, 513	Phosphate titrimetric determination	378
—, in glass	355		
—, in zinc electrolyte	392	Thorium titrimetric determination	433
—, in pyrite	393		
—, in slags	395, 466	Iron titrimetric determination in magnesite	448
—, in tin—nickel electrolyte	414		
—, in hydrochloric acid	424	Sulfate titrimetric determination	564
—, in waste gas	432		
—, in industrial environment	438		
—, in tooth enamel	439, 557		
—, in sewage	490		

Other systems

A citrate electrode can be based on a mixed silver citrate—silver sulfide membrane [361]. A heterogeneous sulfate ion-selective electrode contains barium sulfate and silver sulfide in a polymeric matrix [446]; a phosphate-selective electrode contains a mixture of lead phosphate, lead sulfide and lead oxide [441]. For a monohydrogenphosphate electrode, a copper—thiourea—phosphate complex with silver sulfide has been suggested [558]. A mixed salt sulfate ion-selective electrode has also been described [455].

A cesium ion-selective electrode has been prepared from a crystalline synthetic zeolite of the mordenite type [233, 402]. A rare-earth ion-selective electrode contains cerium(IV) oxide in the membrane [528]. Various ion-selective electrodes have been designed with chalcogenide glasses [474]. For example, the copper ion-selective electrode contains Se_{40-48} Cu_{21-35} As_{25-30} as membrane material while the material of the lead-electrode membrane is Pb_{40-53} Se_{29-37} As_{18-23}. A new pH sensor of the membrane type for high temperatures and high pressures is based on yttria stabilized by zirconia [463]. Two types of thallium(I) ion-selective electrodes with polycrystalline membranes have been designed [367].

LIQUID-MEMBRANE ELECTRODES

Many studies of liquid-membrane electrodes have been reported [26, 71, 81, 86, 101, 152, 163—167, 171—177, 194, 199, 201, 221, 289, 290, 569—852].

Electrodes of the liquid ion-exchanger type have been reviewed [26]. In another review, a full survey of all types of liquid-membrane ion-selective electrodes together with their biomedical applications has been presented [86] (for neutral-carrier systems see [571]). A matrix of selectivity coefficients characterizing liquid-membrane ion-selective electrodes has been published [742]. In a review on macrocyclic compounds in analytical chemistry [71], applications of these compounds to ion-selective electrodes have been described. Electrochemical properties of liquid-membrane anion-selective electrodes have been reviewed [101]. Another review deals with the applications of ion-selective microelectrodes to intracellular ion activity determination [692]. A group of particularly lipophilic ion-carriers suitable for ion-selective electrodes has been described [579, 765]. The use of bis-crown ethers in ion-selective electrodes has been discussed [693, 824].

In the subsequent paragraphs, first the calcium (both ionized ion-exchanger and neutral-carrier systems), nitrate and potassium (based on ionized ion-exchanger and neutral-carrier systems) electrodes will be dealt with; other systems based on ionized ion-exchangers and on neutral carriers will be discussed separately.

Calcium-selective electrodes

Ionized ion-exchanger electrodes. The properties, composition and construction of calcium ion-selective electrodes have been reviewed [747—750, 828]. Several introductory papers have been published [720, 820, 847]. Various modifications of the ion-exchanger have been suggested [602, 603, 640, 836]. A polymeric membrane based on butadiene—styrene rubber [194, 199], a graphite calcium electrode [582] and a calcium electrode without internal reference solution [762] have been described. A modification of the divalent metal (water hardness) electrode has been proposed [660]. The mechanism of the electrode response has been investigated [171—173]. The solvent effect [647] and dynamic calibration and memory effects [835] have been studied. The ion-selective electrode method has been compared with the spectrophotometric determination based on arsenazo-III [770].

Neutral ligand electrodes. The topic has been discussed generally [804]. Various modifications of the electrode and of the ligand have been suggested [569, 617]. A combination ion-selective electrode based on a solvent-polymeric membrane has been designed [618]. Lipophilic di- and tri-amides [629] as well as lipophilic amides of EDTA, NTA and iminodiacetic acid [630] have been evaluated as ionophores for alkali earth metal cations. A neutral carrier-based electrode for magnesium activity determination has

been described [712]. A PVC matrix membrane calcium electrode based on bis-4(1,1,3,3-tetramethylbutyl)-2,6-dinitrophenoxide has been designed [683]. A carbon paste calcium electrode may be based on the theonyltrifluoroacetone—calcium(II) complex [779]. The applications of both types of calcium electrodes are listed in Table 9; applications of the microelectrodes are summarized in Table 10.

TABLE 9

Applications of calcium-selective electrodes

Use	Reference	Use	Reference
(a) Alkylphosphate ion-exchangers			
Calcium determination, in serum	573, 655, 691, 698, 713, 714, 781, 782	—, alkali metal, Zn, Mg, Cu ion interference,	746
—, in teeth	580	—, in dairy products	754
—, in Portland cement	581	—, in soils	772
—, in presence of Mg and chelating effectors of isocitrate dehydrogenase	584	—, by EGTA titration	706
		—, in pancreatic juice	791, 814
		Determination of ion-pair stability, of $CaSO_4$	623, 624, 626
—, in presence of bilirubin	591	—, of $MgSO_4$	624, 625, 626, 627
—, in saliva	598, 711, 791		
—, in presence of complexing ligands	604	Determination of Ca^{2+} and Mg^{2+} in seawater	685
—, in presence of anionic surfactants	605	Binding of Ca^{2+} and Mg^{2+} to cyclic AMP	696
—, for assessment of Ca^{2+} uptake by cells	632	Total water hardness	776
—, in waters	669, 802, 816	Ca binding of charged lipid membranes	841
—, at high pressures	697	Kinetics of mitochondrial Ca transport	843
—, in rocks	702		
—, in ore slurries	705		
(b) Neutral ligand electrodes			
Calcium determination, in serum	723	Alkaline earth titrimetric differential determination	766
—, in pharmaceutical products	778	Study of Ca fluxes in mitochondria	606
Water hardness determinations	739		

TABLE 10

Applications of calcium-selective microelectrodes

Use	Reference	Use	Reference
(a) Ionized ion-exchanger systems		*(b) Neutral ligand systems*	
Calcium determination, in fly salivary gland	577	Determination of extracellular Ca during acute coronary infarction	648
—, in sheep heart Purkinje fibres	578	Extracellular Ca modulation	756
—, in amoeba cytoplasm	596	Intracellular Ca determination	572, 831
—, in heart muscle	725		
—, in Aplysia nerve cells	771		
—, in Xenopus embryos	784		
—, during efflux from smooth muscle	800		

Nitrate-selective electrodes

Three general papers have been published [631, 721, 820]. A coated-wire electrode [817] and an electrode with urushi as membrane matrix [666] have been described. As an important new development, a nitrate electrode with a renewable surface based on nitrobenzene solutions of crystal violet and other cationic dye nitrates has been designed [794] (see Fig. 7). A nitrate electrode based on the copper(I) neocuproine complex has been described [830]. Atomic-absorption, direct potentiometric and polarographic methods [661], and direct potentiometric and cadmium column reduction methods [676] for nitrate determinations have been compared. The detection limit and selectivity of nitrate electrodes have been evaluated [152].

Applications of nitrate ion-selective electrodes are listed in Table 11.

Potassium-selective electrodes

Ionized ion-exchanger electrodes. These electrodes have been used exclusively in the microelectrode version; a review has been published [52]. Various modified constructions have been suggested [221, 289, 290, 785]. Applications are listed in Table 12.

Neutral carrier electrodes. In addition to several theoretical studies [166, 167, 174–177] on the valinomycin electrode, some modifications of the system have been suggested [792, 813, 838]. The response time has been

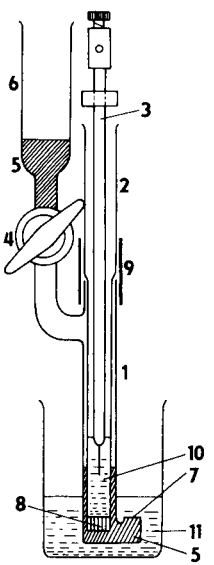

Fig. 7. A nitrate ion-selective electrode [794]. (1) Outer glass jacket; (2) inner glass jacket; (3) inner reference electrode; (4) a stop-cock; (5) the ion-exchanger solution; (6) reservoir for the ion-exchanger solution; (7) orifice of the outer jacket where the membrane–test solution interface is formed; (8) a glass frit; (9) a connecting PVC tube; (10) inner solution; (11) test solution.

TABLE 11

Applications of nitrate-selective electrodes

Use	Reference
Nitrate determination, in waters	583, 621, 664, 726, 803, 829
—, in soils	590, 621, 724, 745, 763, 774, 789, 852
—, in high halide concentrations	619
—, in leaf extracts	676
—, in feeds	740, 788, 851
—, in plant nutrient solutions	740
—, in waste waters	758, 786
—, in plants	763, 788
—, in environmental samples	823, 833
—, in ammonia manufacturing	834
—, in silage	850
Nitrate and nitrite determination	592, 658
Potentiometric titration of hydrogen molybdate	576

TABLE 12

Applications of potassium-selective ion-exchanger microelectrodes

Use	Reference	Use	Reference
Potassium determination,			
—, intracellular	744	—, in transport across bladder membranes	743
—, in kidney proximal tubules	221, 662, 634, 707	—, in heart muscle	751
—, in epithelia	593	—, in nervous system	767
—, in frog ventricular muscle	594, 595	—, in cochlea	787
—, in drone photoreceptor glial cell	597	—, in mammalian CNS	808
—, in toad urinary bladder	604	—, in brain and spinal cord	818
—, effect of local anesthetics	645		
—, effect of drugs and neuro-transmitters	710		

studied [200, 570]. Substitution of valinomycin by crown polyethers in potassium electrodes [759, 761, 832] and by bis-crown polyethers in potassium and cesium electrodes [637, 694, 826] has been investigated. Applications are listed in Table 13. A rubidium ion-selective electrode for assay of polyene antibiotics has been prepared by bathing the valinomycin potassium ion-selective electrode in a rubidium chloride solution [599].

Other systems based on ionized ion-exchangers

In Table 14, systems selective for tetraalkylammonium and other organic base cations are listed. The tetraalkylammonium and analogous compounds of phosphorus and arsenic have been used as ion-exchanging ions for anion-selective electrodes as shown in Table 15.

TABLE 13

Applications of valinomycin potassium-selective electrodes

Use	Reference
Potassium determination, in vanadium catalyst	654
—, in urine	679, 844
—, in blood and serum	757, 768, 773, 790, 844

TABLE 14

Survey of tetraalkylammonium and similar ion-selective electrodes

Type	Reference	Type	Reference
Ion-selective electrode, for cholinesterase study	81, 671	Clobutinol electrode	636
—, for uptake of tetraalkylammonium or tetraphenylphosphonium cations into cells	574, 684, 752, 753	Organic base electrode	651
		Strychnine electrode	662
		Codeine electrode	670
		Histamine electrode	686, 708
		Naphthylazoxine electrode	690
Procylidine, cyclidine and diethylcarbamazine electrodes	588, 727	Chloramine-T electrode for I^- and Os(VIII) determination	704
Surfactant electrodes	607, 682	Liposome immunoelectrode	799
Tetramethylammonium electrode	614	Quaternary ammonium electrodes	806, 807
Creatinium electrode	614		

For organic analysis, the silver liquid-membrane electrode described in Part 3 [1] has been used [601]. A systematic study of homologous trialkylammonium salts as ion-exchangers for chloride, bromide, perchlorate and iodide ion-selective electrodes has been reported [639]. A similar study including solvent effects on perrhenate, sulfate, nitrate, perchlorate and fluoride electrodes has been published [642]. The influence of ion-exchangers (diphosphate, phosphite and phosphonate) and solvent structure on a uranyl-selective electrode has been investigated [641]. Various types of tetrafluoroborate electrode (based on quaternary ammonium or phosphonium, Ni(II) complex of *o*-phenanthroline and brilliant green) have been compared [646]. Micromolar boron determinations with the fluoroborate electrode have been described [649]. In a detailed study, the selectivity and response time of the picrate electrode have been assessed [668]. An ammonium-selective electrode based on tris(2-nitroso-4-chlorophenol)-Fe(II) anion has been suggested [701]. A uranium(VI)-selective electrode is based on tetradecylammonium trisbenzoatodioxouranate [736]. An electrode containing salts of dialkyldithiophosphoric acid can be used for Pb(II), Ni(II) and Cd(II) determinations [737]. An analogous thallium(I) electrode has been described [821]. A copper ion-selective electrode is based on

TABLE 15

Applications of anion-selective electrodes based on tetraalkylammonium salts

Type	Reference	Type	Reference
Benzoate electrode	656	Perchlorate electrode,	677
—, for benzoate determination in pharmaceuticals	575	—, with urushi as membrane matrix	665
Tetrathiocyanato cobaltate(II) electrode for Co(II)	585, 586, 728	High-molecular weight alkylaryl-sulfonate electrode	667
Oxalate electrode	587, 769	Hydrogenchromate electrode	674
Acetate electrode	587, 769	Chromate electrode	677
Chlorocobaltate(II) electrode	589	*N,N*-metallochromic indicator electrode	687
Thiobarbiturate electrode	600	Tetraphenylborate electrode,	688, 77
Bromide electrode,	760	—, for titrations	839, 84
—, effect of interfering anions	610	Bis(2-ethylhexyl)sulfosuccinate electrode	689
Periodate electrode for ethylene glycol and other diols and amino alcohols determination	611, 709	$HgCl_4^{2-}$ and $TlCl_4^-$ electrodes	699
		Thiocyanate electrode,	719, 79
		—, for water analysis	700
Picrate electrode,	653, 668, 672	Iodide electrode,	760
—, for catalytic determination of selenium	612	—, for kinetic determinations	715
—, for determination of alkaloids	613	Perbromate electrode, for citric acid kinetic determination	716
—, for determination of creatinine in serum	615	—, for lactic acid kinetic determination	717
—, for I^-, $Fe(CN)_6^{4-}$, thiourea, cationic surfactants and picrate titrations	616	Hydroxide electrode	729
		Salicylate electrode, for beryllium titration	741
Organic sulfonate electrode, effect of octylphenol	635, 657	Zinc tetrathiocyanate electrode	780
Carbonate electrode	638	Chromium(III) electrode	728
Nicotinate electrode	643, 644	Dodecylsulfate electrode,	755
Anionic surfactant electrode	659	—, for study of micelles	842
Diethyldithiocarbamate electrode, for determination of heavy metals	663	Amino acid electrode	796
		Gold electrode	797
		Niobium(V) acid complex electrode	801
		Alkylsulfate electrode	809

copper(II) complexes with long-chain oximes [819]. In another copper-selective electrode, the complex with benzoylphenylhydroxylamine has been used [822]. In phosphate [848] and arsenate [849] ion-selective electrodes, dialkyltin(IV) compounds are employed in the membrane. In a zinc ion-selective electrode, di(2-ethylhexyl)-phosphoric acid is used [201].

The chloride ion-selective microelectrode (see Part 2 [1]) has been applied to intracellular chloride determination in gall bladder epithelium [620, 783] and in sheep heart Purkinje cells [837].

Several electrodes have been based on ionic hydrophobic dyes dissolved in the membrane. Crystal violet (cf. [794]) has been used in an electrode suitable for titration of acidic and basic dyes [633], of butylammonium bromide, nitrophenols, bromophenols, phenol, picrolonate and laurylsulfate [656] and of fatty acids [652]. In the dodecylbenzenesulfonate electrode, Victoria blue is employed as the counter ion [695].

An anion-selective electrode has been based on an oleophilic anion-exchange resin membrane [675]; this paper is included here because of the analogy of the membrane with liquid ion-exchangers. A tetraphenylborate electrode has been used for detergent titration [777].

Other systems based on neutral ligands

The monensin-based sodium ion-selective electrode (for a general study, see [810]), has been used for intracellular sodium activity in bullfrog kidney [703] and in epithelial cells [718]. Monensin is, of course, an acid and enters the complex in an anionic form (see Part 1 [1]). The neutral carrier suggested for intracellular studies [815] has been employed for sodium activity measurement in Necturus small intestine epithelial cells [764]. The same system has been used to determine sodium in urine [678]. Another ligand, 1,1-oxy-bis(methylene)-bis-benzene in dibutylphthalate has also been suggested for sodium determinations in biological fluids [730—732].

The ammonium electrode based on nonactin has been studied [608, 611, 812]. A thallium(I) electrode has been based on bis-crown ethers [825]. A surfactant ion-selective electrode contains dibenzo-18-crown-6 in the membrane [722]. A liquid-membrane oxonium-selective electrode is based on the synthetic proton carrier [628].

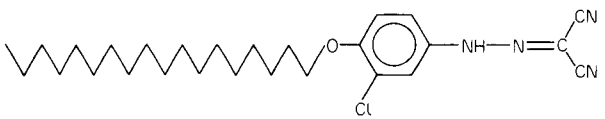

The barium ion-selective electrode (see Part [1]) has been studied with respect to modifications of the ligand [673] and to interferences when this electrode is employed for sulfate titration [681]. The same ligand has been used in an electrode suitable for titration of alkoxylates [680]. A new ionophore for Cd^{2+} has been suggested [793]. Three types of a uranyl ion-selective electrode with heptyldioxaundecane [795], with alkyl sulfoxides [735] and theonyltrifluoracetone [734] as ionophores have been described. Trifluoracetylbenzene derivatives function as ionophores in ion-selective electrodes for organic acids in the presence of tetradecylammonium in the membrane [733, 738].

A number of chiral ionophores has been synthesized and applied to ion-selective electrodes [827] (cf. Part 3 [1]). The treatment of enantiomer selectivity of ion-selective electrodes has been a subject of discussion [805, 845, 846].

OTHER SYSTEMS

Various papers have reported on enzyme electrodes, immuno-chemical electrodes and other devices [5, 70, 80, 94, 95, 106, 111, 124, 136, 184, 254, 853—885].

Enzyme electrodes. Few potentiometric enzyme sensors have been based on the ion-selective electrodes dealt with in this review; most of them contain a glass electrode as the internal electrode. In view of this, only the principles of enzyme sensors will be discussed here.

Enzyme electrodes and their applications have been reviewed in several papers [5, 70, 80, 94, 106, 111, 124, 136, 181]. Morf [254] has presented a simplified theoretical analysis of potentiometric enzyme electrodes and immobilized enzyme sensors, and has formulated the basic parameters governing the steady-state and the dynamic response of these electrodes. The steady-state response of these sensors [184] has been analyzed in a similar way as in an earlier paper (ref. 824 of Part 3 [1]).

Tissue-based membrane electrodes [853—855] have been designed and used for glutamine [853, 855] and adenosine assay [854]. An antidiuretic hormone-specific electrode [885] is based on fitting a toad bladder over the tip of a sodium electrode responding to sodium ions. A bacterial electrode (see Part 3 [1]) based on trimethylphenylammonium cation has been described [863]. Another bacterial electrode has been used for nitrate determination [870].

Enzyme electrodes for acetylcholine [860] and methionine [862] have been described.

Immunochemical electrodes. Several systems have been suggested for antibody assay [858, 879—882].

Miscellaneous. The preceding paragraphs of this [illegible]al with new sensors with interesting possibilities. In contrast, v[illegible]nly heterogeneous membrane electrodes have been based on rat[illegible]d systems which usually show very low stability and reproducibility [856, 857, 859, 864—869, 871—878, 883, 884]. These electrodes can hardly be recommended for practical use.

The assistance of the Technical and Economic Research Institute of Chemical Industry, Prague, who supplied computerized Chemical Abstract condensates dealing with ion-selective electrodes, is highly appreciated. Colleagues from all over the world who send reprints and reports in the field of ion-selective electrodes provide invaluable and much appreciated help for these reviews. I hope that they will continue to assist in this way in the future.

REFERENCES

1 J. Koryta, Anal. Chim. Acta, 61 (1972) 329; 91 (1977) 1; 111 (1979) 1. (Parts 1—3).
2 W. McD. Armstrong and J. F. Garcia-Diaz, Fed. Proc., 39 (1980) 2851.
3 P. L. Bailey, Analysis with Ion-selective Electrodes, 2nd edn., Heyden, London, 1980.
3a P. L. Bailey, Ion-selective Electrode Rev., 1 (1979) 81.
4 D. M. Band and I. Treasure, Ion-selective electrodes in medicine and medical research, in Ref. 24, p. 41.

5 T. Ya. Bart and E. A. Materova, Ion. Obmen Ionometriya, 2 (1979) 73.
6 I. Bergman, Electrochemical gas monitors in occupational hygiene, in W. F. Smyth (Ed.), Electroanalysis in Hygiene, Environmental, Clinical and Pharmaceutical Chemistry, Elsevier, Amsterdam, 1980, p. 167.
7 A. Braat, Continuous trace level analysis using ion-selective electrodes, in J. Albaiges (Ed.), Analytical Techniques in Environmental Chemistry, Pergamon, Oxford, 1980, p. 563.
8 H. M. Brown and J. D. Owen, Ion-selective Electrode Rev., 1 (1979) 145.
9 H. Buehler and H. Galster, Chem.-Tech. (Heidelberg), 8 (1979) 103.
10 R. P. Buck, Crystalline and pressed-powder, solid-membrane electrodes, in Ref. 23, p. 175.
11 R. P. Buck, J. C. Thompsen and O. R. Melroy, A compilation of ion-selective membrane electrode literature, in Ref. 36, pp. 175—288.
12 P. R. Burton, Instrumentation for ion-selective electrodes, in Ref. 23, p. 21.
13 K. Cammann, Working with Ion-selective Electrodes, Springer Verlag, Berlin, 1979.
14 K. Cammann, Gewässerschutz Wasser Abwasser, 39 (1979) 1.
15 W. R. Cattral, Heterogeneous-membrane, carbon-supported and coated-wire ion-selective electrodes, in Ref. 23, p. 131.
16 D. M. Cavagnaro, Natl. Tech. Inf. Serv., Rep. No. NTIS/PS-78/0964, Springfield, VA, 1978, p. 152.
17 D. M. Cavagnaro, Natl. Tech. Inf. Serv., Rep. No. NTIS/PS-78/0965, Springfield, VA, 1978, p. 127.
18 D. M. Cavagnaro, Natl. Tech. Inf. Serv., Rep. No. PB80-815418, Springfield, VA, 1980, p. 210.
19 Y.-H. Chang, Fen Hsi Hua Hsueh, 6 (1978) 313.
20 Chinese Institute of Measurement Science, Fen Hsi Hua Hsueh, 8 (1980) 431.
21 J. Comer, Dev. Food Anal. Tech., 1 (1978) 197.
22 J. Comer, Lab. Equip. Dig., 17 (1979) 73, 75, 77, 79.
23 A. K. Covington (Ed.), Ion-selective Electrode Methodology, 1. CRC Press, Boca Raton, FL., 1979.
24 A. K. Covington (Ed.), Ion-selective Electrode Methodology, 2. CRC Press, Boca Raton, FL, 1979.
25 A. K. Covington, Introduction: Basic electrode types, classification and selectivity considerations, in Ref. 23, p. 1.
26 A. K. Covington and P. Davison, Liquid ion-exchanger types, in Ref. 23, p. 85.
27 D. R. Crow, Lab. Pract., 28 (1979) 1209.
28 B. Csakvári (Ed.), New Developments in Chemistry, Vol. 48, Ion and Molecule-selective Electrodes for Biological Systems (in Hungarian), Akadémiai Kiadó, Budapest, 1980.
29 M. R. Dhaneshwar and R. G. Dhaneshwar. Indian. Chem. Manuf., 18 (1980) 13.
30 A. V. Dolgorev and R. S. Deinekina, Tr. Nauchno-Issled. Inst. Gornokhim. Syr'ya, 47 (1978) 71.
31 Elektródy Ionoselektiwne, Summaries of communications of the 2nd Symposium on Ion-selective Electrodes, Polish Academy of Sciences, Analytical Chemistry, Commission, Warsaw, 1979.
32 D. Eicken, Gewässerschutz Wasser Abwasser, 39 (1979) 181.
33 C.-A. Fang, Fen Hsi Hua Hsueh, 7 (1979) 50.
34 S. N. Fedotova, Khim. Prom., Ser. Prom. Gornokhim. Syr'ya, 3 (1979) 20.
35 M. S. Frant, Ion Selective Electrodes, in M. Grayson and M. Eckrath (Eds.), Kirk-Othmer Encyclopaedia of Chemical Technology, 3rd edn., Vol. 13, Wiley, New York, 1981, p. 720.
36 H. Freiser (Ed.), Ion-Selective Electrodes in Analytical Chemistry, Vol. 2, Plenum, New York, 1980.
37 H. Freiser, Coated-wire ion-selective electrodes, in Ref. 36, pp. 85—105.

38 G. H. Fricke, Anal. Chem., 52 (1980) R259.
39 C. Fuchs, Solid-state ion-selective electrodes in clinical chemistry, in Ref. 74, pp. 93—108.
40 V. Furtula and C. Radenović, Zemljiste Biljka, 29 (1980) 9.
41 M. V. Galiulina and V. K. Leont'ev, Lab. Delo, 6 (1980) 332.
42 H. Galster, Laborpraxis, 3 (1979) 16, 18—21.
43 D. Ghosh, J. Indian Chem. Soc., 56 (1979) 1135.
44 A. V. Gordievskii, Zh. Vses. Khim. Ova., 25 (1980) 616.
45 A. L. Grekovich, E. A. Materova and K. N. Mikhel'son, Ion. Obmen Ionometriya, 2 (1979) 111.
46 A. L. Grekovich, D. E. Morachevskii and V. E. Yurinskaya, Ion. Obmen Ionometriya, 2 (1979) 221.
47 G. G. Guilbault, Enzyme Microb. Technol., 2 (1980) 258.
48 G. G. Guilbault, Use of enzyme electrodes in biomedical investigations, in Ref. 74, pp. 289—323.
49 J. Gulens, Ion-selective Electrode Rev., 2 (1980) 117.
50 K. Hiiro, Kankyo Gijutsu, 8 (1979) 1007.
51 H. Hirata, Natl. Tech. Rep. (Matsushita Electr. Ind. Co., Osaka), 25 (1979) 985.
52 P. Hník, E. Syková, N. Kříž and F. Vyskočil, Determination of ion activity changes in excitable tissues with ion-selective microelectrodes, in Ref. 74, pp. 129—172.
53 A. Hulanicki, Wiad. Chem., 34 (1980) 423.
54 A. Hulanicki, Pr. Kom. Nauk. (Pol. Tow. Glebozn.), 2 (1977) 37.
55 A. Hulanicki and M. Trojanowicz, Ion-selective Electrode Rev., 1 (1979) 207.
56 International Symposium on Electroanalysis in Clinical, Environmental and Pharmaceutical Chemistry, Cardiff, 13—16 April, 1981; Ion-selective Electrode Rev., 2 (1980) 2.
57 M. Ionescu and V. V. Cosofret, Rev. Chim. (Bucharest), 31 (1980) 1005.
58 M. Ionescu and V. V. Cosofret, Rev. Chim. (Bucharest), 31 (1980) 1088.
59 J. D. R. Thomas (Ed.), Ion-selective Electrode Reviews, Pergamon, Vol. 1, 1979; Vol. 2, 1980.
60 N. Ishibashi and A. Jyo, Bunseki, 4 (1978) 210.
61 N. Ishibashi, A. Jyo and K. Kina, Kagaku (Kyoto) Zokan, 78 (1978) 35.
62 IUPAC Analytical Chemistry Division, Pure Appl. Chem., 51 (1979) 1913.
63 IUPAC Analytical Chemistry Division (prep. by G. G. Guilbault), Ion-selective Electrode Rev., 1 (1979) 139.
64 J. Janata and R. J. Huber, Chemically sensitive field effect transistors, in Ref. 36, pp. 107—174.
65 J. Janata and R. J. Huber, Ion-selective Electrode Rev., 1 (1979) 31.
66 R. Kalvoda, F. Opekar, J. Tenygl and A. Trojánek, Chem. Listy, 74 (1980) 785.
67 M. Kataoka and T. Kimihara, Dojin Nyusu, 8 (1978) 1.
68 D. B. Kell, Process Biochem., 15 (1980) 18.
69 Ya. S. Khvorostin, M. S. Skikanova, I. G. Raskina, T. A. Roberts and E. A. Ivanova, Zh. Anal. Kim., 34 (1979) 1694.
70 R. K. Kobos, Potentiometric enzyme methods, in Ref. 36, pp. 1—84.
71 I. M. Kolthoff, Anal. Chem., 51 (1979) 1R.
72 J. Koryta, Basic concepts of electroanalytical methods used in medicine and biology, in Ref. 74, pp. 1—12.
73 J. Koryta, Hung. Sci. Instrum., 49 (1980) 25.
74 J. Koryta (Ed.), Medical and Biological Applications of Electrochemical Devices, Wiley, Chichester, 1980.
75 A. E. Kosov and V. A. Konnov, Okeanologiya, 20 (1980) 943.
76 M. A. Koupparis, C. E. Efstathiou, D. S. Papastathopoulou and T. P. Hadjiioannou, Chem. Chron., Genike Ekdosis, 44 (1979) 45.
77 A. Leiberich, S. M. Hake and A. G. Collins, Rep. No. NTIS-BETC/RT-78/24, Springfield, VA, 1979.

78 D. S. MacIntyre, B. G. Cooksey and J. M. Ottaway, Proc. Anal. Div. Chem. Soc., 16 (1979) 18.
79 M. Mascini, Ion-selective Electrode Rev., 2 (1980) 17.
80 M. Mascini and C. Botrè, Chim. Ind. (Milan), 61 (1979) 542.
81 E. A. Materova and E. B. Nikolskaya, Usp. Khim., 49 (1980) 1937.
82 T. Matsuo, Seinitsu Kikai, 46 (1980) 710.
83 T. Matsuo and M. Esashi, Hyomen, 18 (1980) 495.
84 W. Maurer, GIT Fachz. Lab., 23 (1979) 806.
85 P. C. Meier, Neue Tech., 22 (1980) 11.
86 P. C. Meier, D. Amman, W. E. Morf and W. Simon, Liquid-membrane ion-selective electrodes and their biomedical applications, in Ref. 74, pp. 13—91.
87 A. K. Merzon, V. V. Kolomiets, E. A. Materova and S. E. Didina, Ion. Obmen Ionometriya, 2 (1979) 191.
88 D. Midgley, Anal. Proc. (London), 17 (1980) 306.
89 D. Midgley, Analyst, 104 (1979) 248.
90 G. J. Moody and J. D. R. Thomas, Ion-selective Electrode Rev., 1 (1979) 187.
91 G. J. Moody and J. D. R. Thomas, Ion-selective Electrode Rev., 1 (1979) 251.
92 G. J. Moody and J. D. R. Thomas, Poly(vinylchloride)matrix membrane ion-selective electrodes, in Ref. 23, p. 111.
93 R. Motohashi, Keisaku Gijutsu, 9 (1980) 50.
94 M. Nanjo, Nippon Kinzoku Gakkai Kaiho, 17 (1978) 1039.
95 T. T. Ngo, Int. J. Biochem., 11 (1980) 459.
96 C. Nicholson, Trends Neurosci. (Pers. Ed.), 3 (1980) 216.
97 E. B. Nikolskaya, E. A. Materova, A. L. Grekovich, N. V. Kopylo, A. V. Svyatkovskii, L. V. Ustinova and N. B. Shor, Ion. Obmen Ionometriya, 2 (1979) 208.
98 E. B. Nikolskaya, E. A. Materova, A. L. Grekovich, N. M. Nishchakova, B. V. Pak and N. B. Shor, Ion. Obmen Ionometr., 2 (1979) 215.
99 B. P. Nikolskii and E. A. Materova, Ion-selektivniye elektrody, Khimiya, Leningrad, 1980.
100 A. W. Nobrega and A. M. Da Silva, Quim. Nova, 2 (1979) 45.
101 S. A. Ovchinnikova, Nauchn. Tr., Kuban. Gos. Univ., 232 (1977) 143.
102 D. S. Papastathopoulos, M. A. Koupparis, K. E. Efstathiou and P. Hadjiioannou, Chem. Chron., Genike Ekdosis, 44 (1979) 40.
103 A. Picard-Maureau, MTA-J., 2 (1980) 412.
104 J. Pre, Feuill. Biol., 21 (1980) 73.
105 E. Pungor, K. Tóth and P. Gábor-Klatsmányi, Hung. Sci. Instrum., 49 (1980) 1.
106 G. A. Rechnitz, in Bio-selective Membrane Electrodes in Trace Organic Analysis, NBS Special Publication, No. 519, U.S. Government Printing Office, Washington, 1979, p. 525.
107 K. T. Salikheaev, E. Shermatov, A. A. Abdurakhmanov and A. Ramazanov, Tr. Sredneaziat. Nauchno-Issled. Gidrometeorol. Inst., 61 (1979) 95.
108 R. Sarin, Indian J. Environ. Health, 21 (1979) 244.
109 W. Selig, Ion-selective Electrodes in Organic Elemental and Functional Group Analysis — a Review. Rep. No. UCRL-52393, University of California, Lawrence Livermore Laboratory, 1977.
110 W. Selig, Ion-selective Electrodes in Organic Elemental and Functional Group Analysis — a Review (1975—1978), Rep. No. UCRL-52393, University of California, Lawrence Livermore Laboratory, 1978.
111 D. Skogberg and T. Richardson, J. Food Prot., 43 (1980) 808.
112 O. K. Stefanova, Izmer. Kontrol. Avtomat. (Moscow), 5—6 1980 27.
113 K. Štulík and V. Pacáková. Chem. Listy, 73 (1979) 795.
114 G. Subramanian, N. Avin Chandra and G. P. Rao, J. Electrochem. Soc. India, 27 (1978) 37.
114a Ion-Selective Microelectrodes and Their Use in Excitable Tissues, in E. Syková, P. Hník and L. Vyklický (Eds.), Plenum, New York, 1981.

115 A. Takashi, Hyomen, 18 (1980) 464.
116 3rd Scientific Session on Ion-selective Electrodes, Mátrafüred, October 1980; Hung. Sci. Instrum., 49 (1980).
117 J. D. R. Thomas, Ion-selective electrodes in environmental and toxicological analysis, in J. Albaiges (Ed.), Analytical Techniques in Environmental Chemistry, Pergamon, Oxford, 1980, p. 543.
118 R. C. Thomas, Ion-sensitivie Intracellular Microelectrodes, How to Make and Use Them, Academic Press, London, 1978.
119 R. C. Thomas and W. J. Moody, Trends Biochem. Sci., 5 (1980) 86.
120 K. Tóth, G. Nagy and E. Pungor, Analytical methods involving ion-selective electrodes (including flow methods), in Ref. 24, p. 65.
121 M. Trojanowicz, Chem. Anal. (Warsaw), 25 (1980) 319.
122 M. Trojanowicz, Gaz, Woda Tech. Sanit., 53 (1979) 173.
123 R. Y. Tsien, Trends Neurosci. (Pers. Ed.), 3 (1980) 219.
124 P. Vadgama, Enzyme electrodes, in Ref. 24, p. 23.
125 J. J. Vallon and Y. Pegon, Pharm. Biol., 14 (1980) 531.
126 D. S. Veselinović, Glas. Hem. Drus. (Beograd), 43 (1978) 817.
127 M. Voinov, Use of crystalline solid electrolytes as membranes of ion-selective electrodes, in P. Hagenmüller and W. Van Gool (Eds.), Solid Electrolytes, Academic Press, New York, 1978.
128 J. Vorlíček and A. Dvořák, Rudy, 28 (1980) 74.
129 K. Vytřas, M. Dajková and M. Remeš, Cesk. Farm., 2 (1981) 61.
130 H. Wagner, Laborpraxis, 1 (1977) 24.
131 J. L. Walker, Methods Enzymol., 56, Biomembranes, Part G (1979) 59.
132 J. L. Walker, Single cell measurement with ion-selective electrodes, in Ref. 74, pp. 109—128.
133 G. K. Ward, Proc. Ann. Tech. Meet., Inst. Environ. Sci., 25 (1979) 436.
134 M. Whitfield, The electroanalytical chemistry of seawater, in J. P. Riley and G. Skirrow (Eds.), Chemical Oceanography, Vol. 4, 2nd edn., Academic Press, New York, 1975.
135 P. L. Ying, Fen Hsi Hua Hsueh, 7 (1979) 57.
136 T. M. Yuan, Fen Hsi Hua Hsueh, 7 (1979) 149.
137 M. Xiran Vayreda, Circ. Farm., 36 (1978) 325.
138 T. Zeuthen, How to make and use double-barelled ion-selective microelectrodes, in E. L. Boulpaep, F. Bonner and A. Kleinzeller (Eds.), Current Topics in Membranes and Transport, Vol. 13, Academic Press, New York, 1980. p. 31.
139 I. Ziegler, Gewässerschutz Wasser Abwasser, 39 (1979) 173.
140 G. K. Zykina, V. V. Snakin, T. Bystritskaya and E. A. Materova, Pochv.-Biogeotsenol. Issled. Priazove (Moscow), 1978, p. 136.
141 T. Aomi, Denki Kagaku, 46 (1978) 617.
142 R. P. Buck, Hung. Sci. Instrum., 49 (1980) 7.
143 R. P. Buck, F. S. Stover and D. E. Mathis, J. Electroanal. Chem., 100 (1979) 63.
144 B. D'Epenoux, P. Seta, G. Amblard and C. Gavach, J. Electroanal. Chem., 99 (1979) 77.
145 C. Gavach, P. Seta and B. D'Epenoux, J. Electroanal. Chem., 83 (1977) 225.
146 M. Gros, S. Gromb and C. Gavach, J. Electroanal. Chem., 89 (1978) 29.
146a Le Q. Hung, J. Electroanal. Chem., 115 (1980) 159.
147 A. Hulanicki and A. Lewensztam, Talanta, 24 (1977) 171.
148 M. A. Jensen and G. A. Rechnitz, Anal. Chem., 51 (1979) 1972.
149 P. Joos, J. Electroanal. Chem., 86 (1978) 75.
150 A. Iyo, H. Seta and N. Ishibashi, Nippon Kagaku Kaishi, (1980) 1423.
151 D. E. Mathis, F. S. Stover and R. P. Buck, J. Membr. Sci., 4 (1979) 395.
152 D. E. Mathis and R. P. Buck, J. Membr. Sci., 4 (1979) 379.
153 D. E. Mathis, R. M. Freeman, S. T. Clark and R. P. Buck, J. Membr. Sci., 5 (1979) 103.

154 O. R. Melroy, R. P. Buck, F. S. Stover and H. C. Hughes, J. Electroanal. Chem., in press.
155 J. Mertens, P. van den Winkel and J. Vereecken, Bioelectrochem. Bioenerg., 5 (1978) 699.
156 W. Nernst and E. H. Riesenfeld, Ann. Phys., 8 (1902) 600.
157 U. Oesch and W. Simon, Helv. Chim. Acta, 62 (1979) 754.
158 R. K. Rhodes and R. P. Buck, Anal. Chim. Acta, 110 (1979) 185.
159 Z. Samec, J. Electroanal. Chem., 103 (1979) 1.
160 Z. Samec, J. Electroanal. Chem., 111 (1980) 211.
161 Z. Samec, V. Mareček, P. Vanýsek and J. Koryta, Chem. Listy, 74 (1980) 715.
162 Z. Samec, V. Mareček and J. Weber, J. Electroanal. Chem., 103 (1979) 11.
163 O. K. Stefanova, Elektrokhimiya, 15 (1979) 1707.
164 O. K. Stefanova, Vestn. Leningr. Inst., 22 (1978) 94.
165 O. K. Stefanova and K. H. Mikhelson, Elektrokhimiya, 17 (1981) 554.
166 O. K. Stefanova, N. V. Rozhdestvenskii and I. V. Rusina, Elektrokhimiya, 15 (1979) 1561.
167 O. K. Stefanova and E. D. Suglobova, Elektrokhimiya, 15 (1979) 1822.
168 F. S. Stover, T. R. Brumleve and R. P. Buck, Anal. Chim. Acta, 109 (1979) 259.
169 F. S. Stover and R. P. Buck, J. Electroanal. Chem., 94 (1978) 59.
170 F. S. Stover and R. P. Buck, J. Electroanal. Chem., 107 (1980) 165.
171 N. D. Van Mau and C. Gavach, J. Electroanal. Chem., 97 (1979) 163.
172 N. D. Van Mau and C. Gavach, J. Electroanal. Chem., 97 (1979) 171.
173 N. D. Van Mau and C. Gavach, J. Electroanal. Chem., 97 (1979) 151.
174 V. E. Yurinskaya, O. K. Stefanova and E. A. Materova, Elektrokhimiya, 15 (1979) 723.
175 V. E. Yurinskaya, O. K. Stefanova and E. A. Materova, Elektrokhimiya, 16 (1980) 860.
176 V. E. Yurinskaya, O. K. Stefanova, E. A. Materova and V. V. Glazunov, Elektrokhimiya, 15 (1979) 419.
177 V. E. Yurinskaya, O. K. Stefanova, E. A. Materova and O. A. Yukhno, Elektrokhimiya, 16 (1980) 320.
178 T. Akiyama, T. Lugano and E. Niki, Bunseki Kagaku, 29 (1980) 584.
179 P. W. Alexander and P. Seegopaul, Anal. Chem., 52 (1980) 2403.
180 W. Annan, N. A. Kirwan and W. S. Robertson, Clin. Chem., 25 (1979) 643.
181 I. A. Borisova and I. A. Gurev, Zavod. Lab., 45 (1979) 309.
182 M. Bos, P. Bergveld and A. M. W. van Veen-Blaauw, Anal. Chim. Acta, 109 (1979) 145.
183 G. P. Bound and B. Fleet, Talanta, 27 (1980) 257.
184 J. E. Brady and P. W. Carr, Anal. Chem., 52 (1980) 977.
185 R. P. Buck, Yu. G. Vlasov and D. E. Hackleman, Zh. Prikl. Khim. (Leningrad), 52 (1980) 2465.
186 W. J. Calogero, Advances in Automated Analysis, Technicon International Congress, NY, Vol. 1, 1976, p. 132.
187 S. Caras and J. Janata, Anal. Chem., 52 (1980) 1935.
188 T. F. Chao, K'o Hsueh T'ung Pao, 24 (1979) 212.
189 T. F. Chao, K'o Hsueh T'ung Pao, 24 (1979) 258.
189a R. L. Coleman, Clin. Chem., 25 (1979) 1865.
189b R. L. Coleman, C. C. Young and L. Sidoni, Clin. Chem., 26 (1980) 1922.
190 P. R. Coulet and C. Bertrand, Anal. Lett., 12 (1979) 581.
190a J. D. Czaban and A. D. Cormier, Clin. Chem., 26 (1980) 1923.
191 J. Daroczy, J. Erdelyi, J. Havas, G. Jozan, L. Kecskes and K. Nyiro, Hung. Sci. Instrum., 45 (1979) 47.
192 A. Dencks and R. Neeb, Fresenius Z. Anal. Chem., 297 (1979) 121.
193 A. Dencks and R. Neeb, Fresenius Z. Anal. Chem., 298 (1979) 131.
194 L. Ebdon, A. T. Ellis and G. C. Corfield, Analyst, 104 (1979) 730.

195 M. F. Ebel, W. Gröger, L. Pólos, K. Tóth and E. Pungor, Hung. Sci. Instrum., 49 (1980) 41.
196 M. F. Ebel, K. Tóth, L. Pólos and E. Pungor, Surf. Interface Anal. , 2 (1980) 197.
197 R. D. Edstrom, J. Chem. Educ., 56 (1979) A169.
198 D. L. Eichler, Advances in Automated Analysis, Technicon International Congress, NY, Vol. 1, 1977, p. 51.
199 A. T. Ellis, G. C. Corfield and L. Ebdon, Anal. Proc. (London), 17 (1980) 48.
200 N. A. Fedotov, V. A. Zarinskii, I. Ya. Kolotyrkina, L. M. Khitrov and V. G. Lazarev, Dokl. Akad. Nauk SSSR, 255 (1980) 666.
201 U. Fiedler-Linnersund and K. M. Bhatti, Anal. Chim. Acta, 111 (1979) 57.
202 P. Fievet, A. Truchaud, J. Hersant and G. Glikmanas, Clin. Chem., 26 (1980) 138.
203 J. Fillbach, Int. Lab., Nov./Dec. (1979) 35.
204 T. A. Fjedly and K. Nagy, J. Electrochem. Soc., 127 (1980) 1299.
205 T. A. Fjedly, K. Nagy and J. S. Johannessen, J. Electrochem. Soc., 126 (1979) 793.
206 E. J. Fogt, A. R. Eddy, A. H. Clemens, J. Fox and H. Heath, Clin. Chem., 26 (1980) 1425.
207 A. L. Grekovich, Vestn. Leningr. Univ., Fiz., Khim., 3 (1980) 68.
208 I. A. Gurev, Izv. Vyssh. Uchebn. Zaved., Khim. Khim. Tekhnol., 23 (1980) 1087.
209 I. A. Gurev, E. A. Gushina and E. N. Mitina, Zh. Anal. Khim., 34 (1979) 1184.
210 I. A. Gurev, G. M. Lizanova and N. S. Bulanova, Zh. Anal. Khim., 34 (1979) 1809.
211 I. A. Gurev and T. S. Vyatchanina, Zh. Anal. Khim., 34 (1979) 976.
211a A. Haemmerli, J. Janata and H. M. Brown, Anal. Chem., 52 (1980) 1179.
212 D. Hackleman, Yu. G. Vlasov and R. P. Buck, J. Electrochem. Soc., 125 (1978) 1875.
213 D. E. Hackelman, Thesis, University of North Carolina, Chapel Hill, Univ. Microfilms Int., Order No. 7914355, 1978.
214 J. Harrow, J. Janata, R. L. Stephen and W. J. Kolff, Proc. Eur. Dial. Transplant Assoc., 17 (1980) 179.
215 G. Heidecke, J. Kropf, G. Stork and J. G. Schindler, Fresenius Z. Anal. Chem., 303 (1980) 364.
216 G. Heidecke, G. Stork, J. G. Schindler, M. V. Gulich, W. Schmid, H. Maier, H. O. Lindt and D. Sailer, Fresenius Z. Anal. Chem., 301 (1980) 406.
217 H. B. Herman and J. J. Shoby, Anal. Lett., 13 (1980) 419.
218 H. Hirata, M. Arai and N. Toonooka, Nippon Kagaku Kaishi, 10 (1980) 1475.
219 D. Homolka, Le Q. Hung, A. Hofmanová, M. W. Khalil, J. Koryta, V. Mareček, Z. Samec, S. K. Sen, P. Vanýsek, J. Weber, M. Březina, M. Janda and I. Stibor, Anal. Chem., 52 (1980) 1606.
220 D. Homolka and V. Mareček, J. Electroanal. Chem., 112 (1980) 91.
221 M. Honda, Osaka Ika Daigaku Zasshi, 38 (1979) 202.
222 G. Horvai and E. Pungor, Anal. Chim. Acta, 113 (1980) 287.
223 G. Horvai and E. Pungor, Anal. Chim. Acta, 113 (1980) 295.
224 G. Horvai and E. Pungor, Anal. Chim. Acta, 116 (1980) 87.
225 G. Horvai, K. Tóth and E. Pungor, Anal. Chim. Acta, 107 (1979) 101.
226 G. Horvai, K. Tóth and E. Pungor, Mag. Kem. Foly., 84 (1978) 483.
227 G. Horvai, K. Tóth and E. Pungor, Magy. Kem. Foly., 85 (1979) 382.
228 M. A. Ilyushchenko, V. A. Mirkin and G. S. Zhakipova, Elektrokhimiya, 17 (1980) 862.
229 Y. Inokuma, T. Ochiai, J. Endo and K. Hiiro, Nippon Kagaku Kaishi, (1980) 1469.
230 N. Ishibashi and A. Iyo, Asahi Garasu Kogyo Gijutsu Shoreikai Kenkyu Hokoku, 33 (1978) 47.
231 A. Ivaska, Talanta, 27 (1980) 161.
232 J. S. Johannessen, T. A. Fjedly and K. Nagy, Phys. Scr., 18 (1978) 464.
233 G. Johansson, L. Fälth and L. Risinger, Hung. Sci. Instrum., 49 (1980) 47.
234 L. S. Jovanović, J. D. Fišl and F. F. Gaál, Anal. Chim. Acta, 120 (1980) 81.

235 G. J. Kakabadse, H. A. Maleila, M. N. Khayat, G. Tassopoulos and A. Vahdati, Analyst, 103 (1978) 1046.
236 J. Kalinowski, Ind. Res./Dev., 21 (1979) 105.
237 N. Kamo, Y. Kobatake and K. Tsuda, Talanta, 27 (1980) 205.
238 E. M. Kartchner, Advances in Automated Analysis, Technicon International Congress, NY, Vol. 1, 1976, p. 164.
239 G. Kasseber, Gewässerschutz, Wasser Abwasser, 39 (1979) 159.
240 D. B. Kell, Optimisation of detector systems incorporating ion-selective electrodes, in W. F. Smyth (Ed.), Electroanalysis in Hygiene, Environmental, Clinical and Pharmaceutical Chemistry, Elsevier, Amsterdam, 1980, p. 61.
241 T. Kojima, M. Ichise and Y. Seo, Asahi Garasu Kogyo Gijutsu Shoreikai Kenkyu Hokoku, 32 (1978) 261.
242 J. Koryta, in E. Pungor and E. Burés (Eds.), Electrolysis at the interface of two immiscible electrolyte solutions and its analytical aspects, Akadémiai Kiadá, Budapest, 1981.
243 J. Koryta, M. Březina, A. Hofmanová, D. Homolka, Le Q. Hung, M. W. Khalil, V. Mareček, S. K. Sen, P. Vanýsek and J. Weber, Bioelectrochem. Bioenerg., 7 (1980) 61.
244 I. R. Lauks and J. N. Zemel, IEEE Trans. Electron Devices, 26 (1979) 1959.
245 C. Luca, C. Baloescu, G. Semenescu, T. Tolia and E. Semenescu, Rev. Chim. (Bucharest), 30 (1979) 72.
246 C. R. Martin and H. Freiser, Anal. Chem., 51 (1979) 803.
247 C. R. Martin and H. Freiser, J. Chem. Educ., 57 (1980) 512.
248 W. Matuszewski, A. Zytnikowski and M. Trojanovicz, Chem. Anal. (Warsaw), 25 (1980) 897.
249 P. T. McBride, J. Janata, P. A. Comte, S. D. Moss and C. C. Johnson, Anal. Chim. Acta, 101 (1978) 239.
250 D. Midgley, Analyst, 105 (1980) 417.
251 D. Midgley, Analyst, 105 (1980) 1002.
252 G. J. Moody, N. S. Nassory, J. D. R. Thomas, P. Szeposváry and B. Wright, Analyst, 104 (1979) 1237.
253 G. J. Moody and J. D. R. Thomas, Lab. Pract., 28 (1979) 125.
254 W. E. Morf, Mikrochim. Acta, II (1980) 317.
255 G. Nagy, Zs. Fehér, K. Tóth and E. Pungor, Hung. Sci. Instrum., 49 (1980) 61.
256 G. Nagy, Zs. Fehér, K. Tóth and E. Pungor, Magy. Kém. Foly., 85 (1979) 321.
257 G. Nagy, Z. Lengyel, Z. Fehér, K. Tóth and E. Pungor, Anal. Chim. Acta, 101 (1978) 261.
258 H. Nakajima, M. Esashi and T. Matsuo, Nippon Kagaku Kaishi, (1980) 1499.
259 U. Oesch and W. Simon, Anal. Chem., 52 (1980) 692.
260 M. S. Okunev, T. G. Udartseva and O. I. Kornienko, Mezhvuz. Temat. Sb. Tyumen. Ind. Inst., 62 (1977) 114.
261 D. S. Papastathopoulos, E. P. Diamandis and T. P. Hadjiioannou, Anal. Chem., 52 (1980) 2100.
262 C. J. Preuss and C. Fuchs, J. Clin. Chem. Clin. Biochem., 17 (1979) 639.
263 E. Pungor, Z. Fehér, G. Nagy, K. Tóth, G. Horvai and M. Gratzl. Anal. Chim. Acta. 109 (1979) 1.
264 E. Pungor, K. Tóth, G. Nagy, Z. Fehér and G. Horvai, in A. Varmevuori (Ed.), 27th International Congress of Pure and Applied Chemistry, Pergamon, Oxford, 1980, p. 83.
265 A. U. Ramsing, J. Růžička, J. Janata and M. Levy, Anal. Chim. Acta, 118 (1980) 45.
266 R. A. Robinson and R. G. Bates, Mar. Chem., 7 (1979) 281.
267 J. Růžička and E. H. Hansen, Anal. Chim. Acta, 106 (1979) 207.
268 J. Růžička and E. H. Hansen, Natl. Bur. Stand. (U.S.), Spec. Publ., 519 (1979) 501.
269 Z. Samec, V. Mareček, J. Weber and D. Homolka, J. Electroanal. Chem., 99 (1979) 385.
270 O. F. Schaefer, Fresenius Z. Anal. Chem., 293 (1978) 30.

271 J. G. Schindler and M. v. Gülich, Biomed. Techn., 25 (1980) 283.
272 J. G. Schindler and M. v. Gülich, J. Clin. Chem. Clin. Biochem., 19 (1981) 49.
273 J. G. Schindler, M. v. Gülich, H. Maier, G. Stork, W. Schäl, H. E. Braun, W. Schmid and K. D. Karaschinski, Fresenius Z. Anal. Chem., 301 (1980) 410.
274 J. D. Schindler, G. Stork, R. Dennhardt, W. Schäl, H. E. Braun, K. D. Karaschinski, W. Schmid and E. Fresenius, J. Clin. Chem. Clin. Biochem., 17 (1979) 573.
275 J. G. Schindler, G. Stork, H. J. Struh, W. Schmid and K. D. Karaschinski, Fresenius Z. Anal. Chem., 295 (1979) 248.
276 W. J. Scott, Line analysis in clinical chemistry using ion-selective electrodes, in W. F. Smyth (Ed.), Electroanalysis in Hygiene, Environmental, Clinical and Pharmaceutical Chemistry, Elsevier, Amsterdam, 1980, p. 47.
277 I. Sekerka and J. F. Lechner, Anal. Lett., 12 (1979) 1239.
278 W. Selig, Mikrochim. Acta, II (1980) 133.
279 W. Selig, Talanta, 27 (1980) 914.
280 B. Shiramizu, J. Janata and S. D. Moss, Anal. Chim. Acta, 108 (1979) 161.
281 R. J. Simpson, Application of standard addition technique to ISE calibration in biological fluids, in W. F. Smyth (Ed.), Electroanalysis in Hygiene, Environmental, Clinical and Pharmaceutical Chemistry, Elsevier, Amsterdam, 1980, p. 45.
282 J. Slanina, F. Bakker, J. J. Moels, J. E. Ordelman and A. G. M. Bruyn-Hes, Anal. Chim. Acta, 112 (1979) 45.
283 J. Slanina, W. A. Linderak and F. Bakker, Anal. Chim. Acta, 117 (1980) 91.
284 R. L. Smith, J. Janata and R. J. Huber, J. Electrochem. Soc., 127 (1980) 1599.
285 G. Svehla, Ion-selective electrodes and the law of propagation of errors, in W. F. Smyth (Ed.), Electroanalysis in Hygiene, Environmental, Clinical and Pharmaceutical Chemistry, Elsevier, Amsterdam, 1980, p. 21.
286 J. D. R. Thomas, Hung. Sci. Instrum., 49 (1980) 33.
287 M. Thompson, N. K. Krull and P. J. Worsfold, Talanta, 26 (1979) 1015.
288 M. Trojanowicz, Chem. Anal. (Warsaw), 24 (1979) 649.
289 E. Ujec, O. Keller, N. Kříž, V. Pavlík and J. Machek, Bioelectrochem. Bioenerg., 7 (1980) 363.
290 E. Ujec, O. Keller, J. Machek and V. Pavlík, Pflügers Arch., 382 (1979) 189.
291 Y. Umezawa, J. Takino, Y. Imanishi, Y. Asano, S. Ito and S. Fujiwara, Nippon Kagaku Kaishi, (1981) 182.
292 R. Vaďura and H. Pokorná, Chem. Prům. (Prague), 29 (1979) 194.
293 P. Vanýsek. J. Electroanal. Chem., 121 (1981) 149.
294 P. Vanýsek and M. Behrendt, J. Electroanal. Chem., 130 (1981) 287.
295 J. Veselý, Anal. Lett., 13 (1980) 543.
296 R. Virtanen, Kem.-Kemi, 5 (1978) 460.
297 R. Virtanen, Kem.-Kemi, 5 (1978) 614.
298 Yu. G. Vlasov, Zh. Prikl. Khim., 52 (1979) 3.
299 Yu. G. Vlasov and A. V. Bratov, Elektrokhimiya, 17 (1981) 601.
300 Yu. G. Vlasov, D. E. Hackleman and R. P. Buck, Anal. Chem., 51 (1979) 1570.
301 Yu. G. Vlasov, Yu. A. Tarantov, A. P. Baraban and V. P. Letavin, Zh. Prikl. Khim., 53 (1980) 1980.
302 Yu. G. Vlasov, Yu. A. Tarantov and V. P. Letavin, Zh. Prikl. Khim., 53 (1980) 2345.
302a C. C. Wen, I. Lanks and J. V. Zemel, Thin Solid Films, 70 (1980) 333.
303 C. C. Westcott, Beckman Rep., 2 (1978) 22.
304 K.-L. Wu, Fen Hsi Hua Hsueh, 6 (1978) 266.
305 M. Yamasata and R. Motohashi, Nippon Kagaku Kaishi, (1980) 1532.
306 M. Aihara and Y. Oho, Seikatsu Kagaku, 12 (1979) 95.
307 H. Akaiwa, H. Kawamoto and K. Hasegawa, Talanta, 26 (1979) 1027.
308 H. Akaiwa, H. Kawamoto and K. Hasekawa, Talanta, 27 (1980) 909.
309 S. L. Ali and W. Stock, Pharm. Ztg., 123 (1878) 1815.
310 G. Andreev, A. Stoyanov and V. Simeonov, God. Sofii. Univ., Khim. Fak., (1980) 69.

311 T. B. Andreeva, V. A. Krasnozhen and Yu. M. Trofimov, Fosfornaya prom., (1978) No. 3, 40.
312 T. B. Andreeva, Yu. M. Trofimov, V. G. Pogodaeva and N. V. Sobina, Fosfornaya Promst., 3 (1978) 45.
313 T. Aomi, Denki Kagaku, 47 (1979) 733.
314 T. Aomi, Denki Kagaku, 48 (1980) 491.
315 F. K. Arey, J. W. Chamblee and E. Heckel, Int. J. Environ. Anal. Chem., 7 (1980) 285.
316 Y. Asano and S. Ito, Nippon Kagaku Kaishi, (1980) 1494.
317 C. Baker, S. E. Kahn and E. W. Bermes, Ann. Clin. Lab. Sci., 10 (1980) 523.
318 H. Ballczo and M. Sayer, Fresenius Z. Anal. Chem., 298 (1979) 382.
319 G. I. Bebeshko, V. P. Roze and V. A. Khalizova, Zh. Anal. Khim., 34 (1979) 507.
320 H. Berge, U. Gruenke and P. Hartmann, Z. Phys. Chem. (Leipzig). 261 (1980) 1049.
321 J. L. Bernal, E. Barrado and R. Pardo, Anal. Chim. Acta, 111 (1979) 71.
322 J. L. Bernal, R. Pardo and J. M. Rodrigues, Anal. Chim. Acta, 120 (1980) 367.
323 R. G. Black, J. R. Pasco and R. L. Welton, Aust. J. Dairy Technol., 35 (1980) 64.
324 G. Blazevic, M. Boehner and E. Schenbeck, Fresenius Z. Anal. Chem., 298 (1979) 12.
325 E. I. Babrikova, Fosfornaya Promst., 3 (1980) 26.
326 C. Bohnke, A. Saida and G. Robert, C.R. Acad. Sci., Ser. C, 290 (1980) 97.
327 H. Bourgognon, J.-J. Fombon, F. Lancelot, J. Paris, M. Roubin and J. Tacussel, Analusis, 8 (1980) 296.
328 P. T. Bray, C. F. Clark, J. Moody and J. D. R. Thomas, Arch. Dis. Child., 53 (1978) 483.
329 K. D. Brown and G. A. Parker, Anal. Chem., 51 (1979) 1332.
330 K. D. Brown and G. A. Parker, Analyst, 105 (1980) 1208.
331 L. N. Bykova, N. A. Kazaryan, N. S. Chernova, I. O. Shachova and N. M. Kvasha, Khim. Volokna, 6 (1978) 63.
332 A. Campiglio, Mikrochim. Acta, I (1979) 245.
333 A. Campiglio, Mikrochim. Acta, I (1979) 267.
334 M. Cartwright and A. A. Woolf, J. Fluorine Chem., 13 (1979) 501.
335 N. Cavallaro and M. B. McBride, Soil. Sci. Soc. Am. J., 44 (1980) 881.
336 D. Chakraborti and F. Adams, Anal. Chim. Acta, 109 (1979) 307.
337 D. Chakraborti and F. Adams, Fresenius Z. Anal. Chem., 298 (1979) 397.
338 S. N. K. Chaudhari and K. L. Cheng, Mikrochim. Acta, II (1979) 411.
339 S. N. K. Chaudhari and K. L. Cheng, Mirkochim. Acta, II (1980) 159.
340 H.-Y. Chen, C.-H. Ksiao and T.-L. T'ang, Nan-Ching Ta Hsueh Hsueh Pao, Tzu Jan K'o Hsueh, 2 (1978) 41.
341 T.-Y. Chen, C.-Y. Cheng and L.-Yu I., T'u Jang, 3 (1977) 176.
342 F. W. Cheng, Microchem. J., 25 (1980) 86.
343 K. L. Cheng and S. N. K. Chaudhari, Mikrochim. Acta, I (1981) 185.
344 Chengtu Technological University, Fen Hsi Hua Hsueh, 7 (1979) 116.
345 K. Chiba, K. Tsunoda, H. Haraguchi and K. Fuwa, Anal. Chem., 52 (1980) 1582.
346 K. Chiba, K. Tsunoda, Y. Umezawa, H. Haraguchi, S. Fujiwara and K. Fuwa, Anal. Chem., 52 (1980) 596.
347 R. Ciurlo, E. Tassara, F. Andreoni and G. B. Deferrari, Rass. Chim., 31 (1979) 155.
348 C. J. Coetzee and S. R. Grabler, Tydskr. Natuurwet., 19 (1979) 12.
349 J. F. Coetzee and W. K. Istone, Anal. Chem., 52 (1980) 53.
350 J. F. Coetzee, W. K. Istone and M. Carvalho, Anal. Chem., 52 (1980) 2353.
351 J. F. Coetzee and M. W. Martin, Anal. Chem., 52 (1980) 2412.
352 R. Combes, P. Letellier and N. Baffier, Actual. Chim., 6 (1979) 27.
353 D. C. Cowell, Med. Lab. Sci., 35 (1978) 265.
354 R. W. Dabeka, A. D. McKenzie and H. B. S. Conacher, J. Assoc. Off. Anal. Chem., 62 (1979) 1065.
355 S. I. Dely, Publ. Hung. Min. Res. Inst., 21 (1978) 299.

356 L. A. Demina, N. B. Krasnova and N. N. Mazepova, Khim. Prom., Ser. Reakt. Osobo Chist. Veshchestva, 3 (1979) 38.
357 J.-H. Deng and Y.-S. Yu, T'u Jang Hsueh Pao, 16 (1979) 313.
358 D. Deutsch and S. Zarini, Anal. Chem., 52 (1980) 1167.
359 A. A. Diggens and S. Lichtenstein, Proc. Int. Water Conf., Eng. Soc. West. Pa., 39 (1978) 83.
360 S. M. Donahe, G. E. Janauer, T. D. Zucconi and C. Lewkowicz, Natl. Bur. Stand. (U.S.), Spec. Publ., 519 (1979) 455.
361 L. P. Dorsett and D. E. Mulcathy, Anal. Lett., 13 (1980) 409.
362 E. J. Duffield, G. J. Moody and J. D. Thomas, Anal. Proc. (London), 17 (1980) 533.
363 J. G. Durocher, Ann. Biochim. Clin. Que., 19 (1980) 9.
364 C. E. Efstathiou and T. P. Hadjiioannou, Anal. Chim. Acta, 109 (1979) 319.
365 J. O. Egekeze and F. W. Oehme, Toxicol. Lett., 4 (1979) 461.
366 T. M. Florence and Y. J. Farrar, Anal. Chim. Acta, 116 (1980) 175.
367 J. J. Fombon, Y. Oddon, J. Tacussel and A. Tranquard, Analusis, 7 (1979) 494.
368 N. Fukuzaki, T. Suzuki, R. Sugai and T. Oshina, Bunseki Kagaku, 28 (1979) 60.
369 R. Gallęgo, J. L. Bernal and R. Pardo, Afinidad, 35 (1978) 333.
370 H. Galster, Gewässerschutz Wasser Abwasser, 39 (1979) 143.
371 D. S. Gamble, A. W. Underdown and C. H. Langford, Anal. Chem., 52 (1980) 1901.
372 M. Geissler, Fresenius Z. Anal. Chem., 302 (1980) 188.
373 M. Geissler and E. Lorenz, Z. Chem., 19 (1979) 138.
374 A. Gilak, NUC Compact, Compact News Nucl. Med., 10 (1979) 227, 230.
375 M. Yu. Gorina and L. E. Ryvkina, Zh. Anal. Khim., 33 (1978) 2269.
376 M. Gratzl, F. Rakiás, G. Horvai, K. Tóth and E. Pungor, Anal. Chem. Acta, 102 (1978) 85.
377 S. R. Grabler and S. K. Suri, J. Inorg. Nucl. Chem., 42 (1980) 51.
378 Yu. N. Gusev, A. V. Kopytin, A. F. Zhukov, Yu. I. Urosov and A. V. Gordievskii, Khim. Prom., Ser. Metody Anal. Kontrolya Kach. Prod. Khim. Prom., 1 (1980) 25.
379 I. Haiduci, M. Mioscu and D. Cormos, Stud. Univ. Babes-Bolyai. Ser. Chem., 24 (1979) 59.
380 T. Hashizume, Kitakyushu Kogyo Koto Semmon Gakko Kenkyu Hokoku, 11 (1978) 183.
381 S. S. M. Hassan and M. H. Eldesouki, Mikrochim. Acta, II (1979) 27.
382 S. S. M. Hassan and M. H. Eldesouki, Talanta, 26 (1979) 531.
383 S. S. M. Hassan and M. B. Elsayes, Mikrochim. Acta, II (1978) 333.
384 S. S. M. Hassan and M. T. M. Zaki, Mikrochim. Acta, I (1979) 137.
385 S. S. M. Hassan and M. T. M. Zaki, Talanta, 26 (1979) 91.
386 S. S. M. Hassan, M. T. M. Zaki and M. H. Eldesouki, J. Assoc. Off. Anal. Chem., 62 (1979) 315.
387 T. Hepel, Anal. Chim. Acta, 123 (1981) 151.
388 T. Hepel, Anal. Chim. Acta, 123 (1981) 161.
389 A. Hulanicki, T. Krawczynski and M. Trojanowicz, Chem. Anal. (Warsaw), 24 (1979) 435.
390 A. Hulanicki, R. Lewandowski and A. Lewensztam, Anal. Chim. Acta, 110 (1979) 197
391 A. Hulanicki, A. Lewenstam and M. Maj-Žurawska, Anal. Chim. Acta, 107 (1979) 121.
392 A. Hulanicki, M. Trojanowicz and J. Sztandor, Chem. Anal. (Warsaw), 24 (1979) 617.
393 Human Institute of Chemical Engineering, Fen Hsi Hua Hsueh, 6 (1978) 279.
394 S. Ikeda, N. Matsuda, G. Nakagawa and K. Ito, Denki Kagaku, 47 (1979) 281.
395 V. N. Ioffe and T. D. Rukhtina, Zavod. Lab., 45 (1979) 969.
396 K. Irlweck and H. Soratin, Microchim. Acta, (1977) 25.
397 K. Ito, N. Matsuda, S. Ikeda and G. Nakagawa, Denki Kagaku, 48 (1980) 16.

398 K. Ito, N. Matsuda, T. Maeda, S. Ikeda, T. Iida and G. Nakagawa, Denki Kagaku, 47 (1979) 220.
399 M. Iwaida, K. Ueda and K. Nakamura, Shokuhin Eiseigaku Zasshi, 19 (1978) 524.
400 H. Jager and E. Tschager, Dtsch. Molk. Ztg., 100 (1979) 1658.
401 R. L. Jenkins and R. B. Baird, Anal. Lett., 12 (1979) 125.
402 G. Johansson, L. Risinger and L. Fälth, Anal. Chim. Acta, 119 (1980) 25.
403 A. E. Kochanowskii, Yu. I. Urusov and A. V. Gordievskii, Khim. Prom., Ser. Metody Anal. Kontrolya Kach. Prod. Khim. Prom., 1 (1979) 30.
404 P. Kačmar, A. Samo and J. Legath, Vet. Med. (Prague), 25 (1980) 743.
405 M. Katuoka, S. Miyagata and T. Kambara, Nippon Kagaku Kaishi, 10 (1980) 1520.
406 M. Kataoka, M. Takahashi and T. Kambara, Bunseki Kagaku, 28 (1979) 169.
407 K. Katawaki, I. Fukeda and M. Makita, Semento Gijutsu Nempo, 33 (1979) 151.
408 Y. Kato, Ganseki Kobutsu Kosho Gakkaishi, 74 (1979) 421.
409 S. U. Khan, G. F. Morris and H. Hidiroglon, Microchem. J., 25 (1980) 388.
410 L. Ya. Kheifets and A. E. Vasyukov, Probl. Okhr. Vod, 8 (1977) 79.
411 R. Khristova, M. Novkirishka and M. Ivanova, God. Soffi. Univ., Khim. Fak., 70 (1979) 267.
412 J. R. Kistner, D. E. Longnecker, E. D. Miller and A. D. Lescanic, Anesth. Analg. (Cleveland), 58 (1979) 457.
413 V. V. Kiyanskii, Khim. Prom., Ser. Metody Anal. Kontrolya Kach. Prod. Khim. Prom., 10 (1979) 37.
414 V. V. Kiyanskii, Zavod. Lab., 45 (1979) 205.
415 V. V. Kiyanskii and T. G. Aityurina, Khim. Prom., Ser. Metody Anal. Kontrolya Kach. Prod. Khim. Prom., 12 (1980) 38.
416 W. Klemm, Z. Angew. Geol., 24 (1978) 345.
417 N. Kokubu, T. Kobayasi and A. Yamasaki, Bunseki Kagaku, 29 (1980) 106.
418 N. N. Kolpakova and G. D. Mironova, Geochimya, 12 (1978) 1873.
419 A. Kosturiak and D. Kalavská, Collect. Czech. Chem. Commun., 44 (1979) 1742.
420 M. A. Koupparis, C. E. Efstathiou and T. P. Hadjiioannou, Anal. Chim. Acta, 107 (1979) 91.
421 A. S. Kovalenko and L. P. Tichonova, Teor. Eksp. Khim., 14 (1978) 558.
422 P. A. Kryukov and S. Y. Tarasenko, Izv. Sib. Otd. Akad. Nauk SSSR, (1979) 37.
423 P.-H. Kuang, H.-H. Chang, S.-Y. Yang and K.-K. Po, Fen Hsi Hua Hsueh, 7 (1979) 28.
424 A. I. Kacherova and A. Konovalova, Khim. Prom., Ser. Metody Anal. Kontrolya Kach. Prod. Khim. Prom., 2 (1979) 19.
425 F. Kuhlmann, Lebensm. Gerichtl. Chem., 34 (1980) 95.
426 M. Kurosaki, S. Osaga and T. Kashima, Kyoritsu Yakka Doigaku Kenkyu Nempo, 24 (1979) 1.
427 D. E. Lecroix and N. P. Wong, J. Food Prot., 43 (1980) 672.
428 J. C. Landry, C. Michal and F. Cupelin, Fluoride determination by continuous flow analysis, in J. Albaiges (Ed.), Analytical Techniques in Environmental Chemistry, Pergamon, Oxford, 1980, p. 571.
429 P. Lanza, Anal. Chim. Acta, 105 (1979) 53.
430 J.-P. Li, M.-C. Chow, Y.-L. Chang and M.-M. Chen, Fen Hsi Hua Hsueh, 6 (1978) 433.
431 J. L. F. da C. Lima and A. A. S. C. Machado, Rev. Port. Quim., 21 (1979) 15.
432 A. Kh. Magrilova, V. M. Beglov and P. M. Zaitsev, Uzb. Khim. Zh., 3 (1979) 22.
433 E. Mainka and W. Coerdt, Report Kernforschungszentrum Karlsruhe KFK2709, W. Germany, 1978.
434 G. B. Marshall and D. Midgley, Analyst, 104 (1979) 55.
435 A. Marton, J. Inczedy, T. Damokos and J. Havas, Magy. Kem. Foly., 84 (1978) 380.
436 M. Mascini and G. Palleschi, Ann. Chim. (Rome), 69 (1979) 249.

437 N. Matsuda, G. Nakagawa, S. Ikeda and K. Ito, Denki Kagaku, 48 (1980) 199.
438 D. S. MacIntyre, B. G. Cooksey and J. M. Ottaway, Proc. Anal. Div. Chem. Soc., 16 (1979) 18.
439 J. R. Melberg, Caries Res., 14 (1980) 50.
440 M. E. Meyerhoff and G. A. Rechnitz, Anal. Lett., 12 (1979) 1339.
441 D. Midgley, Talanta, 26 (1979) 261.
442 P. Miles, J. Assoc. Off. Anal. Chem., 61 (1978) 1366.
443 V. A. Mirkin, M. A. Ilyushchenko and I. V. Nenchenko, Zh. Anal. Khim., 35 (1980) 266.
444 V. A. Mirkin, M. A. Ilyushchenko and O. P. Shadrina, Izv. Akad. Nauk Kaz. SSR, Ser. Khim., 6 (1980) 11.
445 V. A. Mirkin, M. A. Ilyushchenko and O. P. Shadrina, Izv. Vyssh. Ucheb. Zaved., Khim. Khim. Tekhnol., 23 (1980) 1511.
446 W. Misniakiewicz and K. Paszka, Pr. Nauk. Inst. Metrol. Elektron. Politech. Wroclaw, 19 (1979) 158.
447 M.-S. Mo and Y.-T. Ho, Fen Hsi Hua Hsueh, 6 (1974) 274.
448 Z. Mokrá and M. Henek, Silikaty (Prague), 23 (1979) 347.
449 Z. Mokrá and M. Henek, Silikaty (Prague), 24 (1980) 81.
450 G. J. Moody and J. D. R. Thomas, Diagnostic screening for cystic fibrosis with a combination chloride ion-selective electrode, in W. F. Smyth (Ed.), Electroanalysis in Hygiene, Environmental, Clinical and Pharmaceutical Chemistry, Elsevier, Amsterdam, 1980, p. 33.
451 G. J. Moody and J. D. R. Thomas, Ion-selective Electrode Rev., 2 (1980) 73.
452 F. Mosey and D. A. Jago, Tech. Rep.-Water Res. Cent. (Medmenham, Engl.), TR53, 28 pp.
453 J. Motonaka, S. Ikeda and N. Tanaka, Anal. Chim. Acta, 105 (1979) 417.
454 J. Motonaka, S. Ikeda and N. Tanaka, Nippon Kagaku Kaishi, (1980) 1525.
455 K. Nagy and T. A. Fjeldly, Talanta, 26 (1979) 811.
456 F. M. Najib, A. T. Faizullah and F. Ahmed, Anal. Lett., 14 (1981) 47.
457 G. Nakagawa, H. Wada and T. Saki, Bull. Chem. Soc. Jpn., 53 (1980) 1303.
458 T. Nakano and Y. Suzuki, Nippon Kagaku Kaishi, (1980) 1485.
459 Nanking Institute of Soil Science, T'u Jang, 1 (1978) 30.
460 A. Napoli, Ann. Chim. (Rome), 68 (1978) 443.
461 M. Neskova and H. Sheytanov, J. Electroanal. Chem., 102 (1979) 189.
462 A. N. Nevzorov and R. A. Shuvalov, Vulkanol. Seismol., 5 (1979) 96.
463 L. W. Niedrach, J. Electrochem. Soc., 127 (1981) 2122.
464 V. A. Nikashina and A. N. Krachak, Zh. Anal. Khim., 34 (1979) 2236.
465 D. P. Nikolelis and T. P. Hadjiioannou, Anal. Lett., 12 (1979) 1169.
466 V. P. Novak, V. I. Bogovina and L. A. Vasileva, Nov. Metody Instrum. Anal. Mater. (Moscow), 1979, 125.
467 V. P. Novak, V. I. Bogovina, L. A. Vasilieva and G. S. Mazharovskaya, 5 Vses. Simpoz. Khim. Neorgan. Ftoridov, Dnepropetrovsk, (1978) 59.
468 M. Novkirishka and R. Khristova, God. Sofii. Univ. Khim. Fak., 69 (1978) 59.
469 M. Novkirishka, G. Michailov and R. Khristova, Fresenius Z. Anal. Chem., 305 (1981) 411.
470 F. Oehme, Gewässerschutz Wasser Abwasser, 39 (1979) 111.
471 F. Oehme, Gewässerschutz Wasser Abwasser, 39 (1979) 213.
472 F. Oehme, TAPPI, (1979) 41.
473 K. Ohzeki, M. Saruhashi and T. Kambara, Bull. Chem. Soc. Jpn., 53 (1980) 2548.
474 A. E. Owen, J. Non-Cryst. Solids, 35—36 (1980) 998.
475 A. Palić and A. Mijatović, Mljekarstvo, 30 (1980) 21.
476 D. S. Papastathopoulos and M. I. Karayannis, J. Chem. Educ., 57 (1980) 904.
477 K.-C. Park, Y.-S. Kwon and W.-D. Huh, Taehan Hwahakhoe Chi, 23 (1979) 385.
478 R. Perez Olmos, An. Bromatol., 32 (1980) 85.

479 R. Perez Olmos, Ing. Quim, (Madrid), 12 (1980) 53.
480 K. J. Peverelli, H. P. van Leeuwen, J. Electroanal. Chem., 99 (1979) 157.
481 K. J. Peverelli and H. P. van Leeuwen, J. Electroanal. Chem., 110 (1980) 119.
482 K. J. Peverelli and H. P. van Leeuwen, J. Electroanal. Chem., 110 (1980) 137.
483 E. Pungor, Z. Fehér, E. Lindner, G. Nagy and K. Tóth, Z. Chem., 19 (1979) 367.
484 E. Pungor, K. Tóth, M. K. Pápay, L. Pólos, H. Malissa, M. Grasserbauer, E. Hoke, M. F. Ebel and K. Persy, Anal. Chim. Acta, 109 (1979) 279.
485 N. Radić, Anal. Lett., 12 (1979) 115.
486 N. Radić and M. Milišić, Anal. Lett., 13 (1980) 1013.
487 P. V. Rakcheev, T. G. Repenkova, G. I. Kravchenko, A. V. Gordievskii and A. A. Vlazneva, Tr. Mosk. Khim. Tekhnol. Inst., 93 (1977) 56.
488 F. Rakiás, K. Tóth and E. Pungor, Anal. Chim. Acta, 121 (1980) 93.
489 D. G. Rands and R. L. Bain, Report NTIS USA No. PB80-113590, VA, 1979.
490 R. E. Rea, Water Pollut. Control, 78 (1979) 139.
491 L. P. Rigdon, C. L. Pomernacki, D. Balaban and J. W. Freiser, Anal. Chim. Acta, 112 (1979) 397.
492 D. Roeske and H. Behrendt, Pharm. Prax., 35 (1980) 162.
493 G. I. Rubeshko and V. A. Khalizova, Zavod. Lab., 45 (1979) 203.
494 V. M. Ryabikova, A. N. Zigela, A. Sverdlova and E. M. Kuznetsova, Okhr. Okruzh. Sredy Pri Proizv. Plastmass (Leningrad), (1978) 57.
495 M. Sager, Fresenius Z. Anal. Chem., 298 (1979) 393.
496 S. Sakura, N. Ichinose, N. Sakurai and G. P. Sato, Bunseki Kagaku, 29 (1980) 659.
497 S. G. Samokhvalov, A. A. Shaimukhametova, A. L. Erinov and I. V. Alekhina, Chim. Selsk. Khoz., 17 (1979) 58.
498 J. R. Sandifer, Anal. Chem., 53 (1981) 312.
499 B. Sapek, Pr. Kom. Nauk, 2 (1977) 51.
500 M. Saruhashi, K. Ohzeki and T. Kambara, Nippon Kagaku Kaishi, (1980) 1490.
501 G. Sbeschni, Acta Hydrochim. Hydrobiol., 8 (1980) 101.
502 O. Scharff, Anal. Chim. Acta, 109 (1979) 291.
503 I. Sekerka and J. F. Lechner, Analyst, 106 (1981) 323.
504 W. Selig, Microchem. J., 25 (1980) 200.
505 Yu. N. Semavin and G. A. Zalazinskaya, Tr. Ural. Nauchno-Issled. Proektn. Inst. Mednoi. Prom., 21 (1978) 134.
506 Y. Seo, Bunseki Kagaku, 28 (1979) 334.
507 Shanghai College of Mechanical Engineering, Shanghai Machine Repair Factory and Shanghai Institute of Metallurgy, Fen Hsi Hua Hsueh, 6 (1978) 441.
508 Shanghai No 2. Analytical Instrument Factory and Tsinhai Institue of Salt Lake Research, Fen Hsi Hua Hsueh, 6 (1978) 6.
509 V. S. Shterman, L. G. Shmidt, I. V. Rosin and L. E. Mikhailova, Izv. Vyssh. Uchebn. Zaved. Pishch. Tekhnol., 2 (1980) 133.
510 L. Singer and R. H. Ophang, Clin. Chem., 25 (1979) 523.
511 D. L. Sorensen, W. A. Kneib and D. B. Porcella, Anal. Chem., 51 (1979) 1870.
512 A. Sovová and N. Kasíková, Sb. Vys. Sk. Zemed. Praze, Fak. Agron., 1 (1976) 13.
513 R. L. Speirs, Arch. Oral Biol., 23 (1978) 1013.
514 R. L. Speirs, Arch. Oral. Biol., 23 (1978) 1019.
515 H. M. Stahr, P. F. Ross and W. Hyde, Microchem. J., 25 (1980) 232.
516 R. Stella and M. T. Ganzerli-Valentini, Anal. Chem., 51 (1979) 2148.
517 R. Stella and M. T. Ganzerli-Valentini. The use of copper ion-selective electrode for determination of copper chemical forms in natural waters, in J. Albaiges (Ed.), Analytical Techniques in Environmental Chemistry, Pergamon, Oxford, 1980, p. 581.
518 E. Still, Anal. Chim. Acta, 107 (1979) 105.
519 E. Still, Anal. Chim. Acta, 107 (1979) 377.
520 J. L. Stuart and E. J. Duff, Analyst, 105 (1980) 1098.

521 G. Subramanian, Navinchandra and G. P. Rao, Trans. Soc. Adv. Electrochem. Sci. Technol., 15 (1980) 243.
522 L. Šůcha, M. Suchánek, Z. Urner and V. Sluka, Sb. Vys. Sk. Chem.-Technol. Praze, Anal. Chem., 12 (1977) 213.
523 I. D. Szucz, Magy. Kem. Foly., 85 (1979) 481.
524 M. Taddia, Microchem. J., 23 (1978) 537.
525 M. Taddia, Fresenius Z. Anal. Chem., 296 (1979) 149.
526 B. Taborska and J. Dojlido, Szklo Ceram., 31 (1980) 53.
527 W.-F. Tai, M.-Y. Chang, T.-P. Kao and H.-K. Liu, Chi Lin Ta Hsueh Hsueh Pao, 1 (1977) 65.
528 Y. Takasaka and Y. Suzuki, Bull. Chem. Soc. Jpn., 52 (1979) 3455.
529 K.-H. Tan, Fen Hsi Hua Hsueh, 6 (1978) 465.
530 K. Tanaka, Shika Gakuho, 78 (1978) 1625.
531 E. Tassarai, R. Ciurlo, F. Andreoni and G. B. Deferrari, Rass. Chim., 30 (1978) 257.
532 S. V. Timofeev, E. A. Materova, L. K. Archangelskii and E. V. Chirkova, Vestn. Leningrad. Univ., Fiz. Khim., 3 (1978) 139.
533 R. L. Tom and P. A. Kapauan, Philipp. A.E.C. [Rep.], IE-77001 (1977) 1.
534 M. Trojanowicz, Anal. Chim. Acta, 114 (1980) 293.
535 M. Trojanowicz, Talanta, 26 (1979) 985.
536 Y. Umezawa and S. Fujiwara, Nippon Kagaku Kaishi, 10 (1980) 1437.
537 Y. Umezawa, Y. Imanishi, K. Sawatari and S. Fujiwara, Bull. Chem. Soc. Jpn., 52 (1979) 945.
538 Y. Umezawa, M. Nagata, K. Sawatari and S. Fujiwara, Bull. Chem. Soc. Jpn., 52 (1979) 241.
539 Y. Usami, T. Tsuzuki, K. Torii and O. Hikosaka, Yosui To Haisui, 22 (1980) 208.
540 W. E. van der Linden and R. Oostervink. Anal. Chim. Acta, 108 (1979) 169.
541 J. Veselý, Collect. Czech. Chem. Commun., 46 (1981) 368.
542 A. E. Villa, Analyst, 104 (1979) 545.
543 W. Vinz and V. Jahn, Pharm. Prax., 35 (1980) 8.
544 T. N. Vladimirskaya, A. P. Gorskaya and I. S. Tishchenko, Met. Anal. Kontr., 9 (1978) 26.
545 Yu. G. Vlasov, Yu. E. Ermolenko and O. A. Iskhakova, Zh. Anal. Khim., 34 (1979) 1522.
546 Yu. G. Vlasov, Yu. E. Ermolenko, V. V. Kolodnikov and M. S. Miloshova, Zh. Anal. Khim., 35 (1980) 691.
547 Yu. G. Vlasov and S. R. Kochergin, Ion. Obmen Ionometr., 2 (1979) 243.
548 G. L. Vogel and W. E. Brown, Anal. Chem., 52 (1980) 377.
549 G. L. Vogel, L. C. Chow and W. E. Brown, Anal. Chem., 52 (1980) 375.
550 K. Vytřas and M. Novotná-Horčicová, Collect. Czech. Chem. Commun., 44 (1979) 1126.
551 R. Wagemann, J. Phys. Chem., 84 (1980) 3433.
552 F. C. Walsh and D. R. Gabe, J. Appl. Electrochem., 11 (1981) 117.
553 D. Weil, Hydrochem. Hydrogeol. Mitt., 3 (1978) 247.
554 D. Weil and K. E. Quentin, Z. Wasser Abwasser Forsch., 11 (1978) 133.
555 J. C. Westall, F. M. M. Morel and D. N. Hume, Anal. Chem., 51 (1979) 1792.
556 S. M. Wheeler, L. R. Fell, G. H. Fleet and R. J. Ashley, Aust. J. Dairy Technol., 35 (1980) 26.
557 G. M. Whitford and K. E. Reynolds, J. Dent. Res., 58 (1979) 2058.
558 A. C. Wilson and K. H. Pool, Anal. Chim. Acta, 109 (1979) 149.
559 F. Yamashita, T. Komatsu and T. Nakagawa, Bull. Chem. Soc. Jpn., 52 (1979) 30.
560 F. Yamashita, T. Komatsu and T. Nakagawa, Bull. Chem. Soc. Jpn., 52 (1979) 1251.
561 Y.-T. Yang, M. Yu. K.-Y. Mo and C.-T. Chiu, Fen Hsi Hua Hsueh, 8 (1980) 112.
562 P.-C. Yi, C.-C. Liu and C.-H. Keh, Fen Hsi Hua Hsueh, 8 (1980) 137.
563 H.-Y. Yiu, Fen Hsi Hua Hsueh, 8 (1980) 73.

564 A. F. Zhukov, A. V. Kopytin, G. K. Zhavoronkova and A. V. Gordievskii, Zavod. Lab., 45 (1979) 492.
565 A. F. Zhukov, A. V. Vishnyakov, Yu. I. Urusov, A. V. Kopytin, L. I. Glasman and A. V. Gordievskii, Zh. Anal. Khim., 34 (1979) 602.
566 A. F. Zhukov, A. V. Vishnyakov, Yu. I. Urusov, A. V. Kopytin and A. V. Gordievskii, Zavod. Lab., 46 (1980) 13.
567 T. J. M. Zimmer, Mess. Preuf., 9 (1978) 521.
568 A.-M. Zou, Y.-Y. Ding, H.-C. Huang, J.-H. Wu and C.-L. Hsia, Huan Ching K'o Hsueh, 1 (1980) 33.
569 H. Affolter and E. Sigel, Anal. Biochem., 97 (1979) 315.
570 T. Akiyama, K. Kinoshita, Y. Horita and E. Niki, Nippon Kagaku Kaishi, (1980) 1431.
571 D. Ammann, H. B. Jenny, P. C. Meier and W. Simon, New Ion-selective electrodes and their clinical biological application, in W. F. Smyth (Ed.), Electroanalysis in Hygiene, Environmental, Clinical and Pharmaceutical Chemistry, Elsevier, Amsterdam, 1980, p. 3.
572 D. Ammann, P. C. Meier and W. Simon, Design and use of calcium selective electrodes, in C. C. Ashley and A. K. Campbell (Eds.), Detection and Measurement of Free Calcium in Cells, Elsevier, Amsterdam, 1979, p. 117.
573 D. M. Band, L. Beynon and P. Skinner, J. Physiol. (London), 293 (1979) 13P.
574 J. E. G. McCarthy and S. J. Ferguson, Biochem. J., 196 (1981) 311.
575 M. T. Benignetti, L. Campanella and T. Ferri, Fresenius Z. Anal. Chem., 296 (1979) 412.
576 J. L. Bernal, R. Pardo and E. Barrado, Anal. Lett., 13 (1980) 241.
577 M. J. Berridge, Cell Calcium, 1 (1980) 217.
578 D. M. Bers and D. Ellis, J. Physiol. (London), 310 (1981) 73P.
579 R. Bissig, U. Oesch, E. Pretsch, W. E. Morf and W. Simon, Helv. Chim. Acta, 61 (1978) 1531.
580 K. Bjorvatn and T. Moerch, Acta Odontol. Scand., 37 (1979) 259.
581 T. Blaż, Chem. Anal. (Warsaw), 25 (1980) 191.
582 T. Blaż and Z. Kowalski, Chem. Anal. (Warsaw), 25 (1980) 121.
583 H. C. Brinkhoff, Environ. Sci. Technol., 12 (1978) 1392.
584 B. A. Bulos and B. Sacktor, Anal. Biochem., 95 (1979) 62.
585 K. Burger and G. Pethö, Anal. Chim. Acta, 107 (1979) 113.
586 K. Burger and G. Pethö, Magy, Kem. Foly., 85 (1979) 424.
587 L. Campanella and T. Ferri, Fresenius Z. Anal. Chem., 302 (1980) 304.
588 M. J. M. Campbell, B. Demetrion and R. Jones, Analyst, 105 (1980) 605.
589 R. W. Cattrall, G. L. Lee and I. C. Hamilton, Anal. Chim. Acta, 116 (1980) 391.
590 E. G. Chagina, R. I. Dubinina, V. A. Galovin, E. A. Materova and A. A. Grekovich, Agrokhimiya, 5 (1980) 134.
591 G. M. Chan, K. O. Ash, W. Hentschel and J. Wu, Clin. Chem., 27 (1981) 204.
592 K. K. Choi and K. W. Fung, Analyst, 105 (1980) 241.
593 M. M. Civan, Fed. Proc., Fed. Am. Soc. Exp. Biol., 39 (1980) 2865.
594 L. Cleemann and M. Morad, J. Physiol. (London), 286 (1979) 113.
595 L. Cleemann and M. Morad, J. Physiol. (London), 286 (1979) 83.
596 P. H. Cobbold, Nature, 285 (1980) 441.
597 J. A. Coles and M. Tsacopoulos, J. Physiol. (London), 290 (1979) 525.
598 M. T. Coroneo, H. Maier, J. G. Schindler and A. Heidland, Adv. Physiol. Sci., 28 (1980) 289.
599 R. F. Cosgrove and A. E. Beezer, Anal. Chim. Acta, 105 (1979) 77.
600 V. V. Cosofret and A. A. Bunaciu, Anal. Lett., 12 (1979) 617.
601 V. V. Cosofret, C. Stefanescu and A. A. Bunaciu, Talanta, 26 (1979) 1035.
602 A. Craggs, B. Doyle, S. K. A. G. Hassan, G. J. Moody and J. D. R. Thomas, Talanta, 27 (1980) 277.

603 A. Craggs, G. J. Moody and J. D. R. Thomas, Analyst, 104 (1979) 412.
604 A. Craggs, G. J. Moody and J. D. R. Thomas, Analyst, 104 (1979) 961.
605 A. Craggs, G. J. Moody, J. D. R. Thomas and B. J. Birch, Analyst, 105 (1980) 426.
606 M. Crompton and E. Carafoli, The application of calcium-selective electrodes and inhibitor stop techniques to the resolution of calcium fluxes in mitochondria, in C. C. Ashley and A. K. Campbell (Eds.), Detection and Measurement of Free Calcium in Cells, Elsevier, Amsterdam, 1979, p. 373.
607 S. S. Davis and O. Olejnik, J. Pharm. Pharmacol., 31 (1979) Suppl. 19P.
608 H. Degawa, N. Sinozuka and S. Kayano, Nippon Kagaku Kaishi, 10 (1980) 1462.
609 J. Delong and M. M. Civan, Intracellular chemical activity of potassium in toad urinary bladder, in E. L. Boulpaep, F. Bonner and A. Kleinzeller (Eds.), Current Topics in Membranes and Transport, Academic Press, New York, 1980, p. 93.
610 D. R. Del Toro, E. M. Rakhmanko and G. L. Starobinec, Vestsi Akad. Navuk B. SSR, Ser. Khim. Navuk, 3 (1979) 29.
611 E. F. Diamandis, C. E. Efstathiou and T. P. Hadjiioannou, Anal. Chim. Acta, 105 (1980) 1203.
612 E. P. Diamandis and T. P. Hadjiioannou, Anal. Chim. Acta, 123 (1981) 143.
613 E. P. Diamandis and T. P. Hadjiioannou, Anal. Chim. Acta, 123 (1981) 341.
614 E. P. Diamandis and T. P. Hadjiioannou, Anal. Lett., 13 (1980) B15, 1317.
615 E. P. Diamandis and T. P. Hadjiioannou, Clin. Chem., 27 (1981) 455.
616 E. P. Diamandis and T. P. Hadjiioannou, Mikrochim. Acta, II (1980) 27.
617 S. E. Didina, E. A. Materova, A. L. Grekovich and L. I. Vatlina, Elektrokhimiya, 17 (1981) 598.
618 R. E. Dohner and W. Simon, Anal. Lett., 12A (1979) 205.
619 A. Duca, E. Doniga and F. Matei, Rev. Chim. (Bucharest), 30 (1979) 916.
620 M. E. Duffey, K. Turnheim, R. A. Frizzell and S. G. Schulz, J. Membr. Biol., 42 (1978) 229.
621 V. Ebock, Chem. Tech. (Leipzig), 32 (1980) 91.
622 A. Edelman, S. Curei, I. Samaržija and E. Frömter, Pfluegers Arch., 378 (1978) 37.
623 B. Elgquist and M. Wedborg, Mar. Chem., 7 (1979) 273.
624 M. M. Emara, N. A. Farid and G. Atkinson, Anal. Lett., 11 (1978) 797.
625 M. M. Emara, N. A. Farid and C. T. Lin, J. Chem. Educ., 56 (1979) 620.
626 M. M. Emara, C.-T. Lin and G. Atkinson, Bull. Soc. Chim. Fr., 1980, 173.
627 M. M. Emara and C.-T. Lin, J. Indian Chem. Soc., 57 (1980) 876.
628 D. Erne, D. Ammann and W. Simon, Chimia, 33 (1979) 88.
629 D. Erne, N. Stojanac, D. Ammann, P. Hofstetter, E. Pretsch and W. Simon, Helv. Chim. Acta, 63 (1980) 2271.
630 D. Erne, N. Stojanac, D. Ammann, E. Pretsch and W. Simon, Helv. Chim. Acta, 63 (1980) 2264.
631 N. A. Fayad and J. F. Tyson, Int. Lab., 1979, 49.
632 U. Flora, R. Gennaro and D. Romeo, Anal. Biochem., 102 (1980) 77.
633 A. G. Fogg and K. S. Yoo, Anal. Chim. Acta, 113 (1980) 165.
634 M. Fujimoto, K. Kotera and Y. Matsumura. The direct measurement of K, Cl, Na and H ions in bullfrog tubule cells, in E. L. Boulpaep. F. Bonner and A. Kleinzeller (Eds.), Current Topics in Membranes and Transport, Vol. 13, Academic Press, New York, 1980, p. 49.
635 T. Fujinaga, S. Okazaki and H. Hara, Chem. Lett., 11 (1978) 1201.
636 K. Fukamachi and N. Ishibashi, Yakugaku Zasshi, 99 (1979) 126.
637 K. W. Fung and K. H. Wong, J. Electroanal. Chem., 111 (1980) 359.
638 N. V. Garbuzova, A. L. Grekovich, L. I. Ishutkina, V. S. Karavan and E. A. Materova, Ion. Obmen Ionometriya, 2 (1979) 156.
639 M. Gerin and J. Fresco, Can. J. Chem., 58 (1980) 1412.
640 T. Goina, S. Hobai, E. Goina and M. Olariu, Rev. Med. (Tirgu-Mures, Romania), 24 (1978) 6.

641 I. Goldberg and D. Meyerstein, Anal. Chem., 52 (1980) 2105.
642 A. V. Gordievskii, Yu. I. Urusov, V. V. Sergievskii, A. F. Zhukov and A. V. Kopytin, Zh. Anal. Khim., 34 (1979) 1252.
643 D. Gozzi, L. Campanella and T. Ferri, Electrochim. Acta, 24 (1979) 817.
644 D. Gozzi and T. Ferri, J. Electroanal. Chem., 109 (1980) 213.
645 R. S. Greenwood, W. E. Dodson and S. Goldring, Brain Res., 165 (1979) 171.
646 A. L. Grekovich, S. E. Didina and E. A. Materova, Ion. Obmen Ionometr., 2 (1979) 150.
647 A. L. Grekovich, O. A. Goncharuk and K. N. Mikhel'son, Ion. Obmen Ionometr., 2 (1979) 125.
648 M. Güggi, M. Kessler, F. Greitschus, V. Wiegand and W. Meesmann, Measurement of extracellular ion activities (potassium ion, sodium ion, calcium ion) during acute coronary occlusion, in P. L. Dutton, J. S. Leigh and A. Scarpa (Eds.), Frontiers of Biological Energy, Vol. 2, Academic Press, New York, 1978, p. 1427.
649 J. Gulens and P. K. Leeson, Anal. Chem., 52 (1980) 2235.
650 I. A. Gurev, A. A. Kalugin and E. A. Gushina, Zavod. Lab., 46 (1980) 497.
651 I. A. Gurev, G. M. Lizunova and I. M. Korenman, Zh. Anal. Khim., 36 (1981) 130.
652 I. A. Gurev and V. R. Naumenko, Zh. Anal. Khim., 35 (1980) 1174.
653 A. L. Gurevich, E. M. Rakhmanko and G. G. Starobinets, Vestsi Akad. Navuk B. SSR, Ser. Khim. Navuk, 4 (1979) 77.
654 Yu. N. Gusev, Yu. P. Korotaeva, E. M. Mavrina and T. G. Repenkova, Khim. Prom., Ser. Metody Anal. Kontrolya Kach. Prod. Khim. Prom., 3 (1979) 20.
655 E. H. Hansen, J. Růžička and A. K. Ghose, Anal. Chim. Acta, 100 (1978) 151.
656 H. Hara, S. Okazaki and T. Fujinaga, Anal. Chim. Acta, 121 (1980) 119.
657 H. Hara, S. Okazaki and T. Fujinaga, Bull. Chem. Soc., Jpn., 53 (1980) 3610.
658 H. Hara, S. Okazaki and T. Fujinaga, Bunseki Kagaku, 30 (1981) 86.
659 H. Hara, S. Okazaki and T. Fujinaga, Nippon Kagaku Kaishi, (1980) 1645.
660 S. K. A. G. Hassan, G. J. Moody and J. D. R. Thomas, Analyst, 105 (1980) 147.
661 S. S. M. Hassan, Talanta, 28 (1981) 89.
662 S. S. M. Hassan and M. B. Elsayes, Anal. Chem., 51 (1979) 1651.
663 S. S. M. Hassan and M. M. Habib, Anal. Chem., 53 (1981) 508.
664 T. Helfgott and J. S. Mazurek, Prog. Water Technol., 8 (1977) 433.
665 K. Hiiro, K. Kawahara and T. Tanaka, Anal. Chim. Acta, 110 (1979) 321.
666 K. Hiiro, A. Kawahare and T. Tanaka, Nippon Kagaku Kaishi, 10 (1980) 1447.
667 S. H. Hoke, A. G. Collins and C. A. Reynolds, Anal. Chem., 51 (1979) 859.
668 D. Homolka, Collect. Czech. Chem. Commun., 44 (1979) 3644.
669 T. Honjo, Fresenius Z. Anal. Chem., 303 (1980) 26.
670 E. Hopirtean and F. Kormos, Chem. Anal. (Warsaw), 25 (1980) 209.
671 E. Hopirtean and M. Miklos, Rev. Chim. (Bucharest), 29 (1978) 1178.
672 E. Hopirtean and E. Radulescu, Stud. Univ. Babes-Bolyai, Ser. Chem., 24 (1979) 23.
673 T. P. Huang, M.-H. Tan, C.-M. Chen and M.-C. Wang, Fen Hsi Hua Hsueh, 6 (1978) 342.
674 T. Iimori, M. Sugawara and T. Kambara, Denki Kagaku, 47 (1979) 549.
675 T. Imato, A. Jyo and N. Ishibashi, Anal. Chem., 52 (1980) 1893.
676 R. K. Jackson, Comm. Soil Sci., Plant Anal., 11 (1980) 127.
677 F. Jasim, Iraq. J. Sci., 20 (1979) 430.
678 H.-B. Jenny, D. Ammann, R. Dörig, B. Magyar, R. Asper and W. Simon, Miktrochim. Acta, II (1980) 125.
679 H.-B. Jenny, C. Riess, D. Ammann, B. Magyar, R. Asper and W. Simon, Mikrochim. Acta, II (1980) 309.
680 D. L. Jones, G. J. Moody and J. D. R. Thomas, Analyst, 106 (1981) 439.
681 D. L. Jones, G. J. Moody, J. D. R. Thomas and M. Hangos, Analyst, 104 (1979) 973.
682 K. M. Kale, E. L. Cussler and D. F. Evans, J. Phys. Chem., 84 (1980) 593.
683 S. Kamata, G. J. Moody and J. D. R. Thomas, Anal. Chim. Acta, 108 (1979) 385.

684 N. Kamo, M. Muratsugu, R. Hongoh and Y. Kobatake, J. Membr. Biol., 49 (1979) 105.
685 S. Kanamari and H. Ikegami, J. Oceanogr. Soc. Jpn., 36 (1980) 177.
686 M. Kataoka and T. Kambara, Bunseki Kagaku, 28 (1979) 705.
687 M. Kataoka, M. Kishigami and T. Kambara, Bunseki Kagaku, 29 (1980) 486.
688 M. Kataoka, M. Kudoh and T. Kambara, Denki Kagaku, 46 (1978).
689 M. Kataoka, S. Ueda and T. Kambara, Nippon Kagaku Kaishi, (1980) 1442.
690 M. Kataoka, T. Watanabe and T. Kambara, Denki Kagaku, 48 (1980) 191.
691 R. A. Kaufman and N. W. Tietz, Clin. Chem., 26 (1980) 640.
692 R. N. Khuri, Intracellular ion activity in kidney tubules, in E. L. Boulpaep, F. Bonner and A. Kleinzeller (Eds.), Current Topics in Membranes and Transport, Academic Press, New York, 1980, p. 73.
693 K. Kimura and I. Shono, Kagaku (Kyoto), 35 (1980) 154.
694 K. Kimura, H. Tamura and T. Shono, J. Electroanal. Chem., 105 (1979) 335.
695 T. Kobayashi, M. Kataoka and T. Kambara, Talanta, 27 (1980) 253.
696 R. K. Kobos and G. A. Rechnitz, Bioelectrochem. Bioenerg., 4 (1977) 87.
697 V. V. Kokovkin, F. A. Kryukov and S. Y. Tarasenko, Izv. Sib. Otd. Akad. Nauk SSSR, Ser. Khim. Nauk, 6 (1979) 30.
698 V. V. Kolomiets, K. A. Merzon, T. N. Lyashevskaya, A. D. Doviner and S. E. Didina, Ion. Obmen Ionometriya, 2 (1979) 202.
699 A. V. Kopytin, A. F. Zhukov, Yu. I. Urusov, L. A. Kopytina and A. V. Gordievskii, Zh. Anal. Khim., 34 (1979) 465.
700 T. Korenaga, Mikrochim. Acta, II (1979) 455.
701 T. Korenaga, Anal. Chim. Acta, 120 (1980) 361.
702 J. Kotek and J. Doležal, Anal. Chim. Acta, 120 (1980) 93.
703 K. Kotera, N. Satake, M. Honda and M. Fujimoto, Membr. Biochem., 2 (1979) 323.
704 M. A Koupparis and T. P. Hadjiioannou, Anal. Chim. Acta, 96 (1978) 31.
705 L. D. Kovalchuk, Izv. Vyssh. Uchebn. Zaved. Tsvetn. Metall., 3 (1980) 111.
706 B. Krungalz and R. Holzer, Limnol. Oceanogr., 25 (1980) 367.
707 T. Kubota, B. Biagi and G. Giebisch, Intracellular potassium activity measurements in single proximal tubules of Necturus kidney, in E. L. Boulpaep, F. Bonner and A. Kleinzeller (Eds.), Current Topics in Membranes and Transport. Academic Press, New York, 1980, p. 63.
708 M. Kudoh, M. Kataoka and T. Kambara, Bunseki Kagaku, 28 (1979) 705.
709 M. Kudoh, M. Kataoka and T. Kambara, Talanta, 27 (1980) 495.
710 T. Kuramoto and B. Haber, J. Neurosci. Res., 6 (1981) 37.
711 F. Lagerlöf, Clin. Chim. Acta, 102 (1980) 127.
712 F. Lanter, D. Erne, D. Ammann and W. Simon, Anal. Chem., 52 (1980) 2400.
713 L. Larsson and S. Ohman, Clin. Biochem., 12 (1979) 138.
714 L. Larsson and S. Ohman, Clin. Chem., 24 (1978) 1962.
715 L. A. Lazarou and T. P. Hadjiioannou, Anal. Chem., 51 (1979) 790.
716 L. A. Lazarou and T. P. Hadjiioannou, Anal. Chim. Acta, 108 (1979) 375.
717 L. A. Lazarou and T. P. Hadjiioannou, Anal. Lett., 12 (1979) 725.
718 S. A. Lewis and N. K. Wills, Biophys. J., 31 (1980) 127.
719 V. L. Lomako, G. L. Starobinets and E. M. Rakhmanko, Vestsi Akad. Navuk B. SSR, Ser. Khim. Navuk, 6 (1980) 5.
720 T. Lu, T.-L. Lin, T.-F. Liu, F.-Y. Li and Y.-Y. Chang, Fen Hsi Hua Hsueh, 6 (1978) 485.
721 W.-Y. Lu, Y.-H. Chang and W.-H. Li, Fen Hsi Hua Hsueh, 8 (1980) 48.
722 T. Maeda, M. Ikeda, M. Shibahara, T. Haruta and I. Satake, Bull. Chem. Soc. Jpn., 54 (1981) 94.
723 H. Maier, A. Roeckel, G. Schmid and A. Heidland, Res. Exp. Med., 173 (1978) 297.
724 M. Maj-Żurawska and A. Hulanicki, Pr. Kom. Nauk. (Pol. Tow. Glebozn.), 2 (1977) 17.
725 E. Marban, T. J. Rink, R. W. Tsien and R. Y. Tsien, Nature, 286 (1980) 845.

726 H. M. Marquas, Gewässerschutz Wasser Abwasser, 39 (1979) 131.
727 C. R. Martin and H. Freiser, Anal. Chem., 52 (1980) 1772.
728 Y. Masuda, E. Ishida, K. Kiraga and E. Sekido, Nippon Kagaku Kaishi, (1980) 1453.
729 E. A. Materova, Z. S. Alagova, G. R. Alekseeva and L. P. Dementeva, Ion Obmen Ionometriya, 2 (1979) 147.
730 E. A. Materova, Z. S. Alagova and G. I. Shumilova, Ion Obmen Ionometriya, 2 (1979) 179.
731 E. A. Materova, Z. S. Alagova, G. I. Shumilova and L. P. Vatlina, Vest. Leningrad. Univ. Fiz. Khim., 4 (1978) 15.
732 E. A. Materova, Z. S. Alagova, G. I. Shumilova, L. P. Vatlina and I. K. Stekolnikova, Vestn. Leningrad. Univ., Fiz. Khim., 4 (1980) 72.
733 E. A. Materova, T. Ya. Bart, E. V. Soboleva, V. S. Kapavan and L. O. Ishutkina, Elektrokhimiya, 17 (1981) 499.
734 E. A. Materova and N. S. Lebedeva, Elektrokhimiya, 16 (1980) 1277.
735 E. A. Materova, N. S. Lebedeva and T. Ya. Bart, Ion Obmen Ionometriya, 2 (1979) 134.
736 E. A. Materova, N. S. Lebedeva and T. Ya. Bart, Ion Obmen Ionometriya, 2 (1979) 138.
737 E. A. Materova, V. V. Makhovnikov and M. G. Grigoreva, Ion Obmen Ionometriya, 2 (1979) 142.
738 E. A. Materova, S. A. Ovchinnikova, V. S. Karavan and L. O. Ishutkina, Elektrokhimiya, 15 (1979) 1185.
739 P. C. Meier, D. Erne, Z. Cimerman, D. Ammann and W. Simon, Mikrochim. Acta, I (1980) 317.
740 V. K. Menakin, I. N. Medvedev, L. T. Migunova and N. P. Buryakov, Mosk. Skh. Akad., 235 (1977) 56.
741 M. Mikesová, J. Petr, J. Šenkýř and M. Bartusék, Scr. Fac. Sci. Nat. Univ. Purkynianae Brun., 9 (1979) 8.
742 V. A. Mikhailov, V. V. Osipov and E. N. Graf, Elektrokhimiya, 15 (1979) 1042.
743 S. Miki, Jpn. J. Nephrol., 21 (1979) 67.
744 S. Miki, G. Kimura, Y. Takamitsu, A. Ando, Y. Orita and H. Abe, Rinsho Kagaku, 7 (1979) 272.
745 H. A. Mills, J. Assoc. Off. Anal. Chem., 63 (1980) 797.
746 G. J. Moody, N. S. Nassory and J. D. R. Thomas, Talanta, 26 (1979) 873.
747 G. J. Moody and J. D. R. Thomas, Anal. Chem. Symp. Ser. 2, Electroanal. Hyg. Environ., Clin. Pharm. Chem., University of Wales Inst. Sci. Technol., Cardiff, 1980, p. 11.
748 G. J. Moody and J. D. R. Thomas, Design principles and behaviour of sensitive calcium ion-selective electrodes, in W. E. Smyth (Ed.), Electroanalysis in Hygiene Environmental, Clinical and Pharmaceutical Chemistry, Elsevier, Amsterdam, 1980, p. 11.
749 G. J. Moody and J. D. R. Thomas, Ion-selective Electrode Rev., 1 (1979) 3.
750 G. J. Moody and J. D. R. Thomas, Proc. Anal. Div. Chem. Soc., 16 (1979) 32.
751 M. Morad, Fed. Proc., Fed. Am. Soc. Exp. Biol., 39 (1980) 1533.
752 M. Muratsugu, N. Kamo, K. Naoki and Y. Kobatake, Maku, 4 (1979) 323.
753 M. Muratsugu, N. Kamo, Y. Kobatake and K. Kimura, Bioelectrochem. Bioenerg., 6 (1979) 493.
754 G. D. Nazarenko and N. I. Isaenko, Assortiment Kachestvo Tovarov (Kiev), (1979) 162.
755 J. E. Newbery, Colloid Polym. Sci., 257 (1979) 773.
756 C. Nicholson, Fed. Proc., Fed. Am. Soc. Exp. Biol., 39 (1980) 1519.
757 B. P. Nikolskii, O. K. Stefanova, E. A. Materova and V. F. Gorshkova, Zh. Anal. Khim., 33 (1978) 1915.
758 Sh. K. Norov, E. S. Gureev and D. M. Aronbaev, Zavod. Lab., 46 (1980) 303.

759 Sh. K. Norov, E. S. Gureev, A. K. Tashmukhamedova, O. G. Vartanova and N. Zh. Saifullina, Elektrokhimiya, 15 (1979) 943.
760 Sh. K. Norov, V. V. Palchevski and A. Pendin, Elektrokhimiya, 14 (1978) 1613.
761 Sh. K. Norov, A. K. Tashmukhamedova, O. G. Vartanova and N. Zh. Saifullina. Elektrokhimiya, 14 (1978) 1615.
762 Sh. K. Norov and O. G. Vartanova, Zh. Anal. Khim., 34 (1979) 1500.
763 O. Nowosielski and E. Szwonek, Pr. Kom. Nauk. (Pol. Tow. Glebozn.), 2 (1977) 3.
764 J. O'Doherty, J. F. Garcia-Diaz, W. McD. Armstrong, Science, 203 (1979) 1349.
765 U. Oesch, D. Ammann, E. Pretsch and W. Simon, Helv. Chim. Acta, 62 (1979) 2073.
766 H. Ohwaki, K. Olimura and T. Kashima, Kyoritsu Yakka Daigaku Kenkyu Nempo, 24 (1979) 20.
767 R. F. Orkand, Fed. Proc., Fed. Am. Soc. Exp. Biol., 39 (1980) 1515.
768 H. F. Osswald, R. Asper, W. Dimai and W. Simon, Clin. Chem., 25 (1979) 39.
769 S. A. Ovchinnikova, Nauchn. Tr. Kuban. Gas. Univ., 232 (1977) 143.
770 J. D. Owen and H. M. Brown, Comparison between free calcium selective microelectrodes and Arsenazo III, in C. C. Ashley and A. K. Campbell (Eds.), Detection and Measurement of Free Calcium in Cells, Elsevier, Amsterdam, 1979, p. 395.
771 J. D. Owen and H. M. Brown, Comput. Biochem. Physiol., 66A (1980) 197.
772 Ya. A. Pachepskii and A. A. Ponizovskii, Pochv.-Biogeotsenol. Issled. Priazove (Moscow), 3 (1978) 160.
773 F. Pavlík and Z. Škodová, Cas. Lek. Cesk., 119 (1980) 467.
774 F. Pedrazzini, A. Castelli and P. Nannipieri, Commun. Soil Sci. Plant Anal., 10 (1979) 883.
775 A. A. Pendin and P. K. Leontevskaya, Zh. Anal. Khim., 34 (1979) 2113.
776 R. Perez Olmos. Ing. Quim. (Madrid), 10 (1978) 233.
777 S. Pinzanti and E. La Porta, J. Pharm. Pharmacol., 31 (1979) 573.
778 Z. Pranjić-Anušić, Acta Pharm. Jugosl., 29 (1979) 29.
779 G. A. Qureshi, Libyan J. Sci., 8A (1978) 37.
780 E. M. Rakhmanko, G. L. Starobinets, V. L. Lomako and A. Beisis, Vestsi Akad. Navuk B. SSR, Ser. Khim. Navuk, 6 (1978) 68.
781 B. W. Renoe, J. M. McDonald and J. H. Ladenson, Clin. Chem., 25 (1979) 1766.
782 B. W. Renoe, J. M. McDonald and J. H. Ladenson, Clin. Chem. Acta, 103 (1980) 91.
783 L. Reuss and T. P. Grady, J. Membr. Biol., 51 (1979) 15.
784 T. J. Rink, R. Y. Tsien and A. E. Warner, Nature, 283 (1980) 658.
785 H. Rosenberg, Anal. Biochem., 96 (1979) 90.
786 V. A. Sakharov and E. K. Mikhaevich, Khim. Prom., Ser. Metody Anal. Kontrolya Kach. Prod. Khim. Prom., 9 (1978) 30.
787 A. N. Salt and T. Konishi, Hear. Res., 1 (1979) 343.
788 S. G. Samokhvalov, V. G. Prizhukova, A. M. Kapustin and G. M. Sorokina, Khim. Sel'sk. Khoz., 18 (1980) 54.
789 B. Sapek and W. Przesmycka, Pr. Kom. Nauk. (Pol. Tow. Glebozn.), 2 (1977) 119.
790 J. G. Schindler, Biomed. Tech., 24 (1979) 203.
791 J. G. Schindler, H. Maier, A. Heidland, G. G. Jaros, O. Aziz and Ch. Steffen, Med. Prog. Technol., 7 (1980) 29.
792 J. G. Schindler, G. Stork and H.-J. Strüh, Fresenius Z. Anal. Chem., 292 (1978) 396.
793 J. K. Schneider, P. Hofstetter, E. Pretsch, D. Ammann and W. Simon, Helv. Chim. Acta, 63 (1980) 217.
794 J. Šenkýř and J. Petr. Chem. Listy, 73 (1979) 1097.
795 J. Šenkýř, D. Ammann, P. C. Meier, W. E. Morf, E. Pretsch and W. Simon, Anal. Chem., 51 (1979) 786.
796 G. M. Sergeev, I. M. Korenman and I. V. Blokhina, Zh. Anal. Khim., 35 (1980) 1184.
797 Yu. V. Shavnya, A. S. Rychkov, O. M. Petrukhin, A. S. Bobrova, V. A. Zarinskii and Yu. A. Zolotov, Gidrometallurgiya Zolota (Moscow), (1980) 179.

798 Yu. V. Shavnya, Yu. M. Chikin and V. A. Pronin, Nauchn. Tr. Irkutsk. Gos. Nauchno-Issled. Inst. Redk. Tsvetn. Met., 31 (1977) 63.
799 K. Shiba, T. Wartanabe, Y. Umezawa, S. Fujiwara and H. Momoi, Chem. Lett., 1980, 155.
800 T. Shiba, T. Uruno, K. Kubata and K. Tákagi, J. Pharmacobio-Dyn., 4 (1981) 109.
801 L. K. Shpigun, E. Pungor, G. Nagy, V. A. Zarinskii and I. V. Volobueva, Zh. Anal. Khim., 35 (1980) 915.
802 V. S. Shterman, S. I. Petrov, I. I. Medvedev and L. T. Krasnoshchenkova, Dokl. TSKhA, 238 (1978) 143.
803 V. Simeonov, G. Andreev and A. Stoianov, Fresenius Z. Anal. Chem., 297 (1979) 418.
804 W. Simon and E. Carafoli, Methods Enzymol., 56, Biomembranes, Part G (1979) 439.
805 W. Simon and V. Prelog, Chem. Lett., 1981, 439.
806 B. S. Smolyakov, Yu. A. Dyadin and L. S. Aladko, Izv. Sib. Otd. Akad. Nauk SSSR, Ser. Khim. Nauk, 6 (1980) 66.
807 B. S. Smolyakov and N. I. Yakovleva, Izv. Sib. Otd. Akad. Nauk SSSR, Ser. Khim. Nauk, 1 (1980) 116.
808 G. G. Somjen, Ann. Rev. Physiol., 41 (1979) 159.
809 G. L. Starobinets, G. A. Laevskaya, F. M. Rakhmanko and A. K. Pirozhnikova, Zh. Anal. Khim., 35 (1980) 154.
810 O. K. Stefanova, V. F. Gorshkova and E. A. Materova, Ion. Obmen Ionometriya, 2 (1979) 183.
811 O. K. Stefanova, N. V. Rozhdestvenskaya and I. V. Rusina, Ion. Obmen Ionometriya, 2 (1979) 166.
812 O. K. Stefanova and I. V. Rusina, Elektrokhimiya, 14 (1978) 882.
813 O. K. Stefanova and E. D. Suglobova, Elektrokhimiya, 15 (1979) 1710.
814 Ch. Steffen, J. G. Schindler and O. Aziz, Biomed. Tech., 21 (1976) 188.
815 R. A. Steiner, M. Oehme, D. Ammann and W. Simon, Anal. Chem., 51 (1979) 351.
816 S.-W. Sun, X. Wang and O.-H. Ge, Hua Hsueh Tung Pao, 2 (1979) 128.
817 K. Suzuki, H. Ishiwada, T. Shirai and S. Yanagisawa, Bunseki Kagaku, 29 (1980) 816.
818 E. Syková, Bioelectrochem. Bioenerg., 7 (1980) 231.
819 K. Sykut, J. Dumkiewicz, R. Dumkiewicz and U. Loboda, Buil. Lubel. Tow. Nauk, Mat-Fiz.-Chem., 21 (1979) 23.
820 K. Sykut, A. Kusak, J. Dumkiewicz and R. Dumkiewicz, Pr. Kom. Nauk. (Pol. Tow. Glebozn.), 2 (1977) 11.
821 W. Szczepaniak and K. Ren, Chem. Anal. (Warsaw), 25 (1980) 449.
822 W. Szczepaniak, M. Ren and K. Ren, Chem. Anal. (Warsaw), 24 (1979) 51.
823 H. Takehara, Y. Hiratskuka and M. Aarazono, Bunseki Kagaku, 29 (1980) 601.
824 H. Tamura, K. Kimura and T. Shono, Bull. Chem. Soc. Jpn., 53 (1980) 547.
825 H. Tamura, K. Kimura and T. Shono, J. Electroanal. Chem., 115 (1980) 115.
826 H. Tamura, K. Kimura and T. Shono, Nippon Kagaku Kaishi, (1980) 1648.
827 A. P. Thoma, A. Viviani-Nauer, K. H. Schellenberg, D. Bedeković, E. Pretsch, V. Prelog and W. Simon, Helv. Chim. Acta, 62 (1979) 2303.
828 J. D. R. Thomas, Lab. Pract., 27 (1978) 857.
829 U. Tietz, U. Gruenke and I. Krause, Acta Hydrochim. Hydrobiol., 8 (1980) 291.
830 M. Trojanowicz, Fresenius Z. Anal. Chem., 297 (1979) 414.
831 R. Y. Tsien and T. J. Rink, Biochim. Biophys. Acta, 599 (1980) 623.
832 Tsinhai Salt Lake Laboratory and Lanchow Chemical Physics Laboratory, Fen Hsi Hua Hsueh, 7 (1979) 20.
833 D. Tuhtar, T. Dobrovoljac and D. Mumcinović, Croat. Chem. Acta, 52 (1979) 401.
834 S.-M. Tung, T.-Y. Pei and H.-F. Chu, Fen Hsi Hua Hsueh, 7 (1979) 242.
835 Y. Umezawa, I. Tasaki and J. Fujiwara, Nippon Kagaku Kaishi, (1980) 1641.
836 O. G. Vartanova, S. Khuzhaev, E. S. Gureev and Sh. K. Norov, Zh. Anal. Khim., 34 (1979) 892.

837 R. D. Vaughan-Jones, J. Physiol. (London), 295 (1979) 111.
838 R. Virtanen, Kemi, 6 (1979) 89.
839 K. Vytřas, Am. Lab., 11 (1979) 93.
840 K. Vytřas, M. Remeš and H. Kubešová-Svobodová, Anal. Chim. Acta, 124 (1981) 91.
841 P. Wooley and M. Teubner, Biophys. Chem., 10 (1979) 335.
842 A. Yamauchi, H. Tokunaga, S. Matsuno and H. Kimizuka, Nippon Kagaku Kaishi, (1980) 388.
843 R. K. Yamazaki, D. L. Mickey and M. Stary, Anal. Biochem., 93 (1979) 430.
844 S. P. Yang, Chung-Hua I Hsueh Chien Yen Tsa Chih, 3 (1980) 32.
845 Y. Yasaka, T. Yamamoto, K. Kimura and T. Shono, Chem. Lett., 1980, 769.
846 Y. Yasaka, T. Yamamoto, K. Kimura and T. Shono, Chem. Lett., 1981, 440.
847 T. Yasaki, R. Ahiko, K. Hara, A. Yamamoto, Y. Yoshio and Y. Iizuka, Koku Eisei Gakkai Zasshi, 27 (1977) 59.
848 V. A. Zarinskii, L. K. Shpigun, V. M. Shkinev, B. Ya. Spivakov, V. M. Trepalina and Yu. A. Zolotov, Zh. Anal. Khim., 35 (1980) 2137.
849 V. A. Zarinskii, L. K. Shpigun V. M. Shkinev, B. Yu. Spivakov and Yu. A. Zolotov, Zh. Anal. Khim., 35 (1980) 2143.
850 K. Zimmermann and J. v. Lengerken, Monatsh. Veterinaermed., 35 (1980) 100.
851 K. Zimmermann and J. v. Lengerken, Nahrung, 24 (1980) 197.
852 G. K. Zykina, T. L. Bystritskaya, E. A. Materova and V. V. Snakin, Issled. Pochv. Pochv. Rezhimov Stepnykh Biogeotsenozakh Priazoviya, (1977) 114.
853 M. A. Arnold and G. A. Rechnitz, Anal. Chem., 52 (1980) 1170.
854 M. A. Arnold and G. A. Rechnitz, Anal. Chem., 53 (1981) 515.
855 M. A. Arnold and G. A. Rechnitz, Anal. Chim. Acta, 113 (1980) 351.
856 M. N. Beg, F. A. Siddiqui, M. Arshad, R. Shyan and M. M. Beg, Fresenius Z. anal Chem., 298 (1979) 157.
857 M. A. Beg, M. Usman and A. Nabi, J. Electroanal. Chem., 112 (1980) 347.
858 J. L. Boitieux, G. Desnet and D. Thomas, Clin. Chem., 25 (1979) 318.
859 W. D'Olieslager and L. Heerman, J. Electrochem. Soc., 126 (1979) 347.
860 P. Durand, A. David and D. Thomas, Biochim. Biophys. Acta, 527 (1978) 277.
861 M. M. Fishman, Anal. Chem., 52 (1980) 185R.
862 K. W. Fung, S. S. Kuan, K. Y. Sung and G. G. Guilbault, Anal. Chem., 51 (1979) 2319.
863 C. R. Gebauer and G. A. Rechnitz, Anal. Biochem., 103 (1980) 280.
864 K.-H. Houng, Bull. Inst. Chem., Acad. Sin., 26 (1979) 31.
865 A. K. Jain, S. Agrawal and R. P. Singh, Anal. Lett., 12 (1979) 995.
866 A. K. Jain, R. P. Singh and S. Agrawal, Fresenius Z. Anal. Chem., 302 (1980) 407.
867 A. K. Jain, R. P. Singh and S. Agrawal, Indian J. Chem., 19A (1980) 1029.
868 A. K. Jain, S. K. Srivastava, S. Agrawal and R. P. Singh, Talanta, 25 (1978) 531.
869 A. K. Jain, S. K. Srivastava, R. P. Singh and S. Agrawal, Anal. Chem., 51 (1979) 1093.
870 R. K. Kobos, D. J. Rici and D. S. Flournoy, Anal. Chem., 51 (1979) 1122.
871 U. S. Lal, M. C. Chattopadhyaya and A. K. Dey, Electrochim. Acta, 26 (1981) 283.
872 U. S. Lal, M. C. Chattopadhyaya and A. K. Dey, Indian J. Chem., 19A (1980) 390.
873 U. S. Lal, M. C. Chattopadhyaya and A. K. Dey, Mikrochim. Acta, 2 (1980) 417.
874 P. Longhi, T. Mussini, F. M. Nardi and S. Rondinini, Nouv. J. Chim., 3 (1979) 649.
875 P. Longhi, T. Mussini, F. M. Nardi and S. Rondinini, Ann. Chim. (Rome), 70 (1980) 315.
876 W. U. Malik, D. K. Rastogi and S. P. Arora, J. Electrochem. Soc. India, 29 (1980) 135.
877 N. A. Polotebnova, O. T. Rudyagina, L. T. Migunova and V. V. Krasnoshchenkov, Izv. Timiryazevsk. Skh. Akad., 2 (1980) 164.
878 B. S. Sharma and A. K. Gurtu, J. Electrochem. Soc. India, 29 (1980) 74.
879 K. Shiba, Y. Umezawa, T. Watanabe, S. Ogawa and S. Fujiwara, Anal. Chem., 52 (1980) 1610.

880 R. L. Solsky, Thesis, Univ. Microfilms Int., Buffalo, NY, No. 8027637, 1980.
881 R. L. Solsky and G. A. Rechnitz, Science, 204 (1979) 1308.
882 R. L. Solsky and G. A. Rechnitz, Anal. Chim. Acta, 123 (1981) 135.
883 S. K. Srivastava, A. K. Jain, S. Agrawal and R. P. Singh, J. Chem. Technol. Biotechnol., 29 (1979) 379.
884 S. K. Srivastava, A. K. Jain, S. Agrawal and R. P. Singh, J. Electroanal. Chem., 90 (1978) 291.
885 S. Updike and I. Treichel, Anal. Chem., 51 (1979) 1643.

Analytica Chimica Acta, 139 (1982) 53—59
Elsevier Scientific Publishing Company, Amsterdam — Printed in The Netherlands

DETERMINATION OF THE PERFORMANCE OF GLASS ELECTRODES IN AQUEOUS SOLUTIONS IN THE PHYSIOLOGICAL pH RANGE AND AT THE PHYSIOLOGICAL SODIUM ION CONCENTRATION

R. SPROKHOLT and A. H. J. MAAS

Department of Cardiology and Cardiovascular Surgery, State University Hospital, 3500 CG Utrecht (The Netherlands)

M. J. REBELO and A. K. COVINGTON*

Department of Physical Chemistry, School of Chemistry, University of Newcastle-upon-Tyne (Gt. Britain)

(Received 19th January 1982)

SUMMARY

A method for testing glass electrodes in the physiological pH range (6.4—7.6) and at the physiological sodium ion concentration (0.15 mol l^{-1}), based on indirect comparison of potentials with the hydrogen gas electrode, is developed according to a scheme described earlier. The hydrogen ion sensitivity and the sodium ion error of a glass electrode can be determined with three different aqueous solutions of amine buffers and their hydrochlorides; two of these have different pH values and one also contains a sodium salt (at the higher pH value). A cell without a liquid/liquid junction, containing silver/silver chloride reference electrodes, is used at 37°C. The accuracy of both determinations is ±0.2 mV (±0.003 pH). The results for some commercial glass electrodes tested with this method are presented.

A glass electrode shows imperfect response or error at both ends of the pH scale, compared to the hydrogen gas electrode. Commonly, the non-ideal behaviour of a glass electrode is described in terms of hydrogen ion sensitivity and acid or alkaline error. The hydrogen ion sensitivity of a glass electrode is the deviation of its observed e.m.f.—pH slope compared to the theoretical slope to which the hydrogen gas electrode conforms in the same cell. This deviation, also described as the electromotive efficiency factor, can be measured with standard buffer solutions [1]. Its value is, however, dependent on the buffer solutions chosen. The alkaline error of a glass electrode is a mixed response to hydrogen ions and alkali metal ions, of which the effect of the sodium ions is most pronounced at high pH [2]. As a result of this error, the pH value of very alkaline mixtures will be too low when measured with most glass electrodes. Maas [1] has already shown that in the physiological pH range (6.4—7.6) in buffer solutions containing various concentrations of sodium ions, a deviation in pH of approximately 0.01 can be measured with a glass electrode and a hydrogen gas electrode. It is therefore important to have a method which determines the performance of a glass electrode very

accurately when pH values are measured by the reference method proposed for blood [3].

The determination of the hydrogen ion sensitivity and the sodium ion error of glass electrodes in aqueous solutions at 25° C has been described by Covington and coworkers [4, 5]. This method is based on indirect comparison of the potentials of the glass electrode and the hydrogen gas electrode, with silver/silver chloride reference electrodes in cells without a liquid/liquid junction. Buffer solutions with different pH, and buffer solutions with nearly equal pH containing sodium ions at different concentrations, are used for determining the hydrogen ion sensitivity and the sodium error, respectively. When the potential differences between the buffer solutions in the cells and the hydrogen electrodes are known, only those with the glass electrode have to be measured.

The method is adapted here for the determination of the performance of glass electrodes in the physiological pH range (6.4—7.6) and at the physiological sodium ion concentration (0.15 mol l^{-1}). Since thermal-electrolytic silver/silver chloride reference electrodes are not commonly available, special attention was given to the silver/silver chloride reference electrodes of glass electrodes and to electrolytic silver/silver chloride electrodes prepared as described by Brown [6].

Hydrogen ion sensitivity

A hydrogen-ion responsive glass electrode behaves ideally when the electromotive force (e.m.f.) of the cell

$$\text{Pt} \mid \text{H}_2(\text{g}) \mid \text{solution} \mid \text{glass electrode} \qquad \text{(I)}$$

is independent of the composition of the solution. An error is indicated by the difference between the e.m.f. values obtained with two different solutions.

For practical reasons, two other cells are set up:

$$\text{Ag} \mid \text{AgCl} \mid \text{solution} \mid \text{H}_2(\text{g}) \mid \text{Pt} \qquad \text{(H)}$$

$$\text{Ag} \mid \text{AgCl} \mid \text{solution} \mid \text{glass electrode} \qquad \text{(G)}$$

When identical solutions and silver/silver chloride electrodes are used, the cells (H) and (G) correspond to the cell (I). The e.m.f. of cell (I) with a solution R (E_I^R) is equal to the differences of the e.m.f.'s of the cells (H) and (G): $E_I^R = E_H^R - E_G^R$. Another solution T of different pH will give a new difference: $E_I^T = E_H^T - E_G^T$. When the glass electrode is assumed to be error-free in solution R, the error of the glass electrode (ΔE) in solution T can be obtained by subtracting E_I^R from E_I^T: $\Delta E = E_I^T - E_I^R$ or $\Delta E = (E_H^T - E_H^R) - (E_G^T - E_G^R)$. From this the relative sensitivity of the glass electrode (g) may be calculated by the equation

$$g = (E_G^T - E_G^R)/(E_H^T - E_H^R) \qquad (1)$$

When the e.m.f. values of cell (H) are known, it is possible to determine the sensitivity of a glass electrode by measuring the e.m.f. of cell (G) with the solutions R and T.

Sodium error

By analogy with the method for the hydrogen ion sensitivity, the sodium error can be determined. The e.m.f. values of cells (G) and (H) are measured with two solutions, T and TNa, with nearly the same pH, containing respectively 0.00 and 0.15 mol l^{-1} sodium ion. The sodium error of the glass electrode (ΔE^{Na}) is obtained from

$$\Delta E^{Na} = (E_H^{TNa} - E_H^T) - (E_G^{TNa} - E_G^T) \quad (2)$$

EXPERIMENTAL

Reagents and buffer solutions

The 1 M HCl solutions were prepared from Titrisol (Merck). 2,2-Bis(hydroxyethyl)imino-tris(hydroxymethyl)methane (Bis-Tris; Aldrich), tris(hydroxymethyl)methylamine (Tris; BDH), and sodium perchlorate monohydrate (BDH) were of analytical-reagent grade. Double-distilled water was used for all dilutions.

As suggested by Covington and Ferra [5], the buffer solutions are coded A*i*, indicating that the pH of a particular buffer solution lies between *i* and *i* + 1. The sodium-containing buffer solutions are coded A*i*Na*j*, where *j* indicates *p*Na = −log [Na^+]. The compositions and pH (at 37° C) of the buffer solutions were as follows:

Buffer	pH	Components
A6	6.36	1 M HCl (50 ml) and Bis-Tris (20.924 g) diluted to 1 l
A7	7.57	1 M HCl (100 ml) and Tris (18.171 g) diluted to 1 l
A7Na0.8	7.58	$NaClO_4 \cdot H_2O$ (10.534 g) in 500 ml of solution A7

Both Bis-Tris and Tris were dried overnight at 80° C [7]. No special precautions were taken to avoid CO_2 contamination. The pH values given are not essential. They were used to check the proper preparation of the buffer solutions.

Apparatus

Following the methods mentioned above [4, 5], the e.m.f. of cell (H) was measured at 37.00 ± 0.01° C. The two compartments of the electrode vessel were connected by a capillary with a tap of 1.5-mm i.d. The tap was greased at the bottom and top in order to leave a central conducting path of solution when it was closed. Before reaching the cell, the hydrogen was passed through a small sintered glass bubbler containing the same solution that was in the cell. The hydrogen was bubbled for 1 h and the e.m.f. of the cell was measured when it reached a steady value. Measurements were made to 0.01 mV with a

Hewlett-Packard digital voltmeter type 3455 A. The hydrogen-responsive electrodes were platinum foils, coated with platinum black by passing 200 mA for 3 min with the electrodes in 3% chloroplatinic acid in 2 M KCl using a similar platinum foil as anode.

The e.m.f. values of cell (G) were measured with a pH (mV)-meter (Radiometer PHM 64, Radiometer) with a discrimination of 0.1 mV. The cell vessel was glass, closed with nylon caps with holes fitted with rubber O-rings, in which the electrodes were placed to avoid evaporation of the buffer solutions. This vessel was thermostatted in a water bath at 37.0 ± 0.1°C. To prevent carryover of the buffer solutions, the electrodes were washed with a little of the buffer solution into which they were to be placed.

Silver/silver chloride electrodes were prepared as described by Brown [6], by electrolytic silvering (4 h), followed by chloridation (0.5 h) of a platinum wire (0.3 mm diameter, 1—2 cm length). In order to obtain stable and useful electrodes, it is important to use proper current densities during both electrolyses [6]: current densities of 0.44 and 0.66 mA cm^{-2}, respectively, were used here. Silver/silver chloride electrodes of the type used as inner reference electrodes in glass pH electrodes were also used.

Procedure for measurements

A glass electrode was tested in combination with a silver/silver chloride reference electrode in the buffer solutions A6, A7 and A7Na0.8, successively. E.m.f. values were measured at 37.0 ± 0.1°C in a cell without a liquid/liquid junction, consisting of a glass electrode, a silver/silver chloride reference electrode and buffer solutions A6, A7 and A7Na0.8. The e.m.f. readings were taken after temperature and chemical equilibrium had been reached; in these experiments, one hour was required. It is recommended that matched silver/silver chloride electrodes be equilibrated in the three buffer solutions at the same time and that the e.m.f. of the glass electrodes in the three cells (G) be measured successively. This will reduce errors arising from a change in asymmetry potential of the glass electrodes with time.

Control pH measurements were done in a water bath thermostatted at 37.0 ± 0.1°C in a cell with a saturated potassium chloride liquid/liquid junction, a calomel reference electrode and a capillary glass electrode. The pH meter was adjusted for both isopotential and slope with standard solutions.

Examples. A glass electrode was tested in cell (G) with the three buffer solutions and the following e.m.f. values and control pH values were observed:

Buffer	E (mV)	pH
A6	62.9	6.37
A7	119.6	7.56
A7Na0.8	123.6	7.57

The calculated e.m.f. differences $E_G^T - E_G^R$ and $E_G^{TNa} - E_G^T$ are 56.7 mV for the change from A7 to A6, and 4.0 mV for the change from A7Na0.8 to A7.

The e.m.f. values for cell (H) are given in the Results section. The error is obtained as $\Delta E = \Delta E_H - \Delta E_G$, being −0.1 mV for the change from A7 to A6 and 0.2 mV for the change from A7Na0.8 to A7. Because the changes in e.m.f. accompanying the buffer change A7 to A6 are equal for cells (H) and (G), within experimental error, the sensitivity of the glass electrode gives a calculated value of $g = 1$. The changes in e.m.f. related to the change A7Na0.8 to A7 are not equal for cells (H) and (G); the error of 0.2 mV corresponds to a pH that is 0.003 too low.

RESULTS AND DISCUSSION

The e.m.f. values of cell (H) for the buffer solutions A6, A7 and A7Na0.8 were measured against thermal-electrolytic silver/silver chloride reference electrodes, which are stable and accurate [8], at 37° C. The e.m.f. differences (ΔE) obtained were 56.6 ± 0.2 mV for the A7 to A6 buffer change, and 4.2 ± 0.2 mV for the A7Na0.8 to A7 buffer change.

When the e.m.f. of cell (G) is measured with a glass electrode, it is important to know the effect of different types of silver/silver chloride reference electrodes on the determination of the e.m.f. differences. To test this, four silver/silver chloride electrodes (from glass electrodes) were compared with one thermal-electrolytic electrode using both types as reference electrodes in cell (G). The calculated e.m.f. differences of cell (G) showed a small range of 2.0 mV (see Table 1). This is caused by the silver/silver chloride reference electrodes from glass electrodes having larger bias potentials than other types, although the potentials are stable and reproducible during an experiment. Therefore, this type is not recommended.

The thermal-electrolytic silver/silver chloride reference electrode was also used in combination with a Radiometer G299A capillary glass electrode to examine the influence of several preparations of buffer solutions on the

TABLE 1

Measured e.m.f. (mV) values and calculated e.m.f. differences (ΔE) of one glass electrode (R1) with five different silver/silver chloride electrodes, in three buffer solutions

Reference electrode	E.m.f. (mV)			ΔE (mV)	
	A6	A7	A7Na0.8	A7 to A6	A7Na0.8 to A7
1	55.4 ± 0.1	111.7 ± 0.2	115.9 ± 0.2	56.3	4.2
2	61.0 ± 0.3	117.6 ± 0.5		56.6	
3	60.4 ± 0.4	115.0 ± 0.3		54.6	
4	60.7 ± 0.2	115.7 ± 0.5		55.0	
Av. ± s.d.	59.4 ± 3.3	115.0 ± 2.5	115.9 ± 0.2	55.6 ± 1.0	4.2
5[a]	57.6 ± 0.1	113.7 ± 0.1	117.8 ± 0.1	56.1	4.1

[a]Thermal-electrolytic electrode.

determination of the e.m.f. of cell (G). The results for four different buffer series (Table 2) showed good reproducibility for the e.m.f. differences, even when measured on different days. This was not always found with some batches of Bis-Tris.

From these results it was calculated that the glass electrode used had a hydrogen ion sensitivity of $g = 1$ and no sodium error, both within experimental error.

Finally, six silver/silver chloride reference electrodes of the electrolytic type were prepared as described by Brown [6]. These showed a maximal difference of 0.1 mV when measured in pairs in sodium chloride solutions of 0.154 and 1.0 mol l^{-1}. These reference electrodes were used to determine the hydrogen sensitivity and the sodium error of commercial glass electrodes (Tables 3 and 4).

The thermal-electrolytic reference electrodes and the electrolytic reference electrodes give identical results within experimental error. The former have been shown to be more reproducible and reliable [9] than the latter. The electrolytic reference electrodes, however, have the advantages of a shorter response time and easier preparation. The glass electrodes showed, within

TABLE 2

Calculated e.m.f. differences (mV) of four buffer series, measured with one glass electrode and a thermal-electrolytic silver/silver chloride reference electrode

Buffer series	A7 to A6	A7Na0.8 to A7
I	56.4, 56.7, 56.5	4.3, 4.4, 4.3
II	56.4, 56.6	4.3, 4.1
III	56.5	4.5
IV	56.8	4.1
Av. ± s.d.	56.5 ± 0.2	4.3 ± 0.2

TABLE 3

Calculated e.m.f. differences (mV) of cell (G) with electrolytic ($n = 6$) and thermal-electrolytic ($n = 2$) silver/silver chloride electrodes and two different glass electrodes

Glass electrode	Calculated e.m.f. change (mV)			
	A7 to A6		A7Na0.8 to A7	
	Electrolytic Ag/AgCl	Thermal-electrolytic Ag/AgCl	Electrolytic Ag/AgCl	Thermal-electrolytic Ag/AgCl
R2	56.6 ± 0.1	56.5 ± 0.1	3.6 ± 0.1[a]	3.9 ± 0.1[a]
R3	55.9 ± 0.1	—	4.3 ± 0.1	—

[a]This glass electrode was new (dry) and was equilibrated in phosphate buffer (pH 7.38) for 6 h instead of 24 h as recommended by the manufacturer.

TABLE 4

Calculated hydrogen ion sensitivities (g) and sodium ion errors of glass electrodes

Glass electrode	Hydrogen ion sensitivity		Sodium error (ΔpH)[a]	
	Electrolytic Ag/AgCl	Thermal-electrolytic Ag/AgCl	Electrolytic Ag/AgCl	Thermal-electrolytic Ag/AgCl
R1	—	0.998, 1.004	—	—0.003, 0.002
R1	—	0.991	—	0.002
R2	1.000	0.998	0.010	0.003
R3	0.998	—	—0.002	—
Russell	—	1.001	—	—0.002
RG202C	—	1.004	—	0.005

[a]Corresponding to error in pH measured.

experimental error, theoretical pH response. The sodium error is theoretical for the R-type glass electrode (Radiometer G299A). The Radiometer G202C electrode showed a slight sodium error of 0.3 mV, as expected from a rough estimation from a nomogram [10] provided by the manufacturers.

It is concluded that the described method is suitable for determining the hydrogen ion sensitivity and the sodium ion error of glass electrodes with an accuracy of ±0.2 mV or 0.003 pH (g value 1.000 ± 0.004), at 37° C. All glass electrodes tested showed, within experimental error, theoretical pH response. It is possible to detect a small sodium ion error of glass electrodes in the physiological pH range, as demonstrated with the G202C electrode.

This work was supported by grant 13-36-27 from The Netherlands Organization for the Advancement of Pure Research, received (by A.H.J.M.) through the Foundation for Medical Research. M.J.R. thanks the Gulbenkian Foundation, Lisbon, for a scholarship award.

REFERENCES

1 A. H. J. Maas, Clin. Chim. Acta, 28 (1970) 373.
2 R. G. Bates, Determination of pH, Theory and Practice, Wiley, New York, 1964, p. 315.
3 O. Siggaard-Andersen, R. A. Durst and A. H. J. Maas, J. Clin. Chem. Clin. Biochem., 18 (1980) 829.
4 M. F. G. F. C. Camoes and A. K. Covington, Anal. Chem., 46 (1974) 1547.
5 A. K. Covington and M. I. A. Ferra, Anal. Chem., 49 (1977) 1363.
6 A. S. Brown, J. Am. Chem. Soc., 56 (1935) 646.
7 R. A. Durst and B. R. Staples, Clin. Chem., 18 (1972) 206.
8 D. J. G. Ives and G. J. Janz, Reference Electrodes, Theory and Practice, Academic Press, New York, 1961, pp. 213—224.
9 A. K. Covington, in R. A. Durst (Ed.), Ion-Selective Electrodes, NBS Spec. Publ. No. 314, U.S. Gov. Printing Office, Washington, 1969, p. 107.
10 N. Linnet, pH Measurements in Theory and Practice, Radiometer, Copenhagen, 1970, p. 81.

Analytica Chimica Acta, 139 (1982) 61—82
Elsevier Scientific Publishing Company, Amsterdam — Printed in The Netherlands

BIPOLAR PULSE CONDUCTOMETRIC MONITORING OF ION-SELECTIVE ELECTRODES

Part 1. Method Development with a Calcium-Selective Electrode and Elucidation of the Basic Principles Involved

CHARLES R. POWLEY and TIMOTHY A. NIEMAN*

School of Chemical Sciences, University of Illinois, Urbana, IL 61801 (U.S.A.)

(Received 8th December 1981)

SUMMARY

The potential generated by a plastic-membrane calcium ion-selective electrode (i.s.e.) is shown to be indirectly measurable by a non-zero current method based on bipolar pulse conductance. Linear current—voltage curves are obtained using 0—5-V pulses; the current axis intercept is related to the i.s.e. potential. A simple electrical contact (e.g., platinum or stainless steel) can be used instead of a poised reference electrode as the counter electrode in this two-electrode system. Long-term exposure of the i.s.e. to calcium solutions causes an upward drift in the measured current. This drift is minimized by avoiding long exposure times to solution, rinsing the electrode between measurements, and constructing current—voltage curves for determination of the current axis intercepts. Voltage pulses lasting 100 μs are optimum for this method. Shorter pulses are subject to error from capacitive charging currents, and longer pulses yield poorer precision, and degrade the electrode through faradaic reactions. The measured signal is dependent upon Ca^{2+} concentration (rather than activity), making ionic strength adjustment unnecessary. The concentration dependence is induced by application of voltage pulses greater than ~15 mV in amplitude. Selectivities of the potentiometric and conductometric methods are shown to be comparable for a variety of interfering monovalent and divalent cations. The conductometric method yields a fast i.s.e. response because of induced migration of Ca^{2+} into the membrane. Response time decreases as the pulse height increases. Pulses greater than 2 V in magnitude yield response times limited by the solution mixing time rather than by the electrode.

The potentiometric (zero current) measurement of ionic activities with ion-selective electrodes (i.s.e.'s) has become a widely used and convenient method [1, 2]. Non-zero current methods are useful in the characterization of i.s.e. properties. Conductivity measurements have been used to determine i.s.e. bulk parameters such as resistance, capacitance, and dielectric constants [3—5]. Alternating current impedance measurements have been useful in the modeling of electrode behavior [6—8]. These non-zero current techniques have not been shown to be useful in determining ionic concentrations in an external bathing solution.

A method based on bipolar pulse conductometric monitoring of a calcium i.s.e. was reported recently [9]. The i.s.e. responded to changes in Ca^{2+} concentration in <10 ms, significantly faster than the potentiometric response

0003-2670/82/0000-0000/$02.75

time of 4—5 s. It was also found that the measured current was a linear function of the logarithm of the Ca^{2+} concentration rather than the logarithm of the Ca^{2+} activity. Still another advantage of this method was that a poised reference electrode, such as a saturated calomel electrode, was not needed.

This paper expands on the results presented earlier [9]. The similarities and differences in the response of the i.s.e. to Ca^{2+} using potentiometric and conductometric monitoring were explored. Further examinations of the instrumental parameters, choice of electrodes, role of interfering ions, and the rapid conductometric response were also performed. Explanations of the observed phenomena are offered where possible; further work is necessary in some instances. Finally, a brief overview of non-zero current work in the literature is presented, and comparisons are made with the bipolar pulse conductance method.

EXPERIMENTAL

Equipment and reagents

Conductance instrument. The bipolar pulse conductance (BICON) technique involves the sequential application to the cell of two short duration voltage (or current) pulses of equal magnitude and duration, but opposite polarity. At the end of the second pulse, the cell current (or voltage) is measured. The current is related to the cell resistance by Ohm's law and is essentially independent of series (double-layer) or parallel capacitances of the cell [10—12].

The BICON instrument used in this work operates in the voltage pulse mode as described earlier [9]. A recent modification is the addition of a "computer expansion" board that contains 8K of RAM and 8K of PROM, in addition to that contained on the INTEL SBC 80/10 computer. All programs used in this work (both in assembly language and in BASIC) are stored in PROM. This board also features an interface to a Digital Equipment Corporation LSI-11 computer, used for storage of additional programs and data manipulation. Another addition to the BICON instrument is a strip-chart recorder interface board.

Calcium electrodes. The calcium electrodes used in this work were of the coated-wire type developed by Cattrall and Freiser [13]. A mixture of calcium liquid ion-exchanger (Orion Research Inc., No. 92-20-02) and poly(vinyl chloride) (Aldrich high molecular weight) weighing a total of 1.2 g was dissolved in 10 ml of tetrahydrofuran. The ratio of ion-exchanger to PVC was typically 70/30 by weight [14, 15], but other ratios were studied. The mixture was coated onto a 14-gauge copper wire inserted through a teflon rod. The exposed wire was about 2.5 cm long, and all exposed metal was coated. After air drying, the electrodes were conditioned by soaking overnight in a 1 M calcium chloride solution. Electrodes were kept in a sealed plastic container when not in use.

The calcium i.s.e. studied earlier [9] was commercially available, based on a neutral carrier developed by Ammann et al. [16]. The coated-wire ion

exchanger-based electrodes used in the present work are inexpensive and easily made. Economy can be an important consideration, as experimentation with various instrumental parameters may shorten the electrode lifetime. Coated-metal i.s.e.'s are also pressure-resistant and can be custom-fabricated in a variety of geometries; these properties are of advantage for application of i.s.e.'s to flowing stream and stopped-flow kinetic measurements.

Counter electrodes. Various counter electrodes (both polarizable and non-polarizable) were studied in this work. The counter electrode used most was a stainless steel rod, 2.5 cm long and 1.6 mm in diameter, mounted in the teflon rod below and parallel to the i.s.e. An additional stainless steel electrode of the same dimensions was mounted below the steel counter electrode for use in solution resistance measurements. The three electrodes were spaced about 5 mm apart. Single-junction Ag/AgCl (Corning Model 476029) and saturated calomel (Corning Model 476109) electrodes were also evaluated as counter electrodes.

Reagents. All solutions were prepared from distilled—deionized water and reagent-grade chemicals.

Measurement techniques

Conductance measurements. Currents were measured using the BICON technique. Pulse height was varied as described in the Results and Discussion section, in order to obtain a current—voltage curve for each solution. The pulse amplitude, measured from the foot of the pulse (instrumental ground) to its plateau, ranged from 0.00 to 5.00 V. Unless otherwise stated, the individual voltage pulses used were 100 μs (edge to edge) in duration. Ten data sets, each representing the average of 16 individual measurements, were taken. The delay between collection of data sets was 10 ms. All conductance measurements were made on solutions stirred with a belt-driven propeller blade.

Potentiometric measurements. Potentiometric measurements were made using an Orion Model 701A pH meter operating in the millivolt mode. The Ag/AgCl or saturated calomel electrodes were used as reference electrodes. Solutions were made 0.1 M in KCl when constant ionic strength was desired. All solutions were stirred during measurements using a magnetic stirrer.

RESULTS AND DISCUSSION

Current—voltage curves

Figure 1 is a set of current—voltage (i/V) curves obtained for various Ca^{2+} concentrations using a calcium i.s.e. made with a mixture containing 70% ion-exchanger and 30% PVC. The data for these curves were obtained by varying the applied voltage pulse height from 0.82 to 4.73 V, and measuring the resulting current. Each voltage pulse was 100 μs in duration. Such current—voltage curves are linear and have slopes equal to the reciprocal of the sum of the solution resistance and the total electrode resistance.

In this figure, the lines have the same slope because the solution resistance was determined separately and subtracted to show that the electrode has a resistance of about 500 kΩ, independent of Ca^{2+} concentration. One explanation for a constant apparent resistance is a constant Ca^{2+} concentration within the membrane, as would be expected from electroneutrality considerations. The only apparent effect of increasing Ca^{2+} concentration is an increase in the current axis intercept, which would be the current at zero applied voltage.

If a working curve is constructed using solutions which are not buffered to have a constant resistance, then the shape of that curve will depend on the magnitude of the voltage pulses used. One approach to solving this problem would be to use a salt such as potassium chloride to buffer each solution to the same resistance; this is operationally the same as buffering to constant ionic strength in potentiometry. A second approach would be to measure separately the resistance of each solution and correct the data, as was done in Fig. 1. The most convenient and useful method is to construct an i/V curve and extrapolate to the current at zero applied voltage. Figure 2 is a plot of this "zero-pulse" current vs. Ca^{2+} concentration; it shows the same general shape, detection limit, and linear range as a potentiometric working curve. The existence of this zero-pulse current is easily explained by remembering that a potential difference is generated across the i.s.e. membrane which depends on the Ca^{2+} concentration in the external solution. If there is no externally applied potential difference between the two electrodes, they are both held at instrumental ground (effectively

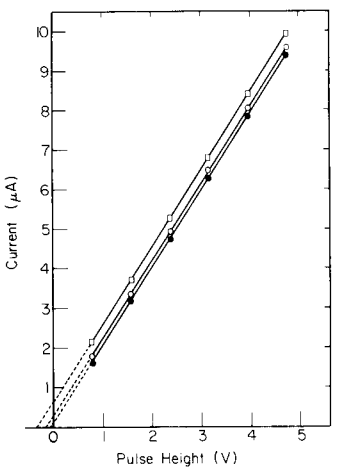

Fig. 1. Current—voltage curves for different Ca^{2+} concentrations: (□) 10^{-2} M; (○) 10^{-4} M; (●) 10^{-6} M.

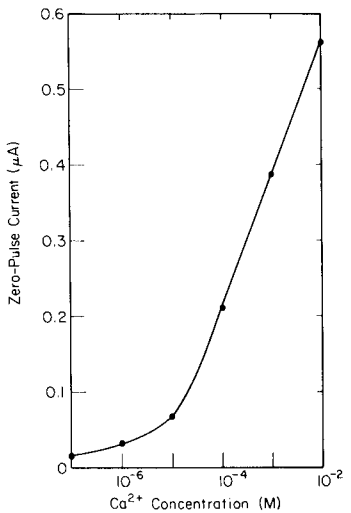

Fig. 2. Plot of i/V curve current axis intercepts vs. Ca^{2+} concentration.

shorted together) and a current will flow simply because of the potential generated at the i.s.e. membrane.

Extrapolation of the i/V curves to zero current yields potentials corresponding to the voltage generated by the i.s.e. Potentials obtained by extrapolation of i/V curves were about 40 mV higher than the values measured potentiometrically when a Ag/AgCl electrode was used as the counter and reference electrode. However, slopes of working curves were the same (32 mV/decade), as were the detection limits (about 1×10^{-5} M Ca^{2+}). Buck and Krull [17] obtained linear i/V curves for glass electrodes, using d.c. voltage steps; a Ag/AgCl counter electrode was used and the values at zero current agreed fairly well with potentiometric values obtained using a Ag/AgCl reference electrode.

Current—voltage curves are a useful diagnostic tool in BICON measurements with i.s.e.'s. The intercepts establish the link between the conductometric method and the classical potentiometric method. Also, the total electrode resistance, as determined from the slope of the i/V curve, does change in the presence of interfering ions, as shown in the results presented below. Variation of the pulse amplitude will also show that voltage-pulsing induces the concentration- (rather than activity-) dependent signal, along with the rapid response to changes in Ca^{2+} concentration.

Electrodes

Calcium electrodes of the type used here, reportedly yield optimum potentiometric performance when the membrane is composed of 70% calcium ion-exchanger and 30% PVC [14, 15]. Evaluation of electrode compositions using the BICON technique gave similar results. The membrane composition was varied from 67% ion-exchanger and 33% PVC to 85% ion-exchanger and 15% PVC. Membranes containing less than 70% ion-exchanger yield working curves showing poor sensitivity and precision. Higher ion-exchanger/PVC ratios yield approximately constant slopes for working curves constructed from the voltage axis intercepts of the i/V curves. Bulk membrane resistance decreased from about 700 kΩ for 67% ion-exchanger to about 200 kΩ for 85% ion-exchanger.

As ion-exchanger content is increased, significant leaching of the ion exchanger into the test solution can occur. Ion-exchanger leaching resulted in higher detection limits and shorter electrode lifetimes. Oesch and Simon [18] varied the composition of their neutral carrier-based plastic membranes [16] over a much wider range than was done here. They also found lower working curve slopes at low carrier concentrations, accompanied by poorer selectivity. Membranes with low PVC content were difficult to fabricate and had short lifetimes.

Potentiometric measurements with i.s.e.'s require a poised reference electrode (typically saturated calomel). Previous non-zero current measurements, based on constant voltage and a.c. impedance techniques, also employed poised, non-polarizable counter electrodes. The most common choice

was a junctionless Ag/AgCl electrode, with test solutions containing a constant chloride concentration (see, e.g., [7] and [17]). It is therefore desirable to compare the performance of polarizable to non-polarizable (Ag/AgCl, saturated calomel) electrodes using the BICON method.

The polarity of the voltage applied across the i.s.e. membrane can be positive or negative at the time of current measurement, depending on which electrode is connected to the pulse driver (see fig. 1 of Ref. 9). The pulse driver generates a negative voltage pulse immediately followed by a positive voltage pulse, with respect to instrumental ground. Ordinarily, the i.s.e. is connected to the virtual ground of the current measurement circuit, so that the voltage drop across the membrane (from internal conducting element to the test solution, with respect to the internal element) will be negative on the first pulse and positive on the second, as shown in fig. 2 of Ref. 9. The effects of reversing this sequence, by reversing the instrumental connections to the cell, were studied with both types of counter electrode.

Table 1 summarizes results obtained by constructing working curves with 10^{-7}—10^{-2} M calcium chloride solutions in decade steps. The detection limit was $\sim 10^{-5}$ M Ca^{2+} with linearity up to 10^{-2} M Ca^{2+} in all cases in which a viable working curve was obtained. The working curves were constructed by determining the voltage axis intercept (where $i = 0$) for i/V curves generated for each solution. The current axis intercept (where $V = 0$) could have been used, but comparisons with potentiometric results would have been difficult. Slopes of working curves constructed using current axis intercepts would be opposite in sign to those constructed using voltage axis intercepts, as is evident from Fig. 1. Otherwise, the working curves would show the same detection limits, precision, and linearity.

Both counter electrode type and i.s.e. polarity reversal were studied. A positive i.s.e. membrane polarity means that at the time of measurement, the applied voltage across the membrane (with respect to the internal element) is positive; a negative polarity means that the membrane is experiencing a

TABLE 1

Summary of results obtained by varying counter electrode and varying i.s.e. polarity

Counter electrode	Polarity of i.s.e. membrane on sampling	Slope of working curve (from voltage axis intercept)
Stainless steel or platinum	Positive	−63 mV/decade
Stainless steel or platinum	Negative	54 mV/decade
Stainless steel or platinum[a]	Positive	−32 mV/decade
Ag/AgCl	Positive	−32 mV/decade
Ag/AgCl	Negative	Poor precision, positive trend
SCE	Positive	−31 mV/decade
SCE	Negative	Poor precision, positive trend
SCE[a, b]	—	32 mV/decade

[a]All solutions 0.1 M in KCl. [b]Potentiometric.

negative applied voltage pulse at the instant of current measurement. The sign of the working curve slope is naturally dependent upon whether the i.s.e. is connected to the current follower amplifier or the pulse driver, because the potential induced by the presence of Ca^{2+} (from membrane interior to exterior, to be consistent with the convention established above) becomes increasingly positive with increasing Ca^{2+} concentration in solution.

The polarity of the voltage applied across the membrane appears to have a significant effect on precision. Use of a stainless steel or platinum counter electrode with the i.s.e. at negative polarity generally yielded poorer precision (an order of magnitude increase in r.s.d. for a set of measurements) than when the i.s.e. was at positive polarity. Use of the Ag/AgCl and saturated calomel electrodes yielded poorer precision (by an order of magnitude) than that obtained with the stainless steel or platinum electrodes, regardless of polarity. A positive i.s.e. membrane polarity implies that Ca^{2+} is flowing from the test solution into the membrane upon current measurement; this may be a more reproducible process than inducing Ca^{2+} flow out of the membrane.

Measurements made with a stainless steel or platinum counter electrode yield working curves with slopes significantly higher in magnitude than the potentiometric slope of 32 mV/decade if ionic strength is not held constant. The BICON working curve has a slope of 31—32 mV/decade when ionic strength is held constant by making each solution 0.1 M in KCl. Apparently, ionic strength can affect the signal of interest when a simple metallic counter electrode is used; this suggests that poorer selectivity would be obtained if ionic strength is not held constant. However, experimental results discussed later in this paper will show that, in fact, selectivity is not affected by ionic strength. The working curves have slopes of 31—32 mV/decade when the Ag/AgCl and saturated calomel electrodes are used as counter electrodes, even if the solution ionic strength is not held constant. These two reference electrodes have the internal conducting element immersed in a constant ionic strength filling solution (saturated KCl solution for the SCE, saturated KCl, AgCl solution for the Ag/AgCl electrode) separated from the external solution by a ceramic plug. The effect that ionic strength has on the slope of the working curve may result from a change in some parameter at the counter electrode/solution interface, such as double-layer capacitance.

The poor performance of the poised reference electrodes is quite surprising. The reversibility and non-polarizability of the Ag/AgCl and Hg/Hg_2Cl_2 couples are well-accepted and the junctionless Ag/AgCl electrodes apparently performed quite well in non-zero current work reported in the literature [7, 17]. The reference electrodes used in our work did have a narrow ceramic junction, and may not be able to support a relatively large current very well, as they were designed for potentiometric use. Further investigations are underway. Stainless steel or platinum electrodes cannot be used as reference electrodes in potentiometric work because their electrochemical potentials are poorly defined and drift in the absence of a redox couple in solution.

They do appear to work quite well in this BICON method, possibly because the double-layer capacitance is never more than 1% charged [12], so that electrochemical potentials cannot be achieved. Future investigations will involve measurements with electroactive species in solution, to hold a polarizable electrode at a characteristic potential.

Measurement techniques

Coated-wire electrodes are known to be simple to make, and have constant potentiometric slopes and detection limits over their useful lifetime of about six months [13]. However, such electrodes do not have a real internal reference element, and this feature has generated some controversy based on both thermodynamic and operational considerations [19, 20]. Absolute potentials of some coated-wire electrodes have been noted to drift significantly with time. The drift is attributed to solvent (water) penetration of the membrane and resulting destabilization of the weak metal/membrane interactive forces which maintain the interior of the i.s.e. at a constant potential [21].

Electrodes prepared for the present work also showed significant drifts in measured signal, under both potentiometric and conductometric monitoring. The drift problem with conductometric monitoring was particularly severe when electrodes were exposed to solution for long periods of time. Drift was reduced significantly when electrode exposure to solution was minimized and electrodes were rinsed between measurements. Electronic non-ideality in the amplifiers connected to the cell can cause potential induced migration of Ca^{2+} into (or out of) the membrane between measurements. Further improvement in precision was achieved when a relay (between the voltage pulse driver and the electrode) was used to close the circuit only when measurements were taken. Otherwise the i.s.e. was disconnected from the instrument. This relay is controlled by software to close 20 ms before a set of measurements is taken, and to open 20 ms after the set is over. The 20 ms delays are necessary to insure that relay switching artifacts do not affect pulse symmetry, and to allow removal of any residual charge built up on the double-layer capacitance.

Apparently, the flow of Ca^{2+} into the membrane with time can cause an upward drift in the measured current. Figure 3 shows drift characteristics over a 200-s interval for a 10^{-3} M Ca^{2+} solution. When total current for the maximum pulse height (5 V) was monitored over time, a relatively high amount of drift (11% in 200 s) occurred. When i/V curves were constructed at 20-s intervals over the same time period, and the current axis intercepts were found, the drift was significantly reduced (to 5%). Evidently, both the ohmic and non-ohmic contributions to the current can drift, and the ohmic part can be eliminated by extrapolation to the intercepts. Further drift reduction (to 3%) was obtained when the relay was used, as it prevented migration of ions into the membrane when measurements were not being taken. The most precise (essentially drift-free) measurements were obtained

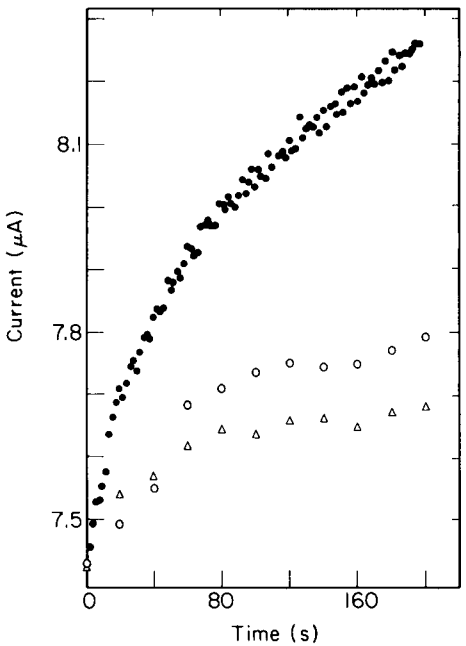

Fig. 3. Plot of current monitored over time for a 10^{-3} M Ca^{2+} solution: (•) current measured with a 5 V pulse; (○) current axis intercept (plus 6.72 μA) of the i/V curve when the switch described in the text is not used; (△) current axis intercept (plus 6.72 μA) when this switch is used.

by taking an entire i/V curve for a particular solution and using as short an exposure time as possible. The i/V curves have the added advantage of allowing solution resistance contributions to be eliminated by extrapolation to either intercept. The BICON hardware and software presently in use can routinely take a i/V curve (6 different pulse heights, 160 measurements at each pulse height) in about 1 s. This time can be further shortened to a lower limit of a few ms with corresponding reduction in the signal-to-noise ratio if less signal averaging is used.

Drift considerations also were found to be important when variation of the pulse width was studied. Pulse widths of 10 μs—100 ms were used to obtain working curves and selectivity coefficients for K^+. The slopes of the working curves (from the current axis intercepts of the i/V curves), detection limits, and K^+ selectivity coefficients are given in Table 2. Calculations of selectivity coefficients were based on the equation recommended for potentiometric use of ion-selective electrodes by IUPAC [22]

$$E = S \log [A_{Ca^{2+}} + k(A_{I^{y+}})^{2/y}] + \text{constant} \quad (1)$$

where E is the measured cell potential, S is the slope of the working curve, k is the selectivity coefficient for an interfering species I^{y+}, and A_i represents the activity of the designated species. The bipolar voltage pulse conductometric analog of Eqn. (1) is

TABLE 2

Working curve parameters and potassium ion selectivity coefficients obtained at different pulse widths

Pulse width (ms)	Working curve slope (μA/decade)	Detection limit (M Ca^{2+})	K^+ selectivity coefficient
0.010	0.706	8×10^{-5}	80
0.10	0.082	7×10^{-5}	0.91
1	0.069	8×10^{-5}	2.1
10	0.069	4×10^{-5}	4.6
100	0.083	1×10^{-5}	2.4

$$i_{zp} = S_{zp} \log ([Ca^{2+}] + k[I^{y+}]^{2/y}) + \text{constant} \quad (2)$$

where i_{zp} is the "zero pulse" current (the current axis intercept of the i/V curve), S_{zp} is the slope of the conductometric working curve, and the quantities in brackets are taken as concentrations.

Calculation of selectivity coefficients for monovalent ions using Eqn. (2) can yield coefficients that are deceivingly high. In the case of the coefficients given in Table 2, a 10^{-4} M Ca^{2+} solution and a 10^{-4} M $Ca^{2+}/10^{-2}$ M K^+ solution were compared. A selectivity coefficient of 100 would therefore have been obtained if the electrode responded equally to potassium and calcium ions.

Measurements made using 10-μs pulse widths are subject to error from parallel capacitance charging currents [12] and yield poor selectivity. The current values are about three times higher than those obtained using longer duration pulses, and the i.s.e. measurements are heavily influenced by the resistance of the solution. This limitation arises, in part, from electronic considerations with the present instrument. The pulse driver amplifier requires a moderately high output impedance for stability, and this output impedance increases the time constant for parallel capacitance charging.

Use of pulse widths in the range 100 μs—100 ms yields approximately constant values for the slopes of the working curves and the selectivity coefficients for K^+. The detection limit is lowered for longer pulse widths, possibly because a longer voltage pulse may induce Ca^{2+} migration deeper into the membrane. However, the use of the longer pulse widths does have serious drawbacks: (1) longer measurement times required for signal averaging make them impractical; (2) the drift over this time period would be significant; and (3) faradaic reactions may occur because of more extensive charging of the double layer.

Faradaic reactions can occur in the bipolar pulse method if the double-layer (or series) capacitances in the cell become appreciably charged. An equivalent circuit for the cell used in these experiments is shown in Fig. 4. (The rationale behind equivalent circuits will be touched on below.) The arrows drawn represent the current path on which measurements should be made (with a positive i.s.e. membrane polarity during the second pulse).

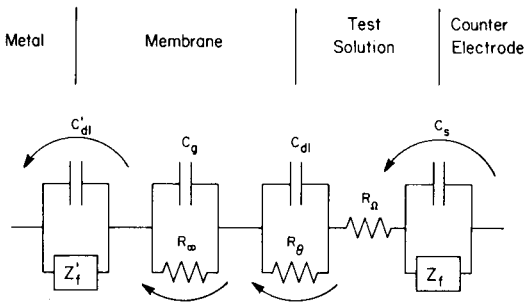

Fig. 4. Equivalent circuit for Ca^{2+} (coated-wire) and metal counter electrode. Arrows indicate desired current path at time of measurement. C'_{dl} = Metal/membrane capacitance, Z'_f = faradaic impedance at metal/membrane interface, C_g = geometric (bulk) capacitance of the membrane, R_∞ = bulk membrane resistance, C_{dl} = membrane/solution interfacial capacitance, R_θ = charge-transfer resistance at membrane/solution interface, R_Ω = solution resistance, C_s = series (double-layer) capacitance of counter electrode, Z_f = faradaic impedance at counter electrode/solution interface.

Very short duration pulses would be expected to result in measurements containing parallel capacitance charging current components, as was observed experimentally with 10-μs pulses. Very long duration pulses would be expected to charge the double-layer capacitances at the metal electrodes significantly, and force current through the faradaic impedances in parallel with these capacitances. Faradaic reactions are undesirable, as non-ohmic behavior will be obtained and electrolytic deterioration of the membrane can result.

Because membrane deterioration at longer pulse widths was anticipated [9], an older electrode was used in this set of pulse width experiments. As a result, somewhat higher detection limits were obtained than that shown in Fig. 2 for a new electrode. After this series of pulse width experiments, the i.s.e. yielded a lower potentiometric slope and an order of magnitude-higher detection limit than it did previously; these observations indicated that some damage had occurred.

Pulse widths of 100 μs were used for the remainder of this work, as the data in Table 2 indicate that 100 μs is the shortest pulse width available that will avoid having measurements influenced by parallel capacitance charging currents. Drift was reduced to an acceptable level by collecting data for i/V curves as quickly as possible (within 6 s) after immersion of the electrode into solution.

Response to concentration instead of activity

It has been reported that bipolar pulse conductometric monitoring of i.s.e.'s results in a response linear with the logarithm of the calcium concentration (log $[Ca^{2+}]$) rather than with the logarithm of the calcium activity (log $A_{Ca^{2+}}$) [9]. However, it might be argued that the working curves shown earlier [9] did not have high enough precision or did not reach a high

enough Ca^{2+} concentration (10^{-2} M was the highest concentration used) to prove unambiguously that the electrode responds to concentration instead of activity. Figure 5 shows working curves obtained both conductometrically and potentiometrically for solutions containing Ca^{2+} in the range 10^{-7}—10^{-1} M. No ionic strength adjustor of any kind was added. The current and potential values are plotted vs. both concentration and activity. Single-ion activity coefficients were calculated using the extended Debye-Hückel equation

$$-\log \gamma = [0.5115z^2(\mu)^{1/2}]/[1 + 0.3291d(\mu)^{1/2}] \quad (3)$$

where γ is the Ca^{2+} activity coefficient, $z = 2$, μ is the ionic strength of the solution, and d is the ion size parameter (4.73 Å for Ca^{2+}) [15]. The standard error estimate (S_E) values for plots of zero-pulse current (or potential) vs. concentration (or activity) are given in Fig. 5. The S_E values were calculated for the 3×10^{-5}—10^{-1} M concentration range in all four cases. The better linear fit (lower S_E) is obtained when zero-pulse current is plotted against $\log[Ca^{2+}]$, instead of $\log A_{Ca^{2+}}$. The S_E values also demonstrate, as expected, that the potential vs. $\log A_{Ca^{2+}}$ plot yields a better linear fit than plotting potential vs. $\log[Ca^{2+}]$.

The response to concentration instead of activity was also demonstrated by measuring electrode response in solutions with a constant concentration of calcium but different ionic strength. For example, the potentiometric response for a 10^{-4} M Ca^{2+}/0.1 M KCl solution was less than that of a 10^{-4} M Ca^{2+} solution, by about 25 mV. Even though K^+ can enhance the i.s.e. potential by a very small amount, the addition of KCl lowers the Ca^{2+} activity coefficient by almost an order of magnitude. Changes in the Ca^{2+} activity coefficient did not have any effect when both of these solutions were measured conductometrically. The zero-pulse current was only enhanced by a small amount in the presence of K^+; the decrease of the Ca^{2+} activity coefficient did not produce any corresponding decreases in the zero-pulse current.

Earlier in this paper, it was stated that the magnitude of the current axis intercept of the i/V curve (Fig. 1) is related to the magnitude of the short-circuit i.s.e. potential. Because the i.s.e. potential is activity-dependent, one would assume that the short-circuit current generated by this potential would also have to be activity-dependent. However, the zero-pulse currents obtained by i/V curve extrapolation are clearly concentration-dependent. Use of a non-zero voltage pulse must therefore cause the concentration dependence.

High-resolution i/V curves using every pulse height achievable by computer control of the BICON instrument were constructed in the −400—+900 mV region for 10^{-2} and 10^{-4} M Ca^{2+} solutions. These curves, which have 39 mV resolution, are shown in Fig. 6. For the 10^{-2} M solution, a negative deviation from the line is evident at the data point closest to zero applied voltage. However, this deviation is barely perceptible for the 10^{-4} M solution. No such

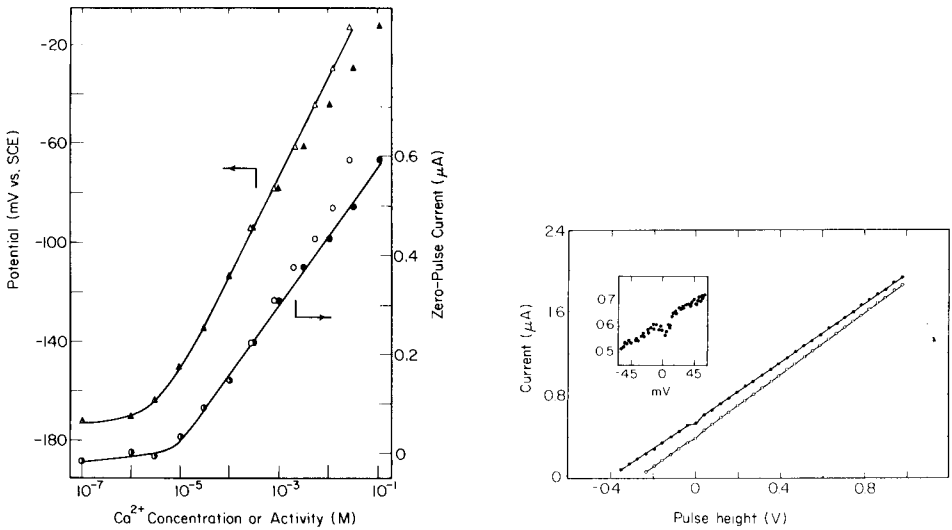

Fig. 5. Conductometric and potentiometric working curves. (△) Potential vs. Ca^{2+} activity, S_E = 1.868; (▲) potential vs. Ca^{2+} concentration, S_E = 2.110; (○) zero-pulse current vs. Ca^{2+} activity, S_E = 0.0179; (●) zero-pulse current vs. Ca^{2+} concentration, S_E = 0.0102.

Fig. 6. High resolution i/V curves: (●) 10^{-2} M Ca^{2+}; (○) 10^{-4} M Ca^{2+}. The inset is an expanded plot of the i/V curve for the 10^{-2} M Ca^{2+} solution in the zero applied voltage region.

deviations were observed for pure resistances, ruling out the possibility of their presence caused by electronic non-idealities in the instrument. An activity dependence in the region of zero applied voltage would account for the negative deviations, as well as their relative magnitudes. A larger deviation would be expected for the 10^{-2} M solution, where Ca^{2+} has an activity coefficient of only 0.53 (calculated from Eqn. 3), whereas the 10^{-4} M solution has a Ca^{2+} activity coefficient of 0.92.

Even higher resolution on the i/V curves was achieved by manual variation of the four least significant bits (non-computer accessible) of the DAC used to control the pulse height [9]. A 39-mV resolution i/V curve was generated at each of the 16 possible combinations of the four lowest bits; superposition of the curves yielded a 2.5-mV resolution i/V curve. The portion of the 2.5-mV resolution i/V curve obtained for the 10^{-2} M solution in the neighborhood of 0.00 V is shown in the inset of Fig. 6. It is evident that the transition from activity to concentration dependence occurs at around ±15 mV applied voltage.

These results indicate that use of the BICON technique with a calcium i.s.e. should allow direct measurement of activity coefficients. Assuming interferences are negligible, Eqn. (2) can be simplified to

$$i_{zp} = S_{zp} \log[Ca^{2+}] + C_{zp} \qquad (4)$$

where i_{zp} is the extrapolated zero-pulse current and S_{zp} and C_{zp} are the slope and intercept parameters from the working curve. Similarly, one can write

$$i^0_{zp} = S^0_{zp} \log A_{Ca^{2+}} + C^0_{zp} = S^0_{zp} \log \gamma[Ca^{2+}] + C^0_{zp} \quad (5)$$

where the superscript zero denotes values resulting from measurements taken at zero applied pulse height. From these two expressions, one can obtain

$$-\log \gamma = [(i_{zp} - C_{zp})/S_{zp}] - [(i^0_{zp} - C^0_{zp})/S^0_{zp}] \quad (6)$$

Once the C and S values for the electrode are evaluated, it is then a simple procedure to determine the activity coefficient. As an example, this procedure was applied to solutions containing between 10^{-1} M and 10^{-4} M $CaCl_2$ and with calcium chloride solutions of the same concentration also containing 0.1 M KCl. The i/V curves at 39 mV resolution were obtained for these solutions. (The pulse height DAC had been adjusted so that the output for a pulse of nominally 0 V differed by no more than 1 mV from 0 V.) A plot of i_{zp} vs. log $[Ca^{2+}]$ was used to obtain S_{zp} and C_{zp}; a plot of i^0_{zp} vs. $\log A_{Ca^{2+}}$ yielded S^0_{zp} and C^0_{zp} values. It was observed that S_{zp} and S^0_{zp} were essentially identical for these solutions; therefore Eqn. (5) simplifies to

$$-\log \gamma = [(i_{zp} - i^0_{zp}) - (C_{zp} - C^0_{zp})]/S_{zp} \quad (7)$$

Table 3 lists the activity coefficients experimentally obtained for these solutions along with theoretical values calculated with the extended Debye-Hückel Equation (Eqn. 3). Uncertainties in the experimentally determined values arise mainly from the one data point obtained at 0 V, i^0_{zp}. The absolute uncertainty is greatest for solutions having an activity coefficient near unity; for such solutions only a very small deflection is observed in the i/V curves near zero applied voltage. A sizeable deflection was obtained for the other solutions studied, and the agreement is quite good.

The dependence on concentration instead of activity is one of the more interesting features of the BICON method. In potentiometric methods, the potential is determined by an ion-exchange equilibrium between the membrane surface and the solution. Therefore, activity considerations are important, as ions in solution interact with each other according to Debye-Hückel

TABLE 3

Activity coefficients for Ca^{2+} obtained from high-resolution i/V curves and from the extended Debye-Hückel equation

Ca^{2+} conc. (M)	γ from Debye-Hückel	γ from i/V curves	Ca^{2+} conc. (M)	γ from Debye-Hückel	γ from i/V curves
10^{-4}	0.92	1.35 ± 0.31	10^{-4} [a]	0.37	0.34 ± 0.10
10^{-3}	0.79	0.92 ± 0.21	10^{-3} [a]	0.36	0.29 ± 0.08
10^{-2}	0.53	0.44 ± 0.10	10^{-2} [a]	0.34	0.29 ± 0.08
10^{-1}	0.25	0.29 ± 0.07	10^{-1} [a]	0.22	0.20 ± 0.06

[a] In 0.1 M KCl.

theory [23]. The conductometric method also indirectly measures the variation of the i.s.e. potential. However, this potential is not achieved by an equilibrium process; it is a potential generated by induced migration of calcium ions into the membrane. The data in Fig. 6 and the decrease in detection limit with increasing pulse width (Table 2) are clear indications that the applied voltage pulses do modify the i.s.e. response to some extent.

A rigorous microscopic explanation of the dependence on concentration has not been attempted as yet. However, it is reasonable to assume that calcium ions are forced to migrate into the membrane, to some extent, upon application of a voltage pulse. The interior of the membrane contains fixed counter-ion sites, and is shielded from the mobile ions in solution which give rise to activity consideration. Therefore, calcium ions bound to these fixed sites experience an environment that, at least to a first approximation, is independent of the ionic strength of the test solution. The amount of Ca^{2+} able to enter the membrane on application of a potential difference across the membrane is primarily determined by the conductivity of the membrane itself, which is independent of the test solution concentration, and by the amount of Ca^{2+} in the solution. The asymmetric coulombic and electrophoretic effects treated by the Onsager theory [24] would therefore be negligible as the solution resistance is much lower than that of the membrane.

The i/V curves shown in Fig. 6 have slopes at negative applied voltages that are about 4% less than those obtained at positive voltages. Apparently, resistance is affected somewhat by the direction of ionic travel, with induction of Ca^{2+} flow into the membrane at a positive applied voltage being somewhat more facile than forcing Ca^{2+} out of the membrane when the voltage across the membrane is negative. The small difference in resistance therefore allows for a net migration of Ca^{2+} into the membrane upon each bipolar voltage pulse.

Evaluation of interferences

Interfering ions appear to play the same role in the BICON method as they do in potentiometry; they shift the induced potential of the i.s.e. so that the i/V curve intercepts change. However, it has been observed that interferents can have additional effects on BICON measurements. Divalent cations have been observed to increase the membrane resistance [9], in addition to enhancing the potential. Table 4 contains the slopes of the i/V curves and intercepts obtained for 10^{-4} M Ca^{2+} solutions containing varying concentrations of lead(II) ions. The current axis intercept increases with increasing Pb^{2+} concentration, reflecting an increase in the i.s.e. potential as expected. However, a decrease in the slope of the i/V curve in the presence of lead was also noted. The i/V curves for the three lead solutions all have the same slope, within the 90% confidence interval shown. The increasing potential and constant slopes obtained for increasing Pb^{2+} concentration indicate that the potential and membrane resistance do not correlate with each other.

TABLE 4

Slopes and intercepts of i/V curves for varying lead(II) concentrations

Concentrations		Slope ± 90% confidence interval (μA/V)	Intercept ± 90% confidence interval (μA)
Ca^{2+} (M)	Pb^{2+} (M)		
10^{-4}	0	1.815 ± 0.032	0.353 ± 0.010
10^{-4}	10^{-3}	1.722 ± 0.035	0.538 ± 0.012
10^{-4}	10^{-2}	1.736 ± 0.032	0.571 ± 0.010
10^{-4}	10^{-1}	1.769 ± 0.036	0.595 ± 0.012

Lead ions, as well as other interfering species, are known to exhibit slow ion-exchange kinetics with the Ca^{2+} exchange sites in i.s.e. membranes [14, 25, 26]. Cations (and anions) reluctant to enter the membrane may migrate into the solution layer immediately adjacent to the membrane upon application of an electric field, replacing the Ca^{2+} that has left this layer to migrate into the membrane. The time scale for the bipolar voltage pulses is too short to allow diffusion to replace the lost Ca^{2+}. Also, radiotracer studies [27] have shown that strongly-bound interferents can block Ca^{2+} entry into the membrane, and would be expected to increase the membrane resistance if their mobility within the membrane was less than that of Ca^{2+}.

Selectivity coefficients for twelve interfering species are given in Table 5. Current axis intercepts were compared for 10^{-4} M Ca^{2+} and 10^{-4} M Ca^{2+}/I^{y+} solutions. Equations (1) and (2) were used to calculate the selectivity coefficients for the potentiometric and conductometric methods, respectively. The value for S_{zp} was 0.109 μA/decade in the solutions containing only Ca^{2+} and interferent, and 0.066 μA/decade in the solutions also containing 0.1 M KCl. Once again, the magnitude of the coefficients for monovalent ions are deceivingly high. A coefficient of 10 would have been obtained for 10^{-1} M K^+, Na^+, and NH_4^+ if the i.s.e. responded equally to Ca^{2+} and those monovalent ions. Similarly, a coefficient of 16 000 would have been obtained for equal H^+ and Ca^{2+} responses.

A negative selectivity coefficient was obtained for Cu^{2+} in the conductometric mode. Copper(II) enhances the i.s.e. potential, as do the other interfering ions, but the i/V curve obtained for the Cu^{2+} solution lies below the i/V curve obtained for the 10^{-4} M Ca^{2+} standard at applied potentials above —40 mV. Therefore, the current axis intercept is actually reduced in the presence of Cu^{2+}. The other interferents yielded i/V curves which crossed the 10^{-4} M Ca^{2+} curve at applied potentials above 0 V. No interference was observed at this "crossing potential," which is determined by both the identity of the interferent and its concentration. This "crossing potential" could conceivably be used to reduce significantly interferences from a particular species, if one knew the identity of that species and its approximate concentration.

TABLE 5

Selectivity coefficients for potentiometric and conductometric methods (All solutions contain 10^{-4} M Ca^{2+})

Interfering species (M)	Potentiometric selectivity coefficients[a]	Conductometric selectivity coefficients[a]	Conductometric selectivity coefficients[b]	Electrode resistance (kΩ)
None (10^{-4} M Ca^{2+} only)	—	—	—	480
K^+ (10^{-1})	1.7×10^{-4}	2.1×10^{-4}	1.3×10^{-4}	489
Na^+ (10^{-1})	0.014	0.040	0.011	492
NH_4^+ (10^{-1})	0.048	0.080	1.6×10^{-3}	485
Ni^{2+} (10^{-2})	8.6×10^{-4}	4.3×10^{-4}	1.1×10^{-3}	492
Ba^{2+} (10^{-2})	1.6×10^{-3}	0.054	0.011	499
Mg^{2+} (10^{-2})	4.6×10^{-3}	8.1×10^{-3}	0.011	494
Sr^{2+} (10^{-2})	9.3×10^{-3}	8.1×10^{-3}	0.036	506
Cu^{2+} (10^{-3})	0.042	−0.085	−0.029	505
Fe^{2+} (10^{-3})	0.088	0.47	0.016	495
Pb^{2+} (10^{-3})	0.77	0.29	0.40	502
Zn^{2+} (10^{-3})	0.92	0.61	0.14	500
H^+ (pH 4.2)	12000	3600	26000	470

[a]All solutions 0.1 M in KCl. [b]No KCl added.

If the potentiometric coefficients and either set of conductometric coefficients are compared, the overall selectivity appears to be about the same. There was some apprehension earlier [9] that the voltage pulses may induce migration of weakly adsorbed interferents into the membrane. Breakdown of selectivity has been observed under non-zero current conditions, both experimentally [3, 4] and by digital simulation [28], but very high electric field values were used, and the voltage was applied over longer time periods than used in BICON. The decrease in working curve slope upon addition of 0.1 M KCl as an ionic strength adjustor (Table 1) was thought to imply selectivity problems caused by ionic strength variation. However, Table 5 shows that overall selectivity is about the same, regardless of the presence of an ionic strength adjustor.

Electrode resistances, obtained by subtracting solution resistance from the inverse of the i/V curve slope, are also reported in Table 5 for the solutions not containing potassium chloride. Interfering species are shown to increase the membrane resistance, as previously noted. Divalent cations appear to have a slightly greater effect on membrane resistance than monovalent ions. Monovalent ions have higher mobilities than divalent ions, and the extremely mobile hydrogen ion actually decreases the electrode resistance.

Response time

The rapid response of the calcium i.s.e. obtained by conductometric monitoring has been previously noted [9]. In subsequent work, response time was

found to depend on the amplitude of the applied voltage pulse. Response times were evaluated by abruptly increasing the Ca^{2+} concentration in the cell from 10^{-4} to 10^{-3} M by addition of a small volume of concentrated calcium solution to the stirred solution in the cell. Conductometric response time curves were obtained by monitoring the current measured for repeated applications of bipolar voltage pulses of a selected amplitude.

Figure 7 shows the times required for the signal to reach 95% of its steady-state value at different pulse amplitudes. The time required for the solutions to mix completely (with a magnetic stirrer) and the potentiometric response time (determined by continuous potentiometric monitoring under the same experimental conditions) are also indicated by the shaded regions. The solution mixing time was determined by continuously measuring the solution resistance between two stainless steel electrodes, which can be assumed to respond instantaneously to changes in solution resistance.

Use of a 0-V pulse (which is equivalent to shorting the electrodes together through the virtual ground of the amplifier) to measure the current yielded the same response time as the potentiometric method. It is evident from Fig. 1 and the related discussion that the current measured at zero volts applied is due to the i.s.e. potential being short-circuited. Therefore direct measurement of this "short-circuit" current would be expected to yield the same response time as the potentiometric method. In Fig. 7, it is also evident that increasing the pulse amplitude decreases the response time, until the response time becomes limited by the solution mixing time at applied potentials of >2 V. Faster response at higher applied voltages is expected if the solutions could be mixed more rapidly.

Potentiometric response times of plastic-membrane electrodes are thought to be controlled by diffusion of ions through a stagnant layer of solution covering the i.s.e. surface [29]. Voltage pulses could be expected to induce ionic migration through these layers, and thus allow achievement of steady-state i.s.e. potentials in much shorter time periods.

Determination of calcium in real samples

In order to demonstrate the analytical capabilities of conductometric monitoring of the calcium electrode, some real samples were assayed for free

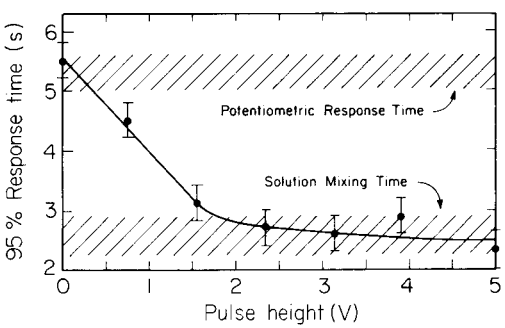

Fig. 7. Conductometric response times at various pulse heights.

(uncomplexed) calcium by using BICON and potentiometry. A direct and simple approach was used with no attempt to eliminate or compensate for matrix problems. Aqueous standards were used to prepare calibration curves over the 3×10^{-4} M—1×10^{-1} M range. The measurement of the potential or the zero-pulse current for the sample was used to obtain the Ca^{2+} concentration from the corresponding calibration curve. All samples and standards were made 0.1 M in KCl to maintain constant ionic strength for potentiometry. Drinking water was run directly. Milk was diluted 1:10. A vitamin pill was dissolved and the solution diluted to 200 ml. The results obtained with conductometric and potentiometric monitoring, respectively, were: drinking water, 19 ppm, 20 ppm; milk, 1100 ppm, 570 ppm; vitamin pill, 1.6%, 2.4%. The values show reasonable agreement to each other and to literature or manufacturer's values, considering the simple technique used.

COMPARISON OF THE BICON METHOD TO OTHER NON-ZERO CURRENT METHODS

In the introductory section, it was mentioned that non-zero current methods have been used to study i.s.e. physical properties and behavior. These methods, based on application of both d.c. and a.c. voltages to the i.s.e., will be compared with the BICON method in this section.

D.c. voltage measurements

Bulk conductivity measurements on liquid-membrane electrodes have yielded useful information about bulk resistance and capacitance, ion transport, ion pairing, and dielectric constants [3—5]. Buck and Krull [17] obtained linear i/V curves for the glass electrode using d.c. voltage steps. However, the d.c. voltage pulses used had to be applied for 2—5 min to charge substantially all capacitances in the cell and to achieve current values reflecting only the resistance.

Figure 8 is a simplified analog circuit of an ion-selective membrane placed between two metal electrodes, with solution contacts on both sides of the membrane. Capacitance C_s and C_s' are the double-layer capacitances at the metal/solution interfaces, Z_f and Z_f' are the corresponding faradaic impedances, and R_Ω and R_Ω' are the solution resistances. The membrane/solution interfaces are modeled as parallel double-layer capacitance/charge-transfer resistance (C_{dl}'/R_θ' and C_{dl}/R_θ) combinations, while the bulk membrane is modeled as a geometric capacitance/bulk resistance combination (C_g/R_∞) [7, 30, 31]. This model does not account for the non-zero i/V curve intercepts; and the membrane capacitances are thought to be of a more diffuse nature [6, 17] than the discrete components shown. Warburg impedances are also included in some models to simulate ion transport through the bulk membrane, solution, and interfaces [6, 31, 32].

A single d.c. voltage step or constant voltage method [3—5, 33] will reflect resistive currents only when all of the capacitances are completely

charged, and Z_f and Z'_f are small, as they would be in the case of the reversible Ag/AgCl couple normally used in d.c. and a.c. methods. The BICON method requires only that the parallel capacitances (C'_{dl}, C_g, C_{dl}) be completely charged; the method can decouple the resistive currents from series capacitance (C_s, C'_s) charging currents. Therefore, bipolar voltage pulses need only be long enough to charge the parallel capacitances, as shown here in the pulse width study. It is not necessary (actually, not even desirable) to charge the series capacitances significantly [12], and faradaic reactions can thus be avoided. The faster measurement time also makes observation of transient phenomena possible.

A.c. impedance measurements

Alternating current impedance measurements are typically used to study an electrochemical system at steady state. A sinusoidal potential of small amplitude is used to perturb the system, and the resulting current signal yields information about the electrochemical processes taking place. A signal of small magnitude assures linearity of the current response from the particular electrode process.

The a.c. impedance method has been used to characterize glass [6, 17], fluoride [7, 30, 31], liquid membrane [8], and silver halide [34] electrodes. Complex plane impedance plots [35] are obtained for an i.s.e./reference electrode combination in solution, as the angular frequency (ω) of the excitation signal is varied. Figure 9 shows a generalized sketch of such a plot. The high frequency semicircle (I) is due to the small RC time constant of the $R_\infty C_g$ combination of Fig. 8. The lowest frequency depressed semicircle (II) is due to the $R_\theta C_{dl}$ interfacial process. Lowering of this semicircle has been attributed to the diffuse nature of the capacitances [6, 17] and to nonequivalence of the two interfaces caused by differing concentrations of ionic species in the two contacting solutions [7, 30, 31]. A finite Warburg impedance arc (III) is sometimes observed at very low frequencies corresponding to transport of ions through solutions and/or membrane.

The various RC time constants obtained relate to the transient response of the i.s.e. The $R_\infty C_g$ term applies to the propagation of potential changes

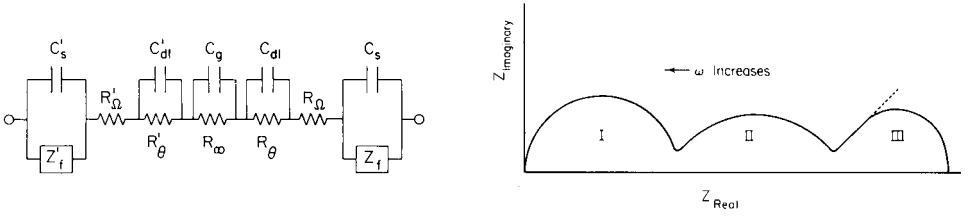

Fig. 8. Analog circuit for an ion-selective membrane between two metal electrodes with solution contacts. The parameters are defined in the text.

Fig. 9. Generalized complex plane impedance plot for an i.s.e.

across the bulk membrane, which is very fast. The $R_\theta C_{dl}$ term reflects attainment of equilibrium at the i.s.e./solution interface, and its magnitude is highly dependent on the nature of the interface. The Warburg quantity reflects adjustment of concentration profiles in the membrane and membrane/solution interfacial area, and is the slowest process. However, the concentration profiles within the membrane usually change by such a small amount that the Warburg process contributes negligibly to the overall potential change [36]. Therefore, the $R_\theta C_{dl}$ process usually controls the response time [6].

It has been observed that variation of test solution composition primarily changes the potential across the membrane, perhaps accompanied by a relatively small change in the physical properties of the membrane. This potential is a d.c. signal, and is usually biased out in a.c. methods by use of a d.c. potentiometer and null detector, as a non-zero i/V curve intercept would complicate the data treatment. Some species in solution may also change the surface-layer resistance of the i.s.e. Surface-layer effects can be observable by a.c. impedance [7, 30, 31], but often cannot be precisely quantified because they appear at low frequencies (typically 1—10 Hz). Changes in both i.s.e. potential and surface-layer resistance can be studied by BICON, because any d.c. offsets can be decoupled from resistive currents by construction of i/V curves. In addition, pulses contain sine waves of all frequencies, so that processes only observable with low frequency sine waves can be observed with pulses and measured more accurately. A successful quantitative method requires accurate measurement of processes related to test solution composition, so that pulse methods would appear to be superior to sine wave methods in this regard.

Use of voltage pulses prohibits resolution of the different processes taking place within the membrane and at the interface. Therefore, only total cell resistance can be determined. Solution resistance can be independently determined and subtracted, but the interfacial and bulk membrane resistances cannot be resolved. Also, there is no convenient way to measure capacitance values. Therefore sine wave methods would be preferable to pulse methods for study of electrode processes and modeling their behavior.

Conclusion

Non-zero current measurements on the calcium i.s.e. by the BICON method yield selectivities and sensitivities comparable to those obtained in the standard potentiometric method. Construction of i/V curves yields information about the electrode potential and resistance, and demonstrates that the concentration-dependent response is due to the application of a non-zero voltage pulse. One of the main advantages of the conductometric method is the short response time which also is shown to be due to the voltage pulses. Another advantage is the elimination of the need for a real reference electrode.

Future papers in this series will deal with bipolar pulse conductometric monitoring of the fluoride electrode, with measurements in flowing streams

using calcium and fluoride i.s.e.'s, with the role of the electrochemical potential of the counter electrode, and with interferences from electroactive species.

The authors thank Richard F. Geiger, Jr. for design and construction of the computer expansion board, and Joy Walker for the design and construction of the recorder interface board. This research was supported in part by the National Science Foundation (CHE78-01614 and CHE81-08816).

REFERENCES

1 R. P. Buck, Anal. Chem., 50 (1978) 17R.
2 G. H. Fricke, Anal. Chem., 52 (1980) 259R.
3 N. D. van Mau and C. Gavach, J. Electroanal. Chem., 97 (1979) 163.
4 N. D. van Mau and C. Gavach, J. Electroanal. Chem., 97 (1979) 171.
5 D. E. Mathis and R. P. Buck, J. Membr. Sci., 4 (1979) 379.
6 J. R. Sandifer and R. P. Buck, J. Electroanal. Chem., 56 (1974) 385.
7 J. Mertens, P. van den Winkel and J. Vereecken, Bioelectrochem. Bioenerg., 5 (1978) 699.
8 D. E. Mathis, F. S. Stover and R. P. Buck, J. Membr. Sci., 5 (1979) 395.
9 C. R. Powley, R. F. Geiger and T. A. Nieman, Anal. Chem., 52 (1980) 705.
10 D. E. Johnson and C. G. Enke, Anal. Chem., 42 (1970) 329.
11 P. H. Daum and D. F. Nelson, Anal. Chem., 45 (1973) 463.
12 K. J. Caserta, F. J. Holler, S. R. Crouch and C. G. Enke, Anal. Chem., 50 (1978) 1534.
13 R. W. Cattrall and H. Freiser, Anal. Chem., 43 (1971) 1905.
14 G. J. Moody, R. B. Oke and J. D. R. Thomas, Analyst (London), 95 (1970) 910.
15 G. H. Griffiths, G. J. Moody and J. D. R. Thomas, Analyst (London), 97 (1972) 420.
16 D. Ammann, M. Guggi, E. Pretsch and W. Simon, Anal. Lett., 8 (1975) 709.
17 R. P. Buck and I. Krull, J. Electroanal. Chem., 18 (1968) 387.
18 U. Oesch and W. Simon, Anal. Chem., 52 (1980) 692.
19 R. W. Cattrall, D. M. Drew and I. C. Hamilton, Anal. Chim. Acta, 76 (1975) 269.
20 M. D. Smith, M. A. Genshaw and J. Greyson, Anal. Chem., 45 (1973) 1783.
21 R. P. Buck, Anal. Chem., 48 (1976) 23R.
22 G. G. Guilbault, Ion-Selective Electrode Rev., 1 (1979) 139.
23 W. E. Harris and H. A. Laitinen, Chemical Analysis, McGraw-Hill, New York, 1975, Ch. 2.
24 D. A. MacInnes, The Principles of Electrochemistry, Dover Publications, New York, 1961, Ch. 18.
25 G. A. Rechnitz and Z. F. Lin, Anal. Chem., 40 (1968) 696.
26 B. Fleet, T. H. Ryan and M. J. D. Brand, Anal. Chem., 46 (1974) 12.
27 A. Craggs, G. J. Moody, J. D. R. Thomas and A. Willcox, Talanta, 23 (1976) 799.
28 F. S. Stover and R. P. Buck, J. Electroanal. Chem., 107 (1980) 165.
29 W. E. Morf, E. Lindner and W. Simon, Anal. Chem., 47 (1975) 1596.
30 J. Mertens and P. van den Winkel, J. Electroanal. Chem., 85 (1977) 277.
31 P. van den Winkel, J. Mertens, F. Boel and J. Vereecken, J. Electrochem. Soc., 124 (1977) 1338.
32 R. P. Buck, J. Electroanal. Chem., 18 (1968) 381.
33 G. D. Carmack and H. Freiser, Anal. Chem., 47 (1975) 2249.
34 R. K. Rhodes and R. P. Buck, Anal. Chim. Acta, 110 (1979) 185; 113 (1980) 55, 67.
35 M. Sluyters-Rehbach and J. H. Sluyters, Electroanal. Chem., 4 (1970) 1.
36 A. Shatkay, Anal. Chem., 48 (1976) 1039.

Analytica Chimica Acta, 139 (1982) 83—96
Elsevier Scientific Publishing Company, Amsterdam — Printed in The Netherlands

BIPOLAR PULSE CONDUCTOMETRIC MONITORING OF ION-SELECTIVE ELECTRODES
Part 2. Studies with the Fluoride-Selective Electrode

CHARLES R. POWLEY and TIMOTHY A. NIEMAN*
School of Chemical Sciences, University of Illinois, Urbana, IL 61801 (U.S.A.)
(Received 8th December 1981)

SUMMARY

Bipolar pulse conductometric monitoring of the fluoride ion-selective electrode (i.s.e.) is evaluated. It is shown that fluoride ion, in addition to affecting the electrode potential, also can have two effects upon the total resistance of the electrode. Fluoride ion can enter a gel layer on the surface of the doped lanthanum fluoride crystal; solution concentrations as low as 10^{-9} M fluoride can significantly decrease the gel resistance. Fluoride concentrations in the potentiometric working range of the i.s.e. can also increase the electrode resistance. The conductometric detection limit is 2—4 decades lower than the potentiometric detection limit. However, because of the resistance factors, the conductometric curve is not monotonic, and shows a maximum at a fluoride concentration in the vicinity of the potentiometric detection limit. The two resistive changes possible have different time dependences; the decrease of the gel layer resistance becomes predominant at long measurement times, while the increase of the crystal resistance predominates within the first minute of exposure to solution. Hydroxide is shown to affect the i.s.e. potential and lower the gel layer resistance. Response time to changes in fluoride concentration are less than 15 s and do not show the strong concentration dependence observed potentiometrically. The i.s.e. is shown to have a slightly lower resistance to fluoride entering the crystal than to fluoride leaving it. The small resistive dependence on direction of ion migration may indicate a directional dependence of activation energy for ion transport across the membrane solution interfaces.

The fluoride ion-selective electrode, based on a doped lanthanum fluoride crystal [1] is one of the best ion-selective electrodes yet developed. The mechanism of charge transport within the pure lanthanum fluoride crystal has been well studied and has been shown to consist of migration of fluoride ions facilitated by the presence of intrinsic Frenkel defects ("holes") in the crystal lattice [2]. Conductivity is enhanced by doping the crystal with europium(II) to create more vacancies than would be present in the pure crystal [1].

Mechanistic studies of the fluoride ion-selective electrode (i.s.e.) have been done with both potentiometric [3—5] and non-zero current methods. Brand and Rechnitz [6] reported the first a.c. impedance results using the fluoride i.s.e. and postulated the existence of a film on the surface of the crystal. Cammann and Rechnitz [7] later used exchange current measure-

ments with the galvanostatic pulse method to show that OH^- interacts with this film. Further a.c. impedance studies [8, 9] yielded a complete equivalent circuit for the electrode and showed that fluoride can significantly lower the resistance of the surface film.

Recently, results have been reported concerning use of bipolar pulse conductance [10] to monitor a calcium i.s.e. [11]. The measured current was shown to be linearly dependent on the logarithm of the Ca^{2+} concentration rather than the logarithm of the Ca^{2+} activity. Response time was decreased significantly, and the need for a real reference electrode was eliminated. The first paper in this series [12] showed that the measured current is directly proportional to the amplitude of the applied voltage pulse. The linear current—voltage (i/V) curves obtained have slopes equal to the reciprocal of the sum of the electrode resistance and the solution resistance. The electrode resistance was shown to be independent of Ca^{2+} concentration. However, the current axis intercepts, or "zero-pulse currents" were shown to result from the short-circuiting of the i.s.e. potentials, to yield a log-linear dependence of total current upon Ca^{2+} activity. The concentration dependence was shown to result from application of a non-zero voltage pulse.

This paper reports results obtained by bipolar pulse conductometric monitoring of a fluoride i.s.e. It will be shown that electrode resistance is not independent of fluoride concentration, and that fluoride plays two distinct roles in determining the total electrode resistance. One of the processes, the lowering of the surface film resistance, is observable at fluoride concentrations as low as 10^{-9} M. The other process involves reduction of the number of charge carrier holes in the crystal, and is observed in the potentiometric working range of the i.s.e. Conductometric monitoring also appears to eliminate the response time dependence on concentration observed in potentiometric measurements.

EXPERIMENTAL

Equipment and reagents

Conductance instrument. The bipolar pulse conductance (BICON) technique has been described [10, 13, 14], as has the application of bipolar pulse conductometric monitoring of ion-selective electrodes [10, 11]. The BICON instrument used in this work [11, 12] operates in the voltage pulse mode.

Electrodes. The fluoride i.s.e. used was obtained commercially from Orion Research Inc. (model 94-09). It has been shown that a poised reference electrode is not necessary for conductometric measurements with i.s.e.'s, and that a simple metallic contact to the solution to complete the circuit is sufficient [11]. The counter electrode used here was a stainless steel rod 1.5-in long and 1/16-in diameter, placed about 5 mm from the crystal surface.

Reagents

Studies were conducted using two different total ionic strength adjustment buffers (TISAB); both were prepared as recommended by Orion Research. TISAB IV (containing hydrochloric acid, sodium tartrate, and tris(hydroxymethyl)amino methane), buffered at pH 8.4 was used for most of the experiments, and TISAB II (containing acetic acid, sodium acetate, sodium chloride, and cyclohexylenedinitrilotetraacetic acid), buffered at pH 5.4, was used to evaluate the effect of pH on the working curves. All test solutions contained 10% (v/v) of the appropriate TISAB, and were prepared from distilled—deionized water, and reagent-grade chemicals. Solutions were transferred to polyethylene labware immediately after being prepared.

Measurement techniques

Conductance measurements. Current measurements were made using the BICON technique. For most studies, a standard addition method was used to obtain conductometric responses to fluoride and other anions. The electrodes were immersed in a stirred solution and small volumes of concentrated solutions were added to produce the final desired concentrations. Bipolar voltage pulses 100 μs in duration and 5 V in amplitude were repeatedly applied across the cell. Current values were measured at the end of the second pulse and averaged in groups of 2048. The analog equivalent of the average was then displayed on a strip-chart recorder. This standard addition method was employed to discriminate against drifting in the i.s.e. potential, which was severe at low fluoride concentrations (below 10^{-5} M) in both the conductometric and potentiometric methods. The electrode responded to changes in test solution concentration in less than 15 s, and yielded sharp deflections from the slowly drifting baseline obtained for the initial solution.

A modification to this standard addition method involved obtaining i/V curves before and after each standard addition, as described in the Results and Discussion section. The pulse amplitude, measured from the foot of the pulse (instrumental ground) to its plateau, ranged from 0.00 to 5.00 V. Ten data sets, each representing the average of 16 individual measurements, were taken. Enough current was added at each pulse height to offset about 90% of the cell current, allowing the sensitivity of the measurement circuit to be increased to obtained higher resolution [14]. Current values at 12 pulse heights were collected in 6 s through use of computer control to increment both pulse height and offset current. All conductance measurements were made on solutions stirred magnetically.

Potentiometric measurements. Potentiometric measurements were made with an Orion Model 701A pH meter operated in the millivolt mode. A single-junction Ag/AgCl electrode (Corning Model 476029) was used as the reference electrode. All solutions were stirred magnetically during measurements.

RESULTS AND DISCUSSION

Working curves

Figure 1 shows the conductometric working curves (at pH 5.4 and pH 8.4) obtained by continuous application of 5-V bipolar voltage pulses across the fluoride electrode. The fluoride concentration in the test solution was increased by decade steps through addition of aliquots of sodium fluoride standards to the stirred solution. All solutions were buffered at pH 8.4 through use of TISAB IV or at pH 5.4 through use of TISAB II. The deviations from the initial "baseline" value created by the reagent blank are plotted as a function of the logarithm of the final fluoride concentration; magnitudes of these deviations 15 s and 60 s after addition are shown. Potentiometric working curves for the same experiments are shown for comparison, where potentials were read 60 s after addition of the appropriate standard.

Two points concerning the conductometric working curves can be noted immediately. First, the conductometric curves show deviations from the blank even at very low fluoride concentrations (down to the nanomolar region). Second, the conductometric working curves are not monotonic,

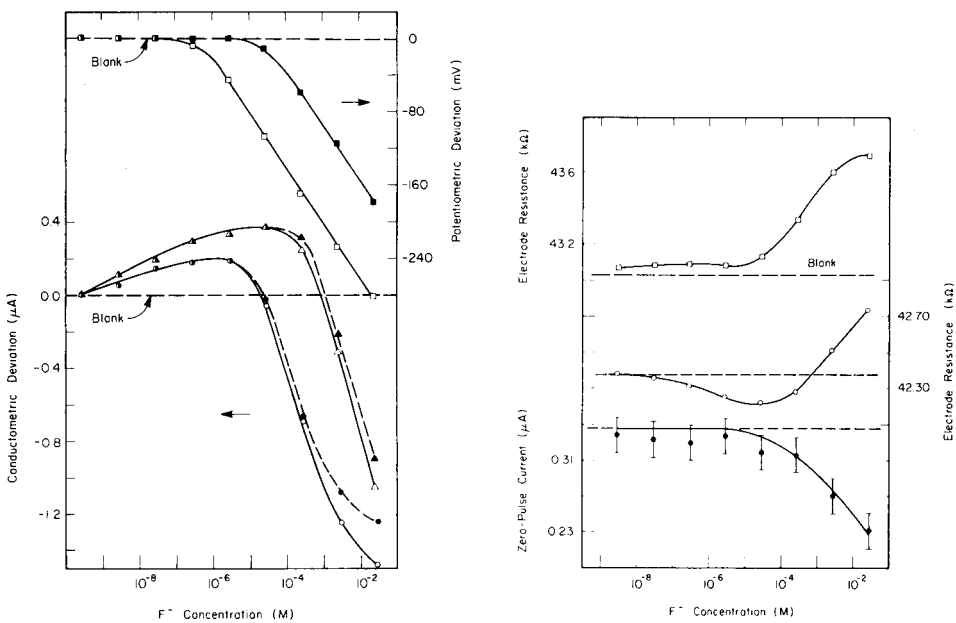

Fig. 1. Conductometric and potentiometric working curves; repeated standard additions and continuous monitoring with 5-V pulses. Potentiometric working curves: (□) pH 5.4; (■) pH 8.4; response 60 s after addition of standard. Conductometric working curves: (○) pH 5.4; (△) pH 8.4; response 15 s after addition of standard; the dashed lines (●, ▲) are conductometric responses 60 s after addition of standard.

Fig. 2. Electrode resistance and zero-pulse current as a function of fluoride concentration: (□) electrode resistance at pH 5.4; (○) electrode resistance at pH 8.4; (●) zero-pulse current at pH 8.4.

but pass through a maximum at a fluoride concentration in the vicinity of the potentiometric detection limit. The potentiometric detection limit is shifted to a lower fluoride concentration at pH 5.4 because of reduction of the hydroxide interference [1]. The maximum in the conductometric working curve also shifts to a lower fluoride concentration at pH 5.4, but the conductometric detection limit remains constant at about 10^{-9} M.

At fluoride concentrations above the potentiometric detection limit, the conductometric working curve consists of current values showing negative deviation from the blank. The value of the negative deviation resulting from each standard addition reached a maximum after 15 s (mixing time was of the order of 1 s), and then the current values slowly became more positive 30—60 s after the addition. The rate of this positive drift increased slightly with increasing fluoride concentration. This positive drift at higher fluoride concentrations was more pronounced at pH 5.4 than pH 8.4. As a result, the "long time" conductometric working curve at pH 5.4 has a deviation from linearity at the highest fluoride concentrations.

Similar conductometric working curves were obtained when individual fluoride standard solutions were measured directly. However, the drift at low concentrations raised the detection limit to about 10^{-8} M, and measurement of i.s.e. exposure time to solution was less precise. Drift at low fluoride concentrations has been noted previously in potentiometric monitoring [3], and was attributed to slow equilibration between free fluoride in the crystal and the solution. Drift was comparable with BICON and potentiometric monitoring, although a slight d.c. offset in the BICON instrument could contribute to the effect by inducing a net migration of fluoride into or out of the electrode.

It is of practical analytical importance that the conductometric detection limit is some two to four decades lower than the potentiometric detection limit. However, because the conductometric working curve is non-monotonic, an understanding of the reason for the curvature is essential for application of the technique. The anomalous appearance of the conductometric working curves suggests that two or more processes may be taking place as the fluoride concentration is increased. It was previously noted [12] that both electrode potential and resistance are reflected in this conductometric method, and that one can resolve these two parameters by obtaining i/V curves.

Current—voltage curves

Current—voltage curves were obtained after each addition of a fluoride standard, and were linear over the applied potential range 0—5 V. The inverse of the slope is equal to the total cell resistance, which is composed of the electrode and solution resistances. However, solution resistance can be assumed to be negligible for these experiments, because of the TISAB. The current axis intercept of the i/V curve, or "zero-pulse current" is generated by the short-circuited electrode potential [12]. Figure 2 shows the electrode resistances and zero-pulse currents for i/V curves obtained at pH 8.4, as well as the electrode resistance obtained at pH 5.4.

The zero-pulse current trend shows the same dependence upon electrode potential that was observed with the calcium i.s.e. [12]. The error bars shown in Fig. 2 represent the 90% confidence intervals calculated from the standard deviations of the i/V curve intercepts. The 90% confidence intervals calculated for the slopes of the i/V curves yield error bars smaller than the size of the data points shown on the electrode resistance plots.

The electrode resistance plots show some unexpected behavior. At pH 8.4, the resistance decreases with increasing fluoride concentration, until it reaches a minimum near the potentiometric detection limit. The resistance then increases with higher fluoride concentration. The combination of the resistance increase and the increasingly negative zero-pulse current yields the negative trends in the working curves shown in Fig. 1, while the resistance decrease at low fluoride concentration yields the positive trend. The decrease in resistance at pH 5.4 and low fluoride concentration is not observed in i/V curves obtained immediately after addition, but does appear to some extent when continuous pulsing is used, as shown in Fig. 1.

Other authors using a.c. impedance [8, 9] and exchange current measurements [7] observed a lowering of the surface layer resistance of the fluoride i.s.e. with increasing fluoride concentration. The existence of a film on the lanthanum fluoride crystal is well accepted, and is thought to have the chemical formula $LaF_x\ (OH)_{3-x}$ $(0 \leqslant x \leqslant 3)$ [3, 6, 15]. An increase in fluoride concentration of the test solution would then be expected to shift the equilibrium

$$LaF_x\ (OH)_{3-x} + yF^- \rightleftharpoons LaF_{x+y}(OH)_{3-x-y} + yOH^-$$

to the right and result in a thinner, less resistant gel layer [3].

Lowering of the gel resistance would account for the decrease in total resistance observed at low fluoride concentrations. The increasing resistance trend in the potentiometric working range is probably due to fluoride from solution interacting with the crystal itself. The doped lanthanum fluoride crystal can support a current by migration of mobile fluoride ions through vacancies in the lattice structure [2]. The behavior of this ionic semiconductor is therefore analogous to that of a p-type electronic semiconductor. This analogy will be used to propose an explanation for the observed increase in resistance.

Raising or lowering of conduction band and valence band (VB) potential energies within an electronic semiconductor, caused by the presence of a space charge, has been described for semiconductor electrodes in solution [16] and metal/semiconductor interfaces [17, 18]. The potential energy curves for a p-type semiconductor that has drawn negative charge from a contacting metal or solution are shown in Fig. 3. The Fermi level, also shown, is that level to which a VB electron must be promoted by thermal energy to have a 50% probability of a charge-carrying hole existing in the VB. The VB energy is pushed farther below the Fermi level by the space charge at the interface. Therefore, the resistance of the surface layer will

increase, as fewer charge-carrying vacancies can be created. Mott and Gurney [17] give the following relationship between the distance x (Fig. 3) and the change in VB potential $\Delta\phi_x$

$$\Delta\phi_x = 2\pi\ (Ne)ex^2/\kappa \tag{1}$$

where e is the electrostatic unit, Ne is the space charge developed, and κ is the dielectric constant of the semiconductor. This theory will now be extended to treatment of the LaF_3 p-type ionic semiconductor. Consideration of fluoride partitioning through the gel layer into the lanthanum fluoride crystal would involve the following equilibria

$$F^-_{(aq)} \overset{K_1}{\rightleftharpoons} F^-_{(gel)};\ F^-_{(gel)} \overset{K_2}{\rightleftharpoons} F^-_{(crystal)}$$

Therefore, the space charge developed would be given by $Ne = K_1 K_2 N_{F^-} e$ where N_{F^-} is the number of fluoride ions per unit volume in solution.

The conductivity at distance x, θ_x, can be expressed as

$$\theta_x = C \exp(-\Delta\phi_x/kT) \tag{2}$$

where C is a constant. Therefore, because the resistance of the increment dx, dR_x, is $dR_x = (1/\theta_x)\,(dx/A)$, where A is the cross-sectional area of the crystal, one obtains by substitution of Eqn. (1) and these expressions for Ne and dR_x into Eqn. (2)

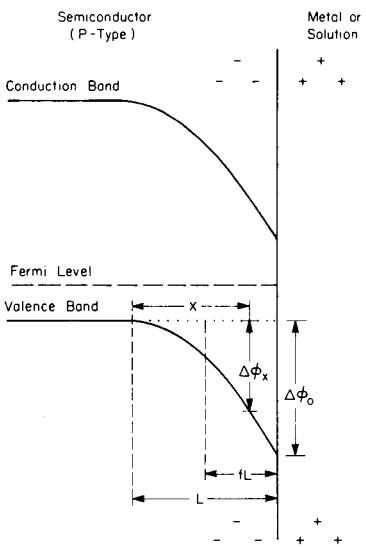

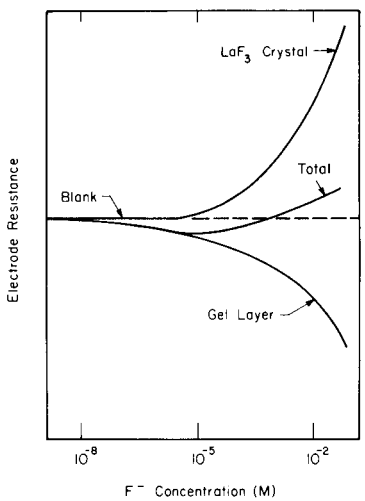

Fig. 3. Lowering of conduction and valence band potentials in a p-type semiconductor by a space charge.

Fig. 4. Combination of gel layer resistance and crystal resistance to yield the total resistance working curves observed with BICON. The situation sketched would be relevant at high pH.

$$dR_x = (dx C/A) \exp [2\pi K_1 K_2 e^2 x^2 N_{F^-}/\kappa kT] \quad (3)$$

The total resistance of the Debye thickness L is given by

$$R = (C/A) \int_0^L \exp [2\pi K_1 K_2 e^2 x^2 N_{F^-}/\kappa kT] \, d\chi \quad (4)$$

Integrals of the form $\int e^{ax^2} dx$ cannot be solved, except by numerical methods. A numerical solution would not be very useful, as accurate values are not available for all of the constants in Eqn. (4). However, an approximate treatment of the model described above will predict the behavior of the R vs. log $[F^-]$ plot.

Instead of considering an infinite number of differential elements, as was done above, let us consider one element of thickness fL, as shown in Fig. 3, in which the VB potential has been lowered by an amount $\Delta\phi_o$. The expression

$$\Delta\phi_o = 2\pi (Ne) eL^2/\kappa$$

as given by Mott and Gurney [17] would then be useful. The resistance of the element fL is given by

$$R_{fL} = (fLC/A) \exp (\Delta\phi_o/kT) \quad (5)$$

and substitution of the expressions for Ne and $\Delta\phi_o$ above into Eqn. (5) yields

$$R_{fL} = (fLC/A) \exp [2\pi K_1 K_2 e^2 N_{F^-} L^2/\kappa] \quad (6)$$

Therefore, a plot of crystal resistance vs. log $[F^-]$ is expected to show some positive curvature, as sketched in Fig. 4. The amount of curvature depends on the magnitude of the constants in the exponential term.

As indicated above, resistance of the gel layer is decreased by fluoride, this effect being especially pronounced at low pH, long measurement times, and/or high fluoride concentrations. Gel resistance is inversely proportional to $[F^-]^y$, where $0 < y < 1$ [7]. The dependence of gel layer resistance on log $[F^-]$ is also sketched in Fig. 4. Superposition of the two effects then yields the total electrode resistance as a function of log $[F^-]$, which apparently is pseudo log-linear in the potentiometric working range at high pH and short measurement times. Low pH values and longer measurement times allow the gel resistance component to become more dominant, and deviations from the log-linear behavior are observed, as in Fig. 1.

Low pH values of the test solution result in a thinner gel layer [4], and low fluoride concentrations did not appear to have any significant effects upon i/V curves taken 15 s after the standard addition. Continuous pulsing yielded more pronounced decreases in electrode resistance at low pH (Fig. 1), probably because of a more rapid accumulation of charge carriers in the gel layer. Current–voltage curves taken 180 s after each standard addition showed a monotonically decreasing trend in electrode resistance with increasing fluoride concentration over the 10^{-9}–10^{-1} M range, at both pH values used. Apparently, the gel resistance component had enough time to become predominant over the crystal resistance component at these longer measurement times.

The results obtained with BICON and with a.c. impedance [7, 8] for the fluoride i.s.e. appear to agree, considering the difference between the two methods. Alternating current impedance requires data collection over a much longer time period than BICON, so that the gel-layer resistance lowering would be more pronounced. The increase of the crystal resistance has not been noted by authors using a.c. impedance. However, Rhodes and Buck [19] obtained results with AgCl and AgBr crystals similar to those results reported here with LaF_3. In these crystals, ionic current can be supported by movement of both interstitial silver ions or vacancies [20]. Therefore, maximum crystal impedance was obtained in a solution of 10^{-3} M $AgNO_3$, where the point of zero charge (i.e., no significant excess of either vacancies or interstitial Ag^+ [21]) was reached. Vacancies were possible at low Ag^+ concentrations in solution, while interstitials were obtained at higher concentrations, and the impedance decreased accordingly.

It is not obvious whether the increase in the lanthanum fluoride crystal resistance would be reflected in the surface layer impedance, as measured by a.c. methods (where it would be "swamped out" by the gel layer resistance), or in the bulk impedance (where the 1% increase in resistance observed here would not be resolved). Unfortunately, BICON cannot resolve surface processes from bulk processes as a.c. impedance can. However, the speed and total resistance resolving power of BICON are far superior to that of the a.c. method.

Evaluation of interferences

The only anion known to interfere in potentiometric measurements with the fluoride i.s.e. is hydroxide [1]. The "mixed solution" method was used to evaluate anionic interferences for the potentiometric and conductometric methods. Measurements made on a solution containing 10^{-2} M Cl^-, Br^-, I^-, ClO_4^-, or CH_3COO^- and 10^{-4} M F^- were compared to those obtained for a 10^{-4} M F^- solution. The conductometric method was also evaluated for interferences in the lower part of its working range, with the fluoride concentration at 10^{-7} M and the anions to be evaluated at 10^{-5} M. All solutions used for interference evaluations contained TISAB IV, a Tris buffer.

No significant interference from Cl^-, Br^-, I^-, or ClO_4^- was observed in the potentiometric method or in both ranges of the conductometric method. Acetate was not observed to interfere potentiometrically, but did yield a small, irreproducible increase in resistance in the conductometric method after a few minutes of continuous monitoring. Anfalt and Jagner [22] observed non-Nernstian, sluggish behavior of the fluoride i.s.e. in the presence of acetate buffers, and attributed this to acetate complexation of lanthanum, blocking fluoride interaction with the crystal. Increases of the calcium electrode resistance in the presence of cationic interferences were observed in previous BICON work [11, 12]. These interferents are thought to have blocking effects [23] at the i.s.e./solution interface.

Hydroxide interference with the fluoride i.s.e. has been characterized potentiometrically by Vesely and Stulik [15], and was shown to consist of two processes. The fastest process involves direct interaction of hydroxide with the crystal, and yields negative potentials analogous to those induced by fluoride. The second process involves hydroxide ions displacing fluoride from the gel layer, and results in a long-term positive drift. Cammann and Rechnitz [7] showed that hydroxide decreases the resistance of the gel layer, but cannot enter the crystal lattice to any great extent.

The present results with the BICON measurements support the dual role of hydroxide. Current–voltage curves were taken at pH 8.43 and pH 9.43, with the fluoride concentration held constant at 10^{-4} M. The potentiometric selectivity coefficient, k, was calculated using the equation recommended by IUPAC [24] $E = S \log ([F^-] + k [OH^-]) + \text{constant}$. The potentiometric selectivity coefficient is comparable to that obtained through use of the conductometric i/V curve intercepts (which reflect the electrode potential), as shown in Table 1. However, a single conductometric measurement at a pulse amplitude of 5 V yielded a negative selectivity coefficient; the total current was increased because of a decrease in electrode resistance.

The electrode resistance changes in Table 1 show that a decade increase in fluoride concentration, within the potentiometric working range of the i.s.e., yielded the previously discussed increase in resistance. However, a decade increase in hydroxide concentration yielded a resistance decrease. Evidently, hydroxide does not lower the VB potential energy of the crystal to a noticeable extent. Measurements taken at fluoride concentrations below the i.s.e. potentiometric detection limit showed that increases in both fluoride and hydroxide concentrations lowered the electrode resistance, presumably by interaction with the gel layer.

TABLE 1

Summary of hydroxide interferences with the fluoride i.s.e.

Measurement technique		Selectivity coefficient[a]
Potentiometric monitoring		1.2
Conductometric monitoring, extrapolate to i/V curve intercept		3.1
Conductometric monitoring, measure current at 5 V pulse only		−0.72
Initial solution	**Final solution**	**Change in electrode resistance (Ω)**
10^{-4} M F^- (pH 8.43)	10^{-3} M F^- (pH 8.43)	+230 ± 20
pH 8.43 (10^{-4} M F^-)	pH 9.43 (10^{-4} M F^-)	−120 ± 20
10^{-7} M F^- (pH 8.43)	10^{-6} M F^- (pH 8.43)	−60 ± 20
pH 8.43 (10^{-7} M F^-)	pH 9.43 (10^{-7} M F^-)	−200 ± 20

[a]Solutions compared were 10^{-4} M F^-, pH 8.43 and 10^{-4} M F^-, pH 9.43 in all three cases.

Response time evaluations

The potentiometric response time of the fluoride i.s.e. has been shown to be heavily dependent on both the magnitude of the fluoride concentration in solution and the direction of the concentration change [3, 25]. The i.s.e. responds almost instantly to fluoride concentrations well above its detection limit, but quite slowly to concentration changes at or near the detection limit. Potentiometric steady-state responses are also reached more quickly when the fluoride concentration of the test solution is increased, rather than decreased. Potentiometric equilibration at low fluoride concentrations may be rate-controlled by dissolution of the LaF_3 crystal [26] or by diffusion of fluoride through the thick $La(OH)_3$ gel layer and equilibration of the fluoride and hydroxide concentrations within this gel layer [3].

Responses times for increases in fluoride concentration were obtained by rapid addition of a concentrated fluoride solution to a less concentrated fluoride solution in which the electrodes were immersed. Decreases in fluoride concentration were achieved by rapidly switching the equilibrated electrodes from the concentrated to the dilute solution. Potentiometric or conductometric measurements were taken continuously during the concentration change and displayed on a strip-chart recorder. Table 2 lists the times to 95% maximum response (t_{95}) for each concentration change. The potentiometric response times show a strong dependence on both fluoride concentration magnitude and direction of change, as expected. However, the conductometric response times are relatively constant. Fast conductometric responses were found for the calcium electrode [12], presumably because of induced migration of Ca^{2+} through the stagnant solution layer covering the membrane [12]. In the case of the fluoride electrode, voltage pulsing may also be inducing fluoride and hydroxide migration into and out of the gel layer, allowing faster equilibration of concentration profiles and surface processes.

The dependence of the potentiometric response time upon the fluoride concentration magnitude and the direction of concentration change has not been conclusively explained. The simple solution-layer diffusion model of

TABLE 2

Potentiometric and conductometric response times of the fluoride i.s.e. for different fluoride concentration changes (All times have a ± 1 s uncertainty)

Concentration change (M)	Potentiometric t_{95} (s)	Conductometric t_{95} (s)
$10^{-2} \rightarrow 10^{-1}$	4	13
$10^{-1} \rightarrow 10^{-2}$	13	14
$10^{-5} \rightarrow 10^{-4}$	39	12
$10^{-4} \rightarrow 10^{-5}$	150	12
$10^{-7} \rightarrow 10^{-6}$	—	10
$10^{-6} \rightarrow 10^{-7}$	—	11

transient behavior [27] useful for precipitate-based and plastic-membrane electrodes, is not applicable because of the presence of the gel layer. More advanced models proposed for the glass electrode [28, 29] and for i.s.e.'s in general [30] all postulate the existence of one or more potential energy barriers to ion transport through the membrane/solution interface. The activation energies for charge transfer in either direction across this barrier would have to be equal for a completely reversible interface. However, it has been noted [12] that the resistance to Ca^{2+} transport out of the calcium membrane i.s.e. is slightly greater than that for Ca^{2+} transport into the membrane. The use of short duration voltage pulses may have revealed a slight amount of irreversibility in the i.s.e./solution interface, if it is assumed that some part of the total resistance of the i.s.e. is related to the activation energy of ion transport across interfaces (referred to in the literature as the charge transfer resistance [6—9]). A small difference in activation energy may go unnoticed in the equilibrium potentiometric response, but could affect the kinetics of transient responses.

The bipolar voltage pulses used here resulted in a negative then positive voltage pulse being applied across the lanthanum fluoride crystal, from internal conducting element to test solution. The current was measured at the end of the positive pulse, with fluoride migrating across the crystal from the internal element to the test solution. Reversal of the leads from the BICON instrument resulted in current measurement upon a negative pulse, with fluoride migrating in the reverse direction. The positive polarity yielded a slightly lower (by about 0.7%) resistance than the negative polarity for test solution concentrations less than 10^{-1} M fluoride. Resistance was independent of applied voltage polarity at a test solution concentration of 10^{-1} M fluoride. The reference solution can provide a greater flux of fluoride into the crystal than a more dilute external solution, and thus yield a correspondingly lower resistance. Apparently, induced fluoride migration into the membrane is more kinetically facile than the reverse process. The differing activation energies may then account for the fact that the electrode responds more slowly to decreases in fluoride concentration (where fluoride ions must leave the crystal) than to increases in fluoride concentration (where fluoride enters the crystal).

Determination of fluoride in real samples

In order to demonstrate the quantitative capabilities of conductometric monitoring with the fluoride electrode, some real samples were assayed for fluoride using BICON and potentiometry. A direct and simple approach was used with no attempt to eliminate or compensate for matrix problems. Aqueous standards were used to prepare calibration curves over the 10^{-3}—10^{-5} M range. The measurement of the potential or the zero-pulse current for the sample was used to obtain the fluoride concentration from the corresponding calibration curve. All samples and standards were diluted 1:1 with TISAB II (pH 5.0). For a toothpaste sample, 480 mg of tooth-

paste was dissolved in 100 ml of boiling, deoxygenated TISAB II; the solution was then diluted to 200 ml with water. The results obtained (all values in ppm) with conductometric and potentiometric monitoring, respectively, were: milk, 1.2, 0.2; drinking water, 1.5, 1.8; toothpaste, 2100, 1300. These values show reasonable agreement to each other and to literature values considering the simple technique used.

Conclusion

Bipolar pulse conductometric monitoring of a fluoride electrode yields significantly lower detection limits than the standard potentiometric method and also reveals some semiconductor properties not observed in previous non-zero current work. The anomalous shapes of the conductometric working curves (Fig. 1) would yield ambiguous results for fluoride determinations in unknown samples. However, ambiguities could be resolved by determination of i/V curve intercepts or the i.s.e. potential (by potentiometry). Fluoride concentrations on the negative sloping part of the curve would yield zero-pulse currents or potentials more negative than those of the blank solution.

A more serious problem is related to the time dependence of the signal, caused by the slowly decreasing resistance of the gel layer. The results reported above were obtained by making measurements at set time intervals after a standard addition or after immersion of electrodes into a fresh solution. A more convenient approach would involve conductometric monitoring of the i.s.e. in a flow-injection or continuous flow system. Timing would be facilitated by adjustment of the sample loop volume, as is done in flow injection [31] or by taking measurements at set time intervals after injection into a continuous flow system. Also, the carrier solution could return the i.s.e. to "baseline" potentials and resistances between samples, eliminating the "memory effect" of the gel layer [15]. The next paper in this series will report results obtained with conductometric monitoring of the calcium and fluoride electrodes in flowing streams.

Special thanks are extended to L. R. Faulkner for helpful ideas and discussions. One of us (C. R. P.) gratefully acknowledges an American Chemical Society, Division of Analytical Chemistry Fellowship sponsored by FACSS. This research was supported in part by the National Science Foundation (CHE-81-08816).

REFERENCES

1 M. S. Frant and J. W. Ross, Science, 154 (1966) 1553.
2 A. Sher, R. Solomon, K. Lee and M. W. Muller, Phys. Rev., 144 (1966) 593.
3 R. C. Hawkings, L. P. V. Corriveau, S. A. Kushneriuk and P. Y. Wong, Anal. Chim. Acta, 102 (1978) 61.
4 J. Buffle, N. Parthasarathy and W. Haerdi, Anal. Chim. Acta, 68 (1974) 253.
5 J. F. Coetzee and M. W. Martin, Anal. Chem., 52 (1980) 2412.
6 M. J. D. Brand and G. A. Rechnitz, Anal. Chem., 42 (1970) 478.
7 K. Cammann and G. A. Rechnitz, Anal. Chem., 48 (1976) 856.

8 J. Mertens, P. van den Winkel, and J. Vereecken, Bioelectrochem. Bioenerg., 5 (1978) 699.
9 P. van den Winkel, J. Mertens, T. Boel and J. Vereecken, J. Electrochem. Soc., 124 (1977) 1338.
10 D. E. Johnson and C. G. Enke, Anal. Chem., 42 (1970) 329.
11 C. R. Powley, R. F. Geiger, Jr. and T. A. Nieman, Anal. Chem., 52 (1980) 705.
12 C. R. Powley and T. A. Nieman, Anal. Chim. Acta, 139 (1982) 61.
13 P. H. Daum and D. F. Nelson, Anal. Chem., 45 (1973) 463.
14 K. J. Caserta, F. J. Holler, S. R. Crouch and C. G. Enke, Anal. Chem., 50 (1978) 1534.
15 J. Vesely and K. Stulik, Anal. Chim. Acta, 73 (1974) 157.
16 A. J. Bard and L. R. Faulkner, Electrochemical Methods, Wiley, New York, 1980, Ch. 14.
17 N. F. Mott and R. W. Gurney, Electronic Processes in Ionic Crystals, Dover Publications, New York, 1964, Ch. 5.
18 J. T. Law, in N. B. Hannay (Ed.), Semiconductors, Reinhold, New York, 1959, Ch. 16.
19 R. K. Rhodes and R. P. Buck, J. Electroanal. Chem., 86 (1978) 349; Anal. Chim. Acta, 113 (1980) 55.
20 M. Koebel, N. Ibl and A. M. Frei, Electrochim. Acta, 19 (1974) 287.
21 E. P. Honig and J. H. Th. Hengst, J. Colloid Interface Sci., 31 (1969) 545.
22 T. Anfält and D. Jagner, Anal. Chim. Acta, 47 (1969) 483.
23 A. Craggs, G. J. Moody, J. D. R. Thomas and A. Willcox, Talanta, 23 (1976) 799.
24 G. G. Guilbault, Ion-Selective Electrode Rev., 1 (1979) 139.
25 J. Mertens, P. van den Winkel and D. L. Massart, Anal. Chem., 48 (1976) 272.
26 J. Buffle and N. Parthasarathy, Anal. Chim. Acta, 93 (1977) 111.
27 W. E. Morf, E. Lindner and W. Simon, Anal. Chem., 47 (1975) 1596.
28 G. A. Rechnitz and H. F. Hameka, Fresenius Z. Anal. Chem., 214 (1965) 252.
29 G. Johansson and K. Norberg, J. Electroanal. Chem., 18 (1966) 239.
30 A. Shatkay, Anal. Chem., 48 (1976) 1039.
31 J. Růžička and E. H. Hansen, Anal. Chim. Acta, 114 (1980) 19.

Analytica Chimica Acta, 139 (1982) 97—103
Elsevier Scientific Publishing Company, Amsterdam — Printed in The Netherlands

ION-SELECTIVE ELECTRODES FOR BASIC DRUGS

LARRY CUNNINGHAM and HENRY FREISER*
Department of Chemistry, University of Arizona, Tucson, AZ 85721 (U.S.A.)
(Received 25th November 1981)

SUMMARY

Coated-wire ion-selective electrodes based on dinonylnaphthalene sulfonic acid (DNNS) are prepared for methadone, methylamphetamine, cocaine and protriptyline in protonated form. In each set, nearly-Nernstian responses are obtained while detection limits range from $10^{-5.5}$ M for cocaine and methylamphetamine electrodes, to $10^{-6.0}$ M for methadone, and $10^{-6.5}$ M for protriptyline electrodes. Selectivity is found to decrease in the order methadone, protriptyline, cocaine and methylamphetamine; these results are consistent with systematic selectivity studies reported earlier for electrodes in this family.

Since the development of DNNS-based poly(vinyl chloride) membrane electrodes as sensors of high molecular weight cations, electrodes responsive to basic lipophilic drugs [1, 2] and to a variety of alkylammonium ions [3] have been prepared. A recent systematic study of selectivity [4] has shown that certain factors in addition to the number of carbon atoms of the cation affect the selectivity displayed by DNNS-based electrodes. These factors included degree of nitrogen substitution, branching of the hydrocarbon chains, and the number and type of hydrophilic substituents; parameters which control the extent to which the analyte (or the interferent) will partition into the PVC membrane.

This paper describes the preparation and evaluation of electrodes selective to methadone, cocaine, protriptyline and methylamphetamine. These compounds were chosen because they are protonated amines in the physiological pH range, and are representative of some important families of pharmaceuticals: methylamphetamine (m.w. = 150) a central nervous system stimulant; protriptyline (m.w. = 263) an anti-depressant; methadone (m.w. = 310) a narcotic analgesic; and cocaine (m.w. = 303) a local anaesthetic.

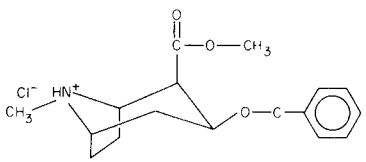

Cocaine HCl

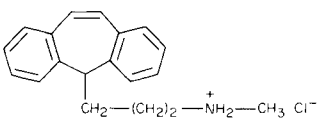

Protriptyline HCl

0003-2670/82/0000-0000/$02.75

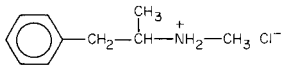

Methylamphetamine HCl

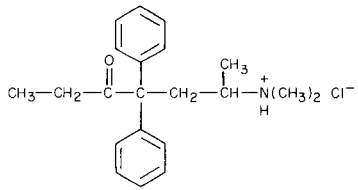

Methadone HCl

EXPERIMENTAL

Stock solutions of the drugs were prepared by dissolving known amounts of the pure hydrochloride salts in 10^{-2} M pH 4.0 acetate buffer. Chromatographic-grade poly(vinylchloride) was obtained from Polysciences (Warrington, PA) and dioctylphthalate from Eastman.

All e.m.f. measurements were made with the previously described Data General Nova 2/10 minicomputer system [4]. To allow use of up to five electrodes in sample volumes as small as 1.0 ml, the following cell was constructed. A 3-mm hole was drilled in the bottom of a 10-ml vial, to which a Ag/AgCl electrode made from two Pasteur pipettes was sealed with silicone rubber cement. Polyacrylamide impregnated with 0.1 M KCl and 0.1 M ammonium nitrate was used for the internal and external junctions, respectively. A 1.000-ml Mettler digital burette capable of adding 1.0-μl increments was used for all titrations.

Coated-wire electrodes were used exclusively, and were prepared as described previously [4]. As before, the electrodes were stored in 10^{-3} M solutions of the species to which they were selective. During the course of calibration and/or selectivity measurements, the electrodes were kept in buffer solution containing no primary ion. All measurements were made at 25.0 ± 0.1°C.

RESULTS

Nearly-Nernstian responses were obtained for all electrodes with excellent linearity (E vs. log C) over the range 10^{-3}—10^{-5} M (Table 1); 10^{-3} M was the

TABLE 1

Response characteristics of coated-wire electrodes for basic drugs

Drug	Slope[a,b] (mV/log C)	Intercept[b] (mV)	Detection limit (M)
Methylamphetamine	58.64 ± 0.67 (0.58)	282 ± 4 (2)	$10^{-5.5}$
Cocaine	59.54 ± 0.83 (0.40)	504 ± 5 (2)	$10^{-5.5}$
Methadone	58.08 ± 1.75 (0.84)	398 ± 22 (4)	$10^{-6.0}$
Protriptyline	58.50 ± 0.74 (0.80)	475 ± 11 (3)	$10^{-6.5}$

[a]Slope for the range 10^{-3}—10^{-5} M. [b]With the standard deviation among several electrodes, and in parentheses the standard deviation for successive measurements with individual electrodes.

highest concentration tested. The electrodes responded rapidly above a concentration of 10^{-5} M, usually equilibrating within 30—60 s after exposure to a new concentration. Below this level, however, longer times were required (2—5 min). For all electrodes, "equilibrium" was assumed when drift was less than 0.4 mV min^{-1}, though at the higher concentrations drift of only 0.1 mV min^{-1} was commonplace.

Selectivity coefficients are reported as log ($k_{i,j}^{pot}$) in Table 2. As expected from earlier studies and by inspection of the structures for the drugs, selectivity decreased in the order methadone, protriptyline, cocaine and methylamphetamine. The very high selectivity of the methadone and protriptyline electrodes over cocaine and methylamphetamine precluded the precise determination of selectivity coefficients for the smaller amines. In fact, interference from methylamphetamine was so slight that no changes in e.m.f. readings for methadone and protriptyline electrodes could be attributed to its presence. The concentrations of primary and interfering ion are reported because the selectivity coefficients varied with each of these values.

It was observed that the detection limits obtained depended on the primary ion. This was not apparent in the earlier studies, because primary ions did not vary in molecular weight or structure to the same extent as those used here. The calibration curve shown in Fig. 1 for a set of five protriptyline electrodes indicates that detection limits of $10^{-6.5}$ M are obtainable. For methadone, slightly higher detection limits were realized (10^{-6} M), and for the cocaine and methylamphetamine electrodes, detection limits were even higher ($10^{-5.5}$ M).

Calibration curves for the individual electrodes were found to be reasonably reproducible from day to day provided that the electrodes were soaked in 10^{-2} M pH 4.0 acetate buffer between calibrations (Table 1). After exposure to strong interferences, however, the calibration curves shifted by several millivolts so that any further measurements would result in erroneously high results. The original response was restored by keeping the electrodes in 10^{-3} M primary ion for several hours followed by soaking overnight in the buffer solution. Electrodes prepared 5 months earlier functioned normally, after regular use.

TABLE 2

Selectivity characteristics (log $k_{i,j}^{pot}$ values) for various coated-wire ion selective electrodes

Ion j	Electrode (ion i)[a]			
	Methylamphetamine	Methadone	Cocaine	Protriptyline
Methylamphetamine	—	<−4[b]	−0.60	<−4[b]
Methadone	2.41	—	1.79	0.40
Cocaine	0.54	−1.96	—	−1.78
Protriptyline	2.16	−0.67	1.37	—

[a]Except where indicated otherwise, [primary ion] = [interferent] = 10^{-3} M. [b][Primary ion] = 10^{-4} M; [interferent] = 10^{-3} M.

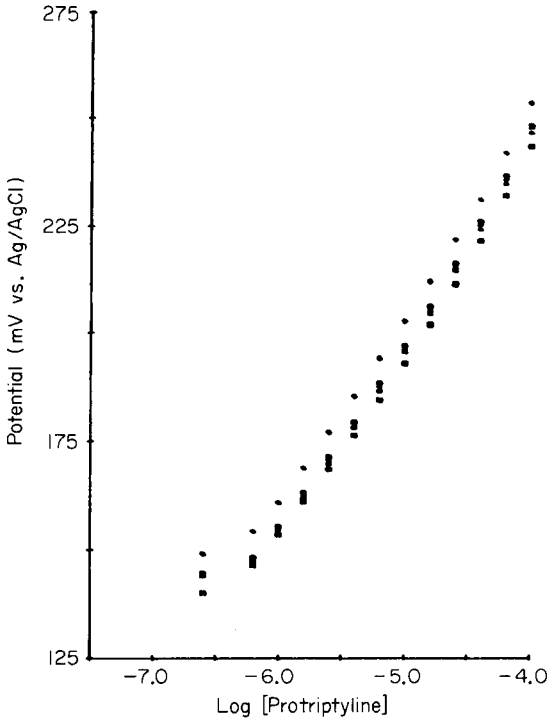

Fig. 1. Potential vs. log concentration for five different protriptyline electrodes.

DISCUSSION

Sternson et al. [5] reported methadone coated-wire electrodes in an earlier paper, using PVC impregnated with dioctylphthalate as the membrane material. Though Nernstian responses to methadone with detection limits of $10^{-6.0}$ M along with high selectivity towards inorganic cations was achieved, selectivity among other high molecular weight cations was poor. For DNNS-based electrodes, selectivity increases with analyte lipophilicity. The $k_{i,j}^{pot}$ values obtained for methadone and protriptyline with respect to cocaine and methylamphetamine attest to this. A larger increase in selectivity is seen for protriptyline over cocaine than for methadone over protriptyline, even though the carbon numbers in each pair differ by only two. This is understandable from the lower distribution constant of cocaine arising from the two carboxylate substituents as well as to the lower degree of substitution of nitrogen in protriptyline. Distribution constants of the drugs in their hydrochloride form for the octanol—water system were calculated by the method of Hansch and Leo [6], in which an overall log K_D value for a compound in a given solvent system is the sum of individual contributions from its molecular fragments. These values increased in the order methylamphetamine (—1.61), cocaine (0.80), methadone (1.37) and protriptyline (1.46).

Because the contributions (or fragment constants) are derived from experiment, small errors can arise with these calculations either from unanticipated molecular interactions or from lack of sufficient experimental data for a given fragment. The latter reason is apparently the case for the methadone/protriptyline pair, because the calculated K_D value for protriptyline is slightly higher than that for methadone yet the methadone electrodes displayed greater selectivity. As pointed out by Hansch and Leo [6], additional data are needed for large fused-ring systems bearing a positive nitrogen. Even so, the high selectivity of both these electrodes over methylamphetamine and cocaine is accurately reflected by the large difference in the distribution constants.

Interference from drug metabolites can also be predicted from their structures. Methylamphetamine does not undergo extensive metabolism and is excreted unchanged [7]. Cocaine, however, is rapidly converted to methylecognine through hydrolysis of the benzoyl group [8]. This represents a decrease in carbon number of seven, which, based on calculated log K_D values, indicates that methylecognine will not be a significant interferent (calculated log K_D = 0.80 for cocaine and −1.64 for methylecognine). Protriptyline is *N*-demethylated [7], and as inferred by previous work [4], this compound would be expected to be a major interferent. Methadone is also *N*-demethylated, but then cyclizes to form 2-ethyl-1,5-dimethyl-3,3-diphenyl-1-pyrroline [9]. Although this is a quaternary ammonium compound it would probably cause significant interference as predicted by its relatively high calculated log K_D value of 2.13. Preparation of electrodes selective to these interfering metabolites which would not respond significantly to the parent drug would be one approach for monitoring metabolism of these substances. Because both species are often at appreciable levels in urine samples, depending upon the individual drug and others which have been ingested [10], each compound must be determined simultaneously. With DNNS electrodes, no interference is possible from inorganic cations even at 10 000-fold concentrations.

Following administration, extremely low levels of drugs are found in serum and urine samples (Table 3). In Table 4, the detection limits of these electrodes are compared to several alternative methods applicable to clinical samples. It should be pointed out that for most of these methods, the

TABLE 3

Concentration of drugs of interest in plasma following therapeutic doses

Drug	Dose	Plasma level	Ref.
Cocaine	Oral: 2 mg kg^{-1}	200 ng ml^{-1} ($10^{-6.2}$ M)	11, 12
	Nasal: 15—150 mg	2—25 μg ml^{-1} (1—8 × 10^{-5} M)	13
Methylamphetamine	10 mg	20 ng ml^{-1} (1.3 × 10^{-7} M)	14
Methadone	1 mg kg^{-1} d^{-1}	100—400 ng ml^{-1} (3 × 10^{-7} M)	15
Protriptyline	2—3 mg kg^{-1} d^{-1}	50—200 ng ml^{-1} (2 × 10^{-7} M)	16

TABLE 4

Detection limits (ng ml^{-1}) various assay procedures for serum and urine

	Protriptylene	Methadone	Cocaine	Methylamphetamine
G.l.c.	10[a] [17]	5[b] [21]	200[b,c] [24]	2 [28]
G.c.—m.s.	5 [18]	5 [15]	2 [25]	0.5 [29]
H.p.l.c.	10 [19]	—	100 [26]	2[e] [30]
R.i.a.	10[f] [20]	1[g] [22]	2 [27]	0.5 [31]
EMIT	—	500 [23]	1000 [23]	2000 [23]
I.s.e[h]	85	350	1000	500

[a]Nitrogen detector. [b]F.i.d. used. [c]Cocaine and metabolites extracted, propylated, and back-extracted. [d]Protriptyline was internal standard for determination of other tricyclic anti-depressants. [e]Preceded by derivatization with β-naphthoquinone-4-sulfonate; u.v. detector. [f]Poor selectivity with respect to other tricyclic anti-depressants. [g]Stereospecific for D- and L-isomers. [h]All 1-ml samples, no preconcentration.

reported values were attained only after sample pretreatment methods such as derivatization or preconcentration, whereas those for the potentiometric ISE method involved none of these. With preconcentration, the detection limit of a potentiometric procedure may equal or surpass that of the EMIT technique. The time and cost of determination using coated-wire electrodes should be substantially reduced. In addition, the electrodes are more than sufficiently sensitive and reproducible for analysis of pharmaceutical preparations. The drugs studied here represent only a fraction of those for which electrodes can be fabricated. Others can easily be made as needed by adding the compound of interest as the primary ion in the polymer membrane solution. Selectivity characteristics are then predicted as described earlier or can be determined experimentally if certain interferences are suspected.

It was interesting to note that the electrode of highest selectivity (methadone) did not have the lowest detection limit (protriptyline). This supports the contention that selectivity is determined primarily by the partition coefficient of the protonated amine, whereas detection limit is determined by solubility of the DNNS—ammonium ion-pair. This suggests that electrodes with lower detection limits could result by using a ligand which can form a more water-insoluble salt with the analyte than can DNNS, or by covalently attaching a ligand to the polymer backbone. Initial studies on ionic polymers in this laboratory [32] have shown promise for this latter approach.

The authors gratefully acknowledge helpful discussions with Dr. Paul Consroe, Associate Professor of Pharmacology and Toxicology, at the University of Arizona. This work was conducted with financial assistance from the Office of Naval Research.

REFERENCES

1 C. R. Martin and H. Freiser, Anal. Chem., 52 (1980) 1772.
2 T. Yamada and H. Freiser, Anal. Chim. Acta, 125 (1981) 179.
3 C. R. Martin and H. Freiser, Anal. Chem., 52 (1980) 562.
4 L. Cunningham and H. Freiser, Anal. Chim. Acta., 132 (1981) 43.
5 L. A. Sternson, T. Higuchi, R. White and S. Srianyata, Anal. Chem., 50 (1978) 232.
6 C. Hansch and J. L. Leo, Substituent Constants for Correlation Analysis in Chemistry and Biology, Wiley, New York, 1979, p. 40.
7 E. G. C. Clarke, Isolation and Identification of Drugs, The Pharmaceutical Press, London, 1969.
8 T. Inaba, D. J. Stewart and W. Kalow, Clin. Pharmacol. Theor., 23 (1978) 547.
9 A. H. Beckett, M. Mitchard and A. A. Shihab, J. Pharm. Pharmacol., 23 (1971) 347.
10 A. E. Robinson and F. M. Williams, J. Pharm. Pharmacol., 23 (1971) 353.
11 J. I. Javaid, M. W. Fischman, C. R. Schuster, H. Dekirmenjian and J. M. Davis, Science, 202 (1978) 227.
12 C. van Dyke, P. Jatlow, J. Ungerer, P. G. Barash and R. Byck, Science, 200 (1978) 211.
13 C. van Dyke, R. Byck, P. G. Barash and P. Jatlow, Clin. Chem., 23 (1977) 241.
14 S. H. Wan, S. B. Matin and D. F. Azarnoff, Clin. Pharm. Ther., 23 (1978) 585.
15 D. L. Hachey, M. J. Kreck and D. H. Matson, J. Pharm. Sci., 66 (1977) 1579.
16 D. R. A. Uges and J. B. G. M. Noten in F. W. H. M. Merkus (Ed.), The Serum Concentration of Drugs, Excerpta Medica, Amsterdam, 1980.
17 D. N. Bailey and P. Jatlow, Clin. Chem., 22 (1976) 1697.
18 J. T. Biggs, W. H. Holland, S. Chang, P. P. Hipps and W. R. Sherman, J. Pharm. Sci., 65 (1976) 261.
19 F. L. Vandemark, R. F. Adams and G. J. Schmidt, Clin. Chem., 24 (1978) 87.
20 J. W. Hubbard, K. K. Midha, J. K. Cooper and C. Charette, J. Pharm. Sci., 67 (1978) 1571.
21 R. K. Lynn, R. M. Leger, W. P. Gordon, G. D. Olsen and N. Gerber, J. Chromatogr., 131 (1977) 329.
22 K. L. McGillard, J. E. Wilson, G. D. Olsen and F. Bartos, Proc. West. Pharmacol. Soc., 22 (1979) 463.
23 S. J. Mule, M. L. Bastos and D. Jukovsky, Clin. Chem., 20 (1974) 243.
24 D. L. von Minden and N. D'Amato, Anal. Chem., 49 (1977) 1974.
25 S. P. Jindal and P. Vestergaard, J. Pharm. Sci., 67 (1978) 811.
26 P. Jatlow, C. van Dyke, P. Barash and R. Byck, J. Chromatogr., 152 (1978) 115.
27 K. Balkrishena, S. J. Millian and B. Davidow, J. Pharmacol. Exp. Ther., 199 (1976) 171.
28 D. B. Campbell, J. Pharm. Pharmacol., 21 (1969) 129.
29 J. Gal, Biomed. Mass Spectrom., 5 (1978) 32.
30 M. Endo, H. Imicmachi, M. Moriyasu and Y. Hashimoto, J. Chromatogr., 196 (1980) 334.
31 B. A. Faraj, Z. H. Israili, N. E. Kight, E. E. Smissan and T. J. Pazdurnik J. Med. Chem., 19 (1976) 20.
32 C. R. Martin and H. Freiser, Anal. Chem., 53 (1981) 902.

Analytica Chimica Acta, 139 (1982) 105—115
Elsevier Scientific Publishing Company, Amsterdam — Printed in The Netherlands

COMBINATION OF FLOW INJECTION ANALYSIS AND VOLTAMMETRY

JIŘÍ JANATA

Department of Bioengineering, University of Utah, Salt Lake City, UT 84112 (U.S.A.)

JAROMÍR RŮŽIČKA*

Chemistry Department A, The Technical University of Denmark, Building 207, 2800-Lyngby (Denmark)

(Received 18th January 1982)

SUMMARY

The flow injection analyzer for students, teaching and research (FIAstar) is used in conjunction with a new micropool mercury flow-through electrode, to explore the possibilities offered by using d.c. polarography, rapid scan and amperometric titrations on a dispersed sample zone in motion. The work outlines the principles of the use of a scanning detector for investigation of the concentration gradients and chemical reactions taking place during the dispersion of sample solution within a carrier stream. The data, which are collected in real time, are displayed in three-dimensional diagrams.

The subject of detectors for flow injection analysis (f.i.a.) has been covered in a recent book [1], while the use of voltammetric detectors for measurement of unsegmented streams has been investigated in detail by Pungor and coworkers [2]. The use of the mercury electrode as a continuous flow polarographic detector has a long tradition [3] which continues through new ingenious designs aimed at h.p.l.c. applications [4] and, more recently, also for f.i.a. work [5]. A micropool mercury electrode is used in the present work, the main purpose of which is to reveal new facets of the combination of f.i.a. and voltammetry, and to draw attention to the hitherto neglected potential of the use of concentration gradients formed at the interface between the injected sample zone and the carrier solution [1, 6]. Further, it will be demonstrated how dynamic detectors can be employed in combination with f.i.a. to yield, in real time, three-dimensional information on the interaction between various species in the sample and the carrier stream solution.

Generally speaking, detectors can be divided into two groups, static and dynamic. The former simply yields an electrical signal which is either linearly or logarithmically related to the concentration of species in the analyte. The most widely used detector of this type is an optical detector operated at a fixed wavelength, or an ion-selective electrode. In order to obtain analytical information on several species simultaneously, potentiometric detectors must be grouped into a multidetector [7]. Spectrophotometric and voltam-

metric (or polarographic) detectors are qualitatively different and belong to the dynamic group. Not only can they detect the concentration of the light-absorbing species at a specific wavelength, or of the electroactive species at a certain potential, but they can also scan their own function on the solution of a given composition; this capability of yielding spectra or voltammograms is one of the most effective tools of instrumental analysis. This feature, combined with the unique ability of the f.i.a. technique to create a perfectly reproducible concentration gradient [1] from an injected sample zone, offers new possibilities for conducting spectrophotometric and electrochemical experiments. Thus, instead of a separate solution being prepared each time, a scan can be done on an element of fluid chosen within the dispersed sample zone (Fig. 1) or, as will be demonstrated below, on a series of successive elements of fluid.

In order to realize the new approach, an electrochemical cell has been designed for operation in a manner compatible with f.i.a. As the line of introducing f.i.a. into teaching and research laboratories continues in this work, the FIAstar system [8] has been used as the central solution processing unit. For the same reason, the stepwise development of the voltammetry—f.i.a. combination is described in didactic form, in order to facilitate the introduction of the method in student courses.

EXPERIMENTAL

Apparatus

The FIAstar system described earlier [8] used nitrogen, the pressure of which was reduced to ca. 2 bar at the inlet side of the liquid propelling mani-

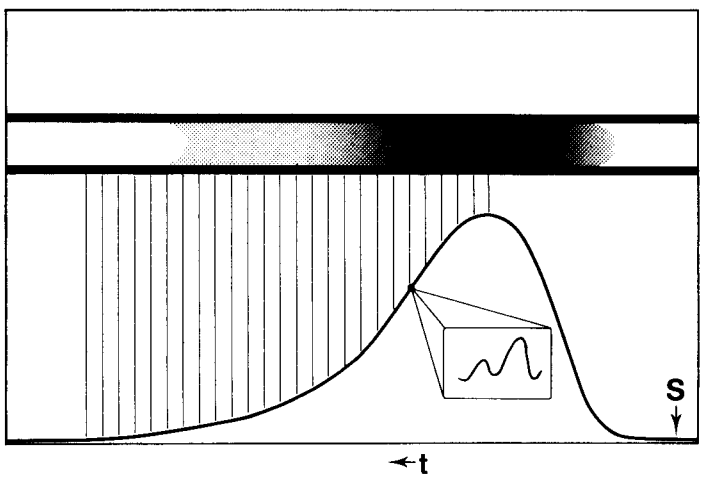

Fig. 1. The principle of the f.i.a. gradient scanning technique. S, point of sample injection; *t*, time.

fold. The fine pressure stabilization and adjustment required to propel the carrier stream in a reproducible manner was effected by a special regulator. The individual components, such as coils, gradient tube, injection valve and flow cell were arranged as shown on the diagrams included in the description of individual experiments. All tubing had an inner diameter of 0.5 mm. The flow cell (Fig. 2) had a volume of <4 μl and accommodated three electrodes: the working electrode (M) was a mercury hemisphere which protruded from the bottom of the flow channel; the reference electrode (R) consisting of a Ag/AgCl wire bathed in saturated potassium chloride was placed in a Pasteur pipette with an asbestos fiber junction; the auxiliary electrode (A) was a stainless steel syringe needle which also served as solution outlet. A suction pipette with an asbestos fiber junction; the auxiliary electrode (A) was a held in place by a screw and silicone rubber washer. The distance between the solution inlet and the surface of the working electrode (*d*, Fig. 2, ca. 3 mm) is a critical parameter and was, therefore, kept constant during all experiments.

The electronic components were assembled to allow either d.c. or rapid scan (linear sweep) voltammetry with a linearly increasing polarization voltage. The three-electrode system was connected to a home-made potentiostat, and the response curves were recorded by a Radiometer REC80 chart recorder equipped with the 112 high-sensitivity unit. The rapid scanning of concentration profiles required more sophisticated equipment. Though the home-made potentiostat still provided the potential ramp, the actual voltage source was a Bruel and Kjaer x—y recorder type 2308, which also delivered a linear potential sweep with a rate of 833 mV s^{-1}, synchronized with the movement of the x-axis, while the y-axis, capable of responding at a rate of 1000 mm s^{-1}, responded to the resulting limiting current. This set-up allowed

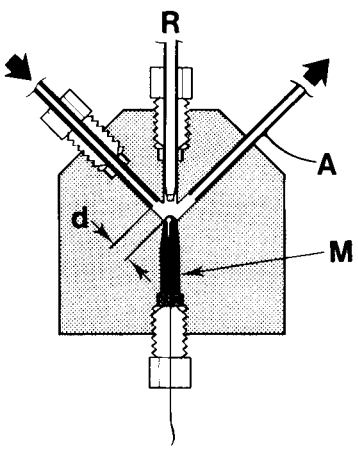

Fig. 2. Voltammetric flow-through cell (machined from 7-mm thick Perspex plate). M, mercury micropool electrode; R, reference electrode; A, auxiliary electrode and outlet.

precise synchronization of the pen position with the electrode potential and recording of i—E curves in real time. A Commodore PET 4032 microcomputer was used with a home-made interface to control the repetition rate of the sweeps and to control the stepwise shift of the starting potential for each scan. In this way, a three-dimensional image was obtained. The time for each individual sweep was 1.8 s, and the time interval between individual sweeps was 0.5 s. It took less than 2 min to obtain an entire three-dimensional recording.

Reagents and solutions

Stock solutions (0.01 M) of cadmium nitrate and copper(II) nitrate in water were diluted by 0.1 M ammonia—ammonium nitrate buffer, pH 9.20, for individual experiments as necessary. The stock 0.01 M solution of EDTA was also prepared in the same ammoniacal buffer. Solutions were deaerated before use under aspiration with vigorous stirring for 5 min. Because the carrier stream was deaerated and because the concentration of the electroactive species was above 10^{-4} M, it was not necessary to make an extra effort to carry out these experiments under nitrogen; however, it would be necessary to deaerate the solutions more rigorously for lower concentrations.

RESULTS

Hydrodynamic d.c. and linear sweep voltammetry

A d.c. voltammogram of an equimolar mixture of the ammine complexes of copper(II) and cadmium (2 mM each) is shown in Fig. 3 (curve 1). The three waves correspond to the reduction of (a) $Cu(NH_3)_2^{2+}$ to $Cu(NH_3)_2^{+}$, (b) $Cu(NH_3)_2^{+}$ to Cu^0 (amalgam), and (c) $Cd(NH_3)^{2+}$ to Cd^0 (amalgam). It is interesting to note that the background electrolyte current for the d.c. voltammogram is shifted towards positive potentials and nearly obliterates the reduction of the cadmium complex. This does not happen if the $Cd(NH_3)_2^{2+}$ complex alone is reduced; in that case, a well resolved two-electron reduction wave is obtained. The complication with the background electrolyte wave is caused apparently by the lowering of the hydrogen overvoltage by formation of copper amalgam during the slow scan. If the scan is rapid, as in linear sweep voltammetry, (Fig. 3, curve 2), the corresponding peaks a, b, and c appear at more negative potentials as does the background current, so that even the cadmium reduction peak is well resolved. For a reversible reduction, the peak potential E_p should be 28.5 mV more negative than the corresponding half-wave potential [9]. In the present experiment, this separation was approximately 30 mV.

For recording of the d.c. and linear sweep voltammograms, the f.i.a. manifold should be assembled as shown in Fig. 3 with a coil length A of 400 cm. With a pressure, P, of 0.4 bar, the assembled line yields a flow rate of ca. 1 ml min^{-1}. As always with the FIAstar, the applied pressure is only reference information, as the exact flow rate, Q, must be measured at the outlet (W) by collecting the effluent for a fixed time period. The role of the

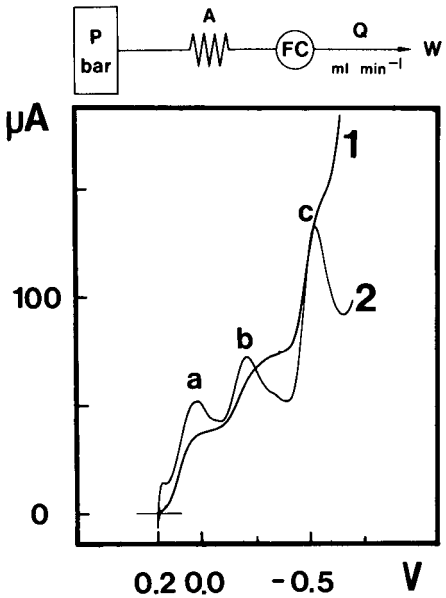

Fig. 3. D.c. voltammogram (1) and a rapid scan voltammogram (2) recorded on a solution of constant composition supplied through the manifold shown. (For details, see text.)

coil A in this and all further experiments is to stabilize the flow rate through hydrodynamic resistance, as voltammetric measurements are sensitive to all changes governing mass transport to the electrode surface.

It should be noted that this is not a flow-injection type of measurement, because the depolarizers were supplied continuously in unchanged concentration throughout the whole experiment which, therefore, represents a "steady state". Thus the 4 mM mixture of copper(II) and cadmium ammine complexes in 0.1 M ammonium nitrate buffer was supplied from the pressurized reagent bottle, while the potential was scanned from +200 mV to −700 mV at a rate of 10 mV s^{-1} (Fig. 3, curve 1). When progressively steeper ramps were used, the linear sweep voltammograms were recorded with scan rates increased to 50 mV s^{-1}, 500 mV s^{-1}, and even 1000 mV s^{-1}. To test the electrode and the flow system further, the flow can be stopped and the linear sweep experiments repeated, to establish the influence of solution movement and sweep rate on the recorded peak shapes and sensitivity of measurement; curve 2 (Fig. 3) was obtained with a scan rate of 50 mV s^{-1} on a stopped flow.

Flow injection

Based on the above experiments, the electrochemical cell was tested as a static linear detector, continuously monitoring the concentration of the copper(II) ammine complex while the electrode potential was kept constant at −300 mV to measure the limiting current past point b on Fig. 3. Thus, if the flow system is supplemented by an injection valve and by a short coil (B = 50 cm) and assembled as shown in Fig. 4, a single-channel flow injection

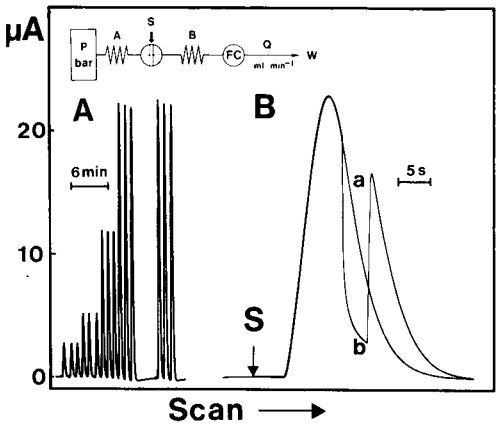

Fig. 4. Flow injection voltammetry: (A) series of standards of increasing concentration; (B) continuous flow (a) and stopped flow (b) measurements.

system can be set up, capable of rapid assay of copper concentrations in injected sample material.

For this purpose, the pressurized reagent bottle was filled with ammonia—ammonium nitrate buffer solution which was propelled (by a pressure of ca. 0.4 bar) at a rate of 1 ml min^{-1}. The samples were injected at regular intervals via an injection valve in the usual way [8] and sharp peaks were formed; the height of the peaks was linearly dependent on the copper concentration. In the recording shown in Fig. 4A, 30-μl aliquots of 0.6, 1.2, 2.5 and 5.0 $\times$ 10^{-3} M Cu^{2+} were injected in triplicate; after a short pause, the most concentrated sample solution was again injected three times. The sampling frequency was 120 samples per hour, the response was strictly linear, and the reproducibility (relative standard deviation) of injections was better than 0.5%. The only objectionable phenomenon is a slight negative shift of the baseline observed during injection of the most concentrated standards; this is apparently due to the formation of copper amalgam. No attempt was made at this stage to increase the sensitivity of measurement. The concentrations of the injected samples were high by any polarographic standard, but the system is only a model and it should be simple to increase the sensitivity considerably.

A continuous flow and a stopped flow measurement were repeated at increased paper chart speed (Fig. 4, B) by injecting twice the most concentrated copper solution, the peaks being traced from the same starting point (S). While the continuous flow curve (a) has a normal shape, the limiting current decreases during the stopped-flow period (b) because of the depletion of copper(II) at the electrode surface.

A simple conclusion may be drawn from these experiments: the concentration profiles formed from the dispersed sample zone can be faithfully and reproducibly recorded providing that the flow injection system and flow-through detector are properly designed.

Flow injection titrations

The theory and practice of flow injection titrations have been described [1] and more detailed experimental descriptions are available in the paper describing the FIAstar instrument [8] where acid—base titrations with a color indicator were included as an exercise. The detector used here is a voltammetric device, which allows amperometric flow injection titrations to be performed. When the metal ion forms a complex during such titrations, the half-wave potential or peak potential (depending on the technique used) is shifted to more negative values, the magnitude of the shift being dependent on the stability of the complex formed [9]. Thus, in a titration with EDTA, if the potential of the mercury electrode is set at —300 mV, as above, the copper present as its ammine complex will be monitored, whereas the Cu—EDTA complex which has a much higher stability constant ($\log K_{\mathrm{Cu\,EDTA}} = 19.1$) than the ammine complexes, will be electro-inactive.

With the manifold shown in Fig. 5, it is possible to record a series of titration curves B, C and D if the carrier stream contains a certain level of EDTA in addition to ammonia buffer. In these experiments, the flow rate (Q) was kept strictly constant (1 ml min^{-1}) and the injected sample volume was 150 μl. The injected copper(II) concentrations were 1×10^{-2} M (a), 7.5×10^{-3} M (b), 5×10^{-3} M (c), and 2.5×10^{-3} M (d). The carrier streams for the different experiments were as follows: A, 0.1 M NH_4OH/0.1 M NH_4NO_3 buffer alone; B, 1×10^{-3} M EDTA in the same buffer; C, 2.5×10^{-3} M EDTA in the same buffer; D, 5×10^{-3} M EDTA in the same buffer. While experiment A is certainly not a titration, because all copper is sensed by the electrode in the absence of EDTA, experiments B, C and D clearly show the increasing influence of a particular concentration of EDTA as the copper(II) concentration decreases. As in all amperometric titrations, the end-point is reached when the limiting current decreases to the level of the background current.

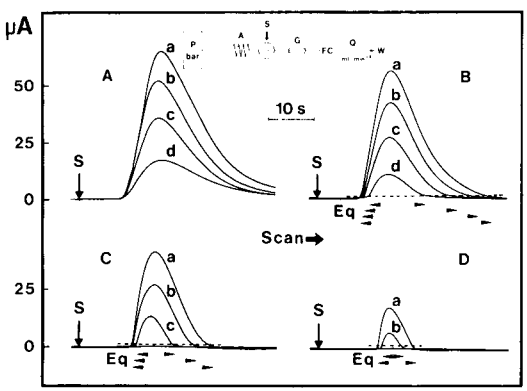

Fig. 5. Flow injection measurement (A) and flow injection amperometric titrations (B, C and D). Concentration of injected Cu(II) solution decreased from a to c and concentration of EDTA in the carrier stream increased from B to D. (For details see text.) In the manifold, G is the gradient tube.

On each flow injection titration curve two such end-points exist [8, 10]. The first is located at the leading edge of the dispersed zone, while the second is located at its tailing section. It is, therefore, the time span between these two points which yields the analytical readout. It has been shown [1, 8] that this equation value increases linearly with the logarithm of the concentration of analyte. This is also true in the present case, as indicated by arrows on Fig. 5, B, C and D. To avoid uncertainty of readout caused by tailing at the base-line level, the time spans were read out at the slightly elevated and arbitarily chosen level indicated by the dotted lines.

Scanning of concentration gradient

It is now well understood that an injected sample zone disperses on the way towards a detector while components of the zone react with the species contained in the carrier stream. So far these phenomena have been monitored by static detectors. Rapid scanning voltammetry of the moving depolarizer solution was discussed above (Fig. 3). Such fast scans can be repeated with a high frequency on a dispersed sample zone and thus the compositions of many elements of the fluid stream can be examined successively. If the starting point of each recording is shifted suitably, a three-dimensional image can be created showing both the voltammogram and the concentration gradient profile simultaneously (Figs. 6—8).

In tests of this approach, the same manifold as in the flow injection titrations (Fig. 5) was used with the same pumping rate and injected sample volume; the copper solution was 1×10^{-2} M. On a single injected zone, 50 scans were repeated within the range of +200 mV to —1.300 mV; each scan lasted for 1.8 s, and was followed by a 0.5-s interval during which the pen (and the potential) returned to the initial point. Thus, each scan was recorded at a sweep rate of 833 mV s^{-1} on a flowing solution. The first curve was recorded with a delay of 19 s after sample zone injection and therefore the scans were recorded only on the descending part of the peak (cf. Fig. 1). Further, it should be noted that the time axis (t) coincided with the concentration axis, thus reflecting the tail section of dispersed sample zone. Figure 6 was obtained in the absence of EDTA in ammoniacal buffer. The three-dimensional recording scan shown in Fig. 7 was obtained with a large excess of EDTA in the carrier stream solution (10^{-2} M EDTA). The experimental conditions were otherwise exactly the same as for the series of scans shown in Fig. 6. As expected, the peaks shifted to more negative potentials because of the strong complexation with EDTA although the stepwise two-electron reduction of copper was preserved. A comparison of the images of Figs. 6 and 7 illustrates clearly the influence of complexation on a voltammetric scan over a wide range of copper concentrations.

There are several reasons why this multiple sweep method on an exponentially descending concentration gradient yields more valuable information than a simple single sweep method. First, this approach can be used for instrument calibration with a single standard solution, instead of preparing

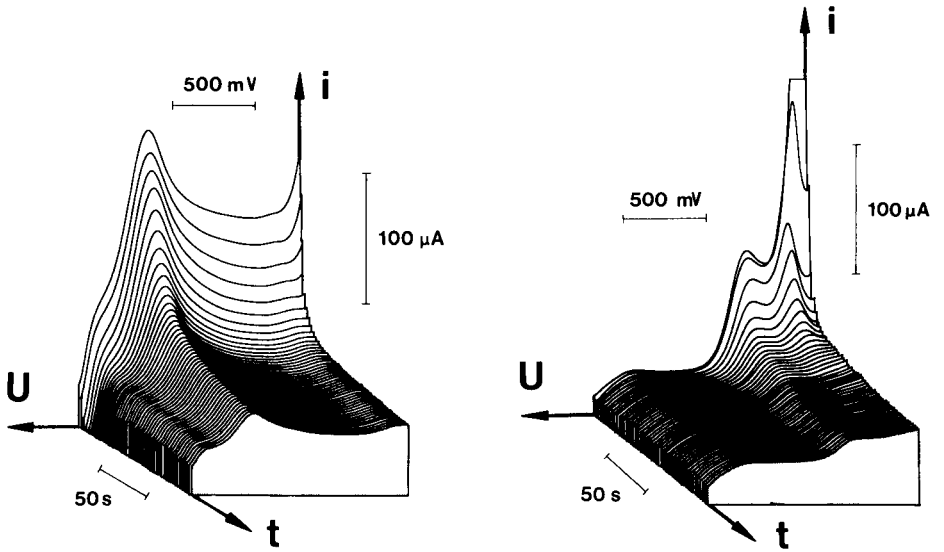

Fig. 6. Successive voltammetric scanning of the descending part of a dispersed zone containing 1×10^{-2} M copper(II) ammine complex. U, positive direction of potential scan: *i*, resulting limiting current; *t*, time (and concentration axis).

Fig. 7. Successive voltammetric scanning of the descending part of a dispersed zone containing copper(II)—EDTA complex. U, *i* and *t* as in Fig. 6.

standards by serial dilution [6]. The next reason may be found by a closer look at Fig. 8, which was recorded using an intermediate concentration of EDTA (5×10^{-4} M EDTA) in the carrier stream. Starting from the farthest curve, recorded in the element of solution containing a large amount of copper(II) ammine complex and a small amount of Cu—EDTA complex, and moving towards the front where an excess of EDTA penetrates into the dispersed tail of the sample zone, one may notice how the peaks at more positive potentials become transformed into peaks at more negative potentials. Though still crude at this stage, this solution-handling technique should be capable of improvement to such an extent that studies of complex formation, electrode kinetics at variable depolarizer concentrations, etc., will be possible on a dispersed continuum of injected solution rather than on separately prepared discrete batches as has been done since polarography began.

The above approach is only one of many possible variants of the flow injection method, where the concentration of a certain species (copper in the above case) can be varied in a reproducible (exponential) manner. Other variable species of interest can also be studied. Thus, if the effect of a change of pH is to be examined, the ammoniacal copper solution can be passed through the system and an acidified copper(II) solution having the same ammonium ion content and the same copper(II) content can be

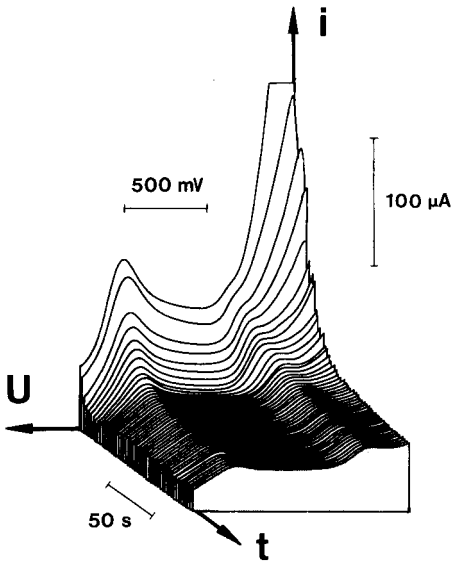

Fig. 8. Successive voltammetric scanning of the descending part of a dispersed zone containing a mixture of copper(II) ammine and EDTA complexes. U, *i* and *t* as in Fig. 6.

injected. Thus, while the copper(II) concentration will remain unchanged, the pH will increase along the *t*-axis during the multiple scanning, yielding easily assimilable information on the complex formation during a pH change.

In this context, the recent paper of Betteridge and Fields [11] on the application of pH gradients in f.i.a. offers interesting reading. Following their earlier work on complex formation at the interface between a carrier stream and an injected sample zone, they outlined possible approaches to complex formation studies using variable concentration gradients monitored by means of a static detector (absorbance at a fixed wavelength). Combination of that approach with the present approach of gradient scanning will obviously expand the applications flow injection analysis outside the field of simple analytical work. In this context, the continuous flow system with a rapid-scanning photodiode-array spectrophotometer designed by Anderson et al. [12] is of interest.

Conclusion

The use of electrochemical detectors in flowing streams has been practised for several decades and there is, therefore, nothing new about the general use of this detector. The justification of this work stems from the realization that by using a well-defined dynamic detector under the rigorous conditions of a flow injection experiment, excellent conditions for doing electrochemical experiments on reaction mixtures can be achieved in a most expeditious manner. Although the present combination has some potential analytical value, as demonstrated in the first half of this paper, the most exciting possibility lies in the use of gradient f.i.a. techniques in conjunction with

modulated electrochemical detectors. In broader terms, the present work outlines future, yet unfathomed, possibilities of scanning spectra along the well defined, perfectly reproducible concentration gradients formed at the interface between a dispersed sample zone and a carrier stream.

The authors express their gratitude to E. H. Hansen for friendly support, to N. Thogersen for programming and skillful assistance, and to C. E. Foverskov for design and construction of vital electronic components (all from Chemistry Department A). This work was supported by the Danish Technical National Science Foundation and partly by the NIGMS Grant Number 22952, which are gratefully acknowledged.

REFERENCES

1 J. Růžička and E. H. Hansen, Flow Injection Analysis, Wiley, New York, 1981.
2 See, e.g., K. Toth, G. Nagy, Z. Fehér, G. Horvai and E. Pungor, Anal. Chim. Acta, 114 (1980) 45.
3 See, e.g., J. V. A. Novak, Continuous Polarographic Analyzers, in P. Zuman and I. M. Kolthoff (Eds.), Progress in Polarography, Wiley, New York, 1962.
4 L. Michel and A. Zatka, Anal. Chim. Acta, 105 (1979) 109.
5 S. J. Lyle and M. I. Salem, Talanta, 28 (1981) 251.
6 J. Růžička, Proceedings of the 1981 Meeting of the Royal Society, London, in press.
7 J. Janata and R. J. Huber, Ion-Selective Electrode Rev., 1 (1979) 31.
8 J. Růžička and E. H. Hansen, Anal. Chim. Acta, 134 (1982) 55.
9 A. J. Bard and L. Faulkner, Electrochemical Methods, Wiley, New York, 1980.
10 A. U. Ramsing, J. Růžička and E. H. Hansen, Anal. Chim. Acta, 129 (1981) 1.
11 D. Betteridge and B. Fields, Anal. Chim. Acta, 132 (1981) 139.
12 L. Anderson, T. Anfält, A. Granéli and N. Strandberg, Anal. Chim. Acta, 109 (1979) 425.

Analytica Chimica Acta, 139 (1982) 117—126
Elsevier Scientific Publishing Company, Amsterdam — Printed in The Netherlands

DETERMINATION OF MOLYBDENUM BY THE CATALYSED PEROXYACETIC ACID—IODIDE—ASCORBIC ACID REACTION

E. LESLIE DICKSON and GYULA SVEHLA*

Department of Analytical Chemistry, The Queen's University, Belfast, Northern Ireland (Gt. Britain)

(Received 17th December 1981)

SUMMARY

A new catalytic method for the determination of 0—10 ppm molybdenum is described. Molybdenum catalyses the peroxyacetic acid—iodide—ascorbic acid Landolt reaction at pH 4.2. The rate is monitored by potentiometry, and results are evaluated from a calibration graph. Optimal conditions for the determination are discussed and interferences are described. The stoichiometry, mechanism and kinetics of both the uncatalysed and the catalysed reactions were investigated, and the rate constants (for 20°C) as well as the entropies and enthalpies of activation of both the uncatalysed and the catalysed reactions are reported.

The advantages associated with the use of Landolt reactions in catalytic analysis are well known [1, 2]. These include not only ease of operation and cheap equipment, but also simplification of the kinetics of reactions involved. Two methods have been suggested for the determination of molybdenum by catalysed Landolt reactions [3, 4] in which the usual monitoring was applied; the hydrogen peroxide—iodide and perborate—iodide reactions were used. The introduction of potentiometric monitoring [5] opens the way not only to automation but to the application of relatively slow reactions which are not feasible with visual measurements. One such reaction is the peroxyacetic acid—iodide reaction, which can be combined with ascorbic acid to form a Landolt system. This Landolt reaction is selectively and sensitively catalysed by traces of molybdenum.

The reaction between peroxyacetic acid and iodide is well known and is often used for the iodimetric determination of peroxyacetic acid [6]. The reaction is rather slow; at the pH value recommended for the determination, it is much slower than the reaction of iodide with hydrogen peroxide. The kinetics of this reaction have not been studied in any detail; Fortnum et al. [7] made only comparative references whereas they treated the reactions with chloride and bromide in detail. In the present investigations, therefore, the kinetics and mechanism were examined in some detail. The catalytic action of molybdenum was also studied, based on the reaction schemes for peroxomolybdate complexes given by Jahr [8].

0003-2670/82/0000-0000/$02.75

EXPERIMENTAL

Reagents

The following reagents were used in the analytical procedure.

Acetate buffer (pH 4.2). This contained 2.51 mol l^{-1} acetic acid and 0.36 mol l^{-1} sodium acetate.

Molybdenum stock solution (1000 ppm). Dissolve 1.8404 g of analytical-grade ammonium molybdate tetrahydrate $[(NH_4)_5Mo_7O_{24}\cdot 4H_2O]$ in water and dilute to 1 l. From this stock, prepare standards containing 2, 4, 6, 8 and 10 ppm by dilution with water. These reagents keep indefinitely.

Ascorbic acid. Standardise an approximately 0.25 mol l^{-1} solution of ascorbic acid against potassium iodate as follows: to 20 ml of 0.083 mol l^{-1} potassium iodate, add 2 g of potassium iodide and 10 ml of 2 mol l^{-1} hydrochloric acid. Titrate the liberated iodine with the ascorbic acid solution until the colour of iodine disappears. Do not use starch or any other indicator. Note the volume (V_A). Prepare this solution daily.

Peroxyacetic acid. Prepare an approximately 0.25 mol l^{-1} solution from the commercial concentrated acid (containing 35—40% active ingredient) by 10—15-fold dilution. The concentrated solution keeps better. Do not use pipettes, as the substance decomposes under reduced pressure. Standardise the solution as follows: dispense 5 ml of the dilute solution from a burette into a small iodine flask. Add 10 ml of glacial acetic acid, 15 ml of chloroform and 1 ml of 1000 ppm molybdenum stock solution, and pass a stream of carbon dioxide over the solution. Now add 2 g of potassium iodide, seal the flask and swirl until all the solid has dissolved. Wait for 1 min and titrate with the 0.25 mol l^{-1} ascorbic acid solution until the colour of iodine disappears from both phases. Note the volume (V_p).

Oxidising reagent. To prepare 100 ml of this reagent, dispense $v = (6.25\ V_A/V_p)$ ml of peroxyacetic acid solution into a 100-ml volumetric flask, and dilute with the acetate buffer to the mark. Prepare daily. The solution contains 0.06 mol l^{-1} peroxyacetic acid.

Reducing reagent. To prepare 100 ml of this reagent, dissolve 3.32 g of potassium iodide in 20 ml of the acetate buffer, add V_A ml of ascorbic acid solution and dilute with the buffer to the mark. Prepare daily. The solution contains 0.02 mol l^{-1} iodide and 0.05 mol l^{-1} ascorbic acid.

Apparatus

A thermostatically controlled potentiometric cell, kept at 20.0 ± 0.2°C is needed. The potential is measured with a bright platinum foil indicator electrode and a saturated calomel electrode, connected to a millivoltmeter, and followed on a chart recorder as a function of time.

Procedure for molybdenum determinations

The following procedure is based on optimization studies [9] concerned with sensitivity, selectivity and precision.

From the sample, prepare a solution containing 0—10 ppm molybdenum in the acetate buffer. Place 5.0 ml of this solution in the cell, add 5.0 ml of reducing reagent, and start stirring and recording the e.m.f. When a steady potential reading is attained, add 5 ml of the oxidising reagent and continue recording. On mixing, some iodine forms but then disappears by reaction with ascorbic acid. On addition of the reagent, the potential changes abruptly, reaches a more or less steady value for a few minutes, and finally decreases, accompanied by liberation of iodine. Typical traces are shown in Fig. 1. After each reaction evacuate the cell, rinse the electrodes and the cell, remove superfluous water and start the next run. A blank test with 5 ml of water (instead of the sample) is made each day.

The calibration graph is obtained by running the 2, 4, 6, 8 and 10 ppm molybdenum standards similarly.

Evaluation. The recorded potentiograms are evaluated as indicated in Fig. 1. The blank reaction time (t_L^0) and the time obtained with a test solution (t_L) may be replaced by the corresponding distances l_L^0 and l_L if constant chart speed is maintained. The t_L^0/t_L (or l_L^0/l_L) values are plotted against molybdenum concentration for the calibration graph. The straight line passes through 1 on the t_L^0/t_L axis, satisfying the equation obtained from theoretical considerations (Eqn. 23, see below). The equation of the line, obtained by linear regression analysis, is $t_L^0/t_L = (0.966 \pm 0.042) + (0.235 \pm 0.007)C_{Mo}$, where C_{Mo} is measured in ppm. The uncertainties around the constants are calculated at the 95% significance level.

It must be mentioned that the plot of reciprocal reaction times ($1/t_L$) vs. molybdenum concentration would also yield a straight line, and according to the law of propagation of errors this would carry lower errors in the final result. However, owing to uncontrollable variations in the concentration of some of the reagents (especially of ascorbic acid and peroxyacetic acid), reaction times (and the slope and intercept of the $^1/t_L$ vs. C_{Mo} lines) tend to vary from day to day, while the t_L^0/t_L vs. C_{Mo} plot is very reproducible. On balance, therefore, the latter plot is recommended.

Procedures for the kinetic study

Concentrations of the reagents were varied as required, but each set of experiments included one test where the initial concentrations of all reagents

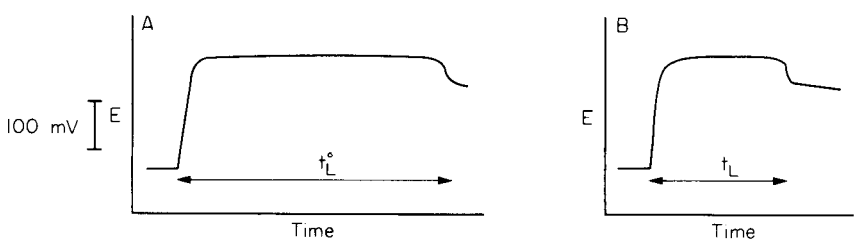

Fig. 1. Potentiometric traces and their evaluation: A, blank; B, 4 ppm Mo.

were the same as in the analytical procedure. Runs with different initial concentrations of all the reagents were made, and from the concentration dependence of reaction times, orders with respect to each reactant were established. Various mechanisms were then postulated and the corresponding rate constants calculated. In the experiments at different temperatures, the initial concentrations were kept constant. Temperatures could be varied only within a very narrow range, because of the danger of decomposition of the peroxyacetic acid at elevated temperatures. It was thought impractical to use very low temperatures and this study was restricted to the 18—29°C range.

RESULTS AND DISCUSSION

Determination of molybdenum

A detailed study of 30 ions enabled their interference on both the uncatalysed and catalysed reactions to be estimated. Each ion was tested at concentration levels of 100, 10, 1 and 0.1 ppm in the absence of molybdenum. From the reaction times measured under these conditions, the ratio t_L^0/t_{LI} was calculated. Results obtained are recorded in Table 1. Obviously the nearer the ratio is to unity, the less pronounced is the catalytic action. Some ten ions interfered with the reaction. Cobalt retarded the reaction while the remaining nine ions accelerated it. Only iron(II) and (III) accelerated it at concentrations of 1 and 0.1 ppm.

A similar survey was done in the presence of molybdenum. The times for molybdenum alone (t_L^{Mo}) were measured in the presence of 4 ppm molybdenum; then the times for 4 ppm molybdenum in the presence of each ion (t_{LI}^{Mo}) were measured. The ratios t_L^{Mo}/t_{LI}^{Mo} were calculated, and are recorded in Table 1. The same ten ions interfered with the reaction under these conditions as in the absence of molybdenum; again only the iron species catalysed the reactions at concentrations of 1 and 0.1 ppm. An attempt was made to suppress these interferences by addition of phosphate ions; 10% (w/v) trisodium phosphate dodecahydrate was introduced into both series of reaction conditions and the ratios were calculated (Table 1). It can be seen that interferences from both forms of iron are suppressed but only that of iron(III) is overcome almost completely at 1 and 0.1 ppm. The presence of trisodium phosphate increases the pH of the reaction. Attempts were made to reduce the effect by using hydrochloric acid but this seriously interfered with the parent reaction and the higher pH did not seem to disrupt the reaction. Concentrations of phosphate higher than 10% also interfered with the stability of the reaction.

When the method is used in practice, matrix effects should be investigated. Table 1 will provide a useful guideline from which to start, but cumulative catalytic effects may occur; these were not investigated systematically here.

Study of reaction kinetics

A study of the stoichiometry, mechanism and kinetics of chemical reactions on which a catalytic method is based, is essential, for it reveals the

TABLE 1

Effect of various ions on the uncatalysed and catalysed reactions ($CH_3COO.OH/I^-$) expressed by the t^0_L/t_{LI} and t^{Mo}_L/t^{Mo}_{LI} ratios, respectively

Ion	t^0_L/t_{LI} ratio at concn. of				t^{Mo}_L/t^{Mo}_{LI} ratio at concn. of			
	100 ppm	10 ppm	1 ppm	0.1 ppm	100 ppm	10 ppm	1 ppm	0.1 ppm
Ag^+	0.97				0.95			
Al^{3+}	1.00				1.02			
Au^{3+}	0.97				1.05			
Ba^{2+}	1.05				1.05			
Ca^{2+}	0.99				0.98			
Cd^{2+}	0.95				0.95			
Ce^{3+}	1.01				0.99			
Co^{2+}	<0.35	0.66	0.93	1.02	0.33	0.61	0.95	
Cr^{3+}	1.01				1.05			
Cu^{2+}	3.01	1.23	1.01		2.27	1.15	0.87	
Fe^{2+}	6.19	2.81	1.52	1.13	3.41	2.00	1.37	1.08
Fe^{3+}	6.50	2.68	1.40	1.04	3.66	2.20	1.42	1.58
Hg^{2+}	0.95				1.00			
La^{3+}	0.97				0.99			
Mg^{2+}	0.99				0.95			
Mn^{2+}	1.01				0.95			
Ni^{2+}	0.98				1.02			
Pb^{2+}	1.03				0.98			
Sb^{3+}	0.90	0.90	0.91		0.90	0.96	0.97	
Se(VI)	1.00				0.95			
Sn^{2+}	0.97	0.98			0.69	0.92		
Sn^{4+}	0.94	0.93			0.78	0.89		
Sr^{2+}	0.97				1.05			
Ti^{3+}	1.21	1.16	1.07	1.04	1.07	0.96	0.96	
U(VI)	1.05				1.04			
V(IV)	<0.39	1.27	0.95		0.38	1.04	0.95	
W(VI)	1.05				0.95			
Y^{3+}	0.96				0.98			
Zn^{2+}	0.95				0.99			
Zr(IV)	1.08	1.05			0.99			
In presence of 10% $Na_3PO_4 \cdot 12H_2O$								
Fe^{2+}	1.42	1.75	1.10	1.04			1.29	1.03
Fe^{3+}	2.43	1.17	1.07	1.02	1.88	1.36	0.95	1.02

most important parameters that influence the reaction rates and so the precision of the method. In studying the peroxyacetic acid—iodide reaction, the mechanism was established by measuring reaction rates and rate constants at different temperatures, and by determining the enthalpies and entropies of activation of the reactions involved.

The uncatalysed reaction. The overall stoichiometry of the reactions can be expressed as

$$CH_3COO.OH + C_6H_8O_6 \rightarrow CH_3COOH + C_6H_6O_6 + H_2O \quad (1)$$

Here $C_6H_6O_6$ is dehydroascorbic acid. The reaction rate depends on the first

power of the concentrations of peroxyacetic acid, iodide and hydrogen ions. Accordingly, two bimolecular steps can be postulated

$$CH_3COO.OH + H^+ \rightleftharpoons CH_3COO.OH_2^+ \text{ (fast equilibrium)} \quad (2a)$$

$$CH_3COO.OH_2^+ + I^- \rightarrow CH_3COOH + HIO \quad (3a)$$

In this scheme, the peroxyacetic acid (pK_a = 8.2 [7]) and acetic acid (pK_a = 4.75) are undissociated which is reasonable at pH 4.2 with a high concentration of acetate ions. Protonation of peroxyacetic acid rather than iodide is suggested, as hydrogen iodide is a strong acid. However, kinetically, it is quite feasible that the two bimolecular steps

$$I^- + H^+ \rightleftharpoons HI \text{ (fast equilibrium)} \quad (2b)$$

$$CH_3COO.OH + HI \rightarrow HIO + CH_3COOH \quad (3b)$$

express the true mechanism [10]. Similarly, the following fast steps are kinetically indistinguishable

$$I^- + H^+ \rightleftharpoons HI;\ HI + HIO \rightarrow I_2 + H_2O \quad (4)$$

$$\text{or } HIO + H^+ \rightleftharpoons H_2IO^+;\ H_2IO^+ + I^- \rightarrow I_2 + H_2O \quad (5)$$

The final step is the reduction of iodine with ascorbic acid (the Landolt step)

$$I_2 + C_6H_8O_6 \rightarrow 2I^- + C_6H_6O_6 + 2H^+ \quad (6)$$

Addition of Eqns. (2—6) yields the stoichiometry of reaction (1). As long as ascorbic acid is present, formation of iodine is not observed; once the ascorbic acid disappears, iodine is formed. The change is visible, but is most conveniently monitored by potentiometry; a sharp change in the oxidation—reduction potential marks the formation of iodine.

The rate of the uncatalysed reaction can be expressed (from 3a) as

$$(-d[CH_3COO.OH]/dt)_{un} = k'_{un}[CH_3COO.OH_2^+][I^-] \quad (7)$$

By application of the law of mass action to reaction (2a), the concentration of the protonated peroxyacetic acid is given by $[CH_3COO.OH_2^+] = K[CH_3COO.OH][H^+]$, where K is a protonation constant. Combination of this with Eqn. (7) gives the differential rate equation

$$(-d[CH_3COO.OH]/dt)_{un} = k'_{un}K[CH_3COO.OH][H^+][I^-] \quad (8)$$

Thus, the reaction is first order with respect to peroxyacetic acid, iodide and hydrogen ions. This equation can be simplified by considering that, during an experimental run, both the hydrogen and iodide ion concentrations are constant. If these are denoted by C_{H^+} and C_{I^-}, respectively, then

$$(-d[CH_3COO.OH]/dt)_{un} = k'_{un}KC_{H^+}C_{I^-}[CH_3COO.OH] \quad (9)$$

Although it was verified experimentally that the reaction is first order with

respect to hydrogen ions at pH 3.8 and pH 4.6 (the experimental values were 0.97 and 1.18, respectively), this pH range was too narrow for valid conclusions to be drawn. Extending the range was not feasible, because the potentiograms became distorted and precise determination of the reaction times was impossible. Altering the pH changed the ionic strength considerably, making comparison of rate constants difficult. Accordingly, the detailed kinetic studies were limited to pH 4.2, which seemed most useful for analytical purposes. Thus, by introducing the notation $k_{un} = k'_{un}KC_{H^+}$, Eqn. (9) can be simplified to

$$(-\mathrm{d}[CH_3COO.OH]/\mathrm{d}t)_{un} = k_{un}C_{I^-}[CH_3COO.OH] \qquad (10)$$

This equation can be integrated with the boundary condition that at t^0_L reaction time (when the Landolt effect occurs) the concentration of peroxyacetic acid is $[CH_3COO.OH]_{t^0_L} = [CH_3COO.OH]_0 - [C_6H_8O_6]_0$, where subscript 0 refers to zero reaction time (i.e., the time of mixing). Integration and rearrangement then gives

$$k_{un} = (t^0_L C_{I^-})^{-1} \ln \{[CH_3COO.OH]_0/[CH_3COO.OH]_0 - [C_6H_8O_6]_0\} \qquad (11)$$

The validity of this equation was tested by measuring reaction times at constant temperature with different initial concentrations of the reagents. Results are shown in Table 2. The tolerance limits around k_{un} were calculated at 95% level of significance. These results indicate that the above mechanism is feasible.

The values of entropy (ΔS^*_{un}) and enthalpy (ΔH^*_{un}) of activation were also determined. These are defined through the Arrhenius-Eyring equation

$$k = \underline{k}T\,h^{-1} \exp(\Delta S^*/R)\exp(-\Delta H^*/RT) \qquad (12)$$

where k is the rate constant, $\underline{k} = 1.381 \times 10^{-23}$ J K^{-1} the Boltzmann constant, $h = 6.626 \times 10^{-34}$ J the Planck constant, $R = 8.314$ J K^{-1} mol^{-1} the gas constant, and T is the absolute temperature.

Equations (11) and (12) can be combined to the form

$$F(T)_{un} = \Delta S^*_{un} - \Delta H^*_{un}T^{-1} = R \ln\{(t^0_{LT}T)^{-1} \cdot h(C_{I^-}\underline{k})^{-1} \ln([CH_3COO.OH]_0/[CH_3COO.OH]_0 - [C_6H_8O_6]_0)\} \qquad (13)$$

TABLE 2

Kinetic study of the uncatalysed reaction

C_{I^-} (mol l^{-1})	$[CH_3COO.OH]_0$ (mol l^{-1})	$[CH_3COO.OH]_t$ (mol l^{-1})	t (s)	k_{un} (l mol^{-1} s^{-1})
6.626×10^{-2}	2.083×10^{-2}	0.500×10^{-2}	182.4	11.81×10^{-2}
6.216×10^{-2}	1.954×10^{-2}	0.469×10^{-2}	218.4	10.51×10^{-2}
5.848×10^{-2}	1.839×10^{-2}	0.441×10^{-2}	266.4	9.16×10^{-2}
5.522×10^{-2}	1.736×10^{-2}	0.417×10^{-2}	273.4	9.45×10^{-2}
5.234×10^{-2}	1.645×10^{-2}	0.395×10^{-2}	302.4	9.02×10^{-2}
4.971×10^{-2}	1.563×10^{-2}	0.375×10^{-2}	330.4	8.70×10^{-2}

Average $k_{un} = (9.77 \pm 1.23) \times 10^{-2}$

where $F(T)_{un}$ is a temperature function of the uncatalysed reaction, t^0_{LT} is the reaction time measured at temperature T. The points of $F(T)_{un}$ when plotted against T^{-1} lie on a straight line (Fig. 2) with the intercept equal to ΔS^*_{un} and the negative slope equal to ΔH^*_{un}. Results of experiments are recorded in Table 3. The values of ΔS^*_{un} and ΔH^*_{un} are as follows

$\Delta S^*_{un} = -134.59 \pm 15.56$ JK^{-1} mol^{-1}; $\Delta H^*_{un} = (39.38 \pm 4.61) \times 10^3$ kJ mol^{-1}

$\Delta S^*_{cat} = -64.56 \pm 18.90$ JK^{-1} mol^{-1}; $\Delta H^*_{cat} = (32.13 \pm 5.60) \times 10^3$ kJ mol^{-1}

The tolerance limits are given for the 95% level of significance.

The catalysed reaction. The stoichiometry is the same for the catalysed reaction as for the uncatalysed reaction. Initially, molybdenum is oxidised first to monoperoxo- then to diperoxo-molybdate [8]

$$MoO_4^{2-} + CH_3COO.OH \rightleftharpoons MoO_5^{2-} + CH_3COOH; \; MoO_5^{2-} + CH_3COO.OH \rightleftharpoons HMoO_6^- + CH_3COO^-$$

During the catalytic reaction cycle, molybdenum oscillates between these two peroxide states, thus the mechanism of the catalysed reaction may be expressed as the sequence of the following bimolecular steps

$$HMoO_6^- + I^- \rightarrow MoO_5^{2-} + HIO \text{ (slow)} \quad (14)$$

$$MoO_5^{2-} + CH_3COO.OH \rightarrow HMoO_6^- + CH_3COO^- \text{ (fast)} \quad (15)$$

followed by reactions (3—5). The sum of these steps results in the same stoichiometry as that of the uncatalysed reaction (1). As reaction (14) represents the only slow step in the mechanism, the rate of this step may be expressed by

$$(-d[CH_3COO.OH]/dt)_{cat} = k'_{cat}[HMoO_6^-]C_{I^-} \quad (16)$$

In this equation the concentration $[HMoO_6^-]$ is not known. If step (15) is regarded as a true chemical equilibrium then

$$K' = [HMoO_6^-][CH_3COO^-]/[MoO_5^{2-}][CH_3COO.OH] \quad (17)$$

and, provided that all the molybdate is oxidized to MoO_5^{2-} or $HMoO_6^-$, the

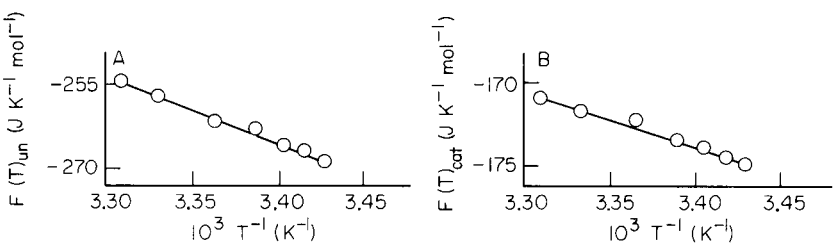

Fig. 2. $F(T)$ vs. T^{-1} lines (Arrhenius plots) for the uncatalysed (A) and catalysed (B) reactions.

TABLE 3

Investigation of the effect of temperature
($[CH_3COO.OH]_0$ = 2.083 × 10^{-2} mol l^{-1}; $[C_6H_8O_6]_0$ = 1.583 × 10^{-2} mol l^{-1}; C_{I^-} = 6.626 × 10^{-2} mol l^{-1}; C_{Mo} = 1.39 × 10^{-5} mol l^{-1})

T (K)	t^0_{LT} (s)	t_{LT} (s)	$F(T)_{un}$ (JK^{-1} mol^{-1})	$F(T)_{cat}$ (JK^{-1} mol^{-1})
291.66	440.4	193.2	−269.8	−174.9
292.66	402.0	182.4	−269.1	−174.5
293.66	384.0	169.2	−268.7	−173.8
295.16	336.0	158.4	−267.7	−173.4
297.16	318.0	139.2	−267.3	−172.3
300.16	265.2	123.6	−265.8	−171.8
302.16	236.4	111.6	−264.9	−171.0

mass balance equation is $C_{Mo} = [MoO_5^{2-}] + [HMoO_6^-]$. Combining this with Eqns. (16) and (17) gives the rate as

$$(-d[CH_3COO.OH]/dt)_{cat} = k'_{cat}K' C_{Mo}[CH_3COO.OH]C_{I^-}/([CH_3COO^-] + K[CH_3COO.OH]) \quad (18)$$

Under the conditions of these experiments, $[CH_3COO^-]$ is constant and large. If k_{cat} is defined as $k_{cat} = k'_{cat}K'/[CH_3COO^-]$, then the rate of the catalysed reaction can be expressed as

$$(-d[CH_3COO.OH]/dt)_{cat} = k_{cat}[CH_3COO.OH]C_{I^-}C_{Mo} \quad (19)$$

It is not possible to examine the catalysed reaction alone experimentally, as under the conditions of the analytical procedure the catalysed and uncatalysed reactions proceed simultaneously, with comparable rates. The overall rate has to be expressed first, from Eqns. (10) and (18)

$$(-d[CH_3COO.OH]/dt) = (-d[CH_3COO.OH]/dt)_{un} + (-d[CH_3COO.OH]/dt)_{cat} = [(k_{un} + k_{cat}C_{Mo})C_{I^-}][CH_3COO.OH] \quad (20)$$

Integration, with the boundary condition that at t_L reaction time $[CH_3COO.OH]_{t_L} = [CH_3COO.OH]_0 - [C_6H_8O_6]_0$, leads to

$$k_{cat} = (C_{Mo}^{-1})\{(t_L C_{I^-})^{-1} \ln([CH_3COO.OH]_0/[CH_3COO.OH]_0 - [C_6H_8O_6]_0) - k_{un}\} \quad (21)$$

This equation was tested by measuring reaction times with different initial concentrations of the reactants (including C_{Mo}). Results are shown in Table 4. The value of k_{cat} (for 20°C) is quoted with tolerance limits taken at the 95% significance level. As all the errors of k_{un} appear also in the value of k_{cat}, the precision of the latter is understandably less than that of the former.

Again, experiments were done at different temperatures, the initial con-

TABLE 4

Kinetic study of the catalysed reaction

C_{I^-} (mol l^{-1})	C_{Mo} (mol l^{-1})	$[CH_3COO.OH]_0$ (mol l^{-1})	$[CH_3COO.OH]_t$ (mol l^{-1})	t (s)	k_{cat} (l^2 mol^{-1} s^{-1})
6.626×10^{-2}	1.390×10^{-5}	2.083×10^{-2}	0.500×10^{-2}	93.0	9.63×10^3
6.216×10^{-2}	1.304×10^{-5}	1.954×10^{-2}	0.496×10^{-2}	112.8	8.11×10^3
5.848×10^{-2}	1.227×10^{-5}	1.839×10^{-2}	0.441×10^{-2}	123.6	8.12×10^3
5.522×10^{-2}	1.158×10^{-5}	1.736×10^{-2}	0.417×10^{-2}	134.4	8.16×10^3
5.234×10^{-2}	1.098×10^{-5}	1.645×10^{-2}	0.395×10^{-2}	140.4	8.78×10^3
4.971×10^{-2}	1.043×10^{-5}	1.563×10^{-2}	0.375×10^{-2}	152.4	8.69×10^3
Average $k_{cat} = (8.58 \pm 0.62) \times 10^3$					

centrations of the reactants being kept the same. Evaluation was based on the equation

$$F(T)_{cat} = \Delta S^*_{cat} + \Delta H^*_{cat} T^{-1} = R \ln \{h(\underline{k} C_{Mo} T)^{-1} [(t_{LT} C_{I^-})^{-1}$$
$$\ln ([CH_3.COO.OH]_0 / [CH_3COO.OH]_0 - [C_6H_8O_6]_0)$$
$$- \underline{k} T h^{-1} \exp (\Delta S^*_{un} R^{-1}) \exp (-\Delta H^*_{un} (RT)^{-1})]\} \quad (22)$$

which results from the combination of Eqns. (12) and (21). The $F(T)_{cat}$ vs. T^{-1} plot is shown in Fig. 2. Table 3 contains the experimental values for all the temperature experiments. Values of ΔS^*_{cat} and ΔH^*_{cat} are reported with tolerance limits at the 95% significance level.

The equation of the calibration graph can be derived from Eqns. (11) and (21)

$$t^0_L / t_L = 1 + k_{cat} C_{Mo} / k_{un} = 1 + a\, C_{Mo} \quad (23)$$

Thus, the theory predicts a linear calibration graph with an intercept of unity, and is confirmed by the calibration graph obtained (see Experimental), which indicates also that the described mechanism is feasible.

E. L. Dickson thanks the Department of Agriculture, Government of Northern Ireland, for financial assistance towards this project.

REFERENCES

1 G. Svehla. Analyst, 94 (1969) 513.
2 G. Svehla and L. Erdey, Microchem. J., 7 (1963) 206.
3 G. Svehla and L. Erdey, Microchem. J., 7 (1963) 221.
4 H. Thompson and G. Svehla, Fresenius Z. Anal. Chem., 247 (1969) 244.
5 E. L. Dickson and G. Svehla, Microchem. J., 24 (1979) 509.
6 D. Swern, Jr., Organic Peroxides, Vol. 1, Wiley—Interscience, New York, 1970, p. 498.
7 D. H. Fortnum, C. J. Battaglia, S. R. Cohen and J. O. Edwards, J. Am. Chem. Soc., 82 (1960) 778.
8 K. F. Jahr, Peroxyverbindungen, Fiat Review of German Science, Part III, Office of Military Government of Germany, Wiesboden, 1948, pp. 170—191.
9 E. L. Dickson, Ph.D Thesis, Queen's University, Belfast, 1981.
10 D. Benson, Mechanisms of Inorganic Reactions in Solution, McGraw-Hill, London, 1968, p. 7.

Analytica Chimica Acta, 139 (1982) 127—132
Elsevier Scientific Publishing Company, Amsterdam — Printed in The Netherlands

AMPEROMETRIC DETERMINATION OF TOTAL CHOLESTEROL IN SERUM WITH USE OF IMMOBILIZED CHOLESTEROL ESTERASE AND CHOLESTEROL OXIDASE

ISAO KARUBE*, KENJI HARA, HIDEAKI MATSUOKA and SHUICHI SUZUKI

Research Laboratory of Resources Utilization, Tokyo Institute of Technology, Nagatsuta-cho, Midori-ku, Yokohama 227 (Japan)

(Received 5th January 1982)

SUMMARY

Cholesterol esterase and cholesterol oxidase were immobilized on octyl-agarose gel, activated with cyanogen bromide and placed in a reactor. The sensor system for total cholesterol was assembled with the immobilized enzyme reactor, a hydrogen peroxide electrode and a peristaltic pump. Characteristics of the sensor system were investigated by using cholesterol palmitate as a standard substrate. A linear relationship was obtained between peak current and cholesterol palmitate concentration below 1000 mg dl^{-1} (10.3 mM). A 10-μl sample could be assayed in 5 min. Total cholesterol in human serum was determined in the range 100—400 mg dl^{-1}. The standard deviation for the determination of 50 samples of 300 mg dl^{-1} was 6 mg dl^{-1} (2%). The system was used for 300 assays without loss of enzymatic activity. The correlation coefficient was 0.94 for 27 samples of human sera analyzed by the system proposed and by the conventional chemical method.

Total cholesterol in serum is an important indicator of abnormality in lipid metabolism, arteriosclerosis and hypertension. Conventional assay methods for total cholesterol are based on spectrophotometry; for example, cholesterol is oxidized with iron(III) chloride in the presence of acetate and concentrated sulfuric acid to form a colored compound [1, 2]. An enzymatic method based on cholesterol esterase and cholesterol oxidase has been proposed. The hydrogen peroxide produced by the enzymatic reaction is treated with phenol and 4-aminoantipyrine to form a red derivative [3, 4].

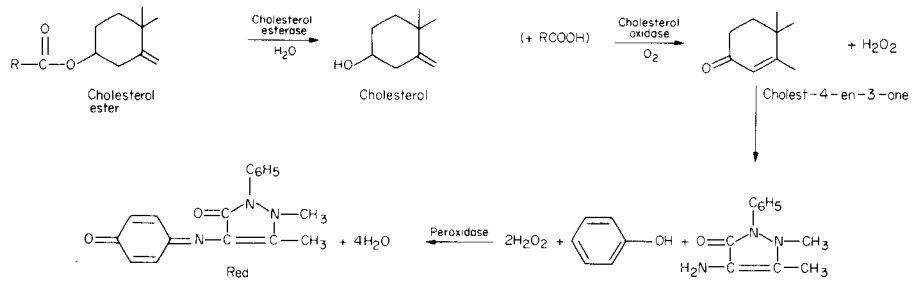

These methods, however, involve complicated and delicate procedures. Assay times are rather long because of the multi-step reactions, and the cost is high

because expensive enzymes must be used in each assay. The development of simple inexpensive assays is important for the determination of total cholesterol in clinical samples. Immobilized enzyme reactors have been used for cholesterol assays with cholesterol oxidase and a thermistor detector [5], and with cholesterol esterase and oxidase and an amperometric detector [6].

Other bioelectrochemical measurement systems with immobilized enzymes have been applied for water-immiscible substrates such as phospholipids [7] or neutral lipids [8]. In the presence of detergents, the enzymes immobilized on a hydrophobic carrier showed good performance. In this paper, a novel bioelectrochemical system for total cholesterol is described, based on the double-enzymatic method described above. An immobilized enzyme reactor containing cholesterol esterase and cholesterol oxidase is coupled with an amperometric detector system. The sensor system is applied to the determination of total cholesterol in human sera. The characteristics of the system are discussed.

EXPERIMENTAL

Materials

The enzymes were cholesterol oxidase (E.C. 1.1.3.6; 3.4 I.U. mg^{-1}; Boehringer Mannheim Yamanouchi Co.), cholesterol esterase (E.C. 3.1.1.13; 1.4 I.U. mg^{-1}; Amano Pharmaceutical Co.) and peroxidase (horseradish, 100 purpurogallin units (P.U.) mg^{-1}; Tokyo Kasei Co.). Triton X-100 (Wako Pure Chemicals and agarose gel (octyl-Sepharose CL-4B; Pharmacia Fine Chemicals) were also used. Cholesterol (Wako Pure Chemicals) and cholesterol palmitate (Nakarai Chemicals) were recrystallized from ethanol and isopropyl alcohol, respectively.

Coupling of enzymes to agarose gel. Agarose gel (octyl-Sepharose CL-4B) was activated with cyanogen bromide [3]. A 1-g portion of the activated gel was added to 1 ml of a phosphate buffer (pH 7.0, 0.05 M) containing 2.0 mg of cholesterol esterase or 10 mg of cholesterol oxidase. After incubation at 4° C for 12 h with stirring, the gel was washed with 0.1 M sodium chloride solution and the phosphate buffer. These immobilized enzymes were stored at 4° C.

Assay of cholesterol oxidase. The activity of cholesterol oxidase was determined spectrophotometrically. An 0.1-ml aliquot of ethanol containing 0.1 mg of cholesterol was added to 3 ml of phosphate buffer solution (pH 6.5, 0.05 M) containing 4-aminoantipyrine (158 mg l^{-1}) phenol (146 mg l^{-1}), peroxidase (10 mg l^{-1}, 100 P.U. l^{-1}) and Triton X-100 (5 ml l^{-1}). A 50-μl aliquot of cholesterol esterase solution (20 mg in 1 ml of the phosphate buffer, pH 6.5) was added to the reaction solution and the mixture was incubated at 37° C. The enzyme activity was estimated from the rate of absorbance increase at 500 nm. The activity of the immobilized oxidase was determined in a similar manner. After incubation of the reaction solution with the immobilized enzyme (0.1 g of agarose gel) at 37 °C for 10 min, the immobilized enzyme was removed by filtration, before measurement at 500 nm, as above.

Assay of cholesterol esterase. The activity of cholesterol esterase was determined by a method developed from that for cholesterol oxidase. An 0.1-ml aliquot of isopropyl alcohol containing 0.1 mg of cholesterol palmitate was added to 3 ml of the same reaction solution described above, containing 50 μl of the cholesterol solution. A 50-μl aliquot of cholesterol esterase solution (20 mg in 1 ml of phosphate buffer solution, pH 6.5, 0.05 M) was added to the reaction solution and the mixture incubated at 37°C. The activity of the enzyme was estimated from the rate of absorbance increase at 500 nm, as described above. The activity of immobilized cholesterol esterase was determined as above, in a similar manner to that for immobilized cholesterol oxidase.

Determination of total cholesterol in serum by the chemical method. Total cholesterol in serum was determined with a cholesterol test kit (Wako Pure Chemicals). An aliquot of serum was added to an iron(III) chloride—acetic acid solution. Concentrated sulfuric acid was added and the red product was measured spectrophotometrically at 550 nm.

Enzyme reactor and procedure for cholesterol determination

A hydrogen peroxide electrode, as shown in Fig. 1, was inserted into the flow line of the continuous assay system used in a previous paper [5]. The hydrogen peroxide liberated by the enzyme reactions was monitored with an

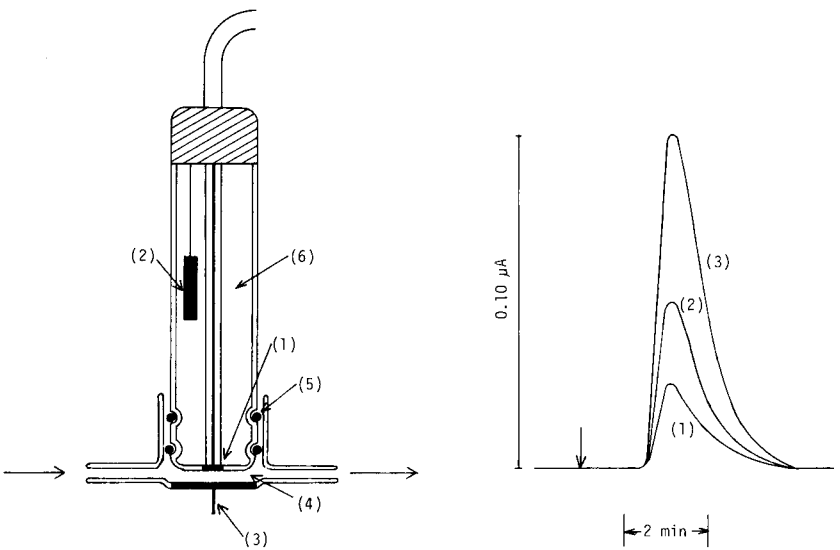

Fig. 1. Schematic diagram of the hydrogen peroxide electrode: (1) Pt anode; (2) SCE; (3) Pt cathode; (4) electrode cell (10 mm × 1 mm diameter); (5) O-ring.

Fig. 2. Response curves. At the arrow, 10 μl of cholesterol palmitate solution containing 5% (w/v) Triton X-100 (pH 8.0) was injected. Flow rate 1.0 ml min^{-1}; 37° C. Cholesterol palmitate concentration: (1) 162, (2) 323, (3) 646 mg dl^{-1}.

amperometric system (Model HA-101, Hokuto Denko Co., Tokyo) based on a platinum electrode (3 mm^2) at 0.60 V vs. SCE. The counter electrode was platinum (78 mm^2). The signal obtained was displayed on a recorder. The immobilized cholesterol esterase (1 g of gel) and the immobilized cholesterol oxidase (0.5 g of gel) were placed in that order in a glass reactor (6 mm i.d., 5.3 cm long) before the electrode cell. The volume of the electrode cell for the determination of hydrogen peroxide was ca. 0.2 ml.

The phosphate buffer (pH 8.0, 0.05 M 5% Triton X-100) was transferred continuously to the system by a peristaltic pump (Model SJ-1121, Mitsumi Scientific Ind.). After the output current reached a steady state, a 10-μl aliquot of cholesterol palmitate in isopropyl alcohol or of human serum was injected into the system and the current changes were recorded. Total cholesterol was estimated from the peak current by using a calibration graph prepared from the results obtained with standard cholesterol palmitate solutions.

RESULTS AND DISCUSSION

Immobilization of enzymes

Table 1 shows the amount of enzymes bound and the specific activities of the free and immobilized enzymes. The concentration of total cholesterol in human serum is about 3 mM, so that 10 μl of serum contains about 0.03 nmol of total cholesterol. The flow rate of the buffer was adjusted to 1.0 ml min^{-1}. The volume of the immobilized enzyme reactor was 1.5 ml, so that it took about 1.5 min for the injected sample to pass through the reactor. The reactor contained 1 g of immobilized cholesterol esterase (0.7 I.U.) and 0.5 g of immobilized cholesterol oxidase (0.19 I.U.). These enzyme activities were sufficiently high for reaction of all cholesterol derivatives in serum.

Response of the system

Typical response curves at various concentrations of cholesterol palmitate are shown in Fig. 2. The peak current increased with increasing choles-

TABLE 1

Activity of free and immobilized enzymes

	Amount of enzyme bound (mg g^{-1})	Activity (I.U. mg^{-1})
Free		
Cholesterol esterase	—	3.4
Cholesterol oxidase	—	1.4
Immobilized		
Cholesterol esterase	7.2[a]	0.70a
Cholesterol oxidase	1.6[a]	0.37[a]

[a]Wet gel.

terol palmitate concentration below 1000 mg dl^{-1}. As shown in Fig. 2, one sample could be assayed in 5 min.

Figure 3 shows the effect of the buffer flow rate on the current. At higher flow rates, the current decreased with increasing flow rate because of incomplete hydrolysis of cholesterol palmitate. A decrease of the flow rate below 0.8 ml min^{-1} also decreased the peak current, because of dilution of the hydrogen peroxide produced by the enzymatic reaction. On the basis of these results, the flow rate was adjusted to 1.0 ml min^{-1} in all further experiments.

Effect of pH, temperature and detergent

To optimize the system, the effects of pH, temperature and detergent were investigated. Figure 4 shows the effect of pH on the current. The optimum pH was 6—7 for the free enzymes, and 8 for immobilized enzymes. This might be attributed to acidification of the microenvironment around the immobilized enzymes by the generation of organic acids. Subsequent work was done at pH 8.0 because the pH of sera is about this value.

The effect of temperature is shown in Fig. 5. The peak current increased with rising temperature up to 43°C. Subsequent experiments were done at 37°C, because human serum was used.

Because Triton X-100 may play an important role in the activity of enzymes (e.g., stabilization of micelles), the effect of Triton X-100 concentration was examined. Free enzymes were easily inactivated with the concentrated detergent. However, the immobilized enzymes were stable and the current increased with increasing detergent concentration, becoming almost constant above 5% Triton X-100, as shown in Fig. 6. Subsequent studies were done with 5% Triton X-100.

Calibration for flow analysis

Human serum was diluted and examined in the system. The concentration of cholesterol in the samples was also determined with the cholesterol

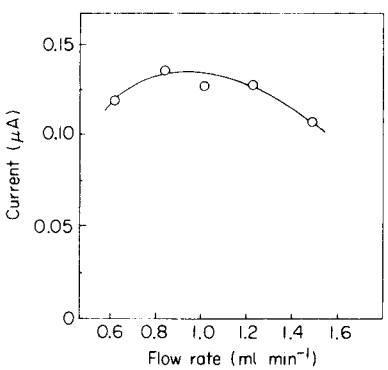

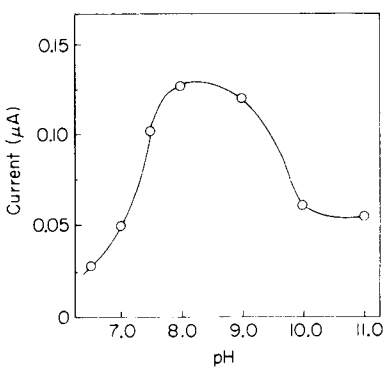

Fig. 3. Effect of flow rate on the peak current; 10 μl of cholesterol palmitate (970 mg dl^{-1}), 5% Triton X-100, pH 8.0, 37°C.

Fig. 4. Effect of pH on the peak current. Conditions as in Fig. 3 except for flow rate (1.0 ml min^{-1}) and pH.

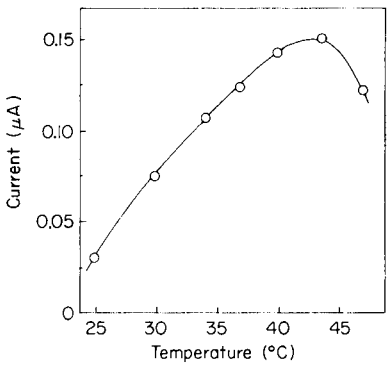

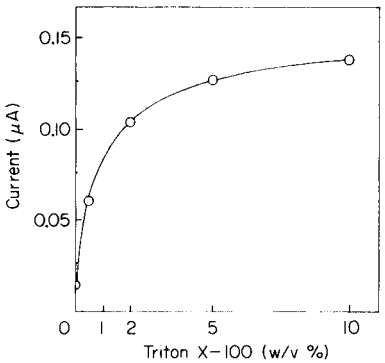

Fig. 5. Effect of temperature on the peak current. Conditions as in Fig. 3 except for temperature and flow rate (1.0 ml min^{-1}).

Fig. 6. Effect of Triton X-100 concentration on the peak current. Conditions as in Fig. 3 except for flow rate (1.0 ml min^{-1}) and Triton X-100.

test kit. A linear relationship was obtained between the peak current and the cholesterol concentration in the range 100—400 mg dl^{-1}; a 200-mg dl^{-1} sample gave a current of 0.05 μA. The standard deviation for the determination of 300 mg dl^{-1} cholesterol was 6 mg dl^{-1} (2%, 50 experiments). Since human serum contains less than 400 mg dl^{-1} of cholesterol, the flow system can be applied for such determinations.

The activity of the immobilized enzymes was retained for at least one month at 4°C. No appreciable decrease of their activity was observed after 300 continual assays. Thus the various components presented in serum had no interfering effects on the sensor.

Comparison of the bioelectrochemical method with a conventional chemical method

Total cholesterol in human sera was assayed by the chemical method and the present system. The correlation coefficient was 0.94 for 27 samples. Therefore, the present system is applicable to a rapid determination of total cholesterol in human sera. When the free cholesterol sensor described previously [8] and the system proposed here are used, the determination of cholesterol esters in sera is also possible.

REFERENCES

1 B. Zak, Am. J. Clin. Path., 27 (1957) 583.
2 B. Zak and R. C. Dickmann, Am. J. Clin. Path., 24 (1954) 1307.
3 C. C. Allain, Clin. Chim. Acta, 20 (1974) 470.
4 M. Takayama, S. Itoh, T. Nagasaki and I. Tanimizu, Clin. Chim. Acta, 79 (1977) 93.
5 B. Mattiasson, B. Danielsson and K. Mosbach, Anal. Lett., 9 (1976) 867.
6 H. Huang, S. S. Kuan and G. G. Guilbault, Clin. Chem., 23 (1977) 671.
7 I. Karube, K. Hara, I. Satoh and S. Suzuki, Anal. Chim. Acta, 106 (1979) 243.
8 I. Satoh, I. Karube, S. Suzuki and K. Aikawa, Anal. Chim. Acta, 105 (1979) 429.

Analytica Chimica Acta, 139 (1982) 133—142
Elsevier Scientific Publishing Company, Amsterdam — Printed in The Netherlands

POLAROGRAPHIC DETERMINATION OF PENICILLOIC ACID IN PENICILLIN PREPARATIONS WITH A FLOW-INJECTION SYSTEM

ULF FORSMAN* and ANDERS KARLSSON

Department of Analytical Chemistry, University of Uppsala, P.O. Box 531, S-751 21 Uppsala (Sweden)

(Received 11th January 1982)

SUMMARY

A flow-injection method for the determination of the penicilloic acid content of benzylpenicillin, phenoxymethylpenicillin, ampicillin, cloxacillin and carbenicillin is described. The penicilloate is detected polarographically at a dropping mercury flow-through detector mounted on a conventional polarographic capillary. A constant potential of +0.04 V vs. SCE is applied and the current is measured in the sampled direct current mode. A pH 9.2 borate buffer containing 0.05% Triton X-100 is used. Triton displaces the reduction wave of oxygen about 400 mV towards negative potentials so that deaeration is not necessary. The penicilloate gives linear calibration graphs for 2×10^{-6} — 1×10^{-4} M solutions. The relative standard deviation for 10 injections of a 5×10^{-5} M solution is 0.2%. Results for the determination of penicilloate in the presence of large amounts of penicillin (the latter in 10—1000-fold excess) are compared with results obtained by two titrimetric procedures.

Penicilloic acid is found in most penicillin preparations as an impurity. The content of penicilloate varies greatly between different penicillins and values between 0.1 and 10% may be found. Since degradation of the penicillin produces penicilloic acid, determination of this product gives much information concerning the stability and purity of the penicillin. Penicilloic acid is at present most often determined by iodimetric [1] or mercurimetric [2] titrations, where its content is obtained merely as a blank value in the determination of the intact penicillin. Penicilloic acid gives rise to an anodic polarographic wave at a dropping mercury electrode [3]. The strong interaction between penicilloic acid and mercury involves oxidation of the electrode material with formation of a mercury complex. Intact penicillin is polarographically inactive, so that a polarographic determination of penicilloate in penicillins becomes possible.

In connection with different flow systems, mercury-based detectors have become increasingly employed [4, 5]. Constructions based on dropping [6] and stationary [7] mercury electrodes have been proposed. In the work reported here, the detector was constructed according to the general principles of the PAR Model 310 polarographic detector, and the detector was mounted on an ordinary dropping mercury capillary. The flow-injection

0003-2670/82/0000-0000/$02.75

determination of penicilloic acid, both in pure form and in the presence of large amounts of penicillin, is evaluated.

EXPERIMENTAL

Apparatus

A PAR-174 polarographic analyzer and a PAR-174/70 drop-timer were used with a Radiometer REC51 X-t recorder. The sampling period of the PAR instrument was modified to 20 ms in order to improve discrimination against 50-Hz noise. The reference electrode was a saturated calomel electrode with a diaphragm tube containing the buffer solution. All potentials given are referred to this electrode. The auxiliary electrode was a platinum wire. All experiments were done at room temperature. The sampled d.c. mode was used throughout. A constant potential of +0.04 V was used unless otherwise stated. When potential-scan voltammograms were recorded, a scan rate of 5 mV s^{-1} and a drop time of 1 s were used.

The flow-injection system. A peristaltic pump (Stålprodukter, Uppsala, Sweden) with a home-made pulse dampener consisting of two cylinders of large volume was used. The injection valve had a sample volume of 30 µl, and was provided with a bypass between the inlet and outlet streams (Bifok FIA-05). The carrier stream was pumped via the injection valve to the detector through 0.5-mm (i.d.) teflon tubing. The length of the tube between injection and detection was 100 cm. With the flow rate employed, 1.0 ml min^{-1}, the dispersion of the system was 5; dispersion is defined according to Růžička and Hansen [8].

The polarographic detector. The detector housing (Fig. 1) was constructed from teflon and was mounted on a capillary immersed in a PAR-G165 flow cell. The flow stream meets the mercury drop in the opposite direction to the mercury flow, and then passes out into the bulk solution of the flow cell. The mercury drops fall out through the oval holes on the side of the teflon body, and are collected at the bottom of the flow cell. The distance between the capillary tip and the flow outlet is about 1 mm. A drain for both mercury and carrier solution ensures a constant level of solution in the flow cell. Auxiliary and reference electrodes were placed in the bulk solution. This principle for a polarographic detector was first introduced by E. G. and G. Princeton Applied Research for use with the static mercury electrode, but is here applied to conventional polarographic equipment.

A mercury column height of 48 cm which gives a mass flow of 1.74 mg s^{-1} was used throughout. This results in electrode areas of 0.8 and 1.2 mm^2 for 0.5 and 1 s drop times, respectively.

Samples and reagents

Benzylpenicillin, ampicillin, cloxacillin, carbenicillin and phenoxymethylpenicillin (ASTRA Pharmaceuticals, Sweden) were used. Penicilloic acid was produced by alkaline hydrolysis of the penicillin as described previously [3]. Borate buffer pH 9.2 was 0.01 M in disodium tetraborate-10-hydrate and 0.1

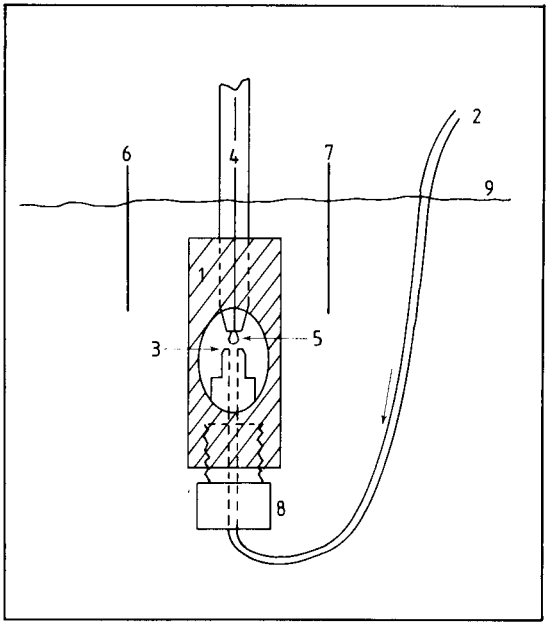

Fig. 1. The detector unit. (1) Teflon body; (2) flow inlet; (3) flow outlet; (4) capillary connected to drop timer; (5) mercury drop; (6) reference electrode; (7) auxiliary electrode; (8) tube fitting; (9) electrolyte level.

M in potassium nitrate. This buffer was chosen because the polarographic behaviour of benzylpenicilloic acid is well defined at this pH whereas it is more complicated in neutral and acidic media [3]. Mercury was of double-distilled quality (Kebo). Triton X-100 (Sigma) was added to the buffers as a surface-active agent. The sample solutions were always diluted with buffer solution of the same Triton content as the carrier stream.

When the penicilloic acid contents of penicillin preparations were determined, penicillin solutions in the concentration range 0.1—1.0 mg ml^{-1} were used. The calibration curve was always constructed from the penicilloate of the penicillin under investigation. When the standard addition technique was used, a second penicillin sample was dissolved in buffer containing the penicilloic acid standard solution. The iodimetric and mercurimetric titrations were done by ASTRA Läkemedel, Södertälje, Sweden.

RESULTS AND DISCUSSION

Polarographic behaviour under flowing solution conditions

The current—potential relations of benzylpenicilloic acid (BPA) solutions and the pure buffer were investigated under flowing solution conditions, by pumping the solutions continuously past the detector. The oxygen wave of the non-deaerated buffer is clearly seen (Fig. 2A). At about +0.1 V, the anodic current rises sharply because of oxidation of mercury.

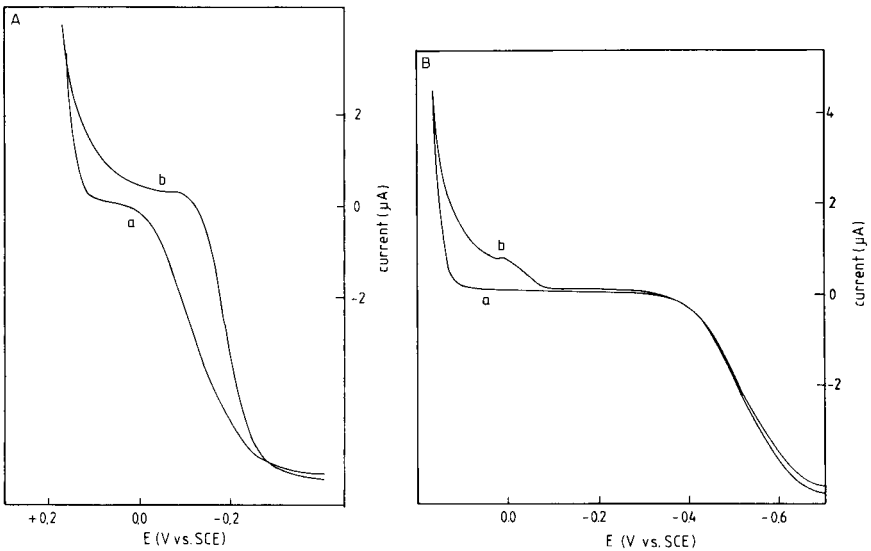

Fig. 2. (A) Polarograms of (a) pH 9.2 buffer, and (b) with 10^{-4} M BPA added. (B) Polarograms of (a) pH 9.2 buffer containing 0.05% Triton X-100, and (b) with 10^{-4} M BPA added. Anodic current is denoted as positive.

It was shown earlier [3] that, in a quiet solution, the anodic wave of BPA is situated at −0.25 V at pH 9.2; the product of the electrode reaction is strongly adsorbed at the mercury surface. In the flow system, this adsorption displaces the oxygen wave in the negative direction. The penicilloate and oxygen waves then overlap (Fig. 2A, curve b).

Addition of Triton X-100 to the buffer solution drastically changes the situation. Figure 2B shows polarograms of the buffer and of 10^{-4} M BPA when 0.05% Triton is present. The oxygen wave is displaced almost 400 mV in the negative direction. Whereas the anodic wave of BPA is displaced about 200 mV in the positive direction and can be seen as a separate wave. The small hump seen on the diffusion plateau is probably due to adsorption effects at this high concentration level, because it disappears at lower concentrations. The half-wave potential of the oxygen wave is easily displaced towards negative potentials by surface-active agents. When Triton X-100 is used, the penicilloate reaction product no longer influences the position of the oxygen wave.

In the absence of Triton, at potentials between the oxygen wave and the background oxidation of mercury, the main contribution to the background is the charging current for the growing mercury surface. Because dA/dt diminishes with time, increased backgrounds accompany shorter drop times. The presence of Triton reduces the charging current and eliminates cathodic background current from reduction of oxygen as stated above. Thus a background level of less than 10 nA at +0.04 V with a noise of ±0.2—0.5 nA is typically recorded.

Flow injection under constant potential conditions

When an injected sample is monitored at the mercury electrode held at a constant potential, the peak obtained is represented by current steps, the number of which depends on the number of mercury drops during passage of the sample zone. According to the PAR Model 310 service manual, a representative peak profile requires at least 10 drops. Peaks obtained after injection of 5×10^{-5} M BPA with 0.5- and 1-s drop times are shown in Fig. 3. In flow injection, the parameter of main interest is the peak height of the signal; the maximum must therefore be sufficiently well defined. With a 0.5-s droptime, 10 drops were employed to achieve the peak value, and with a 1-s droptime, 6 drops were used. Comparison of the relative standard deviations (r.s.d.) of the peak heights obtained with the two drop times showed no significant difference; 10 injections of 5×10^{-5} M BPA gave r.s.d. of 0.2 and 0.3% for 1- and 0.5-s drop times, respectively. Thus it can be concluded that 6 drops is quite sufficient to define the essential parts of the peak. Figure 3 also shows that the current response was higher when the drop time was 1 s. This is, of course, due to the larger drop area. This drop time also gave a lower background level and seems therefore to be the most advantageous. With a 2-s drop time, the peak heights were less reproducible.

The sample hold-up time was 29 s, calculated from the time of injection to when the current had decreased to 1% of its maximum value. This gives a theoretical throughput of 120 samples per hour.

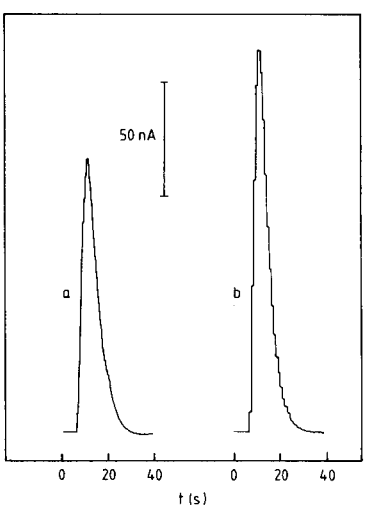

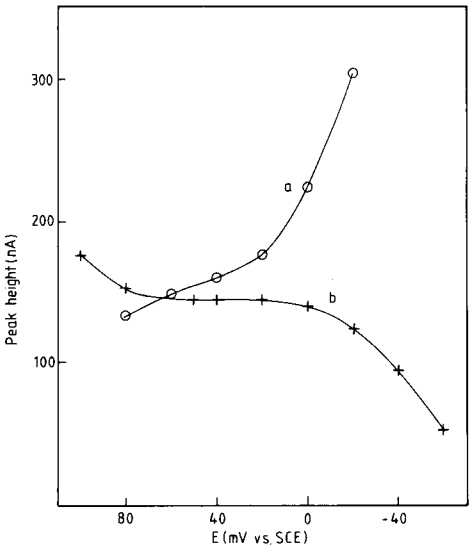

Fig. 3. Flow-injection peaks of 5×10^{-5} M BPA in presence of 0.05% Triton X-100: (a) 0.5 s and (b) 1 s drop time.

Fig. 4. Flow-injection peak height as a function of potential for (a) 6×10^{-5} M BPA; (b) 6×10^{-5} M BPA in presence of 0.05% Triton X-100.

The peak height, i_p, of the flow-injection peak was recorded with different potentials applied to the detector. In the absence of Triton, i_p changes continuously with potential (Fig. 4, curve a). Furthermore, i_p rises drastically at more negative potentials, because of displacement of the oxygen wave by adsorption of the electrode reaction product. This displacement alters the background current in the anodic direction as the sample passes the detector, and therefore contributes to the peak height recorded. In the presence of Triton, the oxygen wave has no effect and i_p changes with potential, similarly to an ordinary polarographic wave (Fig. 4, curve b). The potential of +0.04 V lies on the plateau of the curve and was therefore chosen for the flow-injection determination of the penicilloic acid. The use of Triton is obviously important in decreasing the non-faradaic contributions to the peak height obtained from adsorption of the electrode reaction product.

No deaeration of the solutions is necessary. This is advantageous because efficient elimination of oxygen in a flow system requires exhaustive deaeration of all solutions as well as extensive precautions to avoid diffusion of oxygen through the tubing, etc., into the system [9]. Of course, care must be taken to prevent air bubbles entering the system, because such bubbles may alter the flow pattern.

Effect of flow rate

Figure 5 shows the influence of solution flow rate on the current response. A 1×10^{-5} M BPA solution containing 0.05%. Triton X-100 was continuously pumped and polarograms were recorded; the limiting current, i_l, was then evaluated at +0.04 V. Increased mass transport to the electrode at the higher flow rates obviously increases the limiting current. The effect is less pronounced at the lowest flow rates, suggesting that the current here is still mainly diffusion-controlled. It should be noted that very low flow rates may be employed without the mercury drop coming in contact with the surrounding solution in the flow cell. Only at a flow rate of 0.17 ml min^{-1}, combined with a large distance ($\geqslant$1.5 mm) between the capillary tip and the flow outlet, was interference observed from the bulk solution.

Other penicilloates

Polarograms obtained from potential scans during continuous pumping of solutions of hydrolysed ampicillin, cloxacillin, carbenicillin and phenoxymethylpenicillin are shown in Fig. 6. All penicilloates gave rise to an anodic wave, though small differences in $E_{1/2}$ and wave shape were observed.

The flow-injection method gave linear calibration curves intersecting the origin for 2×10^{-6}—1×10^{-4} M solutions of all the penicilloates examined. The sensitivity for the penicilloates was about 3 μA mM^{-1} with small differences between the penicillins. This overall sensitivity will, of course, change with different dispersion in the flow-injection system. At concentrations above 1×10^{-4} M, the slope of the calibration graph slowly decreased,

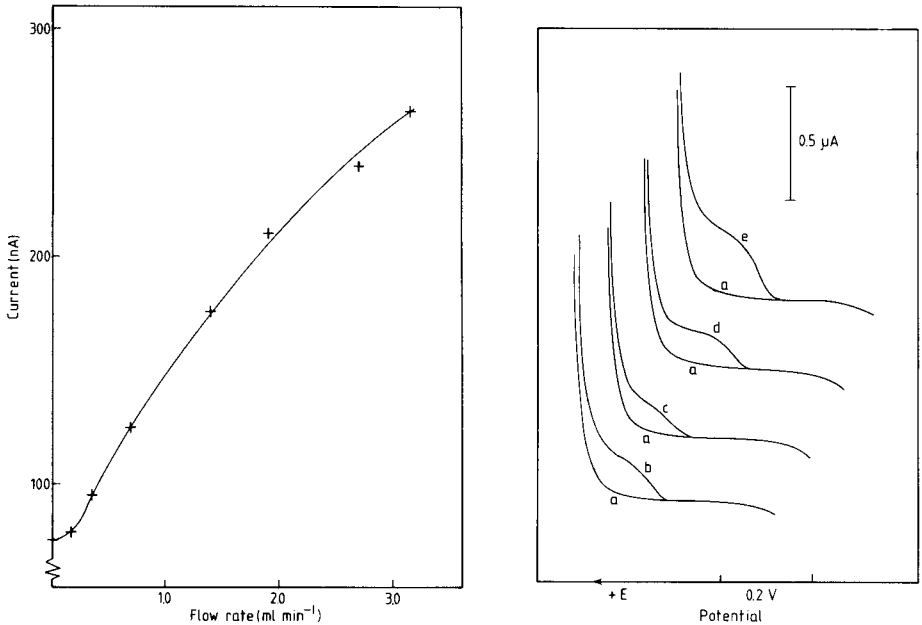

Fig. 5. Limiting current for 10^{-5} M BPA containing 0.05% Triton measured at +0.04 V at different flow rates.

Fig. 6. Polarograms of (a) pH 9.2 buffer, and 10^{-5} M solutions of hydrolysed (b) ampicillin, (c) carbenicillin, (d) cloxacillin; (e) 2×10^{-5} M hydrolysed phenoxymethylpenicillin. Scan started from −0.3 V; 0.05% Triton X-100 added.

and with 1×10^{-3} M solutions, peak splitting was observed. The split peak results from the concentration profile of the sample plug as it reaches the detector, and from adsorption effects. At high concentrations of penicilloate, the mercury drop becomes completely covered with adsorbed material (despite the presence of Triton), and the sensitivity for penicilloate reaching this surface then decreases. At the two sides of the sample plug, the concentration is insufficient for complete coverage to occur; but in the middle of the plug, the mercury drop is covered and the current therefore decreases, giving a split peak.

In the absence of Triton, the calibration graph obtained at pH 9.2 is linear with a small intercept at the Y-axis, whereas at neutral or acidic pH the graph is sigmoidal. However, a linear calibration graph may be obtained in pH 7 phosphate buffer, provided that 0.05% Triton X-100 is present.

Determination of penicilloate in penicillin

Intact penicillin shows no polarographic activity; any current response obtained from injection of unhydrolysed penicillin solutions is therefore attributed to the presence of penicilloic acid in the penicillin preparation.

However, penicillin is adsorbed at the mercury electrode. This adsorption is manifested by displacement of the oxygen wave when Triton is absent. The peak height as a function of the potential is shown in Fig. 7 for injections of unhydrolysed benzylpenicillin (BPN). When Triton is absent, the current rises sharply at more negative potentials because of the oxygen wave; when Triton is present, the curve is similar to that obtained from pure BPA (Fig. 4, curve b).

The penicilloic acid content of BPN was evaluated with the aid of a calibration graph constructed from injections of pure BPA. The linearity of the calibration graph for penicilloic acid was maintained even in the presence of large amounts of penicillin. In Fig. 8 the results of the determination are shown as a function of the injected penicillin concentration. In the absence of Triton, the apparent BPA content decreases with increasing penicillin concentration, possibly because the adsorption of the penicillin displaces the oxygen wave, giving a non-linear contribution to the peak height. As the amount of Triton present in the buffer is increased, this effect diminishes, and at a Triton content of 0.017% the BPA determination gives results that are independent of penicillin concentration.

Penicillins in the dissolved form are amenable to degradation, and injections of the penicillin sample should be done without delay after dissolution. For example, the initial degradation rate of cloxacillin was found to be 1.4% per hour. However, the flow-injection method is rapid and measurements are easily completed within a minute of dissolution.

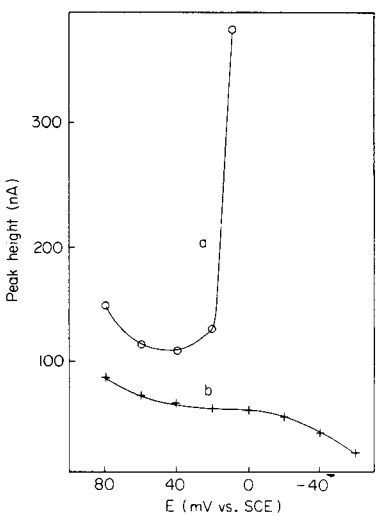

Fig. 7. Flow-injection peak height as a function of potential for (a) 10^{-2} M BPN and (b) 5.6×10^{-3} M BPN in presence of 0.05% Triton X-100.

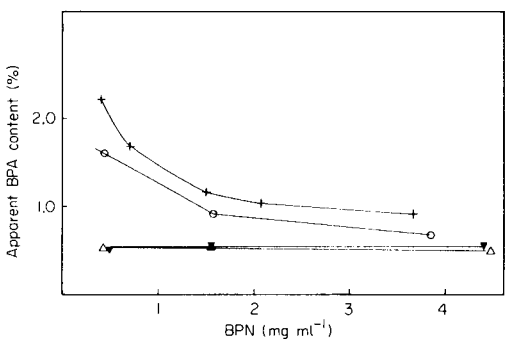

Fig. 8. Apparent content of BPA in BPN as a function of penicillin concentration in the presence of different concentrations of Triton: (+) 0; (○) 0.006%; (△) 0.017%; (▾) 0.05%.

The sensitivity for the penicilloate in the absence and presence of the intact penicillin remained unchanged for BPN and carbenicillin. For cloxacillin and phenoxymethylpenicillin, the sensitivity was about 10% lower in the presence of the penicillin (1 mg ml^{-1}); for ampicillin, a small increase in sensitivity was observed with increasing penicillin concentration. These changes in sensitivity suggest that the standard addition procedure should be more reliable.

The values obtained for the penicilloic acid in various penicillin preparations are given in Table 1. The discrepancies between the standard addition and calibration graph procedures in the flow-injection analyses lie within the experimental error. With penicillin concentrations lower than 1 mg ml^{-1}, the errors are negligible when calibration graphs are used, indicating that this faster procedure is satisfactory. Table 1 also shows the values obtained by the titrimetric methods. For ampicillin the correlation between the methods is excellent, while for cloxacillin and carbenicillin it is fair. The discrepancies are larger for BPN and phenoxymethylpenicillin. A more extended comparative study would be of interest. However, the results obtained by the polarographic technique are very promising.

Conclusions

Flow-injection analysis with polarographic detection provides a rapid and sensitive method for the determination of penicilloic acid, either in pure form or in penicillin preparations. The method seems to be applicable to most penicillins. An advantage of this polarographic system is that deaeration is superfluous, because of the electroactivity of penicilloic acid at potentials positive to the oxygen wave, and due to the presence of Triton X-100. Addition of Triton X-100 is vital when penicillin preparations are to be

TABLE 1

Results from the determination of the penicilloic acid content of some penicillins by the flow-injection, iodimetric and mercurimetric methods

Penicillin		Penicilloic acid found (% w/w)					
		Flow injection[a]				Iodimetry[b]	Mercurimetry[b]
		Graph		St. addn.			
Ampicillin	1	3.8 ± 0.1	(2)	3.7 ± 0.1	(3)	3.6	3.8
	2	2.4 ± 0.1	(2)	2.2 ± 0.1	(3)	2.2	2.2
Cloxacillin		0.5 ± 0.05	(2)	0.6 ± 0.03	(2)	0.8	0.7
Carbenicillin	1	7.0 ± 0.3	(2)	6.8 ± 0.3	(2)	8.3	7.9
	2	7.2 ± 0.3	(8)	7.2 ± 0.3	(8)	8.5	8.0
Benzylpenicillin	1	0.9 ± 0.05	(2)	1.0 ± 0.05	(2)	1.4	0.6
	2	0.4 ± 0.05	(2)	0.5 ± 0.05	(2)	1.2	0.3
Phenoxymethylpenicillin	1	0.9 ± 0.1	(2)	1.1 ± 0.1	(2)	0.6	0.5
	2	1.0 ± 0.1	(2)	1.1 ± 0.1	(2)	1.1	0.6

[a]Results obtained from calibration graphs and by standard addition; number of determinations in parentheses. [b]Mean of two determinations.

analysed. The speed of the flow-injection method makes it of value in studies of the degradation of penicillins.

The polarographic detector used may be constructed to fit any ordinary polarographic capillary and is easily mounted and dismounted. The possibility of using the detector after liquid chromatographic separation of penicillins or penicilloic acids is obvious. Penicillins separated in their intact form may be hydrolysed by a post-column addition of alkali and then detected in the alkaline medium obtained.

REFERENCES

1 J. F. Alicino, Ind. Eng. Chem., Anal. Ed., 18 (1946) 619.
2 B. Karlberg and U. Forsman, Anal. Chim. Acta, 83 (1976) 309.
3 U. Forsman and A. Karlsson, Anal. Chim. Acta, 128 (1981) 135.
4 D. L. Rabenstein and R. Saetre, Anal. Chem., 49 (1977) 1036.
5 R. Samuelsson and J. Osteryoung, Anal. Chim. Acta, 123 (1981) 97.
6 H. B. Hanekamp, W. M. Voogt and P. Bos, Anal. Chim. Acta, 118 (1980) 73.
7 U. Baltensperger and R. Eggli, Anal. Chim. Acta, 123 (1981) 107.
8 J. Růžička and E. H. Hansen, Flow Injection Analysis, Wiley—Interscience, New York, 1981.
9 M. R. Hackman and M. A. Brooks, J. Chromatogr., 222 (1981) 179.

Analytica Chimica Acta, 139 (1982) 143—153
Elsevier Scientific Publishing Company, Amsterdam — Printed in The Netherlands

HIERARCHICAL CLUSTERING OF INFRARED SPECTRA

J. ZUPAN
Institute of Chemistry, "Boris Kidrič", Ljubljana (Yugoslavia)
(Received 4th January 1982)

SUMMARY

The generation of a hierarchical tree of 500 infrared spectra, using the recently proposed fractal or 3-distances-clustering method is described and discussed. The objects of clustering are infrared spectra of polymer compounds which are represented as sets of 80 complex Fourier coefficients, obtained by fast Fourier transformation of digitized absorbance spectra. The generated hierarchical tree, with a maximum height of 20 and an average height of 12 levels, yields a very satisfactory clustering scheme with respect to the structure of the compounds involved. In addition to very good clustering, a 100% retrieval (prediction) ability was obtained. This was achieved by the use of an iterative procedure after the initial tree had been generated. Additionally, the tree was tested with 240 infrared spectra of different compounds which were taken into account during the generation of the tree. The retrieval success of these test runs is discussed with respect to the structural similarity of the compounds to which the "unknown" spectra were linked.

Retrieval problems in complex chemical information systems are normally solved either as sequential searches or by inverted files. Despite their use in almost all applications, each of these approaches has its own drawback which disqualifies it from wider applications. Sequential searches are far too slow for the inspection of large data files, while inverted files are designed for exact matches rather than for applications where wider tolerance limits are permissible or only similarities to the queries are required.

These weak points have led to a search for a better retrieval algorithm that can be implemented on the KISIK chemical information system [1, 2]. The introduction of a hierarchical decision tree seems to be very promising, for it offers the main features which are badly needed in any information system: fast retrieval and competence to give information about items similar to the query in cases where the identical data are not available. The main shortcoming, the generation problem of such a tree for large numbers of objects, has been solved recently by the introduction of a 3-distances-clustering method [3—5].

The purpose of the work described here was two-fold: first, to show that the iterative 3-distances-clustering method is capable of generating a hierarchical tree from a fairly large collection of infrared spectra, allowing 100% retrieval ability; secondly, to demonstrate that the generated tree gives very useful

clusters of structurally similar compounds that can be used successfully in automated structural elucidation processes.

THE METHOD

The 3-distances-clustering method is in principle an update procedure for an existing binary tree [6] involving addition of new objects one at a time. Starting with only two objects linked together in a cluster, represented by the root V_o (Fig. 1a), the tree grows as the objects are added. The only difference between the standard update and the new method is that at each vertex V, instead of only two distances, $d_l = d(V_L, X)$ and $d_r = d(V_R, X)$, an additional distance $d_3 = d(V_L, V_R)$ is calculated. V_L and V_R are descendants of the vertex V and might also be final objects in the tree (leaves or end nodes) (Fig. 1b). A further path for the update of object X is determined according to the minimal distance: $d_3 = \min \{d_l, d_r, d_3\}$.

Any of the three distances can be the minimal one. If it is d_l or d_r, object X proceeds towards one of the vertices V_L or V_R, respectively, where the same calculation and evaluation of the corresponding distances has to be repeated. In the case where d_3 is the smallest distance, the update process stops because X cannot join either V_L or V_R due to the fact that the distance between V_L and V_R is smaller than the distances d_l and d_r (Fig. 2a). It is logically more acceptable for closer clusters to join first rather than to accept a distant object separately and form a cluster with it, since the latter can shift the "center of gravity" considerably. Thus the object X is forced to "bud" a new branch in the tree above the vertex V (Fig. 2b).

When the above update procedure is used, it becomes possible to generate a binary tree containing any number of objects. The problem with this

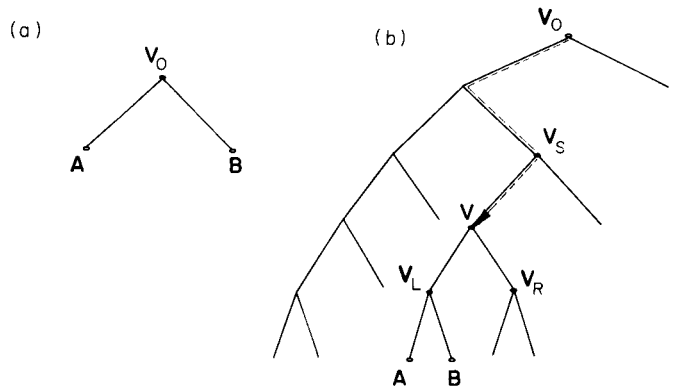

Fig. 1. The growth of the tree starts with two objects, A and B, linked into one cluster represented by V_o (a). The object X is added at the root and continues its path after the decision has been made at each vertex. The vector X (b) has already passed vertex V_s and continues its path toward vertex V. To decide in which direction to move further, both descendants of the vertex V must be considered and three distances calculated.

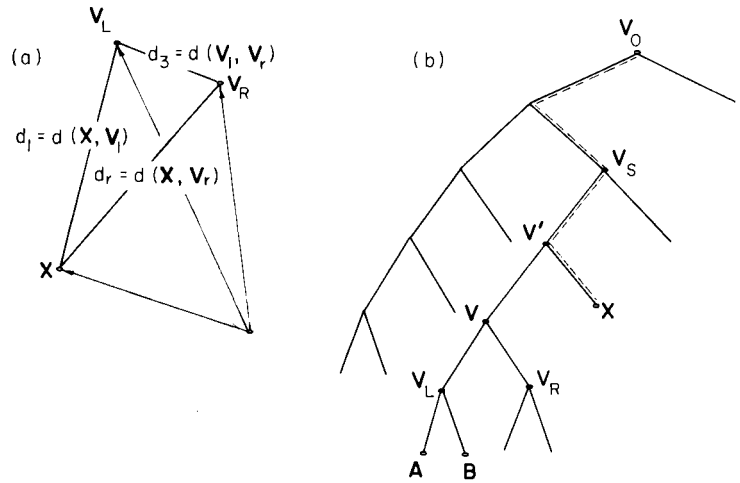

Fig. 2. The decision based on three distances is made at each vertex V on the path of the vector X. If the distance d_3 happens to be the smallest (a), the vector X is not allowed to join the cluster representing V_L and V_R (i.e., the vertex V) but must form a new branch and a new vertex V' between the vertices V and V_s.

method, however, is its heavy dependence on the sequence in which the objects are added to the growing tree. In the great majority of cases, overlapping clusters are generated and these may prevent access to, and retrieval of, many objects. In order to overcome this drawback, an iterative scheme that can be described in the following four steps has been suggested [4].

Step 1. Generation of the binary decision tree of N objects by the 3-distances-clustering method.

Step 2. Testing all N objects to see if they can be accessed and retrieved in the generated tree in the same manner as they were updated into it; all non-accessible objects are put on the "bad list".

Step 3. Removal of all objects stored on the "bad list" from the tree and updating them again.

Step 4. Ending the procedure if the "bad list" is empty, otherwise returning to step 2.

The flow chart of the described algorithm is shown in Fig. 3; more detailed explanations are available elsewhere [4]. As has already been mentioned [3—5], the components $v(M, j)$ of the vertex V_M representing the cluster composed from two smaller clusters K and L are calculated in the following manner:

$$v(K + L, j) = [n(K)\, v(K, j) + n(L)\, v(\mathrm{L}, j)]\,/[n(K) + n(\mathrm{L})]$$

where $n(K)$ and $n(L)$ are the numbers of objects in clusters K and L.

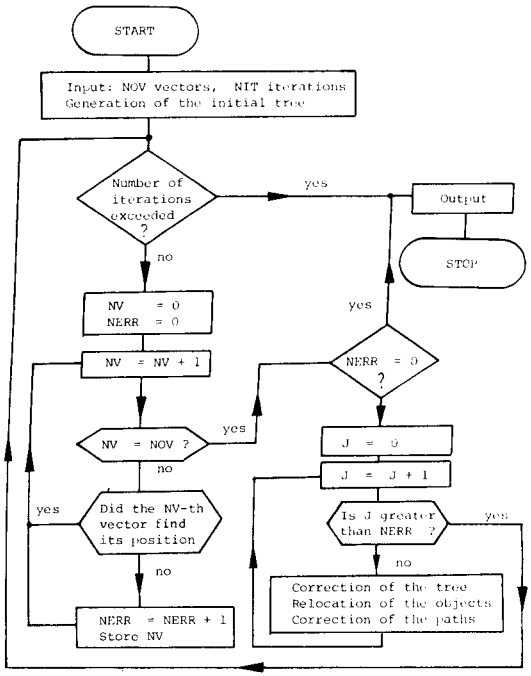

Fig. 3. Flow-chart for the iterative generation of the hierarchical decision tree using the 3-distances-clustering method.

DATA BASE

The method explained in the preceding paragraph was applied to a collection of 740 infrared spectra [7] of polymer compounds. The digitalization of the entire collection and the processing of the computer-readable form of the spectra has been described elsewhere [8]. The file that was used in the present work consists of 740 records (one spectrum per record) of 650 tightly packed intensity values (8 bits = 1 byte per value). Unfortunately, the number of intensities is too large to allow the numerous infrared spectra to be handled efficiently. In order to lower the dimension of the measurement space from 650 components to considerably less, the fast Fourier transform (FFT) was applied to all spectra. Each spectrum was first recalculated to the linear absorbance, then reduced to 512 points and transformed with the fast Fourier algorithm [9]; finally, the 80 leading complex Fourier coefficients were selected as a representation of the spectrum. The decision to take only the first 80 complex Fourier coefficients was made as a trade-off between the time consumption of the iterative 3-distances-clustering method and the reproducibility of the infrared curve. A comparison of the original digitized spectrum and its reproduction from 80 complex Fourier coefficients is shown in Fig. 4. It can be seen that the flat region between the peaks exhibits waves on the reproduced curve because of the absence of

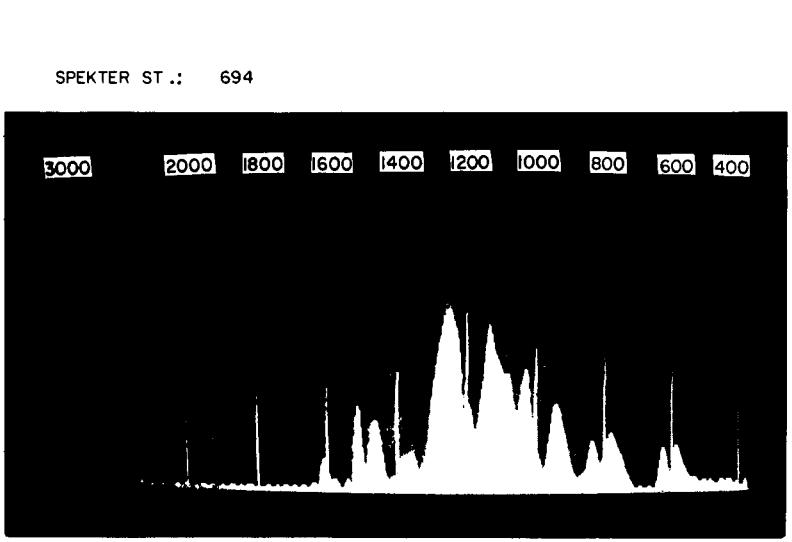

Fig. 4. Comparison between the digitized and reproduced infrared spectra. The upper, gray spectrum is digitized, while the lower, brighter one is recalculated from the 80 complex Fourier-coefficients. The spectra with bands broader than, or separated by more than 10 cm^{-1}, are represented very well, while sharper peaks, or peaks situated close together, are reproduced with considerably less accuracy.

high-order Fourier coefficients. More damaging, is the problem of selectivity between two or more sharp peaks closer than 10 cm^{-1} to each other. In spite of these shortcomings, the reproduction of more than 98% of the spectra was excellent, while the rest was considered acceptable for identification purposes.

The hierarchical decision tree was generated by using the first 500 spectra out of the list containing the randomly mixed complete collection of 740 items. The remaining 240 spectra were used as the spectra of "unknown" compounds for testing the identification and prediction ability of the tree generated.

RESULTS AND DISCUSSION

Generation of the hierarchical tree

In somewhat compressed form (the first 5 levels and the number of objects represented by the vertices on the fifth level), the final tree generated is shown in Fig. 5. To generate it, 26 iterations were needed, starting with 78 (out of 500 possible) errors in the first run. At the fifth iteration, the maximum of 98 non-accessible spectra was detected; after this, almost a monotonous decrease to zero was recorded. The maximal path length in the tree is 20 levels long, requiring 21 comparisons to reach the end node, while the shortest path already ends on the third level (Fig. 5). If the theoretical minimal height of the binary tree of 500 objects (9 levels: 2^9 = 512) is compared with the average path length for the generated tree (12

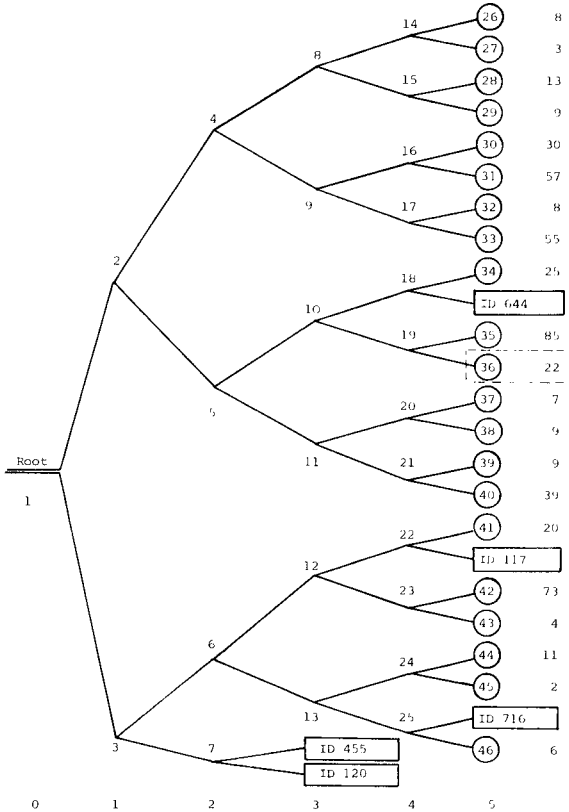

Fig. 5. The first five levels of the generated hierarchical tree containing 500 infrared spectra. The enumeration of vertices on the fifth level is encircled, the numbers on the right side of the circles are the numbers of compounds in each branch or cluster, and the numbers in boxes are the identification numbers of compounds, the spectra of which have already been separated from the rest. The branch from vertex 36 is shown in detail in Fig. 6.

levels), relatively balanced distribution with good representation of objects and a fairly good clustering method are implied simultaneously.

To illustrate this statement, the same set of 500 spectra and the same procedure were used to generate the tree, but the infrared spectra were represented by 300 digitized points instead of by the 80 complex Fourier coefficients. Although the description by 300 digitized points contained almost twice the amount of data per spectrum as the description by the 80 Fourier coefficients, the resulting clusters of chemical structures were considerably worse than those obtained initially. Additionally, the tree had more "chains", resulting in an average path of 22 vertices and a maximal path of 34 vertices.

Inspection of the spectra that split from the rest and ended near the root of the tree (up to the fifth level, Fig. 5), revealed that each spectrum had at least one unique feature that clearly distinguished it from the others in the group. Spectrum number 122, for example, had a very broad band between 3600 and 2300 cm^{-1} that does not appear in any other spectrum in the group.

The 24 subtrees represented as vertices numbers 24—46 (Fig. 5, level 5) differ considerably in size. The size varies from three single-object-clusters (IDs 644, 177, 716) to the largest subtree of 85 spectra that is represented by the vertex 35. Because the number of objects in all the subtrees is too large to be examined in detail here, only the main structural characteristics of 21 subtrees are given in Table 1.

It can be seen readily from Table 1 that clearly separated structural groups are present in the tree. The size of each group having at least one structural feature in common, depends mainly on the actual number of corresponding structures in the data base. However, some inconsistencies in the ordering of groups can also be observed. These are caused by the randomly-generated sequences (certainly not the best possible order) of the spectra taken into consideration during the generation of the tree. A good example of this kind is the small cluster of pigments (vertex 43, Table 1) that should be linked with the other pigments (vertices 26—29). Another, slightly more compli-

TABLE 1

The main characteristics of the 21 sub-trees of the large tree containing 500 objects (The heights of the sub-trees are given relative to level 5 at which the cut was made. The five objects missing in the total sum are those separated from the rest on level 5 or higher (Fig. 5).)

Vertex	No. of objects	Height			Structural properties
		Min.	Av.	Max.	
26	8	2	3.1	4	Pigments, oxides
27	3	1	1.7	2	Pigments, oxides
28	13	2	5.3	6	Pigments, oxides
29	9	2	3.8	5	Pigments, oxides
30	30	2	6.8	11	Oxides, sulphates, silicates
31	57	3	7.5	10	Miscellaneous
32	8	1	4.0	6	Octoates, phthalates, naphthenates
33	55	2	7.5	14	Miscellaneous
34	25	1	6.3	10	Epoxides, rosins, resins
35	85	3	9.1	15	Esters
36	22	2	6.3	10	Acetates
37	7	1	3.6	5	Carbonates, oxides
38	9	2	3.6	5	Alcohols, ketones
39	9	2	3.9	6	Silicones
40	39	2	6.5	9	Esters, alcohols, glycols
41	20	2	6.8	11	Phenolic and epoxy resins
42	73	2	9.1	14	Miscellaneous
43	4	1	2.2	4	Pigments
44	11	1	4.5	7	Formaldehydes
45	2	1	1.0	1	Melamines
46	6	1	3.2	4	Acrylates
Tree	495 + 5	3	12.1	20	

cated, example is given by the four clusters represented by vertices 30—33. The clusters 31 and 33 contain aliphatic and aromatic hydrocarbons with shorter and longer aliphatic chains, respectively. They should, therefore, be linked together after (not before) clusters 30 and 32 are separated. Three of the four largest clusters (vertices 31, 33, and 42) are labelled as "miscellaneous" in Table 1. This label does not imply that the compounds clustered within these groups are not linked according to their structure, but rather that this was done later in the tree.

To give an impression of the clustering ability of the iterative 3-distances-clustering method, one branch of the tree (represented by vertex 36) of medium size (22 compounds) is shown from vertex 36 up to the end nodes in Fig. 6. The structural feature common to all compounds in this cluster without exception, can be recognized immediately: all of them are acetates, present in a monomer, polymer or copolymer. It is fair to say that even in this group, some rearrangements could be made to achieve perfect ordering.

For example, there are six (IDs 287, 288, 289, 290, 292, and 293) vinyl acetate—ethylene copolymers in the cluster not linked together. They occur in the cluster of 18 compounds one level lower, but should actually be linked into a solid group a few levels lower still. Yet it must be noted that copolymer ID 287 contains only 10% of ethylene component and is therefore very appropriately linked to compounds having vinyl acetate as a dominant component (IDs 303, 273, 287, and 266). This example is used to illustrate the difficulties that can arise in trying to determine the best position of a spectrum in a tree.

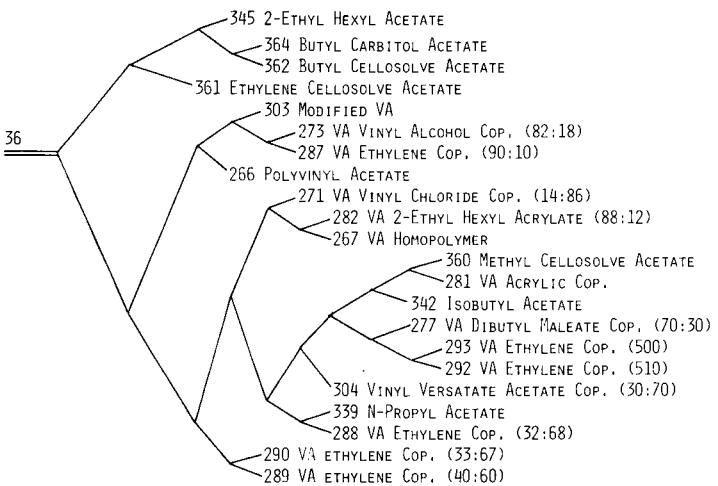

Fig. 6. The sub-tree of 22 acetate compounds (VA stands for vinyl acetate and COP, for copolymer) represented by vertex 36. To this group, 10 remaining acetates from the 240 test compounds were linked correctly.

Tests of predictive ability

To explore the clustering ability of the generated tree further, the prediction ability was tested by using the remaining 240 spectra of the collection as the spectra of the "unknown" compounds. If the tree is used for the prediction of features (i.e., as the decision tree, or for the retrieval of items that are known in advance not to be stored in the tree), the algorithm applied for the calculation and evaluation of three distances at each vertex must be the same as that used for generation of the tree. In the case that distance d_3 (the distance between the two descendants of the vertex at which the decision is made) is the smallest, the retrieval stops, indicating that the closest possible match to the query has been found. In the case of structure prediction (retrieval of spectra of unknown compounds), such a stop means that the vertex at which the stop was made represents a cluster of compounds having the most similar structures to the unknown. Because it is very difficult to determine the best probable location for the spectrum of an unknown compound if an exact match is not found in the tree, only a qualitative description of outcomes for all 240 test runs are given in Table 2. It should be emphasized that no two spectra in the entire collection of 740 items were identical, although there were many duplicate compounds in the collection. Even when the duplicated compounds did not have the same spectra (different conditions, impurities, etc.) they were all linked with their "twins" in the tree generated from the 500 compounds.

The meaning of some terms in Table 2 is of course debatable; expressions like "very similar", "type", "class", or "different" were arbitrarily chosen on the basis of intuitive chemistry. Nevertheless, the results collected in Table 2 give a reasonably good description of the predictive ability of the generated tree.

Prediction about the partial structure of an unknown compound can be made after its spectrum passes (or stops at) a given vertex that represents a group of compounds exhibiting some common structural feature. Ten out of 240 test spectra, for example, passed vertex 36 (Figs. 5 and 6) which represents acetates (Table 1), and all of them were identified as copolymers having

TABLE 2

Results of the retrieval of 240 spectra of "unknown" compounds given in terms of structural similarity between the query and the matched spectrum (or all spectra in the cluster if the query did not reach the end node)

Place where the search stops (level from the end node)	0	1	2	3	4	7	Sum
Identical or very similar	101	34	2	0	0	0	137
Type or class of compound(s)	33	29	9	2	1*	0	74
Different compounds	14	12	0	2	0	1	29
Total	148	75	11	4	1	1	240

vinyl acetate as one of the components. To give another example, the retrieval asterisked in Table 2 stops at the vertex representing five compounds four levels before the most distant end node. Four of these five compounds were polyamides of different origin (IDs 186, 187, 190, and 190), while the fifth was celanese (ID 555). The decision that the spectrum belonged to an amide compound was straightforward. Actually, the "unknown" compound was dimethylacetamide (ID 418). The outcome of all 211 retrievals (137 + 74) listed in the first two rows in Table 2 can be described in a very similar manner as in the above two examples.

The failure of the remaining 29 compounds to find their match or even to yield an indication of their "type" or "class" of structure, does not imply failure in the predictive ability of the tree. The failure is better ascribed to the fact that there were no similar compounds in the training set.

CONCLUSION

The proposed iterative 3-distances-clustering method was used for grouping 500 infrared spectra. The generated hierarchical clustering scheme is shown to have excellent retrieval characteristics: 100% retrieval or recognition ability with only 12 comparisons per search on average. The second advantage is a very adequate predictive ability for structural features of unknown compounds if their digitized (full curve) infrared spectra are available in computer-readable form. To our best knowledge, the clustering scheme discussed is the largest hierarchical tree of infrared spectra available. The computer time and space requirements of the proposed method are roughly linearly dependent on the number of objects in the tree so that even larger groups of objects could be hierarchically clustered. The system has the weakness that the iterative correction procedure reduces the time efficiency for generation of the hierarchical tree in one step significantly, but the 100% retrieval ability and the better clustering scheme of the tree obtained by the iterative method seem to more than compensate for this loss.

Finally, it should be said that for any application of the iterative 3-distances-clustering method, a lot of work has to be done even after the hierarchical decision tree has been obtained. The main efforts should be directed to better clusterings within smaller subtrees, to the generation of trees with different sequences of objects, and to better and more concise representation of objects (not necessarily in that order). Work on the refinement of hierarchical trees based on spectroscopic data is in progress.

The computer program used for this work is completely written in PDP Fortran IV language and is implemented on a PDP 11/34 under OS RSX 11M. Because of the comparatively slow access time of the RK05J disc cartridges, the real time needed to generate the described tree of 999 vertices, from 500 160-dimensional objects, was about 48 h. Listing of the program is available on request.

The author thanks Dr. Matej Penca for his valuable comments on the identification of polymers, and Miss Marjana Janežič, for the FFT programming. Financial support from the Research Community of Slovenia is gratefully acknowledged.

REFERENCES

1 J. Zupan, M. Penca, M. Razinger, B. Barlič and D. Hadži, Anal. Lett., 12 (1979) 109.
2 J. Zupan, M. Penca, M. Razinger, B. Barlič and D. Hadži, Anal. Chim. Acta, 122 (1980) 103.
3 J. Zupan, Anal. Chim. Acta, 122 (1980) 337.
4 J. Zupan, Clustering of Large Data Sets, Research Studies Press, Wiley, Chichester, 1982. in press.
5 M. F. Delaney, Anal. Chem., 53 (1981) 2354.
6 D. E. Knuth, The Art of Computer Programming, Vol. 3, Addison-Wesley, Reading, MA, 1975, p. 422.
7 Infrared Spectroscopy, Its Use in the Coating Industry, Fed. Soc. Paint Technol., Philadelphia, PA, 1969.
8 M. Razinger, M. Penca and J. Zupan, Anal. Chem., 53 (1981) 1107.
9 E. O. Brigham, The Fast Fourier Transform, Prentice-Hall, Englewood Cliffs, NJ, 1974.

Analytica Chimica Acta, 139 (1982) 155—166
Elsevier Scientific Publishing Company, Amsterdam — Printed in The Netherlands

THE RESOLUTION OF CHROMATOGRAMS WITH OVERLAPPING PEAKS BY MEANS OF DIFFERENT STATISTICAL FUNCTIONS

JOAN GRIMALT* and HORTENSIA ITURRIAGA

Department of Analytical Chemistry, Science Faculty, Universitat Autònoma de Barcelona, Bellaterra, Barcelona (Spain)

XAVIER TOMAS

Department of Analytical Chemistry, Institut Químic de Sarrià, Barcelona-17 (Spain)

(Received 23rd March 1981)

SUMMARY

The effectiveness of diverse functions of statistical distribution (log—normal, gamma and Weibull) is examined for the elucidation of chromatograms with overlapping peaks. A Gauss function and a modified Gauss function are used for comparison with the results obtained by the other functions. The generalized least-squares method is applied for adjustment; this is done automatically by the specially designed DAFNA program written in Fortran IV. The use of those functions in the resolution of experimental chromatograms is preceded by an outline of the difficulties involved in the elucidation of overlapping profiles.

Within the field of applications of automated calculation to chromatography, the elucidation of overlapping peaks is a topic which has been approached from several angles but has not yet been totally mastered. The functions used to describe the profile of a chromatographic peak are related, mostly, to the Gauss function. The Gauss function is useful for the resolution of chromatograms with symmetrical peaks [1—8] but it is not satisfactory for describing the profiles of asymmetric or tailing peaks. Diverse functions have been used to achieve better descriptions of such peaks. These include modified Gauss functions [2, 9, 10] as well as others generated by sum, multiplication or linear combination of Gauss and Cauchy functions [2]. The Poisson [11, 12] and bi-Gaussian functions [3, 8, 11, 12] have also been applied. From another angle, some authors have elucidated chromatograms of overlapping peaks from standard peaks [8, 13]. Also, convolution integrals have been widely used in describing chromatographic peak profiles; the Gauss function convoluted with an exponential decay has been used most often [6, 10, 14—21]. Other authors [22, 23] have proposed several polynomial Gauss functions based on the statistical moments of the chromatographic peaks.

*Present address; Department of Environmental Chemistry, Institut de Química Bio-Orgànica, Jordi Girona Salgado St., Barcelona-34, Spain.

0003-2670/82/0000-0000/$02.75

In this paper, the usefulness of various distribution functions currently in use in statistics (Gauss, log—normal, gamma, Weibull) for the resolution of overlapping peaks is described. Generally speaking, the statistical probability functions correspond to given types of phenomena. Accordingly, their utilization in the adjustment of chromatographic peaks may be of interest, for it may help in characterizing some factors in the chromatographic process. The parameters of the functions chosen in each case were adjusted by the generalized least-squares method with a suitable program in Fortran IV. Before the statistical functions were applied to experimental chromatograms, the highest permissible degree of overlapping between peaks to be resolved was evaluated for each statistical distribution. Finally, the procedures were applied to several types of overlapping chromatograms; the more interesting results are presented as examples.

FUNCTIONS OF STATISTICAL DISTRIBUTION STUDIED

Gauss function

This function corresponds to phenomena in which many causes of variation intervene, the variables being independent in their sign and value. It may be expressed by

$$f(t) = h \exp[-(t-\mu)^2/2\sigma^2] \tag{1}$$

where h is the maximum height, μ is the mean, and σ is the standard deviation. The Gauss function is very well known and is used here for comparison with the results obtained by the other functions studied.

Log-normal function

A variable x has a log—normal distribution if the variable $\ln(x)$ has a Gaussian distribution. This function is usually applied in statistics to situations in which some of the independent factors affect the result of an event, not additively but according to the weight of the factor [24]. The log—normal distribution may be expressed by

$$f(t) = h \exp\{-(\ln 2)\,(\ln[(t-t_0)(p^2-1)/wp + 1])^2/(\ln p)^2\}$$

$$\text{for } t > t_0 - wp/(p^2-1) \tag{2}$$

with $f(t) = 0$ for $t \leqslant t_0 - wp/(p^2-1)$. Here h is the maximum height, t_0 is the abscissa reading corresponding to h, w is the width at half-height, and p is the asymmetry coefficient. Some papers [25—27] have reported that this function can be used in the deconvolution of absorption spectra with satisfactory results.

Gamma function

The gamma function may be described by means of the non-normalized expression

$$f(t)=h(t/t_0)^{(\alpha-1)}\exp[-(\alpha-1)(t/t_0-1)] \quad \text{for } 0\leqslant t\leqslant\infty,\ \alpha>0,\ t_0>0 \tag{3}$$

with $f(t) = 0$ for all other cases. Here h and t_0 are as defined above and α is a parameter determining the width of the profile for a given value of t_0.

Weibull function

The non-normalized Weibull function may be expressed by

$$f(t) = h[(t-a)/(t_0-a)]^{(c-1)}\exp\{-([(t-a)/(t_0-a)]^c - 1)[(c-1)/c]\}$$
$$\text{for } a\leqslant t\leqslant\infty,\ t_0>0,\ c>0 \tag{4}$$

with $f(t) = 0$ for all other cases. Here h and t_0 are as defined above, a is the starting point of the function, and c is a parameter defining the width of the function for a given value of t_0.

This function, as well as the gamma function, are usually applied, in statistics, to times of passage, life duration, permanence, etc. These two functions do not seem to have been applied in the deconvolution of absorption spectra or of overlapping chromatographic peaks.

Modified Gauss function

The modified Gauss function proposed by Littlewood et al. [9] was applied for comparison with the other functions. The function is

$$f(t) = h(t_0/t)^{1/2}\exp\{-2[t_0(t_0{}^{1/2} - t^{1/2})^2]/\sigma^2\} \tag{5}$$

where h, t_0 and σ are as defined above.

METHOD OF ADJUSTMENT

The generalized least-squares method was chosen for adjustment. This method has the advantage of taking into account the specific shape of the function to be minimized, thus reducing the number of iterations necessary.

In the present case, the functions to be adjusted are of the type $F(t) = \Sigma_{i=1}^{n} f_i(t)$, where $f_i(t)$ is the specific function to be adjusted to each of the chromatographic peaks. As in all least-squares methods, it is necessary to minimize the residual sum of squares function

$$E(\bar{x}) = \sum_{k=1}^{m} [F^k_{\text{diff}}(\bar{x})]^2 \tag{6}$$

where $F^k_{\text{diff}}(\bar{x}) = F^k_{\text{predicted}}(\bar{x}) - F^k_{\text{observed}}$, $\bar{x}$ is the vector of the n parameters defining $F^k_{\text{predicted}}(\bar{x})$, and k refers to a particular point (abscissa) of the m points of the chromatogram.

If the iteration begins at the starting parameters $\bar{\alpha}$, and the difference with respect to the parameters implying a minimal error is $\bar{\delta}$, the derivation of Eqn. (7) leads to the system of equations

$$\sum_{k=1}^{m} g_i^k(\bar{\alpha}+\bar{\delta})F^k_{\text{diff}}(\bar{\alpha}+\bar{\delta}) = 0 \qquad (\text{for } i = 1,2,\ldots,n) \tag{7}$$

where $g_i^k(\bar{\alpha} + \bar{\delta}) = \partial F_{\text{diff}}^k(\bar{\alpha} + \bar{\delta})/\partial x_i$.

When Taylor's series is used in its first two terms to get an approximation of $F_{\text{diff}}^k(\bar{x})$, and when terms containing second derivatives of this function are neglected, then the system is described by

$$\sum_{j=1}^{n} \left\{ \sum_{k=1}^{m} g_i^k(\bar{\alpha})\, g_j^k(\bar{\alpha}) \right\} \bar{\delta}_j = - \sum_{k=1}^{m} g_i^k(\bar{\alpha}) F_{\text{diff}}^k(\bar{\alpha}) \qquad (\text{for } i = 1,2,\ldots,n) \tag{8}$$

(Further description is available [28].) This system of equations may be represented in matrix form by means of the expression $A\bar{\delta} = B$, where matrix A is defined by $a_{ij} = \Sigma_{k=1}^{m} g_i^k(\bar{\alpha}) g_j^k(\bar{\alpha})$ and matrix B is defined by $b_i = -\Sigma_{k=1}^{m} g_i^k(\bar{\alpha}) F_{\text{diff}}^k(\bar{\alpha})$. Then vector δ is obtained by solution of $A\bar{\delta} = B$, which tells how the initial parameters $(\bar{\alpha})$ have to be incremented so as to obtain the minimum. An iterative process is thus generated: $\bar{\alpha}_{i+1} = \bar{\alpha}_i + \bar{\delta}_i$. The iteration may be considered to end in accordance with a given tolerance in the value of $\bar{\delta}_i$ or by reference to Eqn. (6).

DAFNA program

This program permits the adjustment of any function to a number of data points by the generalized least-squares method. It was written in Fortran IV for an SPC 16/45 computer and, in a parallel version, for a GA 18/30 computer. Both program listings are available on request. In the version from the SPC 16/45 computer, doubled precision is available (four words of two bytes to a real number) and, in the GA 18/30 version, extended precision is available (three words of two bytes to a real number). The general characteristics of the program are as follows.

First, the type of function to be adjusted is described in a function subprogram. Just changing the subprogram makes it possible to adjust any particular function. The rest of the program is general. For a given profile the number of peaks to be adjusted must be indicated. However, the respective function subprogram is such that its description need not be changed according to the peaks to be fitted in.

Secondly, when it is necessary to work with data generated from the functions under study instead of making an adjustment with experimental data (e.g., to examine possibilities of eliminating overlapping), the program contains an option that generates such data from parameters introduced, so that the data can then be manipulated in exactly the same way as experimental data.

Thirdly, so as to avoid the problem of the initial parameters of adjustment in cases where large overlapping makes it difficult to introduce some parameters for generation of a convergent process, the program contains a trial-and-error procedure which provides only the value of the residual sum of squares when some parameters are introduced; if necessary, the program draws a graph reflecting the discrepancy between the data to be adjusted and the values obtained with those parameters.

The program is compiled for user interaction so that the user can decide,

at every step of the calculation, the most appropriate way of completing the calculation, and what information should be given by the computer.

The general working format is as follows (cf. Fig. 1).

(1) The program reads the heading, number of data, number of parameters and precision.

(2) It asks whether a profile generated from a function (2a), or an experimental chromatogram (2b) has to be resolved. In step 2a1, the theoretical chromatogram is generated and the graph of its profile is drawn. In step 2a2, if requested, the integral of each component peak and the integral corres-

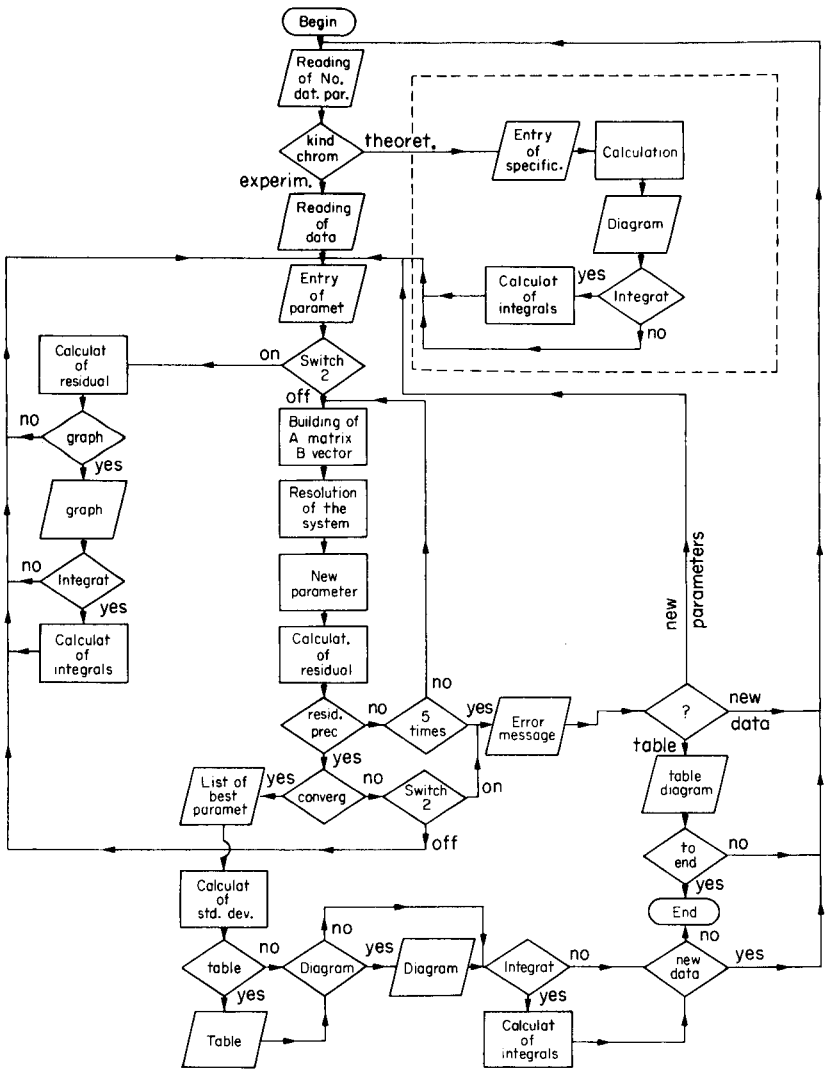

Fig. 1. DAFNA program.

ponding to the overlapping area of two peaks are given. Thereafter the program goes to step 3. In step 2b, the data from the experimental chromatogram are read; thereafter, the program goes to step 3.

(3) The program asks, through the teletype, for the initial adjustment parameters. If the latter are to be estimated then switch 2 on (continued in step 3a), otherwise switch 2 off (continued in step 4). In step 3a, the residual sum of squares is calculated for the parameters entered. In step 3b, the program asks whether the graph of the discrepancy between the experimental data and those corresponding to the parameters entered, should be drawn; if the answer is yes the graph is drawn. In step 3c, the program asks if the integrals under each peak formed by the parameters introduced are of interest. If the answer is yes, it calculates the integral by the Simpson 1/3 method. In step 3d, the program returns to point 3.

(4) The residual sum of squares is calculated.

(5) Matrix A and array B of equation $A\delta = B$ are constructed.

(6) The equation $A\bar{\delta} = B$ is solved by the Gauss-Siedel method.

(7) The vector of the initial parameters is increased (see the equation $\bar{\alpha}_{i+1} = \overline{\alpha_i} + \bar{\delta}_i$), and the new residual sum of squares is calculated. Should the calculation still not converge, the program goes back to step 5. Causes of convergence are a residual sum of squares less than 10^{-10}, or a relative diminution between two residual sums of squares smaller than the precision. Causes of divergence are that matrix A is singular, or that the residual sum of squares in an iteration is greater than the previous one on five occasions (not necessarily consecutively). If the calculation has diverged, or switch 2 is on, the program prints a message and asks if entry of new data is required (returning to step 1), or if entry of new initial parameters is needed (returning to step 3), or if, despite the non-convergence, a global listing is required (proceeding to step 11). If the calculation has converged, then the steps are as follows.

(8) The program calculates the determinant of A by the Gauss-Jordan method.

(9) The standard deviations of the parameters adjusted are calculated.

(10) The program asks, through the teletype, if a global listing of the adjustment is required and, if so, the listing is printed.

(11) The program asks if a graph of the adjustment is wanted and, if so, the graph is drawn.

(12) The program asks if the integrals under each peak defined by the adjusted parameters are of interest, if so, they are calculated by the Simpson 1/3 method.

(13) The program asks if any new data are to be adjusted (returning to step 1). Otherwise, the program ends.

POSSIBILITIES FOR DECONVOLUTION OF PEAKS

Before the five functions outlined above were examined for the resolution of experimental chromatograms, the degree of difficulty found in the decon-

volution was studied for increasingly overlapping profiles of theoretical peaks. The solution of the problem is closely related to the values initially chosen for the adjustment. Thus, in profiles with little overlapping, resolution is easy even if the iterative process begins with parameters very different from the correct values; in contrast, when overlapping is severe, the calculation must be stated with parameters fairly near the real values, if adequate resolution is to be achieved.

Usually, when the operator starts a calculation in order to resolve an overlapping profile, the parameters are selected by direct reading of the profile; a little program of initiation may be established for the convergent process on this basis. It is therefore of interest to evaluate the degree of overlapping at which the diverse pairs of functions used here can still be separated, when directly read parameters are taken as initial parameters. It must be emphasized, however, that the DAFNA program is constructed in such a way that it is possible to comfortably adjust profiles whose overlapping makes it necessary to start the adjustment with parameters nearer the real values than those obtained by direct reading. Thus, as pointed out above, if switch 2 is put on before the initial adjustment parameters are entered, the program generates a trial loop.

To establish the degree of separation possible for two functions when the initial parameters are obtained from direct reading of the overlapping profile, option 2a of the DAFNA program was used; this permits the generation of profiles from some given parameters. For each type of function studied, several overlapping profiles were generated: starting from a pair of each of these, one was taken as fixed, and the other was displaced closer and closer to it (by variation of the retention time). The diverse profiles generated by the DAFNA program were adjusted, by using as initial parameters those obtainable by direct reading of the profile. If a particular parameter could not be obtained in this way, because of the intrinsic definition of the function, the initial parameter used was the value assigned to it for generation of the function; such parameters may be approximated as closely as desired in the test version of the DAFNA program.

The degree of profile overlapping was assessed by two features. The first was the relation between the retention time (t_R) and the sum of half-widths at half-height

$$D = 2(t_{Ra} - t_{Rb})/(H_a - H_b) \tag{9}$$

where t_{Ra} and t_{Rb} are the retention times for peaks a and b, respectively, and H_a and H_b are the respective widths at half-height of the band. The second feature was the relation (in percent) between the overlapping area and the total area of the peaks

$$\%A = 2S_s100/(S_a + S_b) \tag{10}$$

where S_s is the overlapping area between peaks a and b, S_a is the area under peak a, and S_b is the area under peak b. These areas were calculated in the DAFNA program by means of the Simpson 1/3 method.

TABLE 1

Resolution of overlapping profiles

Function	D	$\%A$
Gaussian	0.9	31.7
Log–normal	1.0	26.6
Gamma	0.4	76.2
Weibull	0.9	25.6
Littlewood	1.0	32.1

In Table 1 are listed the maximal degrees of overlapping that can be resolved for each function when the iterative process is initiated with parameters read directly from the profile. However, better performance is possible with the DAFNA program when its estimation parameters loop is used. As can be seen from Table 1, four of the functions perform quite similarly. The discrepancy in the case of the gamma function is due to this function having three parameters, one of which (the α coefficient) is introduced as its real value; this coefficient cannot be read directly on a profile, because of the definition of the function (Eqn. 3), thus the result obtained is not strictly comparable with the corresponding results from other functions.

In the study of the Weibull function, an interesting result was the existence of several minima in the corresponding residual sum-of-squares function (Eqn. 6). Indeed, the wrong adjustment parameters shown in Table 2 were obtained with a precision of 0.001, whereas the correct adjustment parameters were obtained with a precision of 0.0001. The adjusted overlapping profile was generated from the parameters with correct adjustment.

TABLE 2

Parameters obtained with the Weibull function by wrong and correct adjustment

Parameters	First peak		Second peak	
	Value	Std. Dev.	Value	Std. Dev.
Correct adjustment				
Maximum height	1.00000	1.86×10^{-8}	1.00000	1.09×10^{-7}
Corr. t_R	15.0000	4.75×10^{-7}	25.0000	3.57×10^{-7}
Starting point	2.00000	8.80×10^{-7}	15.0000	9.81×10^{-7}
C parameter	3.00000	3.16×10^{-7}	3.00000	1.46×10^{-7}
Residual sum of squares	1.40951×10^{-14}			
Wrong adjustment				
Maximum height	0.784046	2.46×10^{-2}	1.17447	3.61×10^{-3}
Corr. t_R	13.1084	7.69×10^{-2}	23.8727	5.08×10^{-2}
Starting point	1.63029	1.37×10^{-1}	4.84121	1.53
C parameter	3.21477	3.79×10^{-2}	4.38051	2.45×10^{-1}
Residual sum of squares	2.88947×10^{-4}			

The existence of local minima in the residual sum-of-squares function is not an important obstacle in the adjustment of theoretical overlappings. When experimental chromatograms have to be adjusted, however, these minima can cause erroneous solutions because the increase in the precision of the adjustment becomes limited by the number and quality of the points used to describe the profiles.

EXPERIMENTAL CHROMATOGRAMS STUDIED

The criteria for the usefulness of the diverse functions studied were based primarily on the capacity of reproduction of the quantitative composition of the chromatographed mixture, from the resulting areas of the decomposition of the profile (after consideration of the relative molar responses), and secondarily on the value of the residual sum of squares corresponding to the adjustment (Eqn. 6).

Dialkyl adipates

A mixture of 48.84% dimethyl adipate and 51.16% diethyl adipate, in chloroform solution was chromatographed in an EGS column, at 140°C. The chromatographic profile obtained showed fairly symmetrical peaks and little overlapping. The results obtained in the adjustment of the chromatogram by means of the five functions studied are shown in Table 3. Figure 2 shows one of the adjustments obtained by deconvolution of the chromatogram. The profiles obtained were very similar, whichever function was used, and resolution was possible with only small errors. Yet, it is surprising that the functions defined by four parameters (log—normal and Weibull) did not give the minimal errors in the relative areas, although the log—normal distribution gave the least residual sum of squares in the adjustment.

Dialkyl malonates and succinates

Another chromatographic profile studied was that from a mixture of dimethyl malonate (11.80%), diethyl malonate (13.17%), dimethyl succinate (37.98%) and diethyl succinate (36.45%) in chloroform solution, which was chromatographed in an EGS column at 140°C. This chromatogram shows

TABLE 3

Results for a chromatogram of dimethyl adipate and diethyl adipate

Function	Relative error of areas (%)	Residual sum of squares
Gaussian	0.3	0.195
Log—normal	1.1	0.111
Gamma	0.4	0.168
Weibull	1.5	0.161
Littlewood	0.2	0.173

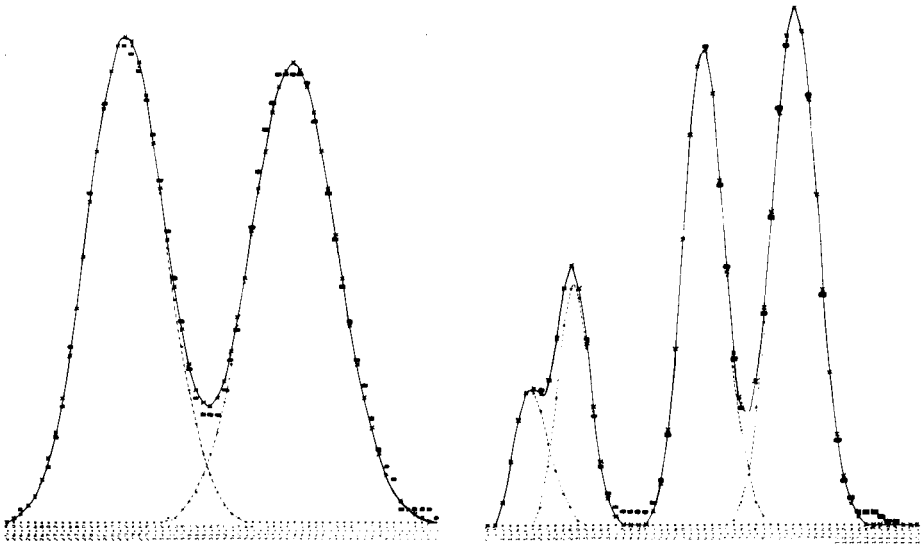

Fig. 2. Adjustment profile of chromatogram for a mixture of dimethyl adipate and diethyl adipate with symmetric peaks and little overlapping. The total adjustment profile and the contour of each component peak are indicated with continuous (——) and dotted (- - - -) lines. (▪) Real points; (×) adjusted points in the chromatogram. Priority pointing rule: × over ▪. Real points are not shown where they coincide with adjusted points.

Fig. 3. Adjustment profile for a mixture of dialkyl malonates and succinates (symmetric peaks and strong overlapping) with the gamma function. Symbols as in Fig. 2.

some fairly symmetric peaks, with strong overlapping in those corresponding to dimethyl malonate and diethyl malonate, and little overlapping in those corresponding to dimethyl succinate and diethyl succinate. The experimental chromatogram is compared with the profile obtained with the gamma function in Fig. 3; the results are very similar to those provided by the Gauss and Littlewood functions. Figure 4 shows the adjustment profile obtained with the log—normal function, which was very close to that afforded by the Weibull function. Table 4 lists the results obtained in the adjustment of each function.

TABLE 4

Results for a chromatogram of dialkyl malonates and succinates

Function	Relative error of areas (%)				
	Dimethyl malonate	Diethyl malonate	Dimethyl succinate	Diethyl succinate	Residual sum of squares
Gaussian	−17.6	9.8	0.1	1.8	0.816
Log—normal	81.6	−40.6	−5.5	−5.4	0.379
Gamma	15.4	−8.9	−0.3	−1.3	0.658
Weibull	83.0	−46.4	−4.8	−4.8	1.124
Littlewood	5.3	−2.9	−0.2	−0.4	0.668

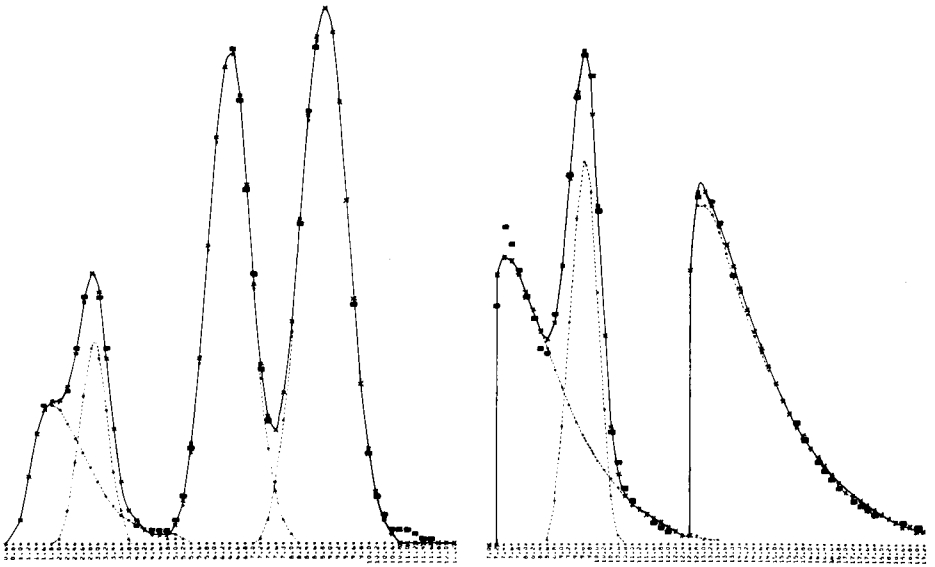

Fig. 4. Adjustment profile of the chromatogram used in Fig. 3 with the log—normal function. Symbols as in Fig. 2.

Fig. 5. Adjustment profile for a chromatogram from acetic acid, butylglycol acetate and propionic acid with the Weibull function. Symbols as in Fig. 2.

In this chromatogram, the relative errors of the ratios of the areas obtained were greater than those in the previous adjustment. The large errors resulting from the utilization of the log—normal and Weibull functions are due to the appearance of a very wide profile describing the peak corresponding to dimethyl malonate. In those two cases, the residual sum-of-squares function presents a minimum which has to be rejected, from a practical chromatographic point of view. It must, therefore, be concluded that neither of these functions is suitable for this adjustment, or that some restrictive criterion must be introduced in the variation of the parameters for the adjustment, so that the minimum adjusted may be coherent with chromatographic intuition.

Acetic acid, butylglycol acetate and propionic acid

In the study of the profile generated from a mixture of 39.57% acetic acid, 17.77% butylglycol acetate and 42.71% propionic acid, chromatographed on a Carbowax 20M column at 80°C, particularly interesting results were obtained (Fig. 5). The Gauss, gamma and Littlewood functions proved ineffective for adjustment of such very asymmetric peaks. The log—normal function and the Weibull function described the chromatographic profile of the mixture to a fair approximation; the errors caused in the area ratios may be considered acceptable, given the extraordinary asymmetry of the component peaks. Table 5 lists the results obtained with these two functions; the adjustment profile corresponding to the Weibull function is shown in Fig. 5.

TABLE 5

Results for a chromatogram of acetic acid, butylglycol acetate and propionic acid

Function	Relative error of areas (%)			
	Acetic acid	Butylglycol acetate	Propionic acid	Residual sum of squares
Log—normal	−7.5	9.4	3.1	9.849
Weibull	−1.0	−0.8	1.3	5.336

Finally, from the practical point of view, it may be emphasized that the method is useful when conventional integrators are unable to determine correctly the areas of the overlapped, asymmetric or tailing peaks. Given that there are no serious problems in linking a computer to a chromatograph, the methods presented above are useful in practical chromatography.

REFERENCES

1 J. C. Bartlet and D. M. Smith, Can. J. Chem., 38 (1960) 2057.
2 R. D. B. Fraser and E. Suzuki, Anal. Chem., 41 (1969) 37.
3 F. Hock, Chromatographia, 2 (1969) 334.
4 S. Polezzo and M. Tamarasso, Chim. Ind. (Milan), 44 (1962) 33.
5 S. M. Roberts, Anal. Chem., 44 (1972) 503.
6 S. M. Roberts, D. H. Wilkinson and L. R. Walker, Anal. Chem., 42 (1970) 886.
7 B. Sen, Anal. Chim. Acta, 22 (1960) 130.
8 A. W. Westerberg, Anal. Chem., 41 (1969) 1770.
9 A. B. Littlewood, A. H. Anderson, T. C. Gibb, in C. L. A. Harbourn (Ed.), Gas Chromatography, 1968, Proc. Seventh Int. Symp., Institute of Petroleum, London, 1969, p. 297.
10 J. C. Sternberg, Adv. Chromatogr., 6 (1968) 173.
11 T. S. Buys and K. Clerk, Anal. Chem., 44 (1972) 1273.
12 E. Grushka, M. N. Myers and J. C. Giddings, Anal. Chem., 42 (1970) 21.
13 A. H. Anderson, T. C. Gibb and A. B. Littlewood, Chromatographia, 2 (1969) 446; J. Chromatogr. Sci., 8 (1970) 640.
14 A. H. Anderson, T. C. Gibb and A. B. Littlewood, Anal. Chem., 42 (1970) 434.
15 E. Cuso, X. Guardino, J. M. Riera and M. Gassiot, J. Chromatogr., 95 (1974) 147.
16 H. M. Gladney, B. F. Dowden and J. D. Swalen, Anal. Chem., 41 (1969) 883.
17 E. Grushka, Anal. Chem., 44 (1972) 1733.
18 L. G. McWilliam and H. C. Bolton, Anal. Chem., 41 (1969) 1755; 43 (1971) 883.
19 R. E. Pauls and L. B. Rogers, Anal. Chem., 49 (1977) 625.
20 W. W. Yau, Anal. Chem., 49 (1977) 395.
21 S. N. Chesler and S. P. Cram, Anal. Chem., 43 (1971) 1943.
22 E. Grushka, M. N. Myers, P. D. Schetteler and J. C. Giddings, Anal. Chem., 41 (1969) 889.
23 O. Grubner, Adv. Chromatogr., 6 (1968) 173; Anal. Chem., 43 (1971) 1934.
24 D. M. Himmelblau, Process Analysis by Statistical Methods, Wiley, New York, 1970, pp. 10—48.
25 D. B. Siano, J. Chem. Educ., 49 (1972) 755.
26 D. B. Siano and D. E. Metzler, J. Chem. Phys., 51 (1969) 1856.
27 X. Tomas, J. Grimalt and R. Fortuny, Afinidad, 36 (1979) 357.
28 G. C. Allen and R. F. McMeeking, Anal. Chim. Acta, 103 (1978) 73.

Analytica Chimica Acta, 139 (1982) 167—176
Elsevier Scientific Publishing Company, Amsterdam — Printed in The Netherlands

THE DETERMINATION OF TECHNETIUM-99 IN SEAWATER AND MARINE ALGAE

J. P. RILEY* and S. A. SIDDIQUI[a]

Department of Oceanography, University of Liverpool, P.O. Box 147, Liverpool, L69 3BX (Gt. Britain)

(Received 28th January 1982)

SUMMARY

Technetium-99 is preconcentrated from acidified seawater containing a trace of bromine by adsorbing it as the pertechnetate ion on the anion exchanger Duolite A101D. After elution with 4 M nitric acid, it is purified from other radionuclides by scavenging with hydrous iron(III) oxide and extracting from 5 M sodium hydroxide medium into methyl ethyl ketone. The organic phase is then evaporated and technetium is electrodeposited from oxalic acid medium onto a bronze disc and counted with a low background β-counter. Overall recovery is >90% and the precision is ± 0.2 pCi l^{-1} at a technetium level of 0.6—1.0 pCi l^{-1}. Concentrations of the radionuclide in the central Irish Sea were found to lie in the range 0.4—2 pCi l^{-1}. The same analytical scheme can be used for determining the element in nitric acid digests of marine algae.

Although technetium is known to be generated in the stars [1], the fact that all its isotopes are radioactive and have relatively short half-lives (maximum 2.6×10^6 y), means that no primordial technetium still exists on earth. Technetium-99 (half-life 2.15×10^6 y) is, however, a major product of the fission of uranium, thorium-232 and plutonium-239 [2] and as a consequence is produced during the explosion of nuclear bombs and in nuclear power plants. It is also produced naturally in negligible amounts by the spontaneous fission of uranium-238 [1]. Bomb-generated technetium-99 has been detected in rainwater [3, 4] and freshwater [5]. However, at present the most important input of this radionuclide to the environment appears to arise from the gaseous [6] and aqueous effluents [7—9] from nuclear power plants. Hunt [10] has reported that an authorization was issued in September 1977 for the marine disposal of waste from the Windscale Processing Works, in which ^{99}Tc was the only significant radioactive component, and this suggests that appreciable amounts of this nuclide must be entering the sea, not only from this plant, but also from many others. Indeed, even as early as 1973 it had been reported to be present in algae from the Irish Sea [11, 12], being particularly strongly concentrated in the Fucoid seaweeds (up to 400 pCi g^{-1} on a wet weight basis). Further work [10] has confirmed

[a]Present address: Institute of Marine Biology, University of Karachi, Karachi 32, Pakistan.

0022-2860/82/0000-0000/$02.75

the existence of this nuclide in a variety of different marine organisms from areas influenced by the discharges from the processing plants at Windscale and Capenhurst. However, no information is available about the concentration and distribution of this nuclide in the sea. This may in part be the result of the lack of a suitable technique for its determination in seawater and the development of such a technique is described in the present paper.

PRECONCENTRATION OF TECHNETIUM

Techniques involving a preliminary evaporative concentration of the alkaline sample, which have been employed for the determination of technetium in freshwater [4, 5], are obviously unsuitable for the analysis of seawater. The close chemical similarity between technetium and rhenium, its neighbour in Group 7b of the Periodic Table, suggested that it should occur in seawater as the pertechnetate ion, TeO_4^-, [13] and that it should be possible to concentrate it by adsorption onto an anion exchanger [14] because of the low degree of hydration of this anion [15]. Accordingly, experiments were carried out in which 1-l samples of bromine-containing seawater which had been spiked with $^{99}TcO_4^-$ and made 0.1 M in hydrochloric acid were passed through 9 cm × 0.3 cm^2 columns packed with the chloride forms of Deacidite FF1P, Duolite A101D, Dowex-1 and AG2-X8. It was found by liquid β-counting that retention of technetium was in each instance >85%, but that the maximum recovery was achieved on the Duolite A101D resin. This resin was therefore adopted for all subsequent work.

Tests were then made to determine the optimum conditions for elution of the adsorbed technetium. Following earlier work [16, 17], elution was done first with 4 M nitric acid, but it was found that although the bulk of the activity was eluted with ~70 ml of the acid, the peak tended to tail, and even after passage of 100 ml only about 88% of the technetium was eluted. As an almost identical elution pattern was observed if the acid strength was increased to 8 M, it was decided to try to improve the recovery by eluting at higher temperatures. This considerably improved the sharpness and efficiency of the elution, and at 65°C a 99% recovery could be achieved with 90 ml of 4 M nitric acid (Fig. 1). This technique was therefore adopted. Since all these tests had been carried out with unrealistically high concentrations of technetium, triplicate 10-l samples of acidified (0.1 M in HCl) seawater containing 25 ml of bromine-saturated water were spiked with 31 pCi of ^{99}Tc. They were then passed through columns of Duolite and eluted at 65°C with 4 M nitric acid. The eluates were neutralized to pH 7.0 ± 0.2 and technetium was prepared for β-counting by electrodeposition as described in the Experimental section. A blank was run in the same way using seawater which had not been spiked with technetium. Comparison of the β-counts with the count obtained from a disc which had been directly plated with the spiked amount of technetium showed recoveries of 98.0, 97.5 and 97.3% (mean 97.6%) after allowance had been made for technetium present in the blank.

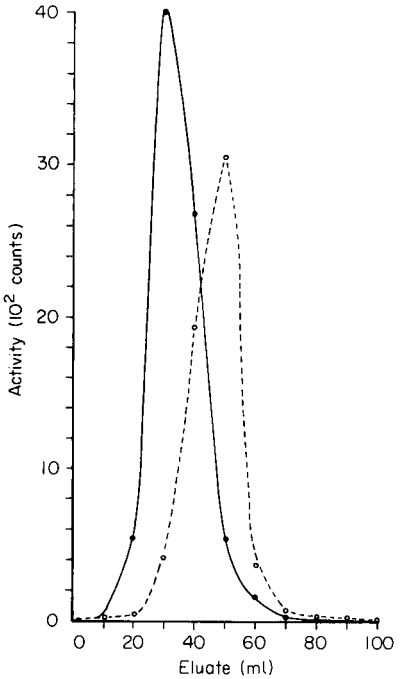

Fig. 1. Elution of technetium from Duolite A101D resin with 4 M nitric acid at (○) 25°C and (●) 65°C. Activity is given as background-corrected counts.

Low activities of a wide range of other radionuclides both naturally occurring and man-made are also present in the sea, many of the latter being waste products of the nuclear industry. Because of this, a study was made of the behaviour of several of the principal elements concerned during the anion-exchange preconcentration process. Aliquots (100 ml) of filtered seawater were acidified to 0.1 M in hydrochloric and 1 ml of bromine water and suitable activities of radionuclides of the appropriate elements were added. The mixtures were submitted to ion exchange as described above. Activities of the percolates and nitric acid eluates were then measured to assess the extent of retention of the nuclide by the resin and the total proportion eluted. The results (Table 1) showed that all the elements concerned were retained to some extent and that most of them were also present in the 4 M nitric acid eluate in significant amounts. This means that it is necessary to employ an efficient clean-up procedure before plating and counting technetium.

Clean-up of technetium

A review of the literature suggested that efficient decontamination of technetium(VII) might be achieved by extracting it from 5 M sodium hydroxide medium with methyl ethyl ketone [18—20]. Gerlit [21] has demonstrated that the distribution coefficient for pertechnetate in this process is

TABLE 1

Uptake of various elements from seawater by anion-exchange resin and their elution with 4 M nitric acid at 65°C

Element	% Retained	% Eluted with 4 M HNO_3	Element	% Retained	% Eluted with 4 M HNO_3
Ce(III)	3.0	1.5	Sb(III)	27.0	27.0
Cr(III)	0.0	0.0	Th(IV)	50.0	0.0
Cu(II)	8.7	9.0	Tl(I)	100.0	0.0
Fe(III)	4.3	0.8	U(VI)	6.7	0.5
Nb(V)	61.0	23.0	Y(III)	85.0	15.0
Nd(V)	5.0	1.0	Zn(II)	28.0	0.0
Ru(VIII)	43.0	3.5	Zr(IV)	2.5	2.5

much greater than that for many other elements (e.g., Ru $<10^{-4}$). Accordingly, experiments were carried out to check the efficiency with which technetium could be extracted. Replicate 40-ml aliquots of 5 M sodium hydroxide solution were spiked with tracer amounts of pertechnetate solution and extracted consecutively with 15-, 5- and 5-ml aliquots of methyl ethyl ketone. The combined organic phases were washed with 5 ml of 5 M sodium hydroxide and then evaporated in a beaker containing 10 ml of water. After the solvent had evaporated, the aqueous phase was evaporated, and the β-activity of a 10-ml aliquot was measured in a liquid geiger counter and compared with that of the appropriately diluted stock technetium solution. It was found that this process gave a recovery of 100.3 ± 0.8%.

The extraction of a range of other elements under these conditions was then tested, using either radiotracer or atomic absorption techniques for the determination of the amount of the possible interferent present in the residue from the evaporation of the ketone. There was no significant extraction of any of the elements tested, (Table 2), with the exception of ruthenium which was extracted to the extent of ~0.5%. It seemed probable therefore that the solvent extraction procedure would provide a satisfactory degree of

TABLE 2

Percentage extraction of fourteen elements from 5 M sodium hydroxide solution into methyl ethyl ketone

Extraction (%)	Element[a]
0.0	Ba^{2+} (1250), Ce^{4+} (737), Co^{2+} (375), Cr^{3+} (250), Fe^{3+} (250), Mn^{2+} (35), Mo^{6+} (350), Nb^{5+} (125), Nd^{3+} (187), Th^{4+} (1000), Zn^{2+} (125), Zr^{4+} (250), U^{6+} (1000)
0.5	Ru^{3+} (100)

[a]The amount tested (in μg) is given in parentheses. Ba, Co, Cr, Fe, Mn, Mo and Zn were measured by a.a.s. and the others radiometrically.

decontamination of the preconcentrated technetium. However, to ensure radiochemical purity, it was decided to add a preliminary purification stage. For this purpose, coprecipitation at pH 8—9 with ~10 mg of iron(III) as its hydrous oxide was employed, as it is known that the precipitate scavenges ruthenium and many other elements very efficiently, and as it was found that technetium is not significantly coprecipitated (<0.1%).

Preparation of technetium for counting

The β-activity of technetium which can be recovered from a volume of sample which is convenient to handle is very low and must be counted with a low-background GM counter equipped with anti-coincidence circuitry. This necessitates presenting the sample to the counter in the form of a disc. Initially, attempts were made to coprecipitate technetium(VII) with either nitron or tetraphenylarsonium perrhenates [21] for counting. However, recoveries proved to be both low and unreproducible. Attention was therefore given to electrodeposition of the element, as this provides a convenient counting source and has been claimed by several workers [22—25] to give high recoveries. The method described by Rogers [22] was first tested. In this, technetium ($>10^{-4}$ M) is plated as the dioxide from 2 M sodium hydroxide medium onto a stainless steel disc. Unfortunately, when the technetium concentration was reduced to 10^{-10} M (the approximate level which would be expected in the concentrates from the separation process), deposition became extremely slow and even after 33 h only ~80% was deposited. Attempts were next made to deposit 1.8 ng of technetium at pH 2.3 and a potential of 0.8 V (vs. SCE) as described by Flagg and Bleidner [23]. It was found that even after 22 h the recovery was only 70% compared with the quantitative yield claimed by these authors. Satisfactory recoveries (~99%) were achieved at pH 2.5 by prolonged (~20 h) electrolysis in the presence of ~0.1% fluoride ion [24]. However, it was felt that a shorter deposition period would be more convenient and the procedure developed by Box [25] was therefore tested. In this, electrolysis is carried out from a medium which is 0.7 M and 0.45 M in oxalic acid and sulphuric acid, respectively. Under these conditions with a bronze disc as cathode and a current density of ~200 mA cm^{-2}, six separate measurements showed that technetium could be deposited with an efficiency of 98.1 ± 0.8% in 8 h. This procedure was therefore adopted for the plating of element from the concentrate in readiness for counting with the low-background GM counter.

Mineralization of organic tissues

It is obviously of importance to know the extent to which technetium discharged into the sea enters the marine food chain. It was thought that the analytical scheme developed above might be applicable to the determination of the element in digests prepared from marine organisms. Tests were therefore made radiochemically with samples of *Fucus vesiculosus* to determine satisfactory conditions for the destruction of the organic tissues

without loss of technetium as its somewhat volatile heptoxide. It was found that adequate mineralization could be achieved by refluxing the sample with concentrated nitric acid for several hours. Under these conditions technetium spikes could be recovered quantitatively.

EXPERIMENTAL

Apparatus

The electrolysis apparatus is shown diagrammatically in Fig. 2. The cell consists of a 75-ml glass beaker contained in a water bath cooled by means of a copper spiral through which tap-water flows. The cathode consists of a bronze disc (2.5 cm diameter) which is placed in the drilled-out screw cap of a plastic specimen tube from which the bottom has been removed. Leakage of electrolyte to the rear of the disc is prevented by an O-ring. Electrical connection to the disc is made by resting a copper rod on it. A piece of platinum foil (1 × 2.2 cm) serves as the anode. Electrolysis is done at ~25°C with a current density of ~200 mA cm^{-2} while stirring magnetically.

Technetium-99 activity was measured with a Nuclear Enterprises low-background β-counter (Type 6016) equipped with anti-coincidence unit (Type 2079) and coupled to a Nuclear Enterprises timer/scaler (Model No. ST6).

Reagents

All water to be used in the analysis and in the preparation of reagents was doubly-distilled from silica. Concentrated nitric acid and constant-boiling (6.5 M) hydrochloric acid were redistilled from a silica still. For the bromine water, redistilled water was saturated with bromine. All chemicals were of analytical-reagent grade.

Formic acid—hydrochloric acid mixture. Mix 475 ml of 98% formic acid with 25 ml of concentrated hydrochloric acid.

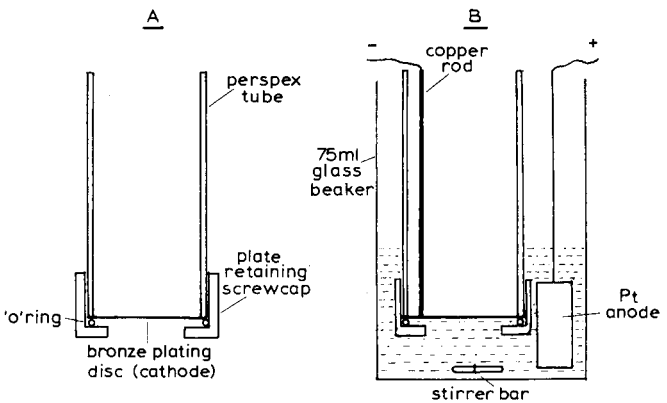

Fig. 2. Cell assembly for electrodeposition of technetium. (A) Construction of cathode; (B) cell.

Acetone—hydrochloric acid mixture. Mix 475 ml of acetone with 25 ml of concentrated hydrochloric acid.

Anion exchanger. Back-wash Duolite A101D resin (50—100 mesh) with a current of water to remove "fines". Purify it by digestion twice on a boiling water-bath with ten times its volume of 2 M hydrochloric acid, and then wash free of acid with redistilled water. Pack a slurry of the resin into 0.6-cm bore ion-exchange columns to give a packed length of ~3 cm.

Method

Filter 10 l of the freshly collected seawater through an acid-washed Whatman GF/F glass fibre filter using gentle suction. Add to the filtrate 150 ml of 6.5 M hydrochloric acid and 50 ml of saturated bromine water. Allow the mixture to flow through the anion-exchange column at a flow rate not exceeding 6 ml min^{-1}. Wash the column with 50 ml of redistilled water and reject the washings. Place the column in a water bath at 65°C, and after thermal equilibrium has been attained, elute technetium with 90 ml of hot (65°C) 4 M nitric acid and wash the column with 10 ml of redistilled water. Combine the eluate and washings in a 150-ml beaker.

Slowly add 14.5 g of sodium hydroxide pellets to the solution while stirring continuously and cooling. Check that the resultant solution is slightly alkaline and then add gradually while stirring a solution of 0.85 ml of iron(III) chloride (59—61% solution) in 10 ml of water. Allow the precipitate of hydrous iron(III) oxide to settle for 5 min. Decant the supernatant liquid through a Whatman GF/F filter and then transfer the precipitate to the filter and wash it with 5 ml of 4 M sodium hydroxide solution. Reject the filter. Combine the filtrate and washings and evaporate to about 50 ml on a water-bath. Dissolve 5.5 g of sodium hydroxide in the cold solution, cool and transfer to a separatory funnel. Extract the solution using successively 15-, 5- and 5-ml portions of methyl ethyl ketone. Wash the combined extracts with 5 ml of 5 M sodium hydroxide. Transfer the organic extract to a small beaker containing 25 ml of distilled water. Evaporate the ketone on the water-bath leaving the technetium in the water.

Dilute the solution to ~40 ml with distilled water, add 10 ml of 4 M sulphuric and 3.2 g of oxalic acid, and stir until the latter has dissolved. Insert the electrodes into the solution and electrodeposit technetium onto the bronze disc using a current of ~0.5 A, while stirring magnetically. After 8 h, switch off the current and rinse the disc first with water and then with methanol. After the methanol has evaporated, count the β-activity of the disc with the low-background counter for at least 3×10^4 s. Carry out a blank in the same manner using 5 l of distilled water instead of the sample. Standardize the method in the same way using 5 l of distilled water which has been spiked with a known activity of ^{99}Tc (2—5 pCi).

Determination of technetium-99 in algae

Weigh out accurately 1 g of the dried (105°C) sample into a 250-ml conical flask, add 25 ml of concentrated nitric acid, and fit a reflux condenser.

Warm cautiously on a hot plate, removing the flask as necessary when the reaction becomes vigorous. Reflux the sample until brown fumes cease to evolve and all the organic tissues have dissolved. Cool, pour into water and neutralize with 5 M sodium hydroxide. Dilute to ~500 ml with water, and add 5 ml of hydrochloric acid and 5 ml of saturated bromine water. Filter the solution to remove any siliceous residue and then pass it through the anion-exchange column. Continue the analysis as described above for seawater. Determine the reagent blank in the same way, but omitting the sample. Standardize the procedure by carrying a blank spiked with a known (pCi) amount of technetium through the whole procedure.

Check on purity of technetium

The purity of the electrodeposited technetium can be checked by determining the aluminium β-absorption curve, and also by testing for the absence of α-emitters by counting the disc in an α-scintillation counter. As a further check, the deposited technetium can be submitted to a further stage of purification and the specific activity again determined. Because the activity isolated from 10 l of seawater is so low, it is advantageous to strip the activity from 4 discs by treating them briefly with 5 M nitric acid, to combine the solutions and to replate the technetium as described previously.

Procedure. After counting, strip the disc with a few drops of 5 M nitric acid and wash it with a few ml of water. Add 1 ml of bromine water and evaporate the solution on the water-bath. Dissolve the residue in 10 ml of formic acid—hydrochloric acid mixture. Pass the solution through a 7 × 0.6-cm column of Duolite A101D resin which has been previously equilibrated by passage of 50 ml of the same mixture. Wash the column with 75 ml of the same mixture followed by 25 ml of 0.5 M hydrochloric acid. Discard the percolate and washings. Elute the column with 45 ml of acetone—hydrochloric acid mixture and then wash it with 25 ml of water. Combine the eluate and washings and evaporate them to dryness on a water-bath. Dissolve the residue in 10 ml of 4 M sulphuric acid, dilute to ~50 ml with water, add 3.2 g of oxalic acid, and electrodeposit technetium as described above. Determine the yield of the separation process by electrodepositing a known amount of technetium on to a disc and, after counting, stripping it and then subjecting it to the process described above. A knowledge of the ratio of the counts of the electrodeposited technetium before and after the ion-exchange process enables allowance to be made for losses occurring with the sample during the purification process. Normally, the recovery is ~75%.

RESULTS AND DISCUSSION

Accuracy and precision of the methods

Seawater. The precision of the method was tested by conducting replicate determinations on 10-l aliquots of a number of samples of filtered coastal water from the Irish Sea. These showed an average standard deviation of

±0.2 pCi l^{-1}. In order to test the accuracy of the procedure, a 10-ml sample of seawater which had been previously found to have an activity of 4.2 pCi ^{99}Tc l^{-1} was spiked with 15.4 pCi ^{99}Tc l^{-1} and analysed again. The spiked sample was found to have a technetium activity of 19.6 pCi l^{-1} corresponding to a technetium recovery of ~97%.

Seaweed. A well-washed dried sample of *Fucus vesiculosus* collected from near Meols, Cheshire, was analysed in quadruplicate. These showed a technetium activity of 17.9 ± 2.2 pCi g^{-1}. Two 1-g portions of the same material were spiked with 15.4 and 30.8 pCi of technetium and analysed again. Activities of 32.6 and 47.9 pCi g^{-1} were found respectively, corresponding to technetium recoveries of 95% and 100%.

Confirmation of identity and purity of technetium

In the analysis of environmental samples for radio-nuclides, it is essential that the radiochemical purity and identity of the activity finally isolated is confirmed. For ^{99}Tc, this presents some difficulties on account of its relatively long half-life and the fact that it is not a γ-emitter. In the present instance, the activities isolated from both the seawater and seaweed samples

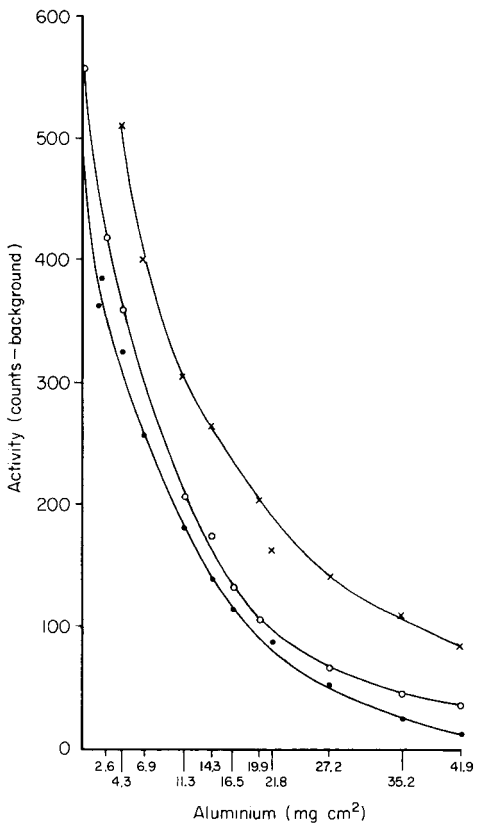

Fig. 3. Aluminium absorption curves for β-energy of ^{99}Tc standard (•) and activities isolated from seawater (○) and *Fucus vesiculosus* (×).

were confirmed in two ways: (i) by determination of the aluminium absorption curves, which for both types proved to be similar to that given by pure ^{99}Tc (Fig. 3); (ii) by submitting the deposited technetium to further purification by non-aqueous ion exchange [14] (see Experimental section) and then counting again after redeposition. If the technetium were pure, then the initial and final counts (after correction for losses in the ion-exchange procedure of ~14%) should be the same. This proved to be the case for both the seawater and the seaweed, thus confirming the radiochemical purity of the ^{99}Tc activity isolated from them.

REFERENCES

1 B. T. Kenna and P. K. Kuroda, J. Inorg. Nucl. Chem., 23 (1962) 142.
2 G. H. Cartledge, J. Am. Chem. Soc., 77 (1955) 2658.
3 M. Attrep, M.Sc. Thesis, University of Arkansas, AR, 1962.
4 M. Attrep, J. A. Enochs and L. D. Broz, Environ. Sci. Technol., 5 (1971) 344.
5 N. W. Golchert and J. Sedlet, Anal. Chem., 41 (1969) 669.
6 F. P. Brauer, R. W. Goles, J. H. Kaye and H. G. Reich, Proc. 4th Joint Conf. on Sensing of Environmental Pollution, 1977, Am. Chem. Soc., Washington, DC.
7 B. G. Blaylock and J. P. Witherspoon, Proc. Symp. on the Impacts of Nuclear Releases into the Aquatic Environment, 1975, Otaniemi, Finland, I.A.E.A., Vienna, ST1/PUB/406.
8 J. J. Anderson and R. L. Walker, Anal. Chem., 52 (1980) 709.
9 W. W. Schulz, Trans. Am. Nucl. Soc., 34 (1980) 395.
10 G. J. Hunt, Aquatic Environment Monitoring Rep. No. 3, 1979, Ministry of Agriculture, Fisheries and Food, London.
11 J. W. R. Dutton and R. B. Ibbett, Proc. Symp. on the Determination of Radionuclides in Marine Biological Materials, 1973, London.
12 N. T. Mitchell, Tech. Rep. Fish. Radiobiol. Lab., 9 (1971) 1.
13 D. R. Turner, M. Whitfield and A. D. Dickson, Geochim. Cosmochim. Acta, 45 (1981) 855.
14 A. D. Matthews and J. P. Riley, Anal. Chim. Acta, 51 (1970) 455.
15 A. K. Lavrukhina and A. A. Posdnyakov, Analytical Chemistry of Technetium, Promethium, Astatine and Francium, Ann Arbor-Humphry, London, 1970.
16 E. H. Huffman, R. L. Oswalt and L. A. Williams, J. Inorg. Nucl. Chem., 3 (1956) 49.
17 F. P. Roberts, F. M. Smith and E. J. Wheelwright, Nucl. Sci. Abstr., 31 (1962) 345.
18 V. V. Bochkarev, E. E. Kulish and I. F. Tupitzyn, Proc. 2nd Int. Conf. on Peaceful Uses of Atomic Energy, 1958, Geneva.
19 A. F. Kuzina, Zh. Anal. Khim., 17 (1962) 489.
20 V. I. Goldanskii, New Elements in the Periodic Table, Atomizdat, Moscow, 1964.
21 J. B. Gerlit, Proc. Int. Conf. on Peaceful Uses of Atomic Energy, 1956, U.N.E.S.C.O., Geneva.
22 L. B. Rogers, J. Am. Chem. Soc., 71 (1949) 1507.
23 J. F. Flagg and W. E. Bleidner, J. Chem. Phys., 13 (1945) 269.
24 E. Anders, The Radiochemistry of Technetium, Nucl. Sci. Ser., Natl. Acad. Sci., Natl. Res. Counc., Washington, DC, 1960.
25 W. D. Box, Nucl. Appl., 1 (1965) 155. (Quoted in G. L. Ruffs, Crit. Rev. Anal. Chem., 1 (1970) 355.)

Analytica Chimica Acta, 139 (1982) 177—186
Elsevier Scientific Publishing Company, Amsterdam — Printed in The Netherlands

DETERMINATION OF CESIUM IN SEAWATER BY RADIOCHEMICAL METHODS

V. I. SHAMAEV* and T. V. CHUDINOVSKICH
Mendeleev Institute of Chemical Technology, Moscow (U.S.S.R.)
(Received 26th October 1981)

SUMMARY

Radiochemical methods for the determination of cesium in seawater are described. Preliminary substoichiometric concentration with nickel hexacyanoferrate(II) and tetraphenylborate and application of selective radiochemical techniques are used. The cesium content in Atlantic Ocean samples is 0.74 ± 0.03 $\mu g\ l^{-1}$. The method is applicable on board ship. The approach should be generally useful.

The determination of cesium in seawater is a difficult analytical problem, as the content of cesium in seawater is $4—9 \times 10^{-10}$ g ml^{-1} whereas the amounts of rubidium, potassium and sodium present are respectively about 10^3, 2×10^6 and 10^8 times greater, when molar ratios are considered. Cesium in seawater has been determined by flame photometry after preconcentration on molybdenyl phosphate and extraction with sodium tetraphenylborate into nitrobenzene [1]. Activation analysis has been applied after concentration of cesium on Amberlite IR105 resin [2]. The low concentration of cesium in seawater and the relatively large concentrations of other alkali elements make such preliminary concentrations essential but uncontrolled losses of cesium are unavoidable.

The determination of cesium in seawater by radiochemical methods has seemed impossible, partly because of insufficient sensitivity (the limit of detection for substoichiometric variants of radiometric correction and isotope dilution methods with extraction processes is about 10^{-6} g ml^{-1}), and partly because of inadequate selectivity; direct determinations of cesium by such methods are possible only in the presence of about equimolar quantities of potassium. Cesium has been determined in the presence of a 60-fold amount of potassium [3] and in the presence of an 8-fold amount of rubidium [4]. Isolation with different quantities of reagent [5] allowed the determination of cesium in the presence of 100-fold amounts of potassium and 20-fold amounts of rubidium; interpolation and comparative methods [6] made it possible to tolerate 150-fold amounts of potassium and 40-fold amounts of rubidium. Combination of these methods with substoichiometric preconcentration [7—9] enabled cesium to be determined in the presence of a 400-fold amount of rubidium and a 10^4-fold amount of potas-

0003-2670/82/0000-0000/$02.75

sium. All these methods were based on extraction with tetraphenylborate or magnesium dipicrylaminate into nitrobenzene. These data indicate that the application of extraction processes alone is not enough to solve the problems of determining cesium in seawater. Further, the exchange constants for cesium with other alkali metals in the tetraphenylborate (TPB) extraction ($\beta_{Cs/K} = 25$, $\beta_{Cs/Na} = 2500$, $\beta_{Cs/Rb} = 5$) do not provide the necessary selectivity. Preliminary concentration of cesium by other methods was therefore examined.

CONCENTRATION OF CESIUM ON HEXACYANOFERRATE(II) SALTS OF TRANSITION METALS

First, the exchange constants (ratios of equilibrium constants) between cesium, rubidium and potassium for mixed hexacyanoferrate(II) precipitates with different metals were determined, and the dependence of these exchange constants (β) on the relative quantities of alkali metal, transition metal and hexacyanoferrate(II) ions was investigated. Precipitations were done at pH 1—2 from hot solutions containing corresponding quantities of potassium (or rubidium), micro quantities of ^{137}Cs and corresponding quantities of transition metal ions, by slow addition of sodium hexacyanoferrate(II) solution with stirring.

The exchange constants were calculated by means of the equation [10]

$$\beta = [(1 - \alpha_{Cs})/\alpha_{Cs}] \{[m_K - m_{HC}/n + m_{Cs}(1 - \alpha_{Cs})]/ [m_{HC}/n - m_{Cs}(1 - \alpha_{Cs})]\} \quad (1)$$

where m_{HC}, m_{Cs} and m_K are the molar amounts of hexacyanoferrate(II), cesium and potassium ions; $\alpha_{Cs} = A_{filtrate}/A_{init.}$ is the unprecipitated fraction of cesium; and n is the stoichiometric ratio in the precipitate (HC/K).

In all experiments, the initial ratio used was $m_{Me}/m_{HC} = 3$; when a large excess of alkali metal is present, this leads to the formation of a precipitate of the composition $Me_3K_2[Fe(CN)_6]_2$ [11]. Therefore, in these experiments, $n = 1$. As micro amounts of cesium were used with $m_{K(Rb)} \gg m_{HC}$, Eqn. (1) can be simplified to

$$\beta = \frac{1 - \alpha_{Cs}}{\alpha_{Cs}} \times \frac{m_K - \frac{m}{n}_{HC} + m_{Cs}(1 - \alpha_{Cs})}{\frac{m}{n}_{HC} - m_{Cs}(1 - \alpha_{Cs})} \quad (2)$$

It is easy to see that the exchange constant then coincides with the crystallization coefficient for the linear law of co-crystallization.

The results of these experiments are given in Tables 1 ($\beta_{Cs/K}$) and 2 ($\beta_{Cs/Rb}$). In both cases, the best selectivity was attained with the mixed precipitate of nickel ($\beta_{Cs/K} \approx 10^5$, $\beta_{Cs/Rb} \approx 3 \times 10^2$). Even with a 2000-fold excess of potassium over hexacyanoferrate(II), precipitation of ^{137}Cs was nearly complete (97.8%). In Fig. 1 are presented the results of a study of the influence of pH on the degree of cesium sorption. The optimal range for the precipitations is pH 1—2.

TABLE 1

Exchange constants ($\beta_{Cs/K}$) for cesium and potassium precipitation with hexacyanoferrate(II) salts of some transition elements

Metal	m_K (mmol)	m_{HC} (mmol)	$\lambda = \frac{m_K}{m_{HC}}$	$1 - \alpha$	β
Cu	6.16	3.096×10^{-3}	1990	0.796	9398
Ni	30.8	1.55×10^{-2}	1990	0.978	88320
Hg	13.73	5.56×10^{-3}	2469	0.726	6539
Co	27.72	1.38×10^{-2}	2016	0.949	37462
Cd	13.73	1.11×10^{-2}	1235	0.128	362
Zn	13.73	1.76×10^{-2}	780	0.366	450

TABLE 2

Exchange constants ($\beta_{Cs/Rb}$) for cesium and rubidium precipitation with hexacyanoferrate(II) salts of some transition elements

Metal	m_{Rb} (mmol)	m_{HC} (mmol)	$\lambda = \frac{m_{Rb}}{m_{HC}}$	$1 - \alpha$	β
Cu	0.21	2.15×10^{-3}	97.68	0.469	127
Ni	2.75	2.75×10^{-2}	100.0	0.768	363
Hg	5.085	4.75×10^{-2}	107.1	0.391	68.1

The dependence of β on the composition of the precipitates was investigated for the mixed potassium—cobalt hexacyanoferrate(II). Constant concentrations of potassium (m_K = 25.74 mmol, V = 15 ml) and hexacyanoferrate(II) ($m_{HC} = 7.04 \times 10^{-3}$ mmol) were used with a variable concentration of cobalt ions. Results are given in Fig. 2, which also shows the relationship

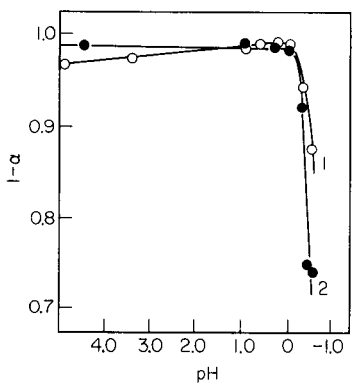

Fig. 1. The influence of pH on the sorption of ^{137}Cs with cobalt hexacyanoferrate(II). (1) Precipitation with sodium hexacyanoferrate(II); (2) precipitation with potassium hexacyanoferrate(II).

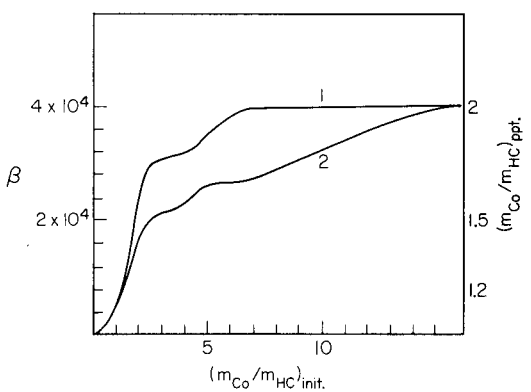

Fig. 2. Dependence of the exchange constant ($\beta_{Cs/K}$) (curve 1) and of the composition of the precipitate (curve 2) on the initial ratio of cobalt to hexacyanoferrate(II) ions.

between the composition of the precipitate and the initial (m_{Co}/m_{HC}) ratio [11]. The latter curve was used to calculate the n value. As can be seen from Fig. 2, the exchange constant increases with increasing $(m_{Co}/m_{HC})_{init.}$ ratio up to $(m_{Co}/m_{HC})_{init.} \approx 6$ and then remains constant. The precipitation of cesium must therefore be done with a big enough m_{Me}/m_{HC} ratio.

The influence of the m_K/m_{HC} ratio on exchange constants was investigated for the precipitates formed with mercury or cobalt hexacyanoferrate(II). The experimental data from the mercury hexacyanoferrate(II) tests are given in Table 3; clearly, β changes very little with varying λ values.

Development of the analytical method

On the basis of the above results, as well as previous data for the separation of alkali metals by extraction with tetraphenylborate into nitrobenzene [6], a general analytical scheme was worked out and model calculations were done by computer in order to choose the best variant of the scheme. The equations were as proposed earlier.

The degree of separation (D_s) of cesium from its mixtures with potassium and rubidium was calculated from the equation [12]

$$D_s = 1 - \alpha/\alpha = [\beta_1\beta_2(1 + m_1/m_2)]/[(\lambda - 1)\beta_1 + \beta_2(m_1/m_2)] \quad (3)$$

where m_1 and m_2 are the molar amounts of the first and second macrocomponents of the mixture (potassium and rubidium); β_1 and β_2 are the exchange constants of the microcomponent (Cs) with the first (K) and the second (Rb) macrocomponents; α is the unisolated fraction of cesium; and $\lambda = (m_K + m_{Rb})n/m_{HC}$.

For calculation of the degree of separation of rubidium at the first stage of cesium preconcentration, when $m_K \gg m_{Rb} \gg m_{Cs}$, the equation, proposed earlier [8] was applied

$$1 - \alpha_{Rb} = \beta_{Rb/K}/[\lambda + (\beta_{Rb/K} - 1)] \quad (4)$$

For calculation of the degree of rubidium separation at the second stage of concentration when its quantity becomes comparable with the amount of potassium but still much greater than the amount of cesium, the equation of the calibration curve method [13] was used

TABLE 3

Influence of the m_K/m_{HC} ratio on the $\beta_{Cs/K}$ value for the precipitation of potassium mercury hexacyanoferrate(II)[a]

m_K (mmol)	m_{HC} (mmol)	$\lambda = \frac{m_K}{m_{HC}}$	$1 - \alpha$	β
13.73	5.56×10^{-3}	2469	0.726	6539
25.74	5.56×10^{-3}	4629	0.600	6944
24.02	4.45×10^{-3}	5401	0.550	6600
26.77	3.89×10^{-3}	6882	0.521	7484
27.11	3.34×10^{-3}	8117	0.499	8083
27.46	2.78×10^{-3}	9876	0.446	7950

[a] $m_{Hg}/m_{HC} = 3$; pH 1—2.

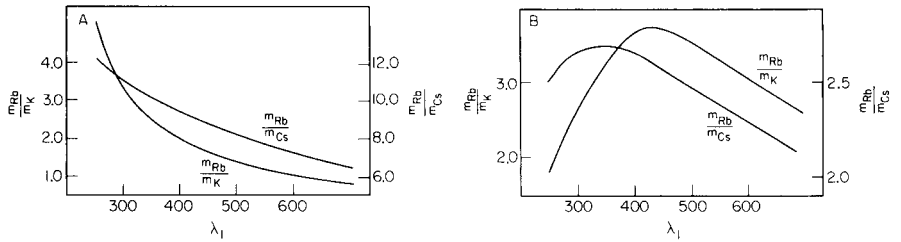

Fig. 3. Model calculations of Rb/Cs and Rb/K ratios after the second and third steps of cesium preconcentration for $\lambda_1\lambda_2 = 1.5 \times 10^6$ = const. and $\lambda_3 = 6$ = const. (A) Second precipitation with nickel hexacyanoferrate(II); (B) extraction with tetraphenylborate.

$$\alpha_{Rb} = \{d + [d^2 + 4\, m_{Rb}(m_0 - m_{HC}/n)(\beta_{Rb/K} - 1)]^{1/2}\}/2\, m_{Rb}(\beta_{Rb/Cs} - 1) \quad (5)$$

where $d = (\beta_{Rb/Cs} - 1)(m_{Rb} - m_{HC}/n) - m_0$, and $m_0 = m_K + m_{Rb}$.

The ratios between the alkali metals were calculated after each stage of preconcentration for two successive precipitations with nickel hexacyanoferrate(II) (λ_1 and λ_2) followed by extraction with tetraphenylborate into nitrobenzene (λ_3). Figure 3 shows the results of these calculations for the conditions $\lambda_1\lambda_2 = 2.5 \times 10^5$ = const. and $\lambda_3 = 6$ = const., where λ is the ratio of the total number of moles of alkali metal to the number of moles of reagent. Table 4 gives the results of calculations for the condition $\lambda_1\lambda_2\lambda_3 = 1.5 \times 10^6$ = const.

The model calculations show that the initial multicomponent system of alkali metals can be reduced by the three-step preconcentration to a two-component system containing cesium and rubidium; the small quantities of potassium remaining at $\lambda_1 < 400$ do not interfere with the determination of cesium. The content of cesium in the final solution is only 3—5-fold less than that of rubidium (see last two lines in Table 4). The extraction step in the scheme for cesium preconcentration is necessary because of technical difficulties in the separation of the hexacyanoferrate(II) precipitate at such low concentrations, and because it is necessary to know the precise value of m_0 in the final solution in order to determine cesium by the comparative or interpolation methods.

EXPERIMENTAL

In the general scheme proposed, the solution of four alkali metals is first treated with nickel hexacyanoferrate(II) ($\lambda_1 \approx 400$). The precipitate containing rubidium and cesium and part of the potassium is dissolved in concentrated sulfuric acid and subjected to a second precipitation of nickel hexacyanoferrate(II) ($\lambda_2 \approx 450$), which leaves most of the potassium and part of the rubidium in solution. Again the precipitate is dissolved in concentrated sulfuric acid, and the solution is extracted with tetraphenylborate ($\lambda_3 = 10$). The solution obtained by re-extraction with 1 M hydrochloric acid contains rubidium, cesium and a little potassium, and is used for the determination of cesium.

TABLE 4

Model calculations for preconcentration of cesium from seawater for $\lambda_1\lambda_2\lambda_3 = 1.5 \times 10^6$ and $(m_0)_3 = 2.67 \times 10^{-5}$ mmol

λ_1	$(m_0)_1$ (mmol)	λ_2	$(m_0)_2$ (mmol)	$\left(\frac{m_{Rb}}{m_{Cs}}\right)_2$	$\left(\frac{m_{Rb}}{m_K}\right)_2$	λ_3	$\left(\frac{m_{Rb}}{m_{Cs}}\right)_3$	$\left(\frac{m_{Rb}}{m_K}\right)_3$
500	0.800	1500	5.33×10^{-5}	3.05	2.08	2.0	1.12	1.06
480	0.833	1040	8.01×10^{-5}	4.50	1.82	3.0	1.35	1.35
460	0.870	815	1.06×10^{-4}	5.99	1.76	4.0	1.75	1.46
440	0.909	682	1.33×10^{-4}	7.55	1.77	5.0	2.17	2.56
425	0.941	590	1.59×10^{-4}	9.09	1.79	6.0	2.62	3.67
410	0.976	523	1.86×10^{-4}	10.7	1.81	7.0	3.13	5.65
400	1.00	469	2.13×10^{-4}	12.29	1.82	8.0	3.65	10.03
390	1.025	427	2.40×10^{-4}	13.9	1.84	9.0	4.22	28.50

A similar, but simpler, scheme can be applied for the determination of rubidium in seawater. Model calculations show that for this purpose one precipitation with nickel hexacyanoferrate(II) ($\lambda \approx 1000$) and one extraction with tetraphenylborate ($\lambda \approx 10$) are sufficient.

The precipitated fraction of rubidium ($\beta_{Rb/K} = 243$) corresponds to $1 - \alpha_{Rb}$ (= 243/(1000 + 242) = 0.196). The amount of rubidium in the precipitate (for 1 l of seawater) is $m_{Rb} = (m_{Rb})_{init.}\ (1 - \alpha_{Rb}) = 2.4 \times 10^{-6} \times 0.196 = 4.6 \times 10^{-7}$ mol. The amount of potassium in the precipitate is $m_K = m_{HC} = 10^{-5}$ mol. The extracted fraction of rubidium ($\beta_{Rb/K} = 5$) is $1 - \alpha_{Rb} = 5/14 = 0.375$. The amount of extracted rubidium is $m_{Rb} = 4.6 \times 10^{-7} \times 0.375 = 1.72 \times 10^{-7}$ mol. The amount of extracted potassium is $m_K = (10 - 1.72) \times 10^{-7} = 8.28 \times 10^{-7}$ mol and the amount of extracted cesium (yield $\approx$ 40%) is about 2.5×10^{-9} mol. At such relative quantities of alkali metals in the final solution, rubidium can easily be determined by any selective radiochemical method, and its concentration in the initial solution of seawater can be calculated by the radiometric correction method [14].

Preliminary work for the determination of cesium

In preliminary experiments the rubidium—cesium mixtures used were prepared containing the absolute and relative concentrations which corresponded to their expected concentrations in the final solution according to the model calculations. The reagents were suitably purified: nitrobenzene by partial freezing, and lithium hydroxide by a three-step fractional crystallization of lithium hydroxide at a molar ratio $m_{ppt.}/m_{init.}$ of 1:3.

The working pH region and the influence of lithium concentration (lithium hydroxide being used to achieve the necessary pH) on the extraction of trace amounts of cesium were first investigated. The results (Fig. 4) show a maximum on the curve, which can be explained as the competing action of hydrogen and lithium ions on the extraction of micro amounts of cesium. At $C_{Cs} = 10^{-6}$ M, this maximum disappears. The best working region was taken as pH 10—11.

The dependence of the unisolated fraction of cesium on its relative concentration (to rubidium) at low concentrations of both elements is shown in Fig. 5. With decrease in this total concentration (m_0), the isolated fraction of cesium decreases and the slope of the curve $\alpha_{Cs} = f(m_{Cs}/m_0)$ decreases also. But, as can be seen, this slope (for the expected concentrations) still suffices for determinations of cesium by the comparative and interpolation methods [7]. In the comparative method

$$m_x = m_{st}(\alpha_{st}/\alpha_x) + 1.25\, m_{TPB}[(1-\alpha_{st})/\alpha_x]/[(1-\alpha_x)(1-\alpha_{st})] \quad (6)$$

where α_x and α_{st} are the unisolated fractions of cesium in the test and standard solutions, and m_x and m_{st} are the quantities of cesium in the test and standard solutions.

For the interpolation method

$$m_x = m_2[(1-\alpha_x)-(1-\alpha_1)]/(1-\alpha_2)-(1-\alpha_1)] + m_1[(1-\alpha_2) - (1-\alpha_x)]/[(1-\alpha_2)-(1-\alpha_1)] \quad (7)$$

where m_1 and m_2 are the amounts of cesium in the first and second standard solutions, respectively.

Application to seawater

The volumes of the seawater were usually 4 l, but if necessary this could be reduced to 1—2 l. Precipitations of nickel hexacyanoferrate(II) were done at pH 1—2 with $m_{Ni}/m_{HC} = 3$; extraction was done at pH 10.5. The first precipitate of nickel hexacyanoferrate(II) was decanted and finally filtered through a Cinpor membrane filter (0.45-μm pore size). The precipitates were then dissolved in the minimum volume of concentrated sulfuric acid (chemi-

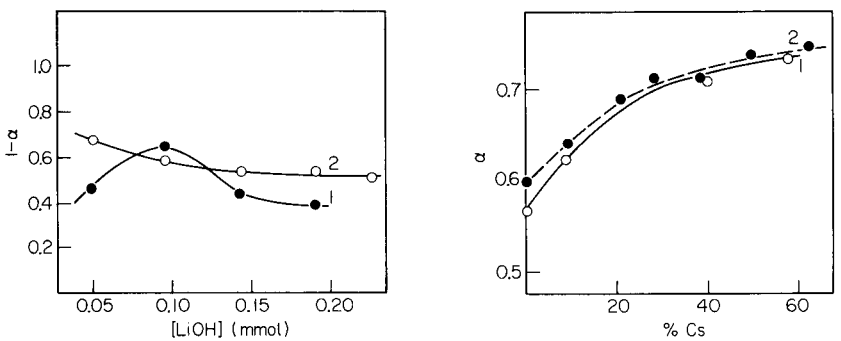

Fig. 4. The influence of the lithium hydroxide concentration on the extraction of cesium with tetraphenylborate into nitrobenzene: (1) ^{137}Cs without carrier; (2) 1.22×10^{-6} M cesium ions.

Fig. 5. Dependence of unextracted fraction of cesium on its absolute and relative (to rubidium) concentration: (1) $C_0 = 1.157 \times 10^{-5}$ M, $m_{TPB} = 2.99 \times 10^{-8}$ mol, $h_0 = 0.259$. (2) $C_0 = 3.85 \times 10^{-6}$ M, $m_{TPB} = 7.84 \times 10^{-9}$ mol, $h_0 = 0.194$.

cally pure) which was then evaporated nearly to dryness. Radioactivities of final solutions (before determinations) were compared with initial radioactivities of the samples for the determination of cesium yield (usually about 30%). The total amount of cesium in the sample volume of seawater was calculated from the equation: $m_{Cs} = m_{det.}A_{init.}/A_{final}$, where $A_{init.}$ and A_{final} are the initial and final (before determination) radioactivities of cesium, and $m_{det.}$ is the amount of cesium found in the "final" solution.

RESULTS AND DISCUSSION

The results of analyses of rubidium—cesium mixtures at low total concentrations of both elements by the comparative and interpolation methods are listed in Table 5. The experimental data show that determinations of cesium are quite possible at the expected cesium concentration in the final solution in the presence of about 10-fold amounts of rubidium.

The proposed scheme of cesium preconcentration and the comparative and interpolation methods for its final measurement were applied in the analyses of 34 samples of seawater taken in different parts of the Atlantic Ocean. The analyses were done directly on board the research ship. In all the tests, the results obtained were practically the same. A slight tendency to increasing cesium concentrations with depth was noted; samples were taken at depths of 10—300 m. However, these differences in cesium concentrations were actually inside the limits of experimental error. Table 6 shows the results obtained for a series of nine samples taken from a depth of 100 m.

The proposed method for cesium determination in seawater was verified by the method of standard additions. The results (Table 7) indicate the absence of systematic error in these determinations.

TABLE 5

Determination of cesium in the presence of rubidium at low concentrations of both elements by means of extraction with tetraphenylborate into nitrobenzene ($C_{TPB} = 1.536 \times 10^{-6}$ M, $V_{org.} = V_{aq.} = 5$ ml, pH 10.5)

m_{Cs} (10^{-8} mol)	m_0 (10^{-8} mol)	$\frac{m_{Rb}}{m_{Cs}}$	$1 - \alpha_{Cs}$	m_{Cs} found (10^{-8} mol)[a]	
				Comparative method	Interpolation method
0	3.56	—	0.417	—	—
0.309	3.504	10.4	0.372	0.445 (44.2)	0.3511 (13.6)
0.515	3.541	5.88	0.351	0.5352 (3.92)	0.5233 (2.0)
0.721	3.569	3.99	0.332	0.7313 (3.20)	0.7272 (0.85)
1.03	3.522	2.42	0.305	1.063 (3.20)	1.069 (3.79)
1.339	3.564	1.66	0.284	1.321 (1.34)	1.393 (4.03)
1.548	3.506	1.265	0.275	1.471 (4.97)	1.549 (0.06)
1.854	3.563	0.92	0.262	1.760 (5.07)	1.837 (0.92)

[a]Values in parentheses are relative standard deviations (%) for $n = 5$.

TABLE 6

Determination of cesium in seawater
(V = 4 l, $(m_{HC})_1$ = 0.103 mmol, λ_1 = 388, $(m_{HC})_2$ = 2.36 × 10^{-7} mol, λ_2 = 436. m_{TPB} = 2.52 × 10^{-8} mol, λ_{TPB} = 9.4)

Sample	Cs yield (%)	Determination of cesium in final solution[a]				
		$1-\alpha$	Comparative method[b]		Interpolation method[c]	
			m_{Cs} (10^{-9} mol)	Cs in water ($\mu g\ l^{-1}$)	m_{Cs} (10^{-9} mol)	Cs in water ($\mu g\ l^{-1}$)
1	31.68	0.368	6.55	0.69	6.61	0.69
2	32.13	0.364	6.91	0.72	7.20	0.75
3	32.53	0.363	6.99	0.71	7.35	0.75
4	33.07	0.360	8.04	0.81	7.80	0.78
5	32.46	0.362	7.87	0.81	7.50	0.77
6	32.34	0.365	6.79	0.70	7.06	0.73
7	35.06	0.359	8.13	0.77	7.95	0.75
8	33.21	0.366	6.74	0.67	6.91	0.69
9	32.89	0.362	7.08	0.72	7.50	0.76

[a] m_0 = 2.52 × 10^{-8} mol; m_{TPB} = 6.72 × 10^{-9} mol; pH 10.5; $V_{org.}$ = $V_{aq.}$ = 5 ml.
[b] Statistical treatment: Cs = 0.73 ± 0.03 $\mu g\ l^{-1}$ (P = 0.9).
[c] Statistical treatment: Cs = 0.74 ± 0.02 $\mu g\ l^{-1}$ (P = 0.9).

The time required for the analysis is mainly determined by the manipulations with the first precipitate (filtration, decomposition with sulfuric acid and evaporation of the solution). The total time of analysis (with precipitation from hot solutions and the use of special vessels with narrow bottoms) is 8—10 h. Several parallel determinations are possible, so that working time per analysis can be reduced significantly.

TABLE 7

Verification of the results by the method of standard additions
(V = 4 l; m_{Ni}/m_{HC} = 3, λ_1 = 388, λ_2 = 436, $(\lambda_3)_{TPB}$ = 9.4)

Cs added (μg)	Total Cs in sample ($\mu g\ l^{-1}$)	Cs yield (%)	Determination of cesium[a]						
			$1-\alpha$	Comparative method			Interpolation method		
				m_{Cs} (10^{-8} mol)	Cs in sample ($\mu g\ l^{-1}$)	δ (%)	m_{Cs} (10^{-8} mol)	Cs in sample ($\mu g\ l^{-1}$)	δ (%)
0	0.74	31.62	0.361	0.795	0.84	13.5	0.765	0.80	8.2
1.44	1.10	28.37	0.352	0.875	1.03	6.3	0.910	1.07	2.72
2.88	1.46	24.65	0.333	1.140	1.54	4.9	1.13	1.53	4.80
4.33	1.82	23.42	0.325	1.160	1.65	9.3	1.19	1.69	7.14
5.77	2.19	18.46	0.314	1.280	2.29	4.6	1.28	2.29	4.6

[a] m_0 = 2.52 × 10^{-8} mol, m_{TPB} = 6.72 × 10^{-9} mol, δ = relative error.

REFERENCES

1 T. R. Folsam, C. Feldman and T. C. Rains, Science, 144 (1964) 538.
2 A. A. Smales and L. Salmon, Analyst, 80 (1955) 37.
3 A. V. Pomerantseva and I. E. Zimakov, Zh. Anal. Khim., 28 (1973) 464.
4 V. I. Spitsyn, V. V. Atraskevich and I. E. Zimakov, Zh. Anal. Khim., 28 (1973) 1465.
5 V. I. Shamaev, J. P. Korchagin and T. V. Chudinovskich, Zh. Anal. Khim., 33 (1978) 286.
6 V. I. Shamaev, V. G. D'Jachkova, Zh. Anal. Khim., 34 (1979) 1065.
7 V. I. Shamaev, Anal. Chim. Acta, 104 (1979) 327.
8 V. I. Shamaev, Anal. Chim. Acta, 106 (1979) 333.
9 V. I. Shamaev, Zh. Anal. Khim., 35 (1980) 885.
10 V. I. Shamaev, Zh. Anal. Khim., 30 (1975) 2069.
11 V. I. Shamaev, Radiokhimiya, 10 (1968) 261.
12 V. I. Shamaev, Zh. Anal. Khim., 34 (1979) 1471.
13 V. I. Shamaev, Zh. Anal. Khim., 27 (1972) 48.
14 V. I. Shamaev, Zh. Anal. Khim., 22 (1967) 988.

Analytica Chimica Acta, 139 (1982) 187—195
Elsevier Scientific Publishing Company, Amsterdam — Printed in The Netherlands

SPECTRAL LINE SHAPE FITTING IN INSTRUMENTAL NEUTRON ACTIVATION ANALYSIS OF POTTERY

JOSEPH YELLIN*

The Hebrew University of Jerusalem, Jerusalem (Israel)

ALBERT E. METZGER

Jet Propulsion Laboratory, California Institute of Technology, Pasadena, CA 91109 (U.S.A.)

(Received 12th December 1981)

SUMMARY

The γ-ray spectrum of a neutron-activated clay standard is analyzed by spectral line shape fitting and the results are compared with an empirical analysis of the spectrum based on detector calibrations. It is concluded that trace element analysis of pottery may be simplified and enhanced by a combination of spectral line shape fitting and detector calibrations.

The complexity of the γ-ray spectra of pottery obtained by instrumental neutron activation analysis (i.n.a.a.) is such that, from a computational point of view, the most expedient way to cope with the γ-ray intensity measurements is by the fractional peak method. In this method, a fixed number of energy channels is summed over the γ-ray photopeak of a particular isotope and, after background subtraction, the intensity is corrected for γ-ray interferences from other isotopes. Only a small portion of the γ-ray spectrum is ever utilized in the fractional peak method. The most useful γ-rays, i.e., those of greatest intensity and relatively free from interferences, are utilized. The method involves a great many calibrations to determine how many channels to sum over a photopeak, where and how to evaluate the background, and the number of interfering counts under the region of peak integration, as well as calibrations for count rate losses caused by peak broadening at higher intensity levels [1]. These calibrations are unique to any detection system and need to be re-evaluated whenever the performance of the detection system is altered. Thus, changing the gain factor of the amplifier (energy/channel) necessitates recalibration, as does any instrumental change that affects the resolution of the detector system. There are many variations to the fractional peak method as applied to isolated photopeaks [2—7]. When the calibrations are done properly, high precision and accuracy are obtained [8, 9].

*On leave at the Jet Propulsion Laboratory, Pasadena, CA 91109, U.S.A.

0003-2670/82/0000-0000/$02.75

An alternative approach is to employ spectral line shape fitting (SLSF) as a means of unfolding the spectrum and removing background interferences. Much or all of the spectrum is fitted by means of least squares to a model of the γ-ray detector response. To the extent that the model faithfully represents the detector response, the spectrum can be accurately unfolded. SLSF is in common use in nuclear research where it is often the only way to interpret unique spectra. It eliminates the need for extensive calibration to account for interferences, except in the case of γ-ray lines which are too nearly coincident in energy to be resolved by the measuring apparatus. In such cases, calibrations are needed to remove the interference by means of a monitor (another γ-ray originating in the same nuclide as the interference, or a γ-ray of an isotope of the interfering nuclide). This paper is designed to show the following points: (1) SLSF may be successfully applied to pottery analysis despite the complexity of the spectra; (2) analysis of pottery for trace elements can be enhanced by recovering information which would be lost in the fractional peak method; (3) SLSF may be used in reverse to extract calibration factors for use in the fractional peak method; (4) combination of SLSF with the fractional peak method leads to significant simplifications in the chemical fingerprinting of pottery by i.n.a.a.

DATA ANALYSIS

Figure 1 is a spectrum of neutron-activated Standard Pottery [8] obtained with a 5-cm^2 Ge(Li) detector approximately eight days after the neutron

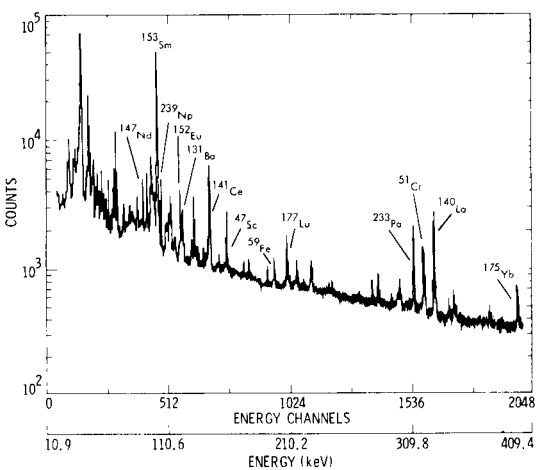

Fig. 1. Part of the γ-ray spectrum of a standard pottery specimen taken with a 5-cm^2 Ge(Li) detector approximately 8 days after neutron irradiation. The weight of the standard was 100 mg and the integrated neutron dose was 1.7×10^{17} n cm^{-2} s^{-1}. The spectrum was accumulated in a 20 min lifetime with the standard 5 mm above the detector window. The FWHM at 121 keV is 780 eV.

irradiation. The spectrum shown covers the energy band from 11 keV to 409 keV. A 20-min live-time data accumulation period was used to take the spectrum. There are 123 measurable γ-ray or x-ray lines in the spectrum, arising from 22 elements. Four elements are normally determined from this spectrum by the fractional peak method: samarium, uranium, barium and lutetium. Other elements are best obtained from higher-energy γ-rays or from other spectra accumulated after the short-lived activities have decayed. The samarium and barium measurements involve interferences and all four elements have serious background problems. The portion of the spectrum from 89 keV to 128 keV (Fig. 2) is quite complex. This energy interval contains the γ-rays that are required to obtain elemental abundance for samarium, uranium and barium, and the problems associated with their measurements are clearly apparent. There is no satisfactory background window for evaluating the baselines, and interferences abound. The ^{153}Sm γ-peak at 103 keV has an interference from the Pu $K\alpha_1$ x-ray which accompanies the decay of ^{239}Np. These two isotopes have similar half-lives (1.95 d and 2.35 d for ^{153}Sm and ^{239}Np, respectively) so it is not possible to eliminate the interference by decay. Both γ-rays must be measured at the same time. For the detector system used in this example and the particular formulae worked out for the peak integrations, the number of interfering Pu x-ray counts is given by 0.70 multiplied by the net ^{239}Np (106-keV) γ-ray count.

For comparison with the fractional peak method, two regions from the portion of the standard pottery spectrum shown in Fig. 1 were processed by the SLSF method. Part of one and all of the second are included in Fig. 2. The first region covers channels 400—500; the second region covers channels 555—600. Region 1, which contains 11 lines, was analyzed in two steps

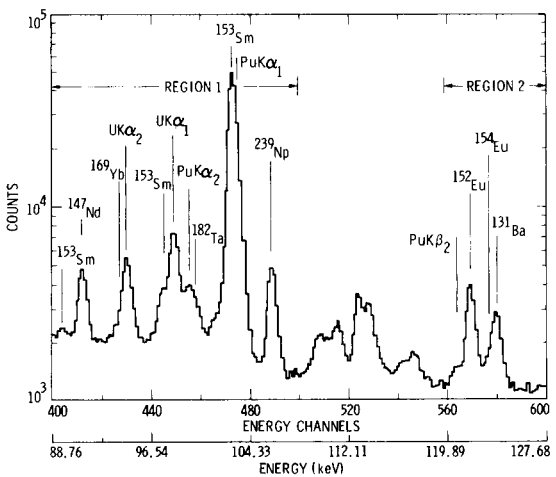

Fig. 2. An exploded view of a portion (88.8—127.7 keV) of the spectrum shown in Fig. 1. Region 1 (88.8—108.2 keV) and region 2 (118.9—127.7 keV) were analyzed by HYPERMET.

because of a programming restriction that no more than 10 photopeaks could be analyzed in any region. In the first step, the region covering channels 420—500 was analyzed for U, Sm, Pu and Np lines; in the second step, channels 346—420 were analyzed, particularly the ^{153}Sm and ^{147}Nd photopeaks centered in channels 403 and 412, respectively. The primary objectives were to compare SLSF intensities with fractional peak intensities where available and, where possible, to compare intensity ratios with expected values. Another objective was to determine whether all interferences known to be in the spectrum could be unfolded by SLSF. The SLSF program chosen to analyze the spectrum was the HYPERMET program of Phillips and Marlow [10]; some other SLSF programs have been reviewed by Lederer [11]. HYPERMET has been applied to the analysis of γ-ray spectra from high-purity germanium γ-ray spectrometers [12].

RESULTS

Table 1 summarizes the SLSF results obtained with HYPERMET. Every γ-ray line known to be in the spectrum was extracted, including lines which are close in energy. Table 2 compares intensity ratios for the U and Pu x-rays, and Sm γ-rays, with expected values from the Table of Isotopes

TABLE 1

Summary of photopeak intensities (counts) analyzed in HYPERMET (SLSF)

Centroid	Energy (keV)	Line	True energy	Intensity
403.70 ± 0.27	89.48 ± 0.05	^{153}Sm	89.48	1175 ± 152
412.02 ± 0.06	91.10 ± 0.13	^{147}Nd	91.10	10841 ± 242
426.53 ± 0.69	93.92 ± 0.13	^{169}Yb	93.61	1197 ± 250
430.31 ± 0.05	94.66 ± 0.01	U $K\alpha_2$ [a]	94.66	14592 ± 398
444.76 ± 0.09	97.47 ± 0.02	^{153}Sm	97.43	6390 ± 244
449.70 ± 0.03	98.43 ± 0.01	U $K\alpha_1$	98.44	23654 ± 403
454.91 ± 0.15	99.44 ± 0.03	Pu $K\alpha_2$ [b]	99.55	6927 ± 448
458.04 ± 0.17	100.05 ± 0.03	^{182}Ta	100.10	4828 ± 402
474.14 ± 0.01	103.19 ± 0.00	^{153}Sm	103.19	208350 ± 2655
477.60 ± 0.14	103.86 ± 0.03	Pu $K\alpha_1$ [c]	103.76	10046 ± 851
489.22 ± 0.03	106.12 ± 0.01	^{239}Np	106.13	14949 ± 302
563.63 ± 0.22	120.60 ± 0.04	Pu $K\beta_2$	120.70	1337 ± 134
569.70 ± 0.04	121.78 ± 0.01	^{152}Eu	121.78	12416 ± 200
576.20 ± 0.21	123.04 ± 0.04	^{154}Eu	123.10	2026 ± 155
580.21 ± 0.06	123.82 ± 0.01	^{131}Ba	123.73	7478 ± 192

[a]The uranium x-rays result from the decay of ^{233}Pa which is produced from neutron capture by ^{232}Th. [b]The plutonium x-rays result from the decay of ^{239}Np which is produced from neutron capture by ^{238}U. [c]The decay of ^{233}Pa is accompanied by a γ-ray at 103.86 keV. The contribution of this γ-ray to the Pu $K\alpha_1$ signal is estimated to be a maximum of 500 counts or 5% of the signal. This estimate is based on an evaluation of the 312 keV γ-ray of ^{233}Pa and the relative production rate of the two γ-rays corrected for detection efficiency.

TABLE 2

Intensity ratios for photopeaks analyzed by HYPERMET (SLSF) and expected values

Ratio	Value	Expected
^{153}Sm (89/98)	0.184 ± 0.025	0.183
^{153}Sm (89/103)	0.0056 ± 0.0007	0.0046
U $K\alpha_2/K\alpha_1$	0.617 ± 0.020	0.619
Pu $K\alpha_2/K\alpha_1$	0.690 ± 0.074	0.625
Pu $K\beta_2/K\alpha_1$	0.133 ± 0.017	0.125
^{239}Np (Pu $K\alpha_1$/106)	0.672 ± 0.058	0.798

[13]. In most cases, the statistics are too poor for the results to be a rigorous test, but the SLSF ratios are in good agreement. Table 3 compares intensities by the SLSF method and the fractional peak method based on detector calibrations. It should be kept in mind when these intensities are compared, that, in the case of the fractional peak method, a finite number of channels is summed over each photopeak, whereas in the case of SLSF the photopeak is integrated over all energies. The number of channels summed over a photopeak by the fractional peak method varies from peak to peak according to energy, and can be approximated by twice the full-width-at-half-maximum (FWHM) except for cases of direct line interference. As a consequence, the SLSF values can be expected to be ~1% higher and the errors are also expected to be somewhat higher. The standard deviation associated with the peak area measurement is dependent on the peak boundaries. Minimum counting errors for an ideal Gaussian line shape are obtained when the number of channels summed over a photopeak is approximately 1.8 × FWHM, with the integration symmetric about the peak channel.

The results by the two methods differ by 1—2.5 SLSF standard deviations (Table 3). This agreement is very good considering the complexity of the spectrum. There is a problem, apparently, with the ^{153}Sm and ^{131}Ba photopeak areas with peaks in channels 474 and 580, respectively. The area of the ^{153}Sm photopeak is larger by the SLSF method than by the fractional peak

TABLE 3

Comparison of photopeak intensities (counts) obtained by HYPERMET (SLSF) and by the fractional peak method

Centroid	Line	SLSF	Fractional peak method
412	^{147}Nd	10841 ± 242	10969 ± 210
474	^{153}Sm	208350 ± 2655	205367 ± 515
489	^{239}Np	14949 ± 302	14838 ± 192
570	^{152}Eu	12416 ± 200	12241 ± 177
580	^{131}Ba	7478 ± 192	7934 ± 151

method by an amount (1.6%) larger than expected from the incomplete peak integration in the latter method. The reason for this difference is almost certainly to be found in the background determination. Most probably, the SLSF background is more reliable. In the other method, one has to rely on a few channels in the narrow background windows to establish the baseline whereas SLSF adjusts the background parameters to obtain a best fit by applying a least-squares analysis to the entire region [10].

Some evidence that the SLSF background determination is more reliable was obtained by analyzing region 1 in one operation. Because the program could not handle more than 10 peaks in a region, the weakest line, the ^{169}Yb photopeak was not extracted and the chi-square of the fit was slightly worse than expected. The ^{153}Sm, ^{147}Nd and U $K\alpha_2$ peak intensities with peaks in channels 403, 412 and 431, respectively, were affected by one standard deviation but none of the other photopeak intensities were significantly affected. In particular, the ^{153}Sm photopeak intensity with a peak in channel 474 was not affected. The region below channel 400 (346—396) has suitable background windows with which both the ^{153}Sm peak in channel 403 and the ^{147}Nd peak in channel 412 are bracketed so that there is little difficulty in fixing the background by either method. Thus there is little question about the SLSF analysis of the region extending from channel 346 to channel 420. The fact that the photopeak intensities were little affected when region 1 was analyzed in one operation, as opposed to a two-step analysis where at least one of the steps included a good background determination, lends support to the validity of the SLSF background value.

DISCUSSION

The SLSF background analysis contrasts with the difficulty in dealing with similar problems by the fractional peak method. In the simple fractional peak method approach, predetermined instruction is employed for background evaluation. Instructions about where to sample the background, how many data channels to average over and the mode of sampling the background (e.g., the minimum sum of N consecutive data channels) are determined by examining a large number of spectra of similar material. Difficulties may arise in dealing with complex spectral regions having narrow background windows (flat regions between peaks) as the windows may further narrow or disappear altogether as a result of peak broadening. Aside from the background problem, there may be another cause for the excessive accumulation in the ^{153}Sm photopeak centered at channel 474, namely interference from the Pu $K\alpha_1$ x-ray line.

A special problem arises with respect to x-ray lines. Included in the spectrum shown in Fig. 2 are five x-ray lines whose analysis by SLSF is inexact in principle. The line shape of an electromagnetic transition observed by the detection system is a convolution of the intrinsic line shape, which is Lorentzian, and the instrumental dispersion, which is essentially Gaussian.

For γ-rays the intrinsic line shape is, for all practical purposes, a delta function, i.e., the intrinsic line width is insignificant compared to the instrumental line width. However, x-ray lines have a finite intrinsic width of about 100 eV owing to their short transition lifetime and this width is an appreciable fraction of the instrumental width. For the measurements reported here, the FWHM was about 780 eV at 122 keV. Thus the x-ray lines should be fitted to a convolution of the instrumental response and the intrinsic Lorentzian line shape [14, 15]. No attempt was made in the methods reported here to treat the x-ray lines differently than the γ-ray lines. While this shortcoming undoubtedly introduces some small error in the SLSF intensity measurements, the errors cannot be large compared to the dispersion in the intensity measurements in the present case. The excellent agreement obtained between intensity measurements by the SLSF and fractional peak methods for γ-ray lines in close proximity to x-ray lines, e.g., ^{152}Eu (Table 3), and for the ratio of x-ray line intensities (Table 2), lends credence to the smallness of the error introduced by ignoring the x-ray line width. Such errors, however, become more pronounced as the instrumental width decreases and as statistics improve. It remains possible, however, that part of the difference observed between the intensities for the 103-keV ^{153}Sm γ-ray line by the two methods is due to the Pu $K\alpha_1$ x-ray.

The Ba, Eu, Pu x-ray quartet of region 2 in Fig. 2 is an interesting example of another type of situation where SLSF is very advantageous. The spectrum shown contains no suitable monitor for unfolding the ^{131}Ba and ^{154}Eu interferences by the fractional peak method. The problem is not how to determine ^{152}Eu (half-life 12.7 y), which can be determined very precisely after the Pu x-ray and ^{131}Ba (half-life 12 d) have decayed, but how to determine barium. The best possibility in the fractional peak method is to truncate the area measurement so as to minimize interferences and to use ^{152}Eu as a monitor for ^{154}Eu. In the present case, this was done by summing only three data channels (3/4 FWHM) on the high energy side of ^{154}Eu and three data channels on the low-energy side of ^{131}Ba (Fig. 2). An empirically determined calibration factor was then used to relate the ^{154}Eu counts under the ^{131}Ba γ-ray peak to the truncated ^{152}Eu integral. The ^{152}Eu integral itself has to be corrected for the Pu $K\beta_2$ x-ray. This method leaves something to be desired as the interference monitor itself has an interference. Furthermore, the factor relating the ^{154}Eu counts to the ^{152}Eu counts depends on the neutron energy distribution of the reactor used for activation and may vary with operating conditions as both ^{151}Eu and ^{153}Eu have strong resonances in their neutron-capture cross-sections. In such a situation, unfolding the quartet of lines by SLSF is a more satisfactory approach. The difference observed for ^{131}Ba in Table 3 is most likely due to an error in the interference factor used to correct ^{131}Ba for the ^{154}Eu interference. When the fractional peak method cannot determine a given element well because of interferences or background problems, that element can usually be determined from another γ-ray in another energy band. Thus for example, barium can be determined

from a 496-keV γ-ray of ^{131}Ba, and europium from a 1408-keV γ-ray of ^{152}Eu. This requires that another spectrum be taken with a coaxial geometry Ge(Li) detector of large volume for adequate detection efficiency at these higher energies. In both these cases, a much larger live-time data accumulation period is needed to achieve statistics comparable to the results shown in Table 3. By using both the fractional peak and SLSF methods, the information recovered from any given spectrum is maximized and the number of calibrations decreased.

A further example of the utility of SLSF is given by the ratio of the Pu $K\alpha_1$ intensity to the ^{239}Np intensity in Table 1. The ratio is 0.67 ± 0.09, comparing favourably with an empirically determined factor of 0.70. This empirical factor was determined by activating a natural uranium glass standard and calibrating the number of Pu $K\alpha_1$ x-rays falling under the ^{153}Sm photopeak in relation to the ^{239}Np photopeak intensity.

Conclusions

Although several specific instances in which the SLSF method yields better results are given above, in most cases the SLSF and fractional peak methods perform comparably. However, the latter method requires many calibrations which, in effect, are never complete because new pottery material of different compositions bring new interferences into play, whereas SLSF requires little calibration. The observed difference between the ^{153}Sm γ-ray intensities by the two methods in Table 3 is partly due to the incomplete peak integration by the fractional peak method. This component of the difference cancels out when the samarium abundance is computed as a ratio of the sample to the standard γ-ray intensity. What remains is insignificant to any conceiveable archaeological application. The much larger error of the SLSF ^{153}Sm γ-ray intensity is only 1% and this is adequate for archaeological application.

The use of SLSF as a routine tool in the i.n.a.a. of pottery is inadvisable if for no other reason that it can greatly increase the computing costs. However, SLSF can be used selectively to great advantage in combination with the fractional peak method. For example, it provides a means of dealing with interferences when no suitable interference monitors exist, and a means of dealing with complex spectral regions with poor background definition. It can be used to extract interference factors for the fractional peak method, or to adjust experimental calibration factors when instrumental changes are made, or as a diagnostic tool for the fractional peak method. An SLSF analysis of the materials in test quickly provides a comprehensive picture of the spectrum and its accompanying problems. However, prior to placing any reliance on SLSF, it is absolutely essential to go through some calibration exercises in order to ascertain that, whichever version of SLSF is used, it faithfully reproduces the detector response.

The evaluation of photopeak areas is a small (though crucial) part of what is involved in data processing of i.n.a.a. spectra [16]. It is a relatively simple

matter to incorporate into a data processing program two area subroutines, one based on fractional peak measurements and one employing SLSF for dealing with problematic spectral regions.

The above results arose from a study intended to establish how well HYPERMET could unfold γ-ray spectra produced by high-energy protons incident on various elemental targets. The use of complex and independently evaluated archaeometric γ-ray spectra provided the answer.

The authors acknowledge the assistance with HYPERMET provided by R. Radocinski and Dr. W. A. Mahoney. This paper is JPL special publication number 326-8174. The Jet Propulsion Laboratory operates under contract with the National Aeronautics and Space Administration.

REFERENCES

1 J. Yellin, Anal. Chim. Acta, 113 (1980) 159.
2 D. F. Covell, Anal. Chem., 31 (1959) 1785.
3 H. P. Yule, Anal. Chem., 40 (1968) 1480.
4 S. Sterlinski, Anal. Chem., 40 (1968) 1995; 42 (1970) 151.
5 P. Quittner, Anal. Chem., 41 (1969) 1504; Nucl. Instrum. Methods, 76 (1969) 115.
6 K. Hoydorn and W. Lada, Anal. Chem., 44 (1972) 2313.
7 P. A. Baedecker, Anal. Chem., 43 (1971) 405.
8 I. Perlman and F. Asaro, Archaeometry, 11 (1969) 21.
9 J. Yellin, I. Perlman, F. Asaro, H. V. Michel and D. F. Mosier, Archaeometry, 20 (1978) 95.
10 G. W. Phillips and K. W. Marlow, NRL Rep. 3198, Naval Research Laboratory, Washington, DC, January 1976.
11 C. M. Lederer, in J. H. Hamilton and J. C. Manthuruthil (Eds.), Radioactivity in Nuclear Spectroscopy, Gordon and Breach, New York, 1972, p. 73.
12 See, e.g., W. Mahony, J. C. Ling and A. S. Jacobson, Nucl. Instrum. Methods, 185 (1981) 449.
13 C. M. Lederer and V. S. Shirley (Eds.), Table of Isotopes, 7th edn., Wiley, New York, 1978.
14 R. Gunnink, Lawrence Livermore Laboratory, Rep. UCRL-76418, June, 1975.
15 D. L. Wilkerson, Nucl. Instrum. Methods, 95 (1971) 259.
16 J. Yellin, J. Radioanal. Chem., 57 (1980) 87.

Analytica Chimica Acta, 139 (1982) 197—205
Elsevier Scientific Publishing Company, Amsterdam — Printed in The Netherlands

A MICROCALORIMETRIC INVESTIGATION OF THE THERMODYNAMICS OF FORMATION OF THE HSO_4^-, $AlSO_4^+$, AND $Al(SO_4)_2^-$ IONS IN AQUEOUS SOLUTIONS AT TEMPERATURES BETWEEN 25 AND 70°C

CHIEN-CHO LO, LOUIS MEITES* and EGON MATIJEVIĆ*

Department of Chemistry and Institute of Colloid and Surface Science, Clarkson College of Technology, Potsdam, NY 13676 (U.S.A.)

(Received 11th February 1982)

SUMMARY

The formation constants and enthalpies of formation of the hydrogen sulfate ion and the mono- and bisulfato complexes of aluminum(III), in aqueous solutions having ionic strengths of 1 M and temperatures ranging from 25 to 70°C, have been evaluated by microcalorimetry.

There is much evidence that the hydrolysis and precipitation of polyvalent metal ions, such as Al^{3+}, Cr^{3+}, and Fe^{3+}, are considerably affected by sulfate ion. For example, much less alkali is needed to produce the first visible precipitate of hydrous aluminum(III) oxide in a solution containing sulfate ion than in one containing only nitrate, chloride, or perchlorate [1—5]. Experience with the preparation of monodispersed particles of the hydrous oxides of aluminum(III) [6], chromium(III) [7], thorium(IV) [8], and iron(III) [9] has shown sulfate ion to have important effects on the shapes and compositions of the particles. It was demonstrated that dissolved metal-sulfate complexes, which act as precursors to the formations of solid phases, are responsible for the observed effects [10, 11].

Specifically, precipitation of aluminum (hydrous) oxides by forced hydrolysis at elevated temperatures of aluminum salt solutions yielded uniform amorphous spherical particles in the presence of sulfate ion [6], while colloidal boehmite of different morphologies was formed in the presence of chloride or perchlorate ions [12]. Furthermore, when a silver iodide sol is coagulated by aluminum(III) ion, the critical coagulation concentration increases at pH values below about 3 if the solution contains sulfate ion, but does not do so if nitrate ion is the only anion present; the effect has been attributed to the formation of the $AlSO_4^+$ complex, and has been used to evaluate its formation constant [13, 14].

The formation of that complex has been studied by several techniques [15—18], and many different values have been obtained for its formation constant. The discrepancies are due partly to interference from hydrolyzed

0003-2670/82/0000-0000/$02.75

species containing aluminum(III), and partly to the failure of some authors to define the experimental conditions adequately. To develop a better understanding of the mechanism of hydrolytic precipitation of aluminum(III), it therefore seemed advisable to re-examine the interaction of aluminum(III) with sulfate ion in solutions having low pH values. Batch microcalorimetry was used to evaluate both the equilibrium constant and the change of enthalpy for the formation of the complex. Both to provide evidence of the reliability of the technique and because data were needed under identical conditions, a similar study was undertaken of the formation of hydrogen sulfate ion.

EXPERIMENTAL

All stock solutions were prepared from the best available reagent-grade chemicals, which were not further purified, and water that had been redistilled in an all-glass apparatus. A 1 M stock solution of aluminum(III) nitrate was filtered through an 0.45-μm Millipore membrane. It was standardized gravimetrically by evaporating a measured volume to dryness under reduced pressure at 40° C and igniting the residue to constant weight in an electric furnace at 1000° C. More dilute (but always at least 0.1 M) working solutions were freshly prepared every few weeks to avoid hydrolysis on aging.

A locally constructed differential twin microcalorimeter was employed. It was similar to one previously described [19, 20], but it incorporated a number of electrical and mechanical refinements. Among these was provision for adding the reagents by means of ampules mounted in specially designed holders that were rotated to stir the solutions and that enabled the ampules in the reaction and reference vessels to be broken simultaneously to initiate a reaction. The temperature coefficients of the matched thermistors (which had resistances very close to 100 000 ohms at 25° C) were evaluated over narrow ranges around each of the temperatures employed, and were used to calculate the sensitivity of the bridge at each temperature.

In all experiments, identical volumes (usually 50 cm^3) of a solution containing a known concentration of sulfate and of predetermined pH were added to the reaction and reference vessels. The ionic strength was kept constant at 1.00 M and was adjusted with sodium perchlorate. The ampule in the reaction vessel contained 0.8 cm^3 of the appropriate reagent, which was perchloric acid in the work on hydrogen sulfate ion, and aluminum nitrate in the work on the aluminum-sulfate complexes. In a few experiments dealing with hydrogen sulfate ion at 25° C, the ionic strength of both solutions was made equal to 0.1 M and the order of addition of the reactants was reversed. The ampule in the reference vessel contained an equal volume of water, or occasionally of a solution of sodium perchlorate of the same concentration as that in the reference vessel. The thermal equivalent of the reaction vessel and its contents was evaluated by electrical calibration [21].

In the work on hydrogen sulfate ion, the compositions of the solutions in the reaction vessel and its ampule were adjusted to give mixtures that contained, at the instant of mixing and before any reaction took place, concentrations of hydrogen ion that ranged from 0.005 to 0.01 M, and of sulfate ion that ranged from 0.03 to 0.3 M. These conditions were chosen after a set of preliminary data that covered wider ranges had been obtained and subjected to pointwise variance analysis [22], which showed that many of the points in that set were nearly devoid of any influence on the values of K and ΔH secured.

All of the calculations were made with the aid of a general computer program for effecting non-linear regression [23] that has been used for many other purposes in these laboratories.

RESULTS AND DISCUSSION

Evaluation of ΔT°

Partly because of the mechanical disturbance that accompanies the breaking of an ampule, partly because only very moderate stirring was employed to minimize the risk of damage of the thermistors by fragments of the ampules, and partly to improve the precision of the result, a non-linear regression procedure was used to evaluate the quantity ΔT°. This denotes the change of temperature that would have occurred if mixing, reaction, and the responses of the thermistors had all been instantaneous, and if there had been no exchange of heat with the surroundings. It is given by the familiar equation

$$\Delta T^\circ = -(\Delta H^\circ)\, N/Q \qquad (1)$$

where ΔH° is the change of enthalpy that accompanies the formation of each mole of product, N is the number of moles of product formed, and Q is the thermal equivalent of the reaction vessel and its contents. Values of ΔT, the measured change of temperature, were obtained from the recorded curve at a number of times t (typically at 18-s intervals from 6 to 258 s) after the reaction had been initiated, and were fitted to the Newtonian heat-exchange equation

$$\Delta T = \Delta T^\circ \exp(-\epsilon t) \qquad (2)$$

where ϵ is the heat exchange coefficient.

Formation of hydrogen sulfate ion

The values of ΔT° thus obtained were first corrected for the heats of dilution of perchloric acid, which were not compensated in the experiments. The corrections were calculated from values given by Parker [24] and were always extremely small.

The number of moles (N in Eqn.1) of hydrogen sulfate ion that is formed in the reaction between hydrogen and sulfate ions at initial concentrations

equal to h and s, respectively, is given by

$$N = V\{h + s + 1/K - [(h + s + 1/K)^2 - 4hs]^{1/2}\}/2 \quad (3)$$

where V is the volume of the reaction mixture (cm^3) and K is the formation constant of hydrogen sulfate ion. Combining this with Eqn. (1), and inserting the known values of V and Q, yields an equation that describes the corrected value of ΔT° as a function of the two independent variables h and s, and that involves two unknown parameters, K and ΔH°. Table 1 summarizes the results thus obtained. For convenience of comparison with values reported in the prior literature, it gives values of K_2^{hs}, the second dissociation constant of sulfuric acid, which is equal to $1/K$, and of the enthalpy of dissociation (rather than formation) of hydrogen sulfate ion.

Only scattered previous results are available for comparison because most earlier workers have chosen to extrapolate their values of K_2^{hs} to infinite dilution. At 25° C the literature values of K_2^{hs} range from 0.0257 to 0.0370 M at an ionic strength of 0.1 M [25—27], and from 0.062 to 0.14 M at an ionic strength of 1.0 M [25, 26, 28]. Each of our values is well within the range of the prior ones. Because ΔH° is unlikely to vary substantially with ionic strength, it seems justifiable to compare our values at 25° C with the average of six published values at the same temperature but at ionic strengths ranging from 0 to 2.0 M [29—34]. That average, −5.48 ± 0.19 kcal mol^{-1}, is nearly identical with the average of the present values at ionic strengths of 0.1 and 1.0 M, which is −5.49 ± 0.08 kcal mol^{-1}. At higher temperatures the data are even scantier. Although Marshall and Jones [35] obtained a value for ΔH° at 50° C that was lower than the average quoted above for 25° C, the general trend of their values is that the exothermic heat of dissociation becomes larger as the temperature increases, and this is confirmed by the results of Lietzke et al. [36]. The same trend may be seen in the present results, which are somewhat larger numerically than those obtained by either of these groups of authors but in better agreement with those of Lietzke et al. For example, whereas the value obtained here was ΔH° = −7.97 kcal mol^{-1} at 70° C, Marshall and Jones [35] obtained −6.79 kcal mol^{-1}, and Lietzke et al. [36] obtained −7.62 kcal mol^{-1}, at 75° C.

TABLE 1

Dissociation constants and enthalpies of dissociation of hydrogen sulfate ion at various temperatures

T (° C)	Ionic strength (M)	K_2^{hs} (M)	ΔH° (kcal mol^{-1})
25	0.1	0.0028_4	−5.57
	1.0	0.103_4	−5.41
35	1.0	0.074_6	−6.13
50	1.0	0.040_1	−6.78
70	1.0	0.028_8	−7.97

The consistency of the present results was evaluated in the following way. First, a least-squares fit of the values of ΔH° to the arbitrary equation

$$\Delta H^\circ = a\,(T - 298.15)^2 + b\,(T - 298.15) + c \qquad (4)$$

provided the values $a = 8.038 \times 10^{-3}$ cal mol^{-1} K^{-2}, $b = -55.61$ cal mol^{-1} K^{-1}, and $c = -5464$ cal mol^{-1}. Evidently c represents the value of ΔH° at 25° C. Combining Eqn. (4) with the familiar equation

$$\mathrm{d} \ln K/\mathrm{d}\, T = \Delta H^\circ/RT^2 \qquad (5)$$

and integrating, yields an expression from which the value of K_2^{hs} at any temperature can be calculated from the value at 25° C. The following results were obtained

Temperature (° C)	25	35	50	70
K_2^{hs}, experimental	0.1034	0.0746	0.0401	0.0288
K_2^{hs}, calculated	(0.1034)	0.0754	0.0462	0.0236

The agreement between the "experimental" values, which are taken from Table 1, and the "calculated" ones, which were obtained in the manner just described, is excellent up to 35° C but deteriorates at higher temperatures. Exactly the same thing is true of the agreement among the corresponding quantities obtained by other authors: at infinite dilution the mean deviation of the literature values is about ±5—10% at 25—35° C but is about ±40% at and above 50° C [30—32, 35, 36].

Formation of aluminum(III)-sulfate complexes

The data resulting on mixing solutions of aluminum(III) and sulfate were analyzed on the basis of several different assumptions about the number of products obtained and their identities. It is generally agreed that $AlSO_4^+$ is formed and is responsible for many of the phenomena observed in such mixtures [13, 16, 17, 37, 38]. However, the literature values of its formation constant at infinite dilution at 25° C range from 370 [14] to 5400 [15] mol^{-1} dm^3, and a reported value [17] of 110 mol^{-1} dm^3 at 30° C seems to increase the uncertainty even more. It was assumed here that $AlSO_4^+$ is the only complex formed, and also that a significant amount of either $Al(SO_4)_2^-$, $Al(HSO_4)^{2+}$, or $Al(OH)(SO_4)$ is formed as well. It was concluded, on grounds to be described below, that the data could not be reproduced satisfactorily except by assuming the formation of both $AlSO_4^+$ and $Al(SO_4)_2^-$ in the mixtures. Thus, only these two complex ions will be considered in the discussions to follow.

Three reactions are assumed to occur

$$Al^{3+} + SO_4^{2-} \rightarrow AlSO_4^+ \qquad K_1, \Delta H_1^\circ \qquad (6)$$

$$AlSO_4^+ + SO_4^{2-} \rightarrow Al(SO_4)_2^- \qquad K_2, \Delta H_2^\circ \qquad (7)$$

$$HSO_4^- \rightarrow H^+ + SO_4^{2-} \qquad K_2^{hs}, \Delta H \qquad (8)$$

Consequently

$$\Delta T^\circ = \Delta T_6^\circ + \Delta T_7^\circ + \Delta T_8^\circ + \Delta T_{\text{diln.}} \tag{9}$$

where ΔT° is the quantity defined above and evaluated by means of Eqn. (2), ΔT_i° is the corresponding change of temperature attributable to the i-th reaction, and $\Delta T_{\text{diln.}}$ is the instantaneous change of temperature caused by the dilution of the solution of aluminum(III) nitrate added to the original contents of the reaction vessel. The enthalpy of dilution of aluminum(III) nitrate was found to be very large: so large, indeed, that the exothermic heat of dilution nearly counterbalances the endothermic heats of formation of the aluminum-sulfate complexes. Very precise enthalpies of dilution of aluminum(III) nitrate were therefore needed but could not be found in the literature. Consequently a value of $\Delta T_{\text{diln.}}$ appropriate to each experiment was obtained from another experiment identical in every way except that sulfate ion was not added to the reaction vessel. Each ΔT_i° is given by an equation of the same form as Eqn. (1)

$$\Delta T_i^\circ = -(\Delta H_i^\circ)\, V\, (\Delta c_i)/Q \tag{10}$$

where V denotes the volume of the reaction mixture and Δc_i denotes the change that takes place in the concentration of a substance involved in the i-th reaction. The concentrations at equilibrium could be calculated by combining expressions for the equilibrium constants with mass-balance equations for sulfate, hydrogen ion, and aluminum(III)

$$s = [SO_4^{2-}] + [HSO_4^-] + [AlSO_4^+] + 2[Al(SO_4)_2^-] \tag{11}$$

$$h = [H^+] + [HSO_4^-] \tag{12}$$

$$m = [Al^{3+}] + [AlSO_4^+] + [Al(SO_4)_2^-] \tag{13}$$

where s and h were defined previously and m denotes the total or analytical concentration of aluminum(III). Combining all these equations and solving for $[SO_4^{2-}]$ yields a quartic equation that was solved by the Newton–Raphson method. It was then easy to compute the equilibrium concentrations of the two aluminum-sulfate complexes and of hydrogen sulfate ion. Because all of the solutions were fairly acidic (pH <3.5) so that the hydrolysis of aluminum(III) would be repressed, the concentration of hydrogen sulfate ion at the instant of mixing was appreciable and had to be subtracted from its equilibrium concentration to obtain the required value of Δc. The latter could be combined with Eqns. (10) and (9) to obtain an expression for ΔT° as a function of the three independent variables s, h, and m, involving four unknown parameters: K_1, ΔH_1°, K_2, and ΔH_2°.

Eight or nine experiments were done at each temperature. Adopting the approach just described, which is exactly parallel to the one used in the work on hydrogen sulfate ion, would therefore have entailed the evaluation of four parameters on the basis of only eight or nine data points. The number of degrees of freedom would have been substantially smaller than it was with hydrogen sulfate ion, for which only half as many parameters had to be calculated from the same amount of data. Each of the changes of enthalpy was

therefore expressed by an equation similar to Eqn. (4). This made it possible to incorporate all of the data into a single fit involving eight adjustable parameters, which were the values of K_1 and K_2 at 25° C and of a_1, b_1, c_1, a_2, b_2, and c_2. In the resulting fit there were 26 degrees of freedom, which suffice to yield reliable results. Values of the dissociation constant and enthalpy of dissociation of hydrogen sulfate ion were also needed, and were taken from Table 1.

The values thus obtained were

$K_1 = 2.84$ mol dm^{-3} $\quad K_2 = 2.02$ mol dm^{-3}

$a_1 = 0.1503$ cal mol^{-1} K^{-2} $\quad a_2 = 1.241$ cal mol^{-1} K^{-2}

$b_1 = -9.60$ cal mol^{-1} K^{-1} $\quad b_2 = 140.6$ cal mol^{-1} K^{-1}

$c_1 = 6925$ cal mol^{-1} $\quad c_2 = 2455$ cal mol^{-1}

Comparison with Eqn. (4) shows that c_i represents the change of enthalpy that accompanies association to form the i-th complex at 25° C. Table 2 lists values of these changes of enthalpy, and of the association constants of the complexes, at other temperatures, obtained by combining these values of the parameters with the integrated form of Eqn. (5).

It was mentioned in an earlier paragraph that the agreement among the values of K_1 in the prior literature is very unsatisfactory. The enthalpies of association seem to have been evaluated only by Izatt et al. [18] who quoted the values $\Delta H_1^\circ = 2.29$ kcal mol^{-1} and $\Delta H_2^\circ = 0.78$ kcal mol^{-1} at 25°C. Both are much smaller than the present values, but their ratio (2.93) is so nearly identical with the ratio found here (2.82) as to suggest that the discrepancy may have been caused by failure to apply an appropriate correction for the large heat of dilution of aluminum(III) nitrate, and the difficulty of applying that correction must also be responsible for the fact that the standard deviation from regression here (0.60 mK) was considerably larger than in the work with hydrogen sulfate ion, where it was 0.2 mK, and that the largest deviations were those at 70° C, where the heat of dilution was largest.

TABLE 2

Association constants and enthalpies of association of $AlSO_4^+$ and $Al(SO_4)_2^-$ ions at various temperatures

(All of the values in this table pertain to an ionic strength of 1.0 M. The value of K_1 and ΔH_1° pertain to the $AlSO_4^+$ ion; those of K_2 and ΔH_2° pertain to the $Al(SO_4)_2^-$ ion.)

T (°C)	K_1 (mol dm^{-3})	ΔH_1° (kcal mol^{-1})	K_2 (mol dm^{-3})	ΔH_2° (kcal mol^{-1})
25	2.84	6.93	2.02	2.46
35	4.14	6.85	2.41	3.99
50	6.95	6.78	3.60	6.75
70	12.9	6.78	8.10	11.3

As was mentioned above, several alternative schemes were investigated. The simplest was that $AlSO_4^+$ is the only complex formed. The standard deviation from regression onto the equation describing this hypothesis was 1.1 mK, and was hardly affected by assuming that either an aluminum hydrogen sulfate or an aluminum hydroxysulfate complex was also formed. Fits to the equations describing the second and third of these hypotheses were ill-behaved: widely different values of the parameters characterizing the "second" complex resulted from different initial estimates. Small values were secured, sometimes for the enthalpy of association and sometimes for the association constant of the "second" complex, indicating that no appreciable change of temperature could be ascribed to the formation of the hydrogen sulfate or hydroxysulfate complex. Such behavior is not uncommon when non-linear regression is used in an attempt to evaluate a parameter having no physical significance. On the other hand, the value $F = 3.24$ was obtained by comparing the variance obtained by regression onto the equation that assumes $AlSO_4^+$ to be the only complex formed with the one obtained by regression onto the equation that assumes $Al(SO_4)_2^-$ to be formed as well. In a one-tailed F-test this corresponds to a level of confidence well above 99% that the bisulfato complex is needed to account for the data.

This work was supported in part by the Electric Power Research Institute under Contract RP-966-2, and in part by the National Science Foundation under grant numbers CHE-7727751 and CHE-8106103. The authors are indebted to Dr. Milan Korn for the construction of the microcalorimeter.

REFERENCES

1 J. H. Hilderbrand, J. Am. Chem. Soc., 35 (1913) 847.
2 H. L. Davis and E. C. Farnham, J. Phys. Chem., 36 (1932) 1037.
3 H. B. Weiser, W. O. Milligan and W. R. Purcell, Ind. Eng. Chem., 33 (1941) 669.
4 P. L. Hayden and A. J. Rubin, in A. J. Rubin (Ed.), Aqueous Environmental Chemistry of Metals, Ann Arbor, Ann Arbor, MI, 1974.
5 H. de Hek, R. J. Stol and P. L. de Bruyn, J. Colloid Interface Sci., 64 (1978) 72.
6 R. Brace and E. Matijević, J. Inorg. Nucl. Chem., 35 (1973) 3691.
7 R. Demchak and E. Matijević, J. Colloid Interface Sci., 31 (1969) 257.
8 N. B. Milić and E. Matijević, J. Colloid Interface Sci., 85 (1982) 306.
9 E. Matijević, R. S. Sapieszko and J. B. Melville, J. Colloid Interface Sci., 50 (1975) 567.
10 A. Bell and E. Matijević, J. Inorg. Nucl. Chem., 37 (1975) 907.
11 R. S. Sapieszko, R. S. Patel and E. Matijević, J. Phys. Chem., 81 (1977) 1061.
12 W. B. Scott and E. Matijević, J. Colloid Interface Sci., 66 (1978) 447.
13 E. Matijević and L. J. Stryker, J. Colloid Interface Sci., 22 (1966) 68.
14 L. J. Stryker and E. Matijević, J. Phys. Chem., 73 (1969) 1484.
15 T. Nishida and R. Tsuchiya, Bull. Chem. Soc. Jpn., 38 (1965) 1398.
16 B. Behr and H. Wendt, Z. Elektrochem., 66 (1962) 223.
17 R. K. Nanda and S. Aditya, Z. Phys. Chem. (Frankfurt am Main), 35 (1962) 139.
18 R. M. Izatt, D. Eatough, J. J. Christensen and C. H. Bartholomew, J. Chem. Soc. A, (1969) 47.
19 T. Meites, L. Meites and J. N. Jaitly, J. Phys. Chem., 73 (1969) 3801.

20 T. Meites and L. Meites, J. Am. Chem. Soc., 92 (1970) 37.
21 L. Lampugnani and L. Meites, Thermochim. Acta, 5 (1973) 351.
22 L. Meites, Anal. Chim. Acta, 74 (1975) 177.
23 L. Meites, Crit. Rev. Anal. Chem., 8 (1979) 1.
24 V. B. Parker, Thermal Properties of Aqueous Uni-univalent Electrolytes, NSRDS-NBS2, U.S. Government Printing Office, Washington, DC, 1965.
25 W. L. Reynolds and S. Fukushima, Inorg. Chem., 2 (1963) 176.
26 D. J. Turner, J. Chem. Soc., Faraday Trans. I, 70 (1974) 1346.
27 M. Kerker, J. Am. Chem. Soc., 79 (1957) 3664.
28 R. W. Ramette and R. F. Stewart, J. Phys. Chem., 65 (1961) 243.
29 J. M. Austin and J. W. Cobble, Inorg. Chem., 66 (1962) 519.
30 V. S. K. Nair and G. H. Nancollas, J. Chem. Soc., (1958) 4144.
31 C. W. Davis, H. W. Jones and C. B. Monk, Trans. Faraday Soc., 48 (1952) 921.
32 J. J. Christensen, R. M. Izatt, L. D. Hansen and J. A. Partridge, J. Phys. Chem., 70 (1966) 2003.
33 K. S. Pitzer, J. Am. Chem. Soc., 59 (1937) 2365.
34 A. G. Zisland, J. Am. Chem. Soc., 81 (1959) 5022.
35 W. L. Marshall and E. V. Jones, J. Phys. Chem., 70 (1966) 4028.
36 M. H. Lietzke, R. W. Stoughton and T. F. Young, J. Phys. Chem., 65 (1961) 2247.
37 S. S. Singh, Can. J. Chem., 47 (1969) 663.
38 J. Miceli and J. Stuehr, J. Am. Chem. Soc., 90 (1968) 6967.

Analytica Chimica Acta, 139 (1982) 207—217
Elsevier Scientific Publishing Company, Amsterdam — Printed in The Netherlands

CONTROLLED ANODIC GENERATION OF THE CATALYST IN KINETIC CONTINUOUS FLOW ANALYSIS

HERBERT WEISZ* and GÜNTER FRITZ

Lehrstuhl für Analytische Chemie, Chemisches Laboratorium der Universität, Freiburg i.Br. (W. Germany)

(Received 4th January 1982)

SUMMARY

Controlled anodic dissolution of copper in a separate generator cell yields well-defined concentrations of catalyst, depending on the voltage applied. This adjustable generation of copper catalyst makes it possible to determine iron over a wide range of concentration (10—1500 μg Fe^{3+} ml^{-1}) via the iron(III)—thiosulphate reaction. By the copper(II)-catalyzed hydrogen peroxide—hydroquinone reaction, EDTA can be determined as an inhibitor (0.5—5 μg ml^{-1}) and cadmium(II) as a reactivator (1—10 μg ml^{-1}). As zinc(II) forms complexes with 2,2'-bipyridine, which activates copper in this reaction, it can be determined (5—50 μg Zn^{2+} ml^{-1}) by measuring the decrease in activation. The electrogeneration of silver ion as a catalyst is also described. The sulphanilic acid—peroxodisulphate reaction is catalyzed by silver(I), which is again activated by 2,2'-bipyridine. Zinc(II) can be determined (0.29—2.9 mg Zn^{2+} ml^{-1}) by the same principle as in the copper(II)-catalyzed reaction.

Many determinations in flow analysis are based on kinetic measurements of catalyzed reactions. This is true for flow-injection techniques [1], for continuous flow techniques [2] and for determinations of continuously changing sample concentrations in an unsegmented sample stream, using one or several unsegmented streams of reagent solution [3]. In all these techniques, a solution of catalyst is usually applied; the only catalysts used in the solid state have been immobilized enzymes. Yet solid catalysts are widely employed in technical chemical processes and in other parts of analytical chemistry, e.g., for the detection of sulphur in the 2— oxidation state in solid samples by the iodine azide reaction [4] and for the decomposition of hydrogen peroxide by elemental platinum.

Efficiency of copper as a catalyst in continuous flow systems

To study the applicability of elemental catalysts in continuous flow systems, the copper(II)-catalyzed reaction of iron(III) with thiosulphate [5] was selected; this has already been applied earlier in flowing systems [3]. The rate of this reaction can easily be followed by measuring the absorbance of the red iron(III) thiocyanate. To investigate the efficiency of elemental copper in this reaction, the metal must be in contact with the flowing solu-

0003-2670/82/0000-0000/$02.75

tion of reagents for a sufficient time. In these preliminary measurements, a small glass-filter tube (1-cm i.d., 2-ml capacity) served as cuvette and reaction chamber, and a copper wire spiral (39-mm long, 0.75-mm diameter, 153 mg in weight) was supported by the filter. The reagent solutions (0.1 mg Fe^{3+} ml^{-1} as iron thiocyanate and a 0.3 mol l^{-1} sodium thiosulphate solution) were pumped into this chamber from the bottom at 1.40 ml min^{-1} each, passing through the filter plate and the catalyst. A small stirrer mixed the solution above the catalyst, where the transmittance of the solution was measured; the light path (i.e., the diameter of the filter tube) was about 1 cm. At the upper end of the tube, the solutions were removed to waste.

The change in the efficiency of the catalyst with time was monitored by pumping the reaction mixtures through this apparatus for several hours, and recording the transmittance of the solution. When the transmittance of the uncatalyzed reaction was set to 0%, these measurements showed a constant transmittance of nearly 100%. This transmittance, which was constant for a few days, was obviously caused by a constant catalytic activity. After a few days, this activity diminished very slowly, while a black coating of copper sulphide was formed on the wire.

The influence of the wire on the reaction was examined as follows. The clean spiral was placed in a test tube and 20 ml of reagent solution (0.1 mol l^{-1} $Na_2S_2O_3$ and 0.5 mol l^{-1} KSCN) was added. The spiral was left in this solution for different times and then removed before the catalytic reaction was started by the addition of 25 ml of iron(III) solution (0.6 mg Fe^{3+} ml^{-1}). The time necessary to decolourize the solution depended on the time that the wire had been in contact with the reagents. Clearly, the catalytic efficiency of the wire was based on copper(II) ions dissolved from the wire.

This constant catalytic efficiency in the flowing system could be used to determine iron(III) continuously. When the above thiosulphate—thiocyanate solution was pumped through the filter tube and copper spiral as outlined above, and sample solutions (0.1—1 mg Fe^{3+} ml^{-1}) were also pumped at a flow rate of 2.43 ml min^{-1}, the concentrations of iron(III) in the samples could be evaluated from a standard graph of the measured signal against iron(III). To simulate a sample stream with continuously changing concentration, the sample solutions were pumped without interruption. The time necessary to reach a constant signal again after the sample had been changed depended on the difference between successive concentrations, but never exceeded 3—4 min. Table 1 gives some results of determinations.

Regulation of the catalytic efficiency of copper by anodic dissolution

As the catalytic efficiency of elemental copper is based on small amounts of copper(II) ions produced by dissolution of the catalyst during contact with the reagent solution, this efficiency should be enhanced by controlled anodic dissolution. Regulation of the efficiency by cathodic removal of the catalyst was described some time ago [6]. During the anodic production of copper(II) ions, the material of the counter electrode must not affect the

TABLE 1

Determination of iron(III)[a]

Taken	0.13	0.26	0.39	0.14	0.91	0.44	0.56	0.75	0.43	0.25
Found	0.10	0.25	0.42	0.10	0.92	0.45	0.60	0.75	0.42	0.25
Diff.	−0.03	−0.01	+0.03	−0.04	+0.01	+0.01	+0.04	0.00	−0.01	0.00

[a]All results are given as mg Fe^{3+} ml^{-1}.

iron(III)—thiosulphate reaction; a platinum cathode was therefore used. In this way, it should be possible to determine a reactant within a shorter reaction time and over a wider range of concentration. Substances which influence the catalytic activity (inhibitors, activators, reactivators) can likewise be determined.

To prevent any influence of the voltage on the reactants, the anodic oxidation of copper had to take place in a separate vessel and the copper(II) ions had to be transferred to the mixing chamber by an inert electrolyte carrier stream. A special generator cell was thus constructed.

EXPERIMENTAL

Equipment

Figure 1 shows the whole apparatus used, as well as details of some components. The generator cell (G), a plexiglas vessel of 35-mm height and 6-mm i.d., contained a platinum wire (0.8-mm diameter, 30 mm long) and a copper wire (0.7-mm diameter, 30 mm long). These were connected to the adjustable direct voltage supply (S) and to a voltmeter (M). The electrolyte solution (0.1 mol l^{-1} sodium sulphate) entered the cell (Fig. 1a) through a hole (I) at the lower end, and left the cell at a point (II) lateral with the tops of the two electrode wires, transferring the copper ions produced to the mixing chamber (MC, Fig. 1b), in which the solutions of reactants and catalyst were mixed. The various debubbling openings (D) served to prevent any gas bubbles from entering the optical system. After mixing, the reaction solution entered the vertical cuvette (C). Light enters via a light pipe (LP) through an appropriate filter (MF, 572 nm, Dr. B. Lange, Berlin) passes through the solution in C and reaches the photo-element (PE). The absorption signal is recorded versus time, and is a measure of the concentration of the indicator substance (iron in this example) and consequently of the rate of reaction. The solution leaves the cuvette via a levelling bottle (LB), the height of which has to be regulated so that the solutions pass the cuvette as quickly as they enter the mixing chamber. If the concentrations of all reactants are kept constant, the signal delivered by the photo-element is a measure of the concentration of the catalyst produced in the generator cell.

Preliminary tests

In the initial experiments, the direct voltage applied to the generator electrodes was increased stepwise, and the corresponding absorbances were

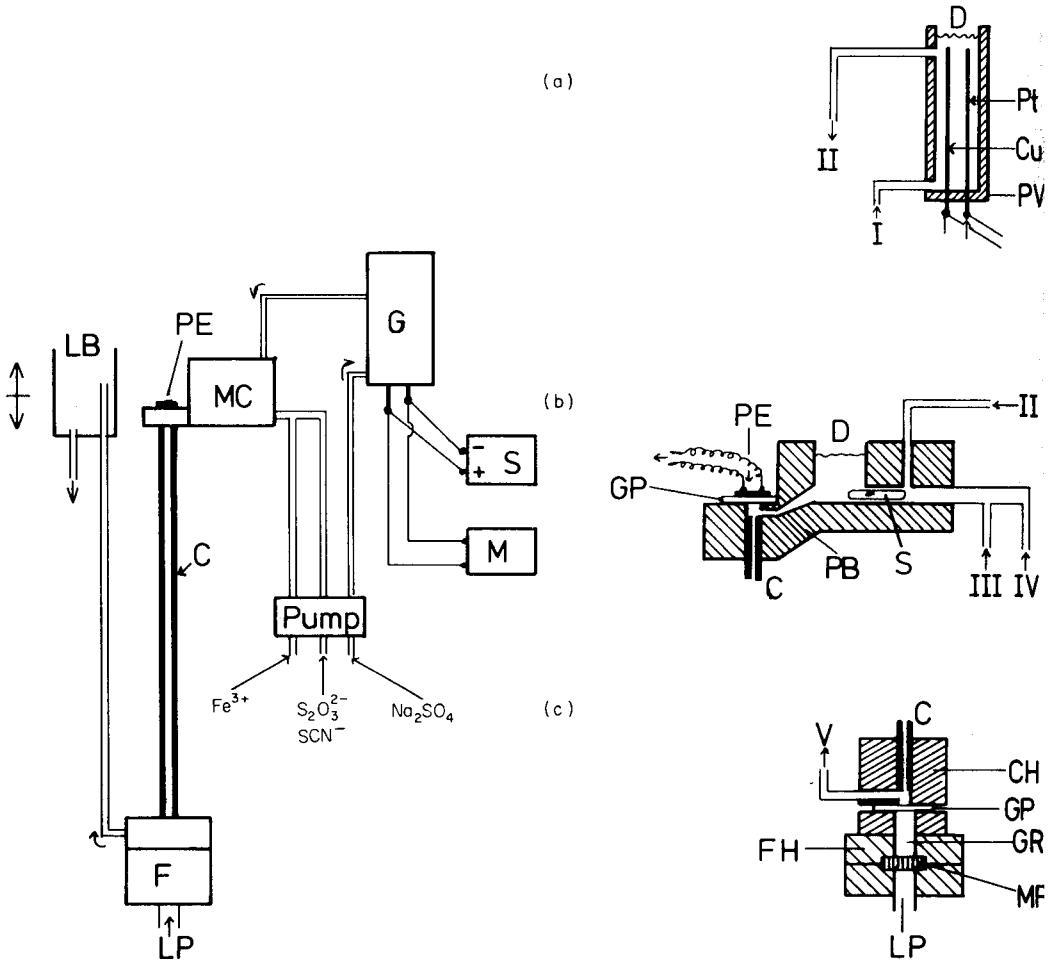

Fig. 1. Apparatus for the electrogeneration of catalyst: LB, levelling bottle; PE, photo-element (Siemens BPX79); MC, mixing chamber; C, cuvette (glass tube, 155 mm long, 1.4-mm i.d.); G, generator cell; S, adjustable direct voltage supply; M, voltmeter; F, filter and cuvette holder; LP, light pipe, coming from a light source (Schott KL150B; 15 V/150 W).

Detailed diagrams are shown for: (a) the generator cell G; (b) the mixing chamber MC; (c) the cuvette and filter holder F. Additional symbols are as follows: D, debubbling opening; PV, plexiglas vessel; GP, glass plate; PE, photo-element; PB, plexiglas block; S, magnetic stirrer; CH, cuvette holder; GR, glass rod; MF, monochromatic filter; FH, filter holder. Solution flows: I, inflow of electrolyte solution; II, connection of generator cell mixing chamber; III, inflow of Fe^{3+} solution; IV, inflow of $S_2O_3^{2-}$ solution; V, connection of cuvette to levelling bottle.

recorded. In these measurements, the solutions used were iron(III) chloride (0.3 mg Fe^{3+} ml^{-1}), thiosulphate/thiocyanate (0.05/0.1 mol l^{-1}) and sodium sulphate (0.1 mol l^{-1}). The pumping rate for each solution was 7.3 ml min^{-1}.

Figure 2 shows the influence of the generating voltage on the transmittance of the reaction mixture. In the range 100—500 mV, every increase in the voltage caused an increase in the concentration of catalyst, and so in higher transmittance of the solution, voltages of 500—900 mV applied to the electrodes, produced a nearly constant concentration of copper(II) ions. To see if this phenomenon was reproducible when other detection systems were used, the generator cell was separated and the electrolyte solutions containing the copper(II) ions produced by anodic oxidation at defined voltages were collected. After the addition of sodium diethyldithiocarbamate to each fraction, the copper was extracted by chloroform and determined spectrophotometrically in the conventional way; the plateau at 500—900 mV was confirmed. Such phenomena can often be observed in electrode processes when the removal of ions from around the electrodes is slow. Voltages exceeding 900 mV produced a rapid increase in the copper(II) concentration. More than 1500 mV could not be applied because of excessive bubble formation.

Determination of iron

When controlled generation of copper catalyst was used, iron could be determined in the range 10—1500 μg ml^{-1}. Iron concentrations up to 300 μg ml^{-1} could be measured without any voltage being applied, as the signal did not exceed 90%. To diminish this signal when higher iron concentrations had to be determined, the copper(II) concentration was augmented by anodic production. At 800 mV, 100—500 μg Fe^{3+} ml^{-1} could be determined, the absorption signals recorded being 15—90%. At 1300 mV, 400—1500 μg Fe^{3+} ml^{-1} could be measured, the absorption signals being 35—95%.

If an unknown sample provided an excessive signal, it was necessary to apply a higher voltage to the electrodes, in order to enhance the catalyst con-

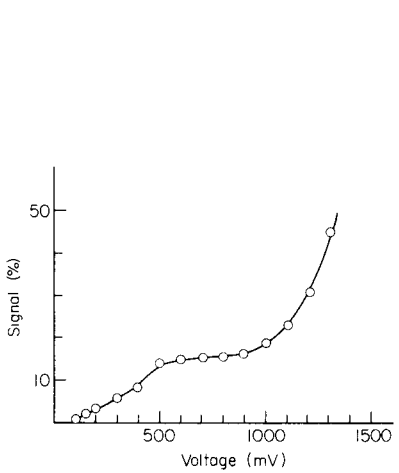

Fig. 2. Transmittance—voltage curve.

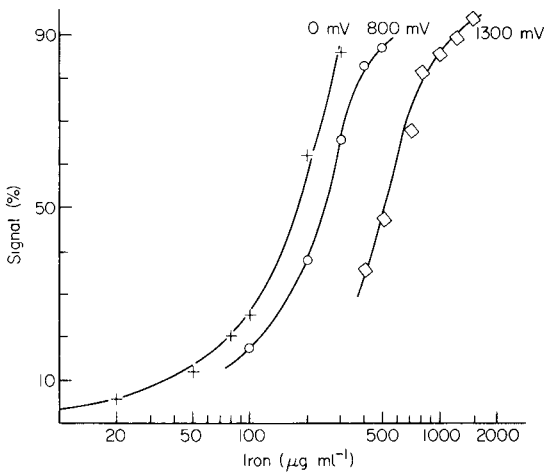

Fig. 3. Standard graph for the determination of iron.

centration and so to diminish the absorption. Conversely, if the absorption signal was too low, then a lower (or no) voltage had to be applied. In the standard graphs (Fig. 3), the absorption signals (in arbitrary units) are plotted versus the corresponding concentrations of iron for each of the three voltages applied. The reagent solution, used for the whole range of iron concentrations, contained sodium thiosulphate (0.2 mol l^{-1}) and potassium thiocyanate (0.2 mol l^{-1}). The sodium sulphate concentration was 0.1 mol l^{-1}. Both solutions and the sample solutions were pumped at 7.3 ml min^{-1}. The time necessary to reach a constant signal again after a change in the sample concentration was about 4 min.

Table 2 gives the results of the determination of some unknown iron samples. The concentrations were measured in a random order to simulate a real changing sample stream. Some samples could be measured at two different voltages; the signals were then evaluated from corresponding standard graphs. In some cases, non-logarithmic calibration curves were used (not shown here). During the determinations, it could be seen that the catalytic efficiency of the copper wire slowly diminished, probably because of changes in the surface of the wire. This could be corrected by regular calibration.

Copper-catalyzed reaction of hydroquinone and hydrogen peroxide

The ability to produce a stream of a constant well-defined concentration of catalyst ions, can be applied to determine many substances that influence the catalytic activity of the solution. The well known copper(II)-catalyzed reaction between hydrogen peroxide and hydroquinone, yielding red—brown oxidation products, has been used as an indicator reaction for such determinations. The copper(II) catalyst is activated by 2,2′-bipyridine [7]. The apparatus used was nearly the same as that shown in Fig. 1. The photometer filter was changed to 492 nm. It was found better to use a sheet of copper (26 × 10 × 0.1 mm; 240 mg) formed to a tube of 3-mm i.d., instead of a copper wire; this was probably due to the larger available surface area. The copper tube was placed into the generator cell and connected to the direct

TABLE 2

Determination of iron with anodic generation of catalyst concentration

Iron conc. ($\mu g\ ml^{-1}$)			Iron conc. ($\mu g\ ml^{-1}$)			Iron conc. ($\mu g\ ml^{-1}$)		
Taken	Found	Diff.	Taken	Found	Diff.	Taken	Found	Diff.
20	26	+6	300	310	+10	790	730	−60
28	28	0	350	320	−30	850	850	0
38	38	0	380	390	+10	1006	1050	+44
41	41	0	410	400	−10	1200	1250	+50
44	43	−1	620	620	0	1350	1500	+150
120	125	+5	650	680	+30	1450	1460	+10
156	148	−8	706	675	−31	1480	1400	+80

voltage supply by copper wire; the platinum cathode was located in the middle of the tube. A reaction coil (100 cm long, 10-mm i.d.) was inserted between the mixing chamber and the cuvette, because the rate of this reaction is lower than that of the iron—thiosulphate reaction; at the given pumping rates it took 1 min for the solution to flow from the mixing chamber to the cuvette.

The following solutions were used: 0.3 mol l^{-1} hydroquinone and 0.4 μmol l^{-1} 2,2′-bipyridine pumped at 2.4 ml min^{-1}; 0.3 mol l^{-1} hydrogen peroxide in disodium tetraborate—hydrochloric acid buffer (pH 8.5; 0.05 mol l^{-1}) pumped at 2.4 ml min^{-1}; 0.1 mol l^{-1} Na_2SO_4 as electrolyte solution pumped at 3.4 ml min^{-1}; water at a flow rate of 2.4 ml min^{-1} was led in through a fourth tube, not shown in Fig. 1, to force the sample solutions into the mixing chamber.

It was necessary to establish how much copper ion was produced at various applied voltages. When the resulting absorption signals from the above procedure were plotted versus the voltages, the curve obtained was similar to that shown in Fig. 2. Direct comparison of these transmittances with the transmittances obtained when electrolyte solutions containing known copper concentrations (not produced by anodic generation) were pumped into the mixing chamber, made it possible to determine the concentration of copper produced by a particular voltage. Table 3 shows the results.

In the following determinations, a voltage of 700 mV was applied, producing nearly 0.23 μg Cu^{2+} ml^{-1} of electrolyte solution; slight changes of the voltage causes practically no change in transmittance (cf. Fig. 2).

Determination of EDTA as inhibitor

As EDTA and copper(II) form a stable complex, EDTA samples can be determined by pumping them continuously into the mixing chamber. Increasing amounts of EDTA decrease the concentration of free copper ions, and so decrease the rate of reaction. The EDTA (sample or standard) was always added to the electrolyte solution (1—10 μg EDTA ml^{-1}) and so passed through the generator cell. The standard graph (Fig. 4) show that 8 or 10 μg

TABLE 3

Comparison of voltages and copper concentrations

Voltage (mV)	Cu^{2+} (μg ml^{-1})	Voltage (mV)	Cu^{2+} (μg ml^{-1})
100	0.01	800	0.23
200	0.07	900	0.25
300	0.15	1000	0.30
400	0.19	1100	0.37
500	0.22	1150	0.50
600	0.24	1200	1.0
700	0.23		

EDTA ml^{-1} sufficed to complex all the copper(II) generated by anodic oxidation at the given voltage, i.e., all the catalyst was inhibited. EDTA in the range 0.5—5 $\mu g\ ml^{-1}$ could be determined from a standard graph, which was nearly linear in this range (Fig. 4). Table 4 gives some results. The time necessary for the determination of a new sample concentration, of course, depends on the concentration of the preceding sample and was usually 6—10 min.

Determination of cadmium as reactivator

The EDTA complexes of cadmium and copper are of similar stability. When cadmium was delivered to the mixing chamber via the sample tube (see above), it released a certain concentration of free copper(II) ions and so enhanced the rate of the reaction, thus decreasing the transmittance recorded. Cadmium itself had no influence on the oxidation of the hydroquinone by hydrogen peroxide. To complex all the copper(II) ions generated at 700 mV, the electrolyte contained 10 μg EDTA ml^{-1}. The concentrations of the reactants and of the electrolyte, and their pumping rates, were the same as described above. Samples containing 1—10 $\mu g\ Cd^{2+}\ ml^{-1}$ were delivered to the mixing chamber at 2.4 ml min^{-1}. Cadmium concentrations were evaluated from a standard graph of transmittance versus standard cadmium concentrations. Table 5 gives some results. The time for a single determination was about 5 min.

Determination of cadmium by measurement of an excess of EDTA

If a known quantity of EDTA, in excess of the amount of cadmium(II), is added to the sample stream, the excess of EDTA complexes part of the copper ions. This decreases the catalytic efficiency of the copper(II)/electrolyte solution, lowers the reaction rate, and thus diminishes the reaction products measured in the cuvette. This decrease in absorbance can be related to the concentration of cadmium in the samples.

To achieve complete reaction of the cadmium (0.6—6 $\mu g\ ml^{-1}$) with the EDTA (10 $\mu g\ ml^{-1}$), these two solutions were pumped to a mixing T at 2.4 ml min^{-1} each, and then through a reaction coil (10 cm, 1.5-mm i.d.) before entering the mixing chamber, in which the reaction with the hydroquinone/2,2′-bipyridine, the hydrogen peroxide and the electrolyte/catalyst solution proceeded. The apparatus, concentrations, voltage and pumping rates were the same as described above. Samples were evaluated from a standard graph of transmittances against cadmium concentrations. Table 5 gives some results.

TABLE 4

Determination of EDTA ($\mu g\ ml^{-1}$) as inhibitor

Taken	0.88	3.92	2.20	4.60	1.40	3.20	0.44	2.75
Found	0.80	4.00	1.90	4.65	1.30	3.45	0.40	3.20
Diff.	−0.08	+0.08	−0.30	+0.05	−0.10	+0.25	−0.04	−0.45

TABLE 5

Determination of cadmium ions ($\mu g\ ml^{-1}$)

By reactivation of the copper(II) catalyst					
Taken	5.6	3.72	2.24	8.36	7.36
Found	4.0	3.50	2.30	6.0	6.80
Diff.	−1.6	−0.22	+0.06	−2.36	−0.56
By measurement of an excess of EDTA					
Taken	5.06	4.00	1.00	2.80	1.50
Found	5.00	3.96	0.90	2.94	1.40
Diff.	−0.06	−0.04	−0.10	+0.14	−0.10

Determination of zinc by diminution of the activation of copper

In the reaction described, the copper(II) catalyst is activated by forming a 2,2′-bipyridine complex [7]. If a second metal is added, which forms a bipyridine complex of similar stability [8], this metal will displace copper and so diminish the activation of the catalyst. The extent of this decrease can then be related to the concentration of the second metal, which can thus be determined. Zinc ions influenced the activation of the catalyst but did not influence the uncatalyzed reaction itself. The zinc(II) solution was pumped into the mixing chamber at 2.4 ml min^{-1} via the sample tube. The electrolyte passed through the generator cell (3.4 ml min^{-1}), where copper ions were produced (at 1500 mV), and transported them to the mixing chamber where these components and the reagent solutions were mixed before passage through the reaction coil and measurement of the transmittance. Higher concentrations of zinc replaced more copper ions in the bipyridine complexes, and so decreased the activation of copper, yielding

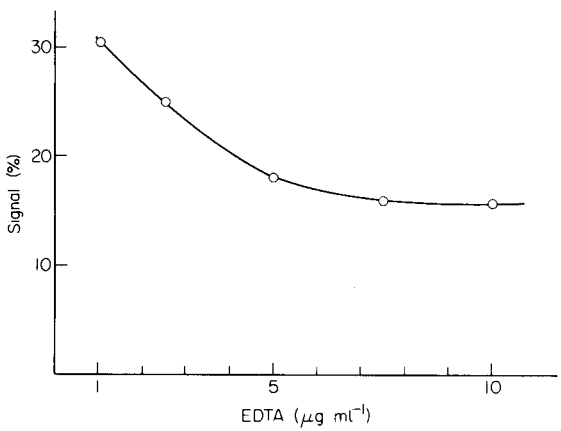

Fig. 4. Standard graph for the determination of EDTA.

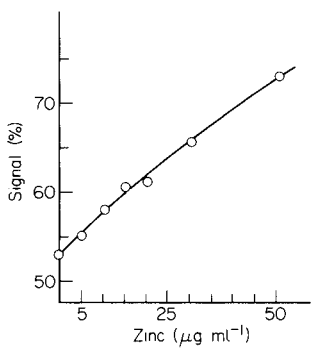

Fig. 5. Standard graph for the determination of zinc.

TABLE 6

Determination of zinc ions

By diminution of the activation of copper $\mu g\ ml^{-1}$										
Taken	5.7	9.7	21.2	42.4	35.6	7.9	46.6	14.5	26.3	9.7
Found	7.5	9.75	20.0	40.0	35.5	7.5	42.0	11.5	23.0	10.0
Diff.	+1.8	+0.05	−1.2	−2.4	−0.1	−0.4	−4.6	−3.0	−3.3	+0.3
By diminution of the activation of silver $mg\ ml^{-1}$										
Taken	0.59	0.39	2.63	2.17	1.25	1.17	0.43	1.10	1.41	2.53
Found	0.77	0.36	2.59	2.36	1.56	1.02	0.51	1.09	1.36	2.40
Diff.	+0.18	−0.03	−0.04	−0.19	+0.31	−0.15	+0.08	−0.01	−0.05	−0.13

higher transmittance. The standard graph (Fig. 5) was prepared with solutions of zinc in the range 5—50 $\mu g\ ml^{-1}$. The time necessary for a single determination was 6—10 min. Table 6 gives the results of some determinations. The concentrations of all reactants used were the same as in the other examples.

The regulation of the catalytic efficiency of silver by anodic dissolution

The principle of the production of a certain concentration of catalyst by anodic oxidation is not limited to reactions which are catalyzed by copper. The technique was also applied to the silver-catalyzed oxidation of sulphanilic acid by ammonium peroxodisulphate. This catalyst is likewise activated by 2,2′-bipyridine [9]. The rate of the reaction could be followed by measuring the concentration of the red oxidation product at 513 nm. The apparatus used was the same as described for the hydroquinone/hydrogen peroxide reaction. The generating electrode was a helix (3-mm i.d., 30 mm high) formed by a silver strip (160 × 3.5 × 0.5 mm; 264 mg) which was connected to the direct voltage supply.

The following solutions were used: a solution of 2.078 g of sulphanilic acid and 0.75 g of 2,2′-bipyridine in 200 ml of sodium citrate/nitric acid buffer (pH 2) diluted to 1 l, stored in a black bottle and pumped at 2.9 ml min^{-1}; ammonium peroxodisulphate (0.1 mol l^{-1}) pumped at 3.6 ml min^{-1}; ammonium nitrate electrolyte solution (0.1 mol l^{-1}) pumped at 2.9 ml min^{-1}; and the sample solution (or water) pumped at 1.6 ml min^{-1}.

To see how the production of silver ions depended on the voltage applied, this voltage was increased stepwise, and the absorbances were registered. Voltages up to 900 mV had no measurable influence on the reaction. Higher voltages caused an increase in reaction rate. By comparisons analogous to those described for the copper-catalyzed reaction, it could be concluded that 1225 mV produced a concentration of about 10 $\mu g\ Ag^{+}\ ml^{-1}$. This was the voltage applied in the following determination. The use of this system for analytical purposes may be illustrated by the example of decreased activation by a second metal. The addition of zinc(II) caused the same effect as mentioned for the hydroquinone/hydrogen peroxide reaction. The standard graph prepared with solutions containing 0.29—2.9 mg $Zn^{2+}\ ml^{-1}$ was similar to the one shown in Fig. 5. Table 6 gives the results of some determinations. It took 6—10 min to determine a new sample concentration.

DISCUSSION

The results of these measurements proved that the catalytic efficiency of metals in these reactions is based on ions produced by oxidation, and that this catalytic efficiency could be regulated by controlled anodic dissolution. A reactant could therefore be determined over a wide range of concentration, using reagent solutions of constant concentrations and different generating voltages for the catalyst. The same is true for determinations of substances which influenced the activity of the catalyst solution (inhibitors, reactivators). Metals (e.g.,zinc) which formed complexes with an activator (bipyridine) could be measured by their influence on the activation of the catalyst.

It may be mentioned here that the applicability of carrier-bound inorganic catalysts in continuous flow analysis was also investigated. Copper(II) was immobilized on different, catalytically inactive substances by adsorption or by precipitation; the influence of these products on the iron(III)—thiosulphate reaction was measured. Carrier substances used were alumina, zeolite, silica gel, titanium dioxide, active charcoal, and iron(III) phosphate. The measurements, carried out in the glass-filter crucible as described above in the example of the copper spiral, showed that the activity of all carrier-bound catalysts diminished continuously. The periods in which they lost all their influence, were between an hour and several days. It is clear, therefore, that electrolytic generation of the catalyst is greatly superior.

REFERENCES

1 J. Růžička and E. H. Hansen, Anal. Chim. Acta, 78 (1975) 145.
2 L. T. Skeggs, Am. J. Clin. Pathol., 28 (1957) 311.
3 H. Weisz and G. Fritz, Anal. Chim. Acta, 123 (1981) 239.
4 F. Feigl, Fresenius Z. Anal. Chem., 74 (1928) 369.
5 A. C. Oudemanns, Fresenius, Z. Anal. Chem., 6 (1867) 129.
6 S. M. Ramasamy, A. Job and H. A. Mottola, Anal. Chem., 51 (1979) 1637.
7 J. F. Dolmanova, V. P. Poddubienko and V. M. Peshkova, Zh. Anal. Khim., 28 (1973) 592.
8 J. Inczedy, Analytical Applications of Complex Equilibria, Horwood, Chichester, 1976, p. 328ff.
9 P. R. Bontchev, A. Alexiev and B. Dimitrova, Talanta, 16 (1969) 597.

Analytica Chimica Acta, 139 (1982) 219—227
Elsevier Scientific Publishing Company, Amsterdam — Printed in The Netherlands

CHROMOGENIC CROWN ETHER REAGENTS FOR SPECTROPHOTOMETRIC DETERMINATIONS OF SODIUM AND POTASSIUM

HIROSHI NAKAMURA, HIROSHI NISHIDA, MAKOTO TAKAGI and KEIHEI UENO*

Department of Organic Synthesis, Faculty of Engineering, Kyushu University, Hakozaki, Higashi-ku, Fukuoka 812 (Japan)

(Received 4th January 1982)

SUMMARY

Crown ethers carrying a phenolic group, 2-hydroxyphenoxymethyl-15-crown-5 and -18-crown-6, were synthesized. Introduction of nitro groups in the 3- and 5-positions of the aromatic nucleus or introduction of a 4-nitrophenylazo group in the 5-position gives a series of chromogenic reagents suitable for the extraction spectrophotometry of sodium and potassium. Sodium in human blood serum was successfully determined by using the (2-hydroxy-3,5-dinitrophenyl)oxymethyl-15-crown-5 reagent. The molar absorptivity of the sodium complex is 14 000 l mol^{-1} cm^{-1} at 423 nm.

Spectrophotometry of alkali metals by using organic reagents has been introduced only recently [1], and is still in the early stages of development. The methods are based on extraction of alkali metal ions into an organic solution by specifically designed crown ether dyes. This molecular absorption spectrophotometry with organic reagents has the advantage over flame photometry in that it does not need special instrumentation, and is easily adapted for automated flow analysis with a membrane separation device [2]. In the present paper, several new crown ether dyes are designed and synthesized in a continuation of earlier work [1, 3—5]. One of the reagents is applied to the extraction-spectrophotometric determination of sodium in human blood serum. Some of the work described below has been reported in a short communication [3].

Synthesis of reagents

The structures and the synthetic routes of the compounds synthesized in this study are shown in Fig. 1. The starting material 1, guaiacol glyceryl ether, is commercially available, and the reactions are generally quite straightforward. However, some of the key procedures should be mentioned. Satisfactory purification of 2 and 3 was attained only by distillation under vacuum, preferably below 0.1 Pa. Crystallization of 4 and 5 from organic solutions was assisted by added water; in particular, 4b and 5b formed crystals only in the presence of water, and the hydrated crystals liquefied in dry air.

Reagents 4 and 5 thus synthesized were readily soluble in ordinary organic solvents, giving yellow and orange solutions, respectively. Reagent 4 was

0003-2670/82/0000-0000/$02.75

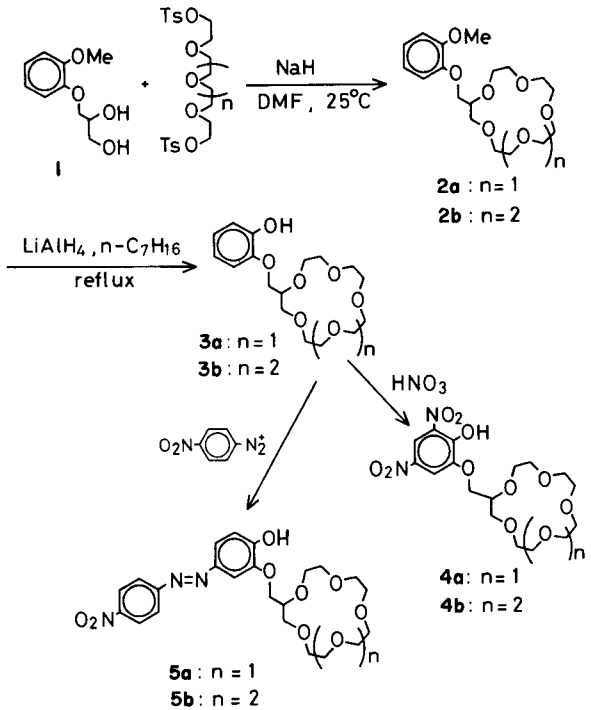

Fig. 1. Synthesis of crown ether dyes.

appreciably soluble in water but the distribution between water and an organic solvent such as chloroform or 1,2-dichloroethane strongly favored the organic phase. Reagent 5 was insoluble in water.

Extraction studies

When a 1,2-dichloroethane solution of 4 or 5 (HL) was brought into contact with an aqueous solution at various pH values, the distribution of the reagent species between the two phases was strongly dependent on the pH and on the nature of the cation present in the aqueous solution. The behavior was also different for 4 and 5, as expected from their inherent difference in lipophilicity.

The distribution of the reagent species in the aqueous phase was negligible for 5 under all the pH conditions studied in this work. When the aqueous solution contained a salt of the metal whose ionic diameter fitted that of the crown ether, the metal became extracted as the pH was raised, giving a violet coloration to the organic phase. When the metal did not fit the crown ether, the organic phase remained yellowish. The distribution of 4 gradually shifted to the aqueous phase as the pH was raised, until the distribution became constant at above pH 10. In this pH region, all the HL species were dissociated in the aqueous phase and the distribution was determined solely

by the distribution behavior of the metal salt or the complex, ML. Thus, when the aqueous solution contained the metal favorable for complex formation with 4, the complex was extracted and the organic phase became orange. Conversely, if the metal did not fit the reagent, the organic phase remained colorless because the reagent stayed in the aqueous phase.

The acid dissociation and the metal extraction equilibria are quantitatively described by

$$HL \rightleftharpoons H^+ + L^-; K_a = \frac{[H^+][L^-]}{[HL]} \quad (1)$$

$$(HL)_0 + M^+ \rightleftharpoons (ML^+)_0 + H^+; K_{ML}^{ex} = \frac{[(ML^+)_0][H^+]}{[(HL)_0][M^+]} \quad (2)$$

The spectral change of the organic phase on the extraction of metal is illustrated in Fig. 2 for the extraction of sodium by 4a. A rigorous isosbestic point was not achieved, because the reagent became increasingly soluble in the aqueous phase as the pH was raised. The spectral data were handled, therefore, by a procedure similar to that described previously [6]. The acidity constants, K_a, and the extraction constants, K_{ex}, obtained are summarized in Table 1. Some spectral data are collected in Table 2.

The general trend in the magnitude of the extraction constants can be reasonably understood by considering the acidity of the phenolic functional groups and the ring size of the crown ethers. The acidity constants of the

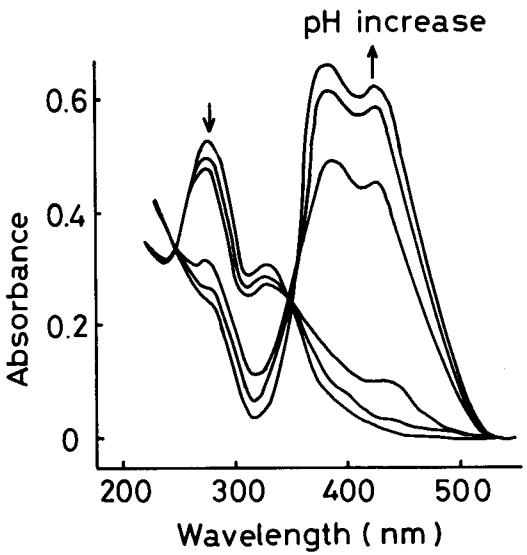

Fig. 2. Spectral change in the organic phase on extraction of sodium. Reagent 4a (1×10^{-5} M) in 1,2-dichloroethane, 5 ml; sodium chloride (0.02 M) in pH buffer solution (pH 2.4—12.5), 10 ml; 25°C. The curves correspond to pH values of 2.4, 3.6, 4.4, 5.7, 9.6 and 12.5.

TABLE 1

Acidity constants and extraction constants

Reagent	$-\log K_a^a$	$-\log K_{ML}^{ex}$				
		Li	Na	K	Rb	Cs
4a	3.16	>5.6	3.60	4.15	4.76	5.6
4b	3.27	4.8	4.01	2.22	2.68	3.76
5a	7.51	9.8	8.40	9.20	9.55	>10
5b	7.54	8.8	8.32	7.11	7.75	>10

[a]10% dioxane, 25°C, μ = 0.1 $(CH_3)_4NBr$.

dinitrophenol-type reagents are larger than those of the 4-(4′-nitrophenylazo)phenol-type reagents by 4.3—4.4 orders of magnitude. This is correctly reflected in the difference in the extraction constants between the reagents of types 4 and 5. The extraction constants of 4 are generally larger than those of 5 by 4—5 orders of magnitude for all the alkali metal ions. The extraction constant defined by Eqn. 2 involves the acid dissociation of the reagents, and it is quite reasonable that the extraction of metals by 4 takes place at lower pH values than extraction with 5.

With regard to the selectivity between sodium and potassium, the 15-crown-5 reagents prefer sodium, whereas the 18-crown-6 reagents prefer potassium. This is simply the expected outcome of the "size selectivity" of the crown ether macrocycles. However, if one looks at the extraction constants for sodium and potassium in Table 1 more closely, it becomes apparent that the selectivity to potassium is higher for 4b than for 5b (log K_{KL}^{ex} − log K_{NaL}^{ex} = 1.79 for 4b and 1.21 for 5b). Similarly, if the selectivity of reagents 4a and 5a is compared, the selectivity to sodium is higher for 5a (log K_{NaL}^{ex} − log K_{KL}^{ex} = 0.55 for 4a and 0.80 for 5a). This means that, for the reagents of the same crown ether structure, the more basic phenolate (5) favors extraction of sodium, while the less basic phenolate (4) favors potassium. This in turn indicates that coordination interaction between the phenolate and the metal is more important for sodium than for potassium in

TABLE 2

Spectral properties of crown ether dyes and their sodium and potassium complexes

Reagent	λ_{max} (ϵ, 10^4 l mol^{-1} cm^{-1})			
	HL[a]	L^{-}[a]	NaL[b]	KL[b]
4a	273(1.2)	385(1.3)	423(1.4)	426(1.3)
4b	273(1.0)	385(1.1)	430(1.3)	433(1.2)
5a	390(1.8)	518(3.0)	560(3.7)	567(3.7)
5b	390(1.8)	518(3.0)	571(3.5)	575(3.5)

[a]10% dioxane, see footnote in Table 1. [b]1,2-dichloroethane.

the extraction process. The structure of the extracted potassium complex is more dependent on intramolecular ion-pair formation. The selectivity between lithium and cesium further strengthens the above ideas on the relative importance of the coordination type (6) and the ion-pair type (7) structures of the extracted metal complexes. For the reagents 4a and 5a of the same 15-crown-5 type, the order of selectivity is Li < Cs for 4a and Li > Cs for 5a. (For the 18-crown-6 reagents, 4b and 5b, the order of selectivity is Li < Cs, probably because the crown ether size is excessively unfavorable for lithium extraction.)

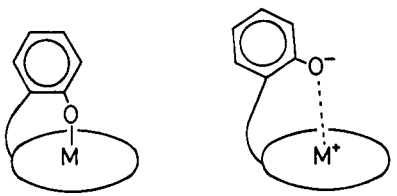

6 (M = Li, Na) **7** (M = K, Rb, Cs)

In conclusion, in order to achieve a high selectivity among alkali metals in solvent extraction with a mono-anionic crown ether reagent, two critical factors must be taken into consideration. The first is a well-known "size selectivity" by the crown ether macrocycle. The second is the coordination interaction (6) and the ion-pair interpretation (7) of the anionic site with the crown ether-bound metal ion. A localized negative charge (high basicity) strengthens the coordination interaction and favors the extraction of lighter alkali metals. A delocalized negative charge (low basicity) favors the formation of ion-pair type complexes and more efficient extraction of the heavier alkali metals.

Application to alkali metal spectrophotometry

In order to prove the usefulness of the reagents in practical analysis, reagent 4a was employed for the determination of sodium in blood serum. A calibration line prepared from standard solutions of sodium chloride under the conditions recommended in the Experimental section, was linear over the range 0—6 ppm sodium ion for measurements at 423 nm (absorbance range, 0—0.3). The sodium concentration of the diluted serum sample subjected to extraction spectrophotometry was 5.44 ppm as determined by standard flame photometry, whereas the concentrations obtained by the proposed method were 5.48 ppm and 5.54 ppm after deproteination by perchloric acid and trichloroacetic acid, respectively. The agreement between these results is excellent. The blood serum contained potassium, but interference was not observed because its concentration was less than a tenth the concentration of sodium.

One of the unusual features of the dinitrophenol-type reagent 4, compared with 5 or other reagents described previously [1, 3, 5—7], is that it does not distribute into the organic phase under the present photometric

conditions in the absence of alkali metals (pH $\geqslant$10). This means a lower reagent blank, which in turn insures a more accurate, sensitive determination of the analyte and better reproducibility. Further, the determination is much less sensitive to pH variation in the extraction procedure. These are the most important advantages of reagent 4 over the others from the practical point of view.

It must be emphasized that only a part (about 17%) of the metal in the original aqueous solution is extracted into the organic phase at equilibrium under the conditions recommended in the Experimental section. Thus, the "apparent" molar absorptivity of the extracted metal complex is only 2200 in contrast to the "true" value of 14 000 l mol^{-1} cm^{-1} shown in Table 2. This means that the sensitivity of the present determination may be increased greatly by increasing the reagent concentration. However, handling of sodium solutions at sub-ppm levels requires special precautions because of contamination problems [4], and experiments to attain the possible ultrasensitivity were not considered worthwhile.

Reagent 4b has not yet been applied in practical determinations of potassium but there is no doubt that it is one of the best photometric reagents so far developed for potassium at ppm levels. The selectivity toward potassium compared to sodium is somewhat lower than that of the picrylamino-substituted reagents [6, 7], but the unusual reagent properties mentioned above should make it useful.

EXPERIMENTAL

Synthesis of crown ethers

The synthetic procedures were essentially the same for the 15-crown-5 and the 18-crown-6 series of reagents. Therefore, the procedures are given below only for the latter series of reagents, which generally needed more skill in handling. Comments will be made when appreciable modifications were involved.

(2-Methoxyphenyl)oxymethyl-18-crown-6 (2b). Guaiacol glyceryl ether (10 g, 50 mmol; Tokyo Kasei Kogyo Co.) was dissolved in dimethylformamide (DMF, 100 ml). Sodium hydride (5.0 g, 100 mmol, 50% in oil) was washed with hexane and added in portions to the solution under a nitrogen atmosphere. After stirring for 1 h, pentaethyleneglycol ditosylate (25.2 g, 50 mmol) in DMF (50 ml) was added slowly to the mixture in an ice bath. After stirring for 10 h under ice cooling, the mixture was heated at 80°C for 1 h. The solvent was removed under reduced pressure. The residue was dissolved in chloroform (300 ml), washed with water, and finally distilled under reduced pressure. B.p. 175—200°C/0.03 Pa, yield 19.8 g (49%). ^{1}H-n.m.r. ($CDCl_3$: δ ppm for internal TMS) δ = 3.64 (23H, broad s, OCH_2, OCH), 3.79 (3H, s, OCH_3), 4.04 (2H, d, J = 2.5 Hz, $ArOCH_2$), 6.84 (4H, s, aromatic H). Found: 56.95% C, 7.6% H; calcd. for $C_{20}H_{32}O_8$, 57.0% C, 8.05% H.

(2-Hydroxyphenyl)oxymethyl-18-crown-6 (3b). Compound 2b (15.2 g, 38 mmol) and lithium aluminum hydride (4 g, 100 mmol) were dissolved in a mixture of benzene (5 ml) and heptane (200 ml). After the mixture was stirred and refluxed for 9 h, methanol (20 ml) was added at room temperature and stirred for 10 min.

Chloroform (300 ml) was then added, followed by 1 M hydrochloric acid (40 ml). The organic layer was separated, washed with water and evaporated under reduced pressure. A distillation of the residue gave two fractions. The first fraction consisted of methyl-18-crown-6 (b.p. 110°C/1 Pa, yield 5.2 g, 49%), the product from a reductive fission of the ArO—CH_2 bond in 2b. The second fraction was the expected product 3b. B.p. 180—200°C/0.04 Pa, yield 6.7 g (47%). ^{1}H-n.m.r. ($CDCl_3$) δ = 3.65 (23H, broad s, OCH_2, OCH), 4.06 (2H, m, $ArOCH_2$), 6.95 (4H, s, aromatic H). Found: 57.4% C, 7.75% H; calcd. for $C_{19}H_{30}O_8 \cdot 0.5\ H_2O$, 57.7% C, 7.9% H.

(2-Hydroxy-3,5-dinitrophenyl)oxymethyl-18-crown-6 (4b). Compound 3b (572 mg, 1.48 mmol) was dissolved in chloroform (10 ml). Concentrated nitric acid (69%, 0.2 ml) was added, and the mixture was stirred and left at room temperature for 10 min. The mixture was then diluted with chloroform (30 ml) and washed with water several times. The organic layer was concentrated, the residue was taken up in carbon tetrachloride (50 ml), and a few drops of water was added. After several days of standing, a white crystalline powder precipitated from the mixture. The solid isolated was kept under moist air, because otherwise it liquefied to a reddish paste losing the hydration water. Yield 200 mg (25%), m.p. 45—50°C. ^{1}H-n.m.r. ($CDCl_3$) δ = 3.5—4.5 (25H, m, OCH_2, OCH), 7.96 (1H, d, J = 2.0 Hz, aromatic H), 8.56 (1H, d, J = 2.0 Hz, aromatic H). Found: 43.4% C, 6.3% H, 5.2% N; calcd. for $C_{19}H_{28}N_2O_{12} \cdot 3H_2O$, 43.0% C, 6.5% H, 5.3% N.

(2-Hydroxy-5-(4-nitrophenylazo)phenyl)oxymethyl-18-crown-6 (5b). *p*-Nitroaniline (1.0 g, 8 mmol) was dissolved in THF—water (1 + 1, 30 ml), to which concentrated hydrochloric acid (1.8 ml) was added. Sodium nitrite (0.55 g, 8 mmol) was added to the ice-cooled solution under stirring. The diazonium salt solution thus prepared was then added to the ice-cooled solution of **3b** (0.72 g, 1.9 mmol) and sodium hydrogencarbonate (2 g) in the THF—water (1 + 1, 30 ml). The mixture was stirred for 1 h and then evaporated under reduced pressure to complete removal of THF. Chloroform (100 ml) was added to the residue, and the mixture was shaken with an aqueous 0.5 M solution of potassium carbonate. The organic layer was collected, washed with a dilute aqueous solution of acetic acid (10^{-2} M) and concentrated to dryness under reduced pressure. The residue was taken into benzene and subjected to column chromatography on silica gel. Elution with benzene and chloroform followed by a mixture of chloroform and ethanol (5 + 1) gave a main band appearing in the chloroform—ethanol fractions. The main band was collected, concentrated, and redissolved in carbon tetrachloride. The addition of a few drops of water and standing for several days gave red crystalline precipitates. Yield 0.7 g (70%), m.p. 88—89°C. ^{1}H-n.m.r.

($CDCl_3$) δ = 3.5—4.4 (25H, m, OCH_2, OCH), 7.05 (1H, d, J = 8 Hz, aromatic H), 7.5—7.8 (2H, m, aromatic H), 7.95 (2H, d, J = 10 Hz, aromatic H), 8.35 (2H, d, J = 10 Hz, aromatic H). Found: 55.2% C, 6.3% H, 7.6% N; calcd. for $C_{25}H_{33}N_3O_{10} \cdot 0.5H_2O$: 55.1% C, 6.3% H, 7.7% N.

(2-Methoxyphenyl)oxymethyl-15-crown-5 (2a). B.p. 203°C/0.1 Pa, yield 47%. ^{1}H-n.m.r. ($CDCl_3$) δ = 3.67 (19H, broad s, OCH_2, OCH), 3.82 (3H, s, CH_3), 4.06 (2H: d, J = 2 Hz, $ArOCH_2$), 6.88 (4H, s, aromatic H). Found: 60.4% C, 8.0% H; calcd. for $C_{18}H_{28}O_7$, 60.7% C, 7.9% H.

(2-Hydroxyphenyl)oxymethyl-15-crown-5 (3a). The final distillation was unnecessary to obtain the analytically pure product. Yield 98%. ^{1}H-n.m.r. ($CDCl_3$) = 3.64 (19H, broad s, OCH_2, OCH), 4.08 (2H, m, $ArOCH_2$), 6.85 (4H, s, aromatic H). Found: 58.1% C, 7.5% H; calcd. for $C_{17}H_{26}O_7$, 59.6% C, 7.65% H.

(2-Hydroxy-3,5-dinitrophenyl)oxymethyl-15-crown-5 (4a). Addition of water was not essential to assist the crystallization. Yield 30%. ^{1}H-n.m.r. ($CDCl_3$) δ = 3.3—4.5 (21H, m, OCH_2), 7.99 (1H, d, J = 2 Hz, aromatic H), 8.58 (1H, d, J = 2 Hz, aromatic H). Found: 45.1% C, 5.8% H, 6.16% N; calcd. for $C_{17}H_{24}N_2O_{11} \cdot H_2O$, 45.3% C, 5.8% H, 6.2% N.

(2-Hydroxy-5-(4-nitrophenylazo)phenyl)oxymethyl-15-crown-5 (5a). Sodium carbonate was used instead of potassium carbonate in washing the chloroform extract of the reaction mixture. Yield 49%, m.p. 45—55°C. ^{1}H-n.m.r. ($CDCl_3$) δ = 3.4—3.7 (21H, m, OCH_2, OCH), 7.02 (1H, d, J = 8 Hz, aromatic H), 7.5—7.75 (2H, m, aromatic H), 7.93 (2H, d, J = 10 Hz, aromatic H), 8.32 (2H, d, J = 10 Hz, aromatic H). Found: 53.4% C, 6.0% H, 8.1% N; calcd. for $C_{23}H_{29}N_3O_{10} \cdot 0.5H_2O$, 53.5% C, 5.85% H, 8.1% N.

Equilibrium measurements

A 1×10^{-5} M solution of a reagent in 1,2-dichloroethane (5 ml) and an aqueous 0.02 M solution of alkali metal chloride (5 ml) were shaken for 5 min. The pH of the aqueous solution was adjusted by a tetramethylammonium salt of tartaric acid, boric acid or Tricine. After centrifugation, the absorption spectra of both the organic and aqueous layer were measured using a standard quartz cell of 1-cm light path [6]. Acidity constants of the reagents were obtained spectrophotometrically in water containing 10% (v/v) dioxane at 25°C and μ = 0.1 (tetramethylammonium bromide) [6].

Determination of sodium in blood serum

Human blood serum (0.2 ml) was mixed with an aqueous perchloric acid or trichloroacetic acid solution (0.33 M, 0.1 ml, deproteinating agent) and centrifuged. An aliquot (0.1 ml) was taken from the supernatant solution, mixed with aqueous tetramethylammonium hydroxide (alkali metal-free 0.2 M, 2 ml) and boric acid (0.2 M, 2 ml), and diluted to 10 ml with distilled water (pH 10.3). The aqueous solution was then shaken with a 1,2-dichloroethane solution of 4a (2×10^{-4} M, 10 ml) for 10 min. After phase separation by centrifugation, the absorbance of the organic layer was measured at

423 nm against the reagent blank. A calibration curve was prepared with aqueous solutions of sodium chloride.

The authors are grateful for a Grant-in-Aid for Scientific Research from the Ministry of Education, Science and Culture of Japan (Project No. 543020).

REFERENCES

1 M. Takagi, H. Nakamura and K. Ueno, Anal. Lett., 10 (1977) 1115.
2 See e.g., J. Kawase, Anal. Chem., 52 (1980) 2124.
3 H. Nakamura, H. Nishida, M. Takagi and K. Ueno, Bunseki Kagaku, 31 (1982) E 131.
4 M. Takagi, H. Nakamura, Y. Sanui and K. Ueno, Anal. Chim. Acta, 126 (1981) 185.
5 H. Nakamura, H. Sakka, M. Takagi and K. Ueno, Chem. Lett., (1981) 1305.
6 H. Nakamura, M. Takagi and K. Ueno, Anal. Chem., 52 (1980) 1668.
7 H. Nakamura, M. Takagi and K. Ueno, Talanta, 26 (1979) 921.

Analytica Chimica Acta, 139 (1982) 229—236
Elsevier Scientific Publishing Company, Amsterdam — Printed in The Netherlands

APPLICATION OF ELECTROGENERATED CHEMILUMINESCENCE OF LUMINOL TO DETERMINATION OF TRACES OF COBALT(II) IN AQUEOUS ALKALINE SOLUTION

KEIJO E. HAAPAKKA

Department of Chemistry, University of Turku, SF-20500 Turku 50 (Finland)

(Received 9th February 1982)

SUMMARY

A selective method for determination of traces of cobalt(II) in aqueous alkaline solution has been developed, based on the electrochemical generation of luminescence from luminol at a rotating ring—disc electrode. The detection limit is 10^{-8} M, and the linear calibration range extends up to 3×10^{-6} M; the r.s.d. for 2.0×10^{-7} M cobalt is 6%. Of 21 metal ions, only chromium(III) and copper(II) interfere seriously; EDTA also interferes.

Metal ions generally have a catalytic effect on the chemiluminescent reaction of luminol with hydrogen peroxide in aqueous alkaline solutions. In the presence of excess luminol and hydrogen peroxide, the chemiluminescent intensity is proportional to metal ion concentration, and trace metal ions can be determined [1—9]. The electrogenerated chemiluminescence of luminol is the light emission generated during the electrolysis of luminol solutions [10—12]. Dallakyan et al. [13] have developed trace methods for certain phenols and thiols based on their inhibitive effects on luminol electrogenerated chemiluminescence, and the feasibility of its use for the trace determination of copper(II) has been demonstrated [14].

In the present paper, a selective method for traces of cobalt(II) in aqueous alkaline solutions is described. The method is based on the cathodic electrogenerated chemiluminescence of luminol, the mechanism of which will be discussed in a later paper.

EXPERIMENTAL

Apparatus and reagents

The apparatus has been described in detail [12].

All water used was quartz-distilled, prepared and stored as described previously [12]. The luminol stock solution was made by dissolving an appropriate amount of purified luminol [12] in 0.04 M sodium hydroxide (Merck, Suprapur) to give a 2.00×10^{-2} M solution, and stored under nitrogen. Sodium chloride, sodium hydroxide and boric acid were Suprapur grade and all other chemicals were pro analysis grade (Merck). The reagents were used

0003-2670/82/0000-0000/$02.75

without further purification. An aqueous 1.00×10^{-3} M stock solution of cobalt(II) was prepared from cobalt chloride hexahydrate. Oxygen (99.999% pure) was passed into test solutions through a soda-lime tube and through a wash bottle filled with water.

Procedure

Before each measurement, the electrolysis vessel was washed with (1 + 1) nitric acid. The ring—disc electrode was washed with ethanol and then water, electrolyzed for 1 min anodically and cathodically in 0.5 M perchloric acid, and finally rinsed carefully with water.

A 40-ml aliquot of the sample solution was pipetted into the cell, which was then transferred to the cell compartment. Oxygen was bubbled through the solution for 10 min. The cell was removed from the cell compartment for the addition of cobalt(II) from a Finnpipette. The cell was returned to the cell compartment, an appropriate rotation rate for the ring—disc electrode was set, and the chosen potentials of the ring and disc electrodes were switched on simultaneously. The intensity of the cathodic luminescence was monitored for 2 min, and the output recorded.

RESULTS AND DISCUSSION

Method of measurement

The rotation of the ring—disc electrode generates the laminar flow of the oxygen-saturated luminol solution from the disc to the ring; the disc is maintained at a negative potential to reduce oxygen to hydrogen peroxide, which is immediately transferred to the ring electrode by the rotation. A symmetric double-step potential is applied to the ring electrode [12]. Figure 1 shows the luminol chemiluminescence generated during the double-step potential at the platinum glassy-carbon ring—disc electrode. The emission during the positive potential pulse is here called the anodic luminescence and that during the negative pulse the cathodic luminescence.

Of twenty-four metal ions studied, only cobalt(II) was capable of stimulating the cathodic luminescence of luminol. Hence the applicability to a selective trace method for cobalt(II) was obvious. The recorder response of the cathodic luminescence is the time average of the light pulse differences between the differently hatched areas in Fig. 1. A typical recorder response—time curve is presented in Fig. 2. In order to achieve good reproducibility, the recorder response was measured 1 min after the beginning of the measurement. This recorder response is hereafter referred to as the intensity and is given in arbitrary units.

The intensities produced with different electrode materials are listed in Table 1 for the conditions of Fig. 1 other than electrode material. The greatest intensity was observed at the Pt—C electrode and all further measurements were done with this electrode pair.

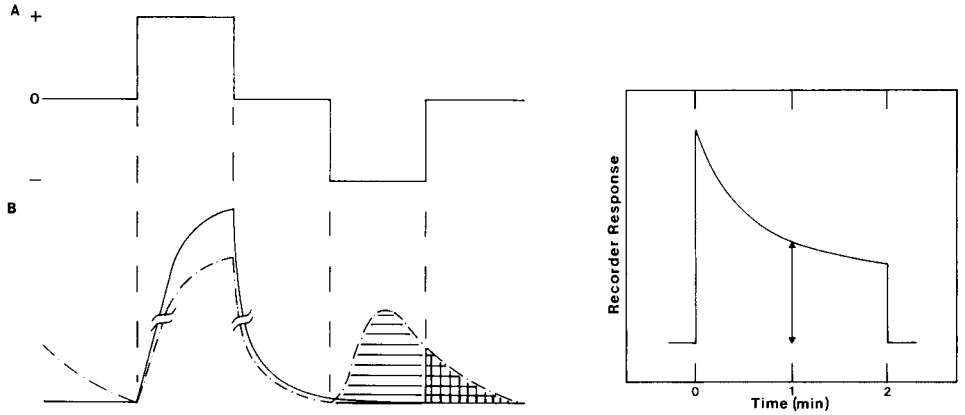

Fig. 1. (A) The symmetrical double-step potential. (B) The electrogenerated chemiluminescence of luminol at the Pt—C ring—disc electrode: (——) without cobalt; (-·-·-) with 5.0×10^{-6} M cobalt(II). 0.100 M NaCl, disc potential −1.00 V, pulse amplitude 0.825 V, pH 10.0, H_3BO_3—NaOH buffer, 1.50×10^{-4} M luminol, rotation rate 350 rpm, pulse length 35.0 ms; solutions saturated with oxygen; for hatching see text.

Fig. 2. Typical recorder response—time curve for the cathodic luminescence of luminol.

TABLE 1

Intensity of cathodic luminescence of luminol at various ring—disc electrodes (cobalt(II) = 5.0×10^{-6} M)

Electrode pair	Pt—C	Pt—Au	Pt—Pt	Au—Au
Intensity	852	313	171	13

Effect of experimental variables on the intensity

In order to establish the optimal conditions for cobalt(II) determinations, the luminescence intensity was measured as a function of disc potential, pulse amplitude, pH, luminol concentration, electrode rotation rate, and pulse length of the double-step potential. The results of these experiments are summarized in Fig. 3. On the basis of these measurements, the values of the variables used in Fig. 4 were selected for cobalt(II) determinations. The pH of 10.0 selected is not the value which gives the highest intensity, but this value is used because at higher pH values the cathodic luminescence of luminol is already induced during the zero potential pulse preceding the negative potential pulse.

Analytical curve, limit of detection and precision

The graph of log intensity vs. log cobalt(II) concentration is shown in Fig. 4. The plot is linear up to 3×10^{-6} M cobalt(II).

The limit of detection of the cobalt(II) determination can be evaluated [15] from $x = x_{bl} + ks_{bl}$, where x is the smallest measure that can be detected with reasonable certainty, x_{bl} is the mean blank measurement, k is a numerical

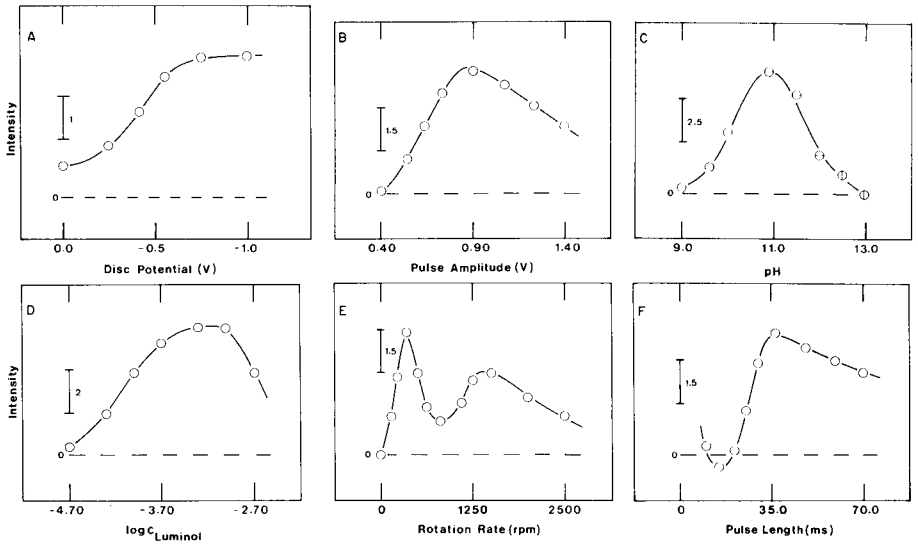

Fig. 3. Effect of variables on the cathodic luminescence from 5.0×10^{-6} M cobalt(II) at the Pt—C electrode: (A) disc potential; (B) pulse amplitude; (C) pH; (D) luminol concentration; (E) rotation rate; (F) pulse length. Except for the variable under consideration, the conditions were: pulse amplitude 0.850 V, pH 10.2 (H_3BO_3—NaOH buffer), 1.00×10^{-4} M luminol, disc potential —1.00 V, rotation rate 500 rpm, pulse length 35.0 ms, solutions saturated with oxygen, 0.1 M NaCl.

factor corresponding to the desired confidence level, and s_{bl} is the standard deviation of the blank. The values of x_{bl} and s_{bl} must be determined from at least 20 measurements. A value of 3 for k is strongly recommended [15], corresponding to a confidence level of about 90%. On this basis, the limit of detection is 1×10^{-8} M cobalt(II) for the proposed method, which is compared with the limits of detection available by other methods in Table 2. The limit of detection by the proposed method is poorer than those reported for other chemiluminescent methods or for inductively-coupled plasma emission spectrometry (on different criteria) but compares favourably with those reported for the other methods.

Twenty-five intensity measurements for 2.0×10^{-7} M cobalt(II) had a relative standard deviation of 6%. Consequently, the precision of the present method is comparable to those of conventional trace methods.

Inorganic interferences

The effects of 21 metal ions on the cathodic luminescence of luminol in the presence of 5.0×10^{-7} M cobalt(II) were determined under the recommended conditions. The results are summarized in Table 3. The effects of chromium(III), copper(II) and iron(III) are presented in Fig. 5. The tolerance limits shown in Table 3 were obtained from the intercept of the interference level and the inhibitive line of a metal ion as presented in Fig. 5. On the basis of Table 3, aluminium(III), antimony(III), bismuth(III), manganese(II),

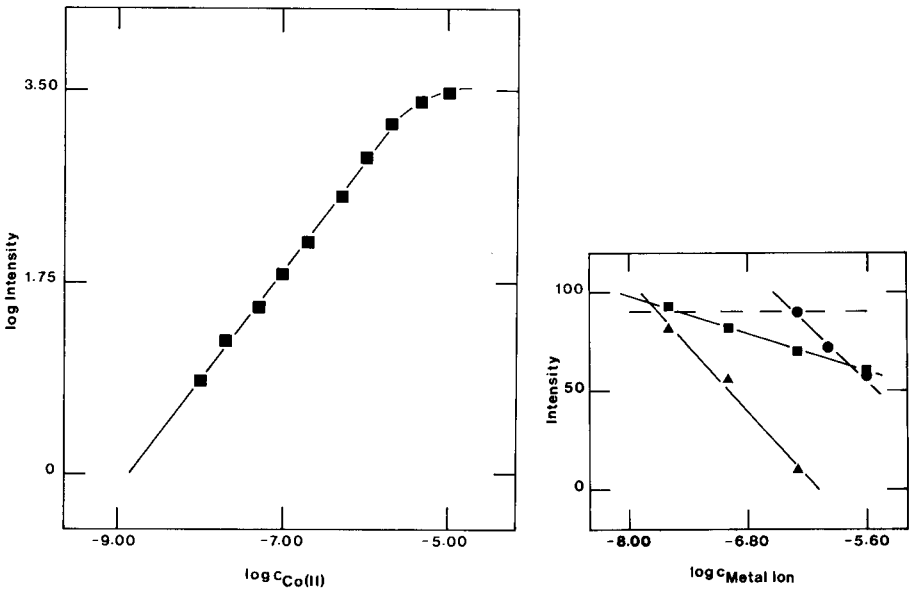

Fig. 4. Logarithmic plot of intensity vs. cobalt(II) concentration. Conditions: 0.100 M NaCl, disc potential −1.00 V, pulse amplitude 0.825 V, pH 10.0 (H_3BO_3—NaOH buffer), 1.50×10^{-4} M luminol, rotation rate 350 rpm, pulse length 35.0 ms, solutions saturated with oxygen.

Fig. 5. Inhibitive effects of (▲) chromium(III), (■) copper(II) and (●) iron(III) on the cathodic luminescence of luminol with 5.0×10^{-7} M cobalt(II). (- - -) Interference level of 10%. Conditions as in Fig. 4.

mercury(I), mercury(II), nickel(II), uranium(VI) and vanadium(V) have no effect on cobalt(II) determinations at a five-fold molar concentration; all the other metal ions inhibit the cathodic luminescence to some extent.

TABLE 2

Detection limits for cobalt(II) by various methods

Method	Detection limit (M)	Ref.
Proposed method	1×10^{-8}	—
Chemiluminescence		
Luminol + H_2O_2	1×10^{-10}	9
Lucigenin + H_2O_2	3×10^{-10}	16
Lophine + H_2O_2	2×10^{-9}	17
Gallic acid + H_2O_2	7×10^{-9}	18
Atomic absorption spectrometry	8×10^{-8}	19
Atomic emission spectrometry	5×10^{-7}	19
Atomic fluorescence spectrometry	8×10^{-8}	19
Electrothermal atomic absorption spectrometry	1×10^{-8}	20
Inductively-coupled plasma emission spectrometry	2×10^{-9}	21

TABLE 3

Effects of other ions on the cathodic luminescence of luminol with 5.0×10^{-7} M cobalt(II)

Ion	Conc. ($\times 10^{-6}$ M)	Relative intensity	Tolerance limit ($\times 10^{-7}$ M)	Ion	Conc. ($\times 10^{-6}$ M)	Relative intensity	Tolerance limit ($\times 10^{-7}$ M)
—	—	100		Pb(II)	2.5	56	
Al(III)	2.5	101			1.0	72	
Sb(III)	2.5	92			0.5	90	5
Bi(III)	2.5	92		Sn(II)	2.5	38	
Mn(II)	2.5	107			1.0	70	
Hg(I)	2.5	99			0.5	87	3
Hg(II)	2.5	96		Cd(II)	1.0	52	
Ni(II)	2.5	100			0.5	74	
U(VI)	2.5	104			0.25	91	3
V(V)	2.5	100		Ce(III)	1.0	68	
Zn(II)	2.5	64			0.5	77	
	1.0	88			0.25	85	
	0.5	102	9		0.1	93	2
Ag(I)	2.5	79		Tl(I)	2.5	70	
	1.0	88	8		1.0	78	
In(II)	2.5	55			0.5	83	
	1.0	79			0.25	90	2
	0.5	92	6	Cu(II)	0.5	71	
Fe(III)	2.5	29			0.1	82	
	1.0	66			0.025	93	0.3
	0.5	95	6	Cr(III)	0.5	10	
Fe(II)	1.0	53			0.1	56	
	0.5	76			0.025	82	0.2
	0.25	86					
	0.1	101	2				

However, the tolerance limits for zinc(II), silver(I), indium(III), iron(III), lead(II) and tin(II) are at least as high as the cobalt(II) concentration and, those of cadmium(II), cerium(III), iron(II) and thallium(I) are only slightly below the cobalt(II) concentration. Only chromium(III) and copper(II), with tolerance limits of 3×10^{-8} M and 2×10^{-8} M, interfered seriously with the determination of 5.0×10^{-7} M cobalt(II).

The interference of copper(II) is due to alteration of the intensity—time profile; the intensity does not level off after 1 min but falls linearly to zero after the peak. Thus the interference can be avoided by measuring the peak intensity but this leads to poor precision.

Organic interferences

The effects of EDTA, iminodiacetic acid and aminoacetic acid on the cathodic luminescence of luminol with 5.0×10^{-6} M cobalt(II) (Fig. 6) were determined. EDTA forms a 1:1 chelate with cobalt(II) ($pK = 16.3$ [22]). Iminodiacetic acid and aminoacetic acid form 1:2 and 1:3 metal:ligand

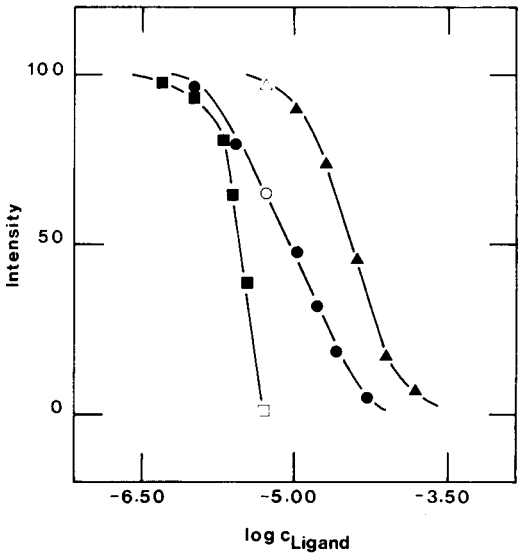

Fig. 6. Inhibitive effects of (▪) EDTA, (•) iminodiacetic acid and (▲) on the cathodic luminescence of luminol with 5.0×10^{-6} M cobalt(II). (□, •, ○) Indicate the points where the concentrations of cobalt(II) and ligands are equal. Conditions as in Fig. 4.

chelates, the stability constants being $pK_1 = 7.0$ and $p\beta_2 = 12.3$, and $pK_1 = 4.8$, $p\beta_2 = 8.6$ and $pc_3 = 11.0$ [22], respectively. The results show serious interference from EDTA, which binds with all the coordination sites of cobalt(II) necessary for the formation of the cobalt(II)—hydrogen peroxide complex which participates in the generation of the cathodic luminescence of luminol. The interfering effect of organic ligands, however, is decreased when the ligand has only two or three chelating groups, and is quite small for aminoacetic acid.

Financial aid from the Emil Aaltonen Foundation is gratefully acknowledged.

REFERENCES

1 W. R. Seitz and D. M. Hercules, in M. J. Cormier, D. M. Hercules and J. Lee (Eds.), Chemiluminescence and Bioluminescence, Plenum Press, New York, 1973, p. 427.
2 U. Isacsson and G. Wettermark, Anal. Chim. Acta, 68 (1974) 339.
3 W. R. Seitz and M. P. Neary, Anal. Chem., 46 (1974) 188A.
4 D. B. Paul, Talanta, 25 (1978) 377.
5 A. Hartkopf and R. Delumyea, Anal. Lett., 7 (1974) 79.
6 W. R. Seitz, W. W. Suydam and D. M. Hercules, Anal. Chem., 44 (1972) 957.
7 S. D. Hoyt and J. D. Ingle, Jr., Anal. Chim. Acta, 87 (1976) 163.
8 C. A. Chang, H. H. Patterson, L. M. Mayer and D. E. Bause, Anal. Chem., 52 (1980) 1264.
9 V. Nau and T. A. Nieman, Anal. Chem., 51 (1979) 424.
10 N. Harvey, J. Phys. Chem., 33 (1929) 1456.

11 B. Epstein and T. Kuwana, Photochem. Photobiol., 4 (1965) 1157; 6 (1967) 605.
12 K. E. Haapakka and J. J. Kankare, Anal. Chim. Acta, 138 (1982) 253.
13 G. A. Dallakyan, S. I. Pogosyan, V. A. Veselovskiy and B. N. Tarusov, Gidrabiol. Zh. (English Translation), 14 (1979) 90.
14 K. E. Haapakka and J. J. Kankare, Anal. Chim. Acta, 118 (1980) 333.
15 H. M. N. H. Irving, H. Freiser and T. S. West (Eds.), IUPAC Compendium of Analytical Nomenclature, Pergamon Press, Oxford, 1978, p. 117.
16 L. A. Montano and J. D. Ingle, Jr., Anal. Chem., 51 (1979) 919.
17 D. F. Marino, F. Wolff and J. D. Ingle, Jr., Anal. Chem., 51 (1979) 2051.
18 S. Stieg and T. A. Nieman, Anal. Chem., 49 (1977) 1322.
19 V. A. Fassel and R. N. Kniseley, Anal. Chem., 46 (1974) 1110A.
20 F. D. Posma, H. C. Smit and A. F. Rooze, Anal. Chem., 47 (1975) 2087.
21 K. W. Olson, W. J. Haas, Jr. and V. A. Fassel, Anal. Chem., 47 (1975) 1011.
22 A. Martell and L. Sillén (Eds.), Stability Constants of Metal—Ion Complexes, The Chemical Society, London, 1964.

Analytica Chimica Acta, 139 (1982) 237—246
Elsevier Scientific Publishing Company, Amsterdam — Printed in The Netherlands

EXTRACTION OF METAL IONS BY *N*-PHENYL-, *N*-METHYL-, AND *N*-UNSUBSTITUTED HYDROXAMIC ACID RESINS

RICHARD J. PHILLIPS and JAMES S. FRITZ*

Ames Laboratory and Department of Chemistry, Iowa State University, Ames, IA 50011 (U.S.A.)

(Received 28th January 1982)

SUMMARY

Procedures are described for preparing macroreticular chelating resins with hydroxamic acid or *N*-methylhydroxamic acid functional groups. The chelating properties of the resins are compared with each other and with an *N*-phenylhydroxamic acid resin reported earlier. The extraction of 19 metal ions was studied as a function of pH for the *N*-methylhydroxamic acid resin. Several analytical applications of this resin have been demonstrated including the purification of chemical reagents, concentration of trace metal ions, and chromatographic separation of metal-ion mixtures.

The relationship between the structure of hydroxamic acids and their ability to act as complexing agents for metal ions has received little attention. Bass and Yoe [1] studied 36 hydroxamic acids with various structural features for use as colorimetric reagents. They concluded that color formation is a function of pH, solvent, and reagent concentration, and that *N*-substitution is relatively unimportant. The available stability-constant data, however, suggest that the *N*-substituted hydroxamic acids should be more effective complexing agents than their *N*-unsubstituted analogues in strongly acidic media [2, 3].

Most of the research on polyhydroxamic acids has been concentrated on primary, or *N*-unsubstituted, compounds. Exceptions to this are found in the work of Vernon and Eccles [4], Winston and Mazza [5], and Winston and McLaughlin [6]. In no case has the relationship between *N*-substitution and complexing ability been explored systematically. Such a study is reported in this paper. Synthetic methods are described for attaching hydroxamic acid and *N*-methylhydroxamic groups to a macroporous polystyrene–divinylbenzene resin. The properties of these resins and the *N*-phenylhydroxamic acid resin reported earlier [7] are compared. The extraction behavior of the *N*-methyl resin with 19 metal ions is studied and various analytical applications of this new resin are reported.

0003-2670/82/0000-0000/$02.75

EXPERIMENTAL

Apparatus and reagents

Gravity-flow columns were constructed of glass with appropriate reservoirs and glass wool for holding the resin. The columns were 5 mm i.d. and were packed with 100—200-mesh hydroxamic resin to a height of ca. 5 cm.

A liquid chromatograph especially designed for inorganic separations was used for the separation of thorium(IV) and uranium(IV) [8]. A solution of 0.004% (w/v) arsenazo-III in 3 M hydrochloric acid served as the color-forming reagent [9].

Hydroxylammonium chloride and calcium hypochlorite were obtained from Fisher Scientific Co., and *N*-methylhydroxylammonium chloride from Aldrich. A commercial laundry bleach was used as 5% sodium hypochlorite. Potassium hypochlorite was prepared as an approximately 1.5 M solution by the reaction of calcium hypochlorite and potassium carbonate [10]. The XAD-4 resin and other reagents used for the synthesis of the chelating resins were described previously [7].

Synthesis

Acetyl XAD-4 was prepared by the acetylation procedure described previously [7]. This was oxidized to carboxy XAD-4 by repeated treatment with sodium or potassium hypochlorite at 60—70°C. Carboxy XAD-4 was then converted to chloroformyl XAD-4 by heating a mixture of the resin and thionyl chloride at reflux for one hour.

The *N*-unsubstituted hydroxamic acid resin was synthesized by adding ca. 1 g of chloroformyl XAD-4 to a 50-ml beaker containing 2.1 g of sodium carbonate, 1.4 g of hydroxylammonium chloride, and 10 ml of diethyl ether. On addition of 2.5 ml of water, the mixture began to effervesce. After about 10 min, the product was isolated by suction filtration, washed with water and methanol, and stored under methanol.

The *N*-methylhydroxamic acid resin was synthesized by substituting 1.68 g of *N*-methylhydroxylammonium chloride for the hydroxylammonium chloride in the above procedure. The preparation of the *N*-phenylhydroxamic acid resin described earlier [7] has now been improved [11].

Procedures

Characterization. The hydrogen ion capacity of the carboxy XAD-4 and the nitrogen contents of the final products were determined as described previously [7].

Batch extraction. A 50 ± 2 mg portion of resin was accurately weighed into a 60-ml polyethylene bottle and 10 ml of a 10^{-4} M solution of the test ion was added. The bottle was placed in the automatic shaker for 4 h. After being filtered through glass wool to remove the resin, the solutions were analyzed for the test ion by colorimetry or atomic absorption spectrometry.

Purification of reagents. Concentrated solutions of various reagents were spiked with the test ion, filtered through Whatman No. 5 paper, and passed through a short column of the *N*-methylhydroxamic acid resin. The concentration of the test ion in the column effluent was determined spectrophotometrically. Percentage of metal ion removed was calculated by the formula

$$R = \frac{100\,(A_s - A_c)}{(A_x - A_b)}$$

where R is the percentage removed, A is the absorbance of the solution indicated, and subscripts s, c and b indicate the spiked solution, the column effluent and the blank, respectively.

Concentration and recovery of uranium(VI). Synthetic seawater was prepared by a standard procedure [12]. Samples were spiked with 120 μg of uranium(VI) dissolved in dilute acid or sodium hydrogencarbonate. The latter was preferred for the seawater samples because it did not decrease the pH. The sample was passed through a gravity column packed with the *N*-methylhydroxamic acid resin at a flow rate of ca. 1 ml min^{-1}. The column was eluted with ca. 5 ml of water, followed by two 5-ml aliquots of a wash solution containing 0.025 M ammonium acetate, 0.075 M acetic acid, and 0.5 M ammonium chloride. It was rinsed again with water, and the sorbed uranium was removed by elution with 5 ml of 0.2 M hydrochloric acid. The uranium content of this solution was determined spectrophotometrically.

Concentration and determination of aluminium. A 200-ml sample was buffered by adding 1 ml of acetic acid and adjusting the pH to 4.0 with ammonium hydroxide. This was passed through a gravity column and washed as in the experiment described above with 5 ml of water followed by two 5-ml aliquots of the above wash solution. The column was rinsed again with water and the sorbed aluminum was removed by elution with 5 ml of 0.1 M oxalic acid. The aluminum content of this solution was quantified by atomic absorption spectrometry.

Concentration and determination of titanium. A gravity column was packed to a depth of 5 cm with the *N*-unsubstituted hydroxamic acid resin. A small plug of Dynel (Union Carbide) modacrylic staple fiber, which resists attack by hydrofluoric acid, was used to hold the resin in place. The sample was treated with 1.0 mg of ascorbic acid per milliliter to reduce iron(III). The sample (5—200 ml) was adjusted to pH 1.0, and was passed through the column. The column was eluted with two 5-ml aliquots of 0.1 M hydrochloric acid followed by 5 ml of 0.3 M hydrofluoric acid. The effluent from the hydrofluoric acid elution was analyzed for titanium spectrophotometrically.

Chromatographic separation of uranium(IV) and thorium(IV). The liquid chromatograph described earlier was used. A 2-mm i.d. by 10-cm column containing 200—325 mesh *N*-methylhydroxamic acid resin was used for the separation. The column was eluted with 3 M hydrochloric acid. A sample containing 10^{-4} M each of uranium(VI) and thorium(IV) was injected with a

50-μl sample loop. After 5 min, the eluent was switched to 3 M hydrochloric acid plus 0.1 M oxalic acid to elute uranium(IV). The column effluent was automatically mixed with a solution of arsenazo-III, as described earlier [8] and its absorbance at 665 nm was monitored continuously.

RESULTS AND DISCUSSION

Resin capacity

Exchange isoplanes, or breakthrough curves, were used to obtain the capacity of each resin for copper(II) at pH 6. The results of these experiments are shown in Table 1. The carboxy intermediate has some capacity for copper and so, presumably, do the unreacted carboxy groups in the hydroxamic acid resins. The *N*-methylhydroxamic acid resin has the highest capacity. The copper(II) capacity is lower in each case than the hydroxamic acid capacity as deduced from the nitrogen content of the resin. Part of this difference is because two hydroxamic acid groups can combine with one copper(II). The remaining difference may be due to steric factors which limit the near approach of copper(II) to some of the hydroxamic acid groups.

All of the resins showed good stability; the capacities were not affected by treatment with 2 M hydrochloric acid or 1 M ammonium hydroxide. Prolonged exposure of the resins to light and air produced some decrease in capacity.

Comparison of resins

Batch-extraction experiments were used to compare the complexing ability of the three hydroxamic acid resins. The extraction data for titanium(IV) and iron(III) are plotted as functions of pH in Fig. 1. These data show that the most stable complexes are formed by the *N*-methyl resin. Similar results were obtained for the extraction of copper(II), aluminum(III), uranium(VI), and thorium(IV) by the three resins.

The superiority of the *N*-methylhydroxamic acid resin in complexing ability is quite interesting, because virtually all work previously reported on

TABLE 1

Copper(II) capacity at pH 6.3 as determined by exchange isoplanes

Functional group	Nitrogen content (mmol g^{-1})	Cu(II) capacity (mmol g^{-1})
	—[a]	0.15
—CONHOH	1.68	0.48
—$CON(CH_3)OH$	1.78	0.69
—$CON(C_6H_5)OH$	1.08	0.40

[a]Carboxylic acid resin intermediate.

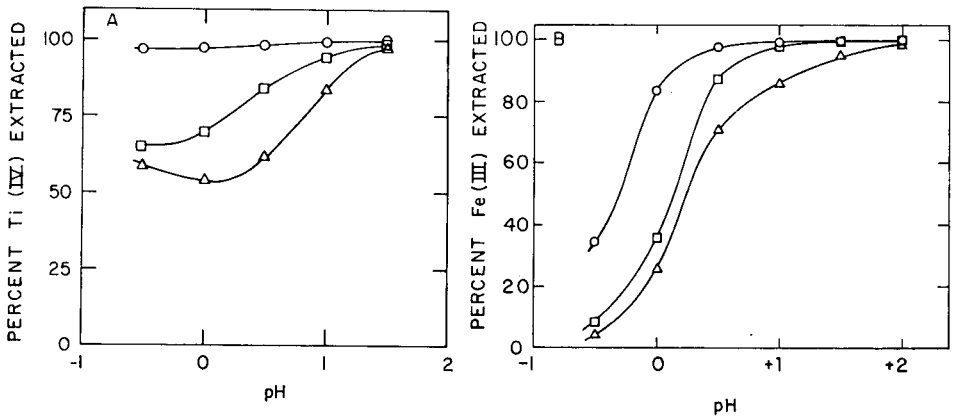

Fig. 1. Extraction of (A) titanium(IV), and (B) iron(III), by *N*-phenyl (△), *N*-unsubstituted (□), and *N*-methyl (○) hydroxamic acid resins vs. pH.

monomeric hydroxamic acid chelating reagents has been with *N*-phenyl- or *N*-hydrogen derivatives. The *N*-methyl chelating resin was chosen for the remaining studies reported here.

Effect of pH on metal-ion uptake

Extraction of several metal ions by the *N*-methylhydroxamic acid resin is shown in Figs. 2 and 3. Figure 2A shows that iron(III) is retained from more acidic solution than is aluminum(III) or copper(II). The extraction curve for copper(II) is normal, but the curves for nickel(II) and calcium(II) are spread out. For nickel, there could be a combination of chelation at the lower pH range and simple ion exchange towards the higher pH range. The calcium curve might be explained by ion exchange with the carboxyl hydrogen and possibly with the hydrogen of the N—OH group. The extraction curves for thorium(IV) and uranium(VI) in Fig. 3A indicate the possibility of separating these two ions using the *N*-methylhydroxamic acid resin.

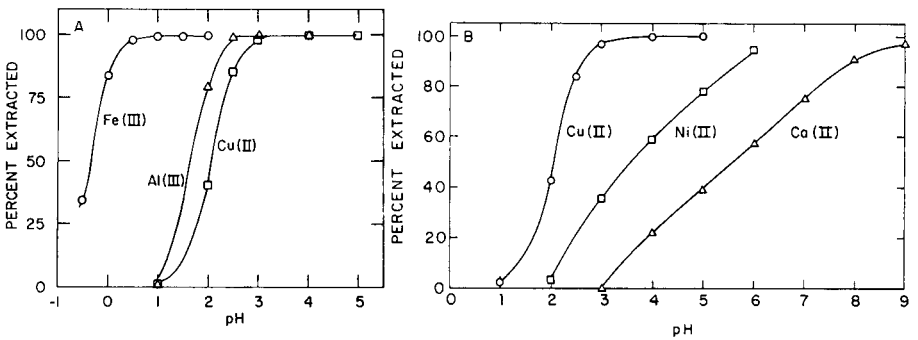

Fig. 2. Extraction of Fe(III), Al(III), Cu(II), Ni(II) and Ca(II) by *N*-methylhydroxamic acid resin vs. pH.

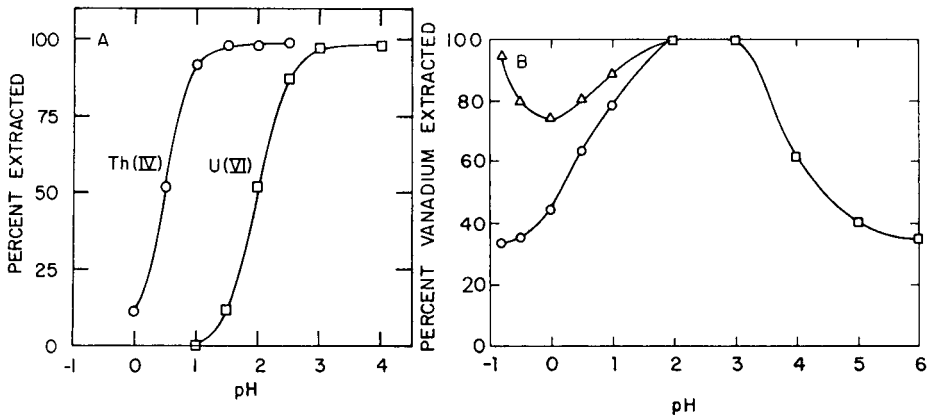

Fig. 3. Extraction of (A) U(VI) and Th(IV), and (B) vanadium, by *N*-methylhydroxamic acid resin vs. pH. For (B): (△) $HClO_4$; (○) HCl; (□) HCl—HOAc—NaOAc.

The extraction of vanadium(V) from both weakly and strongly acidic solutions is shown in Fig. 3B. It reaches a maximum at pH 3. Extraction from solutions of hydrochloric acid may be complicated by reduction to vanadium(IV). Vanadium(V) is extracted more efficiently from perchloric than from hydrochloric acid. Vanadium(IV) extraction was also studied at pH 1—3 and gave results nearly identical to those found with vanadium(V) in this pH range. Here it appears that vanadium(IV) was oxidized to vanadium(V). Brandt [13] has reported that vanadium(IV) reacts only extremely slowly with benzohydroxamic acid when exposed to air. The vigorous shaking used in the batch-extraction experiments may have accelerated this process.

The pH values for 50% extraction by the *N*-methylhydroxamic acid resin of 16 ions are shown in Table 2. This is a convenient way of comparing the relative affinity of various ions for the resin. In general, the results correlate well with published data on the stability constants of hydroxamic acid complexes with metal ions [14]. Vanadium(V) is not included in this table because, unlike the other ions, its extraction does not increase continuously as the pH is raised. Titanium(IV) and zirconium(IV) are not included because their extraction exceeds 95% even in 3—4 M acid. The extraction of zirconium(IV) can only be described as remarkable. More than 99% of the zirconium was extracted from solutions in 1—4 M hydrochloric acid.

TABLE 2

pH for 50% extraction of ions by *N*-methylhydroxamic acid resin

Ion	Mg(II) Ca(II) Mn(II) Co(II) Ni(II) Zn(II) Cr(III) La(III)
pH (50% ext.)	6.4 5.6 5.2 4.0 3.6 3.6 3.0 2.5
Ion	Lu(III) Eu(III) Cu(II) U(VI) Al(III) Sc(III) Th(IV) Fe(III)
pH (50% ext.)	2.4 2.3 2.1 2.0 1.8 1.0 0.5 —0.4

The batch-extraction data were used to estimate distribution coefficients for several ions by the following formula, where E is the percentage extracted: $D_g = 200(E)/(100 - E)$. The factor of 200 is the ratio of solution volume (ml) to resin weight (g) used in the experiments. Plots of log D_g vs. pH are shown in Fig. 4 Iron(III), thorium(IV) and scandium(III) give linear plots with slopes of 1.98, 1.98, and 1.95, respectively. In other plots, copper(II) was essentially linear with a slope of 1.46. The plots for uranium(VI) and lanthanum(III) were not quite linear but gave slopes which approached a value of 2. The plot for nickel(II) was non-linear.

These results indicate that extraction of several of the ions is accompanied by the release of two protons [15]. It seems likely that in these cases two adjacent hydroxamic acid groups are involved in complexation. Precipitation or extraction with monomeric hydroxamic acids usually involves complexes with the formula ML_n, where M is the metal cation, n is its charge, and L is the hydroxamate anion [16]. In the resin, however, there are obvious limitations to the number of immobilized groups that can approach the same metal ion closely enough for chelation. While the formation of a neutral complex is necessary for solvent extraction or precipitation, this may not be the case for a chelating resin. Excess charge at the chelation site could be balanced by counter ions from the solution.

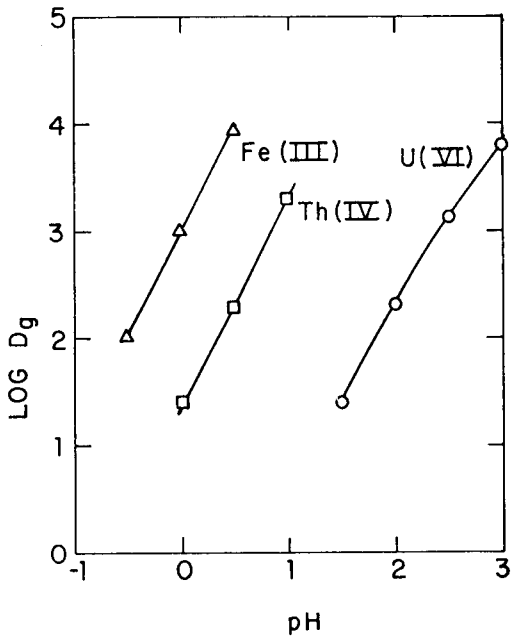

Fig. 4. Log D_g vs. pH for extraction of Fe(III), Th(IV) and U(VI) by *N*-methylhydroxamic acid resin.

Analytical applications

Purification of reagents. An attractive use for the hydroxamic acid resins is in purification of reagents by selective extraction of the metallic impurities. By passing a solution of the reagent through a column of the chelating resin, the metal-ion impurities could be removed without contamination of the reagent solution with the addition of a soluble chelating agent. The results of several experiments (Table 3) demonstrate the feasibility of this approach. The removal of iron(II) from 1,2-ethanediammonium dichloride seems especially noteworthy. This selectivity for inorganic versus organic cations is a unique feature of chelating ion exchangers.

Concentration of metal ions. Tables 4 and 5 show the effectiveness of the hydroxamic acid resins for the selective concentration of metal ions. Uranium(VI) was extracted by the *N*-methyl resin from synthetic seawater and dilute hydrogencarbonate at pH 7—8 with recoveries of 99—101%. A concentration of 200-fold was achieved in one of the extractions from seawater. Extraction of uranium(VI) from a pH 10 carbonate buffer was incomplete. Aluminum(III) was efficiently concentrated by the *N*-methyl resin at pH 4 in the presence of either calcium or phosphate. This procedure should be applicable to the determination of trace aluminum in biological samples [17]. Titanium(IV) was efficiently complexed by both the *N*-methyl and the *N*-unsubstituted resins. It was more readily eluted from the latter, however, with 0.3 M hydrofluoric acid. The recovery of titanium from concentrated aluminum chloride solutions was slightly low, ranging from 97% to 99%.

Chromatographic separations. Figure 5 shows the chromatographic separation of uranium(IV) from thorium(IV) on a column of *N*-methylhydroxamic acid resin. Based on the results from batch- and column-extraction experiments, it should be possible to separate uranium(IV) from many other ions, including uranium(VI), iron(II), and the rare earths. The possibility of

TABLE 3

Removal of aluminum, zirconium, and iron from concentrated reagent solutions

Solution	Ion added	Concentration (10^{-5} M)	% removed
5% $Ca(NO_3)_2 \cdot 4\ H_2O$	Al(III)	1	97
5% NaCl	Al(III)	1	103
5% $NaC_2H_3O_2 \cdot 3\ H_2O$	Al(III)	1	105
10% $AlCl_3 \cdot 6\ H_2O$	Zr(IV)	4	100[a]
10% $AlCl_3 \cdot 6\ H_2O$	Fe(III)	5	90[b]
10% $Na_2C_4H_4O_6 \cdot 2\ H_2O$	Fe(III)	5	102
10% $C_2H_{10}N_2Cl_2$	Fe(II)	5	101[c]

[a]Solution in 1 M hydrochloric acid. [b]Solution in 0.1 M hydrochloric acid. [c]Solution at pH 3.5.

TABLE 4

Recoveries of uranium from various media by *N*-methylhydroxamic acid resin

Medium	Volume extracted (ml)	U(VI) recovered (%)
0.1 M acetate pH 4	5	100
0.01 M CO_3^{-2} + 0.01 M HCO_3^- pH 10.1	5	68
Synthetic seawater pH 7	100	101
Synthetic seawater pH 8.1	1000	99
0.005 M HCO_3^- pH 8.3	5	101

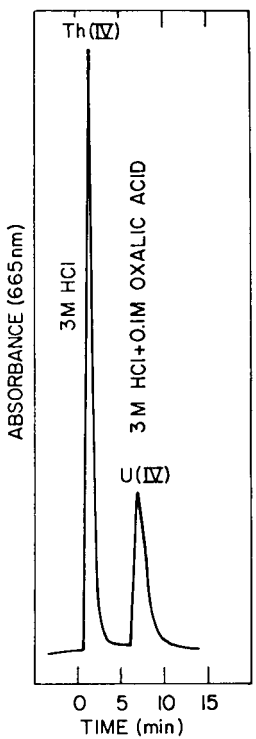

Fig. 5. Chromatographic separation of Th(IV) and U(IV) with *N*-methylhydroxamic acid resin.

TABLE 5

Concentration and determination of aluminum(III) and titanium(IV)
(Samples analyzed for aluminum were pH 4 and those analyzed for titanium were 0.1 M HCl)

Solution	Ion determined	Added (ppm)	Found (ppm)
Tap water	Al(III)	0.00	0.00
	Al(III)	0.34	0.34
Distilled water	Al(III)	0.00	0.00
	Ti(IV)	47.9	47.9
1000 ppm Ca(II)	Al(III)	1.05	1.05
1000 ppm PO_4^{3-}	Al(III)	1.05	1.05
5% $AlCl_3 \cdot 6\ H_2O$	Ti(IV)	0.0	1.7
	Ti(IV)	47.9	48.2

extending the use of these resins from analytical separations to larger scale processing of nuclear fuels should certainly be considered. Such applications have already been found for solvent extraction with hydroxamic acids [18].

The Ames Laboratory is operated for the U.S. Department of Energy by Iowa State University under contract No. W-7405-Eng-82. This research was supported by the Director of Energy Research, Office of Basic Energy Sciences, WPAS-KC-03-02-03.

REFERENCES

1 V. C. Bass and J. H. Yoe, Talanta, 13 (1966) 735.
2 G. Schwarzenbach and K. Schwarzenbach, Helv. Chim. Acta, 46 (1963) 1390.
3 I. G. Perkov, N. P. Komar and V. V. Melnik, J. Anal. Chem. USSR (Engl. Trans.), 22 (1967) 429; Zh. Anal. Khim., 22 (1967) 485.
4 F. Vernon and H. Eccles, Anal. Chim. Acta, 77 (1975) 145; 79 (1975) 229.
5 A. Winston and E. T. Mazza, J. Polym. Sci., Polym. Chem. Ed., 7 (1975) 1035.
6 S. Winston and G. R. McLaughlin, J. Polym. Sci., Polym. Chem. Ed., 14 (1976) 2155.
7 R. J. Phillips and J. S. Fritz, Anal. Chim. Acta, submitted.
8 J. N. King and J. S. Fritz, J. Chromatogr., 50 (1978) 507.
9 S. B. Savvin, Talanta, 8 (1961) 673.
10 M. S. Newman and H. L. Holmes, in A. H. Blatt (Ed.), Organic Synthesis, Wiley, New York, 1943, Collect. Vol. 2, p. 429.
11 R. J. Phillips, Ph.D. Dissertation, Iowa State University, Ames, IA, 1980.
12 G. Dietrich, General Oceanography, An Introduction, Interscience, New York, 1963, Ch. 2.
13 W. W. Brandt, Rec. Chem. Prog., 21 (1960) 159.
14 G. Anderegg, F. L'Eplattenier and G. Schwarzenbach, Helv. Chim. Acta, 46 (1963) 1400.
15 A. Ringbom, Complexation in Analytical Chemistry, Interscience, New York, 1963.
16 A. K. Majumdar, *N*-Benzoylphenylhydroxylamine and Its Analogues, Pergamon, Oxford, 1972.
17 K. Garmestani, A. J. Blotchky and E. P. Rack, Anal. Chem., 50 (1978) 143.
18 S. Cao, H. Dworschak and A. Hall, Com. Naz. Energ. Nucl., 10 (1973) 73; Chem. Abstr., 80 (1974) 151734v.

Analytica Chimica Acta, 139 (1982) 247—256
Elsevier Scientific Publishing Company, Amsterdam — Printed in The Netherlands

PROFILE ANALYSIS OF ORGANIC VOLATILES IN URINE OF TOBACCO SMOKE-EXPOSED BEAGLES

R. S. BRAZELL* and R. A. JENKINS

Analytical Chemistry Division, Oak Ridge National Laboratory, Oak Ridge, TN 37830 (U.S.A.)

C. K. BAYNE

Computer Science Division, Oak Ridge National Laboratory, Oak Ridge, TN 37830 (U.S.A.)

(Received 7th December 1981)

SUMMARY

Volatile organic components were determined in the urine of beagle dogs exposed to cigarette smoke and sham in an effort to identify possible biochemical changes resulting from the exposures. The data obtained from high-resolution chromatograms were subjected to principal component and discriminant analysis. Principal component analysis was used to reduce the dimensionality of the data and discriminant analysis was used to develop a classification model. Classification of the profiles into their respective exposure groups based on quantitative variations was 92% correct using only five peaks in the chromatograms. Compounds present in the urine of smoke-exposed dogs were identified by mass spectrometry.

The metabolic profiling of biological fluids has progressed over the last several years to become recognized as an important means of studying clinical diseases. It has been used to recognize inborn errors of metabolism and to obtain information on the etiology of certain diseases [1—5]. In some instances profile data have also been used to suggest medical treatment [2].

Of the various classes of compounds that have been profiled, the volatile organic fraction has proven to be one of the most challenging. This fraction is a complex mixture of compounds containing the lower-molecular-weight (b.p. $<250^{\circ}C$) metabolic intermediates and byproducts. The complexity of this fraction increases the probability of detecting differences between normal and pathological states. However, the volatility of the compounds poses problems in terms of sample-handling and collection and has required the development of new techniques for isolation and concentration. The necessary methods are now well established and have been used to characterize the differences among normal individuals and patients with diabetes, renal insufficiency, and respiratory virus infections [3].

A difficulty involved in examining complex profile data is the extraction of information relating to pathological changes over the large variations in data found among individuals in a given sample population. In order to fully

evaluate and assess differences, the background or normal levels of individual compounds in a metabolic profile need to be established. These levels generally cover a broad range and will dictate the confidence with which profile changes can be interpreted as resulting from biochemical alterations. This variation has prompted some investigators to use animal models which allow better control over environmental, dietetic, and genetic factors. Pattern recognition techniques have also aided in reducing and extracting the significant differences.

Biochemical changes that may occur as a result of tobacco smoking are under investigation in the laboratory, by determining the volatile constituents found in urines of animals exposed to whole cigarette smoke. While the relationship between smoking and increased incidence of disease has been well established, only a few biochemical alterations have been identified as occurring as a result of the exposures. Most recently, Assenza and Brown [6] have found elevated levels of low-molecular-weight ultraviolet-absorbing compounds in sera of beagles exposed to tobacco smoke. It is the purpose of this paper to use gas chromatography to examine the volatile components extracted from samples obtained from beagles differing only in their level of exposure, and to define the variation found in a well controlled animal study for the volatile compounds. Additionally, a feature selection method is described that reduces the dimensionality of the data and determines the importance of selected volatile compounds as classification variables.

EXPERIMENTAL

Inhalation exposures

Urine samples were obtained from healthy male beagle dogs housed under strict laboratory environmental conditions at the Veterans Administration Hospital in East Orange, NJ. The animals were from the same strain and were similar in age and weight. Three different exposure groups were sampled and were designated control, high nicotine, and medium nicotine. Animals were exposed with the ADL/II—cuffed cannula smoke exposure system, as depicted elsewhere [7]. Briefly, cigarette smoke is generated by the ADL/II smoking machine under standard puffing parameters (35-cm^3 volume, 2-s duration). Cigarettes were smoked at two puffs per minute until the burn line was within 3 mm of the filter overwrap. The smoke is delivered to the head of a large-bore stand tube, through which the animals breath via a cuffed, intertracheal cannula. Animals were exposed to the smoke of 12 cigarettes per day, half of which were administered sequentially in the morning and the remainder in the afternoon. The group designated control was sham-smoked. The high nicotine group was exposed to the smoke of A-1 cigarettes (85 mm filter NCI S&HP) which offered under these smoking conditions an average of 30 mg of total particulate matter (TPM) and 2.2 mg of nicotine per cigarette. The medium nicotine group was exposed to the smoke of A-2 cigarettes (85 mm filter, NCI S&HP) which offered approximately 16 mg of

TPM and 1.1 mg of nicotine per cigarette. Procedures for the determination of the amounts of TPM and nicotine available to the animal for inhalation have been described elsewhere [8]. The beagles were exposed routinely for a period of 144 to 292 days prior to sample collection.

Sampling and sample preparation

Urine samples (24 h) were obtained from each beagle using stainless steel collection pans installed in individual cages. All samples were collected on ice and shipped frozen. On arrival here, the samples were thawed, filtered through medium glass frits, and aliquoted into 100-ml glass bottles for storage at −10°C until all samples were ready for analysis.

The volatile organics were extracted with a dynamic headspace sampling procedure. The volume of urine purged per 24-h sample was adjusted for creatinine content to correct for errors in the collection of the specimens. This correction was necessary because it was observed that the volume of urine recovered was incomplete. It was also observed that in some cases the urine was diluted with spilled drinking water of the animal. Creatinine was determined as described by Tietz [9], and urine volumes equivalent to 35 mg of creatinine were used for extraction. Helium adjusted to a flow of 20 cm^3 min^{-1} was used as the purge gas and sampling time was 30 min per 50 ml of urine. The sample was heated in a water bath at 60°C in a headspace collection apparatus [3] and the condenser was cooled with chilled water at 12°C. The extracted volatiles were trapped and concentrated on 12.5 cm × 9 mm i.d. glass tubes containing 1.8 ml of Tenax (60—80 mesh; Applied Science Laboratories, State College, PA). The volatiles were then thermally desorbed in a chamber maintained at 250°C by purging with helium at 12 cm^3 min^{-1} for 10 min. The desorbed volatiles were subsequently trapped in a cryogenically cooled uncoated nickel precolumn (15 cm × 0.38 mm i.d.) that, when attached to the analytical column, served to introduce the sample.

Instrumentation

Separations were done in a Perkin-Elmer 3920 gas chromatograph equipped with a flame ionization detector, and a 60 m × 0.28 mm i.d. glass capillary column coated with 2% w/w UCON 50-HB-2000. The column was operated at 35°C for 2 min, then programmed at 2°C min^{-1} to 180°C where it was held isothermally for 16 min. Helium was used as the carrier gas at a flow of 1 cm^3 min^{-1}. Peak areas were integrated with a Hewlett-Packard 3390A reporting integrator.

Mass spectrometry was done with an HP-5985A instrument coupled with an HP-5840A gas chromatograph. Spectra were recorded at 70 eV in a linear scan mode for a mass range of 40—400 a.m.u. every 4 s. Identifications were based upon comparisons to reference spectra and known retention volumes.

For data analysis, an IBM 3033 computer was employed with the statistical analysis system (SAS) software package [10].

RESULTS AND DISCUSSION

The chromatographic profiles obtained from the urine samples were complex, containing well over 100 peaks, and visual inspection did not reveal any obvious differences between the exposure groups. Although there were some qualitative differences found among subjects they were not consistent within a group. Figure 1 shows a typical chromatogram obtained from a smoke-exposed dog and Table 1 lists some of the compounds identified by mass spectrometry. Several of these constituents have been previously reported in urines [3].

To analyze the data further and to discriminate between 5 control and 13 exposed samples (including 3 high and 10 medium nicotine profiles), 15 chromatographic peaks were selected to form a data base. These peaks (shown in Fig. 1) were easy to distinguish in the chromatograms and were well resolved from neighboring compounds. Their retention times ranged from 13 to 52 min and covered the mid to latter section of the profiles. Outside of these few considerations, the peaks were chosen arbitrarily prior to identification. Principal component and discriminant analyses [11, 12] were then applied to the data. Principal component analysis was used to rank the peaks in order of their importance in representing the data variation, and discriminant analysis was used to select the minimum number of peaks from the 15 selected for a reasonable misclassification probability.

In principal components analysis, the dispersion of N-points (e.g., 18 samples) in P-dimensional space (e.g., 15 peaks) is described with a new set of P-orthogonal linear coordinates so that the variances of the given points with respect to these derived coordinates are in decreasing order of magnitude. Thus the first principal component is such that the projection of the given points onto it has maximum variance; the second principal component has maximum variance subject to being orthogonal to the first; and so on. Algebraically, the principal components analysis involves finding the eigen-

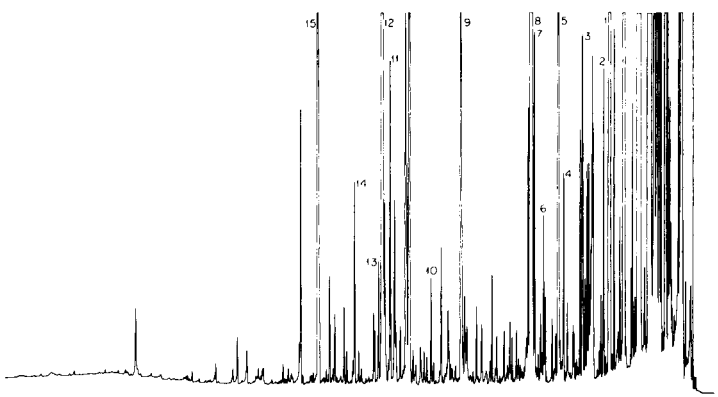

Fig. 1. Chromatogram of organic volatiles isolated from urine of smoke-exposed dogs. Numbers refer to compounds in Table 1.

TABLE 1

Volatile constituents in dog urine

Peak no.[a]	Compound	Peak no.[a]	Compound
	2-Butanone	8	2-Heptanone
	Thiabutane		Octanone
	4-Methyl-2-pentanone	9	C_8H_{16}
	Toluene	10	Decanone
1	Thiapentane		Octenone
2	3-Hexanone		Nonanone
	2-Hexanone	11	Benzaldehyde
3	Thiahexane	12	C_6H_6S[b]
4	Unsaturated C_7 sulfide ($C_7H_{10}5$)[b]	13	Unidentified component
	4-Heptanone	14	Unidentified component (m.w. 134)
6	3-Heptanone	15	Undecanone
7	C_6 cyclic ketone ($C_6H_{10}O$)[b]		Carvone

[a]Peak numbers refer to Fig. 1. [b]Tentative.

values and eigenvectors of the covariance matrix. The eigenvalues represent the amount of variance explained by the corresponding principal component. The eigenvector of the corresponding eigenvalue is the vector of coefficients for that principal component.

To apply this analysis to the profile data, a logarithmic transformation (base e) was first used to reduce the large variance of the original peak area measurements and equalize the variance between the control and exposed samples. Figure 2 shows the percent relative standard deviation, %RSD (100% standard deviation/mean) versus the peak number for the original and transformed data. The original data were found to have a large %RSD that exceeded 100% for peaks 3, 5, 6, 7, 10, 11 and 14, and the logarithmic transformation reduced this variation to under 15% in most cases. The two exceptions, peaks 4 and 7, arise because these two peaks were absent in two of the thirteen exposed samples. Replicate analysis of three aliquots of a control urine sample showed that the within sample measurement error was relatively small for the 15 original peaks with a %RSD ranging from 1% to 11%. The primary source of variation was attributed to dog-to-dog differences. The pooled covariance matrix [11] of the transformed data was then formed using the chromatograms obtained from both control and exposed samples. This matrix has estimated variances as the diagonal elements and estimated covariances as the off-diagonal elements.

The principal components were formed as linear sums of the 15 transformed peak areas with the coefficient corresponding to each peak being an element of the eigenvector. Table 2 lists the eigenvectors and eigenvalues for the covariance matrix of the profile data. Although the first few principal components explain the majority of the variation, they do not necessarily

TABLE 2

Eigenvectors and eigenvalues of the pooled covariance matrix

Peak	Principal components (eigenvectors × 10^2)[a]														
	1	2	3	4	5	6	7	8	9	10	11	12	13	14	15
1	−6	−4	16	−25	49	−1	−2	−37	−10	8	19	−43	22	−48	14
2	−9	−3	44	−4	−17	−8	13	1	3	15	−25	−29	36	14	−66
3	−2	−2	40	−12	−9	−9	28	43	25	40	34	0	11	10	43
4	−6	95	2	23	5	3	15	−2	2	2	2	−5	2	−9	−1
5	−4	8	−18	−21	−57	−22	2	−57	−17	32	25	8	9	10	6
6	−7	−3	53	6	−29	−2	−8	−25	27	−11	−18	8	−53	−39	7
7	−97	−7	−16	4	−1	2	4	8	1	2	−5	−4	−4	−1	5
8	−3	7	9	−41	−17	47	19	−12	7	−36	−33	16	39	7	31
9	1	5	2	−38	8	25	40	−2	−23	−6	16	−27	−59	32	−15
10	−10	16	14	−40	−7	19	−48	26	−10	−12	46	30	3	−17	−32
11	−2	5	16	−12	−9	−59	15	23	−57	−39	−12	4	3	−12	14
12	−5	4	7	−24	45	−16	17	−14	−3	37	−28	65	−8	2	−13
13	−10	0	20	9	24	−28	2	−33	33	−48	37	12	9	44	−3
14	−5	11	32	3	12	7	−58	−7	−30	18	−22	−14	−7	48	30
15	4	17	−28	−51	0	−39	−24	14	49	−1	27	−27	−10	5	2
Eigenvalue	14.339	9.751	3.578	1.777	0.662	0.565	0.488	0.245	0.190	0.167	0.060	0.022	0.015	0.009	0.003
% of total variation	45.0	30.6	11.2	5.6	2.1	1.8	1.5	0.8	0.6	0.5	0.2	0.07	0.05	0.03	0.01

[a]The original eigenvectors are found by multiplying the entries by 10^{-2}.

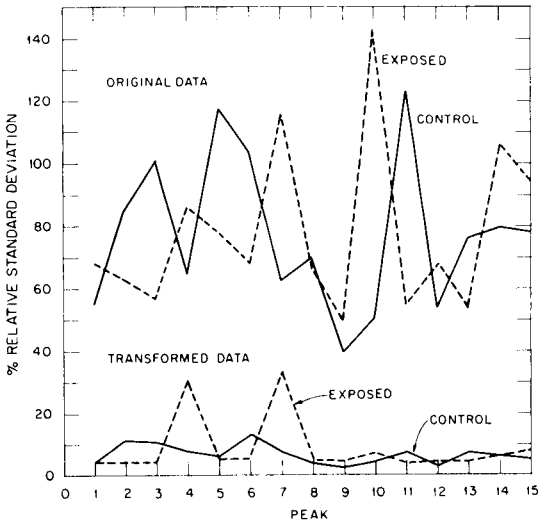

Fig. 2. Relative standard deviation for 15 selected peaks for original integration counts and logarithmic transformation of counts.

identify the most important individual peaks. To make this identification, a ranking procedure was used to rank the peaks in order of importance based on both the eigenvalues and eigenvectors. The sum of the squared elements in each eigenvector adds up to one. Therefore, the magnitudes of the squares of the coefficients represent the importance a particular principal component places on each of the 15 peaks. If for a particular peak, the squared coefficients of each principal component were added together, a measure of the importance of that peak would be obtained. Because all principal components are not equally prominent, the ranking procedure used the sum of the squared coefficients with each coefficient weighted by the fraction of the total variation explained by the corresponding eigenvalue. The ordered peaks are given in Table 3 with their ranking values.

TABLE 3

Ranking order of profile peaks based on principal components

Rank	Peak	Ranking value	Rank	Peak	Ranking value
1	7	0.433	9	5	0.020
2	4	0.282	10	8	0.019
3	15	0.039	11	13	0.015
4	6	0.037	12	1	0.015
5	10	0.028	13	11	0.014
6	2	0.027	14	9	0.013
7	3	0.024	15	12	0.012
8	14	0.023			

The minimum number of peaks necessary to distinguish between control and exposed samples was determined by discriminant analysis using the principal components. Fisher's linear discriminant function was formed from the principal components using subsets of the original 15 peaks. The number of peaks in each subset ranged from 1 to 15 where a subset of K peaks was made up of the first K ordered peaks determined from the ranking procedure. Figure 3 plots the misclassification probability versus the number of peaks used to determine the discriminant function. When the first ten ordered peaks were used, perfect classification was obtained. However, only an 8% error rate was made when the first five peaks were used. This was considered reasonable, and it reduced the number of original peaks to be measured by 1/3.

The principal components corresponding to the eigenvalues (13.96, 9.43, 1.65, 0.89, and 0.16) for the first five ordered peaks are:

$$Y1 = 0.04\ln(P4) + 0.05\ln(P6) + 0.99\ln(P7) + 0.09\ln(P10) - 0.03\ln(P15)$$
$$Y2 = -0.97\ln(P4) + 0.03\ln(P6) + 0.05\ln(P7) - 0.16\ln(P10) - 0.17\ln(P15)$$
$$Y3 = -0.13\ln(P4) - 0.75\ln(P6) + 0.07\ln(P7) - 0.02\ln(P10) + 0.64\ln(P15)$$
$$Y4 = -0.19\ln(P4) + 0.42\ln(P6) - 0.07\ln(P7) + 0.73\ln(P10) + 0.49\ln(P15)$$
$$Y5 = 0.02\ln(P4) + 0.50\ln(P6) + 0.05\ln(P7) - 0.66\ln(P10) + 0.56\ln(P15)$$

These five principal components were used to classify the control and exposed samples. Fisher's linear discriminant function used to classify observations into the two groups based on the principal components of the first 5 ordered peaks is:

$$D(\mathrm{Y}) = 54.99 + 0.03\ Y1 - 0.12\ Y2 - 0.34\ Y3 - 0.76\ Y4 - 6.37\ Y5$$

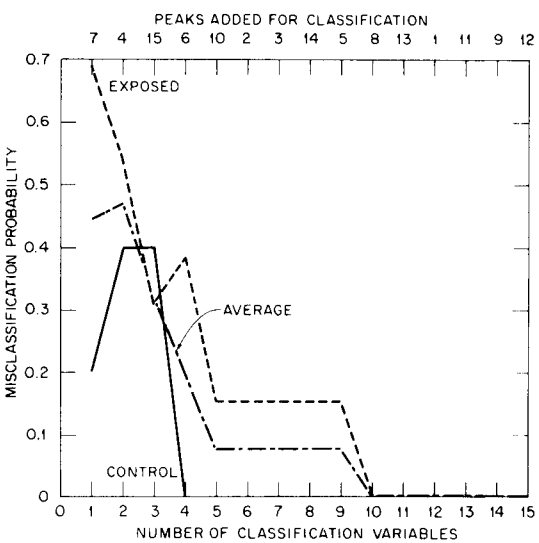

Fig. 3. Plot of misclassification probability versus classification variables for determining discriminant functions.

The decision rule for an unknown vector, Y, of the first 5 principal components is to classify the observation as coming from a control sample if $D(Y)$ is greater than zero, and as coming from an exposed sample if $D(Y)$ is less than zero.

Manual comparisons of the mean values and standard deviations for the 5 transformed peak areas did not show any clearly elevated or reduced levels for one exposure group relative to the other. Because principal component analysis takes into account the contributions from all five peaks for classification, it is the combined relationship of the peaks that is important. The significance of the five peaks selected by principal component analysis is presently unknown.

CONCLUSION

The quantitative variations found in the volatile constituents of urines obtained from this well defined animal smoke-exposure study were very high despite the large number of variables which were controlled. Genetic, dietetic, and environmental factors were minimized and the urine samples were the best obtainable under routine exposure conditions. Although several investigators have reported high levels of variation in studies involving the volatile fraction in urines, the variation has been generally attributed to subject-to-subject differences [3]. These studies have involved human subjects, and genetic differences could not be ruled out as a source of the variation. Volatile profiling studies using other animal species where such differences can be limited have not been previously reported. Our data indicate that large quantitative deviations will be encountered for this class of compounds regardless of the number of factors controlled. The variation will in turn affect data interpretation and will require pattern recognition techniques for data evaluation. Although the variation prevents obvious recognition of differences between sample groups, it was found here that a logarithmic transformation of the data reduces the variation so that differences can be extracted with computational techniques. This type of preprocessing or transformation is preferable to normalizing the peak areas in a chromatogram, which has been the practice of some investigators [13], because the latter would introduce an artificial correlation among the normalized peak areas.

The combined use of principal component and discriminant analysis was both effective and efficient. It resulted in a classification scheme which led to a 92% correct categorization of the data when only five peaks were used. In view of the complexity and variability of the original chromatograms, a successful classification model based upon such a limited number of data points is encouraging. It suggests that the chemical differences in the volatile fraction may be related to smoke exposure, either as constituents or metabolites of smoke, or as biochemical changes which the exposure produces. Additional data may be used in future studies to test the classification model

further. The combined data analysis method also decreases the amount of computer time needed for feature extraction to reduce the dimensionality of the data relative to other pattern recognition techniques. Finally, although 15 peaks were arbitrarily selected for testing, the number can be easily increased to include a larger number of compounds or compounds with a known significance.

The authors thank Dr. M. V. Buchanan for providing mass spectral data. This research was sponsored by the National Cancer Institute under Interagency Agreement DOE No. 40-485-74, NIH(NCI) No. Y01 CP 60206 under Union Carbide Corporation Contract W-7405-eng-26 with the U.S. Department of Energy.

REFERENCES

1 E. Jellum, O. Stokke and L. Eldjarn, Clin. Chem., 18 (1972) 800.
2 E. Jellum, J. Chromatogr. Biomed. Appl., 143 (1977) 427.
3 A. Zlatkis, R. S. Brazell and C. F. Poole, Clin. Chem., 27 (1981) 789.
4 E. Jellum, P. Strseth, J. Alexander, P. Helland, P. Stokke and E. Teig, J. Chromatogr., 126 (1976) 487.
5 A. Zlatkis, C. F. Poole, R. Brazell, K. Y. Lee, F. Hsu and S. Singhawangcha, Analyst, 106 (1981) 352.
6 S. P. Assenza and P. R. Brown, Anal. Chim. Acta, 123 (1981) 33.
7 R. A. Jenkins and T. M. Gayle, Proc. 19th Annual Hanford Life Sci. Symp., Richland, WA, 1979, p. 68.
8 W. B. Wartman, E. C. Cogbill and E. S. Harlow, J. Assoc. Off. Anal. Chem., 31 (1959) 1705.
9 N. W. Tietz (Ed.), Fundamentals of Clinical Chemistry, W. B. Saunders Co., Philadelphia, PA, 1970, p. 722.
10 J. T. Helwig and K. A. Council (Eds.), SAS User's Guide, SAS Institute Inc., Raleigh, NC, 1979.
11 D. F. Morrison, Multivariate Statistical Methods, Hafner Press, New York, 1967.
12 P. A. Lachenbruch, Discriminant Analysis, McGraw-Hill, New York, 1975.
13 A. Zlatkis, K. Y. Lee, C. F. Poole and G. Holzer, J. Chromatogr., 163 (1979) 125.

Analytica Chimica Acta, 139 (1982) 257—266
Elsevier Scientific Publishing Company, Amsterdam — Printed in The Netherlands

DETERMINATION OF SELECTED ORGANICS IN TREATED SLUDGES AND ASSOCIATED LEACHATES FROM COAL CONVERSION FACILITIES

M. P. MASKARINEC*, R. S. BRAZELL and R. W. HARVEY

Analytical Chemistry Division, Oak Ridge National Laboratory, P.O. Box X, Oak Ridge, TN 37830 (U.S.A.)

D. K. BROWN

Environmental Science Division, Oak Ridge National Laboratory, P.O. Box X, Oak Ridge, TN 37830 (U.S.A.)

(Received 8th January 1982)

SUMMARY

Methods have been developed for the determination of organic compounds in solid wastes and sludges. The methods involve sequential extraction with acid, base, and organic solvent, as well as dynamic headspace stripping of the volatile components. Methods for assessing the mobility of organic compounds in the environment have been evaluated, including four batch extractions and an upward-flow column extraction. Batch extractions in closed vessels are most effective for the determination of volatile components. The upward-flow column arrangement is shown to be the most aggressive leaching procedure for semi-volatile organic compounds.

Because of the relatively large volume of solid waste which will be generated by future coal conversion facilities, adequate assessment of environmental consequences will be necessary before disposal options are considered. Under current regulations, many solid wastes associated with coal conversion may be declared hazardous because of the similarity to oil refinery wastes. Because disposal options for hazardous wastes are much more restrictive than those for non-hazardous wastes, the economy of a particular conversion technology will certainly be affected by the classification of the associated solid wastes. The classification of a solid waste with respect to degree of hazard, involves qualitative and quantitative analysis for potentially toxic materials in the waste and, subsequently, assessment of the mobility of these materials in the environment. The objectives of this work were the development of analytical methods for organic compounds in coal conversion solid wastes, and the development of procedures for assessing the mobility of these compounds in the environment.

Steps in the determination of organic compounds in solid wastes and sludges (once an appropriate sample is obtained) may be divided into two categories: (a) extracting the organics from the sample, and (b) quantifying the individual

components in the extract. The method of extraction is crucial to the reliability of the analytical data. Methods such as Soxhlet extraction [1], ultrasonic extraction [2], steam distillation [3], and three-phase extraction systems [4—6] have been used for the separation of target compounds in solid wastes: all have limitations in terms of recovery and/or discrimination of certain classes of compounds and none provide quantitative recovery of volatile components. Further separation and determination of the individual components of the extracts can be made by any of several well-established techniques such as open-tubular gas chromatography, gas chromatography/mass spectrometry, and high-performance liquid chromatography, although the complexity of most samples requires high separation power. Assessing the mobility of organic components of solid wastes requires (a) quantification of low-boiling constituents which might be volatilized into the atmosphere at the disposal site, and (b) quantitative analysis of aqueous extracts of the solid waste, which contain potential water contaminants.

EXPERIMENTAL

Materials and samples

All solvents used (including water) were distilled-in-glass. Materials used for leachate generation were as follows: Ultrex acetic acid (J. T. Baker, Phillipsburg, NJ), ACS reagent-grade citric acid, and analytical-grade Chelex-100 ion-exchange resin in the Na^+ form (Bio-Rad Laboratories, Richmond, CA). The XAD-2 resin was obtained in pre-filled, pre-cleaned cartridges of 4-ml volume (Isolab, Akron, OH) and in bulk form (Polysciences, Warrington, PA) which was Soxhlet-extracted with methanol and acetone prior to use. All standards used were of 97% purity or better.

All samples were collected from operating, wastewater treatment plants. The samples consisted of various solid wastes from direct liquefaction of coal: (A) a final wastewater treatment plant sludge, (B) a filtered biological treatment plant sludge, and (C) centrifuged heavy oil residuals. All samples were stored in sealed glass bottles at 4°C. Where possible, aqueous discharges into and out of the solid waste collection point were also sampled.

Procedures

Aqueous extraction. Five extraction techniques were applied to the three solid wastes using the conditions listed in Table 1. The apparatus used for the pH 5 extraction (EP), the water extraction and the Na-resin displacement extraction was a 4.0-l glass vessel, fabricated at Oak Ridge National Laboratory and described elsewhere [7]. The citrate buffer extraction was done in a rotary tumbler (Associated Design & Manufacturing, Alexandria, VA). For column extractions, a 2.5-cm i.d. glass column with adjustable end plungers was used with a constant displacement pump and a pressure-relief valve set at 60 psi (Fig. 1). In this case, the weighed sludge mixed with acid-washed sand (1 + 1) was added to the column, with a bed of sand

TABLE 1

Extraction procedures: identification of variable and constant leaching factors[a]

Extraction	Variable factors			
	Initial leaching medium	Mode of extraction	pH adjustment	Treatment of leachate solutions for extract analysis
1. EP	Distilled—deionized water	Batch: magnetically stirred, open vessel	Adjust to pH 5 with 0.5 M acetic acid; maximum limit of 2 meq g^{-1} sample	Pressure-filtered[b]
2. Water	Distilled—deionized water	Batch: magnetically stirred, open vessel	None	Pressure-filtered[b]
3. Na-resin displacement	Distilled—deionized water with 1 g calculated dry wt. Chelex-100/10 g sample	Batch: magnetically stirred, open vessel	Adjust to pH 7 with 0.1 M HCl	Pressure-filtered[b]
4. Citrate buffer	0.5 M citrate buffer	Batch: rotary extractor, closed vessel	None	Pressure-filtered[b]
5. Column	Distilled—deionized water	Column: upward flow	None	Leachate directly onto XAD-2 resin

[a]Constant factors were as follows: <9.5 mm sample particle size; extraction at room temperature; batch extraction for 24 h; column extraction until effective solid:solution ratio was reached; only one leaching on same sample; 1:20 effective solid:solution ratio.
[b]Through 0.4-μm Nuclepore filter.

below and above the sludge. The column effluent was isolated directly on XAD-2 resin.

Direct analysis of solids. Solids were Soxhlet-extracted with methylene chloride for 24 h. Alternatively, the wastes were sequentially extracted using the procedure shown in Fig. 2. Extraction with acid, base, and organic solvent produced three fractions.

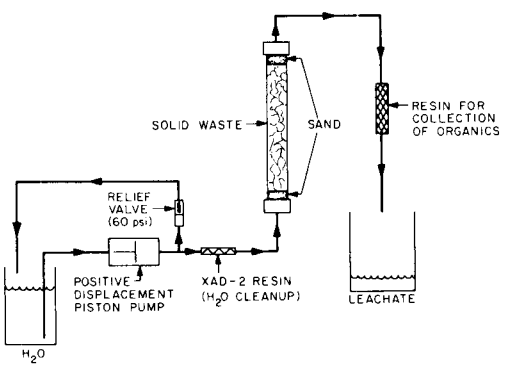

Fig. 1. Apparatus for upward-flow column extraction.

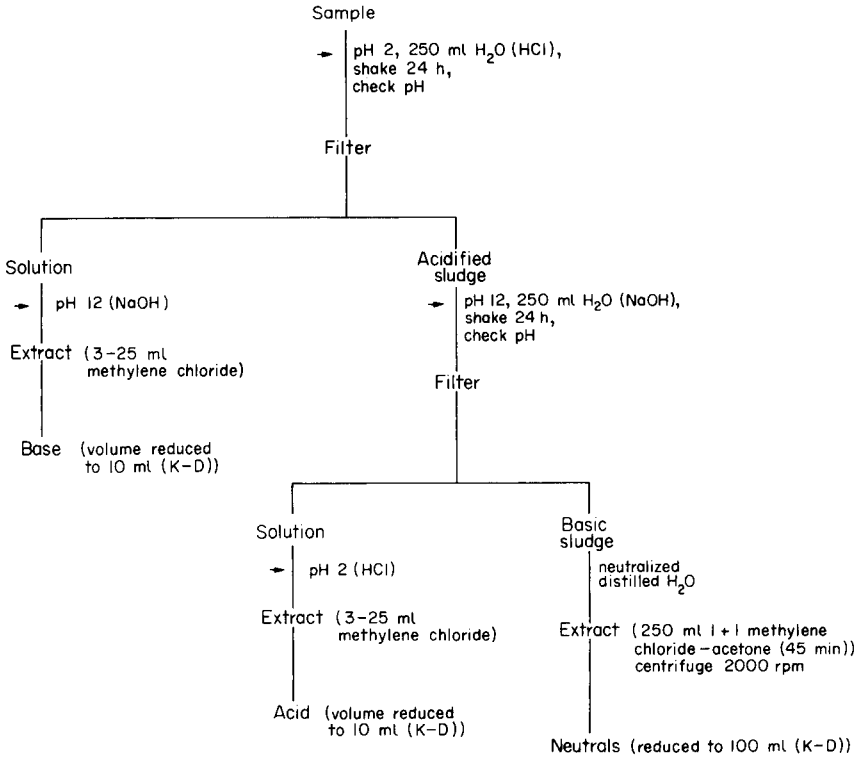

Fig. 2. Procedure for analysis of solid wastes and sludges. Filtrations were done through 0.45-μm Millipore filters.

Volatiles in the solid wastes were determined by using a dynamic headspace technique [8]. The solid wastes (15—30 mg) were placed in a closed vessel and purged at 50° C with helium. The volatile organics were collected on a Tenax cartridge, and desorbed thermally at 250° C.

Aqueous extract analysis. The aqueous extracts of the solid wastes were stored at 4° C. Separate aliquots of 40-ml were taken for the determination of volatile organics. These aliquots were collected in glass bottles with no headspace and analyzed as soon as possible after collection. Volatile organics were determined by standard purge and trap techniques [9]. The organics were isolated from the aqueous extracts by adjusting the pH of the extract to 6.8 with phosphate buffer and the conductivity to 20 mS with sodium chloride. Aliquots (500 ml) of the adjusted extract were passed through a column containing 4 ml of XAD-2 resin. Adsorbed organics were eluted with 15 ml of acetone. The acetone eluate was dried with sodium sulfate and evaporated to less than 1 ml under nitrogen to minimize evaporative losses. The residue was adjusted to 1 ml with methylene chloride. The XAD-2 resin cartridge from the column was treated in an identical manner. All gas chromatography was done on a Hewlett-Packard Model 5736 instrument equipped

with a 30-m fused silica open tubular column coated with SE-52 silicone gum and a Hewlett-Packard 3390 recording integrator. Gas chromatography/mass spectrometry was conducted on a Hewlett-Packard 5985 g.c./m.s./d.s. using electron impact ionization (20 eV) and direct introduction of the capillary column effluent.

RESULTS AND DISCUSSION

Direct analysis of solid wastes

One of the major objects of this work was to develop methods for the determination of organic compounds in solid wastes and sludges, to demonstrate the applicability of these methods to coal conversion solid wastes, and to quantify the leachability of organic compounds from the wastes using a variety of aqueous extraction techniques. The sequential extraction procedure shown in Fig. 2 was compared with the Soxhlet extraction in terms of the amount of material recovered. Aliquots of the Soxhlet extract and each of the sequential fractions were applied to a pre-weighed filter pad. The solvent was evaporated and the pads weighed. Thus, a crude measure of mass was obtained. The results are shown in Table 2. In each case, the mass of material by the sequential extraction procedure was greater than that extracted by the Soxhlet procedure. In fact, the mass of the neutral fraction alone exceeded the mass of the Soxhlet extract. The various fractions were also chromatographically compared. (Fig. 3 shows the comparison for the solid waste from sample C.) Compounds in the fractions were identified by g.c./m.s., and are listed in decreasing order of concentration.

Sample A. Biphenyl, C_5-phenol, C_1-tetrahydronaphthalene, C_1-naphthalene, tetrahydronaphthalene and C_1-naphthalene. Minor components were C_3-hydroxybiphenyl, C_2-biphenyl, isopropylcyclohexane, C_3-benzenes (3), indane, naphthalene, hydroxyanthracene, acenaphthene, C_2-biphenyl, dibenzofuran, fluorene, C_2-biphenyl, phenanthrene, hydroxyfluorene, C_1-phenanthrene (2) and methoxyphenanthrene.

Sample B. Methylfluoranthrene, methylbiphenyl, trimethylnaphthalene, biphenyl, and various aliphatic hydrocarbons.

TABLE 2

Comparison of Soxhlet extraction with sequential equilibration scheme: gravimetric data on solid waste extracts

Sample	Concentration (mg g^{-1})			
	Sequential extraction			Soxhlet extraction
A	2.7	0.24	368	151
B	0.25	0.4	16	4.1
C	0.48	0.31	344	25.8

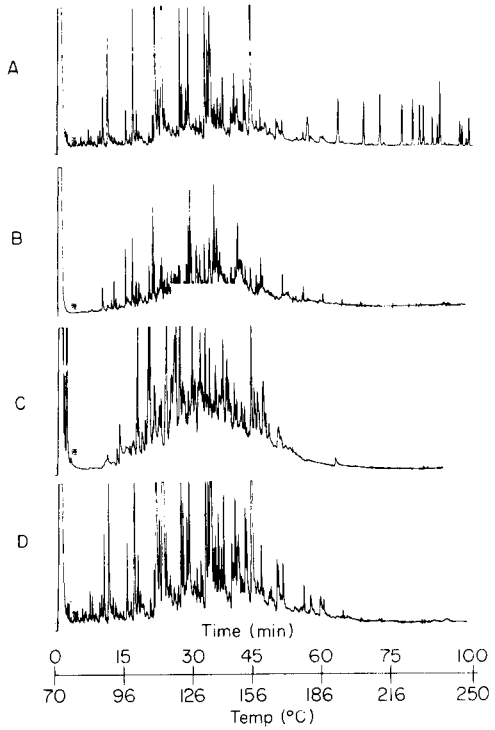

Fig. 3. Chromatograms of extracts from sample C: (A) Soxhlet extract; (B) acid fraction; (C) base fraction; (D) neutral fraction.

Sample C. Biphenyl ether, biphenyl, phenanthrene, tetrahydronaphthalene, cresol, C_3-phenol, xylenols (3), phenylphenol, tolylphenols (5), C_5-phenol, bipyridine, acridine and benzoquinolines (6), dibenzofuran, acenaphthene, fluorene, dibenzothiophene, phenanthrene, fluoranthene, and pyrene.

The sequential extraction method has several advantages over Soxhlet extraction beyond enhanced recovery: the scheme provides some measure of fractionation, which is important in dealing with complex mixtures; the recovery of organics by this technique is much less dependent on the physical state (e.g., water content) of the matrix; and the method provides for the removal of basic compounds from the sludge first, thus reducing the possibility of hydrolytic losses of this important class of compounds.

The procedure described above allows the determination in solid wastes of most of the organic compounds suitable for chromatography. However, one exception is the class of compounds with very low boiling points: these volatile compounds are lost during solvent volume reduction in any of the commonly used isolation techniques. Yet, these compounds are of interest in an environmental evaluation because they may be released into the atmosphere after disposal. Thus, a technique was developed [8] which allows the stripping of volatiles from the solid wastes, and subsequent chro-

matographic separation. The solid waste sample is placed into a purging device and sparged with an inert gas. The volatiles are collected on an adsorbent cartridge (Tenax). The resultant chromatograms for sample B are shown in Fig. 4. The system blank is quite clean, and the sample shown here contains such volatile compounds as benzene, toluene, and other alkylbenzenes, as well as phenol and the cresols. An important point is that all of the wastes studied here contained significant levels of these compounds. Thus, disposal of these wastes must be done with attention to the release of volatile compounds. Reproducibility was about 3% for individual compounds. When combined with the sequential extraction scheme, the technique allows relatively comprehensive characterization of the organic content of solid wastes.

Analysis of aqueous extracts

A second major object of this work was to define the mobility of the organic compounds out of the solid waste and into the aqueous environment. This is usually done by using aqueous extraction tests. Several such techniques were evaluated. The factors involved in laboratory extractions included the leaching medium itself, the vessel used, the method of agitation, and the method of separation of the aqueous extract from the leached solid. All have an effect on contaminants found in the resulting extracts. Variable and constant extraction factors used in this study are defined in Table 1. Both the pH 5 and citrate buffer extractions are intended to simulate the disposal of solid wastes co-disposed with municipal wastes. The other extractants are intended to reflect disposal conditions dominated by the inherent chemical and physical characteristics of the waste itself.

Current regulations for identifying toxic hazardous wastes under RCRA (40 CFR 261.24) utilize analyses of pH 5 extracts for elements listed in the

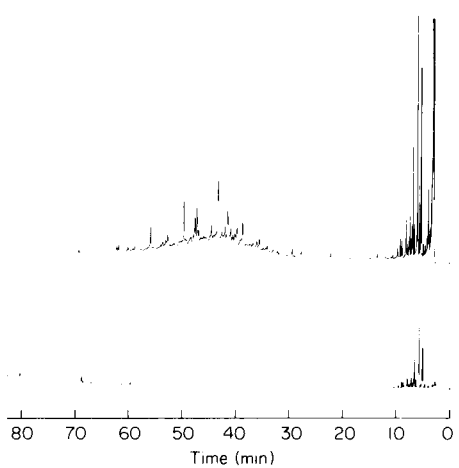

Fig. 4. Chromatograms of volatile organics from sample B (upper chromatogram) and from a blank (lower chromatogram).

National Interim Primary Drinking Water Regulations. Other than two herbicides and four pesticides, no organic compounds are listed to define a toxic hazardous waste.

Because the pH 5 extraction (EP) is the extraction method specified by current regulations, it was used for baseline comparison with the other extraction methods in terms of organic content. Table 3 contains the results for percent total elutable organics found in the water, Na-resin, citrate buffer, and column extracts, relative to that found in the pH 5 extracts. In the case of sample B, the water extract was used. In all cases, more organics were found when the column leaching technique was used. The Na-resin displacement extraction produced the lowest amount of organic material, except for the pH 5 extract from sample B (where no peaks were found). A comparison between the batch and column techniques, with distilled–deionized water as the extractant, indicated that the column method yielded higher amounts of total organics. The precision (3 replicates) was 10% for the batch extraction and 13% for the column extraction. Figure 5 compares the chromatograms of the four batch extracts from sample C. The qualitative similarity is remarkable, in terms of the type of compounds extracted.

The extracts were also compared with respect to the quantity of individual organic compounds extracted, and the results are also shown in Table 3. In general, the results parallelled the results of the total organics suitable for chromatography. Again, in every case, the upward-flow column was more

TABLE 3

Organics found in water, Na-resin displacement, citrate buffer, and column extracts, versus that found in EP extracts[a]

Sample	Compound	% vs. EP				
		H_2O	Na-resin	Citrate buffer	Column	Estimated total in EP ($\mu g\ l^{-1}$)
A	Total	151	62	90	230	754
	C_3-Pyridine[b]	467	312	394	1310	80
	Naphthalene	320	143	156	1493	130
	Quinoline	564	129	230	673	65
	1-Methylnaphthalene	197	116	151	673	55
B	Total	100	42	44	468	37
C	Total	49	40	69	891	2740
	Cresol	33	68	134	1450	600
	Xylenol	10	13	51	965	120
	Quinoline	52	106	74	433	190
	C_3-Phenol[b]	71	68	68	865	220
	Naphthol	70	51	58	880	25
	Biphenyl	347	275	85	1655	50

[a]Except for sample B, EP is taken as 100%. For sample B, the EP (pH 5) extract showed no peaks. [b]C_3 = trimethyl, methylethyl or propyl.

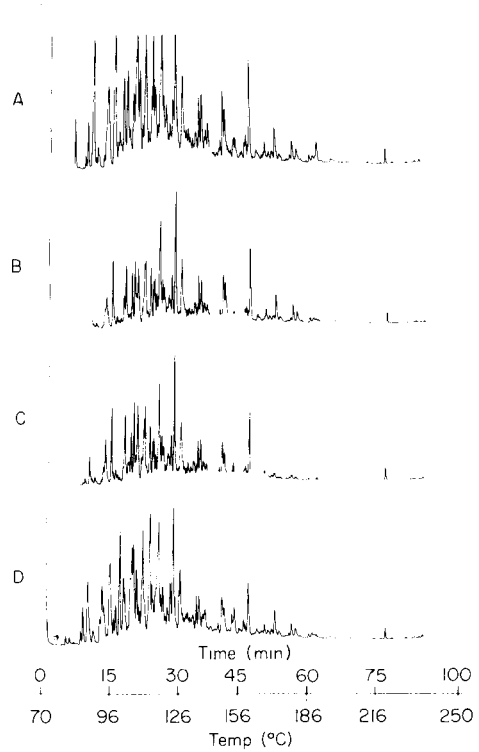

Fig. 5. Chromatograms of organics extracted from leachates of sample C: (A) EP; (B) H_2O; (C) Na-resin displacement; (D) citrate buffer.

effective in extracting organics than any of the batch extracts. It must be noted that the compounds listed in Table 3 are the major components of the extracts. They are not the only compounds present. However, it is apparent that the major concern in terms of mobility of organics from coal conversion solid wastes will be phenolic compounds, because of the relatively large amounts present as well as their toxicity. Blanks were extracted on all systems. No artifacts were produced by any of the procedures except the citrate buffer, which contained phthalates at levels of ca. 50 $\mu g\ l^{-1}$. Volatile organic compounds were also determined in the batch aqueous extracts. In every case, the level of volatile organic matter was more closely tied to the extraction vessel used than to the extractant. The citrate buffer extract contained 3—5 times higher levels of volatile components, compared to the other batch extraction procedures. This is probably due to the closed nature of the extraction vessel, as well as the tendency of the citrate buffer to disperse solid material. Distilled water extracts in the closed system were also 3—4 times higher in volatile content than the distilled water extracts in the open magnetically stirred system. Thus, the rotary tumbler is the preferred vessel for the extraction of volatile organic materials, regardless of the extractant.

Research sponsored by the U.S. Environmental Protection Agency, DOE No. 40-1087-80, EPA No. AD-84-F-1-058, under Union Carbide Corp. Contract W-7405-ENG-26 with the U.S. Department of Energy, Environmental Sciences Division, Publication No. 1952.

REFERENCES

1 Test Methods for Evaluating Solid Waste, USEPA SW-846, 1980, Method 8.86.
2 Test Methods for Evaluating Solid Waste, USEPA SW-846, 1980, Method 8.85.
3 G. D. Veith and L. M. Kiwus, Bull. Environ. Contam. Toxicol., 18 (1977) 631.
4 Development of Analytical Test Procedure for the Measurement of Organic Priority Pollutants in Sludge and Sediments, Midwest Res. Inst. Final Rep. EPA Contract No. 68-03-2695, June 26, 1979.
5 Development of Analytical Protocols for Organic Priority Pollutants in Municipal Sludges, Battelle—Columbus Laboratories, Final Rep. EPA Contract No. 68-03-2624, March 30, 1979.
6 Presence of Priority Pollutants in Sewage and Their Removal on Sewage Treatment Plants, University of Washington, Ann. Rep. Grant R.806102, July 31, 1979.
7 D. K. Brown, C. W. Francis, M. P. Maskarinec and F. W. Larimer, Toxicity of Leachates, Comparison of Extraction Procedure Extracts and Landfill Leachates, ORNL/TM-7563, June, 1981.
8 R. S. Brazell and M. P. Maskarinec, High Res. Chromatogr. Chromatogr. Comm., 4 (1981) 404.
9 T. A. Bellar and J. J. Lichtenberg, J. Am. Water Works Assoc., 66 (1974) 739.

Analytica Chimica Acta, 139 (1982) 267—277
Elsevier Scientific Publishing Company, Amsterdam — Printed in The Netherlands

TUNING OF A VOIGT EFFECT OPTICAL FILTER AROUND THE SODIUM 589.0-NM LINE

C. H. CHISHOLM and R. STEPHENS*

Trace Analysis Research Centre, Dalhousie University, Halifax, N.S. B3H 4J3 (Canada)

(Received 6th August 1981)

SUMMARY

The methods of the Jones calculus are used to show that the output of a Voigt effect optical system can be frequency-tuned. Rotation of a retardation plate inserted in the optical train provides the tuning mechanism. Transmission profiles are calculated for various magnetic field strengths, retarder displacements and atom densities in the magneto-optic cell. The tuning effect is demonstrated experimentally by using the filter as a light source and observing changes in sensitivity of flame atomic absorption spectrometry as the filter output frequency is altered. The data are used to demonstrate the feasibility of measuring atomic line profiles by this means.

Magneto-optic rotation (m.o.r.) in an atomic vapour enables optical transmission to be observed in the neighbourhood of the atomic resonance frequencies. The effect can be utilized to produce high-resolution optical filters [1]. At low transverse magnetic field strengths, the transmission profile of such a filter has the qualitative form of a normal Zeeman triplet, even when the associated atomic line shows anomalous Zeeman splitting. Under suitable conditions, coherence narrowing causes the greater portion of the transmission profile to be located within the central line of the triplet, and to show a half-width below that of the parent zero field absorption line. These filters are potentially useful in analytical atomic spectroscopy because they combine high resolving power with a large optical aperture. These characteristics are of interest in both emission and absorption measurements because of the high signal-to-noise ratio and increased freedom from spectral interferences which can be obtained. The optical simplicity of the filter also offers the multichannel capability needed for simultaneous multi-element determination.

It is possible that an ability to tune a m.o.r. filter would improve its usefulness. This possibility does not appear to have been explored yet. For example, a m.o.r. filter can act as the tuning element of a dye laser. If the filter were tunable, then a corresponding control of the laser output frequency would become available. Other possible spectroscopic applications include the high-resolution measurement of absorption line profiles. An analogous technique has been demonstrated by using absorption

measurements of the σ_+ and σ_- components of the longitudinal Zeeman effect [2, 3]. However, the simplicity of the latter approach can be offset by the difficulty of deconvolution when the source multiplet shows a complex hyperfine structure [4]. The profile of the m.o.r. filter appears to be less complicated than that of the associated Zeeman multiplet, and therefore the necessary deconvolution may prove to be less sensitive to an exact knowledge of the hyperfine splitting pattern (particularly if measurements are carried out at fixed magnetic field strength). Of specific analytical interest, tuning of a m.o.r. filter would enable emission or absorption signals to be maximized, by ensuring that the transmission maximum of the optical system coincided with the peak of the emission or absorption line to be observed. This could improve sensitivity, and, perhaps more importantly, permit correction for spectral interferences to be made. Corrections of this nature can be carried out by taking measurements of more than one frequency around the line centre [5—7]; they are applicable to both emission and absorption signals and, under suitable circumstances [8], they can be used even when the interference is caused by sharp line overlap.

The recognition of possibilities such as those outlined above was felt to warrant an examination both of the feasibility of tuning a m.o.r. filter and of the type of behaviour which might be expected from such a device. The results of this study are given below.

THEORY

For technical convenience, the filter used here comprised an evacuated, electrically heated, sodium vapour cell contained in a transverse magnetic field. The cell and its associated optical system are shown in Fig. 1. It will be shown that the tuning element of this system is the retardation plate, X. This device comprises any birefringent medium, i.e., one which possesses different refractive indices along its x and y axes, and which therefore introduces a phase difference between the x and y vibrations of an electromagnetic wave travelling through the device in the z direction. Tuning is accomplished by rotation of this element by some angle, θ.

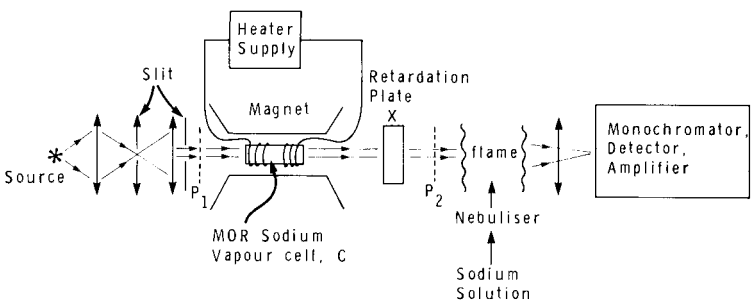

Fig. 1. The m.o.r. cell and associated optical system; P_1 and P_2 are the polarizers.

The following variables are defined. The x axis of the optical system is defined by the transmission axis of polariser, P_1; a is the peak absorbance in the m.o.r. cell at zero magnetic field strength (used as a measure of atom density in Fig. 3 below); n_x and n_y are the refractive indices of the retardation plate along its x and y axes; $\tilde{n}_x$ and $\tilde{n}_y$ are the complex refractive indices of the atomic vapour along its x and y axes ($\tilde{n}_x$ and $\tilde{n}_y$ being distinguished by the external magnetic field and $\tilde{n} = n' + in''$; $i = \sqrt{-1}$); p is the angle between the transmission axis of P_2 and the y axis of the optical system; θ is the angle between the n_x axis of the retardation plate and the transmission axis of P_1; and ϕ is the angle between the $\tilde{n}_x$ axis of the atomic vapour and the transmission axis of P_1.

The centre of the zero magnetic field atomic absorption line, ν_0, will be used as reference frequency.

The optical behaviour of the system shown in Fig. 1 is conveniently described by using the Jones matrix formalism [9]. The Jones matrix [J] of the system is given by

$$[\mathbf{J}] = [\mathbf{P}_2][\mathbf{R}(p)][\mathbf{R}^{-1}(\theta)][\mathbf{X}][\mathbf{R}(\theta)][\mathbf{R}(\phi)]^{-1}[\mathbf{C}][\mathbf{R}(\phi)][\mathbf{P}_1] \tag{1}$$

and the intensity, I_T, transmitted through the output polarizer P_2 is given by $I_T = \frac{1}{2}I_0[\mathbf{J}][\mathbf{J}^\dagger]$, where I_0 is the source intensity at a single specified frequency and [J†] is the transpose of the complex conjugate of [J]. In Eqn. (1), $[\mathbf{P}_1]$, $[\mathbf{P}_2]$, [X], and [C] are respectively the Jones matrices of the polarizers P_1 and P_2, of the retardation plate X, and of the atom cell, C, in Fig. 1, and $[\mathbf{R}(p)]$, $[\mathbf{R}(\theta)]$ and $[\mathbf{R}(\phi)]$ are rotation matrices which serve to align the x and y vectors of the incident wave with the x, y axes of, respectively, P_2, X, and C. The matrices are expressed as

$$[\mathbf{P}_1] = \begin{pmatrix} 1 & 0 \\ 0 & 0 \end{pmatrix} \qquad [\mathbf{P}_2] = \begin{pmatrix} 0 & 0 \\ 0 & 1 \end{pmatrix}$$

$$[\mathbf{X}] = \begin{pmatrix} \exp i\tilde{n}_x & 0 \\ 0 & \exp i\tilde{n}_y \end{pmatrix} \qquad [\mathbf{C}] = \begin{pmatrix} \exp i\tilde{n}_x & 0 \\ 0 & \exp i\tilde{n}_y \end{pmatrix} \tag{2}$$

$$[\mathbf{R}(\theta)] = \begin{pmatrix} \cos\theta & \sin\theta \\ -\sin\theta & \cos\theta \end{pmatrix} \qquad [\mathbf{R}^{-1}(\theta)] = \begin{pmatrix} \cos\theta & -\sin\theta \\ \sin\theta & \cos\theta \end{pmatrix}$$

with similar expressions for $[\mathbf{R}(p)]$ and $[\mathbf{R}(\phi)]$, $[\mathbf{R}^{-1}(\phi)]$. Further details on the origin and behaviour of the above notation are available [10].

Substitution of Eqn. (2) into Eqn. (1), and assuming an optimum value of $\phi = 45°$ C leads to the result

$$[\mathbf{J}] = \begin{pmatrix} 0 & 0 \\ j & 0 \end{pmatrix}$$

where

$$j = \left[\exp \frac{i}{2}(\tilde{n}_x + \tilde{n}_y + n_x + n_y)\right] \{[i \sin(2\theta - p) \sin \tfrac{1}{2}\Delta n - \sin p \cos \tfrac{1}{2}\Delta n] \times [\cosh \tfrac{1}{2}\Delta n'' \cos \tfrac{1}{2}\Delta n' - i \sinh \tfrac{1}{2}\Delta n'' \sin \tfrac{1}{2}\Delta n'] - [i \cos(2\theta - p) \sin \tfrac{1}{2}\Delta n - \cos p \cos \tfrac{1}{2}\Delta n] \times [-\sinh \tfrac{1}{2}\Delta n'' \cos \tfrac{1}{2}\Delta n' + i \cosh \tfrac{1}{2}\Delta n'' \sin \tfrac{1}{2}\Delta n']\} \quad (3)$$

and Δn, $\Delta n'$ and $\Delta n''$ represent $n_x - n_y$, $n'_x - n'_y$, and $n''_x - n''_y$ respectively. Substitution of Eqn. (3) into Eqn. (1) leads to

$$[J][J^\dagger] = jj^* \text{ and } I_T = \tfrac{1}{2} I_0 jj^* \quad (4)$$

Existence of frequency tuning

Tuning effects will be considered, in particular, on the central (π) transmission maximum of the system. One reason for this is that the central maximum covers the zero field atomic line frequency whereas the outer satellites do not. In addition, it transpires that tuning of the central line is best accomplished at positive values of θ, because this causes the intensity of the central line to be enhanced at the expense of its satellites. Thus, as the transmission profile is shifted, it becomes increasingly dominated by the central line; the outer satellites cease to be available (see below). Because of this process, reversal of the tuning effect is best accomplished by rotating the retardation plate by 90° and retaining a positive displacement of θ.

Equations (1) to (4) describe the transmission profile of the optical system in Fig. 1. That this profile is subject to frequency tuning can be demonstrated by setting $p = 0$ in Eqn. (3) and substituting the result into Eqn. (4). After manipulation, this gives

$$4I_T/I_0 = [\exp -(n''_x + n''_y)][\cosh \Delta n'' + \sin 4\theta \sin^2 \tfrac{1}{2}\Delta n \sinh \Delta n'' - \cos \Delta n' (\cos 4\theta \sin^2 \tfrac{1}{2}\Delta n + \cos^2 \tfrac{1}{2}\Delta n) + \sin 2\theta \sin \Delta n \sin \Delta n'] \quad (5)$$

The last term, $\sin 2\theta \sin \Delta n \sin \Delta n'$, is asymmetric about zero in θ and $\Delta n'$. Thus for positive θ this term will enhance transmission at frequencies for which $\Delta n'$ is positive, and vice versa. Because $n' - 1$ and $\Delta n'$ are both asymmetric about ν_0 [11], this leads to a corresponding displacement of the central transmission maximum of the optical system, i.e., the system can be tuned simply by rotating the retardation plate.

It can be noted that rotation of one of the polarizers does not achieve an analogous effect. Thus putting $\theta = 0$ in Eqn. (3) and substituting the result into Eqn. (4) gives $4I_T/I_0 = [\exp -(n''_x + n''_y)][\cosh \Delta n'' - \cos \Delta n' \cos 2p + \sinh \Delta n'' \sin 2p]$. This expression contains only symmetric terms in $\Delta n'$ and $\Delta n''$ (at least when the absorption profile n'' is itself symmetrical, as in the present case), and varying p simply causes two transmission maxima to separate symmetrically and simultaneously on the high and low frequency sides of ν_0.

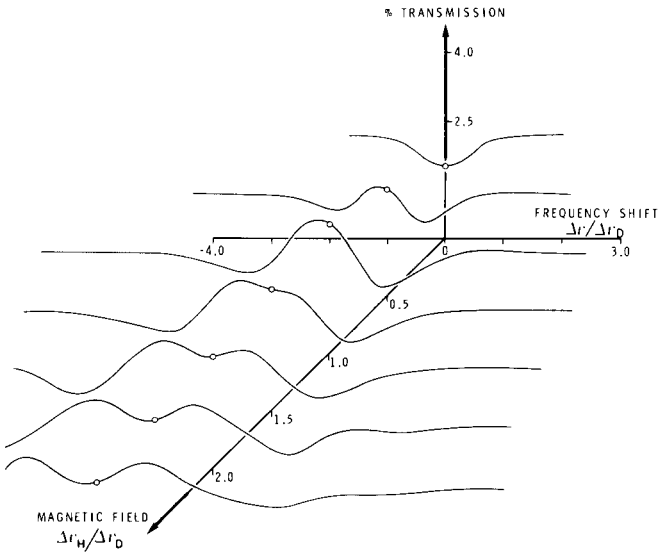

Fig. 2. Transmission profiles at various magnetic field strengths calculated from Eqn. (5). Open circles mark ν_0. The frequency shift from ν_0, $\Delta\nu$, is expressed relative to the Doppler half-width, $\Delta\nu_D$, of the atomic line of the species in the m.o.r. cell. The magnetic field is expressed as the frequency displacement of the normal Zeeman effect, $\Delta\nu_H$, which that field would cause, again in units of $\Delta\nu_D$. Values of θ and a were fixed at 0.15 and 2.0, respectively.

Effect of magnetic field strength, atom density and θ on the central transmission line

The individual influences of the above variables on the filter transmission profile, calculated from Eqn. (5), are shown in Figs. 2—4. Asymmetry caused by the tuning effect of θ is evident in each figure. The splitting which develops with increasing field strength (Fig. 2) is due to separation of the two π components of the $^2p_{3/2}$—$^2s_{1/2}$ transition. The effect is of practical interest because it permits the tuning range obtained by varying θ to be shifted if required by altering the magnetic field. Changing the atom density (Fig. 3) appears to have little effect other than altering the intensities of the π and σ envelopes. Figure 4 shows the enhancement of the π envelope (i.e. the middle portion of the transmission profile centred approximately at $\Delta\nu/\Delta\nu_D = 0$) at the expense of the σ satellites at positive values of θ, already mentioned, and the reverse process at negative θ.

EXPERIMENTAL

A block diagram of the apparatus is shown in Fig. 1. Apart from the addition of the retardation plate, the apparatus is identical to that described previously [1], and details will not be repeated. The retardation plate was a stress birefringent device comprising a block of pyrex glass of 3-cm path,

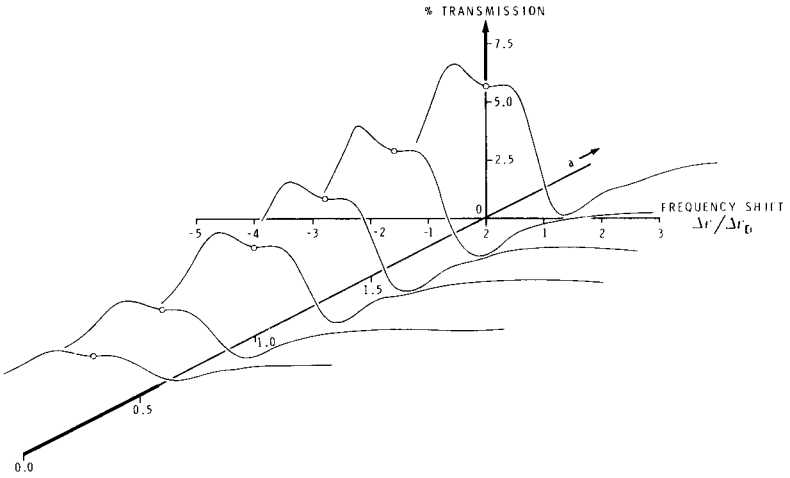

Fig. 3. Transmission profiles at various atom densities calculated from Eqn. (5). Magnetic field strength and θ were fixed at $\Delta\nu_H/\Delta\nu_D = 1.6$ (i.e., the same units as in Fig. 2) and 0.15, respectively.

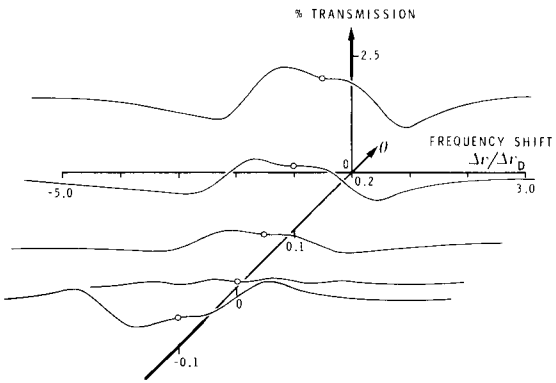

Fig. 4. Transmission profiles at various θ calculated from Eqn. (5). Magnetic field strength and a were fixed at $\Delta\nu_H/\Delta\nu_D = 1.6$ and 2.0, respectively.

held in a clamp to maintain a steady, uniform stress. The magnitude of the stress controls Δn.

In operation, the monochromator (Fig. 1) was set to pass the 589.0-nm line, and the stress on the retarder was set to give $\Delta n = \pi/2$. Then, in a series of experiments, sodium solutions were aspirated into the air—acetylene flame (Fig. 1), and the resulting flame atomic absorption signals were measured as θ was varied from zero. Experiments were repeated over a range of field strengths, sodium concentrations introduced into the flame, and sodium atom density in the m.o.r. cell. Two light sources were used: a quartz—halogen continuum and a sodium vapour discharge lamp. The latter gave the better results, because its emission profile does not extend much beyond the range of the Zeeman absorption multiplet in the m.o.r. cell.

RESULTS

Tuning the filter by rotation of the retardation plate in the manner used above causes wide band background transmission of the source to occur in addition to the m.o.r. signal of interest. The background intensity increases as $\sin^2 \theta$; its presence is included in Eqn. (1) et seq. Because the present experimental procedure does not isolate flame atomic absorption on the m.o.r. transmission from that on the background, and because flame atomic absorption is lower on the background than on the m.o.r. signal (because of the broad emission profile of the former), than in the absence of any frequency shift of the m.o.r. transmission profile, maximum flame atomic absorption is observed exactly at the point of minimum background transmission, as seen in Fig. 5. Conversely, any shift of the absorption maximum from this point is evidence of a tuning effect, as the m.o.r. transmission is frequency-shifted towards the absorption maximum of the flame profile. This procedure is convenient because it automatically locates the origin ($\theta = 0$) with great exactness, and makes any shift of the absorption maximum correspondingly easy to detect.

Some typical results from the above experiments are shown in Fig. 5. They show the expected shift in the absorption maximum when the retarder angle, θ, but not the polarizer angle, p, is varied. The data from the other experiments done here were quite analogous, and appeared to be consistent with the type of behaviour shown in Figs. 2—4. In view of these results, it appears that the tuning process described by Eqn. (5) is quite easily observed in practice, and is probably capable of offering modest advantages for analytical purposes along the lines suggested in the introduction.

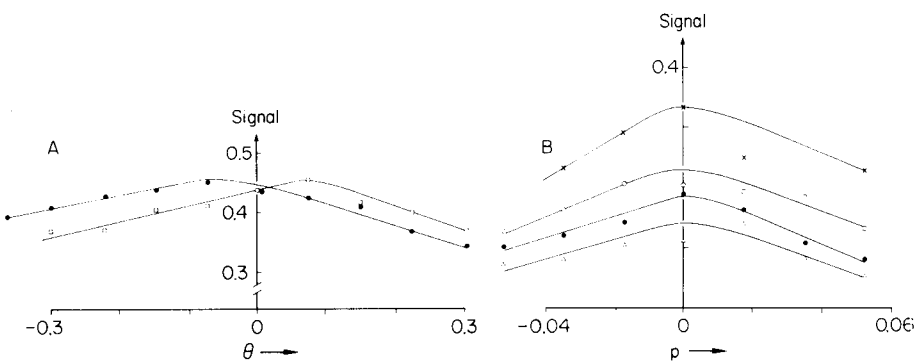

Fig. 5. (A) Dependence of experimental flame atomic absorption signals from 0.5 μg Na ml^{-1} on the retarder displacement, θ; solid and open points represent values obtained at θ and at $\theta + \pi/2$. (B) Dependence of experimental flame atomic absorption signals on polarizer displacement, p, measured at field strengths of (×) 2.4, (○) 4.2; (•) 5.8; (△) 8.2 kG, successive curves being displaced by 0.05 units on the y axis.

Frequency scanning

Apart from any direct analytical implications it may have, the data in Fig. 5 illustrate another of the potential applications mentioned in the introduction, namely, the frequency scanning of a spectral line at fixed magnetic field strength. It is clear from Fig. 5 that the magnitude of flame atomic absorption depends on θ and hence, by virtue of Eqn. (5), on the corresponding frequency shift of the filter transmission profile. Therefore, these data contain information on the frequency dependence of the flame atomic absorption signal. This information can be deconvoluted by using Eqn. (5) to obtain the approximate form of that frequency dependence (i.e., to give the corresponding flame atomic absorption line profile). The method used to carry out the deconvolution is given in the Appendix; the results are shown in Fig. 6. At the magnetic field strength used (4.6 kG), results are concentrated in the wings of the profile. They extend sufficiently to show the asymmetry of the line quite clearly, although its frequency shift is less obviously apparent.

Combined rotation of the polarizer and retarder

The increased background transmission caused by varying θ or p from zero also increases photon noise. Once this photon noise reaches a magnitude comparable to the other noise sources in the system, a marked degradation of the output signal-to-noise ratio occurs. The effect is particularly obtrusive when a continuous source is used, especially at large values of θ, to the point where it places an upper limit on the maximum frequency displacement that can be achieved. Various ways were sought to avoid this problem. In particular, it might appear that a combined, simultaneous variation of p and θ could allow the tuning effect to occur while blocking the background. Unfortunately, this proved not to be the case.

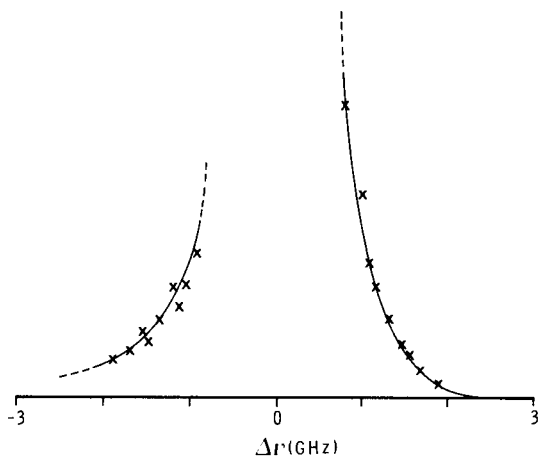

Fig. 6. Wings of the sodium flame absorption profile determined from the data in Fig. 5A.

When atom density is zero, Eqns. (3) and (4) become

$$j = i \sin(2\theta - p) \sin \tfrac{1}{2}\Delta n - \sin p \cos \tfrac{1}{2}\Delta n$$

and $$2I_T/I_0 = \sin^2(2\theta - p) \sin^2 \tfrac{1}{2}\Delta n + \sin^2 p \cos^2 \tfrac{1}{2}\Delta n \quad (6)$$

The only solution to Eqn. (6) which gives $I_T = 0$ when neither θ nor p is zero is

$$2\theta = p, \Delta n = (2N + 1)\pi \quad (N = 0, 1, 2...\pi) \quad (7)$$

Substitution of the condition $2\theta = p$ into Eqns. (3) and (4) gives

$$4I_T/I_0 = [\exp -(n_x'' + n_y'')][\cosh \Delta n'' + \sin 4\theta \cos^2 \Delta n/2 \sinh \Delta n''$$
$$- \cos \Delta n' (\cos 4\theta \cos^2 \Delta n/2 + \sin^2 \Delta n/2) - \sin 2\theta \sin \Delta n' \sin \Delta n]$$

which shows the tuning term $\sin 2\theta \sin \Delta n \sin \Delta n'$ to be retained intact. However, this term is incompatible with the second requirement of Eqn. (7), that $\Delta n = (2N + 1)\pi$. Thus the procedure of simultaneously varying p and θ may allow an optimum signal-to-noise ratio to be obtained, by judicious selection of p, θ and Δn, but it does not allow the tuning term to be retained while eliminating the background altogether. These conclusions were confirmed experimentally. With $\Delta n = \pi$, the background transmission could indeed be eliminated for any value of θ. However, no evidence for a tuning effect could be found when the data shown in Fig. 5 were measured again using this procedure.

CONCLUSIONS

The present technique permits a Voigt effect m.o.r. optical filter to be tuned. Rotation of a retardation plate provides the actual tuning mechanism. The maximum frequency displacement is of the order of the half-width of the atomic line profile within the m.o.r. cell. This range is superimposed on the frequency displacement caused by Zeeman splitting of that line.

For the sodium 589.0-nm line, the filter transmission frequency could be shifted sufficiently to cause changes in flame atomic absorption signals of about ±20% after correction for the absorption on the background transmission. This may be sufficient to warrant future consideration of the technique as a method for correcting spectral interferences in emission or absorption measurements, provided that other atomic lines of potential interest behave in a similar fashion. This possibility has not been examined yet; however, theory suggests no reason why the technique should not be generally applicable.

This type of usage may be somewhat restricted by the continuous background transmission associated with the tuning process, which limits the maximum frequency displacement that can be obtained before photon noise starts to degrade the signal-to-noise ratio of the system. The point of onset for this effect will depend on the nature of the spectral source to be observed. No technique could be found to avoid this effect.

Frequency scanning with the filter enabled portions of the sodium 589.0-nm flame absorption profile to be determined. The method appears to have some advantages over the technique of longitudinal Zeeman scanning. In particular, it allows measurements to be made at fixed magnetic field strengths; at the same time the transmission spectrum can be simplified by coherence narrowing which reduces contributions from weak lines in the multiplet. By making use of these simplifying properties, some of the complexities of calculating the exact form of a Zeeman multiplet under circumstances where the necessary field strengths cover the Back-Goudsmit transition (or enter a Paschen-Back transition) may be avoided.

The authors are indebted to the Natural Sciences and Engineering Research Council of Canada for support of this work.

Appendix

The data in Fig. 5 were measured at a field strength of 4.6 kG. At this field strength, Eqn. (5) shows the π transmission envelope to consist of two separated lines. The two lines are assumed to be monochromatic at frequencies ν_1, ν_2, with intensities I_1, I_2. This assumption demands that the unknown profile should vary only slowly over the range of measurement. If $K(\nu_1)$ and $K(\nu_2)$ are defined as the flame atomic absorption coefficients at ν_1 and ν_2, and a_1 and a_2 are the experimental absorbances at retarder angles of θ and $\theta + \pi/2$, corrected for the effect of absorption on the background transmission, then

$$\exp -a_1 = [I_1 \exp -K(\nu_1) + I_2 \exp -K(\nu_2)]/(I_1 + I_2)$$

$$\text{and } \exp -a_2 = [I_2 \exp -K(\nu_1) + I_1 \exp -K(\nu_2)]/(I_1 + I_2)$$

$$\text{Hence } K(\nu_1) = \ln \{(r_1^2 - r_2^2)/[r_1 (\exp -a_1) - r_2 (\exp -a_2)]\}$$

$$\text{and } K(\nu_2) = \ln \{(r_2^2 - r_1^2)/[r_2 (\exp -a_1) - r_1 (\exp -a_2)]\} \quad (8)$$

where $r_1 = I_1/(I_1 + I_2)$ and $r_2 = I_2/(I_1 + I_2)$. These equations cannot be used immediately because at high magnetic field strengths, I_1 and I_2 are essentially equal for a continuum source. The problem was resolved by use of a vapour discharge source. This gave a strongly self-reversed emission profile which, upon multiplication by Eqn. (5), led to different values of I_1 and I_2 as required by Eqn. (8) if $\nu_1 \neq \nu_2$. This procedure enabled I_1 and I_2 to be calculated from Eqn. (5) as a function of θ. Hence, for a known source profile, Eqn. (8) permitted $K(\nu)$ to be determined as a function of frequency, to give the flame atomic absorption profile shown in Fig. 6. The source profile was determined by the longitudinal Zeeman scanning technique.

REFERENCES

1 G. Jolly and R. Stephens, Anal. Chim. Acta, 116 (1980) 365.
2 Tj. Hollander, B. J. Jansen, J. J. Plaat and C. Th. J. Alkemade, J. Quant. Spectrosc. Radiat. Transfer, 10 (1970) 1301.
3 H. F. van Heek, Spectrochim. Acta, 25B (1970) 107.
4 Tj. Hollander and H. P. Broida, J. Quant. Spectrosc. Radiat. Transfer, 7 (1967) 965; Combust. Flame, 13 (1969) 63.
5 W. Snelleman, T. C. Rains, K. W. Yee, H. D. Cook and O. Menis, Anal. Chem., 42 (1970) 394.
6 A. T. Zander, T. C. O'Haver and P. N. Keliher, Anal. Chem., 48 (1976) 1166.
7 R. G. Michel, J. Sneddon, J. K. Hunter, J. M. Ottaway and G. S. Fell, Analyst, 106 (1981) 288.

8 R. Stephens and G. F. Murphy, Talanta, 25 (1978) 441.
9 R. S. Longhurst, Geometrical and Physical Optics, 3rd edn., Longman, London, 1973.
10 J. Kankare and R. Stephens, Appl. Spectrosc., 34 (1980) 590.
11 D. J. Caldwell and H. Eyring, The Theory of Optical Activity, Wiley—Interscience, New York, 1971.

Analytica Chimica Acta, 139 (1982) 279—285
Elsevier Scientific Publishing Company, Amsterdam — Printed in The Netherlands

COMPARISON OF ASCORBIC ACID AND RELATED COMPOUNDS AS INTERFERENCE SUPPRESSORS IN ELECTROTHERMAL ATOMIC ABSORPTION SPECTROMETRY

MAMORU TOMINAGA* and YOSHIMI UMEZAKI

National Research Institute for Pollution and Resources, Yatabe, Tsukuba-gun, Ibaraki 305 (Japan)

(Received 2nd February 1982)

SUMMARY

Suppression of interferences from sodium, calcium and iron(III) chlorides by addition of ascorbic acid and related compounds was investigated for the determination of Pb, Sn, Mn, V and Mo. Absorption—time curves for these metals with and without ascorbic acid and other compounds showed that the peak appeared earlier for Pb, and later for Sn, Mn, Mo and V when ascorbic acid was present. Suppression of interferences was also achieved, but usually less effectively, by lactones, carboxylic acids, ammonium carbonate and formaldehyde. Carbon monoxide or dioxide generated by pyrolysis of the suppressors may participate in the suppression of interferences.

Graphite-furnace atomic absorption spectrometry, suffers from various interference effects such as background absorption from molecular absorption or light scattering, and atomization interferences. Several workers have reported means of overcoming these interferences. Separation procedures, including liquid—liquid extraction [1], ion exchange [2] and co-precipitation [3] are time-consuming and error-prone. Selective atomization [4] requires correct temperature control, and has limited application. Matrix modification, which achieves suppression of interferences by the reaction between analyte or matrix and a reagent added directly into the graphite tube, has been reported for several elements. Modifiers investigated include ammonium peroxodisulfate [5], ammonium nitrate [6], nitric acid [7, 8], EDTA [9], thiourea [10] and L-ascorbic acid [11, 12]. Ascorbic acid was very effective for suppression of interferences in the determination of lead [13], tin [14] and manganese [15]. However, little explanation of the processes involved in such interferences or their removal has been given. This report describes a study of the suppression of interferences by ascorbic acid and related compounds.

EXPERIMENTAL

Apparatus and reagents

A Perkin-Elmer graphite furnace (HGA-2100) was used in conjunction

0003-2670/82/0000-0000/$02.75

with a Perkin-Elmer 403 atomic absorption spectrometer and a Hitachi 056 recorder. The light sources were Hamamatsu TV single-element hollow-cathode lamps. A deuterium lamp was used for background correction. Sample solutions were injected into the graphite tube by an autosampler (Perkin-Elmer AS-1) and a micropipette (Rainin Co. P-20). The absorption signal in the atomization step was analyzed by using a transient memory (Tokyo Kagaku TM-706).

Lead nitrate (1.60 g), manganese nitrate (3.26 g), and ammonium heptamolybdate tetrahydrate (1.84 g) were each dissolved in the minimum amount of concentrated hydrochloric acid and diluted to 1 l with distilled water. Tin and vanadium metal (1 g each) were each dissolved in 100 ml of concentrated hydrochloric acid and diluted to 1 l with distilled water. These solutions were diluted as necessary with (1 + 9) hydrochloric acid. All acids used were of super-special grade (Wako Pure Chemicals). L-Ascorbic acid and other reagents were of analytical-reagent grade.

General procedure

The instrumental parameters used are summarized in Table 1. A 20-μl portion of modifier solution was injected into the graphite tube by micropipette followed by the sample (20—40 μl) from the autosampler. Argon was used as sheath gas at 80 ml min^{-1}. The peak height was recorded. In the study of the signal—time profile, lower atomization temperatures were adopted for lead, tin and manganese, because it was difficult to record the profiles obtained at the rapid temperature rises given in Table 1. The atomization temperatures were 1400°C for lead, 2300°C for tin and 2000°C for manganese. The signals for the atomization step were introduced into a transient memory with an input time of 20 ms, and were recorded at an output time of 200 ms.

RESULTS AND DISCUSSION

Figure 1 shows the atomic absorption—time profiles for lead, tin and manganese, with and without additions of ascorbic acid (curves 1—3). For lead, the absorption profile showed a shoulder with the addition of 0.05%

TABLE 1

Instrumental parameters

Element	Pb	Sn	Mn	V	Mo
Lamp current (mA)	10	10	10	10	15
Wavelength (nm)[a]	283.3	286.3	279.4	318.4	313.2
Char (°C)[b]	400	700	900	1300	1500
Atomize (°C)	2000	2500	2500	2500	2500
(s)	6	10	10	20	20

[a]Slit width 0.7 nm. [b]After drying at 100°C for 40 s.

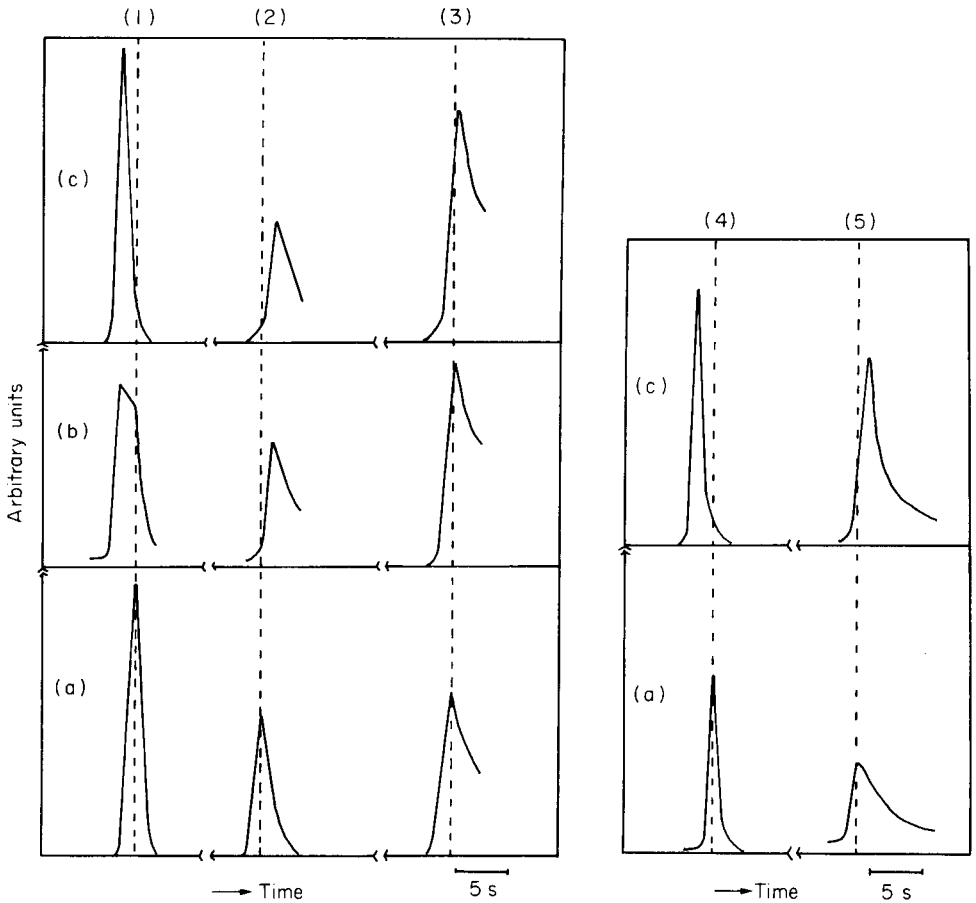

Fig. 1. Absorption–time profiles of: (1) 0.2 mg Pb l^{-1}; (2) 0.02 mg Mn l^{-1}; (3) 0.1 mg Sn l^{-1}; (4) 0.2 mg Pb l^{-1} in the presence of 0.05% NaCl; (5) 0.02 mg Mn l^{-1} in the presence of 1% NaCl. (a) In the absence of ascorbic acid; (b) with 0.05% ascorbic acid present; (c) with 5% ascorbic acid present.

ascorbic acid solution. Addition of 5% ascorbic acid solution gave a single peak which appeared earlier than previously. For manganese, the peak appeared later as the ascorbic acid concentration increased. For tin, the tendency was similar to manganese, but was less marked. Figure 1 also shows the results of similar experiments in the presence of sodium chloride which depressed the peaks; curves 4 and 5 show that ascorbic acid decreased the depressive effect.

In the determination of tin and manganese described previously [14, 15], ascorbic acid was much more effective in suppressing interferences than other carbohydrates. Regan and Warren [16] suggested that pyrolysis of ascorbic acid left a carbonaceous residue, which accelerated the reduction of metal oxides during the atomization step. However, it seems that the

TABLE 2

Effect of various lactones on the removal of interferences on tin and lead

Lactone[a]	Sn recovery (%)[b] in presence of			Pb recovery (%)[c] in presence of	
	NaCl	$CaCl_2$	$FeCl_3$	NaCl	$CaCl_2$
—	72	75	52	46	32
Levulinic acid	90	80	68	98	93
γ-Butyrolactone	85	118	103	23	117
D-Glucuronolactone	95	100	94	91	88
D-isoascorbic acid	96	111	107	130	110
L-Ascorbic acid	100	100	101	94	104

[a]Added as aqueous 10% (w/v) solution. [b]0.1 mg Sn l^{-1}, 100 mg l^{-1} Na, Ca or Fe. [c]0.2 mg Pb l^{-1}, 200 mg l^{-1} Na or Ca.

suppression of interferences may be ascribed to characteristic properties of ascorbic acid itself and not to a general property of carbohydrates. Lactones, which have the same intramolecular ester bond as ascorbic acid, could also be effective for suppression of interferences. Table 2 shows how several

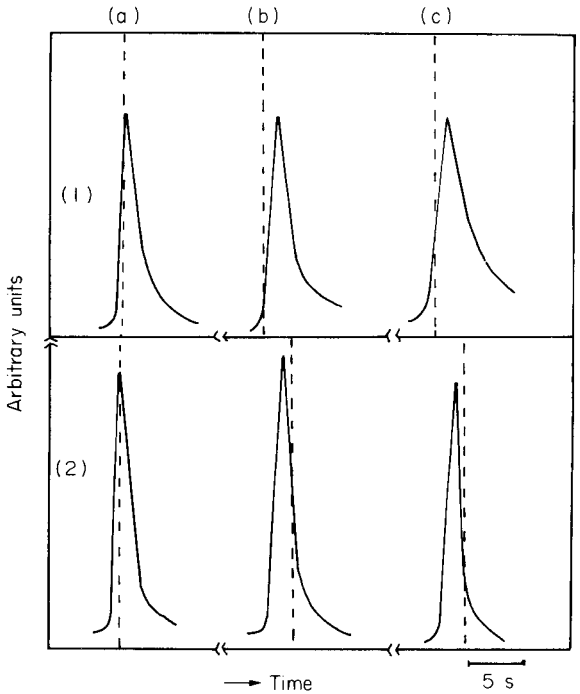

Fig. 2. Absorption—time profiles of: (1) 0.02 mg Mn l^{-1}; (2) 0.2 mg Pb l^{-1}. (a) In the absence of suppressor; (b) in the presence of 5% ascorbic acid; (c) in the presence of 10% glucuronolactone.

lactones suppressed the interferences of sodium chloride, calcium chloride and iron(III) chloride in the determination of lead and tin. These lactones are soluble in water and mixed readily with the sample solution after injection into the graphite tube. Suppression of interferences was not so marked as with ascorbic acid, but nevertheless was measurable. Figure 2 shows the atomic absorption profiles with glucuronolactone. The lead peak appeared earlier, and the manganese peak later, than in the absence of lactone, the results being very similar to those shown in Fig. 2 for ascorbic acid.

Lactones generate carbon monoxide and carbon dioxide on pyrolysis. As the evolution of these gases may have a role in interference suppression, carboxylic acids, which also evolve these gases on pyrolysis, were also investigated as interference suppressors. Table 3 shows the results for various carboxylic acids and formaldehyde on the determination of lead. As the number of carbon atoms in the compound increases, both the sensitivity and the suppressive effect become poorer. Best suppression was obtained with formic or acetic acid.

Application to other elements was briefly investigated. Table 4 shows that interference of iron in the determination of vanadium and molybdenum was suppressed with ascorbic acid. In the atomic absorption profile of vanadium and molybdenum, the absorption peaks appeared later with ascorbic acid

TABLE 3

Suppression of sodium chloride interference (200 mg Na l^{-1}) on the determination of lead (0.2 mg Pb l^{-1}) by carboxylic acids and formaldehyde

Compound tested[a]	Recovery (%)	Sensitivity[b] ($\mu g\ l^{-1}$)	Compound tested[a]	Recovery (%)	Sensitivity[b] ($\mu g\ l^{-1}$)
—	46	3.9	Caproic acid	74	4.7
Formaldehyde	69	4.7	Oxalic acid	41	3.8
Formic acid	89	3.4	Fumaric acid	28	3.8
Acetic acid	81	3.4	Tartaric acid	51	3.8
Propionic acid	73	5.3	Citric acid	29	4.9
Butyric acid	62	4.9			

[a]Aqueous 5% (w/v) solution added. [b]Concentration giving an absorbance of 0.0044.

TABLE 4

Suppression of iron interference by ascorbic acid in the determination of vanadium (5 mg l^{-1}) and molybdenum (2 mg l^{-1})

Salt added[a]	Vanadium recovery (%)		Molybdenum recovery (%)	
	No suppressor	5% ascorbic acid	No suppressor	5% ascorbic acid
$FeCl_3$	81	103	46	105
$Fe(NO_3)_3$	85	96	—	—

[a]1000 mg Fe l^{-1}.

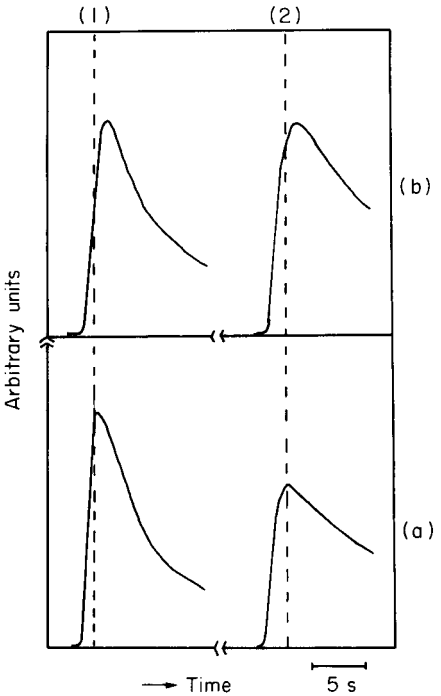

Fig. 3. Absorption—time profile of: (1) 5 mg V l^{-1}; (2) 2 mg Mo l^{-1}. (a) In the absence of ascorbic acid; (b) with 5% ascorbic acid present.

(Fig. 3). It would be possible to determine vanadium and molybdenum directly in the presence of ascorbic acid.

In Table 5, the effects of sodium and iron(III) chlorides were compared to aid in the elucidation of the mechanism of suppression of interferences. The suppressors used were formaldehyde, formic and acetic acids, ammonium carbonate and ascorbic acid. The effects of formaldehyde and the carboxylic

TABLE 5

Percentage recoveries of different elements after suppression of interferences from sodium and iron by various compounds

Interference suppressor	Pb (0.2 mg l^{-1}) +200 mg Na l^{-1} [a]	Sn (0.5 mg l^{-1}) +100 mg Na l^{-1} [a]	Mn (0.02 mg l^{-1}) +1% NaCl	V (5 mg l^{-1}) +1 g Fe l^{-1} [b]	Mo (2 m +1 g Fe
—	46	72	44	81	46
Formaldehyde [c]	69	98	100	97	44
Formic acid [c]	89	53	92	104	88
Acetic acid [c]	81	47	94	100	92
$(NH_4)_2CO_3$ [d]	77	78	67	60	90
Ascorbic acid [d]	104	100	100	103	105

[a] Added as NaCl. [b] Added as $FeCl_3$. [c] Concentrated solution. [d] Aqueous 5% (w/v) solution.

acids were different for different elements. Ascorbic acid was remarkably effective for all the elements. This suggests that carbon monoxide or dioxide generated by pyrolysis of the suppressors participates in the suppression of interferences, and that ascorbic acid is superior to the other suppressors in this process. The exact mechanism, however, has still not been elucidated.

REFERENCES

1 T. K. Jan and D. R. Young, Anal. Chem., 50 (1978) 1250.
2 J. P. Riley and D. Taylor, Anal. Chim. Acta, 40 (1968) 479.
3 V. Hudnik, S. Gomišćek and B. Gorenc, Anal. Chim. Acta, 98 (1978) 39.
4 D. A. Segar and J. G. Gonzalez, At. Absorpt. Newsl., 10 (1971) 94.
5 K. R. Sperling, Fresenius Z. Anal. Chem., 287 (1977) 23.
6 J. R. Montgomery and G. N. Peterson, Anal. Chim. Acta, 117 (1980) 397.
7 A. Le Bihan and J. Courtot-Coupez, Analusis, 3 (1975) 59.
8 V. B. Stein, E. Canelli and A. H. Richards, Int. J. Environ. Anal. Chem., 8 (1981) 99.
9 R. Guevremont, Anal. Chim. Acta, 115 (1980) 163.
10 M. Suzuki, K. Ohta and T. Yamakita, Anal. Chem., 53 (1981) 9.
11 J. G. T. Regan and J. Warren, At. Absorpt. Newsl., 17 (1978) 89.
12 D. J. Hydes, Anal. Chem., 52 (1980) 959.
13 J. G. T. Regan and J. Warren, Analyst, 101 (1976) 220.
14 M. Tominaga and Y. Umezaki, Anal. Chim. Acta, 110 (1979) 55.
15 M. Tominaga and Y. Umezaki, Nippon Kagaku Kaishi, 1 (1981) 7.
16 J. G. T. Regan and J. Warren, Analyst, 103 (1978) 447.

Analytica Chimica Acta, 139 (1982) 287—295
Elsevier Scientific Publishing Company, Amsterdam — Printed in The Netherlands

THE DETERMINATION OF BISMUTH IN SERUM AND URINE BY ELECTROTHERMAL ATOMIC ABSORPTION SPECTROMETRY

ROGER L. BERTHOLF and BRIAN W. RENOE*

Departments of Pathology and Chemistry, University of Virginia, Charlottesville, VA 22908 (U.S.A.)

(Received 28th September 1981)

SUMMARY

A method for the determination of bismuth in serum and urine is presented. The method includes 1 + 1 dilution of the sample with 1 mM EDTA followed by charring in a graphite furnace under an oxygen atmosphere. The use of oxygen results in the formation of more homogeneous bismuth salts (probably bismuth oxides) during charring, and more efficient burning of the protein and organic components of the sample matrix. The procedure formulated is a standard additions method and is verified for serum and urine samples. The method reduces matrix interferences, gives a detection limit of 0.05 $\mu g\ l^{-1}$, and has a relative standard deviation of less than 5% for bismuth in the reference range of 2.6—6.0 $\mu g\ l^{-1}$. The method displays a recovery accuracy of 91, 96, and 100% for urine, serum, and aqueous samples, respectively.

Clinical/medical interest in bismuth dates back about 50 years, when the element was first introduced in a pharmaceutical used in the treatment of syphillis. Since then, its pharmaceutical uses have expanded to antacids, peptic ulcer treatments, and topical dermatological creams [1]. There have been several reported cases of nephrotoxic and neurotoxic symptoms attributable to the use of bismuth-containing pharmaceuticals [2—6]. These cases underscore the necessity for a method to determine bismuth concentrations in biological fluids such as serum or urine. The importance of reliable methods for bismuth in biological samples extends beyond the clinical laboratory, however, because the modes of biochemical interactions of bismuth have not yet been elucidated [7]. Investigations into the biochemical mechanisms responsible for bismuth-induced toxic symptoms require methodology for trace determination of bismuth in biological matrices.

While bismuth may be determined by many methods with detection limits adequate for clinical determinations ($\leqslant 1\ \mu g\ l^{-1}$), most methods suffer from either prohibitive cost or technical difficulty. The cost of bismuth determinations by atomic absorption is compensated by widespread availability of instrumentation and its adaptability to many elemental determinations using electrothermal atomization. Microprocessor control of the atomic absorption instrument and autosampling devices make this method technically simple, which can help enhance precision. Because of these considera-

tions, electrothermal atomic absorption seems attractive for determinations of bismuth in biological samples.

The reactions that occur during the desolvation and charring/ashing steps in graphite-furnace atomic absorption determine the atomic vapor formed during the atomization step. Among the attractive features of the graphite furnace are the instrumental control of the physical and chemical sample manipulations during these steps. Chemical manipulations can be controlled during desolvation and charring by the choice of time, temperature and sample diluent, and during charring by the choice of purge gas. In this work, sample manipulations prior to the measurement step were minimized and the physical and chemical conditions within the graphite furnace were used to minimize matrix interferences and to achieve minimum detection limits.

EXPERIMENTAL

Instrumentation and reagents

All measurements were done with a Perkin-Elmer Model 5000 atomic absorption spectrometer equipped with a Model HGA500 furnace unit, a Model AS40 autosampler/sequencer, PRS10 printer, and strip-chart recorder. The instrumental settings are given in Table 1.

Bismuth added to serum or urine, or in aqueous standards was from a 1 g l^{-1} bismuth certified atomic absorption standard (Fisher Scientific, Fairlawn, NJ 07410). The stock 1 mM EDTA solution (tetra-acid; Fisher) was prepared by addition of 0.29 g of EDTA to 1 l of deionized water. The bismuth solutions used for standard additions were prepared by addition of the appropriate volume of 1 g l^{-1} bismuth standard to 100 ml of EDTA solution (e.g., 10 μl for a 100 μg l^{-1} solution).

Procedures

Three standards were prepared by additions of 0, 5, and 10 μl of the 1 g l^{-1} bismuth standard to 100 ml of the 1 mM EDTA diluent, giving 0-, 50-, and

TABLE 1

Instrumental settings for the PE 5000 atomic absorption spectrometer, autosampler and HGA 500 furnace

Wavelength	223.1 nm	Operation mode	AA/BG (Background-corrected absorbance)
Slit width	0.2 nm		
Lamp current	10 mA	Read time	6 s
Recorder output mode	Rec ABS	Signal mode	Peak height
Signal mode	ABS	Sample volume	25 μl

	(°)	Ramp(s)	Hold(s)	Purge gas
Drying	120	30	90	Ar
Charring	650	120	0	O_2
Flushing	650	0	20	Ar
Atomizing	2500	1	5	Stopped

100-μg l^{-1} standards. Three aliquots of serum or urine were then mixed with equal volumes of each of the three standards. The standard additions to the samples can then be considered to be 0, 50, and 100 μg l^{-1} of bismuth (this accounts for dilution by the factor of 2).

Several serum pools were prepared as needed from sera submitted to the University of Virginia Hospital Clinical Chemistry Laboratory. These pools consisted of 100—200 individual samples drawn in evacuated test tubes containing no preservatives or anticoagulants. They were selected at random without knowledge of origin or pathology. Urine was obtained on several occasions from healthy male laboratory employees.

Fifty serum samples from patients were selected to establish a reference range for "normal" serum bismuth concentration. The criterion for selection of "normal" samples was that results for glucose, potassium, sodium, carbon dioxide, chloride, calcium, phosphorus, creatinine, urea, uric acid, total protein, albumin, and total bilirubin all be within normal limits established for this laboratory. The patients were not known to be taking any bismuth-containing drugs.

RESULTS

The concerns were to develop a method which would minimize manual manipulations of samples, and improve the performance for the bismuth determinations.

Pretreatment and drying

The drying studies involved selection of a drying temperature, time, and ramp time for three possible matrices: aqueous, serum, and urine. A mirror was used to view the samples during drying. Sera proved to be the most difficult samples to dry, so the parameters were optimized for this matrix. A 30-s ramp from ambient to a final drying temperature of 120°C avoided spattering of the liquid and resulted in a uniform solid deposit on the surface of the graphite furnace. Longer ramp times yielded no apparent advantage, but shorter ramp times caused spattering. The sample is held at 120°C for 90 s to complete the drying cycle (complete dryness was defined as that point at which no further changes were observed in the sample). Drying of serum at 110°C required 180 s, and a temperature of 130°C caused spattering. When this drying cycle was used, both aqueous standards and urines were observed to dry evenly and completely in a much shorter time (approximately 30 s). Thus a drying program using a 30-s ramp to 120°C and holding for 90 s was chosen for use with the three matrices.

The enhancement of the final bismuth absorption signal from the use of EDTA in the sample diluent was suggested by Ramirez-Muñoz [8]. A bismuth signal enhancement of 13—18% resulted from the use of EDTA with the present specimens.

Charring/ashing

The charring step is probably the most critical in the entire program for bismuth determinations. The chemical reactions occurring during this step were controlled by using an oxygen atmosphere to ensure the combustion of matrix components and the homogeneity of bismuth compounds formed. The dramatic effects of using oxygen are shown in Fig. 1. The figure shows both a profound bismuth absorption signal increase for all three matrices, and an improvement in the reproducibility of the signal. The most dramatic effect of the oxygen char is observed for urine with an approximately 20-fold increase, followed by lesser but still dramatic increases for serum and aqueous matrices.

The effect of oxygen charring on the bismuth determinations was further demonstrated by slowly increasing the temperature from the 650°C charring temperature to the atomization temperature both with and without oxygen charring. Figure 2 shows the recorder tracings obtained during a 30-s ramp from 650°C to 2500°C for aqueous standards. The relative signal responses with and without oxygen charring are superimposed in the figure. For both tracings, there are at least three and perhaps more peaks revealed as the temperature is increased. This may indicate the presence of different bismuth compounds, each decomposing at different temperatures to yield

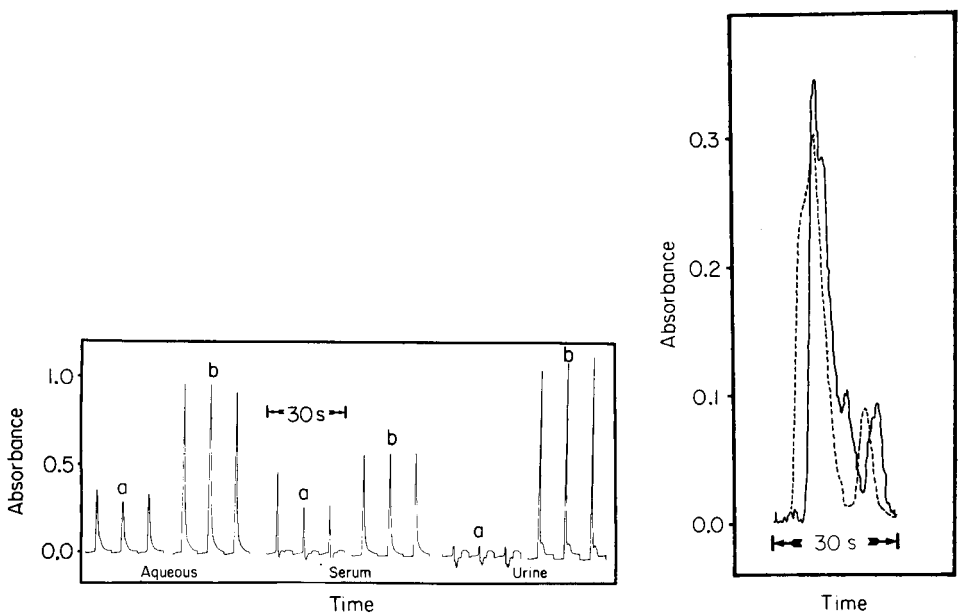

Fig. 1. Absorbance peaks obtained for three consecutive determinations of 200-μg l^{-1} spiked aqueous, serum and urine matrices without oxygen (a) and with oxygen (b) charring conditions.

Fig. 2. Absorbance peaks obtained during a 30-s atomization cycle from 650°C to 2500°C for a 100-μg l^{-1} aqueous sample after charring with (——) and without (------) oxygen.

atomic bismuth in a manner similar to that reported for zinc species by Sohler et al. [9]. The superimposed tracings reveal that the multiple bismuth peaks appear at different, higher temperatures with oxygen charring vs. without.

Of course the multiple peaks presented above could be due to different physical phenomena such as layering of the bismuth species or the relative geometry of the bismuth species on the graphite surface, and not the formation of different molecular bismuth species. To test this explanation, the same slow temperature ramp was run with three different rates of argon gas flowing. The results of this study for 0-, 20-, and 50-ml min^{-1} argon flows are shown in Fig. 3. The figure reveals the loss of the multiple peaks and an apparent decrease in signal magnitude with increasing argon flow rate. With an argon flow of 50 ml min^{-1}, only the first (lowest temperature) of the bismuth peaks is detected. The disappearance of the later bismuth peaks with increasing flow is indicative of the formation of volatile molecular bismuth species, which are flushed from the graphite furnace prior to their decomposition to elemental bismuth.

Figure 4 illustrates the effect of charring temperature on the signal observed during atomization. A char temperature of 650—700°C gives maximum absorbance, with better precision at 650°C. Figure 5 shows the precision attained at varying ramp times during the char cycle of 10—180 s. Although relative standard deviations are less than 1% for aqueous bismuth standards at short or long ramp times, good precision for serum bismuth standards was obtained only by raising the temperature very slowly (>90-s ramp time). The charring cycle was thus set for a 120-s ramp from 120°C

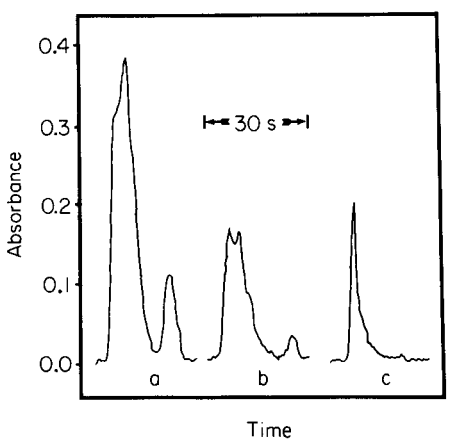

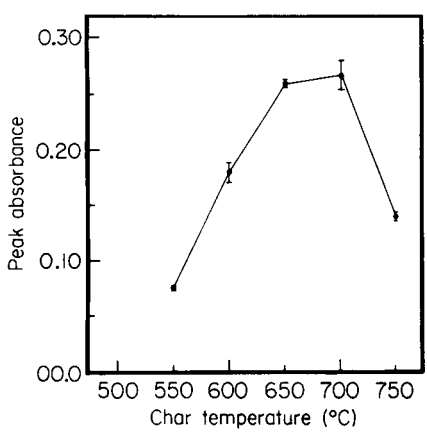

Fig. 3. Absorbance peaks obtained during a 30-s atomization cycle from 650°C to 2500°C for a 100-$\mu g\ l^{-1}$ aqueous sample with purge gas (argon) flow rates of (a) 0, (b) 20, and (c) 50 ml min^{-1}.

Fig. 4. Bismuth absorbance vs. char temperature. A serum sample with 100 $\mu g\ l^{-1}$ bismuth was run in triplicate for each point (bars indicate range of the values). A 120-s ramp time was used.

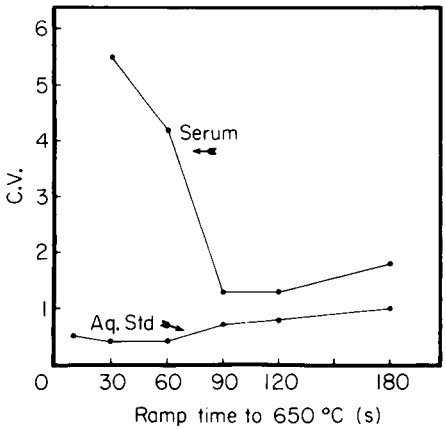

Fig. 5. Dependence of precision on the ramp time of the char cycle. Precision for a serum sample with 100 μg l^{-1} bismuth is compared to that for an aqueous standard with the same bismuth concentration (n = 5).

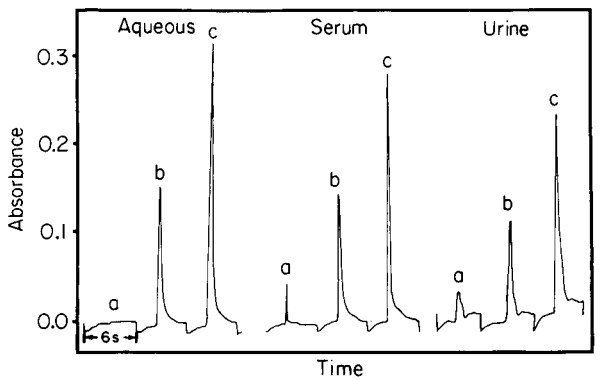

Fig. 6. Absorbance peaks obtained for aqueous, serum and urine samples with standard additions of (a) 0, (b) 25, and (c) 50 μg l^{-1} bismuth.

to 650°C, followed by a 20-s hold at 650°C to allow the oxygen gas to be flushed from the furnace by argon prior to atomization.

Atomization

The atomization cycle was selected by considering the apparent atomization efficiency of bismuth, the graphite tube life, and the instrumental characteristics of the atomic absorption spectrometer. Increasing the atomization temperature above 2500°C offered no enhancement in either sensitivity or precision, but lower temperatures resulted in decreased signals. Thus 2500°C was chosen as the atomization temperature. The mode of attaining 2500°C was found to have significant effects on the signal. A very slow ramp from the charring temperature to 2500°C resulted in poor precision, especially when using the area encoding mode of the instrument. Full-power heating

(0-s ramp), however, resulted in poor precision and inconsistent results between the recorder output, and the spectrometer display. A 1-s ramp from 650°C to the final atomization temperature followed by holding for 5 s at 2500°C yielded the best precision. This ramp will sometimes result in a second trailing "peak" for some samples, as seen in Fig. 1 for the urine specimens, but it had no measurable effect on the precision of the observed peak height.

Both pyrolytically-coated and uncoated graphite tubes were used, and no difference was observed in either sensitivity or precision.

Standard additions methodology and evaluation of the method

Standard additions were used because there is a small residual background absorbance signal from some samples even after oxygen charring. Typical signals are shown in Fig. 6 for aqueous standard additions to aqueous standard, serum, and urine. The relative differences in the signals are probably due to the small residual matrix effects from the samples.

To evaluate the accuracy of this method, aqueous, serum and urine samples were run through the entire procedure; the samples were used neat and with standard additions of 25 $\mu g\ l^{-1}$ bismuth (nitrate salt). The recovery data are summarized in Table 2. These data can be summarized as showing recoveries of over 90% for the added bismuth.

The entire procedure was used to determine bismuth in serum samples from 50 patients in order to establish a reference range. The mean serum bismuth concentration was found to be 4.2 $\mu g\ l^{-1}$, with 95% of values falling between 2.6 and 6.0 $\mu g\ l^{-1}$. The utility of the procedure for urine samples was also verified because it could prove useful in monitoring the clearance of bismuth in therapeutic or toxic cases, but no attempt was made to establish a reference range for these specimens because of the heavy dependence of the results on the completeness of urine collections.

The precision of the bismuth determination was evaluated for serum in the reference range by running ten different serum pools a minimum of 10 times each. The coefficients of variation from these pools were less than 5%. A urine specimen with a bismuth concentration of 50 $\mu g\ l^{-1}$ revealed a precision of 3%. A serum sample with an elevated bismuth (added bismuth to yield 50 $\mu g\ l^{-1}$) had a coefficient of variation of 4.6%.

TABLE 2

Results for bismuth added to aqueous, serum, and urine samples

Bi added ($\mu g\ l^{-1}$)	Bi found ($\mu g\ l^{-1}$)		
	Aqueous	Serum	Urine
0	1.1	9.9	5.1
25	26.0	33.8	27.9
Recovery (%)	100	96	91

DISCUSSION

The possibility of improving the reliability of electrothermal a.a.s. by careful control of the chemistry of the desolvation and charring steps has been greatly neglected in developing methods for complex biological matrices. As noted above, EDTA can have profound effects. The power of the oxygen charring technique was demonstrated first by Beaty and Barnett [10]. The use of oxygen, introduced as a reagent gas during the charring stage here, offers two advantages in the analysis of biological matrices. First, the organic components of the matrix are more efficiently and completely burned in an oxygen atmosphere. Secondly, charring with oxygen favors metal oxide formation. Metal oxides are, in general, thermally stable compounds that will not volatilize or decompose at charring temperatures. Further, metal oxide formation should make the procedure less susceptible to variations in matrix constituents which under an inert atmosphere, can affect the metal species remaining after charring. A similar advantage is gained by using EDTA in the diluent.

Figures 2 and 3 require further comment. As stated before, the occurrence of multiple peaks during a slow temperature increase to 2500°C can have two explanations: varying bismuth species present or a physical phenomenon related to the distribution of the sample on the tube surface. The former explanation seems more likely for several reasons. First, the appearance of multiple peaks was quite reproducible from run to run and from one graphite tube to another. Such reproducibility would seem unlikely in a process governed by the placement of the sample on the tube surface, the heating characteristics of the tube, etc. Secondly, the fact that the number and character of the peaks observed changes when oxygen is introduced in the charring stage indicates a chemical, rather than physical process. Finally, Fig. 3 demonstrates how the spectrum collapses as an argon flow is introduced during atomization. The disappearance of certain peaks indicates the removal of a particular bismuth species responsible for the peak before decomposition and subsequent detection occurs. While the occurrence of multiple peaks is an interesting subject for further investigation, the uncertainties associated with this observation can be circumvented, in a practical sense, by making the rate of temperature increase during atomization sufficiently rapid.

Previously a wet digestion was required to ensure homogeneity and reproducibility as studied by Rooney [11]. The present results, which demonstrate better precision, indicate the ability to avoid this tedious, error-prone step. Simplicity is especially important in a routine laboratory because of considerations of cost, time, and operator skill, and most of the chemistry required for sensitive determinations of bismuth in serum and urine can, in fact, be done inside the graphite tube, provided that a standard additions method is applied to compensate for different residual effects of matrix constituents.

REFERENCES

1 D. W. Thomas, T. F. Hartley, P. Coyle and S. Sobecki, in S. S. Brown (Ed.), Clinical Chemistry and Toxicology of Metals, Elsevier/North-Holland Biomedical Press, Amsterdam, 1977, pp. 293—296.
2 R. Urizar and R. L. Vernier, J. Am. Med. Assoc., 198 (1966) 207.
3 R. Burns, D. W. Thomas and V. J. Barron, Br. Med. J., 1 (1974) 220.
4 W. J. Serfontein and R. Mekel, Res. Comm. Chem. Path. Pharm., 26 (1979) 391.
5 H. L. Boiteau, J. M. Cler, J. F. Mathe, R. Delobel and J. R. Feve, Europ. J. Tox., 9 (1976) 233.
6 B. A. Fowler and V. Vouk, in L. Friberg (Ed.), Handbook on the Toxicology of Metals, Elsevier/North-Holland and Biomedical Press, Amsterdam, 1979, pp. 345—353.
7 G. Kruger and D. J. Thomas, Lancet, 2 (1976) 485.
8 J. Ramirez-Muñoz, Atomic Absorption Spectroscopy, Elsevier, Amsterdam, 1968, p. 309.
9 A. Sohler, R. Wolcott and C. C. Pfeiffer, Clin. Chim. Acta, 70 (1976) 391.
10 M. Beaty and W. Barnett, At. Spectrosc., 1 (1980) 72.
11 R. C. Rooney, Analyst, 101 (1976) 749.

Analytica Chimica Acta, 139 (1982) 297—305
Elsevier Scientific Publishing Company, Amsterdam — Printed in The Netherlands

MULTI-ELEMENT ANALYSIS OF MANGANESE NODULES BY ATOMIC ABSORPTION SPECTROMETRY WITHOUT CHEMICAL SEPARATION

JEAN S. KANE*

U.S. Geological Survey, Reston, VA 22092 (U.S.A.)

J. M. HARNLY

Nutrient Composition Laboratory, BHNRC, U.S. Department of Agriculture, Beltsville, MD (U.S.A.)

(Received 13th January 1982)

SUMMARY

Five manganese nodules, including the USGS reference nodules A-1 and P-1, were analyzed for Co, Cu, Fe, K, Mg, Mn, Na, Ni and Zn without prior chemical separation by using a simultaneous multi-element atomic absorption spectrometer with an air—acetylene flame. The nodules were prepared in three digestion matrices. One of these solutions was measured using sixteen different combinations of burner height and air/acetylene ratios. Results for A-1 and P-1 are compared to recommended values and results for all nodules are compared to those obtained with an inductively coupled plasma. The elements Co, Cu, Fe, K, Mg, Mn, Na, Ni, and Zn are simultaneously determined with a composite recovery for all elements of 100 ± 7%, independent of the digestion matrices, heights in the flame, or flame stoichiometries examined. Individual recoveries for Co, K, and Ni are considerably poorer in two digests than this composite figure, however. The optimum individual recoveries of 100 ± 5% and imprecisions of 1—4%, except for zinc, are obtained when Co, K, Mn, Na and Ni are determined simultaneously in a concentrated digest, and in another analytical sequence, when Cu, Fe, Mg, Mn and Zn are measured simultaneously after dilution. Determination of manganese is equally accurate in the two sequences; its measurement in both assures internal consistency between the two measurement sequences. This approach improves analytical efficiency over that for conventional atomic absorption methods, while minimizing loss of accuracy or precision for individual elements.

Great interest exists in manganese nodules as sources of the technologically important metals Mn, Co, Cu, and Ni. In order to elucidate varied aspects of the chemistry and geology of these marine sediments and to evaluate the economics of their exploitation, rapid but accurate determinations of several minor and trace elements are needed. This paper describes the application of simultaneous multi-element atomic absorption spectrometry with continuum source (SIMAAC) [1—3], to the determination of several elements in manganese nodules.

The elements Co, Cu, Mn, and Ni are highly enriched in manganese nodules over the abundance levels found in many other geological materials. This enrichment is evident from the comparison to crustal abundances presented

0003-2670/82/0000-0000/$02.75

in Table 1. Chromium is, by contrast, exceptionally depleted in manganese nodules. Other elements such as K, Mg, and Na are neither greatly enriched nor depleted. The patterns of enrichment with respect to average crustal abundances, the Fe/Mn ratio, and its correlation to nickel concentration provide information to the geochemist regarding the geographic source of the nodule and its rate of growth. Trace element composition with respect to that of associated sediments aids in understanding the chemistry of transition metals in seawater.

Conventional atomic absorption spectrometry (a.a.s.) is a well-established technique for determining high and low concentrations of most metals. It has, however, a limited dynamic range under any one set of experimental conditions and is a multi-element technique only in the sense of sequential determinations. Furthermore, background correction of line-source a.a.s. using a continuum source is often inadequate for samples with highly complex matrices [7, 8].

The SIMAAC system uses wavelength modulation to correct for all broad-band, non-specific background absorption interferences [9] and to achieve dynamic analytical ranges of 4—6 orders of magnitude for each element [2]. These capabilities are achieved without significant deterioration of the detection limits from those for conventional single-element a.a.s.

Korkisch et al. [10—13] employed ion-exchange separations to separate individual elements or small groups of elements from the bulk matrix and from one another. They reported errors from chemical interferences when separations were not used prior to determination of the elements of interest by atomic absorption.

This paper reports results for Co, Cu, Fe, K, Mg, Mn, Na, Ni, and Zn determined simultaneously with an air—acetylene flame. U.S. Geological Survey (USGS) reference nodule A-1 and P-1 from the Atlantic and Pacific Oceans,

TABLE 1

Geological sample enrichments over crustal abundance levels for a variety of sample types (Depletions appear as enrichment factors of less than 1.0)

Crustal abundance levels (wt. %) [4]		Average enrichment factors for			
		Granites [4]	Basalts [4]	Coal ash [5]	Mn nodules [6]
Mn	0.095	0.048	1.58	⩽0.63	170
Zn	0.007	0.714	1.43	⩽19	10.1
Fe	5.63	0.389	1.54	⩽5.5	2.77
Cu	0.0055	0.200	1.58	⩽2.9	46.6
Cr	0.010	0.130	1.70		0.14
Ni	0.0075	0.133	1.73		65.2
Co	0.0025	0.160	2.08		119
Na	2.36	1.15	0.763	⩽8.77	0.822
K	2.09	0.397	1.24	1.58	0.307
Mg	2.33	1.97	2.36	3.62	0.782

respectively, and three Atlantic Ocean nodules, one each collected from the Blake Plateau, the Caryn Seamount, and the Gillis Seamount were included in the study.

The results are assessed in two ways. First, A-1 and P-1 SIMAAC analyses are compared with the recommended concentrations for the reference nodule [14], determined almost exclusively by a.a.s. An intermethod comparison was also made between SIMAAC results for all five nodules and those from inductively-coupled plasma emission spectrometry (i.c.p.e.s.) done at USGS [15].

EXPERIMENTAL

Instrumentation and software

The SIMAAC system [1] uses a xenon arc continuum source, an echelle polychromator modified for wavelength modulation, and a dedicated minicomputer for data acquisition, storage, and manipulation. The software package described previously [3] is a critical element of the system. For each atomization, intensities are measured at 20 points across the modulation interval. From these intensities, six absorbances of differing sensitivity are calculated, enabling the simultaneous generation of a family of calibration curves covering 4—6 orders of magnitude for as many as 16 elements [2]. These calibration curves are comparable to those which result from repeated determinations of any element at less sensitive wavelengths in conventional line-source atomic absorption spectrometry.

Elements determined

Selection of the elements for simultaneous determination was based on geochemical interest in the element, on availability on the exit slit cassette of the spectrometer predetermined at the time of purchase, and on the detection limits for air—acetylene flame atomization. The wavelengths used were: Co, 240.7 nm; Cr, 357.9 nm; Cu, 324.7 nm; Fe, 248.3 nm; 302.0 nm; K, 404.4 nm; Mg, 285.2 nm; Mn, 279.5 nm; Na, 589.6 nm; Ni, 232.1 nm and Zn, 213.8 nm. The Na and K lines were selected specifically for the reduced sensitivity they provide, anticipating the high concentrations of these elements in biological materials, for which the SIMAAC system was designed. The less sensitive nickel line resulted from accidental misalignment of the exit slit.

Sample preparation

Two sample digestion techniques were used. One, a quite severe high-temperature procedure [16] routinely used on coal ash samples of high iron oxide content, assured total dissolution of the nodules and complete volatilization of silicon. Fluoride ion is incompletely removed during this digestion procedure, as evidenced by sodium contamination when glassware is used for dilution and storage of the solutions. The digest is therefore unsuitable for aspiration into a conventional glass i.c.p. torch.

The second procedure was the same room-temperature digestion with nitric and hydrofluoric acids used for i.c.p.e.s. [17]; the intermethod comparison was then possible without introducing sample preparation as a variable. Silicon is retained in solution after this digestion. This is potentially a disadvantage for a.a.s., in which silicon is known to cause chemical interferences for many elements.

For nodules A-1 and P-1, triplicate preparations were made by each procedure. Single preparations of the other three nodules were made. Both digestions were done at the same 2000 factor dilution from solid to solution used for i.c.p.e.s. [15]. The high-temperature digestion and SIMAAC measurement were repeated for A-1 and P-1 at a 200 factor dilution.

High-temperature digestion. Weigh into a PTFE digestion beaker 50 mg (500 mg) of manganese nodule which has been ground to 100 mesh and dried at 110° C overnight. Add 5 ml of hydrochloric acid, 2.5 ml of perchloric acid and 7 ml of hydrofluoric acid, and heat uncovered for 1 h at 200°C on a hotplate. Add 2 ml of nitric acid, and heat until heavy fumes of perchloric acid appear; evaporate to a residual volume of 2 ml. Cool slightly and add 1 ml of nitric acid and 2.5 ml of hydrochloric acid. Heat uncovered overnight at 200° C. Cool slightly and add 5 ml of hydrochloric acid. Rinse the beaker wall with a small amount of distilled water and warm briefly to dissolve salts. Transfer quantitatively to a 100-ml linear polyethylene volumetric flask and fill to volume. The concentration in solution is a factor of 2000 (200) more dilute than in the solid sample. All acids used were concentrated reagent grade.

Room-temperature digestion. Weigh into a screw-cap PTFE digestion bomb 50 mg of manganese nodule which has been ground to 100 mesh and dried at 110° C overnight. Add 1 ml of perchloric acid and 2 ml of hydrofluoric acid, both concentrated reagent grade; screw the cap on tightly and leave at room temperature overnight. Open the bomb and add 4 ml of 6% boric acid solution. Transfer quantitatively to a 100-ml linear polyethylene volumetric flask and fill to volume. The concentration in solution is a factor of 2000 more dilute than in the solid nodule.

Calibration standards. For each digestion matrix, a matched series of multi-element calibration standards was prepared. First, 10000 ppm single-element stock solutions of Ca, Co, Cr, Cu, Fe, K, Mg, Mn, Na, Ni, and Zn were prepared from high-purity metals and compounds as described by Jeffery [18]. Appropriate aliquots of these were used to prepare four calibration standard solutions in 5% (v/v) hydrochloric acid. The first contained Ca, Fe, Mg, and Mn (2000 μg ml^{-1}), Co, Cu, K, Na, Ni, and Zn (200 μg ml^{-1}), and Cr (20 μg ml^{-1}). The remaining three solutions were 50, 35, and 25% the concentration of the first for all elements. These four stock calibration standards were diluted by factors of 10 three successive times. The dilution was done with 5% (v/v) hydrochloric acid for the standards matched to the high-temperature digest. In matrix-matching the room-temperature digest, 4 ml of 6% (w/v) boric acid and 2 ml of hydrofluoric acid were added to the stock solution aliquots before diluting to volume with 5% (v/v) hydro-

chloric acid. For each digestion matrix, three orders of magnitude were covered per element, with four calibration standards per decade.

Atomic absorption measurements

Each run involved a series of atomizations as follows. First, 5—10 atomizations of a distilled water blank were followed by a single atomization of each of the calibration standards. Then the manganese nodule samples, the water blank, and the calibration standards were atomized several times each in a somewhat random sequence. No more than 99 atomizations were included in any one run.

From 10—15 repeat atomizations of the distilled water blank, the standard deviation of the baseline absorbance, S_B, was calculated. The detection limits, defined as $3S_B$, as well as the lower limits of determination, defined as $15S_B$, were then measured for the individual elements. Absorbance measurements were made at a height of 1.5 mm above the burner head in a lean flame (air/acetylene volume ratio of 4.2). Each of the sample preparations was analyzed by comparison with the appropriately matrix-matched series of multi-element calibration standards in 2—3 different analytical runs. Thus, reported A-1 and P-1 analyses are based on 6—9 replicate measurements; however the remaining nodule results represent only duplicate measurements.

Additionally, A-1 and P-1 in the high-temperature digestion matrix were analyzed once at each of the varied conditions of air/acetylene ratio and measurement height previously described [16].

RESULTS AND DISCUSSION

Matrix variation

Results for the USGS reference manganese nodules at both dilution factors after high-temperature dissolution are compared in Table 2 to recommended concentrations [14] and i.c.p.e.s. results [15]. Recoveries for the SIMAAC determinations were 100% with ±5% accuracy and ±3% precision for most elements in both A-1 and P-1.

Poorer accuracy and precision for cobalt and nickel in the 2000 factor digest were seen A-1 recoveries of 108 ± 21% and 143 ± 29%, respectively. Accuracy improved considerably for Ni, Co, and K when the 200 factor digest was used. Inaccuracy in the more dilute digest for the three elements was due to imprecision near the detection limit, and for potassium was also due to the insensitivity of the 404.4-nm line. If chemical interferences such as those reported by Korkisch et al. [10, 11] had caused the inaccuracy noted in the more dilute digest, increasing the concentration ten-fold would have increased the error.

Comparable accuracies for Mn, Zn, Cu, and Na at the two dilutions of A-1 and P-1 imply a lack of chemical interferences of analytical consequence for these elements. For zinc and sodium, some improvement of precision was noted when the more concentrated sample solution was used. At the higher

TABLE 2

SIMAAC results for A-1 and P-1 compared to i.c.p. results [15] and recommended concentrations [14] (Measurement at 1.5 nm; air—acetylene volume ratio 4.2)

Element	Results for A-1				Results for P-1			
	SIMAAC				SIMAAC			
	200 dilution	2000 dilution	I.c.p.	Recommended	200 dilution	2000 dilution	I.c.p.	Recommended
Mn	18.3 ± 0.3	17.8 ± 0.2	18.7	18.54	30.4 ± 0.3	29.6 ± 0.6	29.6	29.00
Zn	0.080 ± 0.012	0.062 ± 0.016	0.061	0.0586	0.190 ± 0.013	0.146 ± 0.022	0.164	0.1600
Fe	11.4 ± 0.2	10.4 ± 0.4	10.7	10.72	6.62 ± 0.11	5.55 ± 0.32	6.00	5.78
Cu	0.113 ± 0.001	0.108 ± 0.006	0.121	0.1098	1.24 ± 0.01	1.13 ± 0.01	1.32	1.150
Ni	0.676 ± 0.030	0.684 ± 0.200	0.700	0.6360	1.43 ± 0.03	1.69 ± 0.21	1.56	1.336
Co	0.318 ± 0.003	0.336 ± 0.070	0.348	0.3100	0.230 ± 0.005	0.254 ± 0.052	0.258	0.224
Mg	2.68 ± 0.22	2.93 ± 0.12	3.00	2.87	1.85 ± 0.07	1.81 ± 0.07	2.00	1.99
Ca	8.34 ± 0.15	10.3 ± 0.45	10.5	11.03	0.618 ± 0.017	1.07 ± 0.09	2.14	2.180
Na	0.798 ± 0.007	0.758 ± 0.080	0.846	0.774	1.58 ± 0.03	1.48 ± 0.16	1.67	1.640
K	0. 476 ± 0.026	Not detected	0.510	0.5000	1.05 ± 0.02	0.901 ± 0.17	0.908	1.050
Cr (ppm)	33 ± 12	Not detected	—	24	28 ± 12	Not detected	—	20

concentration, results for magnesium show a lower percent recovery in A-1 (93% vs. 103%) as expected in the absence of lanthanum matrix modification. The accuracy of the magnesium results for P-1 does not change with the dilution factor. For iron, A-1 and P-1 both show high recoveries in the more concentrated digest. Accuracy is still within the ±5% limit for A-1; however, P-1 at the 200 factor dilution in outside this range. A chemical interference is a possible cause, because the calibration standards were a better matrix match for A-1 than for P-1.

Chromium and potassium, not detected in the more dilute digest, are detectable (though below the lower limit of determination) at the 200 factor dilution. Accuracy is acceptable in view of the precision of measurement so close to the detection limit.

These same results and the SIMAAC results for the room-temperature digests of A-1 and P-1 are expressed in Table 3 as percent recovery of recommended concentrations [14]. Results for the room-temperature digest showed no interference from the silicon in this digest. The variations in accuracy found for most elements cannot be attributed to matrix changes, as the between-matrix variation was no greater than the within-matrix imprecision of measurement. Iron is the one exception. For iron, the 2000 factor high-temperature digest provided a more accurate result than the more concentrated solution. Lack of precision for zinc in all three matrices was due to the low intensity of the EIMAC continuum source in the low ultraviolet [19]. The direct spectral overlap of the iron 213.859-nm and zinc 213.685-nm lines, well documented in line-source a.a.s. [20], is insignificant in analysis of manganese nodules, affecting only the round-off error. Correction was not made. Three other spectral interferences identified by using SIMAAC [21] are also insignificant.

TABLE 3

Elemental percentage recoveries from different solutions
(Measurement height 1.5 mm, air—acetylene volume ratio 4.2)

Element	High-temperature digest (2000)		High-temperature digest (200)		High-temperature digest (2000)	
	A-1	P-1	A-1	P-1	A-1	P-1
Mn	96 ± 1	102 ± 2	99 ± 2	105 ± 1	103 ± 1	108 ± 4
Zn	107 ± 25	92 ± 15	120 ± 15	132 ± 7	99 ± 13	93 ± 8
Fe	98 ± 4	97 ± 4	106 ± 2	114 ± 2	108 ± 4	129 ± 5
Cu	99 ± 3	98 ± 1	103 ± 1	107 ± 1	100 ± 3	80 ± 3
Ni	143 ± 29	126 ± 12	107 ± 4	106 ± 2	68 ± 30	88 ± 14
Co	108 ± 21	113 ± 20	103 ± 1	103 ± 2	104 ± 4	112 ± 5
Mg	103 ± 8	95 ± 4	93 ± 4	93 ± 4	102 ± 2	107 ± 11
Ca	94 ± 2	49 ± 8	76 ± 4	28 ± 2	101 ± 3	102 ± 7
Na	98 ± 10	90 ± 11	103 ± 1	96 ± 2	130 ± 17	95 ± 8
K	Not detected	91 ± 19	95 ± 5	100 ± 2	119 ± 5	60 ± 9

TABLE 4

Comparison of SIMAAC and i.c.p. results for the Blake, Caryn, and Gillis nodules

Element	Concentration in solution (ppm)			Element	Concentration in solution (ppm)		
	High-temp. digest[a]	Low-temp. digest[a]	I.c.p.		High-temp. digest[a]	Low-temp. digest[a]	I.c.p.
Mn Blake	65.4	77.9	64.7	Co Blake	0.80	1.07	1.1
Caryn	51.2	51.0	54.3	Caryn	0.81	0.92	1.0
Gillis	35.9	35.4	34.4	Gillis	0.57	0.69	0.70
Zn Blake	0.34	0.34	0.41	Ca Blake	95.0	89.3	82.8
Caryn	0.28	0.32	0.24	Caryn	2.23	7.7	6.4
Gillis	0.21	0.17	0.17	Gillis	15.6	18.1	22.0
Fe[b] Blake	29.6	30.6	27.1	Mg Blake	9.43	9.48	9.11
Caryn	77.3	77.9	80.4	Caryn	5.37	7.65	5.13
Gillis	45.6	44.5	46.0	Gillis	6.37	8.45	6.27
Cu Blake	0.52	0.405	0.36	Na Blake	4.24	4.85	4.37
Caryn	0.53	0.524	0.55	Caryn	5.19	6.08	6.01
Gillis	0.57	0.540	0.60	Gillis	6.67	6.93	6.68
Ni Blake	2.2	2.12	2.6	K Blake	2.64c	2.93[c]	1.94
Caryn	0.71[c]	0.72[c]	1.0	Caryn	3.69[c]	3.28	2.57
Gillis	1.0[c]	0.48[c]	0.85	Gillis	5.48	4.83	5.31

[a]2000 factor dilution. [b]Fe at 248.3 nm and at 302.0 nm; reported value is average of the two lines. [c]Between detection limit and lower limit of quantitative measurement.

Results obtained by SIMAAC and i.c.p.e.s. for the Blake, Caryn, and Gillis nodules are given in Table 4. No precision estimates are given for the SIMAAC values because only two results were obtained per element per nodule. Comparison between the two methods for these nodules shows generally the same accuracy for the SIMAAC results as seen for the nodules A-1 and P-1.

Compromise analytical conditions

It was previously found that changes in the measurement height and in the flame fuel:air ratio had no significant effect on the accuracy of Co, Cu, Fe, K, Mn, Na, Ni, and Zn determinations in several geological samples prepared by high-temperature digestion [16]. As Table 1 demonstrates, however, the manganese nodule matrix is markedly different from many geological matrices. For this reason, the same study was undertaken for A-1 and P-1 analyses, using the 2000 factor dilution with high-temperature digestion. Again, no significant effect on the accuracy of the results for these elements was found as parameters were varied.

The authors thank P. A. Aruscavage and A. F. Dorrzapf, Jr. for permission to include their i.c.p. data, and for providing a portion of the Atlantic Ocean nodules submitted to them by the Branch of Marine Geology. They also thank D. W. Golightly, F. E. Lichte, and T. C. O'Haver for helpful reviews of the manuscript.

REFERENCES

1 J. M. Harnly, T. C. O'Haver, B. Golden and W. R. Wolf, Anal. Chem., 51 (1979) 2007.
2 J. M. Harnly and T. C. O'Haver, Anal. Chem., 53 (1981) 1291.
3 J. M. Harnly, N. J. Miller-Ihli and T. C. O'Haver, J. Autom. Chem., 4 (1982) 54.
4 R. A. Horne, The Chemistry of the Environment, Wiley-Interscience, New York, 1978, pp. 562—563.
5 E. M. Magee, H. J. Hall and G. M. Varga, Potential Pollutants in Fossil Fuels, Esso Research and Engineering, Linden, N.J. (EPA Report #EPA-R2-73-249), 1973.
6 J. P. Riley and R. Chester (Eds.), Chemical Oceanography, Academic Press, New York, 1976, pp. 240—241.
7 A. T. Zander, Am. Lab., 11 (1976) 11.
8 F. Vajda, Anal. Chim. Acta, 128 (1981) 31.
9 J. M. Harnly and T. C. O'Haver, Anal. Chem., 49 (1977) 2187.
10 J. Korkisch, H. Huber, I. Steffan, G. Arrhenius, M. Fisk and J. Frazer, Anal. Chim. Acta, 83 (1976) 83.
11 J. Korkisch and A. Sorio, Anal. Chim. Acta, 79 (1975) 207.
12 J. Korkisch, I. Steffan and G. Arrhenius, Anal. Chim. Acta, 94 (1977) 237.
13 J. Korkisch, I. Steffan and M. B. Fisk, Anal. Chim. Acta, 108 (1979) 63.
14 F. J. Flanagan and D. Gottfried, USGS Professional Paper 1155, U.S. Geological Survey, Reston, VA, 1980.
15 P. A. Aruscavage and A. F. Dorrzapf, Jr., written communication, 1980.
16 J. M. Harnly, J. S. Kane, N. J. Miller-Ihli and T. C. O'Haver, Federation of Analytical Chemistry and Spectroscopy Societies, paper 287, Philadelphia, PA, Sept. 1981.
17 H. Uchido, T. Uchido and I. Chuzo, Anal. Chim. Acta, 108 (1979) 87.
18 P. G. Jeffery, Chemical Methods of Rock Analysis, Pergamon, Oxford, 1970.
19 R. L. Cochran and G. M. Hieftje, Anal. Chim. Acta, 49 (1977) 2040.
20 W. R. Kelly and C. B. Moore, Anal. Chem., 45 (1973) 1274.
21 N. J. Miller-Ihli, T. C. O'Haver and J. M. Harnly, Anal. Chem., 54 (1982) 799.

Analytica Chimica Acta, 139 (1982) 307—313
Elsevier Scientific Publishing Company, Amsterdam — Printed in The Netherlands

Short Communication

SUBSTITUENT EFFECTS ON COMPLEXATION AND EXTRACTION OF ALKALI METALS WITH CHROMOGENIC CROWN ETHERS

B. P. BUBNIS, J. L. STEGER, Y. P. WU, L. A. MEYERS and G. E. PACEY*
Department of Chemistry, Miami University, Oxford, OH 45056 (U.S.A.)
(Received 17th July 1981)

Summary. The placing of chromogenic tags on crown ethers makes it possible to incorporate the natural selectivities of crown ethers into extractions with detection by visible spectrophotometry. The structures of these reagents include a monobasic amine linkage which, upon dissociation and complexation, gives a color change. The parent compound, 2″,4″,6″-trinitrophenyl-4′-aminobenzo-15-crown-5, provides a linear range for 10—800 ppm potassium ion in the presence of >2000 ppm sodium ion. Changes in substituents on the chromophore (e.g., nitrile or trifluoromethyl for nitro) and the effects of these substituents on the visible spectra, extraction constants, equilibrium constants, the wavelength of maximum absorption, and the molar absorptivity are presented. Application of a compound to the determination of potassium ion in blood serum is reported.

Crown ethers have been used for numerous applications including phase-transfer systems [1], ion-selective electrodes [2], chromatographic resins [3], and the introduction of naked anions [4] in organic solutions. The attachment of a chromophoric tag to a crown ether [5, 6] has demonstrated that solution spectrophotometry of alkali metals is possible as an alternative to flame photometry, atomic absorption, and ion-selective electrodes. The general structure of the substituted crown ethers tested here is illustrated in Table 1 which summarizes those compounds that have been synthesized to incorporate the monobasic amine linkage between the benzo-15-crown-5 ether and the chromophore. An investigation into this type of system rather than the azo-type linkages previously reported [7] seemed to be preferable, because the monobasic amine linkage has greater aqueous solubility as well as larger shifts in the wavelength of maximum absorption after complexation.

In an extraction system involving such ligands, the protonated amine species (HL) dissociates when introduced into a pH-buffered aqueous phase, and the L^- species then reacts with the alkali metal ions to give a neutral species that is extracted into an organic layer. The visible absorption spectrum of L^- also exhibits a bathochromic shift relative to HL because of increased conjugation. A change in molar absorptivity (ϵ) also accompanied the shift in the wavelength of maximum absorption (λ_{max}). The linear range for compound 1 (Table 1) has been reported to be 10—800 ppm K^+ in the presence of >2000 ppm Na^+ [5].

0003-2670/82/0000-0000/$02.75

TABLE 1

Substitutions made on the chromophore of chromogenic crown ethers

Compound	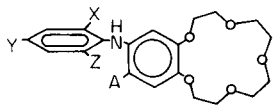			
	A	X	Y	Z
1	H	NO_2	NO_2	NO_2
2	H	NO_2	CN	NO_2
3	H	NO_2	CF_3	NO_2
4	H	NO_2	NO_2	CF_3
5	H	NO_2	NO_2	H
6	NO_2	NO_2	NO_2	NO_2 [7]
7	Br	NO_2	NO_2	NO_2 [7]

Because it was found that deprotonation was a necessary requirement for the extraction of alkali metals, compound 6 was synthesized [6] in an attempt to lower the pK_a of the monobasic amine proton. While the addition of the nitro group at the 5′-position did lower the pK_a of the amine proton from 10.55 to 8.63 and improved the extraction constants (K_{ex}) somewhat, the selectivity of the reagent was lessened.

It was believed that by changing the substitution on the chromophore, it would be possible to increase the spectral separation of the HL and L^- species, making the effective molar absorptivity for L^- greater and improving the reagent sensitivity. In addition, changes in pK_a and the formation constants of ML and MHL were expected.

Experimental

The synthesis of compounds 1—7 (Table 1) has been described [6, 9]. All reagents were used as received. Infrared (i.r.) spectra were obtained on a Perkin-Elmer 683 instrument. Nuclear magnetic resonance (n.m.r.) spectra were recorded on a Varian 360A. Ultraviolet—visible spectra were determined with a Hewlett-Packard 8450A spectrophotometer. All pH values were measured with a Corning 12 pH meter. All water for dilutions was deionized and distilled with a Barnstead glass-still. Atomic absorption measurements for blood serum determinations were made on a Perkin-Elmer 560 instrument. All n.m.r. and i.r. spectra for compounds 2[8], 3 and 4[9] are consistent. Compound 5,2″,6″-dinitrophenyl-4′-aminobenzo-15-crown-5, showed the expected n.m.r. and i.r. spectra; the calculated elemental composition is 53.45% C, 5.15% H, 9.3% N, compared with 53.3% C, 5.2% H, 9.1% N found (Galbraith Laboratories).

Visible spectra. Visible spectra were obtained by dissolving a weighed quantity of the crown ether in either acetonitrile/water or dioxane/water mixtures that contained a fixed concentration of a lithium salt. Two spectra were recorded, at pH 2 and at another pH necessary for complete dissociation of the amine proton.

Determination of extraction constants and complex stoichiometry. An aliquot (5 ml) of 0.1 M alkali metal solution was extracted using 5 ml of chloroform solution which contained varying crown ether concentrations and a constant buffer concentration. The absorption spectrum of the chloroform layer was recorded between 200 and 800 nm. The extraction constant, K_{ex}, and the apparent molar absorptivity, $\Delta\epsilon$, were then calculated using the equations of Nakamura et al. [6]. A second experiment, in which the pH and metal concentration were constant and the concentration of the crown ether reagent in the organic phase was varied, produced data that were used to calculate the ratio of crown ether to metal in the complex.

Determination of K_a, K_{ML} and K_{MHL}. Approximately 2.5×10^{-4} M crown ether was dissolved in a 25% dioxane/water or 40% acetonitrile/water solution; 10 ml of this solution was diluted to 25 ml with deionized water. The K_a value can be experimentally determined, according to the equation $K_a^{app} = K_a\,(1 + K_{ML}\,[M^+])/(1 + K_{MHL}\,[M^+])$, if the dilute solution also contains a cation which will not be complexed by the crown. For the compounds reported, $K_a^{app} = K_a$ when 0.01 M LiCl is used. Once K_a has been determined, K_a', K_{ML}, and K_{MHL} can be determined by varying the concentrations of an alkali metal salt (KCl at 0.1, 0.08, and 0.06 M) present in solution. The absorbance was measured at the wavelength of maximum apparent molar absorptivity, $\epsilon_{ML} - \epsilon_{HL}$, at varying $[H^+]$; pH was adjusted with lithium hydroxide or hydrochloric acid. Linear regression analysis was used and K_a^{app}, K_{ML}, and K_{MHL} were determined from appropriate plots [10].

Linear range and sodium ion interference. The linear range was determined by mixing 5 ml of 2×10^{-3} M crown ether in chloroform, which contained 1 M triethylamine, with 5 ml of a solution containing 0—800 ppm potassium ion. A portion (1 ml) of the collected organic layer was diluted with the chloroform/1M triethylamine solution to 25 ml and the absorbance was measured at the appropriate wavelength. Sodium ion interference was studied by determining a constant concentration of potassium ion with increasing amounts (0—3000 ppm) of sodium ion present.

Potassium level in blood serum. Blood serum (1 ml), 2 ml of 100% ethanol, and 2 ml of deionized water were mixed and centrifuged. The liquid was decanted into a separatory funnel and shaken with 5 ml of 2×10^{-3} M compound 4 in chloroform/1 M triethylamine for 5 min. Standards were prepared in the same manner, substituting 1 ml of K^+ stock solution for the serum. After phase separation, 1 ml of the organic phase was diluted to 10 ml with the chloroform/1 M triethylamine solution. The absorbances of the serum and standards were measured at 480 nm.

Results and discussion

Visible spectra. Table 2 summarizes the changes in λ_{max} and ϵ. The protonated HL species undergo a bathochromic shift on dissociation because of increased conjugation of the chromophoric system. The data also indicate that the largest shifts ($\Delta\lambda_{max}$) were observed when substitutions were

TABLE 2

Wavelength of maximum absorption (λ_{max}) and molar absorptivities (ϵ, in l mol^{-1} cm^{-1}) of chromogenic crown ethers

Compound	HL		ML		$\Delta\lambda_{max}$ (nm)
	λ_{max} (nm)	ϵ	λ_{max} (nm)	ϵ	
1 [6]	390	13000	445	20000	55
2	420	11000	550	8500	130
3	425	6400	585	4400	150
4	380	13250	460	20800	80
5	373	14760	416	14822	43

made at the 4''-position; substitutions at the 2''- and 6''-positions affect $\Delta\lambda_{max}$ less. Larger molar absorptivities were observed when the nitro group was in the 4'' position. Substitution of nitrile or trifluoromethyl at the *p*-position decreased the molar absorptivities.

Extraction constants and complex stoichiometry. Examination of the absorption spectra and pK_a values (Table 3) suggests that compounds 1, 2 and 4 should have potential for quantifying potassium ions. The extraction constants for compounds 1 and 4 indicate similar efficiencies. That compound 2 was less efficient as an extractant can be attributed to the increased ionic strength of the extraction system which included lithium hydroxide instead of triethylamine as a buffer. The pK_{ex} values for potassium and rubidium ions in all cases differed by only an order of magnitude but this should not cause problems in most samples.

The stoichiometry of the complex seems to depend on the buffer system employed. The use of triethylamine as buffer resulted in 1:1 or 1:2 metal—ligand complexes. When lithium hydroxide was used, the stoichiometry was 1:1. The increase in ligand content in the complex when triethylamine is used indicates that triethylamine is involved in the complex. This has been observed with other chromogenic crown ethers [5]. The extent and mechanism of this interaction is not completely understood.

Aqueous complexation. The pK_a values of compounds 1—5 are presented in Table 3. The monobasic amine proton could be dissociated easily from three reagents (1, 2 and 4). The buffer system necessary to attain deprotonation could be established by using an amine with a pK_a greater than the pK_a of the reagent. Compounds 3 and 5 with pK_a values greater than 12 were not easily deprotonated, and a suitable buffer system for complete deprotonation could not be found. The pK'_a values for compounds 1, 2 and 4 were less than the respective pK_a values, indicating that the alkali metal ion has some electron-withdrawing effects on the 4'-amine proton.

Table 3 summarizes the aqueous complexation of compounds 1, 2, and 4. In all cases, K_{MHL} is less than K_{ML}, as would be expected, because of

TABLE 3

Equilibrium constants for the chromogenic crown ethers

Compound	K_a	pK_a	pK'_a	K_{ML}	$\log K_{ML}$	K_{MHL}	$\log K_{MHL}$	pK_{ex}	
								K^+	Rb^+
1	2.818×10^{-11}	10.55 [6]	—	—	—	—	—	7.55 [6]	8.5 [6]
	3.388×10^{-11}	10.47 ± 0.01	9.543	80.54	1.9 ± 0.10	9.54	0.98 ± 0.21	7.5	8.5
2	3.548×10^{-12}	11.45 ± 0.09	11.017	22.52	1.34 ± 0.09	8.32	0.91 ± 0.074	9.44	10.4
3	4.168×10^{-13}	12.38 ± 0.62	—	—	—	—	—	—	—
4	6.025×10^{-11}	10.22 ± 0.06	9.522	131.3	2.11 ± 0.06	26.34	1.41 ± 0.076	7.5	8.3
5	1.698×10^{-13}	12.77 ± 0.1	—	—	—	—	—	—	—
A[a]	—	—	—	—	3.44	—	—	—	—
B[b]	—	—	—	—	1.92	—	1.62	—	—

[a]Benzo-15-crown-5. [b]4′-Picrylaminobenzo-18-crown-6 [10].

the greater affinity of an alkali metal cation for the deprotonated reagent. The formation of an intermolecular ion-pair is more favorable than the electrostatic attraction exhibited by a protonated crown ether. The formation constants in Table 3 suggest that reagent 4 most readily forms a metal—ligand complex in both the protonated (K_{MHL}) and deprotonated (K_{ML}) species; thus compound 4 with a trifluoromethyl group at the 6″-position is potentially the best extraction reagent. Reagent 2 with a CN group at the 4″-position has the least favorable formation constants.

The formation constants for potassium complexes of chromogenic crown ethers can be compared to these for unmodified crown ethers in Table 3. Reagent 4 exhibits better stability toward potassium ions than reagent 1 and its 18-crown-6 analog. It should also be noted that the placement of a chromophoric tag on benzo-15-crown-5 seems to improve the selectivity toward K^+ over Na^+. This enhanced selectivity was evident in Na^+ interference studies.

Linear range and sodium ion interference. The linear ranges were 10—300, 10—600, and 5—700 ppm K^+ for reagents 1, 2, and 4, respectively. Takagi et al. [5] extended the linear range for compound 1 from 10 to 800 ppm K^+ by using an additional equation. Reagents 2 and 4 exhibit adequate linear ranges for most analytical procedures. Sodium ion interference levels for compounds 1, 2, and 4 were 680, 2200, and 3000 ppm Na^+, respectively.

A typical calibration curve for the determination of potassium with reagent 4 exhibited a linear range of 5—700 ppm. The equation for the line was $A = (7.62 \pm 0.1) \times 10^{-4} C_{K^+ppm} - (7.04 \pm 3) \times 10^{-4}$ with standard error of 0.005 and correlation coefficient of 0.9974.

Potassium ion levels in blood serum. The results for blood serum by the colorimetric crown technique were similar to the results obtained by atomic absorption spectrometry of the same sample. Four serum samples yielded average values of 149, 194, 141, and 109 ppm K^+ by the extraction—colorimetric procedure compared with 155, 196, 150, and 115 ppm K^+ by atomic absorption spectrometry. Relative standard deviations for three measurements on each sample ranged between 3 and 5%. The values obtained fall within the normal 137—207 ppm K^+ range for human blood serum [11].

Conclusion

The colorimetric crown ether technique for potassium determination is a viable alternative to conventional methods at the ppm level. The effect of changing the substituents on the chromogenic tag appears predominantly in the spectral character of the particular reagent. Reagent 4 is a better reagent than the model reagent 1, while reagent 2 is somewhat poorer. The addition of a trifluoromethyl group improves aqueous solubility.

The authors thank Miami University Faculty Research Committee and Sigma Xi for support of this project.

REFERENCES

1 S. Shinkai, et. al., J. Am. Chem. Soc., 103 (1981) 111.
2 See e.g., W. E. Morf and W. Simon, in H. Freiser (Ed.), Ion-Selective Electrodes in Analytical Chemistry, Plenum Press, New York, 1978, p. 211.
3 K. Funazo, K. Kusano, M. Tamaka and T. Shono, Anal. Lett., 13A (1980) 741.
4 C. L. Liotta, E. E. Grisdale and H. P. Hopkins, Tetrahedron Lett., (1975) 4205.
5 M. Takagi, H. Nakamura and K. Ueno, Anal. Lett., 10 (1977).
6 H. Nakamura, M. Takagi and K. Ueno, Talanta, 26 (1978) 921.
7 J. P. Dix and F. Vogtle, Angew. Chem., 90 (1978) 893.
8 G. E. Pacey and B. P. Bubnis, Anal. Lett., 13 (1980) 1085.
9 G. E. Pacey, B. P. Bubnis and Y. P. Wu, Analyst, 106 (1981) 636.
10 H. Nakamura, M. Takagi and K. Ueno, Anal. Chem., 52 (1980) 1668.
11 N. W. Tietz, in N. W. Tietz (Ed.), Fundamentals of Clinical Chemistry, 2nd edn., 1976.

Analytica Chimica Acta, 139 (1982) 315—321
Elsevier Scientific Publishing Company, Amsterdam — Printed in The Netherlands

Short Communication

ROOM-TEMPERATURE PHOSPHORESCENCE OF SELECTED AROMATIC CARBOXYLIC ACIDS ADSORBED ON SILICA GEL AND POLYACRYLIC ACID—SODIUM CHLORIDE MIXTURES

ROBERT J. HURTUBISE* and GEORGE A. SMITH[a]

Department of Chemistry, The University of Wyoming, Laramie, WY 82071 (U.S.A.)

(Received 14th December 1981)

Summary. Several aromatic carboxylic acids give room-temperature phosphorescence when adsorbed on silica gel chromatoplates that contain a polymeric binder. Terephthalic acid is used as a model compound to investigate the interactions with such chromatoplates and various polyacrylic acid—sodium chloride mixtures. The results indicate that under some conditions, hydrogen bonding appears to be operative, whereas under other conditions room-temperature phosphorescence can be detected without hydrogen bonding interactions.

Room-temperature phosphorimetry (r.t.p.) is a rapidly developing analytical technique [1—12]. A review covering the physical aspects of room-temperature phosphorescence and practical analytical considerations has been published [13, 14]. In addition, the instrumentation for r.t.p., some interactions responsible for room-temperature phosphorescence, and analytical applications have been discussed in detail [15].

In this communication, the room-temperature phosphorescence of some aromatic carboxylic acids is considered. The mechanisms of interactions of terephthalic acid with silica gel chromatoplates that contain a polymeric binder and with polyacrylic acid—NaCl mixtures are discussed. A previously reported mechanism [16] for inducing room-temperature phosphorescence from aromatic carboxylic acids adsorbed on silica gel chromatoplates is apparently incorrect.

Experimental

Apparatus. Room-temperature phosphorescence measurements at appropriate excitation and emission wavelengths were obtained with a modified Schoeffel SD3000 spectrodensitometer [17]. Room-temperature phosphorescence excitation and emission spectra were obtained with a Farrand MK-2 spectrofluorimeter fitted with a phosphorescence rotary chopper and a thin-layer chromatogram scanner. With the MK-2, a slit program of 5 nm, 5nm (entrance) and 5 nm, 5 nm (exit) was used. In addition, the largest slit

[a]National Science Foundation Undergraduate Research Participant, Cameron University, Lawton, OK 73505, U.S.A.

(2.0 mm) provided by the manufacturer was used in the optical head just below the chromatoplate. Ultraviolet absorption spectra were obtained with a Hitachi 100-80 spectrophotometer. The pH values were measured with an Orion model 501 pH meter and glass—calomel electrodes.

Reagents. Ethanol was purified by distillation, and SpectAR grade dimethylformamide (Mallinckrodt, St. Louis, MO) was used. All the aromatic carboxylic acids were recrystallized from ethanol prior to use. The aluminum-backed silica gel chromatoplates (EM Laboratories, Elmsford, New York) and plastic-backed chromatoplates (Brinkmann Sil-G, Westbury, New York) employed were developed in ethanol before use, to concentrate impurities at one end. Polyacrylic acid (Scientific Polymer Products, Ontario, New York) and column-chromatography silica gel (mesh size 100—200; Grace-Davison Chemical, Baltimore, MD) were used.

Solutions for r.t.p. Standard solutions of terephthalic acid (1 $\mu g\ \mu l^{-1}$) were prepared in ethanol—dimethylformamide (4 + 1) and in ethanol—water (1 + 1). The solutions were warmed gently to hasten dissolution. The solutions were spotted on the chromatoplates as described previously [17]. The spotted chromatoplates were usually dried for 30 min at 100° C prior to the phosphorescence measurements. Terephthalic acid was excited at 290 nm and the phosphorescence was measured at 415 nm with the spectrodensitometer [16, 17]. Coumarin-3-carboxylic acid was treated similarly except that ethanol was used as solvent, and it was excited at 350 nm and the phosphorescence was measured at 460 nm.

Polyacrylic acid—NaCl mixtures. Mixtures of 1% (w/w) polyacrylic acid in NaCl were prepared and mixed thoroughly to assure homogeneity. Terephthalic acid was adsorbed onto this mixture by the following procedure. An aliquot (20 μl) of ethanol—water (1 + 1) was introduced into a 40 × 4-mm test tube, followed by 2 μl of an appropriate terephthalic acid solution and a fixed amount of 1% polyacrylic acid—NaCl (~10 mg). The contents were mixed well, and the solvent was evaporated at 100° C. After the samples were dried, the powders were transferred to depressions in a blackened brass plate [18]. The brass plate with samples was dried and then the phosphorescence was measured with the densitometer.

pH adjustment. Samples of polyacrylic acid were dissolved in water and the pH was adjusted to 7.0 with 0.01 M NaOH. Terephthalic acid was dissolved in ethanol—water (1 + 1) before pH adjustment in the same way. The solvents were evaporated to dryness and the resulting residues were used for r.t.p.

Results and discussion

Compounds giving room-temperature phosphorescence. Coumarin-3-carboxylic acid, 4-biphenylcarboxylic acid, 4-biphenylacetic acid, indole-5-carboxylic acid, 4-hydroxy-3-methoxybenzoic acid, and xanthrene-9-carboxylic acid gave observable phosphorescence when adsorbed on EM silica gel chromatoplates which contained a salt of polyacrylic acid as binder.

The phosphorescence was measured with a spectrodensitometer or viewed after excitation with a u.v. hand lamp [17]. Details on the use of these chromatoplates to induce room-temperature phosphorescence from nitrogen heterocycles have been reported [1, 11, 16, 17, 19]. For conditions used in this work, several aromatic carboxylic acids did not give the phosphorescence (Table 1).

Results with acidic, basic, and neutral conditions. It was previously shown that room-temperature phosphorescence could be obtained from terephthalic acid spotted from an ethanol solution onto EM silica gel chromatoplates that contain a salt of polyacrylic acid as a binder [16]. Table 2 gives the relative intensities from terephthalic acid under several conditions. It can be seen that the phosphorescence is completely quenched when spotted from 0.1 M HBr. Also, samples spotted from NaBr solutions and NaOH solutions gave smaller signals than those from neutral solutions. The 0.1 M NaOH solution gave a white precipitate and thus could not be used to obtain accurate data. Most of the samples from neutral solutions gave strong signals; the variation in the relative intensity from these solutions was mainly caused by plate-to-plate variation. Terephthalic acid spotted from 0.1 M HCl gave a slightly stronger signal than a sample spotted from a neutral solution. Coumarin-3-carboxylic acid gave similar results, and most of the samples spotted from neutral solutions yielded strong phosphorescence. Samples spotted from the hydrochloric acid solutions yielded signals about twice as strong as those from neutral solutions. A 0.1 M NaOH solution of coumarin-3-carboxylic acid gave a yellow precipitate and could not be used to obtain accurate data.

TABLE 1

Compounds not showing room-temperature phosphorescence on EM silica gel chromatoplates[a]

4-Aminosalicylic acid	*m*-Hydroxycinnamic acid
2,6-Dihydroxybenzoic acid	2,3-Pyrazinedicarboxylic acid
4-Aminophthalic acid	3,5-Pyrazoledicarboxylic acid
p-Hydroxyphenylacetic acid	*p*-Phenyloxybenzoic acid
4-Amino-3-methylbenzoic acid	2-Indolebutyric acid
9-Hydroxy-9-fluorenecarboxylic acid	Benzoic acid
Anthranilic acid	3-(*p*-Hydroxyphenyl)propionic acid
1-Methylindole-2-carboxylic acid	*o*-Hydroxybenzoic acid
p-Nitrobenzoic acid	Salicylic acid/sodium salt
Isophthalic acid	2,5-Pyridinecarboxylic acid
3,5-Pyrazinedicarboxylic acid	Salicylic acid
	4-Dimethylaminobenzoic acid

[a]Samples of either 1.0 μg or 0.1 μg spotted from ethanol solutions and then dried for 30 min at 100° C. Samples either visually observed or measured with a spectrodensitometer.

TABLE 2

Relative intensities (RI) for terephthalic acid adsorbed on silica gel chromatoplates[a]

Condition	RI	Condition	RI
Neutral	3.0	Neutral	3.4
0.1 M HCl	3.4	0.01 M NaOH	1.0
0.01 M HCl	2.9		
Neutral	3.6	Neutral	3.4
0.1 M HBr	0.0	0.1 M NaBr	1.6
0.01 M HBr	1.1	0.01 M NaBr	2.8

[a]Relative intensities compared to the 0.01 M NaOH sample. A 1.0-μg sample was spotted from ethanol—dimethylformamide (1 + 1) solution and then dried at 100° C for 45 min.

Interactions in room-temperature phosphorescence. Terephthalic acid was used as a model compound because it was investigated previously by r.t.p. [16]. The proposed mechanism of interaction was hydrogen bonding of the carboxyl groups of terephthalic acid with silanol hydroxyl groups of the silica gel chromatoplate. Because it was recently found that a salt of polyacrylic acid was present in these chromatoplates and polyacrylic acid was largely responsible for inducing room-temperature phosphorescence from nitrogen heterocycles [1], it was important to re-examine the previously reported mechanism for terephthalic acid.

Neutral, basic (0.1 M), and acidic (0.1 M) terephthalic acid and coumarin-3-carboxylic acid solutions were adsorbed in duplicate on Brinkmann Sil-G chromatoplates and Grace column-chromatography silica gel and then dried. The Brinkmann Sil-G chromatoplates were known to contain a binder other than polyacrylate [1]. The Grace silica gel contained no binder. If silanol hydroxyl groups were responsible for inducing the phosphorescence from terephthalic acid, then the Grace silica gel would induce a signal. Measurements with the spectrodensitometer showed that little or no phosphorescence was obtained from terephthalic acid or coumarin-3-carboxylic acid adsorbed on either support under all conditions tested. The lack of phosphorescence from the two carboxylic acids on the Grace silica gel indicated that hydrogen bonding of the carboxyl groups with silanol hydroxyl groups is not the mode of interaction which induces the phosphorescence. The results with the Brinkmann Sil-G chromatoplates show that the combination of binder in the chromatoplates and the silica gel induce little phosphorescence.

Solid-surface room-temperature phosphorescence excitation and emission spectra, solution low-temperature phosphorescence excitation and emission spectra, and solution u.v. absorption spectra permitted no specific conclusions to be drawn because the differences in the spectra were minor.

Polyacrylic acid—sodium chloride mixtures. Because the chromatoplates that induced room-temperature phosphorescence from terephthalic acid con-

tained a salt of polyacrylic acid, mixtures of polyacrylic acid and NaCl were investigated. Two polyacrylic acid—NaCl mixtures, one containing unneutralized and one containing neutralized polyacrylic acid were examined, along with the dianion of terephthalic acid. The data obtained (Table 3) indicate that polyacrylic acid—NaCl mixtures induce phosphorescence from terephthalic acid. In addition, because the EM silica gel chromatoplates contained a salt of polyacrylic acid, the evidence in Table 3 and the results discussed earlier for Grace silica gel, strongly suggest that the salt of polyacrylic acid is responsible for inducing the phosphorescence. In other experiments, it was shown that terephthalic acid adsorbed only on sodium chloride or only on polyacrylic acid from neutral, acidic (0.1 M HCl), and basic (0.1 M NaOH) solutions gave little or no phosphorescence. It was observed previously for benzo[f]quinoline that only mixtures of polyacrylic acid and silica gel or polyacrylic acid and sodium chloride induced strong phosphoresence [1]. The role of sodium chloride and silica gel is presently under investigation.

The data in Table 3 suggest several modes of interaction of terephthalic acid and its dianion with polyacrylic acid, and with the sodium salt of polyacrylic acid. Terephthalic acid should form hydrogen bonds with polyacrylic acid both in the initial "wet" state and final dry state. Its dianion should react to some extent with polyacrylic acid in the "wet" state to form terephthalic acid. Polyacrylic acid behaves like an aliphatic carboxylic acid and can be readily titrated with a solution of sodium hydroxide [20]. It is possible, depending on the extent of the reaction of the dianion with polyacrylic acid, that a mixture of terephthalic acid, the dianion and monoanion would remain on the dried surface with various combinations of hydrogen bonds being formed. Terephthalic acid added to the sodium salt of polyacrylic acid, again in the "wet" state, could react with this sodium salt to form the monoanion and/or dianion. In the dry state, there could be a mixture of terephthalic acid, the monoanion and dianion, with various combinations of hydrogen bonds. For the final case (Table 3) in which the dianion was added to the sodium salt of polyacrylic acid, a relatively high phosphorescence signal was obtained. This is surprising because the dianion would not give an acid—base reaction with the sodium salt of polyacrylic acid in the "wet" state and no hydrogen bonds can be formed. Von Wandruszka

TABLE 3

Relative intensities (RI) for terephthalic acid and its dianion adsorbed on polyacrylic acid—NaCl mixtures[a]

Polyacrylic acid—NaCl	RI	Sodium salt of polyacrylic acid—NaCl	RI
Acid	1.3	Acid	1.0
Dianion	2.8	Dianion	2.4

[a] 2 μg of terephthalic acid adsorbed from ethanol—water (1 + 1) solution.

and Hurtubise [8] have shown that the anion of *p*-aminobenzoic acid has a strong affinity for sodium acetate, and room-temperature phosphorescence can be observed from *p*-aminobenzoate adsorbed on sodium acetate. In this work, no phosphorescence was observed from terephthalic acid adsorbed on sodium acetate under a variety of conditions.

The results of this and earlier work [8] do not allow a simple interaction mechanism to be proposed for all the conditions studied. While hydrogen bonding appears to be the main interaction holding the compound rigid, for neutral terephthalic acid adsorbed on polyacrylic acid—NaCl, it cannot explain the dianion adsorbed on the sodium salt of polyacrylic acid—NaCl mixture. Niday and Seybold [21] proposed that various salts or sugars packed into filter paper could inhibit internal molecular motions of the phosphorescence compound and thus enhance room-temperature phosphorescence. This may occur with the terephthalate dianion adsorbed on the sodium salt of the polyacrylic acid—NaCl mixture. However, as mentioned above, terephthalic acid gives essentially no phosphorescence when adsorbed on sodium acetate. If a simple "matrix packing" mechanism were occurring with sodium acetate, e.g., protecting terephthalic acid from collisions with oxygen, then room-temperature phosphorescence should have been observed.

Some practical implications of the results in Table 3 are important. Obviously, a single species should be adsorbed. Terephthalic acid adsorbed on polyacrylic acid—NaCl should be in the form of the diprotic acid. Its dianion adsorbed on the sodium salt of polyacrylic acid should be present as the dianion. With the EM silica gel chromatoplates that contain a salt of polyacrylic acid, acidic solutions of aromatic carboxylic acids should be spotted, so that the polyacrylate will be converted to the acid and only the acid form of the aromatic carboxylic acid will be adsorbed. Table 2 shows that terephthalic acid spotted from a 0.1 M HCl solution gave the largest signal on a particular plate.

The authors thank S. M. Ramasamy for obtaining some of the experimental data. This work was supported by the Department of Energy (Office of Basic Energy Sciences) under contract No. DE-AC02-80ER10624 and the National Science Foundation, Undergraduate Research Participation Grant No. SPI-8026276.

REFERENCES

1 C. D. Ford and R. J. Hurtubise, Anal. Chem., 52 (1980) 656.
2 R. A. Paynter, S. L. Wellons and J. D. Winefordner, Anal. Chem., 46 (1974) 736.
3 R. T. Parker, R. S. Freedlander, E. M. Schulman and R. B. Dunlap, Anal. Chem., 52 (1979) 1921.
4 T. Vo-Dinh and J. R. Hooyman, Anal. Chem., 51 (1979) 1915.
5 M. L. Meyers and P. G. Seybold, Anal. Chem., 51 (1979) 1609.
6 E. M. Schulman and R. T. Parker, J. Phys. Chem., 81 (1977) 1932.

7 C. G. de Lima and E. M. Nicola, Anal. Chem., 50 (1978) 1658.
8 R. M. A. von Wandruszka and R. J. Hurtubise, Anal. Chem., 49 (1977) 2164.
9 E. L. Bower and J. D. Winefordner, Anal. Chim. Acta, 102 (1978) 1.
10 L. J. Cline Love, M. Skrilec and J. G. Habarta, Anal. Chem., 52 (1980) 754.
11 R. J. Hurtubise, Talanta, 28 (1981) 145.
12 R. J. Hurtubise and R. A. Dalterio, Am. Lab., 13 (1981) 58.
13 R. T. Parker, R. S. Freedlander and R. B. Dunlap, Anal. Chim. Acta, 119 (1980) 189.
14 R. T. Parker, R. S. Freedlander and R. B. Dunlap, Anal. Chim. Acta, 120 (1980) 1.
15 R. J. Hurtubise, Solid Surface Luminescence Analysis: Theory, Instrumentation, Applications, Dekker, New York, 1981, Ch. 3, 5, 7.
16 C. D. Ford and R. J. Hurtubise, Anal. Chem., 50 (1978) 610.
17 C. D. Ford and R. J. Hurtubise, Anal. Chem., 51 (1979) 659.
18 R. M. A. von Wandruszka and R. J. Hurtubise, Anal. Chem., 48 (1976) 1784.
19 C. D. Ford and R. J. Hurtubise, Anal. Lett., 13 (1980) 485.
20 K. J. Saunders, Organic Polymer Chemistry, Chapman and Hall, London, 1973, p. 121.
21 G. T. Niday and P. G. Seybold, Anal. Chem., 50 (1978) 1577.

Analytica Chimica Acta, 139 (1982) 323—327
Elsevier Scientific Publishing Company, Amsterdam — Printed in The Netherlands

Short Communication

THE SUITABILITY OF A FLAME ATOMIZER IN A VOIGT EFFECT OPTICAL FILTER

G. S. JOLLY and R. STEPHENS*

Trace Analysis Research Centre, Department of Chemistry, Dalhousie University, Halifax, N.S. B3H 4J3 (Canada)

(Received 6th August 1981)

Summary. A Voigt effect optical filter is described which uses a small flame as a tuning device. The filter selectively transmits the atomic spectra of the element(s) introduced into the flame. Under favourable conditions, e.g., when an atomic spectrum is isolated from a hollow-cathode emission source, no additional wavelength discrimination is needed. The performance of the system is described for emission and absorption measurements.

Several recent papers have discussed the theory, behaviour and instrumental requirements of magneto-optic rotation (m.o.r.) in atomic vapours [1—7]. Any m.o.r. system is characterized by an optical transmission profile whose maxima occur in the immediate vicinity of the resonance absorption frequencies of the vapour. Because of this behaviour, any m.o.r. cell can function as an optical filter.

A filter of this type, that utilized a sealed electrothermal sodium cell as the tuning element, has been described [8]. The device offered some advantages for quantitative work; specifically, a high resolving power combined with a large optical aperture. Despite these advantages, such a filter is unlikely to be of real use unless it can be easily applied to a variety of elements, and can be switched readily from one element to the next. The present communication describes one method by which this aim might be achieved.

Experimental

Filter design. In the filter, an air—acetylene flame was used as the atomizer, and coarse wavelength selection was provided either by an interference filter or by a Jarrell-Ash 0.25-m monochrometer from which the slits had been removed (Fig. 1). Both arrangements gave a large aperture, compatible with that of a m.o.r. filter, and an optical bandwidth of around 10 nm. There was little to choose between the performance of the interference filters and that of the monochromator, although the flexibility of the latter is an advantage. The interference filter or monochromator can usually be omitted altogether when hollow-cathode sources are used.

Use of a flame atomizer permits the m.o.r. filter to transmit any atomic

0003-2670/82/0000-0000/$02.75

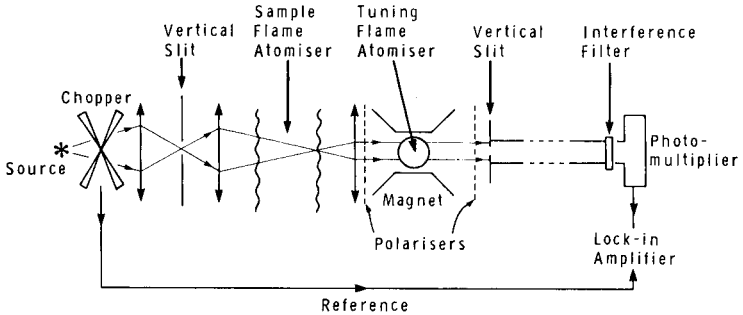

Fig. 1. Block diagram of the filter.

line, or combination of lines, simply by aspirating a solution of the appropriate composition. Because the flame does not atomize a sample, the requirements for path length, atomization efficiency, etc., are less stringent than usual. This permits the system to be miniaturized, which in turn allows its use with a correspondingly small electromagnet.

One problem caused by the flame is its background emission, which is not blocked because it only passes through one polarizer before reaching the detector (Fig. 1). This background produces both a d.c. offset and increased noise at the detector output. The former can be eliminated by the usual phase-sensitive detection. The latter can be dealt with in one of two ways: either source intensity must be increased, or the flame background must be reduced. The latter option is particularly attractive with a m.o.r. system because the transmitted (signal) beam can be collimated independently of the background. This permits the signal-to-background intensity ratio to be increased by extending the physical separation between the m.o.r. cell and the detector. The separation used here was about one metre. Longer distances were not worthwhile with the present apparatus, because the reduction in the effective aperture of the system caused the signal to decrease as well as the background; at this point, no further advantage is to be gained.

A schematic diagram of the filter is shown in Fig. 1. The magnet (Hammond, Guelph, Ontario) gave a maximum field of 16 kG with a gap size of 1.5 × 1 cm area × 5 mm wide. The size of the burner slot accommodated by this gap was 1 cm × 2 mm. The polarisers were 8 mm aperture calcite Glan prisms (Oriel) with an extinction ratio better than 1×10^{-5}.

Operation. Operation of the filter was similar to that described previously [8]. In use, the polarizers were fully crossed, and the magnetic field and solution composition to be aspirated into the filter were set to the values appropriate to the particular experiment. Atomic absorption of the transmitted radiation was observed by aspirating suitable solutions through a conventional nebulizer—10-cm burner assembly (Varian-Techtron) mounted in the optical path. The latter is referred to below as the absorption flame, to distinguish it from the m.o.r. atomiser.

Results

Performance of the m.o.r. filter. Table 1 gives 1% absorption values, obtained by aspirating standard solutions into the absorption flame after the filter had been optimized for each line. The two sets of values given in Table 1 were obtained by using hollow-cathode sources and with a xenon arc continuum. The similarity between the two sets of values is clear evidence that the bandwidth of the filter is comparable to the emission line width of the hollow-cathode lamp.

Table 1 also gives estimates for the transmission efficiency of the filter. This was measured as the ratio of the line intensity transmitted by the filter when operating normally, to that transmitted with the two polarizers aligned and no solution aspirated into the filter flame. The latter value was averaged over the two available orthogonal orientations of the polariser axes. Transmission efficiencies are well below the maximum attainable with this type of optical configuration (ca. 5%) suggesting that the filter design used here is not optimal. Poor homogeneity both of the magnetic field and of the atom distribution within the field are probably at least partly responsible for this observation.

Noise sources in the filter. The 1% absorption concentrations given in Table 1 were found essentially to represent the detection limits also, due to the high associated noise levels. Two major sources of noise were found; photon noise associated with background emission from the filter flame, and transmission noise caused by fluctuations of atom density in the same flame. Photon noise is reduced, but is not completely eliminated, by the collimation technique described above. Transmission noise is particularly apparent because the transmission efficiency of a m.o.r. filter is approximately proportional to the square of the absorbance in the m.o.r. flame under the

TABLE 1

Summary of filter performance

Elements	Wavelength (nm)	1% Absorption (μg ml^{-1})		% Transmission efficiency of m.o.r. filter
		Hollow-cathode lamp with m.o.r. filter	Xenon arc with m.o.r. filter	
Ca	422.7	0.1	0.1	1.5
Cd	228.8	0.04	0.04	0.8
Cu[a]	324.8 327.4	0.08	0.1	1.5
Li[a]	670.78 670.79	0.02	0.03	1.2
Na[a]	589.0 589.6	0.01	0.01	0.95

[a]Both lines are transmitted by the m.o.r. filter. This reduces absorption sensitivities for Cu and Na relative to their standard values, which were measured on the best single line in each case.

conditions used here; hence fluctuations of atom density cause correspondingly large variations of the output signal.

Atomic emission measurements. The high noise levels are less obtrusive with atomic emission than with absorption measurements provided that an intense source is available. This happens because transmission noise falls with decreasing intensity of the emission signal to be measured, and because contributions to photon noise from the filter flame become progressively less significant as the intensity (i.e., signal plus background) of the emission source increases. These comments are illustrated by the results in Fig. 2 which show emission signals from 3×10^{-10} g of calcium from a carbon arc source using, respectively, the m.o.r. filter and a 0.5-m Ebert monochromator (reciprocal dispersion of 3.3 nm mm^{-1}; 15 μm slit). It is apparent in this case that the advantages of high resolving power and large aperture conferred by the m.o.r. filter outweigh the increased noise caused by its use.

Conclusions

The filter described here is straightforward to assemble and use, and enables different atomic lines to be readily selected. The 1% absorption sensitivities given in Table 1 show the bandwidth of the filter to be narrow, of the order of the emission line width of a hollow-cathode lamp. This is despite the pressure broadening in the m.o.r. flame. This tolerance towards a broadened profile in the m.o.r. atomizer is attributed to coherence narrowing of the transmitted line. The characteristics of the present device seem to make it suitable for use with high-intensity atomic emission sources, an application for which high resolving power is important, and in which the

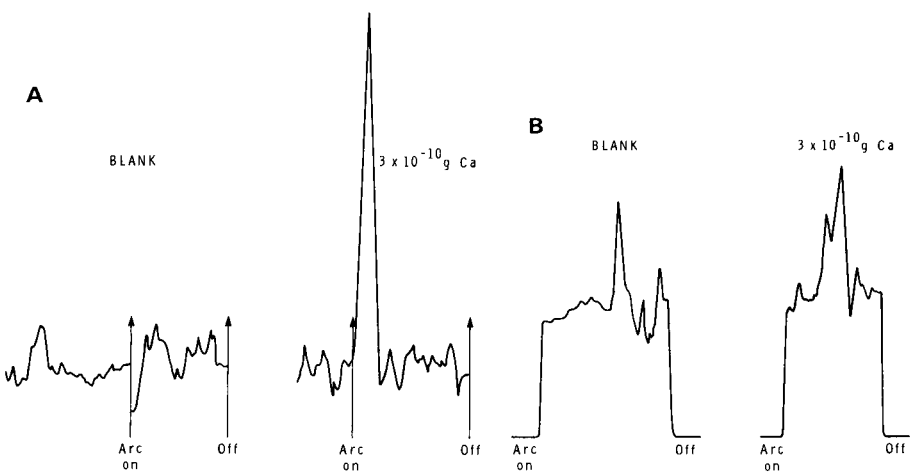

Fig. 2. (A) Blank and emission signal from 3×10^{-10} g Ca with the m.o.r. filter. The absence of a background signal on the blank when the arc is fired is an indication of the narrow bandwidth of the filter. (B) Equivalent results obtained with a 0.5-m Ebert monochromator.

type of internal noise generated by the filter does not automatically limit the sensitivity of the system.

The authors are indebted to the Natural Sciences and Engineering Research Council of Canada for support of this work.

REFERENCES

1 D. A. Church and T. Hadeishi, Appl. Phys. Lett., 24 (1974) 185.
2 M. Ito, S. Murayama, K. Kayama and M. Yamamoto, Spectrochim. Acta, 32B (1977) 347.
3 R. Stephens, Anal. Chim. Acta, 98 (1978) 291.
4 K. Kitagawa, T. Shigeyasu and T. Takeuchi, Analyst, 103 (1978) 1021.
5 M. Yamamoto and S. Murayama, J. Opt. Soc. Am., 69 (1979) 781.
6 M. Yamamoto, S. Murayama, M. Ito and M. Yasuda, Spectrochim. Acta, 35B (1980) 43.
7 J. Kankare and R. Stephens, Appl. Spectrosc., 34 (1980) 590.
8 G. Jolly and R. Stephens, Anal. Chim. Acta, 116 (1980) 365.

Analytica Chimica Acta, 139 (1982) 329—332
Elsevier Scientific Publishing Company, Amsterdam — Printed in The Netherlands

Short Communication

INTERFERING EFFECTS ON THE DETERMINATION OF LOW CONCENTRATIONS OF MERCURY IN GEOLOGICAL MATERIALS BY COLD-VAPOUR ATOMIC ABSORPTION SPECTROMETRY

A. BARTHA* AND K. IKRÉNYI

Hungarian Geological Survey, P.O. Box 106, 1442 Budapest (Hungary)

(Received 5th November 1981)

Summary. Gold, platinum, selenium and tellurium interfere with the determination of mercury in geological materials by cold-vapour atomic absorption spectrometry. These elements can be reduced together with mercury by tin(II) chloride, and surface adsorption and amalgamation then hinder the vaporization of mercury from acidic media. In strongly alkaline media, the interfering effect does not appear even when considerable concentrations of these elements are present.

The average concentration of mercury in the earth's crust is about 0.07 g/tonne, but in ore deposits containing minerals of the polymetallic type, mercury contents can reach the 1—100 g/tonne range. Widespread primary and secondary dispersed rings of mercury can form around such ore deposits. This is why mercury is an important geochemical indicator in prospecting for ore deposits, not only for the mercury deposits themselves but for hydrothermal deposits generally. Anomalies in the mercury concentration can often be recognized even in zones some kilometres away from the ore deposit [1, 2].

Although mercury at low concentrations can be determined by neutron activation or spectrophotometric methods, cold-vapour atomic absorption spectrometry (a.a.s.) is very selective and is widely applied. In the case of indirect determinations [3—5], mercury is released by heating the rock sample and then collected on gold or silver; when this collector is heated, the evaporated mercury is swept into the absorption cell. However, if several elements are to be determined in the rock or ore, the sample is usually decomposed in a teflon-lined acid digestion bomb, and mercury is generated directly from the stock solution by reduction with tin(II) chloride [6—8]. Several papers on this method have mentioned the interfering effects of noble metals [7—9] but neither the degree nor the elimination of the interference has been detailed. The problems of mercury determination in connection with geological ore prospecting and how to overcome the interferences are discussed in this communication.

Experimental

Instrumentation. A Pye-Unicam SP-192 atomic absorption spectrometer was used with a Pye-Unicam mercury cold-vapour analyzer, which has a 100-

0003-2670/82/0000-0000/$02.75

mm long absorption cell with silica windows, and a recirculation system (air). A three-way tap makes ventilation possible between determinations. Parr acid digestion bombs were used for the decompositions, the volume of the teflon cup being 25 cm^3.

Reagents. All reagents were analytical-reagent grade. Solutions were prepared with distilled water and blanks were negligible.

Procedure. Transfer 200—500 mg of ground sample into the teflon cup. Add 9 cm^3 of distilled water, 2.5 cm^3 of concentrated nitric acid and 2.5 cm^3 of concentrated hydrochloric acid. Seal the bomb, mix by shaking, and heat at 140° C for an hour. Cool to ambient temperature, and dilute to 50 cm^3 with distilled water in a volumetric flask.

For determinations in an acidic medium, transfer 0.2—10-cm^3 aliquots into the reaction flask containing 30 cm^3 of distilled water, 2 cm^3 of (1 + 1) sulphuric acid and 2 cm^3 of 10% (w/v) tin(II) chloride solution. Immediately close the flask and start the recirculating apparatus. After 1.5—2 min the system reaches equilibrium and the absorbance is displayed. Open the recirculating gas system to purge the mercury vapour for about 3 min.

For determinations in an alkaline medium, the reaction flask contains 30 cm^3 of 40% (w/v) potassium hydroxide solution and 2 cm^3 of 10% (w/v) tin(II) chloride solution. The procedure is otherwise identical with that for an acidic medium.

To calibrate the instrument, add 1 cm^3 of mercury standard solution (0.1 mg dm^{-3}, prepared daily) into the reaction flask and repeat the procedure so that measurements of the standards and the samples are done from the same solution.

Results and discussion

Although Omang and Paus [8] suggested total decomposition of the samples, there is no real need to decompose the siliceous matrix for the determination of mercury. Mercury is normally present as the sulphide or metal; it cannot form natural silicate minerals because of its large ionic radius. The mixture of hydrochloric and nitric acids quantitatively extracts the mercury from rocks and ores.

The influence of gold, silver, platinum, selenium and tellurium on the determination of mercury was examined for acidic and alkaline media. The depressing effects of these elements (except silver) on the absorbance of mercury with reduction in the acidic medium are shown in Fig. 1; 50% decreases in the absorbance signals are caused by 1.5×10^{-6} g of gold or platinum, 5×10^{-6} g of selenium or 0.3×10^{-6} g of tellurium. Silver is precipitated as the chloride, which is not reduced by tin(II) and so does not interfere. After the reduction, the mercury is more or less adsorbed, depending on the concentration of interfering ions on the surface of platinum, gold, selenium or tellurium particles, possibly forming amalgams, so that part of the mercury atoms cannot form the vapour. If the determination is repeated in the presence of interfering material, the depressing

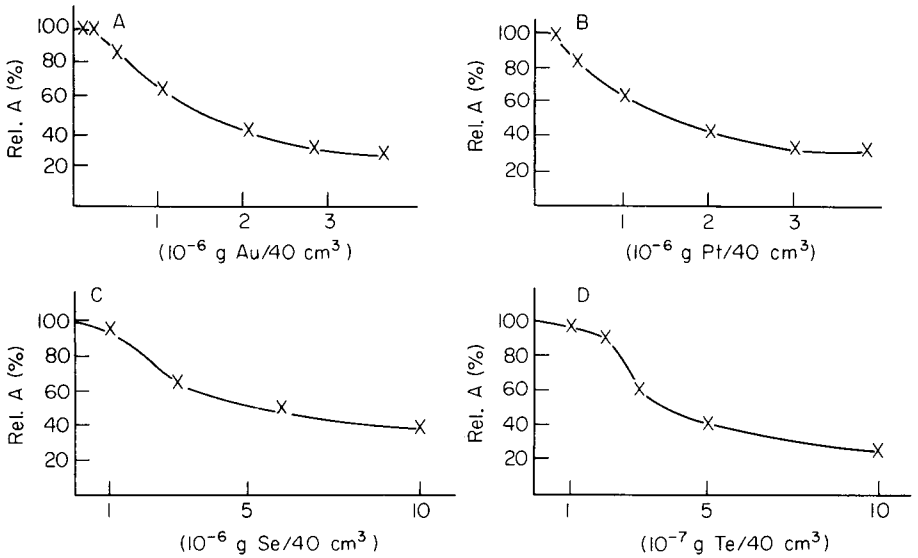

Fig. 1. Depressing effects on the absorbance of mercury after reduction in an acidic medium in presence of: (A) gold; (B) platinum; (C) selenium; (D) tellurium.

effect diminishes: e.g., 3×10^{-6} g of gold caused a 70% decrease in the signal of mercury on the first run, whereas when further mercury was added after purging, the decreases were 54%, 38% and 30% on successive runs. Thus it appears that the number of active mercury-adsorbing sites on the interfering metal depends on the amount of mercury adsorbed. This is why the standard addition method is not useful for the cold-vapour determination of mercury in geological samples.

The mechanism of the reduction reactions depends on the pH of the solution, and a high concentration of hydroxide ions helps to eliminate the interfering effects. The metal ions examined form hydroxides or complexes (possibly colloidal precipitates) which are reduced only very slowly, whereas the atomization of mercury is fast. The determination of mercury in a strong alkaline medium is not affected, even by 10^{-3} g of platinum, gold or selenium, and only more than 6×10^{-4} g of tellurium interferes (Fig. 2). The determination is more sensitive (about 50%) than in an acidic medium, probably because of differences in the gas—liquid phase equilibrium constants of mercury in acidic and alkaline media.

If 10^{-4} g of tellurium is added to the reaction mixture previously, the tellurium is reduced from the solution after some hours and the cold-vapour mercury determination then becomes impossible. It is interesting that previously reduced platinum, gold or selenium (10^{-2} g) does not interfere because the aggregated particles do not adsorb mercury in a strongly alkaline medium.

More than 10^{-4} g of silver could interfere with this determination, but most of the silver does not reach the stock solution because it is precipitated

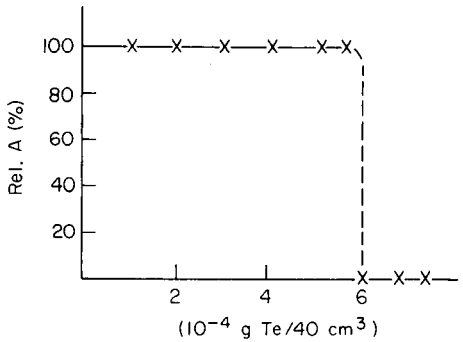

Fig. 2. Depressing effect of tellurium on the absorbance of mercury after reduction in an alkaline medium.

as silver chloride. Other precipitates that may form in alkaline solution do not interfere because there is no measurable mercury adsorption on the surface of hydroxides.

The real detection limit for mercury determinations by the recommended procedure in various kinds of geological samples is 0.02—0.03 g/tonne, and the relative standard deviation is about 1%.

REFERENCES

1 A. A. Saukov, Tr. Inst. Geol. Nauk AN SSR, Ser. Min. Geokhim., 17 (1946) 129.
2 M. Földvári-Fogl, Theory and Practice of Regional Geochemical Exploration, Akademiai Kiadó, Budapest, 1978, pp. 64—66.
3 H. G. Henry, K. R. Stever, W. L. Borry and H. H. Heady, Appl. Spectrosc., 26 (1972) 288.
4 V. I. Muscat, T. J. Vickers and Anders Andren, Anal. Chem., 44 (1972) 218.
5 J. Olafsson, Anal. Chim. Acta, 68 (1974) 207.
6 W. R. Hatch and W. L. Ott, Anal. Chem., 40 (1968) 2085.
7 J. Y. Hwang, P. A. Ullucci and A. L. Malenfort, Can. Spectrosc., 16 (1971) 100.
8 S. H. Omang and P. E. Paus, Anal. Chim. Acta, 56 (1971) 393.
9 G. Lindstedt, Analyst, 95 (1970) 264.

Analytica Chimica Acta, 139 (1982) 333—339
Elsevier Scientific Publishing Company, Amsterdam — Printed in The Netherlands

Short Communication

MULTI-ELEMENT ANALYSIS BY INDUCTIVELY-COUPLED PLASMA EMISSION SPECTROMETRY IN ANIMAL DIETS AND FAECES CONTAINING CHROMIUM MARKER

M. T. FISHER* and J. LEE

Applied Biochemistry Division, D.S.I.R., Private Bag, Palmerston North (New Zealand)

(Received 23rd November 1981)

Summary. A simple fusion method is given for the dissolution of chromium(III) oxide marker in animal diets and faeces. Chromium is determined by inductively-coupled argon plasma emission spectrometry and, for comparison, by flame atomic absorption spectrometry. The feasibility of simultaneous multi-element analysis is investigated. Data on interferences and recovery are presented.

The importance of using a continuous, non-absorbed, non-toxic faecal marker in balance studies to correct for variations is well recognized [1—4]. By comparing the quantity of a marker administered in the diet, with that recovered in the collected faecal material, a correction or digestibility factor may be obtained. When this factor is applied to other chemical determinations [5], the effects of varying rates of solid-phase excretion from one collection to the next are accounted for.

In this work, powdered chromium(III) oxide (Cr_2O_3) was used as the solid dietary marker in balance studies on rats. A simple method for the dissolution of Cr_2O_3 in rat diets and in solid rat excreta is described; it is a modification of a clinical method based on sodium peroxide fusion [4]. The dissolved chromium is determined by inductively-coupled argon plasma emission spectrometry (i.c.p.e.s.), the results being compared with those obtained by flame atomic absorption spectrometry (a.a.s.). The suitability of i.c.p.e.s. for simultaneous multi-element determinations on the digests from the Cr_2O_3 dissolution was studied along with potential interferences.

The advantages of i.c.p.e.s. are high sensitivity, minimum sample preparation, and relative freedom from many chemical interferences often encountered in flame a.a.s. The latter attribute is of particular significance in the determination of chromium in the presence of variable concentrations of concomitant ions such as aluminium, silicate, phosphate and iron, which are well known to cause specific interferences involving the condensed phase and interfere seriously with chromium determinations by both flame emission and absorption methods [6].

The corundum structure of strongly ignited Cr_2O_3 is inert toward both acids and bases; this precludes the use of common wet digestion methods, such as nitric/perchloric acid. Other methods based on the use of perchlorate

0003-2670/82/0000-0000/$02.75

or phosphoric acid—bromate mixture [4, 7] involved too many time-consuming steps and often gave poor recoveries. An added disadvantage of these methods is the undesirable effect of phosphoric acid or saturated potassium perchlorate solutions on the nebulization and transport properties in the i.c.p.e.s. method.

Experimental

Reagents. Stock solutions of chromium (250 μg ml^{-1}) were prepared by dissolving potassium dichromate in 2 M HCl containing 25 mg ml^{-1} sodium chloride. Multi-element standards for calibrating the i.c.p. spectrometer were prepared from 1000 μg ml^{-1} stock solutions of the metal chloride in 2 M HCl made from the redistilled constant-boiling acid. Sodium peroxide was in the granular form. All reagents were of analytical grade.

Instrumentation. A Techtron AA4 atomic absorption spectrometer with an AA6 nebulizer and burner was used under the following instrumental conditions: chromium wavelength, 357.87 nm, slit width, 25 μm; single element chromium hollow-cathode lamp current, 6 mA; reducing air—acetylene flame.

An Applied Research Laboratories (ARL) 34000 emission spectrometer system was used with an argon plasma (1.6 kW). The polychromator has a 1-m Paschen-Runge mount, with a Bausch and Lomb grating (1080 lines/mm), equipped with a movable primary slit operated under computer control, enabling the immediate vicinity of emission lines to be scanned for possible spectral interferences.

Dissolution of chromium(III) oxide. Oven-dried faecal (0.1 g) or feed material (3.0 g) was ashed at 460°C for 12 h to decompose organic material; the resulting ash containing the chromium oxide marker was fused at 520°C with 600 mg of sodium peroxide for 45 min. Chromium(III) is oxidized to chromium(VI) in the strongly alkaline flux. The crucible contents were leached with deionized water and boiled gently on a hot plate for 5 min to remove most of the excess of peroxide. The solution was cooled and acidified with constant-boiling hydrochloric acid, transferred to a 100-ml volumetric flask and diluted to volume. The resulting solution was 2 M in hydrochloric acid which provided a constant concentration and minimized transport and nebulization effects in the i.c.p.e.s.

The dissolutions for simultaneous chromium and trace metal determinations were done in 20-ml platinum crucibles. For the determination of chromium alone, cheap 20-ml glazed porcelain crucibles were satisfactory. Previous studies [4] had shown that at least 6 parts of Na_2O_2 to 1 part of Cr_2O_3 was needed for the Cr_2O_3 dissolution.

Results and discussion

Interferences. Faecal and diet samples provide chemically and physically complex matrices and numerous interelement effects may occur during the spectrometry. Interferences related to stable-compound formation in the

condensed phase in flame emission spectroscopy are virtually negligible in a toroidal inductively-coupled plasma [8, 9].

Relatively high levels of aluminium, silicate and sodium are present in the faecal and diet solutions following the sodium peroxide fusion in the porcelain crucibles. The effect of these elements on the intensity of the Cr II 267.716-nm line was examined. Cobalt was added as an internal reference standard to correct for the relative quantity of analyte arriving in the plasma. The signal intensity of a Cr(III) solution (5 μg ml^{-1}) in 2 M HCl was monitored in the presence of increasing amounts of Al, Si and Na. The chromium emission intensity was not suppressed by the presence of up to a 200-fold molar ratio of aluminium. A 9% suppression was observed for 100-fold levels of silicate (as silicic acid), but when the net chromium signal was compared to the cobalt internal reference, 100% recovery was obtained. Hence the effect was largely a result of transport to the plasma rather than a consequence of atomization interference. The effect of sodium on the emission intensity at 267.716 nm of a 5 μg Cr ml^{-1} solution in 2 M HCl is illustrated in Fig. 1. High concentrations cause changes in nebulization efficiency. There was no significant difference in the background intensity at 267.716 nm when 2 M HCl was aspirated with or without sodium at concentrations up to 10 000 μg ml^{-1}. This was also observed for all the emission lines in the optical array.

At analyte concentrations in the low μg ml^{-1} range, spectral interferences may arise from high concentrations of concomitant elements. The interfering emission usually lies within 0.04 nm of the analyte wavelength [10]. The spectral environment about the Cr II 267.716-nm emission line in the presence of various concomitants is illustrated in Fig. 2. The relatively weak Mn 267.725-nm and P I 267.712-nm lines fall within the spectral window of the Cr II 267.716-nm line, resulting in spectral overlap. There is no overlap from the weak Fe 267.687-nm, line although the background was enhanced when high concentrations of iron were aspirated into the plasma.

Broadband emission was observed when high concentrations of a magnesium salt were aspirated into the plasma. The Cr II 267.716-nm emission line lies in a region which is influenced by the presence of a series of broad

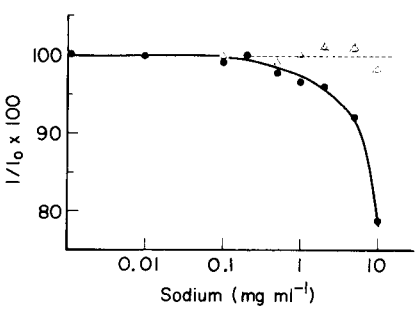

Fig. 1. Effect of increasing sodium concentration on the net emission intensity of 5 μg Cr ml^{-1} with (I) and without (I_0) NaCl in 2 M HCl.

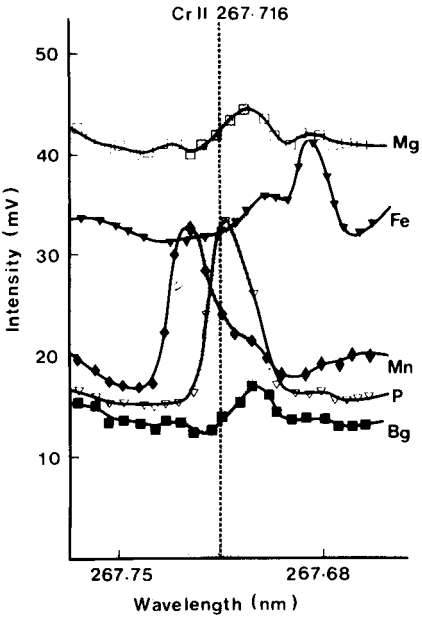

Fig. 2. The spectral environment about the Cr II 267.716-nm emission line obtained whilst aspirating Mg (10 mg ml^{-1}), Mn (1 mg ml^{-1}), Fe (10 mg ml^{-1}) and P (10 mg ml^{-1}) into the plasma (Bg = background). The band-pass region of the spectrum about the Cr II 267.716-nm emission line is shown by the shaded area.

$3p^{\circ}—^{3}d$ Mg triplets resembling molecular bands [11]. Line broadening from these triplet states results in a spectral background shift around the Cr II 267.716-nm line. An empirical software correction must be made in samples with widely varying magnesium composition; this is particularly important at low chromium concentrations.

In practical analysis, the contribution of the interfering elements to the analyte emission signal was established and simple correction factors were applied to the analyte signal. Potential interelement interferences arising from faecal and diet matrices are summarized in Table 1.

Recovery and accuracy. The fusion method employed was examined for the accuracy and precision of chromium recoveries from known amounts of Cr_2O_3 powder added to diet and faecal material. The concentrations of chromium (10—60 mg g^{-1}) were those usually encountered in the rat faeces. Chromium was determined by i.c.p.e.s. The results (Table 2) indicate that the method produces an adequate level of recovery and precision for most studies of animal digestion. No variability of signal intensity or background level was observed among individual faeces or diet batches.

The fusion method in porcelain crucibles, gave excellent recoveries of chromium, but resulted in greatly enhanced aluminium levels in the final digest solution through corrosion of the crucible. Such levels and the high

TABLE 1

Spectral interelement interferences found in i.c.p.e.s. of faecal and diet matrices

Element	Spectral order	Wavelength (nm)	Interferent	Tolerable ratio (ppb/ppm)
Al	2	308.215	Fe	0.06
			Mn	1.6
Co	2	228.62	Fe	0.08
			Cr	0.33
Cr	3	267.716	Fe	0.06
			Mg	0.16
			Mn	0.17
			P	0.06
Cu	2	324.754	Ca	0.04
Fe	2	259.939	Mn	0.22
Mo	3	202.03	Al	0.21
Ni	3	231.603	Fe	0.05
			Mn	4.0
Pb	2	220.35	Fe	0.6
			Al	3.6
Zn	2	213.856	Al	0.08

TABLE 2

Recovery of chromium from chromium(III) oxide in diet and faecal material (0.5% Cr_2O_3)

Sample	Chromium recovery (%)		
	N	$\bar{x}$	RSD
Faeces	18	97.7	3.7
Diet			
Batch 1	10	101.9	2.3
Batch 2	10	101.3	2.9
Total (3 diets, 12 batches)	117	101.2	5.4

levels of sodium inherent in the method might cause interferences in the a.a.s. determination of chromium. The two techniques were therefore compared for the determination of chromium in faecal and diet material. However, when using the flame stoichiometry optimized for chromium absorption, there was no significant difference between the two methods (Table 3).

The effect of matrix interferences on the determination of various trace elements in the faecal and diet material by i.c.p.e.s. was assessed by spiking the material before ashing with aliquots from stock solutions of the elements. Possible background shifts caused by the sample matrix were also examined

TABLE 3

Comparison between i.c.p.e.s. and flame a.a.s. for the determination of chromium in rat faeces (N = 4; Cr in the range 5—50 μg ml^{-1})

Cr concn. (mg g^{-1} dry wt.)				
I.c.p.e.s.		Flame a.a.s.		A.a.s./i.c.p.e.s. recovery (%)
$\bar{x}$	RSD (%)	$\bar{x}$	RSD (%)	
47.5	2.1	46	4.9	97.8
71	2.3	68	2.2	95.8
100	6.7	98	3.3	98.0
143	2.1	128	5.6	89.5
178	3.1	165	3.7	92.7
239	1.8	215	10.2	89.9
283	0.9	261	4.8	92.2
333	0.8	301	6.8	90.4
423	1.9	377	5.6	89.1
493	3.0	465	1.9	94.3

by scanning the near vicinity of each analytical line. No enhancement or suppression of the plasma background was observed. Typical recovery data for a number of element spikes are reported in Table 4. The recoveries obtained indicate that for these samples, matrix effects are negligible and that the fusion method employed allows satisfactory recoveries of a number of trace elements.

TABLE 4

Recovery of multi-element spikes by i.c.p.e.s.

Element	Mean concentration (μg g^{-1} dry wt.)				Mean concentration (μg g^{-1})			
	Sample diet	Sample spike	Amount added	Mean recovery (%)	Sample faeces	Sample spike	Amount added	Mean recovery (%)
Al	36	702	667	99.8	770	20560	20000	99.0
Co	<0.9[a]	31.3	33.3	94.0	<21	960	1000	96.0
Cu	12.3	45	33.3	98.1	210	1190	1000	98.0
Fe	289	412	133.3	92.1	5350	8965	4000	90.4
Mn	23	90	66.6	100.5	490	2425	2000	96.8
Mo	1.3	34.7	33.3	100.1	<15	965	1000	96.5
Ni	<1.0	32	33.3	96.2	<22	980	1000	98.0
Pb	<7.3	30	33.3	89.0	<170	965	1000	96.5
Sr	2.2	35.5	33.3	99.9	40.5	1043	1000	100.3
Zn	58	126	66.6	102.5	880	2925	2000	102.3

[a]Below the limit of determination (10 sigma detection limit) for a dilution factor of 33 and 500, diet and faeces respectively.

The authors are grateful to Dr. K. James for providing the samples and to Miss Sandra Gordon for her technical assistance.

REFERENCES

1 H. Edin, G. Kihlen and S. Nordfeldt, Ann. Agric. Coll. Sweden, 12 (1944) 186.
2 A. F. Schurch, L. E. Lloyd and E. W. Crampton, J. Nutr., 41 (1950) 629.
3 C. R. Barnicoat, N.Z. J. Sci. Technol., 27 (1945) 202.
4 M. T. Fisher, P. R. Atkins and G. F. Joplin, Clin. Chim. Acta, 41 (1972) 109.
5 M. T. Fisher, Anne Tondowski and G. F. Joplin, Clin. Chim. Acta, 70 (1976) 311.
6 C. Th J. Alkemade and R. Herrmann, Fundamentals of Analytical Flame Spectroscopy, Adam Hilger, Bristol, 1979.
7 C. H. Williams, D. J. David and O. Iismaa, J. Agric. Sci., 59 (1962) 381.
8 V. A. Fassel and R. N. Knisely, Anal. Chem., 46 (1974) 1100A, 1155A.
9 R. L. Dahlquist and J. W. Knoll, Appl. Spectrosc., 32 (1978) 1.
10 M. A. Floyd, V. A. Fassel and A. P. D'Silva, Anal. Chem., 52 (1980) 2168.
11 G. F. Larson and V. A. Fassel, Appl. Spectrosc., 33 (1979) 592.

Analytica Chimica Acta, 139 (1982) 341—346
Elsevier Scientific Publishing Company, Amsterdam — Printed in The Netherlands

Short Communication

INTERNAL REFLECTANCE SPECTRA ASSOCIATED WITH STAIRCASE VOLTAMMETRY IN ANODIC OXIDATION OF AROMATIC AMINES IN ACETONITRILE

TERUO HINOUE,* SATOSHI OKAZAKI and TAITIRO FUJINAGA

Department of Chemistry, Faculty of Science, Kyoto University, Kyoto, Sakyo-ku 606 (Japan)

(Received 12th November 1981)

Summary. Dynamic transformation profiles of internal reflectance spectra were observed for anodic oxidation of triphenylamine, *N*-methyldiphenylamine, and *N*,*N*-dimethylaniline in acetonitrile. Absorption bands appearing in these spectra are compared with those in conventional absorption spectra of the electrolyzed aromatic amine solutions by controlled-potential electrolysis. From this comparison, the internal reflectance bands are assigned to a tetraphenylbenzidine radical monocation and dication, a dimethyldiphenylbenzidine radical monocation and dication, etc.

A combination of internal reflectance spectroscopy in the visible region with staircase voltammetry (i.r.s.—s.c.v.) was developed recently [1, 2]. The present communication describes an attempt to acquire and interpret dynamic transformation profiles of internal reflectance spectra of electrogenerated species by anodic oxidation of aromatic amines in acetonitrile.

Experimental

Details of a computer-controlled system for i.r.s.—s.c.v. have been reported [2]. A multi-reflection cell was used here with a tin oxide optically-transparent electrode (OTE). In the measurements, one internal reflectance spectrum was measured each time the staircase wave was stepped and its dynamic transformation profile was recorded over a certain potential range. Each spectrum was obtained by accumulating spectral signals from a photodetector, which consisted of a 256-part photodiode array. Because of the accumulation, the step interval of the staircase wave was several tens of seconds, which is much longer than in conventional staircase voltammetry. Each i.r.s.—s.c.v. measurement covered a wavelength range of 92 nm because of the limited field of the diffraction grating and the photodetector. The visible region was, therefore, covered by several measurements. Conventional absorption spectra were observed with a Shimazu UV 200 spectrophotometer.

*Present address: Department of Materials Science and Technology, Technological University of Nagaoka, Kamitomioka, Nagaoka 949-54, Japan.

Triphenylamine, *N*-methyldiphenylamine, *N*,*N*-dimethylaniline, and 3,3′-5,5′-tetramethylbenzidine (all analytical grade) were tested without further purification. The acetonitrile was dried with calcium hydride and then distilled twice from phosphorus pentoxide. The supporting electrolyte was 0.1 M tetraethylammonium perchlorate for all experiments. Sample solutions were bubbled with nitrogen to remove oxygen and a nitrogen atmosphere was maintained during all measurements. The reference electrode was the conventional silver/0.01 M silver perchlorate—0.1 M tetraethylammonium perchlorate in acetonitrile; its potential against an aqueous saturated silver/silver chloride electrode was +337 mV in acetonitrile containing 0.1 M tetraethylammonium perchlorate.

Results

Figure 1 A—C illustrates the dynamic transformation profiles for triphenylamine, *N*-methyldiphenylamine, and *N*,*N*-dimethylaniline solutions. Figure 2

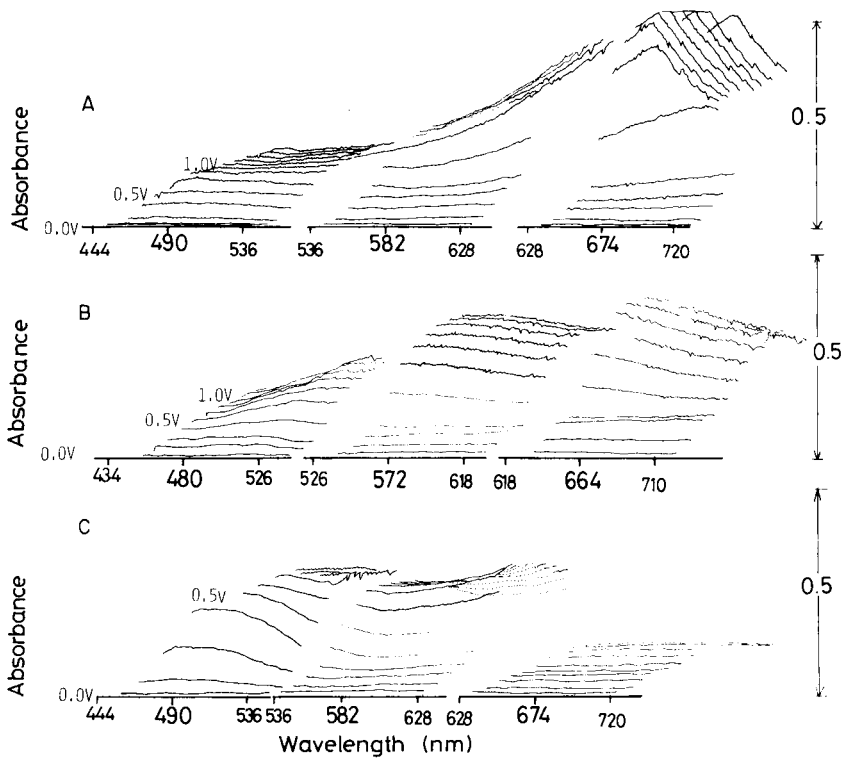

Fig. 1. Dynamic transformation profiles of the internal reflectance spectra by i.r.s.—s.c.v. measurements: (A) triphenylamine; (B) *N*-methyldiphenylamine; (C) *N*,*N*-dimethylaniline. Successive lines correspond to internal reflectance spectra observed at the given electrode potentials of the staircase wave. Parameters of the staircase wave: step potential E_s = 0.1 V; step interval τ = 20 s; delay time τ' = 10 s; sampling time (accumulation) $\Delta\tau$ = 5 s. Sample solutions were ca. 2 mM in the aromatic amine with 0.1 M tetraethylammonium perchlorate in acetonitrile.

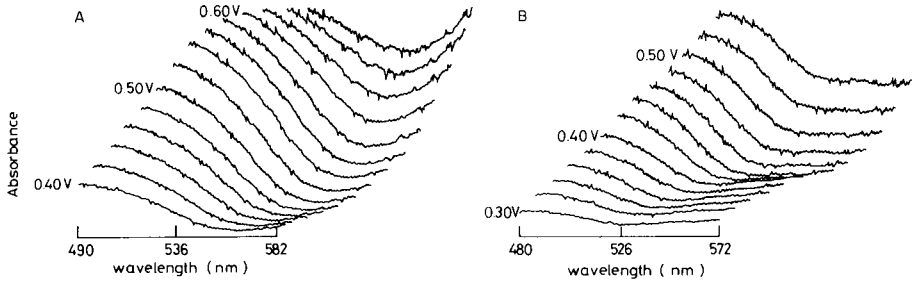

Fig. 2. Dynamic transformation profiles of internal reflectance spectra by i.r.s.—s.c.v. measurements: (A) triphenylamine; (B) *N*-methyldiphenylamine. Successive lines correspond to internal reflectance spectra observed at the given electrode potentials of the staircase wave. Step potential E_s = 0.02 V; other s.c.v. parameters as for Fig. 1. Sample solutions were ca. 2 mM in the aromatic amine with 0.1 M tetraethylammonium perchlorate in acetonitrile.

shows the profiles in the spectral ranges 490—582 nm for triphenylamine and 480—572 nm for *N*-methyldiphenylamine. Table 1 lists the absorption maxima appearing in the dynamic transformation profiles by the i.r.s.—s.c.v. measurements for solutions of aromatic amines, and the potential ranges where the maxima grow. In the profiles for triphenylamine and *N*-methyldiphenylamine, the weak bands at 490 nm and 485 nm grow in the less anodic potential ranges, whereas the strong bands at 690 nm and 520 nm increase at the more anodic potentials. At very positive potentials, the band growth increases only slightly or even stops. In the profile for *N*,*N*-dimethylaniline, only one band at 470 nm grows in the potential range 0.20—0.40 V. As the electrode potential becomes more anodic, blue insoluble products deposit on the optically transparent electrode.

The dynamic transformation profiles of these spectra show not only what species are generated at the electrode/solution interface but also the potential at which the species are produced. In contrast, conventional controlled-potential electrolysis gives information about the final products. Controlled-potential electrolysis was applied for triphenylamine, *N*-methyldiphenyl-

TABLE 1

Absorption maxima in transformation profiles and potential ranges where the maxima grow

Compound	Potential range (V vs. Ag electrode specified)	Maximum wavelength (nm)
Triphenylamine	0.35 ~ 0.60	490
	0.50 ~ 0.70	690
***N*-Meth**yldiphenylamine	0.30 ~ 0.50	485
	0.40 ~ 0.80	530
***N*, *N*-Di**methylaniline	0.20 ~ 0.40	470

amine, *N*,*N*-dimethylaniline, and 3,3′,5,5′-tetramethylbenzidine solutions with a platinum gauze electrode. During electrolysis, color changes were observed by the naked eye. The color of the solution around the electrode varied to blue followed by yellow for triphenylamine, and to yellow for *N*-methyldiphenylamine in the first few seconds of electrolysis; finally, the electrolyzed triphenylamine solution was blue and the *N*-methyldiphenylamine solution was wine-red. For the *N*,*N*-dimethylaniline solution, such color changes were not observed and the final color was yellow.

Conventional absorption spectra were recorded immediately after electrolysis and after standing for ca. 24 h in air. Absorption maxima appearing in these spectra are shown in Table 2, together with electrochemical information. For triphenylamine, the band at 680 nm was very strong and the band at 476 nm was weak in the spectrum recorded immediately after electrolysis, but after 24 h, the former had decreased while the latter increased. In the spectra of *N*-methyldiphenylamine, a strong band at 520 nm was observed immediately after electrolysis but a new band, which had a maximum at 490 nm and a shoulder near 520 nm, appeared after 24 h. With *N*,*N*-dimethylaniline and 3,3′5,5′-tetramethylbenzidine, the spectra did not change with time, except for a slight decrease in the band intensities.

Discussion

As shown in Table 3, the absorption maxima appearing in the transformation profiles of the i.r.s.—s.c.v. and the absorption spectra of electrolyzed solutions were assigned and identified on the basis of the above results and information in the literature [3—6]. Adams et al. [3] examined anodic oxidation pathways of many substituted aromatic amines electrochemically and spectrochemically and proposed the following e.c.e. mechanism. For example, in the case of anodic oxidation of triphenylamine (TPA),

TABLE 2

Absorption bands in conventional spectra recorded immediately after electrolysis and after standing for ca. 24 h in air, with electrochemical information[a]

	TPA	MPA	DMA	TMB
Immediately after	680(s)	520	465	458
electrolysis (nm)	476(w)		440(sh)	435(sh)
After standing for	680	490	465	458
ca. 24 h in air (nm)	476	520(sh)	440(sh)	435(sh)
Electrode potential (V)	1.10	1.10	0.60	0.40
Electron number	2.09	2.01	0.918	1.00

[a]TPA, triphenylamine; MPA, *N*-methyldiphenylamine; DMA, *N*,*N*-dimethylaniline; TMB, tetramethylbenzidine. Bands are indicated as strong (s) or weak (w) or shoulders (sh). Electrode potential means the potential where controlled-potential electrolysis was done, and is given vs. the cited Ag electrode in acetonitrile.

TABLE 3

Assignment and identification of the maxima in conventional spectra, and internal reflectance spectra by the i.r.s.—s.c.v. measurements

Species[a]	Conventional spectra (nm)	I.r.s.—s.c.v. (nm)	Literature data (nm)
$TPA^{+\cdot}$	—	—	640 [3], 660 [5], 656 [6]
$TPB^{+\cdot}$	476	490	480 [3], 480 [4], 485 [5]
TPB^{2+}	680	690	700 [4]
$MPA^{+\cdot}$	—	—	650 [6]
$MPB^{+\cdot}$	490	485	
MPB^{2+}	520	530	
$DMA^{+\cdot}$	—	—	
$TMB^{+\cdot}$ or TMB^{2+}	465 (458)	470	

[a]TPA, triphenylamine; TPB, tetraphenylbenzidine; MPA, *N*-methyldiphenylamine; MPB, dimethyldiphenylbenzidine; DMA, *N,N*-dimethylaniline; TMB, tetramethylbenzidine.

$$TPA - e^- \rightleftharpoons TPA^{+\cdot} \text{ (at } E_1\text{)} \quad (1)$$

$$2TPA^{+\cdot} \rightarrow TPB + 2H^+ \quad (2)$$

$$TPB - e^- \rightleftharpoons TPB^{+\cdot} \text{ (at } E_3\text{)} \quad (3)$$

$$TPB^{+\cdot} - e^- \rightleftharpoons TPB^{2+} \text{ (at } E_2\text{)} \quad (4)$$

Here TPB denotes 3,3′,5,5′-tetraphenylbenzidine and the oxidation potentials E_3 to E_1 become increasingly positive. In this e.c.e. scheme, the light-absorbing species are considered to be a parent cation radical ($TPA^{+\cdot}$), a benzidine radical ($TPB^{+\cdot}$), and a benzidine dication (TPB^{2+}).

The maxima in the conventional spectra at 680 nm for triphenylamine and 520 nm for *N*-methyldiphenylamine are assigned to a tetraphenylbenzidine dication and a dimethyldiphenylbenzidine cation, respectively; the electron numbers (see Table 2) agree with the above e.c.e. requirement of 2.00. The maxima at 476 nm for triphenylamine and 490 nm for *N*-methyldiphenylamine are not due to their cation radicals, because these radicals undergo a coupling reaction (Eqn. 2) very rapidly [3] but the maxima were observed even after 24 h. Moreover, the blue color in the first few seconds of electrolysis for triphenylamine has been attributed to the cation radical [3]. The maxima at 476 nm and 490 nm are, therefore, assigned to a tetraphenylbenzidine and a dimethyldiphenylbenzidine cation radical, respectively. The absorption spectra for *N,N*-dimethylaniline and tetramethylbenzidine were superimposable except for a difference in the maximum wavelength. The maximum at 465 nm for *N,N*-dimethylaniline is, therefore, assigned to a tetramethylbenzidine dication or a cation radical; it is not possible to decide which is correct on the basis of the electron numbers shown in Table 2.

Srinivasan and Kuwana [7] pointed out that erroneous conclusions might be drawn from direct comparisons of internal reflectance with conventional absorption spectra. Considering the potential ranges where the bands grow (see Table 1) and the e.c.e. mechanism mentioned above, the maxima which appeared in the dynamic transformation profiles of the i.r.s.—s.c.v. are identified with those in the conventional spectra, as shown in Table 3. The internal reflectance spectra of parent aromatic amine cation radicals were not observed by i.r.s.—s.c.v. here. This is attributed to the fact that these cation radicals are very unstable, so that the reaction layers containing them are thin compared with the observation zone of the internal reflectance spectroscopic equipment used here. The "effective thickness" was ca. 200 nm from the surface of the optically transparent electrode, and the photodetector may have lacked adequate sensitivity.

This work was supported by a Grant in Aid, Scientific Research No. 243010 from the Ministry of Education, Science and Culture.

REFERENCES

1 T. Hinoue, S. Okazaki and T. Fujinaga, Bull. Inst. Chem. Res., Kyoto Univ., 58 (1980) 211.
2 T. Hinoue, S. Okazaki, T. Nagaoka, K. Masuda and T. Fujinaga, Anal. Chim. Acta, 136 (1982) 385.
3 E. T. Seo, R. F. Nelson, J. M. Fritsch, L. S. Marcoux, D. W. Leedy and R. N. Adams, J. Am. Chem. Soc., 88 (1966) 3498.
4 H. Hasegawa, J. Phys. Chem., 66 (1962) 834.
5 F. R. Dollish and W. K. Hall, J. Phys. Chem., 69 (1965) 2127.
6 G. N. Lewis and E. Lipken, J. Am. Chem. Soc., 64 (1942) 2801.
7 V. S. Srinivasan and T. Kuwana, J. Phys. Chem., 72 (1968) 1144.

Analytica Chimica Acta, 139 (1982) 347—352
Elsevier Scientific Publishing Company, Amsterdam — Printed in The Netherlands

Short Communication

FLOW INJECTION SAMPLE PROCESSING WITH NICKEL OXIDE ELECTRODE AMPEROMETRIC DETECTION OF AMINO ACIDS SEPARATED BY ION-EXCHANGE CHROMATOGRAPHY

J. B. KAFIL and C. O. HUBER*

Department of Chemistry, University of Wisconsin-Milwaukee, Milwaukee, WI 53201 (U.S.A.)

(Received 11th December 1981)

Summary. A new automatic post-column sampler has been designed and used for interfacing the column outlet to a flow injection system. Segments of the effluent from the column are injected into the flow injection apparatus at regular intervals. Separation and detection of several amino acids are described. A nickel oxide electrode detector yields characteristic, useful signals for concentrations as low as 10^{-6} M. Samples containing 20—35 μg of total amino acids in 1 ml were chromatographed.

Chemiluminescence or fluorescence properties of amino acid derivatives are most commonly used to detect amino acids after chromatographic separation. A pre- or post-column treatment of amino acids is essential for these methods [1]. Other methods, such as refractive index detection, are also used. Refractive index detection is very insensitive and is not applicable at low concentrations. Potentiometric detectors have recently been proposed [2, 3].

Oxidation of amines and alcohols at a nickel electrode was reported by Fleischmann et al. [4]. Investigations of amino acids, amines, and alcohols using the flow injection techniques have shown that amino acids are reactive and can be determined at the nickel oxide electrode [5, 6].

This communication describes a system in which amperometric detection of chromatographically separated amino acids is aided by interfacing the ion-exchange column to a flow injection system. The linear amperometric response of the nickel oxide electrode to amino acids at low concentrations is used for detection. The advantages of the proposed system include ease of detector maintenance, low cost of components, direct detection of amino acids in column eluate, and detector sensitivity.

Experimental

Instrumentation. A schematic representation of the apparatus indicating major components and flow path is shown in Fig. 1. Solutions were moved with a multi-head peristaltic pump (Cole-Palmer Instrument Co.). Other components used without modification were a Tracor 100 UV detector (Tracor Inc., Winfield, IL), and strip-chart potentiometric recorders. The

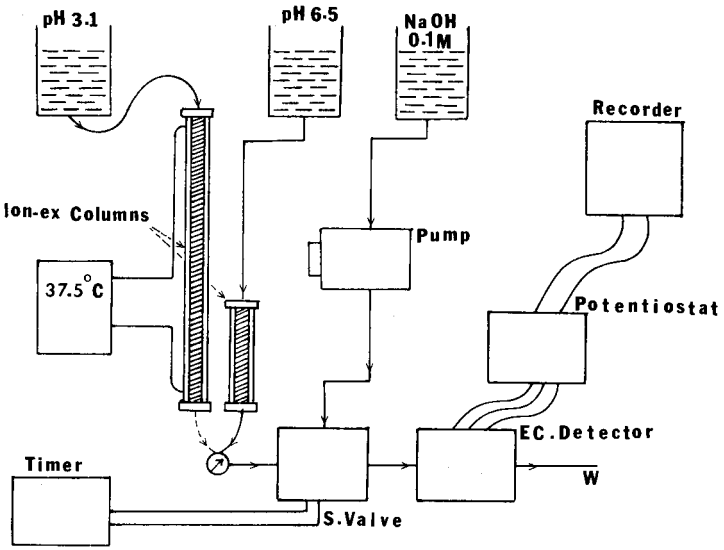

Fig. 1. Schematic diagram of apparatus.

flow-through amperometric detector was made in this laboratory and was essentially the same as that described earlier [5, 6].

Automatic injection of the column eluate requires a solenoid-activated four-way stream-exchange valve. Commercial units of appropriate size and chemical inertness were not available. Accordingly, an automatic four-way valve was designed and built using two modified three-way valves (Angar Scientific Co. Model 368, Cedar Knolls, NJ). The new valve was made by the following modification on two 368 solenoid valves. Each valve had three openings marked NC, NO, and COMM. A fourth boring of diameter similar to the other openings was made directly opposite the hole marked COMM on each valve. The new opening should join the NC outlet as near as possible to the opening of the valve cavity at a common point. Two 8-cm long 0.8-mm i.d. teflon tubes with fitting on both ends connected the NC on one valve to the NO of the other valve. The two COMM openings were used for inlets and the two new openings for outlets. An alternative compact four-way valve was also designed and built. This valve operated on only one solenoid. To make this valve, the same procedures as for the two-solenoid four-way valve were applied. However, the two modified teflon head pieces were bolted together on one solenoid. A 3-mm long 1.5-mm diameter teflon spacer was placed in the cavity between the two heads. This effectively extended the solenoid action to the second head. The adjustment for proper positioning of the pistons inside the valve heads can be made by the screw at the end of the solenoid opposite the valve head (see Fig. 2).

The chromatographic column eluate was sampled by timed injections into the otherwise continuous electrolyte stream. Injection occurred during the energized (state II) time interval. Timing of state I and II intervals was

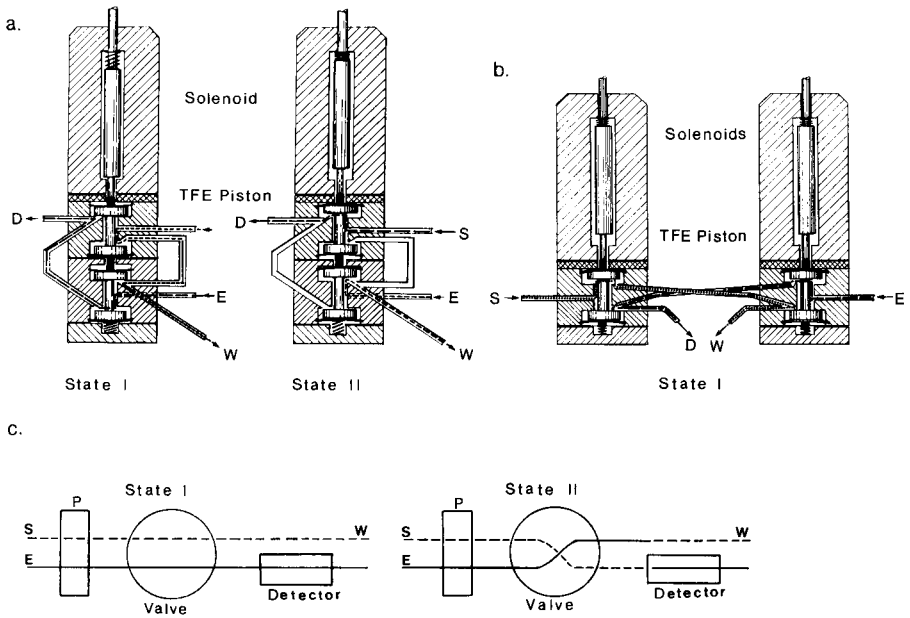

Fig. 2. Four-way valve assembly: (a) cut-away one solenoid; (b) cut-away two solenoid; (c) logic. E, carrier electrolyte; S, sample; D, detector; W, waste; P, pump.

accomplished using the circuit shown in Fig. 3. Sample size and rate of sampling can be adjusted via R5 and R2, respectively.

The flow-through nickel oxide amperometric electrode cell allows for detection of amino functional groups to very low concentrations. The main stream electrolyte is alkaline (0.1 M hydroxide), but samples with moderate pH injected into the stream can readily be accommodated. Construction and further particulars have been described [6].

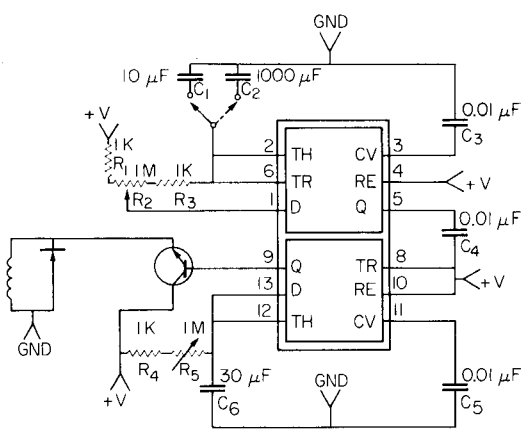

Fig. 3. Timing circuit. Marked connections are for 556 dual timer IC.

The chromatographic technique used was based on those described by Schormüller and Hofmeister [7]. In the present case, the buffer solutions used were 0.1 M sodium arsenite (pH 6.9, 6.5), 0.2 M sodium oxalate (pH 5.0), sodium acetate (pH 5.4), and 0.2 M potassium hydrogenphthalate (pH 4.2, 3.1). A three-way valve and teflon tubing (3-cm long 0.8-mm i.d.) connected the column outlets to the eluate sampling valve system.

Reagents. All amino acids were obtained from Sigma Chemical Co. (St. Louis, MO) except glycine from Aldrich Chemical Co. (Milwaukee, WI). Cation-exchange resin (AG50-X8, Bio-Rad Laboratories, Richmond, CA) with sulfonate sites, 8% cross-linking and 200—400 mesh was used.

Results and discussion

Detector response. It was shown previously [6] that when a blank sample plug of lower pH than the carrier electrolyte reaches the electrode, a negative peak precedes a positive peak signal. These background peak heights depend upon both pH and buffer concentration, but will not change throughout the experiment unless the pH or the buffer concentration is changed. Table 1 shows the signal obtained as a function of pH and buffer concentration for buffers suitable as eluting agents for the amino acid chromatographic separation. The series of positive peaks from the elution buffer alone defines the baseline for the chromatogram obtained (see Fig. 4). Sampling segments of the chromatogram eluate is preferred to continuous pH adjustment and detection because of the long-term electrode effects of buffer species in the latter approach.

When the apparatus was used in a straightforward flow injection mode, a linear quantitative response was found for glycine and serine for concentrations from 1×10^{-6} M and 5×10^{-6} M, respectively, up to 1×10^{-3} M in 0.05 M oxalate buffer solution of pH 5. The sensitivities were 85 and 62 nA μM^{-1}, respectively. The range of linear response for the various amino acids can be expected to differ somewhat [6].

TABLE 1

Nickel oxide electrode response to buffer solutions

Buffer	Concentration (M)	pH	Positive peak (μA)	Negative peak (μA)
Acetate	0.20	5.4	1.40	0.24
	0.05	5.1	0.70	0.05
	0.01	5.1	0.57	0.14
Oxalate	0.20	5.0	0.80	0.30
	0.05	5.0	0.27	0.30
Phthalate	0.20	4.2	0.86	—
	0.20	3.1	0.92	—
Arsenate	0.10	6.9	0.91	0.76
	0.10	6.5	0.90	0.63
Phosphate	0.05	6.9	0.85	0.60
	0.02	6.5	0.76	0.60

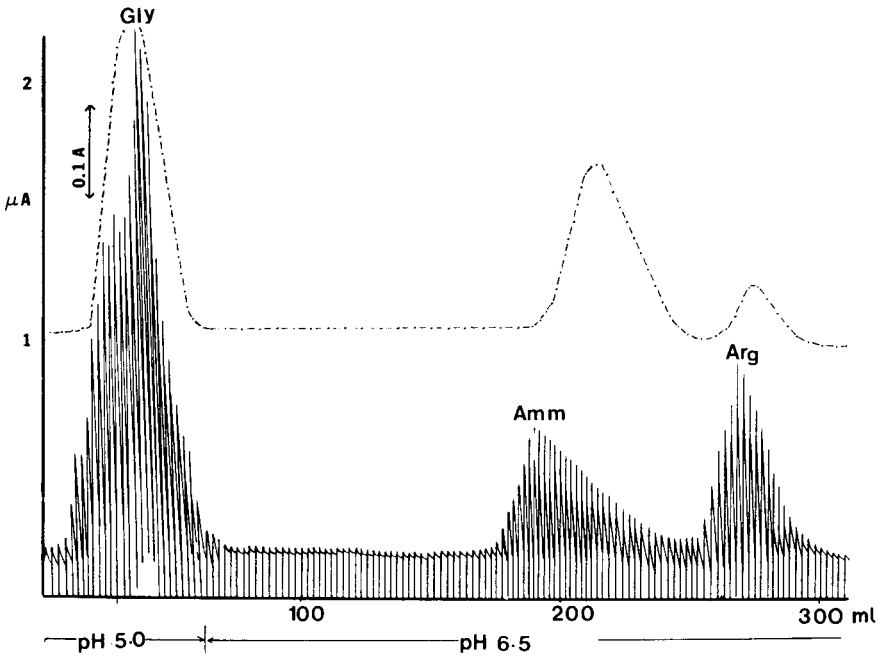

Fig. 4. Chromatogram of glycine (Gly), ammonia (Amm) and arginine (Arg). (-·-·-) U.v. detection; (—) nickel oxide electrode detection. Column: AG50-X8, 200—400 mesh, 0.9 × 20 cm. Flow rate 48 ml h^{-1}; sample, 22 μg total in 1 ml.

Flow rate effects. One feature in the system is that the time during which the column outlet is opened to the flow injection is used to establish the sample volume. Thus, a constant flow rate is essential for eluate samples of equal size throughout the chromatogram. Other effects of flow rate on the system are that sample dispersion and chromatographic resolution [8, 9] are also significant. In order to prevent intermittent backflow when the four-way valve changes state, it is necessary to have equal pressure on the eluent stream and the carrier electrolyte stream. Accordingly, a flow rate of 1.2 ml min^{-1} of carrier electrolyte was found to be optimum. The eluent was sampled for 3.0 s, corresponding to a 20-μl sampling volume. The sampling interval was 1.5 min.

Precision. The precision of the sample was tested by 100 replicate injections of 50 μM glycine in 0.1 M NaOH at 1.5-min intervals. A coefficient of variation of 2.3 was obtained. Precision is probably limited by variations in electrode response or flow rate or sampler timing.

The precision of the detector for sampling intervals as low as 30 s was observed to be similar to that for 1.5-min intervals. For sampling time intervals shorter than 30 s, a smaller sample size should be used. Decreasing the sample segment size or the sampling interval was not necessary for the system described here. Limits for such decreases would be expected because of dispersion and/or rate of electrode response. The flow path between the column and the detector should be kept as small as possible both in diameter

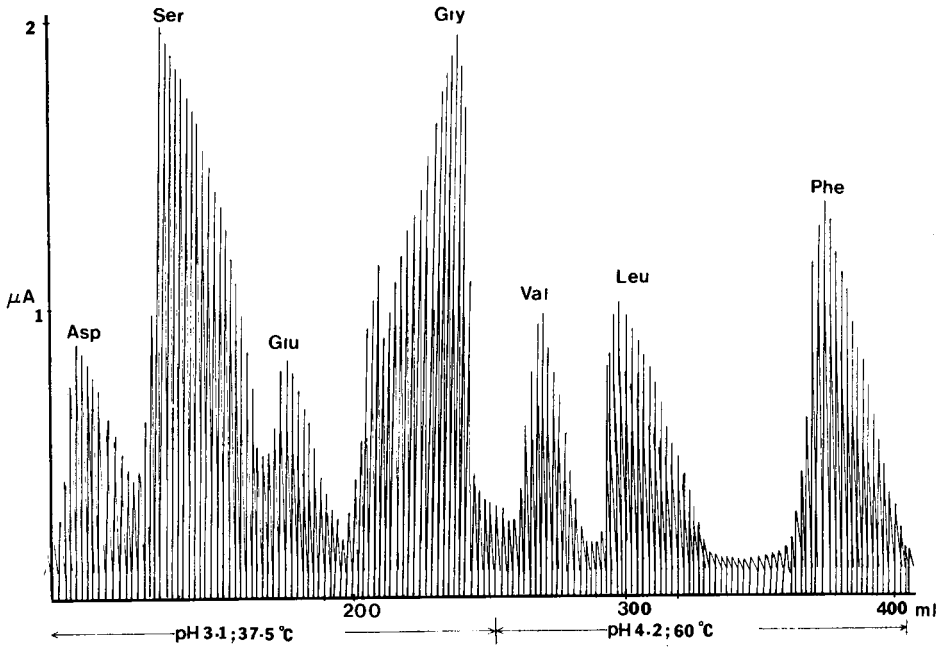

Fig. 5. Chromatogram of seven amino acids from an AG50-X8 (200—400 mesh, 0.9 x 100 cm) column. Acids were aspartic (Asp), serine (Ser), glutamic (Glu), glycine (Gly), valine (Val), leucine (Leu), phenylalanine (Phe). Flow rate 15 ml h^{-1}; sample, 35 μg total in 1 ml; nickel oxide electrode.

and length in order to minimize dispersion of the sampled segment of the chromatographic band.

Chromatograms. A chromatogram of glycine, ammonia and arginine with simultaneous detection by post-column ninhydrin injection with a photometric detector in series with the nickel oxide electrode is shown in Fig. 4. A typical chromatogram showing separation of seven acidic and neutral amino acids is shown in Fig. 5. The sampling and detection system described here can be applied to other sample streams, chromatographic or otherwise, provided that analyte species yield anodic currents in excess of the background.

The authors thank Dr. A. Thompson for technical advice on the timing circuitry.

REFERENCES

1 K. T. Hsu and B. L. Currie, J. Chromatogr., 166 (1978) 555.
2 P. W. Alexander, P. R. Haddad, G. K. C. Low and C. Maitra, J. Chromatogr., 209 (1981) 29.
3 C. R. Loscombe, G. B. Cox and J. A. W. Dalziel, J. Chromatogr., 166 (1978) 403.
4 M. Fleischmann, K. Korinek and D. Pletcher, J. Chem. Soc. Perkin Trans. II, (1972) 1396
5 T. N. Morrison, K. G. Schick and C. O. Huber, Anal. Chim. Acta, 120 (1980) 75.
6 B. S. Hui and C. O. Huber, Anal. Chim. Acta, 134 (1982) 211.
7 J. Schormüller and E. Hofmeister, Z. Lebensm. Unters. Forsch., III (1959) 20.
8 R. Tijssen, Anal. Chim. Acta, 114 (1980) 71.
9 M. Martin, C. Eon and G. Guiochon, J. Chromatogr., 108 (1975) 229.

Analytica Chimica Acta, 139 (1982) 353—357
Elsevier Scientific Publishing Company, Amsterdam — Printed in The Netherlands

Short Communication

POTENTIOMETRIC DETERMINATION OF SULFONAMIDES WITH A SILVER SULFIDE ELECTRODE

F. MAŁECKI* and R. STAROŚCIK
Department of Analytical Chemistry, School of Medicine, 50-139 Wrocław (Poland)

(Received 23rd November 1981)

Summary. The silver sulfide membrane electrode shows well-defined responses to several pharmaceutically important sulfonamides over the concentration range 10^{-1}—10^{-4} M. Both direct and titrimetric determinations of sulfonamides are described and applied to pharmaceutical dosage forms.

Numerous methods are available for the determination of sulfonamide drugs in both biological samples and pharmaceutical dosage forms [1, 2], but few of these are based on reactions with silver ions, and the indirect methods proposed to date have limited applications. Silver-selective electrodes have not been used, even though these sensors may provide many advantages in comparison to other methods. The only attempt to use ion-selective electrodes has involved a liquid-state electrode containing an appropriate ion-pair with the bathophenanthroline—iron(II) complex for determinations of sulfizomidine and sulfamerazine [3].

The present communication reports the application of the silver sulfide membrane electrode as an indicator electrode for both direct potentiometric measurements and for monitoring potentiometric titrations of some pharmaceutically important sulfonamides. It is well known that the presence of a complexing agent can seriously influence the electrode potential of a potentiometric sensor. In the case of silver compound membranes, this effect can be explained by a model developed by Morf et al. [4], according to which the total activity of silver ion at the sample solution—membrane interface comprises the sum of three silver ion activities: (a) in the sample solution, (b) from dissolution of the membrane, and (c) defect or interstitial silver ions. When silver sulfide membrane electrodes are used in solutions free of silver ions but containing a ligand forming relatively weak complexes with silver, the ligand does not dissolve the membrane but may react with the interstitial silver ions. The equation describing the response of the silver sulfide electrode to ligands [5] is

$$E = E^0_{Ag^+} + RT\mathrm{F}^{-1} \ln (\alpha_{Ag^+}/\beta_p) - p\ RT\mathrm{F}^{-1} \ln (L - p\alpha_{Ag^+}) + RT\mathrm{F}^{-1} \ln \gamma_{Ag^+}$$

where p is the coordination number and β_p the formation constant of the complex formed, α_{Ag^+} is the silver ion activity from interstitial silver ions,

0003-2670/82/0000-0000/$02.75

L is the total ligand activity and γ_{Ag^+} is the silver ion activity coefficient. Because silver generally forms linear 1:2 complexes, a slope of −118.3 mV (25° C) for the response to the ligand has to be expected. The experimental data can be used to estimate the coordination number as well as the formation constant of the silver complex. The effect of complexing agents on the function of ion-selective electrodes can be utilized analytically [5, 6]. The cyanide response of silver halide electrodes seems to be the most widely studied example.

Experimental

The all-solid state silver sulfide membrane electrodes were prepared as described earlier [7]. These electrodes responded linearly both to sulfide in the usual anti-oxidant buffer solutions and to silver over concentration ranges of 10^{-1}—10^{-6} M with slopes 28.5 and 58.5 mV/decade, respectively. The performance of the electrode against the known systems $Ag(CN)_2^-$ and $Ag(S_2O_3)_2^{3-}$ was checked; calculation of the defect ion activity α_{Ag^+} was based on the constants 18.75 and 13.2, respectively [8]. The evaluated α_{Ag^+} value was $10^{-6.09}$ M and the $E^0_{Ag^+}$ was 553 mV. The reference electrode was a double-junction saturated calomel electrode (Radiometer K503).

The sulfonamides used were of pharmacopeial grade (Polfa, Poland); other reagents were of analytical grade. Water was purified by deionization followed by distillation. The sulfonamide stock solutions were prepared by dissolving weighed samples in a little 1 M sodium hydroxide and diluting to volume with water.

All e.m.f. measurements were made with a high-impedance digital millivoltmeter (Meratronik V533; Poland); pH was measured with a Mera 512 pH meter and a Radiometer G202 glass electrode. Solutions were stirred during each measurement and maintained at 25° C by a constant temperature bath. The final potential of each test solution was read when the measured potential changed less than 0.1 mV over a 3-min period. Replicate measurements were reproducible to ±0.5 mV. Discrete increments of stock solutions and/or titrant were added from an automatic burette (Radiometer ABU12). The electrode was calibrated against increasing concentrations of the relevant sulfonamide by a titration procedure. The ionic strength of the solutions used in the direct potentiometric measurements was kept constant at 1 M with potassium nitrate. The pH was adjusted with 0.1 M NaOH or 0.1 M HNO_3.

Results and discussion

The response of the silver-selective electrode to sulfonamide drugs was studied for sulfonamides forming soluble complexes with silver (sulfacetamide, acetozolamide, furosemide and hydrochlorothiazide) and for those precipitating silver ions (sulfathiazole and sulfadimethoxine). Alkaline media (pH 9—12) were used to increase both the solubility and ionization of the sulfonamides; the electrode potentials were not affected by pH changes within this range. The response times of the electrode were studied for different

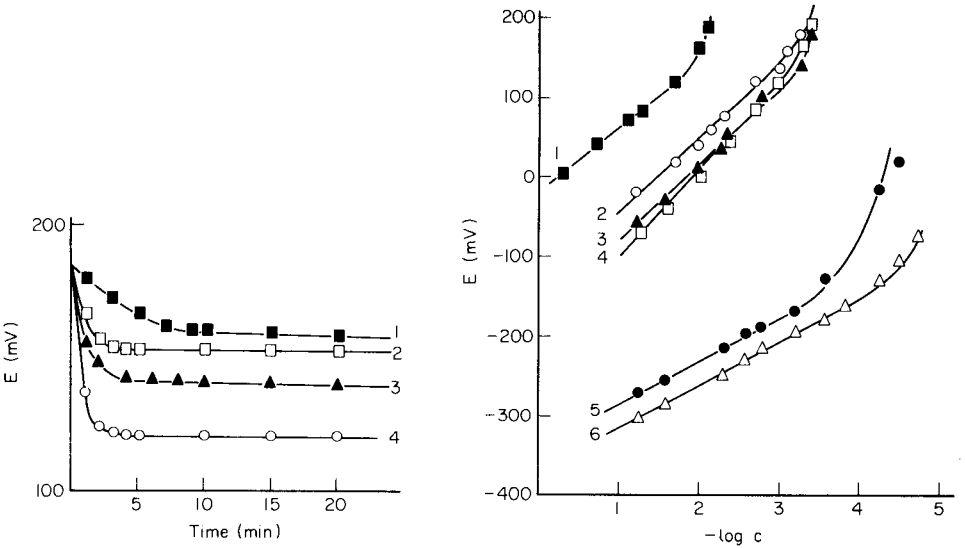

Fig. 1. Response times of the Ag_2S membrane electrode for different sulfonamides: (1) 8.3 × 10^{-3} M sulfacetamide; (2) 5 × 10^{-4} M hydrochlorothiazide (3) 5.4 × 10^{-4} M acetazolamide; (4) 1.9 × 10^{-3} M furosemide. pH 9.5.

Fig. 2. Response of the Ag_2S membrane electrode to different sulfonamides: (1) sulfacetamide; (2) furosemide; (3) acetazolamide; (4) hydrochlorothiazide; (5) sulfadimethoxine; (6) sulfathiazole. pH 9.5; I = 1 M (KNO_3); 25°C.

concentrations of the sulfonamides; Fig. 1 shows that 90% of the expected response was usually obtained within 1—2 min and that steady potentials were established within 5 min, except for sulfacetamide. Plots of the measured potentials against log c for the sulfonamides tested are shown in Fig. 2; as can be seen, the slope of the linear portion of the response curve as well as the linear range depended on the sulfonamide.

These data were used to calculate [5] the complex formation constants (Table 1). The evaluated stability constants compare well with results evaluated by an alternative procedure [9]. The E_L^0 values given in Table 1 were shown to depend linearly on log $(\beta_2)^{1/2}$; the slope of the plot was 118 mV, which is in close agreement with theoretical prediction [4]. It can be concluded that the electrode potential is controlled mainly by the reaction of interstitial silver ions with the respective sulfonamide, resulting in a 1:2 complex. However, it must be noted that the response slopes were only partly in agreement with those predicted by Morf's model. Because of the high pH level used and the similar stabilities of the silver—sulfonamide and silver—hydroxo complexes, it seems probable that the hydroxide ions compete with the sulfonamide for interstitial silver ions, thereby producing the decrease in response slope. The slopes for sulfathiazole and sulfadimethoxine, which form AB precipitates, are almost Nernstian, because of the relatively high pK_{so} values of the precipitates.

TABLE 1

Results of evaluation of the response curves and stability constants ($\log \beta_2$) of the silver—sulfonamide complexes
(pH 9.5, I = 1 M (KNO_3), 25°C)

Sulfonamide	E_L^0[a] (mV)	Limit of detection (M)	Slope (mV/decade)	Log β_2 values	
				This work	Other method [9]
Sulfacetamide	+3.0	2.14	86	3.31	3.43
Furosemide	−116.0	3.28	93	5.34	5.58
Acetazolamide	−157.0	3.30	97	6.04	6.19
Hydrochlorothiazide	−182.0	3.34	109	6.47	6.52
Sulfadimethoxine	−332.0	4.24	51	—	—
Sulfathiazole	−360.0	4.74	54	—	—

[a]Values obtained by extrapolation to 1.0 M activity of the sulfonamide.

The electrode exhibits very little selectivity for the different sulfonamides. An indication of the order of selectivity is given by the selectivity coefficients related to sulfathiazole, taken arbitrarily as the primary ion (Table 2). The relatively high selectivity for some sulfonamides over chloride means that interference may occur when direct potentiometry is used to determine halide ions in the presence of sulfonamides.

Analysis of drugs. The characteristics of the silver sulfide electrode towards sulfonamides seem to make the electrode useful for drug analysis. Commercially available hydrochlorothiazide tablets (containing 25 mg per tablet) were therefore analyzed by the direct method. The sample was prepared by simply mixing with 1 ml of 0.1 M NaOH diluting to 25 ml with 1 M KNO_3. The results listed in Table 3 indicate that the formulation excipients had no effect on the electrode potential.

The silver sulfide electrode can also be used to detect the end-point in titrations of sulfonamides which form sparingly soluble precipitates with silver(I) solution. Potential jumps of about 200 mV were obtained in titrations of 10^{-2} M sulfadimethoxine at pH 12.5, and the end-points could be readily located even for 10^{-4} M solutions. In the procedure suggested, the solid sample (tablet or substance) containing 100—200 mg of the sulfonamide is mixed with 50 ml of 0.1 M NaOH and the solution or suspension is titrated

TABLE 2

Selectivity coefficients by the separate solutions method for sulfathiazole as the primary ion i
($c_i = c_j$ = 0.1 M, pH 9.5, I = 1.0 M, KNO_3)

Ion j	Sulfadimethoxine	Hydrochlorothiazide	Acetazolamide	Furosemide	Sulfacetamide	Chloride
$-\log k_{ij}^{pot}$	0.45	3.07	3.83	4.54	6.60	2.60

TABLE 3

Determination of sulfonamides in some commercial tablets

Tablet	Sulfonamide component	Method used	Amount (mg)		Recovery (%)	R.s.d. (%)
			Stated	Found[a]		
Madroxin	Sulfadimethoxine	Titrimetric	500	500.2	100.0	1.2
Merafin	Sulfamerazine[b]	Titrimetric	375	381.1	101.8	1.2
Hydrochloro-thiazide	Hydrochloro-thiazide	Direct	25	25.4	101.6	2.9

[a]Average of at least 5 determinations. [b]These tablets also contain sulfaproxyline (375 mg per tablet).

with standard silver nitrate solution. Typical results for two commercial formulations are listed in Table 3. The tablet excipients did not interfere nor did sulfaproxyline, a second sulfonamide component of the Merafin tablets. The procedure above was also used for sulfadimidine tablets with satisfactory results.

Efforts to employ solid-state copper-selective electrodes for similar purposes were unsuccessful.

REFERENCES

1 S. Ebel, Handbuch der Arzneimittel-Analytik, Verlag Chemie, Weinheim, 1977.
2 V. Bekárek and H. Kalová, Chem. Listy, 70 (1976) 17.
3 N. Hazemoto, N. Kamo and Y. Kobatake, J. Pharm. Sci., 65 (1976) 435.
4 W. E. Morf, G. Kahr and W. Simon, Anal. Chem., 46 (1974) 1538.
5 P. K. C. Tseng and W. F. Gutknecht, Anal. Chem., 47 (1975) 2316.
6 M. F. El-Taras, E. Pungor and G. Nagy, Anal. Chim. Acta, 82 (1976) 285.
7 R. Starościk and F. Małecki, Acta Pol. Pharm., 34 (1977) 643.
8 L. R. Sillen and A. E. Martell, Stability Constants of Metal-Ion Complexes, Spec. Publ. No. 17, The Chemical Society, London, 1964.
9 F. Małecki and R. Starościk, Pharmazie, submitted.

Analytica Chimica Acta, 139 (1982) 359—362
Elsevier Scientific Publishing Company, Amsterdam — Printed in The Netherlands

Short Communication

AMPEROMETRIC DETERMINATION OF CHOLINESTERASE WITH USE OF AN IMMOBILIZED ENZYME ELECTRODE

FUMIO MIZUTANI* and KEISHIRO TSUDA

Research Institute for Polymers and Textiles, 1-1-4, Yatabe-Higashi, Tsukuba, Ibaraki 305 (Japan)

(Received 18th February 1982)

Summary. A choline-sensitive electrode consisting of an immobilized choline oxidase layer and an oxygen electrode is described. Cholinesterase (0.5—60 I.U. l^{-1}) is measured by addition of acetylcholine, and detection of the choline produced. The precision is 3%, and the electrode is stable for more than 2 weeks (140 assays).

The determination of cholinesterase (acylcholine acyl-hydrolase, E.C. 3.1.1.8) in serum is of clinical importance for a variety of disorders, e.g., depressed levels of the enzyme are often indicative of liver disease [1—3]. Numerous methods have been proposed for the assay of cholinesterase [4, 5]. While some spectrophotometric methods [6—8] have been commonly accepted for routine use, electrochemical monitoring has the advantage of providing simple, rapid assays. Gibson and Guilbault [9] have described an improved electrochemical method. The rate of pH decrease of a weak buffer caused by enzymatic liberation of protons is monitored by a glass electrode. However, this method is of limited use because the electrode responds erroneously in the presence of biological fluids, as in the case of the acetylcholine- [10] and thiocholine-sensitive [11] systems.

Choline oxidase (E.C. 1.1.3.17) has been employed as a homogeneous catalyst for the amperometric determination of cholinesterase as well as its spectrophotometric measurement [8]. However, an enzyme electrode constructed from an immobilized choline oxidase layer and an amperometric device has not previously been examined as a sensor for cholinesterase, although this system provides a compact and substrate-specific device.

Experimental

Materials. The enzymes used were choline oxidase (E.C. 1.1.3.17, from *Alcaligenes* sp., 7 I.U. mg^{-1}; Toyobo), cholinesterase (E.C. 3.1.1.8, from human serum, 8 I.U. mg^{-1}; Sigma Chemical), and peroxidase (E.C. 1.11.1.7, from horseradish, 270 I.U. mg^{-1}; Toyobo). Human sera used were commercially available lyophilized (Böhringer Mannheim). Acetylcholine chloride (Sigma Chemical) and the other reagents (analytical grade, Nakarai Chemicals) were used as received.

0003-2670/82/0000—0000/$02.75

Enzyme assays. Choline oxidase was determined by the method of Ikuta et al. [12]; hydrogen peroxide generation was assayed by using a peroxidase—phenol—4-aminoantipyrine system. Cholinesterase was determined by the method of Dietz et al. [7]; the thiocholine liberated was detected by its chromogenic reaction with 5,5′-dithio-bis(nitrobenzoic acid). A Hitachi model 323 spectrophotometer was used for these assays.

Assembly of enzyme electrode. The enzyme solution (100 μl, containing 20 I.U. of choline oxidase in 0.2 M phosphate buffer, pH 7.7) was dropped onto a porous filter membrane (Millipore, type GS, 10-mm diameter) which was placed on a dialysis membrane (Visking, 15-mm diameter) with suction. The filter membrane (inside) and the dialysis membrane (outside) were attached to the teflon membrane of an oxygen electrode (battery-type, with a platinum cathode of 3-mm diameter; Ishikawa Manufacturing) and fastened with rubber rings, so that the enzyme was trapped in the filter membrane, sandwiched between the other membranes. The enzyme electrode thus prepared was stored in 0.2 M phosphate buffer (pH 7.7) at 5° C when not in use.

Procedures. The system consisted of a cylindrical cell (volume ca. 20 ml), enzyme electrode and recorder (Yokogawa Electric Works, model 3066). The enzyme electrode was inserted into the test solution (10 ml) which was saturated with oxygen by bubbling air continuously (ca. 100 ml min^{-1}) and was stirred magnetically. The temperature of the solution was kept at 30 ± 0.1° C. The current obtained from the enzyme electrode was recorded through a 2-kΩ resistance.

The solutions used were 0.2 M phosphate buffer (pH 7.7) for the assay of choline (as chloride) and the same buffer solution containing 10 mM acetylcholine (as chloride) for the assay of cholinesterase. The pH of the buffer used was very close to the optimal pH for choline oxidase [12] and cholinesterase [5]. The concentration of acetylcholine is several times larger than the K_m value of cholinesterase for this substrate [9]. Acetylcholine was added to the buffer solution several minutes before the enzyme assay in order to minimize its non-enzymatic decomposition, which became significant if the solution containing acetylcholine was left for several hours.

Results and discussion

Response to choline. The assay of cholinesterase is based on monitoring choline generated from the enzymatic hydrolysis of acetylcholine. Therefore, the response of the electrode to choline was first examined. Figure 1 shows the response curves obtained by the addition of different concentration of choline. The current began to decrease a few seconds after the addition of choline, and ca. 2 min was required to restore a steady-state current. The oxidation of choline, which took place in the immobilized choline oxidase layer, caused a decrease in dissolved oxygen in the layer and thus a decrease in the current. A linear relationship was observed between the current decrease (the difference between the initial current and the steady-state current during the assay) and the concentration of choline up to 0.3 mM

(current decrease 1.78 μA). The minimum concentration of choline which could be determined was ca. 2 μM (signal:noise = 5).

Response to cholinesterase. Figure 2 shows the response curves of the enzyme electrode in solutions containing different concentrations of cholinesterase. The initial current in this case was somewhat less than in the buffer without acetylcholine (Fig. 1). This might be attributed to the presence of choline in the acetylcholine. As shown in Fig. 2, the addition of cholinesterase caused a discernible decrease in the current from the initial level. The current decreased linearly with time at least from 2 to 5 min after the addition of the enzyme. The rate of current decrease in the linear region is proportional to the rate of increase in the concentration of choline, i.e., proportional to the activity of cholinesterase added.

When the enzyme electrode used for the assay was rinsed in water and then inserted in the solution without cholinesterase, the current returned to its initial level within a few minutes.

Calibration. A linear relationship was obtained between the rate of the current decrease, $\Delta i/\Delta t$, between 2 and 4 min after the addition of cholinesterase, and the activity of cholinesterase from 0.5 to 60 I.U. l^{-1}. The equation was $\Delta i/\Delta t = 5.75a + 9.80$ nA min^{-1}, where a is the activity of cholinesterase in the solution (I.U. l^{-1}). The term 9.80 reflects the non-enzymatic hydrolysis of acetylcholine; the current decreased at 9.8 nA min^{-1} in the acetylcholine-containing solution when cholinesterase was absent. The relative standard deviation of the response for 10 successive assays of 10 I.U. l^{-1} cholinesterase was 3%.

Stability and application of the enzyme electrode. The long-term stability of the enzyme electrode was examined; cholinesterase (10 I.U. l^{-1}) was

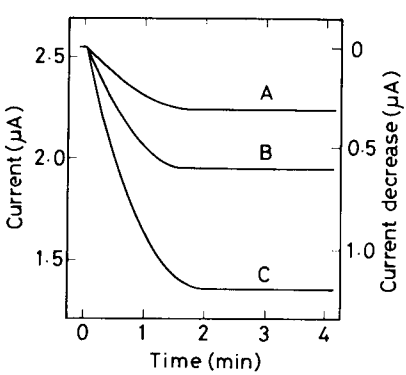

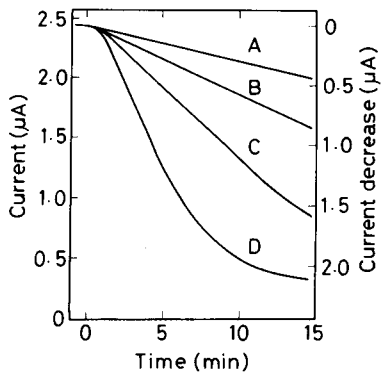

Fig. 1. Typical response curves of the enzyme electrode to: (A) 0.05 mM; (B) 0.10 mM; (C) 0.20 mM choline.

Fig. 2. Typical response curves of the enzyme electrode after the addition of: (A) 5.1; (B) 10.0; (C) 20.5; (D) 51.0 I.U. l^{-1} cholinesterase to a 10 mM acetylcholine solution, pH 7.7 (0.2 M phosphate buffer).

TABLE 1

Comparison of results obtained for cholinesterase in human sera

Serum no.	Activity of cholinesterase in serum (I.U. l^{-1})	
	Present method	Spectrophotometry [7]
1	4360	4280
2	3500	3560
3	3740	3830
4	3660	3670

measured 10 times a day, every day for 3 weeks. The average rate of the current decrease over the 10 successive assays was unchanged for more than 2 weeks.

Cholinesterase activities in human sera were determined by the proposed method and the conventional spectrophotometric method [7]. In the proposed method, 50 μl of serum was added to the solution containing acetylcholine. The results, summarized in Table 1, agreed satisfactorily. These results show that cholinesterase can be determined accurately by the proposed method, and that is useful for a reasonable time.

The authors are grateful to Mr. T. Yamanaka, Drs. K. Sasaki and Y. Shimura for their helpful discussions.

REFERENCES

1 R. V. LaMotta, H. M. Williams and H. J. Weststone, Gastroenterology, 33 (1957) 50.
2 H. J. Weststone, R. V. LaMotta, A. Bellucci, R. Tennant and B. V. White, Ann. Int. Med., 52 (1969) 102.
3 V. Fintelmann and H. Linder, Dtsch. Med. Wochenschr., 95 (1970) 469.
4 K. B. Augstinsson, in D. Glick (Ed.), Methods of Biochemical Analysis, Suppl. Vol., Interscience, New York, 1970, pp. 217—273.
5 G. G. Guilbault, Handbook of Enzymatic Methods of Biochemical Analysis, Dekker, New York, 1976, pp. 86—92.
6 F. Rappaport, J. Fische and N. Pinto, Clin. Chim. Acta, 4 (1959) 227.
7 A. A. Dietz, H. M. Rubinstein and T. Lubrano, Clin. Chem., 19 (1973) 1309.
8 H. Okabe, K. Sagehara, N. Nakajima and A. Noma, Clin. Chim. Acta, 80 (1977) 87.
9 K. Gibson and G. G. Guilbault, Anal. Chim. Acta, 76 (1975) 245.
10 G. Baum, F. B. Ward and S. Yaverbaum, Clin. Chim. Acta, 36 (1972) 405.
11 G. G. Guilbault and H. von Storp, Anal. Chim. Acta, 62 (1972) 425.
12 S. Ikuta, S. Imamura, H. Misaki and Y. Horiuchi, J. Biochem., 82 (1977) 1741.

Analytica Chimica Acta, 139 (1982) 363—366
Elsevier Scientific Publishing Company, Amsterdam — Printed in The Netherlands

Short Communication

CONTINUOUS-FLOW ANALYSIS FOR ETHANOL WITH IMMOBILIZED ALCOHOL DEHYDROGENASE

TOSHIO YAO*, YOSHIAKI KOBAYASHI and SOICHIRO MUSHA

Department of Applied Chemistry, College of Engineering, University of Osaka Prefecture, Mozu-Umemachi, Sakai 591 (Japan)

(Received 4th January 1982)

Summary. Alcohol dehydrogenase is immobilized by reaction with glutaraldehyde onto silica gel, which is packed in a column in a flow system. Ethanol (0.1—5 mmol) is determined by catalysis of the reaction with NAD^+, the NADH produced being detected amperometrically. The reproducibility is ca. 1%.

Alcohol dehydrogenase catalyzes the reaction

$$CH_3CH_2OH + NAD^+ \rightleftharpoons CH_3CHO + NADH + H^+$$

This reaction is often used to determine ethanol by measuring the NADH produced. The concentration of NADH is proportional to the original ethanol concentration if NAD^+ is in sufficiently high concentration to keep the reaction pseudo-first order. NADH is oxidizable at a variety of solid electrode materials [1—3], and can be monitored amperometrically.

Immobilization of enzymes onto water-insoluble matrices by covalent bonding has several advantages over the use of soluble enzymes. These include longer lifetimes and less temperature sensitivity [4]. If the immobilized enzyme is used in a continuous-flow system, handling is minimized and reproducibility is enhanced. Packed-bed reactors [5—12] and open tubes with enzymes immobilized on the wall [8, 9, 13—20] have been used in various flow systems, including those involving alcohol dehydrogenase.

This communication describes a continuous-flow method for the determination of ethanol, in which alcohol dehydrogenase is immobilized by the widely used aminoalkyl-bonded silica gel—glutaraldehyde procedure [21].

Experimental

Reagents. Alcohol dehydrogenase (E.C. 1.1.1.1, 100 I.U. mg^{-1}), NAD^+ and NADH were commercial preparations (Oriental Yeast Co., Tokyo) used as received. Pyrophosphate buffers (0.1 M) were prepared from sodium pyrophosphate (Wako Pure Chemical) in distilled water and adjusted to the desired pH values with 6 M hydrochloric acid. All other reagents were of analytical-reagent grade.

0003-2670/82/0000-0000/$02.75

Apparatus. The equipment included a high-performance liquid chromatograph (Yanagimoto L-2000), a voltammetric detector (Yanagimoto VMD-101; a thin-layer electrochemical flow cell consisting of a glassy carbon working electrode, a silver—silver chloride reference electrode, and a platinum auxiliary electrode) and a strip-chart recorder (Hitachi 056-3001). The stainless steel column (12.5 cm long, 4.00 mm i.d.) packed with the immobilized alcohol dehydrogenase was positioned just after the point of sample introduction. Samples were injected with a 100-μl sample loop injection valve.

Immobilization of alcohol dehydrogenase on silica gel. The method was similar to that described before [12]. Silica gel was boiled in 6 M hydrochloric acid for 2 h, and refluxed with stirring for 5 h in a 10% (v/v) solution of 3-aminopropyltriethoxysilane (Tokyo Kasei Co.) in toluene. The resulting aminoalkyl-bonded silica gel was activated for binding the enzyme by reaction with an aqueous 5% (v/v) solution of glutaraldehyde. The activated silica gel was packed into the stainless steel column, and alcohol dehydrogenase was loaded onto the column by circulating a solution of the enzyme (10 U. ml^{-1}) in sodium hydrogencarbonate solution (0.1 M, pH 8.5), 0.1 M in sodium chloride through the column at 2 ml min^{-1} for 24 h at room temperature. The column was washed for 12 h with a 0.1 M sodium hydrogen carbonate solution at pH 8.5 and was stored at 5° C in the same solution when not in use.

Results and discussion

Selection of experimental conditions. Experiments were conducted to establish the optimum pH, under flow conditions, for the determination of ethanol. Figure 1 evaluates the effect of pH in terms of peak current. Maximum activity of the immobilized alcohol dehydrogenase occurred at a pH close to 8.5 and this pH was used in all later work. As the NAD^+ concentration in the buffer was increased, the peak current increased gradually. However, the peak current fell off above 1 mM because of electrode fouling. Also, the peak current increased with an increase in the sodium chloride concentration in the buffer up to 0.5 M, but remained constant at higher concentrations. Therefore, a pyrophosphate buffer at pH 8.5, 0.5 mM in NAD^+ and 0.5 M in sodium chloride was selected as the carrier solution. Maximum sensitivity was obtained at applied potentials above 0.8 V vs. Ag/Ag^+, and so this potential was applied to the flow cell for NADH monitoring. The effect of flow rate on the peak current obtained for injections of a 1.0 mM ethanol solution is shown in Fig. 2. As the peak current decreased sharply with an increase in the flow rate, 1.5 ml min^{-1} is recommended as a suitable flow rate for achieving relatively good sensitivity and a reasonable determination rate (about 1 every 2 min).

The peak current was nearly proportional to the injected sample size from 5 to 100 μl. The sample size preferred was 100 μl, because it provides reasonable sensitivity without much sacrifice in the time of return to baseline that determines the rate of sample throughput.

Calibration curve and precision. Figure 3 shows a typical calibration curve for ethanol obtained for freshly prepared solutions by measurements of peak

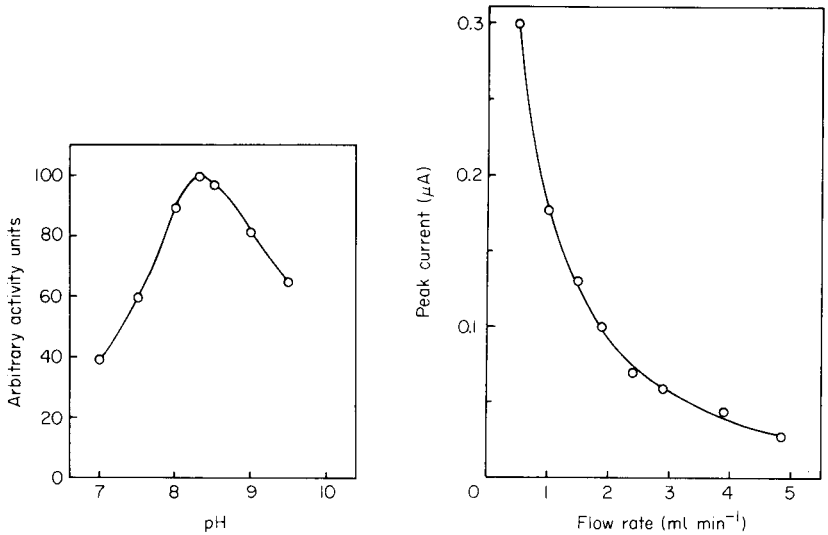

Fig. 1. pH profile for the activity of alcohol dehydrogenase immobilized on silica gel, with sodium pyrophosphate buffers, 0.5 mM in NAD^+.

Fig. 2. Effect of flow rate on the peak current for 1.0 mM ethanol.

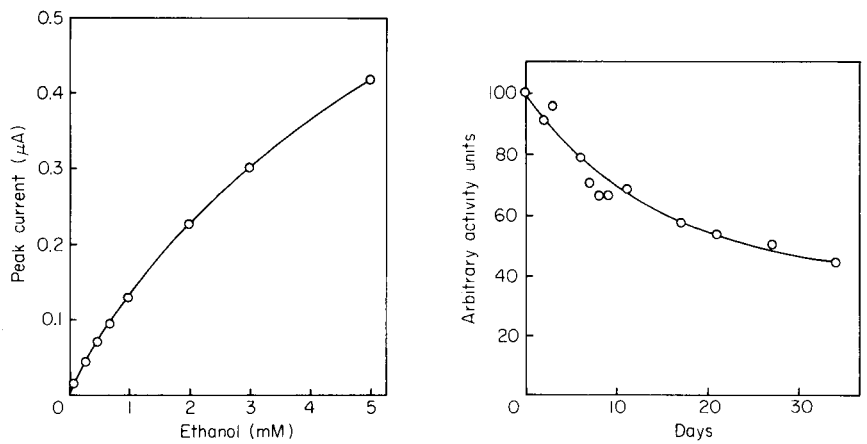

Fig. 3. Peak current vs. ethanol concentration.

Fig. 4. Storage stability of alcohol dehydrogenase immobilized on silica gel.

currents. The peak current is a non-linear function of ethanol concentration over the range 0.1—5 mM. However, the relative standard deviation for 10 replicate injections was 1.2% at the 0.3 mM level and 0.54% at the 3 mM level.

Selectivity and stability of immobilized alcohol dehydrogenase. The selectivity of the alcohol dehydrogenase immobilized on silica gel was evaluated

TABLE 1

Selectivity of the immobilized alcohol dehydrogenase

Compound[a]	Relative activity	Compound[a]	Relative activity
Methanol	0	1-Butanol	10.9
Ethanol	100	1-Pentanol	3.9
1-Propanol	24.2		

[a]At the 2 mM level.

by measuring the response to other alcohols. Table 1 shows that 1-butanol and 1-pentanol were only slightly oxidized and methanol was unaffected. 1-Propanol was 24% as reactive as ethanol.

The stability of the immobilized alcohol dehydrogenase under the defined storage conditions is shown in Fig. 4. The useful lifetime was ca. 30 days. This was considerably poorer than the highly stable immobilized lactate dehydrogenase reported previously [12].

This work was supported by a Grant-in-Aid for scientific research from the Ministry of Education, Japan.

REFERENCES

1 W. J. Blaedel and R. A. Jenkins, Anal. Chem., 47 (1975) 1337.
2 J. Moiroux and P. J. Elving, Anal. Chem., 51 (1979) 346.
3 D. N. Grag, D. H. Keyes and B. Watson, Anal. Chem., 49 (1977) 1067A.
4 O. R. Zaborsky, Immobilized Enzymes, CRC Press, Cleveland, Ohio, 1973.
5 R. S. Schifreen, D. A. Hanna, L. D. Bowers and P. W. Carr, Anal. Chem., 49 (1977) 1929.
6 R. E. Adams and P. W. Carr, Anal. Chem., 50 (1978) 944.
7 A. Iob and H. A. Mottola, Anal. Chem., 52 (1980) 2332.
8 A. S. Attiyat and G. D. Christian, Analyst, 105 (1980) 154.
9 E. L. Gulberg and G. D. Christian, Anal. Chim. Acta, 123 (1981) 125.
10 L. Ögren, Anal. Chim. Acta, 125 (1981) 45.
11 A. O. Lindberg, Anal. Chim. Acta, 131 (1981) 133.
12 T. Yao, Y. Kobayashi and S. Musha, Anal. Chim. Acta, 138 (1982) 81.
13 M. D. Joseph, D. J. Kasprzak and S. R. Crouch, Clin. Chem., 23 (1977) 1033.
14 L. P. Leon, M. Sansur, L. R. Snyder and C. Horvath, Clin. Chem., 23 (1977) 1556.
15 G. A. Noy, A. L. J. Buckle and K. G. M. M. Alberti, Clin. Chim. Acta, 89 (1978) 135.
16 P. V. Sundaram and M. P. Igloi, Clin. Chim. Acta, 94 (1979) 295.
17 R. Chirillo, G. Caenaro, B. Pavan and A. Pin, Clin. Chem., 25 (1979) 1744.
18 R. Bais, N. Potezny, J. B. Edwards, A. M. Rofe and R. A. J. Conyers, Anal. Chem., 52 (1980) 508.
19 L. P. Leon, D. K. Chu, L. R. Snyder and C. Horvath, Clin. Chem., 26 (1980) 123.
20 W. Hinsch, A. Antonijević and P. V. Sundaram, J. Clin. Chem. Clin. Biochem., 19 (1981) 307.
21 I. Chibata, Immobilized Enzymes, Halsted Press, New York, 1978.

Analytica Chimica Acta, 139 (1982) 367—372
Elsevier Scientific Publishing Company, Amsterdam — Printed in The Netherlands

Short Communication

DIFFERENTIAL PULSE VOLTAMMETRIC STUDY OF THE COMPLEXATION OF AN IRON PORPHYRIN AT SUBSTOICHIOMETRIC LEVELS OF LIGAND

LAWRENCE A. BOTTOMLEY[a] and KARL M. KADISH*

Department of Chemistry, University of Houston, Houston, TX 77004 (U.S.A.)

(Received 7th December 1981)

Summary. A new approach is presented for elucidating the complex identities of iron porphyrins when both the electrode reactant and product are strongly coordinated by an equal number of ligands. The current is monitored for each electroactive form of the complex at substoichiometric levels of ligand. The increased resolution afforded by the differential pulse technique is used to elucidate the stepwise formation of complexes. Current—voltage curves are described for perchlorato(2,3,7,8,12,13,17,18-octaethylporphinato)iron(III), in the presence of low levels of imidazole. At imidazole:porphyrin ratios of less than 2, the mono-adduct is reduced at a peak potential of —0.11 V while the bis-ligand adduct is reduced at —0.38 V. This marks the first electrochemical evidence for a mono-ligated imidazole—Fe(III) species.

Since the pioneering work of DeFord and Hume [1], electroanalytical methods have been widely used in the study of metal complexation equilibria. Several theoretical approaches [2—7] have been developed for elucidating complex stoichiometry and stability constants from current—voltage data. These approaches mainly depend on an accurate determination of the potential associated with either reduction or oxidation of the complex as the concentration of ligand is increased. The concentration of ligand is usually in excess. In the course of electrochemical investigations of synthetic metalloporphyrins [7—10], cases were frequently encountered in which both the oxidized and reduced species involved in the electron transfer were strongly coordinated by the same type of axial ligand. This type of reaction can be described in general terms by

$$ML_p^{(n+1)} + e^- \rightleftharpoons ML_q^{(n)} + (p - q)L \quad (1)$$

The stability constants of the two species at the electrode surface are defined as

$$\beta_{ML_p} = [ML_p^{(n+1)}]/[M^{(n+1)}][L]^p \text{ and } \beta_{ML_q} = [ML_q^{(n)}]/[M^{(n)}][L]^q$$

The measured $E_{1/2}$ value at any concentration of ligand is shifted from the $E_{1/2}$ value determined in the absence of ligand by an amount commensurate with the concentration of L, and the stoichiometry of both the reactant and

[a]Present Address: Department of Chemistry, The Florida State University, Tallahassee, FL 32306, U.S.A.

0003-2670/82/0000-0000/$02.75

product at the electrode and their respective stabilities, according to the equation

$$E_{1/2}(\text{complex}) = E_{1/2}(\text{free}) - RT(n\text{F})^{-1} \ln (\beta_{\text{ML}_p}/\beta_{\text{ML}_q}) - RT(n\text{F})^{-1} \ln [\text{L}]^{(p-q)} \quad (2)$$

This is the well-known Lingane treatment for the determination of coordination numbers and stability constants of metal complexes [2]. The treatment assumes that the activity coefficients of all species and the square root of the ratio of diffusion coefficients ($D_{\text{ML}_p}/D_{\text{ML}_q}$) do not deviate substantially from unity. When $(p - q) \neq 0$ in Eqn. (2), the stoichiometry of the reaction can be determined in a straightforward manner by conventional potential–concentration methodology. This methodology can still be useful when $p = q$ and either β_{ML_p} or β_{ML_q} is small [8]. However, when both β_{ML_p} and β_{ML_q} are large (greater than 10^5), the conventional method is not applicable because the halfwave potential is independent of free ligand concentration.

This communication presents a new approach for elucidating complex stoichiometry when both the electrode reactant and product are strongly coordinated by an equal number of ligands. Conventionally, the potential for reduction or oxidation of the complexes is measured in the presence of excess ligand; here, the current is monitored for each electroactive form of the complex at less than stoichiometric levels of ligand. The increased resolution afforded by the differential pulse technique is utilized to elucidate the stepwise formation of complexes.

Experimental

Perchlorato(2,3,7,8,12,13,17,18-octaethylporphinato)iron(III), OEPFeClO_4, was synthesized from (OEPH_2), the free base, in accordance with standard literature procedures [11]. The starting material was used as received from Strem Chemical Company. The solvent, dichloromethane, was stripped of its stabilizer by extraction first with concentrated sulfuric acid, then twice with distilled water and finally fractional distillation under nitrogen from phosphorus(V) oxide. Solvent treated in this manner was stored over activated 3-Å molecular sieves, in the dark, prior to use. The supporting electrolyte, tetrabutylammonium perchlorate (TBAP), was recrystallized from ethyl acetate and dried in vacuo at 100°C prior to use. *N*-Methylimidazole was used as received from Aldrich Chemical Company.

Cyclic voltammetric measurements were obtained with the apparatus previously described [9]. For differential pulse voltammetry, an EG & G PAR Model 174A Polarographic Analyzer was used with a conventional three-electrode configuration. A scan rate of 10 mV s^{-1}, a pulse interval of 0.5 s, and a pulse amplitude of 25 mV were the instrumental parameters imposed on the working (Pt button) electrode. All potential measurements were referenced to a commercial saturated calomel electrode (SCE) which contained a porous asbestos fiber junction. Aqueous contamination of por-

phyrin solutions was minimized by isolating the reference electrode in a bridge having a porous glass junction (medium porosity). The bridge was filled with dichloromethane, 0.1 M in TBAP. Oxygen was purged from solutions by passing nitrogen presaturated with solvent for 10 min; solutions were blanketed with similar nitrogen during measurements.

Aliquots of an *N*-methylimidazole solution in dichloromethane, 0.1 M in TBAP, were added to 5.00 ml of test solution which was 2.27 mM in $OEPFeClO_4$ and 0.1 M in TBAP. Precise volumes of the reagent solution were delivered via a 10-μl Hamilton syringe. The solution was stirred for ~20 s and allowed to come to rest for ~5 s, and then the differential pulse voltammogram was recorded. All experiments were done at 23 ± 1°C.

Results and discussion

In the non-coordinating solvent, dichloromethane, reduction of $OEPFeClO_4$ occurs quasi-reversibly at $E_{1/2}$ = 0.08 V vs. SCE [12]. At *N*-methylimidazole (N—MeIm):$OEPFeClO_4$ ratios greater than 2, a single quasi-reversible process is observed at $E_{1/2}$ = —0.38 V which corresponds to the electro-reduction of an axially complexed iron(II) porphyrin

$$OEPFe(N—MeIm)_2^+ClO_4^- + e^- \rightleftharpoons OEPFe(N—MeIm)_2 + ClO_4^-$$

At substoichiometric levels of ligand, however, up to three distinct single electron-transfer processes are observed in the range of +0.30 to —0.60 V with differential pulse voltammetry. Differential pulse voltammograms obtained during the addition of the *N*-methylimidazole solution to $OEPFeClO_4$ are depicted in Fig. 1. As the ligand:metalloporphyrin molar ratios increased from 0 to 2, the peak current observed at +0.08 V decreased with a concomitant increase in current at —0.38 V. At interim ratios, a third process at —0.11 V first increased and then decreased with increasing ligand concentration. Evaluation of the peak width at half current for each process yielded identical values, indicating no change in electron transfer kinetics upon complexation. The peak current for the process at E_p = —0.38 V is about 1.5 times the peak current for the reduction of the uncomplexed species. The increase in peak current was also seen in the cyclic voltammogram and reflects an increase in the diffusion coefficient. Differential pulse peak currents for each process were normalized and are plotted (Fig. 2) against the ligand:metalloporphyrin molar ratio.

The results of Fig. 2 clearly indicate that the process at —0.11 V involves the reduction

$$OEPFe(N—MeIm)ClO_4 + e^- \rightleftharpoons OEPFe(N—MeIm) + ClO_4^-$$

Interestingly, this marks the first electrochemical evidence for a mono-ligated imidazole—Fe(III) species. Walker et al. [13] have previously shown that complexation of iron(III) porphyrins with non-sterically hindered imidazoles is concerted. Addition of the second imidazole is thermodynamically favored over addition of the first. Thus, only a bis-ligated species has previously been observed.

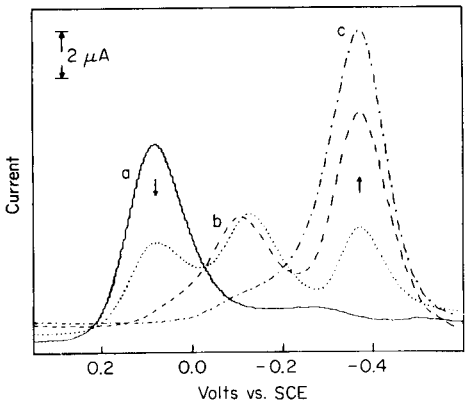

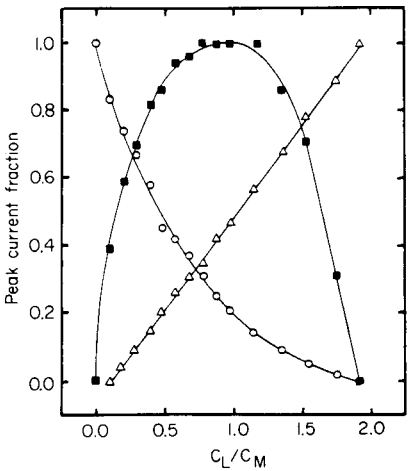

Fig. 1. Differential pulse voltammetric monitoring of the reaction of 2.27 mM $OEPFeClO_4$ with *N*-methylimidazole in CH_2Cl_2 containing 0.10 M TBAP. The concentrations of *N*-methylimidazole were: (—) 0.00 mM; (....) 1.32 mM; (- - - -) 3.06 mM; (-·-·-) 4.54 mM. Peak a corresponds to the reduction of $OEPFeClO_4$; peak b corresponds to the reduction of $OEPFe(N—MeIm)ClO_4$; peak c corresponds to the reduction of $OEPFe(N—MeIm)_2^+ClO_4^-$.

Fig. 2. Plot of the normalized current for each peak vs. ratio of equivalents of N—MeIm, L, to $OEPFeClO_4$, M. The symbols (○), (▪) and (△) denote the normalized current observed for the electron-transfer processes at 0.08 V (peak a, Fig. 1), —0.11 V (peak b) and —0.38 V (peak c).

The lability of the investigated ligand with $OEPFe^+$ has been previously determined by proton n.m.r. line width analysis [14]. Line broadening by ligand exchange of $(N—MeIm)_2^+Cl^-$ was reported. An intermediate species, $OEPFe(N—MeIm)_2^+Cl_4^-$). The driving force for this process is the ease of was shown to have a lifetime of 1.05 ± 0.08 ms. This lifetime was reported to be independent of counter-ion and was determined with the ligand concentration in excess.

In the differential pulse experiments with the instrumental parameters defined above for the Model 174A, current samples are taken over 17-ms periods just before the start and end of the 57-ms pulse. At substoichiometric levels of *N*-methylimidazole, this time window is more than sufficient for dissociation of *N*-methylimidazole from $OEPFe(N—MeIm)_2^+ClO_4^-$ to occur at the electrode (assuming that the rate is similar to that observed for $OEPFe(N—MeIm)_2^+Cl^-$). The driving force for this process is the ease of reduction of the intermediate mono-adduct as compared to the di-adduct (—0.11 vs. —0.38 V). This exchange process can be represented by

$$OEPFe(N—MeIm)_2^+ClO_4^- \rightleftharpoons OEPFe(N—MeIm)ClO_4 + N—MeIm \quad (3)$$

$$OEPFe(N—MeIm)ClO_4 + N—MeIm^* \rightleftharpoons OEPFe(N—MeIm)(N—MeIm^*)^+ClO_4^- \quad (4)$$

where N—MeIm and N—MeIm* are different molecules of *N*-methylimidazole.

Isolation of the intermediate at the electrode, and subsequent reduction of this species is not observed at higher levels of ligand simply because the equilibrium concentration of this component is too low. The rate of the reaction in Eqn. (4) is proportional to the free ligand concentration. At higher levels of ligand, the lifetime of the intermediate becomes infinitesimal.

From the data of Fig. 1, and the relationship [15] of the differential pulse voltammetric peak potential to $E_{1/2}$, the ratio of complex stabilities of Fe(II) and Fe(III) can be determined ($\log \beta_1^{III}/\beta_1^{II} = 3.04$ and $\log \beta_2^{III}/\beta_2^{II} = 7.60$). Brault and Rougee [16], have previously shown $\log \beta_1^{II}$ and $\log \beta_2^{II}$ to be 3.94 and 4.90, respectively, for addition of imidazole to 5,10,15,20-tetraphenylporphinato iron(II) (TPPFe). Walker et al. [13] have previously shown that there is little difference in formation constants for adduct formation of $OEPFe^+$ and $TPPFe^+$. Use of Eqn. (2) and Fig. 1, with the values of Brault and Rougee as reasonable estimates for the formation of OEPFe(N—MeIm) and $OEPFe(N—MeIm)_2$, gives calculated $\log \beta_1^{III}$ and $\log \beta_2^{III}$ values of 7.0 and 12.5, respectively. These values agree with the predicted values of Walker et al. [13].

In summary, the intermediate iron(III) mono-ligand porphyrin $OEPFe(N—MeIm)^+$ was observed electrochemically for the first time. This complex can be reduced to a similar mono-ligated Fe(II) complex, OEPFe(N—MeIm). For redox systems in which both species at the electrode are complexed by an equivalent number of ligands, it can be predicted that a separate process will be observed for each intermediate species whenever the production of the intermediate is rate-limiting [6]. Identification of the stoichiometry of each species encountered is readily accomplished by monitoring the current dependence on the ligand:metal molar ratios for each process observed. The results in this study, as well as similar studies now in progress on rhodium and ruthenium complexes, suggest that differential pulse voltammetry may be the method of choice for unravelling complexation reactions at low levels of ligand.

Acknowledgement is made to the National Institutes of Health (Grant GM-25172) for support of this work. We also acknowledge several helpful discussions with Dr. Tadeusz Malinski.

REFERENCES

1 D. D. DeFord and D. N. Hume, J. Am. Chem. Soc., 73 (1951) 5321.
2 D. R. Crow, Polarography of Metal Complexes, Academic Press, New York, 1969.
3 D. J. Leggett, Talanta, 27 (1980) 787.
4 J. E. Spell and R. H. Philip, Jr., J. Electroanal. Chem., 112 (1980) 281.
5 K. Osura, Y. Fukusima and I. Aomizu, J. Electroanal. Chem., 107 (1980) 271.
6 N. G. Elenkova and T. K. Nedelcheva, J. Electroanal. Chem., 69 (1976) 271, 395.
7 K. M. Kadish, L. A. Bottomley and J. S. Cheng, J. Am. Chem. Soc., 100 (1978) 2731.
8 K. M. Kadish, L. A. Bottomley and D. Beroiz, Inorg. Chem., 17 (1978) 1124.
9 K. M. Kadish and L. A. Bottomley, Inorg. Chem., 19 (1980) 832.

10 K. M. Kadish, L. R. Shiue, R. K. Rhodes and L. A. Bottomley, Inorg. Chem., 20 (1981) 1274.
11 D. H. Dolphin, J. R. Sams and T. B. Tsin, Inorg. Chem., 16 (1977) 711.
12 K. M. Kadish, L. A. Bottomley, S. Kelly, D. Schaeper and L. R. Shiue, Bioelectrochem. Bioenerg., 8 (1981) 213.
13 F. A. Walker, M. W. Lo and M. T. Ree, J. Am. Chem. Soc., 98 (1976) 5552.
14 J. D. Satterlee, G. N. LaMar and T. J. Bold, J. Am. Chem. Soc., 99 (1977) 1088.
15 G. A. Heath and G. Hefter, J. Electroanal. Chem., 84 (1977) 295.
16 D. Brault and M. Rougee, Biochem. Biophys. Res. Commun., 57 (1974) 654.

Analytica Chimica Acta, 139 (1982) 373—377
Elsevier Scientific Publishing Company, Amsterdam — Printed in The Netherlands

Short Communication

A CHELATING GEL FOR COLLECTION OF COPPER FROM SEAWATER

C. H. CULBERSON* Y.-J. LIANG, T. M. CHURCH and R. H. WOOD
College of Marine Studies, University of Delaware, Newark, DE 19711 (U.S.A.)
(Received 12th October 1981)

Summary. An affinity chromatographic gel is coupled to carboxymethyl(imino)-bis(ethylenenitrilo)tetraacetic acid (DTPA) by a carbodiimide reaction. This gel is successful in extracting copper from seawater with high selectivity over alkaline earths such as magnesium. It is useful over a wide range of pH (4—9), and is stable and reversible over a period of nine months. Up to 20 μmol of copper can be adsorbed and recovered with greater than 99% efficiency with gel—DTPA prepared from 1 g of dry gel.

The very low levels of trace metals in waters such as seawater and the necessity of separating trace metals from alkali and alkaline earth elements in seawater prior to quantitation, make the determination of trace metals in seawater difficult without preconcentration. Preconcentration can be done by chelation and extraction [1, 2], coprecipitation [3], and chelating ion-exchange [4, 5]. Of the preconcentration techniques used, the ion-exchange method (essentially a two-step procedure) is simpler and less time-consuming than solvent extraction; it allows higher concentration factors to be attained, and it is amenable to use at sea. In addition, the sample is not subjected to contamination with heavy metal impurities from multiple reagents such as buffers and organic reagents. The most popular ion-exchange resin used for extracting trace metals from seawater (Chelex-100 [4, 6, 7]) has an affinity for alkali and alkaline earths that causes matrix problems during atomic absorption spectrometry of trace metals [6]; it will not remove metals held as organic and inorganic colloids which can be present even after ultrafiltration [2, 7]; and it swells and contracts, under various conditions, causing inconvenience [4, 5].

This communication describes a technique by which affinity chromatography [8] is used to prepare a new chelating resin which is easy to use and which is more selective for trace metals than Chelex-100. An insoluble bed material, AH-Sepharose 4B gel (Pharmacia Fine Chemicals, Piscataway, NJ) is coupled with a chelating agent, carboxymethyl(imino)-bis(ethylenenitrilo)-tetraacetic acid (diethylenetriamine-*N*,*N*,*N*′,*N*′,*N*′-pentaacetic acid; DTPA) through a carbodiimide promoted reaction [8, 9]. This reaction couples each of the terminal amine groups on the gel to one of the carboxyl groups on DTPA to form a peptide linkage

0003-2670/82/0000-0000/$02.75

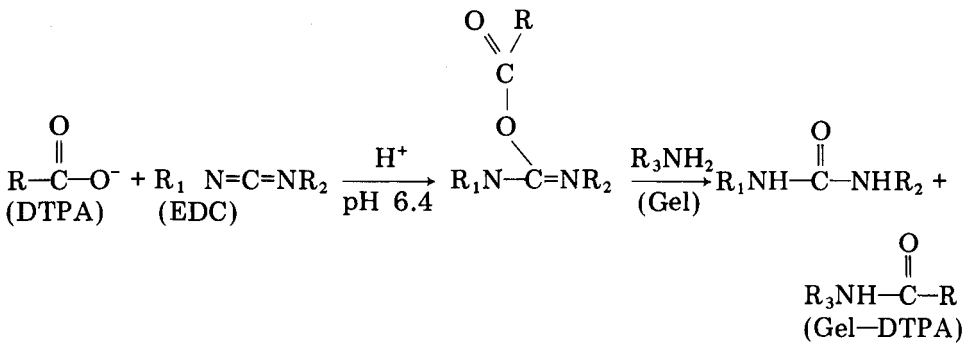

The coupled chelating gel (gel—DTPA) can be used to extract copper from seawater. Future papers will describe utilization of the gel for trace metal extraction and activity measurements in marine waters.

Experimental

Apparatus. A digital pH meter was used in conjunction with a combination pH electrode for the measurement of pH. Teflon-coated magnetic stirring bars (20 mm) were modified by suspension on plastic washers near each end to avoid grinding the gel while stirring in solution. Nuclepore filters (0.4 μm) prewashed with 4 M HCl were used in conjunction with a Millipore filter holder for all filtrations. A Millipore filter holder (ca. 20 ml in volume) was also used as a column when the column technique was used to elute copper from the gel with DTPA solution. Trace metals were quantified by atomic absorption spectrometry (a.a.s.) by either the flame or the electrothermal technique. The spectrometer used was a dual channel model with deuterium background correction (Instrumentation Lab., model-751, Wilmington, MA) equipped with a flameless atomizer (IL-555), and a flatbed recorder.

Solutions and reagents. All chemicals were reagent grade unless otherwise noted. Distilled water was double-distilled in a quartz still. Reagent-grade hydrochloric and nitric acids were ultra-purified in a quartz sub-boiler before use. The 1-ethyl-3-(3-dimethylaminopropyl)carbodiimide hydrochloride (EDC; Pierce Chemical Company, Rockford, IL), and AH-Sepharose 4B gel (Pharmacia Fine Chemicals) were used as received. The chelating reagent, DTPA, was purified by dissolving in sodium hydroxide solution (pH 12) followed by recrystallization at pH 0.5 using concentrated hydrochloric acid. Recrystallized DTPA was filtered, washed with distilled water, dried (85—90°C, overnight), dissolved in base solution (final pH > 4), and diluted to concentration.

Coupling DTPA to gel. The general procedures for the treatment of the gel and for the carbodiimide reaction were as described [8]. However, the coupling conditions must be optimized for each ligand. Dry gel (1 g) was permitted to swell in 100 ml of 0.5 M NaCl solution for 30 min. The gel was filtered off, washed with 200 ml of 0.5 M NaCl to insure complete removal of

lactose and dextran, and then washed with 100 ml of distilled water (pH 6.4). The swollen gel had a volume of about 4 ml g^{-1} of dry gel. Then DTPA (10 ml, 0.176 M) was adjusted to pH 6.4, and mixed with the swollen gel and with 1.0 g of EDC for the carbodiimide reaction. The pH of the solution, which tended to decrease during the first hour of the reaction, was held constant by the addition of sodium hydroxide (0.05 M). The suspension was stirred, and the coupling reaction was allowed to proceed at room temperature overnight. At the end of the reaction, the coupled gel—DTPA was collected by filtration and washed with 50 ml of the reaction medium before being used for the adsorption of copper from solution.

Adsorption of copper and regeneration of gel—DTPA. A batch technique was used to test the efficiency of gel—DTPA to adsorb copper from solution. The gel—DTPA, washed as above, was added to 100 ml of the sample solution containing various amounts of copper in 0.7 M $NaClO_4$. The solution was stirred, the pH was adjusted to the desired value, the stirring was stopped and copper adsorption was allowed to proceed at constant temperature (25 ± 0.06° C) overnight. The sample was then filtered and the filtrate was saved for measurement of the copper left in the solution. Then dilute sodium hydroxide solution (20 ml, pH 9) was passed through the gel to leach any reaction medium trapped in the pores. The gel was then rinsed with 40 ml of DTPA solution (pH 8) to elute the adsorbed copper using a Millipore filter holder as the column. Finally the gel was rinsed with 100 ml of distilled water to remove any DTPA trapped in the pores and to complete regeneration of the gel for future use.

Handling of the gels. The gel should not be exposed to extreme pH ranges ($3 < pH < 9$) [8]. Early tests of the acid leaching of copper from the gel—DTPA showed that the gel did not absorb copper after treatment with 1×10^{-3} M HCl, nor could DTPA be re-coupled to this gel. This indicates that acidic conditions denatured the gel. When the gel—DTPA—Cu was washed with pH 9 NaOH, however, no degradation of the adsorption property of the coupled gel—DTPA was observed, and the same gel—DTPA could be used to adsorb copper repeatedly for a period of nine months. The raw gel and the coupled gel—DTPA were stored in distilled water at 8° C, without freezing, when not in use. This storage technique was found satisfactory for the preservation of the gel and the gel—DTPA complex for up to 9 months.

Atomic absorption spectrometry of copper. The electrothermal technique used to determine copper was first found to be difficult because the high salt content of the sample caused spattering during the drying stage, and the sodium perchlorate used as the reaction medium corroded the graphite rod at high atomization temperatures, giving irreproducible results. These difficulties were overcome by extending the drying time (Table 1) and by replacing sodium perchlorate by sodium chloride. This medium (0.7 M NaCl) was further modified by addition of 3% (v/v) nitric acid and 0.25% DTPA. Table 1 lists the parameters used for the determination of copper left in the solution.

TABLE 1

Parameters used for electrothermal atomic absorption spectrometry of copper

Wavelength	324.7 nm	Pyrolysis	125—350(45), 350—550(45)°C
Bandwidth	5 nm	Atomization	850—2200(0), 2200(5)°C (s)
High voltage setting	620	Argon (SCFH)	20
Current	2 mA	Sample size	10 μl
Mode	AA, Normal, L	Scale expansion	2 X
Integration	Auto, 1/16	Auto clean mode	No
Drying	25—75(30), 75—125(45)°C (s)		

Results and discussion

The primary goal of this study was to synthesize a chelating reagent which would contain a strong ligand for chelating trace metals such as copper. The uncoupled gel itself adsorbed insignificant amounts of copper (adsorption $\leqslant$8.25% for a total copper content of 40 μmol). The gel—DTPA, as prepared here, however, adsorbed copper almost stoichiometrically and was used

TABLE 2

Uptake of copper by the gel—DTPA complexes prepared at various conditions[a]

Sample No.	Coupling conditions[b]		Copper adsorbed	
	EDC (mg)	pH	(%)[c]	(μmol)
1	6	4.82	0.00	0.00
2	15	4.82	5.40	1.08
3	127	4.82	16.15	3.23
4	240	4.82	21.40	4.28
5	240	4.80	21.88	8.75
6	500	4.80	31.50	12.60
7	240	4.80	24.63	9.85
8	1000	4.80	38.38	15.35
9	1000	5.50	99.39	19.88
10	500	5.50	98.72	19.74
11	1000	6.24	98.99	19.80
12	500	6.24	98.92	19.78
13	1000	6.39	98.99	19.80
14	500	6.39	98.92	19.78
15	1000	5.50	18.97	37.93
16	500	5.50	16.56	33.12
17	1000	6.24	26.75	53.50
18	500	6.24	24.49	48.97
19	1000	6.39	26.82	53.65
20	500	6.39	25.98	50.96

[a]The coupling reaction and the copper adsorption were allowed to proceed overnight at room temperature and at constant temperature, respectively. [b]DTPA: samples 1—6, 888 μmol; samples 7—20, 1763 μmol. [c]Copper added: samples 1—4 and 9—14, 20 μmol; samples 5—8, 40 μmol; samples 15—20, 200 μmol.

repeatedly for nine months without losing its adsorption capacity. Table 2 shows the efficiency of copper adsorption by gel—DTPA complexes which were prepared under various coupling conditions. It can be seen that higher concentrations of EDC and DTPA used for the coupling reaction enhanced the ability of the coupled gel—DTPA to adsorb copper from solution; higher pH (>5.5) of the coupling reaction was necessary for production of a satisfactory gel—DTPA complex; and the optimum conditions for the coupling reaction include maintaining the solution pH at 6.4 and using 1.0 g and 1763 μmol of EDC and DTPA, respectively, for up to 54 μmol of copper.

Several experiments with gel—DTPA prepared from 1 g of gel at optimum conditions demonstrated that 20 μmol of copper was absorbed with greater than 99% efficiency. When the gel—DTPA on which copper was adsorbed was washed with distilled water prior to elution with DTPA, recoveries of copper after washing averaged 95.3% with a standard deviation of 1.4% for five experiments. When similar samples were washed with 1×10^{-5} M NaOH, recoveries after washing averaged 101.8% with standard deviation of 2.1%. Apparently, distilled water contains enough acid to elute some of the copper bound to the gel—DTPA system.

The ultimate goal of this study is to use the coupled gel—DTPA to determine the activity of copper in seawater. This possibility is being examined and results will be reported at a later date.

This work was supported by the Office of Naval Research Contract N0014-77-C-0290. We thank Dr. Meares (University of California, Davis) for suggesting the use of DTPA in preparing the gel.

REFERENCES

1 P. G. Brewer, D. W. Spencer and C. L. Smith, Atomic Absorption Spectrometry, Am. Soc. Testing Materials, STP 443, 1969, p. 70.
2 K. W. Bruland, R. P. Franks, C. A. Knauer and J. H. Martin, Anal. Chim. Acta, 107 (1979) 233.
3 E. A. Boyle and J. M. Edmond, in T. Gibbs (Ed.), Analytical Methods in Oceanography, Adv. Chem. Series, Vol. 147, Ch. 6, pp. 44—55.
4 J. P. Riley and D. Taylor, Anal. Chim. Acta, 40 (1968) 479.
5 H. M. Kingston, I. L. Barnes, T. J. Brady and T. C. Rains, Anal. Chem., 50 (1978) 2064.
6 J. H. Martin, K. W. Bruland and W. W. Broenkow, in H. L. Windom and R. A. Duce (Eds.), Marine Pollutant Transfer, Ch. 7, D. C. Heath and Co., Lexington, MA, 1976, pp. 159—184.
7 T. M. Florence and G. E. Batley, Talanta, 22 (1975) 201; 23 (1976) 179.
8 Pharmacia Fine Chemicals, Affinity Chromatography: Principles and Methods, Piscataway, NJ, 1976, 71 pp.
9 C. R. Lowe and P. D. G. Dean, Affinity Chromatography, Wiley, New York, 1976, 272 pp.

Analytica Chimica Acta, 139 (1982) 379—382
Elsevier Scientific Publishing Company, Amsterdam — Printed in The Netherlands

Short Communication

DETERMINATION OF THE SECOND ACIDITY CONSTANT OF LUMINOL

KEIJO E. HAAPAKKA*, JOUKO J. KANKARE and JYRKI A. LINKE
Department of Chemistry, University of Turku, SF-20500 Turku 50 (Finland)
(Received 9th February 1982)

Summary. The second acidity constant of luminol, determined by a graphical spectrophotometric method at 25.0°C and an ionic strength of 5.0, is $pK_{a,2}$ = 15.1. A method for purification of luminol is also given.

The chemiluminescent reaction of luminol, 5-amino-2,3-dihydro-1,4-phthalazinedione or 3-aminophthalhydrazide, has been extensively studied [1—3] and its analytical applicability investigated [4—8]. However, there are few studies on the acidity constants of luminol. Weber [9] and Erdey et al. [10] using a fluorimetric technique, reported nearly identical values for the first acidity constant. Babko and Lukovskaya [11] using a spectrophotometric method obtained a somewhat higher value and also reported a value for the second acidity constant.

The principal purpose of the present study was to determine the second acidity constant of luminol by a spectrophotometric method. A method for purifying luminol by crystallization of its monosodium salt is also presented.

Experimental

Apparatus. The Cary 17D spectrophotometer (Varian Associates, CA) used was calibrated with didymium glass and standard potassium dichromate solutions [12].

Reagents. Luminol (Fluka, pract.) was purified as described below. The luminol stock solution was stored under nitrogen. Sodium chloride, sodium hydroxide and boric acid (Suprapur, Merck) were used as received. The accurate molarity of the sodium hydroxide stock solution was determined by conventional potentiometric titration; sample solutions were diluted with a calibrated Finnpipette. Ethanol and nitrogen were of the purest grade available.

Procedure. The sample and reference solutions were prepared simultaneously in quartz-distilled water using calibrated Finnpipettes and volumetric flasks. The absorbance measurements were carried out at 25.0° C.

Results and discussion

Purification of luminol. In numerous studies commercial luminol has been used without further purification, probably because it is difficult to find a

0003-2670/82/0000-0000/$02.75

suitable solvent from which to crystallize luminol. However, it can be purified by crystallization from concentrated hydrobromic acid as its hydrobromide or from 5% (w/v) sodium hydroxide as its sodium salt, after which the crystals are redissolved in excess of aqueous ammonia, the solution is diluted with ethanol and finally luminol is precipitated by slow addition of acetic acid. The molar absorptivity values reported for purified luminol, however, differ considerably. Lee and coworkers [13, 14] using the hydrobromic acid method reported 7600 l mol^{-1} cm^{-1}; Epstein and Kuwana [15] and Haapakka and Kankare [16], using the sodium hydroxide method, found values of 7440 and 7750 l mol^{-1} cm^{-1}, respectively.

The sodium salt of luminol crystallizes as long (1 cm), colourless, needles from its 0.1 M solution in 5 M sodium hydroxide over two weeks. The crystals were washed with ethanol under a nitrogen atmosphere and dried carefully under reduced pressure. Elemental analysis gave the results: 48.1% C, 3.1% H, 16.1% O, 21.15% N, 11.8% Na; required for the monosodium salt 48.25% C, 3.0% H, 16.1% O, 21.1% N, 11.5% Na. The molar absorptivity of the purified luminol was 7720 l mol^{-1} cm^{-1} at the wavelength of maximum absorbance of 348.5 nm in aqueous 0.05 M potassium hydroxide solution.

Second acidity constant of luminol. If LuH_2 is regarded as the neutral luminol molecule, acidity constants K_{a_1} and K_{a_2} correspond to the formation of LuH^- and Lu^{2-}, respectively. The pK_{a_1} values reported earlier were 6.20 at ionic strength 0.1 [10] and 6.74 at ionic strength 1.0 [11]; the pK_{a_2} value reported was 14.2 at ionic strength 4.0 [11].

The usual spectrophotometric method is unsuitable for determining the pK_{a_2} value of luminol, because the conditions necessary for the isolation of the pure luminol dianion would be too alkaline for accurate work. The pK_{a_2} value, however, can be determined by using a modified graphical spectrophotometric method [17], which utilizes the equation $A = A_{Lu^{2-}} - [c_{H^+}(A - A_{LuH^-})]/K_{a_2}$, where A is the absorbance of a luminol test solution with a certain hydrogen ion concentration (c_{H^+}), $A_{Lu^{2-}}$ is the absorbance of the luminol dianion, and A_{LuH^-} is the absorbance of the luminol monoanion. A plot of A vs. $c_{H^+}(A - A_{LuH^-})$ should be linear and the pK_{a_2} value of luminol could be calculated from the slope.

Figure 1 shows the spectrum obtained from the luminol test solution in pH 10.0 buffer, i.e., the spectrum of the luminol monoanion, as well as the spectra obtained from solutions of stronger sodium hydroxide concentrations. The difference in spectra between the luminol test solutions in 4.0 M sodium hydroxide and in pH 10.0 buffer (Fig. 2) shows that 370.5 nm is the most sensitive wavelength for following the formation of the luminol dianion. The utilization of this wavelength in determining the pK_{a_2} value of luminol, however, is not reasonable because of the rapid absorbance changes with changes in wavelength shown in Fig. 1. Hence the absorbance measurements were carried out at 323.0 nm, where such absorbance changes are small, but there is a reasonable change in absorbance with pH.

In order to determine the pK_{a_2} value of luminol from the above equation, the absorbances of the luminol test solutions were measured at the hydroxide

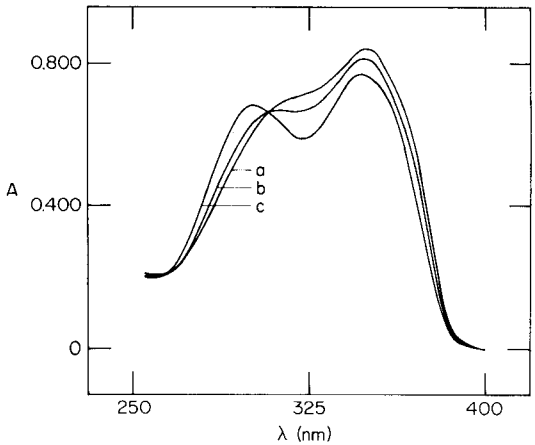

Fig. 1. Luminol spectra in (a) 5.0 M NaOH; (b) 3.0 M NaOH; (c) pH 10.0, H_3BO_3—NaOH buffer. Ionic strength 5.0 adjusted with NaCl, 1.00×10^{-4} M luminol, scan rate 0.2 nm s^{-1}, 25.0° C.

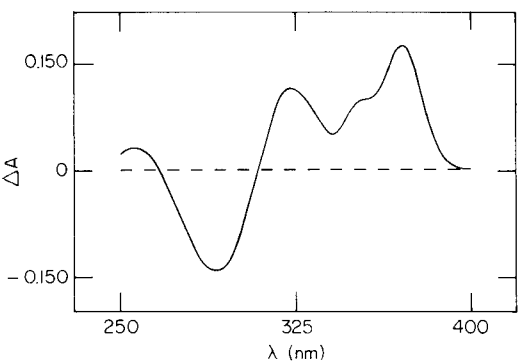

Fig. 2. Difference between spectra of luminol in 4.0 M NaOH and pH 10.0 buffer. Conditions as in Fig. 1.

TABLE 1

Determination of the $pK_{a,2}$ value of luminol
(Ionic strength 5.0 adjusted with NaCl, 1.00×10^{-4} M luminol, measured at 323.0 nm, 25° C.)

c_{OH^-} (M)	c_{H^+} (M)	A	$c_{H^+}(A - A_{LuH^-})$ (M)
4.882	1.292×10^{-15}	0.7072	1.753×10^{-16}
3.906	1.615×10^{-15}	0.6899	1.912×10^{-16}
2.929	2.154×10^{-15}	0.6679	2.076×10^{-16}
1.953	3.231×10^{-15}	0.6377	2.139×10^{-16}
0.976	6.465×10^{-15}	0.6100	2.489×10^{-16}

concentrations stated in Table 1. The absorbance of the luminol monoanion, A_{LuH^-} = 0.5715, was measured in the H_3BO_3—NaOH buffer at pH 10.0 All the test solutions were adjusted to an ionic strength of 5.0 by sodium chloride. The hydrogen ion concentrations were calculated using the pK_w value of 14.20 [18]. The slope of the linear plot of A vs. $c_{H^+}(A - A_{LuH^-})$ based on the data in Table 1, gives $pK_{a,2}$ = 15.1 for luminol at this ionic strength. The intercept on the y-axis gives an absorbance of 0.9486 for the luminol dianion under these conditions.

The $pK_{a,2}$ value of luminol obtained in this study differs approximately one order of magnitude from the value 14.2, reported by Babko and Lukovskaya [11] but it is almost the same as the value 15.0 reported by Dubovenko et al. [19] for 4-dimethyl-phthalhydrazide.

REFERENCES

1 See, e.g., F. McCapra, Essays Chem., 3 (1972) 101.
2 K.-D. Gundermann, Top. Current Chem., 46 (1974) 63.
3 D. F. Roswell and E. H. White, Methods Enzymol., 57 (1978) 409.
4 U. Isacsson and G. Wettermark, Anal. Chim. Acta, 68 (1974) 339.
5 W. R. Seitz and M. P. Neary, Anal. Chem., 46 (1974) 188A.
6 D. B. Paul, Talanta, 25 (1978) 377.
7 J. L. Burguera, A. Townshend and S. Greenfield, Anal. Chim. Acta, 114 (1980) 209.
8 D. Pilosof and T. A. Nieman, Anal. Chem., 52 (1980) 662.
9 K. Weber, Chem. Ber., 75 (1942) 565.
10 L. Erdey, I. Buzas and K. Vigh, Talanta, 13 (1966) 463.
11 A. K. Babko and N. M. Lukovskaya, Ukr. Khim. Zh. (Russ. Ed.), 29 (1963) 479.
12 A. J. Gordon and R. A. Ford, The Chemist's Companion, Wiley, New York, 1972, p. 213.
13 I. B. C. Matheson and J. Lee, Photochem. Photobiol., 12 (1970) 9.
14 J. Lee and H. H. Seliger, Photochem. Photobiol., 15 (1972) 227.
15 B. Epstein and T. Kuwana, Photochem. Photobiol., 4 (1965) 1157.
16 K. E. Haapakka and J. J. Kankare, Anal. Chim. Acta, 118 (1980) 333.
17 A. Albert and E. P. Serjeant, The Determination of Ionization Constants, Chapman and Hall, London, 1971, p. 44.
18 A. Martell and L. G. Sillen (Eds.), Stability Constants of Metal-Ion Complexes, The Chemical Society, London, 1964, p. 14.
19 L. I. Dubovenko, L. A. Pilipenko and O. S. Tsyndrovskaya, Ukr. Khim. Zh. (Russ. Ed.), 47 (1981) 755.

Analytica Chimica Acta, 139 (1982) 383—385
Elsevier Scientific Publishing Company, Amsterdam — Printed in The Netherlands

Announcement

WORKING PARTY ON ANALYTICAL CHEMISTRY (WPAC), FEDERATION OF EUROPEAN CHEMICAL SOCIETIES (FECS)

EUROPEAN ANALYTICAL COLUMN 5

By January 1982, the WPAC consisted of 27 national chemical societies of 21 European countries represented by 26 delegates. Among the FECS member societies, only the Portuguese Chemical Society, the Pancyprian Union of Chemists, and the Turkish Chemical Society are not represented in the WPAC. The Rumanian Chemical Society sent an observer to the last WPAC meeting.

The 12th meeting of the WPAC was held in Helsinki, August 23, 1981, during the Euroanalysis IV conference. At this meeting, Prof. Dr. E. Pungor (Budapest) was elected as WPAC chairman for the period 1981—1984, and the following issues were discussed.

Euroanalysis IV, August, 1981, Helsinki

This conference, the 25th event of FECS [conference chairman, Prof. Dr. L. Niinistö (Helsinki); further presidium members, D. Carroll (Dublin), A. Hulanicki (Warszaw), H. Malissa (Vienna)], was organized on behalf of the WPAC by the Association of Finnish Chemical Societies as a widely ranging conference, and was attended by 750 participants (including 100 accompanying persons) from 39 countries. The number of presented papers was well over 250, including 17 invited plenary and keynote lectures. The latter will be published in a joint East—West issue of the series *Review on Analytical Chemistry* with the title *Euroanalysis IV*, by Akademia Kiado (Budapest) and the Association of Finnish Chemical Societies. The conference program also included three special sessions (Analytical Chemistry, the Analyst and Society; Symbolism in Analytical Chemistry; and Mass Spectrometry in Inorganic Analysis) and a commercial exhibition of analytical equipment and literature.

FECS lecture 1981

The FECS lecture, which is delivered annually on the occasion of a major event of FECS, was given in 1981 by Prof. Bengt Samuelson (Karolinska Institutet, Stockholm), by invitation of the Association of Finnish Chemical Societies. Professor Samuelson presented an outstanding survey on *Leukotrienes: A New Group of Biologically Active Compounds*, at the Finlandia Hall, Helsinki, during Euroanalysis IV.

Euroanalysis V, 1984

It was announced that the next conference will be held in Cracow, Poland,

August 26—31, 1984, at the Jagellonian University and the Technical University Cracow. The decision will be considered at the next WPAC meeting on April 26, 1982, in Munich. Depending on the report of the Polish delegation, the topics of special sessions will be decided.

Euroanalysis VI, 1987

According to a decision at the last WPAC meeting, Euroanalysis VI will be organized on behalf of the WPAC by the host society of the French Chemical Societies in 1987 in France. The actual location will be decided later.

Euroanalysis VII, 1990

There has been an official bid from the Austrian Society of Microchemistry and Analytical Chemistry to hold this conference in 1990 in Vienna.

COBAC II (FECHEM conference on computer-based analytical chemistry), Munich, April 28—29, 1982

The conference will be organized by WPAC in cooperation with the Analytical Chemistry Division of the Gesellschaft Deutscher Chemiker, under the chairmanship of Dr. Ziegler (Mühlheim) for Prof. Fahr (who died in July 1981) and Prof. Breuer (Bonn). The following topics will be discussed: on-line coupling of computers and analytical equipment, integrated process control systems, peripheral equipment; desk computers and their application in computer-based interpretation of spectra; library search procedures, and identification of substances by means of spectroscopic data; programs for analytical chemistry; pattern recognition; present status of computerization in clinical analysis; interpretation of clinical data; control of significance of clinical data; role of computerization in the economics of a large laboratory.

COBAC III

This FECHEM conference is planned to be held as a special session of the Euroanalysis V conference. Professor Hippe (Rzeszow, Poland) has been proposed as conference chairman. Scientists interested in this active field of research are invited to contact the secretary of WPAC (address below).

Education in analytical chemistry

As part of the preparation for the next FECHEM conference on education in analytical chemistry (in connection with Euroanalysis V), a questionnaire has been prepared in an attempt to establish the new developments in this field in Europe after the last FECHEM conference in Vienna 1980. All institutions active in the field of higher education in analytical chemistry are invited to apply for a copy of the questionnaire. Please write to the secretary of WPAC if copies are required.

Chemometrics and analytical chemistry

A definition of chemometrics (as approved by the Chemometrics Society)

and a model curriculum for chemometric studies were presented by Dr. Christie (Oslo) and will be further discussed at the next meeting.

Pending FECS sponsorship

On request of the new chairman, Prof. Pungor, WPAC should ask for FECS sponsorship for:

(a) symposium on electrochemical detection in flow analysis, Matrafüred (Hungary), October 17—20, 1982;

(b) symposium on pattern recognition, Matrafüred (Hungary), October 20—22, 1982;

(c) FECHEM conference on good laboratory practices (date and location to be specified).

Next (13th) meeting of the WPAC

The Fachgruppe Analytische Chemie of the Gesellschaft Deutscher Chemiker invited WPAC to hold the 13th meeting in München in connection with the "Biochemische Analytik" and the "Analytika" on Monday, April 26, 1982.

PROF. DR. R. KELLNER, WPAC Secretary,
Institut für Analytische Chemie,
Technische Universität Wien,
A-1060 Wien, Getreidsmarkt 9, Austria

ANALYTICA CHIMICA ACTA, Vol. 139 (1982)

AUTHOR INDEX

(continued from outside of cover)

Short Communications

CONTENTS

(*continued on inside back cove*